JACC
Basic to Translational Science

A Journal of the American College of Cardiology

JACC
Basic to Translational Science
A Journal of the American College of Cardiology

CORRESPONDENCE FOR AMERICAN COLLEGE OF CARDIOLOGY

All correspondence for the College, other than that related to *JACC: Basic to Translational Science* should be sent to Resource Center, American College of Cardiology, 2400 N Street, NW, Washington, DC 20037

JACC: BASIC TO TRANSLATIONAL SCIENCE VOL. 4, NO. 3, 2019

CLINICAL RESEARCH

Breastfeeding, Cellular Immune Activation, and Myocardial Recovery in Peripartum Cardiomyopathy

Agnes Koczo, MD,[a] Amy Marino, MD,[a] Arun Jeyabalan, MD,[a] Uri Elkayam, MD,[b] Leslie T. Cooper, MD,[c] James Fett, MD, MPH,[a] Joan Briller, MD,[d] Eileen Hsich, MD,[e] Lori Blauwet, MD,[f] Charles McTiernan, PhD,[a] Penelope A. Morel, MD,[a] Karen Hanley-Yanez, BS,[a] Dennis M. McNamara, MD, MS,[a] for the IPAC Investigators

JACC: BASIC TO TRANSLATIONAL SCIENCE CME/MOC/ECME

This article has been selected as this month's *JACC: Basic to Translational Science* CME/MOC/ECME activity, available online at http://www.acc.org/jacc-journals-cme by selecting the *JACC* Journals CME/MOC/ECME tab.

Accreditation and Designation Statement

The American College of Cardiology Foundation (ACCF) is accredited by the Accreditation Council for Continuing Medical Education (ACCME) and the European Board for Accreditation in Cardiology (EBAC) to provide continuing medical education for physicians.

The ACCF designates this Journal-based CME/MOC/ECME activity for a maximum of 1 AMAPRA Category 1 Credit or 1 EBAC Credit. Physicians should only claim credit commensurate with the extent of their participation in the activity.

Successful completion of this CME activity, which includes participation in the evaluation component, enables the participant to earn up to 1 Medical Knowledge MOC point in the American Board of Internal Medicine's (ABIM) Maintenance of Certification (MOC) program. Participants will earn MOC points equivalent to the amount of CME credits claimed for the activity. It is the CME activity provider's responsibility to submit participant completion information to ACCME for the purpose of granting ABIM MOC credit.

Breastfeeding, Cellular Immune Activation, and Myocardial Recovery in Peripartum Cardiomyopathy will be accredited by the European Board for Accreditation in Cardiology (EBAC) for 1 hour of External CME credits. Each participant should claim only those hours of credit that have actually been spent in the educational activity. The Accreditation Council for Continuing Medical Education (ACCME) and the European Board for Accreditation in Cardiology (EBAC) have recognized each other's accreditation systems as substantially equivalent. Apply for credit through the post-course evaluation.

Method of Participation and Receipt of CME/MOC/ECME Certificate

To obtain credit for JACBTS: Basic to Translational Science CME/MOC/ECME, you must:

1. Be an ACC member or JACBTS subscriber.
2. Carefully read the CME/MOC/ECME-designated article available online and in this issue of the *journal*.
3. Answer the post-test questions. At least 2 questions provided must be answered correctly to obtain credit.
4. Complete a brief evaluation.
5. Claim your CME/MOC/ECME credit and receive your certificate electronically by following the instructions given at the conclusion of the activity.

CME/MOC/ECME Objective for This Article: Upon completion of this activity, the learner should be able to: 1) list the risk factors for peripartum cardiomyopathy; 2) identify appropriate treatment strategies for women diagnosed with peripartum cardiomyopathy during pregnancy; and 3) discuss the changes in the T cell population in the postpartum period with and without breastfeeding.

CME/MOC/ECME Editor Disclosure: CME/MOC/ECME Editor L. Kristin Newby, MD, is supported by research grants from Amylin, Bristol-Myers Squibb Company, GlaxoSmithKline, Sanofi, Verily Life Sciences (formerly Google Life Sciences), the MURDOCK Study, NIH, and PCORI; receives consultant fees/honoraria from BioKier, DemeRx, MedScape/TheHeart.org, Metanomics, Philips Healthcare, Roche Diagnostics, CMAC Health Education & Research Institute; serves as an Officer, Director, Trustee, or other fiduciary role for the AstraZeneca HealthCare Foundation and the Society of Chest Pain Centers (now part of ACC); and serves in another role for the American Heart Association and is the Deputy Editor of *JACC: Basic to Translational Science*.

Author Disclosures: This investigation was supported by the National Heart, Lung, and Blood Institute through contract HL102429. The authors have reported that they have no relationships relevant to the contents of this paper to disclose.

Medium of Participation: Online (article and quiz).

CME/MOC/ECME Term of Approval

Issue Date: June 2019
Expiration Date: May 31, 2020

From the [a]University of Pittsburgh Medical Center, Pittsburgh, Pennsylvania; [b]University of Southern California, Los Angeles, California; [c]Mayo Clinic, Jacksonville, Florida; [d]University of Illinois, Chicago, Illinois; [e]Cleveland Clinic, Cleveland, Ohio; and the [f]Mayo Clinic, Rochester, Minnesota. This investigation was supported by the National Heart, Lung, and Blood Institute through contract HL102429. The authors have reported that they have no relationships relevant to the contents of this paper to disclose.

ISSN 2452-302X https://doi.org/10.1016/j.jacbts.2019.01.010

JACC: BASIC TO TRANSLATIONAL SCIENCE VOL. 4, NO. 3, 2019
JUNE 2019:291–300

Breastfeeding, Cellular Immune Activation, and Myocardial Recovery in Peripartum Cardiomyopathy

Agnes Koczo, MD,[a] Amy Marino, MD,[a] Arun Jeyabalan, MD,[a] Uri Elkayam, MD,[b] Leslie T. Cooper, MD,[c] James Fett, MD, MPH,[a] Joan Briller, MD,[d] Eileen Hsich, MD,[e] Lori Blauwet, MD,[f] Charles McTiernan, PhD,[a] Penelope A. Morel, MD,[a] Karen Hanley-Yanez, BS,[a] Dennis M. McNamara, MD, MS,[a] for the IPAC Investigators

VISUAL ABSTRACT

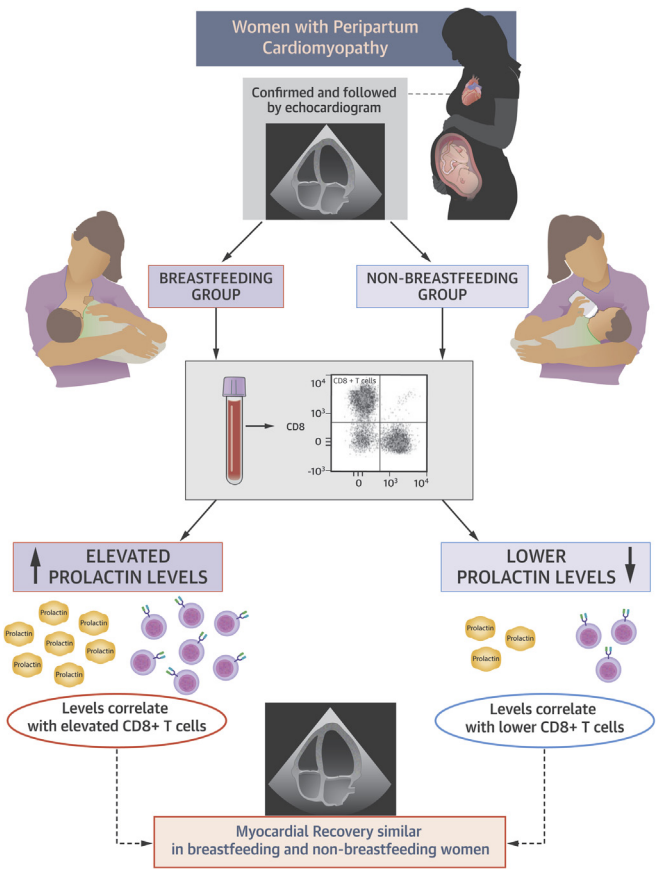

Koczo, A. et al. J Am Coll Cardiol Basic Trans Science. 2019;4(3):291–300.

HIGHLIGHTS

- **The impact of breastfeeding on prolactin, cellular immune activation, and myocardial recovery was analyzed in 100 women with peripartum cardiomyopathy**
- **Cardiac function was assessed by echocardiography at presentation and at serial intervals over the first year postpartum**
- **The levels of circulating prolactin were assessed by ELISA, and cellular immunophenotyping by flow cytometry, and compared between breastfeeding and nonbreastfeeding women**
- **Prolactin levels were higher in breastfeeding women and correlated with significant increases in CD8+ T cells**
- **Despite significantly higher prolactin levels and increased CD8+ cells, myocardial recovery was similar in breastfeeding and nonbreastfeeding women**

All authors attest they are in compliance with human studies committees and animal welfare regulations of the authors' institutions and U.S. Food and Drug Administration guidelines, including patient consent where appropriate. For more information, visit the *JACC: Basic to Translational Science* author instructions page.

Manuscript received August 22, 2018; revised manuscript received January 10, 2019, accepted January 11, 2019.

SUMMARY

The etiology of peripartum cardiomyopathy remains unknown. One hypothesis is that an increase in the 16-kDa form of prolactin is pathogenic and suggests that breastfeeding may worsen peripartum cardiomyopathy by increasing prolactin, while bromocriptine, which blocks prolactin release, may be therapeutic. An autoimmune etiology has also been proposed. The authors investigated the impact of breastfeeding on cellular immunity and myocardial recovery for women with peripartum cardiomyopathy in the IPAC (Investigations in Pregnancy Associated Cardiomyopathy) study. Women who breastfed had elevated prolactin, and prolactin levels correlated with elevations in $CD8^+$ T cells. However, despite elevated prolactin and cytotoxic T cell subsets, myocardial recovery was not impaired in breastfeeding women. (J Am Coll Cardiol Basic Trans Science 2019;4:291–300)

ABBREVIATIONS AND ACRONYMS

BF = breastfeeding

LVEF = left ventricular ejection fraction

NBF = nonbreastfeeding

PPCM = peripartum cardiomyopathy

Peripartum cardiomyopathy (PPCM) is a rare complication of pregnancy that remains a major cause of maternal morbidity and mortality. PPCM is classically defined as a nonischemic cardiomyopathy presenting toward the end of pregnancy or in the months following delivery, without previously known structural heart disease (1). An examination of the Nationwide Inpatient Sample database analysis of PPCM in the United States found that the incidence ranges from approximately 1 in 1,000 to 1 in 4,000 live births (2). It is more prevalent in Africa and Asia, with an incidence of about 1 in 1,000 live births. There are also particular "hot spots" of PPCM, including Haiti, in which the incidence of PPCM may be closer to 1 in 300 live births (3).

SEE PAGE 301

Much research has been dedicated to understanding the pathophysiology of PPCM, but the etiology remains unknown. Several hypotheses have been proposed, from hemodynamic stress to viral myocarditis and underlying autoimmune processes (3–5). A theory of unbalanced oxidative stress and hormonal interaction leading to vasculopathy was proposed in a 2007 study, which postulated that the cathepsin-cleaved 16-kDa form of prolactin may be crucial to the development of the condition. It further showed that the inhibition of prolactin with bromocriptine, a dopamine D_2 receptor agonist, inhibited the development of PPCM in a murine model (6). Recent studies have suggested that inhibition of prolactin with bromocriptine improves myocardial recovery (7–9). Given this postulate, a recent European study group recommendation advised against breastfeeding (BF) in women with PPCM, but these recommendations regarding BF in women with PPCM remain controversial (10).

In addition to its role in lactation, prolactin plays an important role in resetting maternal immunity in the peripartum and early postpartum periods. Despite the potential impact of prolactin on cellular immunity and the autoimmune hypothesis, there has been little investigation regarding the impact of BF on maternal cellular immunity in patients with PPCM. It also remains unclear as to whether prolactin-induced alterations of cellular immunity adversely affect recovery in these patients. We investigated the impact of BF and prolactin on cellular immunity and myocardial recovery in the prospective, multicenter IPAC (Investigations in Pregnancy Associated Cardiomyopathy) study.

METHODS

COHORT. One hundred women with newly diagnosed PPCM were enrolled within the first 13 weeks postpartum at 30 centers (Supplemental Material) between December 2009 and September 2012. All women were at least 18 years of age, had no histories of cardiac disease, had estimated left ventricular ejection fractions (LVEF) of ≤45% at the time of enrollment, and had evaluations consistent with recent-onset nonischemic cardiomyopathy presenting in late pregnancy or early postpartum without evidence of pre-existing structural heart disease. Women with significant valvular disease, coronary disease (>50% stenosis of a major epicardial vessel or positive results on noninvasive study), evidence of ongoing bacterial septicemia (positive blood cultures), ongoing drug or alcohol abuse, history of chemotherapy or chest radiation within 5 years of enrollment, or histories of previous cardiomyopathy were excluded.

PROTOCOL. The study protocol was approved by the Institutional Review Boards at all participating

TABLE 1 Demographics and Clinical Phenotype of the Breastfeeding and Nonbreastfeeding Cohorts

	Breastfeeding at Entry (n = 15)	Nonbreastfeeding at Entry (n = 85)	p Value
Age (yrs)	32 ± 6	30 ± 6	0.23
Race (black)	27	31	0.76
Days postpartum	20 ± 16	33 ± 25	0.07
Gravida	3.1 ± 2.5	2.8 ± 1.8	0.89
Para	2.0 ± 1.4	2.2 ± 1.4	0.53
NYHA functional class (I/II/III/IV)	13/67/20/0	12/42/26/20	0.06
LVEF (at entry) (%)	0.39 ± 0.06	0.34 ± 0.10	0.06
BP systolic (mm Hg)	117 ± 12	111 ± 18	0.09
BP diastolic (mm Hg)	77 ± 12	69 ± 3	0.02
HTN	42	60	0.26
BMI (kg/m^2)	27 ± 4	29 ± 8	0.30
ACE inhibitor	67	82	0.17
Beta-blocker	80	89	0.38

Values are mean ± SD or %, unless otherwise indicated.

ACE = angiotensin-converting enzyme; BMI = body mass index; BP = blood pressure; HTN = hypertension; LVEF = left ventricular ejection fraction; NYHA = New York Heart Association.

centers, and informed consent was obtained from all subjects. At the time of enrollment, demographic information including self-designated race, previous clinical evaluation, and current medical therapy were recorded. Women were followed until 1 year postpartum. All hospitalizations and major cardiac events including death, cardiac transplantation, and implantation of a left ventricular (LV) assist device were recorded.

LV FUNCTION. All subjects underwent echocardiography to assess LVEF at entry and 6 and 12 months postpartum. Echocardiograms were reviewed in a core laboratory at the University of Pittsburgh for assessment of ventricular volumes and calculation of ejection fraction. LV volumes and LVEF were assessed using the biplane Simpson's rule with manual tracing of digital images.

FLOW CYTOMETRY. Patients with PPCM (n = 67) enrolled early (during the first 6 weeks postpartum) had immunophenotyping repeated at 2 and 6 months postpartum. The remaining 33 subjects, enrolled at 2 months postpartum, had immunophenotyping performed at 2 and 6 months postpartum. For the early time point, all 67 women had blood collected (postpartum 16.6 ± 10.6 days), while 73 women were sampled at 2 months (postpartum 62.1 ± 11.5 days) and 77 women at the 6-month time point (postpartum 179.2 ± 33.2 days).

Immunophenotyping of circulating cells was performed on whole blood collected and stabilized in Cyto-Chex BCT tubes, approximately 3 days prior to multicolor flow cytometry. Antibodies against CD3, CD4, CD8, CD16, and CD56 were used for determination of cellular subsets: overall T cells ($CD3^+$), T helper cell subset ($CD3^+CD4^+$), cytotoxic T cells ($CD3^+CD8^+$), "double-negative" T cells ($CD3^+CD4^-CD8^-$), classical monocytes ($CD14^+CD16^-$), nonclassical monocytes ($CD14^-CD16^+$), and natural killer cells ($CD3^-CD56^+CD16^+$, $CD3^-CD56^+CD16^-$). Cell "activation" status was assessed by expression of CD25, CD38, or human leukocyte antigen DR isotype. Antigen-specific and compensation antibodies used in flow cytometry were previously published (11). Flow cytometry data were acquired using a BD FACS ARIA 1 and analyzed using FACSDiva version 6.1.3 software (BD Biosciences, Ashland, Oregon). Data are presented as the percentage of all events within a particular immunophenotyping "gate."

BIOMARKER ASSAYS. Serum was collected from 98 of 100 subjects at the time of entry, shipped overnight at room temperature to the core laboratory (University of Pittsburgh), and stored at −80°C until the time of analysis. Enzyme-linked immunosorbent assays for human prolactin were obtained from R&D Systems (Minneapolis, Minnesota), run with 50 μl of undiluted sample per well in duplicate, and read at 450 nm on a Packard Spectracount instrument (ALPCO, Salem, New Hampshire).

STATISTICAL ANALYSIS. All analyses were done in SPSS version 24 (IBM, Armonk, New York). For analysis of clinical and demographic variables, Fisher exact tests were used to compare categorical variables by BF status, BF versus non-BF (NBF). The Mantel-Haenszel test for trend was used for comparison of New York Heart Association functional class by BF status. For continuous variables, we examined the distribution of data for normality using the Shapiro-Wilk test. Given the skewed distributions of several clinical variables (e.g., days postpartum, gravida, para), the nonparametric Mann-Whitney *U* test was used to compare groups for all continuous clinical variables. Given similar skewed distributions of cellular activation and biomarker data, the Mann-Whitney *U* test was also used for comparison of the percentage of circulating immune cells and prolactin levels in BF versus NBF subsets. To evaluate the role of prolactin in immune activation, a regression model with prolactin levels and percentage $CD3^+CD8^+$ at entry was used with percentage $CD3^+CD8^+$ as a continuous outcome variable and prolactin levels as the predictor to examine the relationship between these 2 variables. We examined this relationship first in the overall cohort and in the subset of women BF at entry. The impact of BF on myocardial recovery was examined by comparing LVEF at entry, 6 months, and 12 months and change in LVEF from entry to 6 and 12 months between the BF and NBF subsets. LVEF and

TABLE 2 Flow Cytometry Analysis of Circulating Cells From Breastfeeding Women and Nonbreastfeeding Women

	Entry			2 Months			6 Months		
Cell Subset	**BF (n = 13)**	**NBF (n = 54)**	**p Value**	**BF (n = 12)**	**NBF (n = 61)**	**p Value**	**BF (n = 14)**	**NBF (n = 63)**	**p Value**
T cells									
$CD3^+$	54.7 ± 14.1	49.8 ± 15.1	0.24	**65.6 ± 7.1**	**56.3 ± 14.7**	**0.02**	**59.9 ± 13.1**	**54.8 ± 13.7**	**0.04**
$CD3^+CD4^+$	54.7 ± 9.0	59.1 ± 11.1	0.08	**49.7 ± 9.1**	**56.6 ± 10.6**	**0.02**	**54.6 ± 8.8**	**59.8 ± 8.3**	**0.03**
$CD3^+CD4^+HLA\text{-}DR^+$	2.8 ± 1.6	2.5 ± 1.9	0.33	3.0 ± 2.1	2.5 ± 1.3	0.77	2.4 ± 1.8	3.0 ± 3.2	0.63
$CD3^+CD4^+CD38^+$	47.6 ± 9.3	44.4 ± 12.4	0.52	46.3 ± 9.7	43.1 ± 13.2	0.60	**51.2 ± 8.2**	**43.3 ± 14.0**	**0.03**
$CD3^+CD4^+CD25^+$	3.1 ± 2.0	4.1 ± 3.0	0.38	4.3 ± 4.4	4.3 ± 4.2	0.89	5.9 ± 4.0	5.3 ± 6.1	0.14
$CD3^+CD8^+$	**37.4 ± 9.3**	**29.0 ± 6.1**	**0.003**	**37.0 ± 7.8**	**31.4 ± 6.1**	**0.02**	**36.4 ± 7.3**	**31.0 ± 7.0**	**0.01**
$CD3^+CD8^+HLA\text{-}DR^+$	7.9 ± 5.9	6.2 ± 7.7	0.29	6.7 ± 6.3	4.7 ± 3.3	0.66	6.5 ± 9.1	5.0 ± 4.3	0.86
$CD3^+CD8^+CD38^+$	33.6 ± 13.9	31.1 ± 13.2	0.48	32.6 ± 17.0	28.3 ± 14.2	0.44	35.0 ± 15.1	28.4 ± 14.1	0.10
$CD3^+CD8^+CD25^+$	0.3 ± 0.4	0.3 ± 0.5	0.85	0.3 ± 0.3	0.4 ± 1.2	0.44	0.4 ± 0.3	0.5 ± 1.3	0.16
$CD3^+CD4^+/CD8^+$	1.6 ± 0.7	2.2 ± 0.7	0.01	1.4 ± 0.4	1.9 ± 0.6	0.01	1.6 ± 0.5	2.1 ± 0.7	0.01
$CD3^+CD4^-CD8^-$	9.6 ± 16.0	7.4 ± 6.6	0.67	10.0 ± 6.7	9.1 ± 7.5	0.33	6.2 ± 3.5	7.6 ± 4.8	0.43
$CD3^+CD4\text{-}8^-HLA\text{-}DR^+$	5.7 ± 5.2	4.1 ± 5.4	0.26	4.1 ± 5.1	3.8 ± 2.8	0.54	4.2 ± 4.2	4.0 ± 3.6	0.98
$CD3^+CD4\text{-}8^-CD38^+$	28.4 ± 16.7	23.6 ± 11.2	0.41	23.2 ± 15.5	19.8 ± 10.2	0.70	24.2 ± 11.6	20.1 ± 11.5	0.15
$CD3^+CD4\text{-}8^-CD25^+$	0.6 ± 1.3	0.4 ± 0.5	0.82	0.4 ± 0.6	0.4 ± 0.8	0.98	1.0 ± 1.7	0.4 ± 0.5	0.26
$CD3^+CD56^+$	4.2 ± 8.5	2.2 ± 2.5	0.69	3.6 ± 3.2	2.8 ± 2.6	0.36	1.9 ± 0.9	3.7 ± 4.7	0.38
$CD3^+CD56^+CD8^+$	1.6 ± 2.2	1.2 ± 1.8	0.41	2.3 ± 2.5	1.8 ± 1.7	0.64	1.3 ± 0.9	2.4 ± 3.1	0.80
Monocytes									
$CD14^+$	15.9 ± 6.4	15.1 ± 8.1	0.60	10.4 ± 3.4	13.2 ± 5.9	0.06	13.3 ± 2.3	14.5 ± 6.1	0.62
$CD14^+CD16^-$	**91.4 ± 2.9**	**86.0 ± 7.8**	**0.005**	**89.4 ± 9.2**	**87.6 ± 5.2**	**0.04**	88.3 ± 3.3	86.4 ± 8.4	0.97
$CD14^+CD16\text{-}HLA\text{-}DR^+$	48.8 ± 9.5	45.6 ± 21.1	0.34	60.0 ± 16.6	52.7 ± 17.6	0.18	64.6 ± 18.1	60.7 ± 15.6	0.51
$CD14^+CD16^-CD38^+$	92.4 ± 11.3	91.8 ± 15.4	0.32	93.8 ± 6.0	91.7 ± 12.2	0.92	96.2 ± 5.1	95.1 ± 7.7	0.82
$CD14^+CD16^+$	**8.9 ± 3.1**	**13.7 ± 6.0**	**0.005**	11.0 ± 9.3	12.5 ± 5.4	0.07	12.0 ± 3.6	14.0 ± 8.7	0.93
$CD14^+CD16^+HLA\text{-}DR^+$	65.0 ± 12.0	58.2 ± 20.7	0.34	**74.4 ± 17.6**	**62.1 ± 19.4**	**0.03**	71.3 ± 23.0	70.0 ± 17.1	0.55
$CD14^+CD16^+CD38^+$	79.5 ± 16.3	80.5 ± 17.0	0.57	78.3 ± 19.1	75.0 ± 18.1	0.42	79.1 ± 16.5	80.8 ± 14.5	0.82
NK cells									
$CD3^-CD56^+CD16^+$	8.2 ± 4.2	6.2 ± 3.9	0.11	8.5 ± 3.0	8.5 ± 4.9	0.80	8.8 ± 4.0	8.8 ± 4.8	0.94
$CD3^-CD56^+CD16^+HLA\text{-}DR^+$	7.3 ± 5.3	7.8 ± 7.1	0.86	8.4 ± 4.9	6.1 ± 3.8	0.10	7.9 ± 4.9	8.3 ± 6.8	0.91
$CD3^-CD56^+CD16^+CD38^+$	93.4 ± 5.6	93.5 ± 13.5	0.47	91.9 ± 3.9	91.5 ± 7.4	0.49	90.4 ± 7.3	89.2 ± 9.4	0.87
$CD3^-CD56^+CD16^-$	2.6 ± 0.8	2.2 ± 1.5	0.08	3.1 ± 1.7	2.3 ± 1.3	0.11	2.0 ± 0.7	2.2 ± 1.1	0.34

Values are mean ± SD. Values with $p < 0.05$ are in **bold**.
BF = breastfeeding; NBF = nonbreastfeeding; NK = natural killer.

the percentage of $CD3^+CD8^+$ cells were compared between BF and NBF women for the entire cohort and for the subset with complete data at all time points. The relationship of initial prolactin level and percentage $CD3^+CD8^+$ cell to subsequent myocardial recovery was examined by linear regression using both as predictors with 6- and 12-month LVEFs as the outcome variables.

RESULTS

COMPARISON OF BF AND NBF COHORTS. Of the overall IPAC cohort, 15 women were BF at time of entry, and the remaining 85 were not. There were no significant differences in age, race, body mass index, parity, or medical therapy on the basis of BF (Table 1).

Women who breastfed tended to present earlier postpartum (days postpartum: BF, 20 ± 16; NBF, 33 ± 25; $p = 0.07$) and also demonstrated a nonsignificant trend toward higher LVEF at entry ($p = 0.06$) as well as a lower New York Heart Association functional class ($p = 0.06$). Diastolic blood pressure ($p = 0.02$) was higher in BF women, but the difference in systolic blood pressure was not significant ($p = 0.09$). The percentage of women treated with beta-blockers (BF, 80%; NFB, 89%; $p = 0.38$) and angiotensin-converting enzyme inhibitors (BF, 67%; NFB, 82%; $p = 0.17$) was similar between groups.

DIFFERENCES IN BF AND NBF CIRCULATING IMMUNE CELLS. Comparison of cellular subsets revealed a significant increase in the percentage of $CD3^+CD8^+$ cells in BF women (Table 2). This was evident at entry ($p = 0.003$) and remained significant at 2 ($p = 0.02$) and 6 ($p = 0.01$) months postpartum (Figure 1). When evaluated only in women with complete cellular data at all 3 time points, the mean values of percentage $CD3^+CD8^+$ cells were similar and

FIGURE 1 Percentage $CD3^+CD8^+$ T Cells at Entry and 2 and 6 Months for the Breastfeeding and Nonbreastfeeding Cohorts

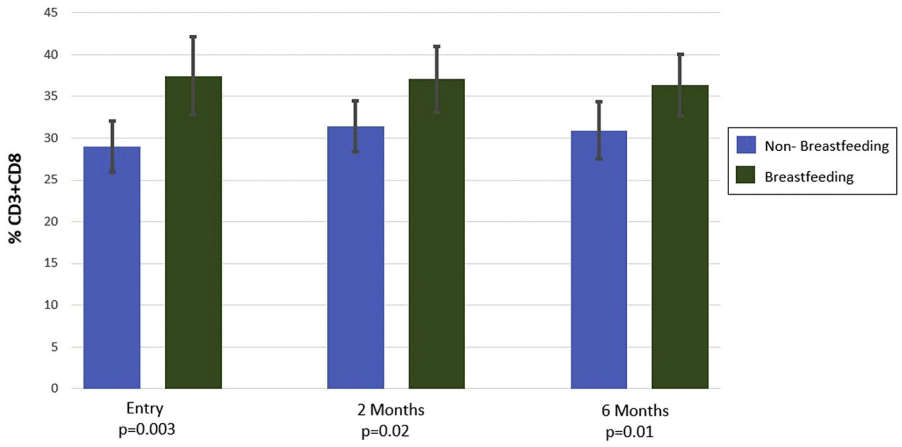

$CD3^+CD8^+$ cytotoxic T cells in breastfeeding women were significantly higher at entry ($p = 0.003$) and remained significant at 2 ($p = 0.02$) and 6 ($p = 0.01$) months postpartum.

remained significantly higher in BF women ($n = 41$; BF vs. NBF percentage $CD3^+CD8^+$ cells at entry, 40.7 ± 7.3 vs. 28.8 ± 6.3 [$p < 0.001$]; at 2 months, 38.0 ± 8.6 vs. 30.1 ± 5.9 [$p = 0.01$]; and at 6 months, 36.8 ± 6.9 vs. 30.3 ± 6.6 [$p = 0.02$]). In comparison, percentage $CD3^+CD4^+$ T helper cells were not significantly different at entry ($p = 0.08$) but were lower in BF women at 2 ($p = 0.02$) and 6 ($p = 0.03$) months. When evaluated in women with complete data at the 3 time points ($n = 39$), the mean values of percentage $CD3^+CD4^+$ cells were significantly lower in BF women at all time points (BF vs. NBF percentage $CD3^+CD4^+$ cells at entry, 51.0 ± 7.7 vs. 56.8 ± 13.2 [$p = 0.04$]; at 2 months, 49.3 ± 10.7 vs. 57.5 ± 10.1 [$p = 0.03$]; at 6 months, 53.6 ± 8.8 vs. 61.0 ± 8.3 [$p = 0.03$]). The percentage of nonclassical monocytes ($CD14^+CD16^+$) was significantly lower ($p = 0.005$) and the percentage of classical monocytes ($CD14^+CD16^-$) higher ($p = 0.005$) in the BF cohort at entry. Similar trends remained at 2 months, which remained significant for classical monocytes ($p = 0.04$) but not nonclassical monocytes ($p = 0.07$). These differences were no longer significant at 6 months.

A prior analysis (11) comparing circulating immune cells from women with PPCM in the IPAC cohort with healthy postpartum women revealed a significant

FIGURE 2 Correlation of the Percentage $CD3^+CD8^+$ T Cells With Prolactin Levels in the Overall and Breastfeeding Peripartum Cardiomyopathy Cohorts

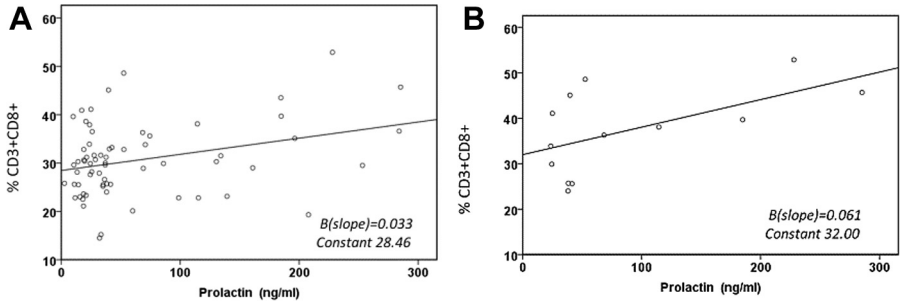

(A) In the overall peripartum cardiomyopathy cohort, higher serum levels of prolactin at entry were associated with a higher percentage of $CD3^+CD8^+$ cells ($n = 98$; $p = 0.01$). **(B)** In the smaller breastfeeding subset, higher serum prolactin levels remained significantly associated with a higher percentage of $CD3^+CD8^+$ cells ($n = 13$; $p = 0.04$).

FIGURE 3 Left Ventricular Ejection Fraction at Entry and 6 and 12 Months for the Breastfeeding and Nonbreastfeeding Cohorts

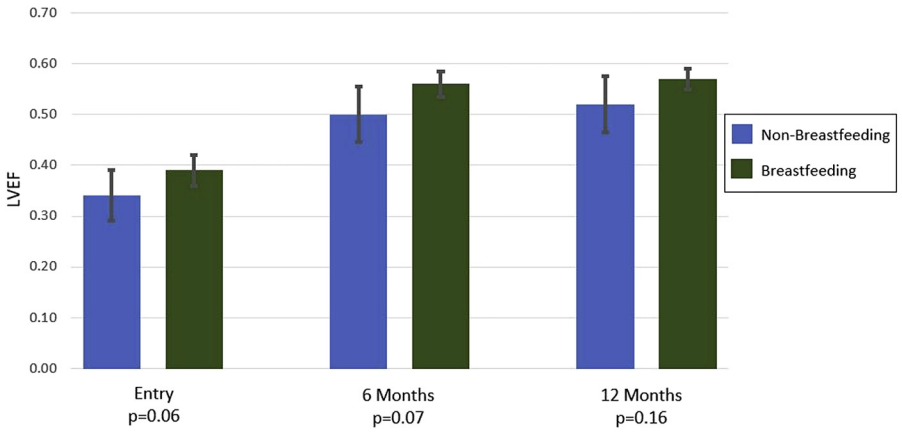

Mean left ventricular ejection fraction (LVEF) at entry displayed a trend toward a higher mean LVEF in the breastfeeding subset ($p = 0.06$), which was significant at 6 months ($p = 0.07$) but not 12 months ($p = 0.16$) postpartum.

reduction in natural killer cells ($CD3^-CD56^+CD16^+$) and an increase in $CD3^+CD4^-CD8^-$ double-negative T-cells in patients with PPCM. There was no observed difference in the percentage of either natural killer cells or double-negative T cells between the NBF and BF subsets in the present analysis. Prolactin levels at entry were significantly higher in BF women (NBF 50 ± 59 ng/ml vs. BF 82 ± 84 ng/ml; $p = 0.02$). Higher levels of prolactin at entry correlated with a greater percentage of $CD3^+CD8^+$ cells overall ($n = 66$; $p = 0.01$) (Figure 2A), and this remained significant when this analysis was limited to the smaller BF subset ($n = 13$; $p = 0.04$) (Figure 2B).

MYOCARDIAL RECOVERY: IMPACT OF BF, PROLACTIN, AND $CD3^+CD8^+$ CELLS. BF women had a trend toward higher LVEF at entry (BF 39 ± 6% vs. NBF 34 ± 10%; $p = 0.06$), with a similar difference at 6 months (BF 56 ± 5% vs. NBF 50 ± 11%; $p = 0.07$) and 12 months (BF 57 ± 4% vs. NBF 52 ± 11%; $p = 0.16$) postpartum (Figure 3). When evaluated only in women with complete LVEF data at all time points, the mean values of LVEF and p values were very similar to the analysis of the overall cohort ($n = 71$; BF vs. NBF at entry, 39 ± 6% vs. 34 ± 9% [$p = 0.07$]; 6 months, 56 ± 5% vs. 50 ± 12% [$p = 0.07$]; and 12 months, 57 ± 4% vs. 52 ± 12% [$p = 0.19$]). There were no differences noted by BF status in the mean change increase in LVEF from entry to 6 months (ΔLVEF: BF, 17 ± 9%; NBF, 16 ± 11%; $p = 0.46$) or in the mean change increase in LVEF from entry to 12 months postpartum (ΔLVEF: BF, 18 ± 8%; NBF, 17 ± 11%; $p = 0.68$). Analysis of linear regression models demonstrated that prolactin levels at entry did not predict subsequent LVEF at either 6 ($p = 0.47$) or 12 ($p = 0.40$) months. In a similar fashion, the percentage of $CD3^+CD8^+$ cells at entry also did not predict subsequent LVEF at 6 ($p = 0.59$) or 12 ($p = 0.84$) months.

DISCUSSION

This study revealed that in the women enrolled in the IPAC study who breastfed, there was a significantly higher percentage of circulating $CD3^+CD8^+$ cells at entry, and this higher percentage persisted through 6 months postpartum. Prolactin appears to be the driving force for this elevation, as there was also a linear relationship between percentage $CD3^+CD8^+$ cells and levels of prolactin for both the BF subset as well as the whole IPAC cohort. Despite the impact of prolactin and BF on maternal immunity, there was no clear evidence that BF (or prolactin) had any impact on subsequent LVEF at 6 or 12 months. Not surprisingly, the subset of women who breastfed had higher ejection fractions at entry and tended to be less ill than women who did not breastfeed. This difference persisted at 6 and 12 months. Overall in the IPAC study, there was no evidence that BF had any adverse impact on subsequent myocardial recovery.

The diagnosis of PPCM is made in late antepartum or early postpartum at a time when the adaptive down-regulation of maternal cellular immunity allowing fetal tolerance is ending and maternal cellular immunity is being restored. Prior studies have found differences in peripheral circulating subsets of T cell populations in women with PPCM

compared with healthy postpartum women (11). One preliminary study found that patients with PPCM had marked reductions of $CD4^+CD25^{lo+}$ T regulatory cells during the third trimester compared with normal healthy pregnant patients, which persisted for more than 1 month postpartum (6). $CD4^+CD25^+$ cells, also known as professional suppressor T cells, are a subset of regulatory T cells that have been found to suppress T cell activation in an antigen-independent manner. $CD4^+CD25^+$ cells are thought to have profound suppressive effects on $CD3^+CD8^+$ cells. Therefore, persistent low levels of regulatory T cells may be one mechanism for the greater numbers of $CD3^+CD8^+$ cells among BF women, which was demonstrated in our study.

Prolactin receptors are expressed on a number of immune cells, including T and B lymphocytes and thymic epithelial cells. Interestingly, some studies suggest that prolactin up-regulates Th1-type cytokines, which play a role in stimulating $CD3^+CD8^+$ cells (12–14), as found in our study. One study on patients with systemic lupus erythematous revealed that prolactin receptors were expressed on both $CD4^+CD25^+$ regulatory and effector T cells (15). Another study showed that when adding prolactin to cocultures of regulatory and effector T cells, prolactin seemed to impair regulatory T cell suppression of effector T cells via increased production of Th1 cytokines (16). In patients with PPCM who have marked reduction in $CD4^+CD25^+$ T regulatory cells, prolactin may play a role in enhancing the Th1 cytokine response, which could result in up-regulation of $CD3^+CD8^+$ T cells, as seen in our study.

Although BF and prolactin appear to affect $CD3^+CD8^+$ levels, there was no evidence in our study that this had clinical impact in terms of LVEF at presentation or subsequent myocardial recovery. Our data do not support a significant role for cytotoxic T cells in the pathogenesis of PPCM or subsequent recovery. Recently, we reported that a decrease in natural killer cells was evident in patients with PPCM compared with healthy postpartum control subjects, but in contrast, circulating cytotoxic T cell and T helper cell levels were not significantly different between the 2 cohorts (11). The present study found higher circulating cytotoxic T cells in patients with PPCM who breastfed than those who did not. Overall, the analysis of circulating cellular subset data did not support the autoimmune hypothesis. Consistent with the data from circulating cells, examination of myocardial inflammation in a subset of 39 women from IPAC who underwent cardiac magnetic resonance imaging revealed little evidence of myocardial inflammation for the majority of women (17). Although the prevalence of myocarditis on endomyocardial biopsy studies in PPCM varies from 10% to 62%, the pathological evidence mirrors what is seen in other forms of nonischemic cardiomyopathies and is positive only in a minority of subjects (18,19).

A pilot study of prolactin inhibition with bromocriptine in 20 South African women suggested that this strategy improved outcomes (20). A recent German study comparing high-dose versus low-dose bromocriptine in 63 women showed benefit compared with historical control subjects but did not show differences between the treatment groups and was limited by the absence of a control group not treated with bromocriptine (9). In addition, a German registry comprising 96 patients with PPCM showed that 67% (64 of 96) were treated with bromocriptine and revealed no difference in major adverse events, including advanced therapies, transplantation, or mortality among treatment subgroups (21). A randomized controlled trial enrolled 96 women in Burkina Faso in West Africa and revealed significant improvements in LVEF and end-diastolic LV diameter in the bromocriptine-treated group (8), though the control group had a lower recovery rate compared with European and U.S. cohorts. Despite limitations noted in each study, a recent publication from the Heart Failure Association of the European Society of Cardiology Study Group on PPCM discouraged BF and recommended the use of bromocriptine to block prolactin in patients with PPCM (10). Our study, in which women who breastfed had significantly higher LVEFs at 6 months, does not support this recommendation, nor does a retrospective Internet-based study in the United States that showed better outcomes among women with PPCM who breastfed (22). In addition, a recent single-center study showed that 27 of 63 patients with PPCM who breastfed had no significant difference in recovery status at 1 year compared with their NBF counterparts (23).

BF in postpartum women provides numerous maternal (24) and newborn benefits that may affect health far beyond the months spent actually BF, particularly in parts of Africa, Asia, and Haiti, where PPCM is endemic. In developing countries, where PPCM is more common than the United States, BF is of essential importance, not only as food and nutrition but also for neonatal immunity (25). Indeed, a recent report from the World Health Organization

stressing the importance of BF for neonatal health in the developing world stated that BF has the potential to save 800,000 lives for children in developing countries every year. The negative health effects on infants of women with PPCM who are prohibited from BF remains high (26–28).

STUDY LIMITATIONS. The 16-kDa prolactin fragment was not measured in the present analysis, and although we found no evidence that prolactin influenced myocardial recovery, we cannot address whether an increase in the 16-kDa fragment might be associated with poorer recovery. However, the present study uncovered no evidence that enhancing prolactin levels by continuing to breastfeed had any adverse impact on subsequent LVEF. Additionally, although $CD4^{+}CD25^{+}$ cells were measured, staining with antibodies for Foxp3, the most specific marker for regulatory T cells, was not done (29). Finally, the subset of women from IPAC who breastfed was small (15%), and in general they represent a healthier subset of IPAC with a trend toward a higher LVEF and lower New York Heart Association functional class. This healthier subset would be expected to do better than the more acutely ill subset that either could not, or chose not, to breastfeed. Comparisons of outcomes between these different subsets is limited; however, we can still confidently report that no hazard was evident in the BF group.

CONCLUSIONS

This study is the first to demonstrate the impact of BF on maternal cellular immunity in a cohort of women with PPCM and that this change in cellular immunity (increased cytotoxic T cells) was correlated with prolactin. To the extent that PPCM is an autoimmune form of myocarditis, one would expect this change in cellular immunity to affect outcomes. The fact that BF did not seem to affect outcomes argues against the inflammatory hypothesis. Indeed, the absence of any hazard for BF in IPAC argues against a significant role for prolactin as a mediator and bromocriptine as a therapy. For women presenting with PPCM who are well compensated, we find no evidence to support a recommendation against BF. Women with PPCM who are more gravely ill at the time of diagnosis may potentially benefit from prohibition of BF via bromocriptine therapy, but a recommendation regarding the use of bromocriptine in these patients with PPCM should be based on a rigorous large randomized controlled study comparing the use of bromocriptine versus placebo in patients with PPCM who are at higher risk for poor outcomes, all of whom should also be concomitantly treated with guideline-directed heart failure therapies.

ADDRESS FOR CORRESPONDENCE: Dr. Dennis M. McNamara, University of Pittsburgh Medical Center, Scaife Hall, Room S-566, 200 Lothrop Street, Pittsburgh, Pennsylvania 15213. E-mail: mcnamaradm@upmc.edu.

PERSPECTIVES

COMPETENCY IN MEDICAL KNOWLEDGE: This study provides further evidence that BF does not adversely affect myocardial recovery for patients with PPCM. This result has implications on an international scale, particularly in resource-limited countries, where PPCM has been shown to be more prevalent. Bromocriptine has been promoted as a treatment for PPCM. However, a randomized placebo-controlled trial regarding the efficacy of bromocriptine for treatment of all, or a certain subset of, patients with PPCM must be completed before any recommendations regarding the use of bromocriptine for treatment of PPCM can be confidently supported.

TRANSLATIONAL OUTLOOK: In this study we explored the impact of BF has on cellular immunity, which is likely mediated by prolactin. Our study found that neither $CD3^{+}CD8^{+}$ cells nor prolactin has an impact on myocardial recovery in patients with PPCM. This argues against an autoimmune or inflammatory hypothesis for the etiology of PPCM. More research is needed to further explore alternative etiologies of this condition.

REFERENCES

1. Hilfiker-Kleiner D, Sliwa K. Pathophysiology and epidemiology of peripartum cardiomyopathy. Nat Rev Cardiol 2014;11:364–70.

2. Kolte D, Khera S, Aronow WS, et al. Temporal trends in incidence and outcomes of peripartum cardiomyopathy in the United States: a nationwide population-based study. J Am Heart Assoc 2014;3:e001056.

3. Arany Z, Elkayam U. Peripartum cardiomyopathy. Circulation 2016;133:1397–409.

4. McNamara DM, Elkayam U, Alharethi R, et al. Clinical outcomes for peripartum cardiomyopathy in North America: results of the IPAC Study (Investigations of Pregnancy-Associated Cardiomyopathy). J Am Coll Cardiol 2015;25;66:905–14.

5. Ansari A, Fett JD, Carraway RE, et al. Autoimmune mechanisms as the basis for human peripartum cardiomyopathy. Clin Rev Allergy Immunol 2002;23:301–24.

6. Hilfiker-Kleiner D, Kaminski K, Podewski E, et al. A cathepsin cleaved 16kDa form of prolactin mediates postpartum cardiomyopathy. Cell 2007;128:589–600.

7. Haghikia A, Podewski E, Berliner D, et al. Rationale and design of a randomized, controlled multicentre clinical trial to evaluate the effect of bromocriptine on left ventricular function in women with peripartum cardiomyopathy. Clin Res Cardiol 2015;104:911–7.

8. Yaméogo N, Kagambèga L, Seghda A, et al. Bromocriptine in management of peripartum cardiomyopathy: a randomized study on 96 women in Burkina Faso. J Cardiol Clin Res 2017;5:1098.

9. Hilfiker-Kleiner D, Haghikia A, Berliner D, et al. Bromocriptine for the treatment of peripartum cardiomyopathy: a multicentre randomized study. Eur Heart J 2017;38:2671–9.

10. Sliwa K, Petrie MC, Hilfiker-Kleiner D, et al. Long-term prognosis, subsequent pregnancy, contraception and overall management of peripartum cardiomyopathy: practical guidance paper from the Heart Failure Association of the European Society of Cardiology Study Group on Peripartum Cardiomyopathy. Eur J Heart Fail 2018;20:951–62.

11. McTiernan C, Morel P, Cooper LT, et al. Circulating T-cell subsets, monocytes, and natural killer cells in peripartum cardiomyopathy: results from the multicenter IPAC study. J Card Fail 2018;24:33–42.

12. Peeva E, Zouali M. Spotlight on the role of hormonal factors in the emergence of autoreactive B-lymphocytes. Immunol Lett 2005;101:123–43.

13. Lahat N, Miller A, Shtiller R, Touby E. Differential effects of prolactin upon activation and differentiation of human B lymphocytes. J Neuroimmunol 1993;47:35–40.

14. Orbach H, Shoenfeld Y. Hyperprolactinemia and autoimmune diseases. Autoimmun Rev 2007;6:537–42.

15. Legorreta-Haquet MV, Chavez-Rueda K, Chavez-Sanchez L, et al. Function of Treg cells decreased in patients with systemic lupus erythematosus due to the effect of prolactin. Medicine (Baltimore) 2016;95:e2384.

16. Legorreta-Haquet MV, Chauvez-Rueda K, Montoya-Diaz E, et al. Prolactin down-regulates $CD4^{+}CD25^{hi}CD127^{low}$ regulatory T cell function in humans. J Mol Endocrinol 2012;48:77–85.

17. Schelbert E, Elkayam U, Cooper LT, et al. Myocardial damage detected by late gadolinium enhancement cardiac magnetic resonance is uncommon in peripartum cardiomyopathy. J Am Heart Assoc 2017;6:e005472.

18. Bultmann BD, Klingel K, Nabauer M, Wallweiner W, Kandolf R. High prevalence of viral genomes and inflammation in peripartum cardiomyopathy. Am J Obstet Gynecol 2005;193:263–5.

19. Hilfiker-Kleiner D, Haghikia A, Nonhaff J, Bauersachs J. Peripartum cardiomyopathy: current management and future perspectives. Eur Heart J 2015;7;36:1090–7.

20. Karen S, Blauwet L, Tibazarwa K, et al. Evaluation of bromocriptine in the treatment of acute severe peripartum cardiomyopathy: a proof-of-concept pilot study. Circulation 2010;121:1465–73.

21. Haghikia A, Podewski E, Libhaber E, et al. Phenotyping and outcome on contemporary management in a German cohort of patients with peripartum cardiomyopathy. Basic Res Cardiol 2013;108:366.

22. Safirstein JG, Ro AS, Grandhi S, et al. Predictors of left ventricular recovery in a cohort of peripartum cardiomyopathy patients recruited via the Internet. Int J Cardiol 2012;154:27–31.

23. Kawamoto K, Langen E, Jackson EA, et al. Breastfeeding is not associated with worse outcomes for women with peripartum cardiomyopathy (abstr). Circ Cardiovasc Qual Outcomes 2017;10:A237.

24. Perrine C, Nelson J, Corbelli J, et al. Lactation and maternal cardio-metabolic health. Annu Rev Nutr 2016;36:627–45.

25. Black RE, Victora CG, Walker SP, et al. Maternal and child undernutrition and overweight in low-income and middle-income countries. Lancet 2013;382:427–51.

26. Binns CW, Lee MK. Exclusive breastfeeding for six months: the WHO six months recommendation in the Asia Pacific region. Asia Pac J Clin Nutr 2014;23:344–50.

27. Victora CG, Bahl R, Barros AJ, et al. Breastfeeding in the 21st century: epidemiology, mechanisms, and lifelong effect. Lancet 2016;387:475–90.

28. Fett JD, Murphy JG. Infant survival in Haiti after maternal death from peripartum cardiomyopathy. Int J Obstet Gynecol 2006;94:135–6.

29. Rudensky A. Regulatory T cells and Foxp3. Immunol Rev 2011;241:260–8.

KEY WORDS breastfeeding, immune activation, peripartum cardiomyopathy

APPENDIX For a list of IPAC investigators, please see the online version of this paper.

Go to http://www.acc.org/jacc-journals-cme to take the CME/MOC/ECME quiz for this article.

JACC: BASIC TO TRANSLATIONAL SCIENCE VOL. 4, NO. 3, 2019

EDITORIAL COMMENT

To Breastfeed or Not to Breastfeed With Peripartum Cardiomyopathy*

Zoltan Arany, MD, PhD,[a] Arthur M. Feldman, MD, PhD[b]

Peripartum cardiomyopathy (PPCM) is a disease of maternal cardiac systolic dysfunction, often accompanied by ventricular dilation, that afflicts ~1 in 2,000 births worldwide (1,2). PPCM accounts for most cases of cardiogenic shock in pregnancy (3) and is increasingly a leading cause of peripartum maternal death in the United States and abroad (4,5). Gestational hypertension, multiparous pregnancies, and African heritage are the strongest known risk factors for PPCM. Treatment mirrors that of dilated cardiomyopathy, focusing on supportive measures, neurohormonal blockade, and, when necessary, mechanical support or even cardiac transplantation. Prognosis is relatively favorable, with recovery of systolic function in the majority of women. However, a significant subset of women, who are typically otherwise young and healthy, and with a new infant to nurture, do not recover and are faced with prolonged cardiac insufficiency, need for cardiac transplantation, or premature mortality.

The cause of PPCM remains poorly understood. Approximately 10% of women with PPCM bear truncating mutations in the gene TTN, encoding for the sarcomeric protein titin, indicating a genetic cause to PPCM in at least a subset of cases (6). In addition, numerous studies in model organisms have advanced the hypothesis that PPCM is caused by vasculotoxic hormones, released from the placenta and pituitary during late gestation and early postpartum periods (1,7–10). These toxic hormones damage the cardiac microvasculature, in turn leading to cardiomyocyte dysfunction and contractile failure. One of these potentially toxic hormones is prolactin (10). The maternal pituitary secretes prolactin late in gestation and continues to do so postpartum in response to breastfeeding. Prolactin acts directly on mammary glands to promote generation of milk. However, in some contexts, prolactin can be cleaved by extracellular proteases to yield a 16 kD peptide that is profoundly vasculotoxic. Studies in mice suggest that this action may occur in certain predisposed individuals, leading to loss of cardiac microvasculature, global ischemia, and cardiomyopathy.

SEE PAGE 291

These studies have raised the possibility that suppressing prolactin production may benefit patients with PPCM by removing a key mechanistic driver of this disease. There are 2 readily available ways to suppress prolactin production: 1) treatment with dopamine agonists, such as bromocriptine, which act directly on the pituitary to suppress dopamine synthesis; or 2) cessation of breastfeeding. We refer the reader to recent sources for discussions on the use of dopamine agonists in PPCM (11–15); controversy remains on this topic.

What of breastfeeding in PPCM? On the basis of the preclinical experimental findings with prolactin, and of suggestive studies with bromocriptine, the 2010 European position statement on PPCM recommended cessation of breastfeeding in PPCM (16). A more recent European Society of Cardiology study group recommended that breastfeeding should be "encouraged in women with mild cardiac dysfunction" but is "not advisable in cases of severely

*Editorials published in *JACC: Basic to Translational Science* reflect the views of the authors and do not necessarily represent the views of *JACC: Basic to Translational Science* or the American College of Cardiology.

From the [a]Perelman School of Medicine, University of Pennsylvania, Philadelphia, Pennsylvania; and the [b]Lewis Katz School of Medicine, Temple University, Philadelphia, Pennsylvania. Dr. Feldman is the director of and holds equity in Renovacor, Inc. Dr. Arany has reported that he has no relationships relevant to the contents of this paper to disclose.

All authors attest they are in compliance with human studies committees and animal welfare regulations of the authors' institutions and Food and Drug Administration guidelines, including patient consent where appropriate. For more information, visit the *JACC: Basic to Translational Science* author instructions page.

ISSN 2452-302X https://doi.org/10.1016/j.jacbts.2019.03.005

impaired systolic function" (17). However, there are remarkably few published data that directly address the question of breastfeeding in PPCM, in part because most PPCM studies do not report on breastfeeding. A single, small (N = 55) retrospective Internet-recruited study in the United States that directly addressed the question suggested that breastfeeding was associated with better, rather than worse, maternal outcome (18); and a similar single-center retrospective study (N = 27) suggested no difference in outcome based on breastfeeding status (19). Both studies are retrospective and therefore may have been biased by ascertainment. Prospective studies were entirely lacking.

Enter the IPAC (Investigations of Pregnancy-Associated Cardiomyopathy) study. IPAC is a U.S.-based, multicenter prospective study that followed 100 women for 12 months immediately after the diagnosis of PPCM (20). A number of important studies have emanated from this cohort. In this issue of *JACC: Basic to Translational Research*, Koczo et al. (21) focus on the question of breastfeeding. Of 100 women, 15 were breastfeeding at entry, and 85 were not. This percentage is substantially below the U.S. national rate of breastfeeding at 6 months (57.6%; CDC report card [22]). Only 1 woman received a dopamine agonist. There were no obvious differences in demographic, hemodynamic, or obstetric parameters between women who breastfed and those who did not. The women who breastfed had a trend toward higher ejection fraction at presentation (breastfeeding 0.39 ± 0.06 vs. nonbreastfeeding 0.34 ± 0.10; $p = 0.06$). The key observation of the study, however, is that no difference was seen in mean change in left ventricular ejection fraction from entry to 6 months (breastfeeding 0.17 ± 0.09 vs. nonbreastfeeding 0.16 ± 0.11; $p = 0.46$) or 12 months (breastfeeding 0.18 ± 0.08 vs. nonbreastfeeding 0.17 ± 0.11; $p = 0.68$). In other words, breastfeeding seemed to have no impact whatsoever on recovery rates.

The strength of this study (21) lies in the fact that participants were followed up prospectively and all subjects underwent comprehensive phenotyping, and it thus provides important new data to instruct decision-making in a clinical setting that lacks clear guidelines. Nonetheless, the study has limitations. First, the small size of the trial provides limited power. It should be noted, however, that the lack of even a trend toward an adverse effect of breastfeeding makes it unlikely that a type II error biased the statistical outcome of the study. Second, the study is observational (i.e., it is not randomized). Is it possible, for example, that self-selection of a less ill cohort to breastfeeding could have biased the outcome to favor breastfeeding? This possibility is suggested by the relatively low percentage of women breastfeeding, and the trend to higher ejection fraction at entry in this group. The only way to conclusively address this question is a prospective and randomized trial, an unlikely outcome. In sum, the study does not definitively report that breastfeeding is safe in women with PPCM, but it strongly suggests that it is so.

The decision of whether to breastfeed with PPCM must also consider the potential benefits of breastfeeding to both mother and infant. Critical nutrients and factors, both known and unknown, pass from mother to child via breast milk. In developing countries, where undernutrition and unsafe water supplies account for the majority of childhood mortality and where breast milk substitutes are expensive, discontinuation of breastfeeding can be catastrophic to the infant (23). Breastfeeding promotes bonding, immunoprotection, metabolic protection, an appropriate microbiome population, and profound protection against diarrheal and respiratory diseases and otitis media, while reducing risk of sudden infant death (24). Most of these findings are true in both high- and low-income countries. In addition, in high-income countries, breastfeeding is associated with protection from obesity and diabetes and with higher performance on intelligence tests. Strong evidence also implicates breastfeeding in maternal protection from breast and ovarian cancer. Prolactin itself has been implicated in many of these processes, in particular immunoprotection, and indeed Koczo et al. (21) show in their study that $CD8^+$ cytotoxic T cells were higher in breastfeeding women with PPCM (in contrast to $CD4^+$ helper cells, which tended to be lower). Both the World Health Organization and the American Academy of Pediatrics recommend exclusive breastfeeding for 6 months, and continued breastfeeding for at least 1 to 2 years. In short, discontinuation of breastfeeding should not be taken lightly.

Conversely, women with PPCM are a special case, because the majority are taking medicines for heart failure. Are these drugs transmitted to the fetus, and if so, are they safe? Levels of loop diuretics expressed in breast milk are likely too low to have an effect in the infant (25). Similarly, negligible amounts of bioactive derivatives of most angiotensin-converting enzyme inhibitors, mineralocorticoid receptor antagonists, beta-blockers, hydralazine, or nitrates are detected in milk, typically leading to <1% infant exposure on a weight-adjusted basis. With judicious choice of drugs, and appropriate monitoring of the infant, standard PPCM therapy thus seems safe for the infant and should not be a contraindication for breastfeeding.

Finally, returning to the context of the possible use of dopamine agonists such as bromocriptine, 2 points should be made about breastfeeding. First, once the decision has been made to use dopamine agonists, the question of whether to breastfeed is then obviously moot, as these drugs will suppress lactation. However, second, the observations that breastfeeding seems to be safe in PPCM suggests that continued stimulation of prolactin secretion into the maternal circulation is not harmful, somewhat calling into question the rationale for using dopamine agonists. Once again, only a placebo-controlled, randomized trial will adequately resolve this quandary. The lost benefits of breastfeeding should therefore be factored into the decision of using a dopamine agonist.

In conclusion, few direct clinical data exist to guide the decision of whether a woman with PPCM should breastfeed. The study by Koczo et al. (21) provides substantially more data than existed in aggregate in the antecedent literature, but it still leaves us without certainty. To date, there is no direct evidence that breastfeeding in women with PPCM is harmful, and in fact increasing evidence that it is safe. Cessation of breastfeeding should thus be recommended only with caution.

ADDRESS FOR CORRESPONDENCE: Dr. Zoltan Arany, Cardiovascular Metabolism Program, Cardiovascular Institute, and Institute for Diabetes, Obesity, and Metabolism, Perelman School of Medicine, University of Pennsylvania, Smilow Center for Translational Research, 11-106, 3400 Civic Boulevard, Philadelphia, Pennsylvania 19104. E-mail: zarany@pennmedicine.upenn.edu.

REFERENCES

1. Arany Z, Elkayam U. Peripartum cardiomyopathy. Circulation 2016;133:1397–409.

2. Arany Z. Understanding peripartum cardiomyopathy. Ann Rev Med 2018;69:165–76.

3. Banayan J, Rana S, Mueller A, et al. Cardiogenic shock in pregnancy: analysis from the National Inpatient Sample. Hypertens Pregnancy 2017;36:117–23.

4. Soma-Pillay P, Seabe J, Sliwa K. The importance of cardiovascular pathology contributing to maternal death: confidential enquiry into maternal deaths in South Africa, 2011-2013. Cardiovasc J Afr 2016;27:60–5.

5. Schellpfeffer MA, Gillespie KH, Rohan AM, Blackwell SP. A review of pregnancy-related maternal mortality in Wisconsin, 2006-2010. WMJ 2015;114:202–7.

6. Ware JS, Li J, Mazaika E, et al. Shared genetic predisposition in peripartum and dilated cardiomyopathies. N Engl J Med 2016;374:233–41.

7. Bello NA, Arany Z. Molecular mechanisms of peripartum cardiomyopathy: a vascular/hormonal hypothesis. Trends Cardiovasc Med 2015;25:499–504.

8. Patten IS, Rana S, Shahul S, et al. Cardiac angiogenic imbalance leads to peripartum cardiomyopathy. Nature 2012;485:333–8.

9. Hilfiker-Kleiner D, Sliwa K. Pathophysiology and epidemiology of peripartum cardiomyopathy. Nature Rev Cardiol 2014;11:364–70.

10. Hilfiker-Kleiner D, Kaminski K, Podewski E, et al. A cathepsin D-cleaved 16 kDa form of prolactin mediates postpartum cardiomyopathy. Cell 2007;128:589–600.

11. Hilfiker-Kleiner D, Haghikia A, Berliner D, et al. Bromocriptine for the treatment of peripartum cardiomyopathy: a multicentre randomized study. Eur Heart J 2017;38:2671–9.

12. Koenig T, Bauersachs J, Hilfiker-Kleiner D. Bromocriptine for the treatment of peripartum cardiomyopathy. Card Fail Rev 2018;4:46–9.

13. Ersboll AS, Arany Z, Gustafsson F. Bromocriptine for the treatment of peripartum cardiomyopathy: comparison of outcome with a Danish cohort. Eur Heart J 2018;39:3476–7.

14. Hilfiker-Kleiner D, Sliwa K, Bauersachs J. Reply to 'Bromocriptine for the treatment of peripartum cardiomyopathy: comparison of outcome with a nationwide Danish cohort'. Eur Heart J 2018;39:3478.

15. Fett JD. More study still needed on the use of bromocriptine in the treatment of peripartum cardiomyopathy. Eur Heart J 2018;39:3904.

16. Sliwa K, Hilfiker-Kleiner D, Petrie MC, et al. Current state of knowledge on aetiology, diagnosis, management, and therapy of peripartum cardiomyopathy: a position statement from the Heart Failure Association of the European Society of Cardiology Working Group on peripartum cardiomyopathy. Eur J Heart Fail 2010;12:767–78.

17. Sliwa K, Petrie MC, Hilfiker-Kleiner D, et al. Long-term prognosis, subsequent pregnancy, contraception and overall management of peripartum cardiomyopathy: practical guidance paper from the Heart Failure Association of the European Society of Cardiology Study Group on Peripartum Cardiomyopathy. Eur J Heart Fail 2018;20:951–62.

18. Safirstein JG, Ro AS, Grandhi S, Wang L, Fett JD, Staniloae C. Predictors of left ventricular recovery in a cohort of peripartum cardiomyopathy patients recruited via the internet. Int J Cardiol 2012;154:27.

19. Davis M, Kawamoto K, Langen E, Jackson E. Breastfeeding is not associated with worse gy, outcomes in peripartum cardiomyopathy. J Am Coll Cardiol 2017;69 Suppl 842.

20. McNamara DM, Elkayam U, Alharethi R, et al. Clinical outcomes for peripartum cardiomyopathy in North America: results of the IPAC study (Investigations of Pregnancy-Associated Cardiomyopathy). J Am Coll Cardiol 2015;66:905–14.

21. Koczo A, Marino A, Jeyabalan A, et al. Breastfeeding, cellular immune activation, and myocardial recovery in peripartum cardiomyopathy. J Am Coll Cardiol Basic Translational Sci 2019;4:291–300.

22. Centers for Disease Control and Prevention. Breastfeeding Report Card. Available at: https://www.cdc.gov/breastfeeding/data/reportcard.htm. Accessed April 23, 2019.

23. Black RE, Victora CG, Walker SP, et al. Maternal and child undernutrition and overweight in low-income and middle-income countries. Lancet 2013;382:427–51.

24. Victora CG, Bahl R, Barros AJ, et al. Breastfeeding in the 21st century: epidemiology, mechanisms, and lifelong effect. Lancet 2016;387:475–90.

25. Kearney L, Wright P, Fhadil S, Thomas M. Postpartum cardiomyopathy and considerations for breastfeeding. Card Fail Rev 2018;4:112–8.

KEY WORDS breastfeeding, peripartum cardiomyopathy, pregnancy, prolactin

JACC: BASIC TO TRANSLATIONAL SCIENCE VOL. 4, NO. 3, 2019

CLINICAL RESEARCH

Inflammasome-Driven Interleukin-1α and Interleukin-1β Production in Atherosclerotic Plaques Relates to Hyperlipidemia and Plaque Complexity

Xintong Jiang, MD,[a,*] Feilong Wang, MD,[b,*] Yajuan Wang, MD, PhD,[a] Anton Gisterå, MD, PhD,[a] Joy Roy, MD, PhD,[c] Gabrielle Paulsson-Berne, PhD,[a] Ulf Hedin, MD, PhD,[c] Amir Lerman, MD,[b] Göran K. Hansson, MD, PhD,[a] Joerg Herrmann, MD,[b,†] Zhong-qun Yan, MD, PhD[a,†]

VISUAL ABSTRACT

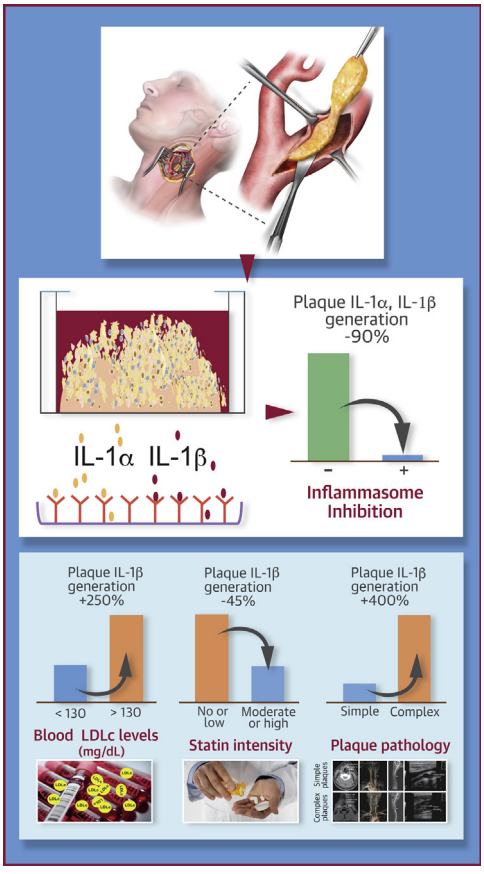

Jiang, X. et al. J Am Coll Cardiol Basic Trans Science. 2019;4(3):304-17.

HIGHLIGHTS

- **Genetic and functional evidence suggests that there are additional inflammasome pathways, besides NLRP3, that contribute to IL-1 generation in human atherosclerotic plaques.**
- **Plaque generation of mature IL-1β is accompanied by secretion of similar levels of IL-1α, through a mechanism controlled by NLRP3 and caspase-1.**
- **Plaque IL-1β production is higher in patients with uncontrolled hyperlipidemia, on no or low-dose statin therapy, or with complex plaque imaging features.**
- **The present study lends support to high-intensity cholesterol lowering and anti-IL-1-directed therapies for patients at high cardiovascular risk.**

ISSN 2452-302X https://doi.org/10.1016/j.jacbts.2019.02.007

SUMMARY

CANTOS (Canakinumab Antiinflammatory Thrombosis Outcome Study) confirmed interleukin (IL)-1β as an appealing therapeutic target for human atherosclerosis and related complications. However, there are serious gaps in our understanding of IL-1 production in atherosclerosis. Herein the authors show that complex plaques, or plaques derived from patients with suboptimally controlled hyperlipidemia, or on no or low-intensity statin therapy, demonstrated higher recruitable IL-1β production. Generation of mature IL-1β was matched by IL-1α release, and both were attenuated by inhibition of NLR family pyrin domain containing 3 or caspase. These findings support the inflammasome as the main pathway for IL-1α/β generation in atherosclerosis and high-intensity lipid-lowering therapies as primary and additional anti-IL-1-directed therapies as secondary interventions in high-risk patients. (J Am Coll Cardiol Basic Trans Science 2019;4:304–17) © 2019 The Authors. Published by Elsevier on behalf of the American College of Cardiology Foundation. This is an open access article under the CC BY-NC-ND license (http://creativecommons.org/licenses/by-nc-nd/4.0/).

ABBREVIATIONS AND ACRONYMS

ASC = apoptosis-associated speck-like protein containing a CARD

ATP = adenosine 5′-triphosphate disodium salt hydrate

BiKE = Biobank of Karolinska Carotid Endarterectomies

CT = Computerized tomographic scanning

IL = interleukin

LDL = low-density lipoprotein

LPS = lipopolysaccharide

mRNA = messenger ribonucleic acid

NLRC = nucleotide-binding oligomerization domain, leucine-rich repeat and CARD domain-containing protein

NLRP = nucleotide-binding oligomerization domain, leucine-rich repeat and pyrin domain-containing protein

PBS = phosphate-buffered saline

The innate immune cytokine interleukin (IL)-1β plays key roles in an extended spectrum of inflammatory conditions, including atherosclerosis and its complications. IL-1β blockade in patients with atherosclerosis reduces the burden of inflammation and recurrence of cardiovascular events, establishing an important role for IL-1 signaling in the pathogenesis of atherosclerosis (1).

Generation of mature IL-1β is a dynamic process controlled by inflammasome activation. In the context of atherosclerosis, cholesterol crystals and oxidized low-density lipoprotein (LDL) have the properties of danger signals that can activate the nucleotide-binding oligomerization domain, leucine-rich repeat and pyrin domain-containing protein (NLRP) 3 inflammasome in macrophages (2–4), leading to caspase-1-mediated IL-1β maturation and secretion. Alternatively, IL-1β generation can be induced in macrophages by lipopolysaccharide (LPS) via activation of caspase-4 (5,6). In a prior, primarily messenger ribonucleic acid (mRNA) profiling-based study, our group demonstrated the expression of the NLRP3 inflammasome and IL-1β in atherosclerotic plaques and provided initial evidence that IL-1β can be released in response to cholesterol crystals (5). Despite these advances, important gaps remain in our understanding of the generation of IL-1β and the regulation of inflammasome function in human arthrosclerosis.

Herein, using a plaque explant culture system that retains much of the cellular connections and functions in a near-native microenvironment and extending to a larger cohort of patients at 2 different study sites in Europe and the United States, we investigated the biology of inflammasome-mediated IL-1 signaling in human atherosclerotic plaques, including the connection with clinical parameters such as hyperlipidemia and clinical plaque imaging parameters that allow for a correlation with plaque complexity. The present study shows that progression of atherosclerosis is linked to up-regulation of lesional inflammasome activity and NLRP3-mediated generation of IL-1β and IL-1α. These findings provide novel insights into the pathogenesis of atherosclerosis and the therapeutic merit of high-intensity lipid lowering and anti-IL-1 therapy.

METHODS

GENE EXPRESSION ANALYSIS. Microarray-based unbiased gene expression analysis was performed on

From the [a]Experimental Cardiovascular Research Unit, Center for Molecular Medicine, Department of Medicine, Karolinska Institutet, Karolinska University Hospital, Stockholm, Sweden; [b]Department of Medicine, Division of Cardiovascular Diseases, Mayo Clinic, Rochester, Minnesota; and the [c]Department of Vascular Surgery, Karolinska University Hospital, Stockholm, Sweden. *Drs. Jiang and Wang contributed equally to this work and are joint first authors. †Drs. Herrmann and Yan contributed equally to this work and are joint senior authors. This work was supported by the KI-Mayo collaboration project, the Swedish Research Council, the Swedish Heart-Lung Foundation, European Union Seventh Framework Programme projects AtheroFlux (HEALTH-F2-2013-602222) and VIA (HEALTH-F2-2013- 603131), the Foundation for Strategic Research in Sweden, and the National Institutes of Health (HL116952-04). Dr. Jiang was supported by the Chinese Scholarship Council. All other authors have reported that they have no relationships relevant to the contents of this paper to disclose.

All authors attest they are in compliance with human studies committees and animal welfare regulations of the authors' institutions and U.S. Food and Drug Administration guidelines, including patient consent where appropriate. For more information, visit the *JACC: Basic to Translational Science* author instructions page.

Manuscript received October 9, 2018; revised manuscript received November 24, 2018, accepted February 11, 2019.

total ribonucleic acid obtained from 127 carotid arterial atherosclerotic plaques and from 10 macroscopically nonatherosclerotic biopsies of the iliac artery and the aorta in the BiKE (Biobank of Karolinska Carotid Endarterectomies) as described previously (7–9). The full data of the transcriptome analysis are available in Gene Expression Omnibus (accession number GSE21545). All biopsies were collected with written consent from all participants according to the Declaration of Helsinki and with the approval of the Ethical Committee of Northern Stockholm.

EX VIVO CULTURE OF ATHEROMA-DERIVED TISSUE AND CELLS. Ex vivo atheroma cultures were set up as previously described (10). In brief, atheromatous plaques were cut into small pieces (about 1.0 mm^3), and calcified tissue was separated out by centrifugation. The decalcified tissue was washed with cold phosphate-buffered saline (PBS) prior to transfer to culture. In some experiments, an enzymatic digestion procedure with collagenase type I (400 U/ml), elastase type III (4 U/ml), deoxyribonuclease (300 U/ml), trypsin inhibitor (1 mg/ml), and polymyxin B (2.5 μg/ml) in 10% fetal calf serum Roswell Park Memorial Institute medium was performed for cell isolation. Atheromatous tissue or isolated cells were distributed on 48-well plates with about 0.1 g tissue/well or 5,000 cells/well. After 2 h incubation in Roswell Park Memorial Institute medium with 10% fetal calf serum, plaque tissues or cells were treated for 24 h with 100 ng/ml LPS (serotype O111:B4, Enzo Life Sciences, Farmingdale, New York), 30 min with 5 mmol/L adenosine 5′-triphosphate disodium salt hydrate (ATP, Sigma-Aldrich, St. Louis, Missouri), or 4 h with 10 μmol/l *Salmonella typhimurium* (InvivoGen, San Diego, California) or 10 μg/ml poly(deoxyadenylic-deoxythymidylic acid) (LyoVec, InvivoGen). In some experiments, MCC950 (PZ0280, Sigma-Aldrich) or the caspase inhibitor Z-Val-Ala-Asp fluoromethyl ketone (ALX-260-154-R100, Enzo Life Sciences) was applied at indicated concentrations 2 h prior to adding LPS or ATP. Thereafter, supernatants and tissues and cells were snap-frozen and kept at −80°C.

FUNCTIONAL ATHEROSCLEROTIC PLAQUE STUDIES. Functional characterization of IL-1 production (and inflammasome activity) in atherosclerosis was conducted on: 1) 17 plaques obtained from patients who underwent carotid or femoral endarterectomy at the Karolinska University Hospital; and 2) 24 carotid artery plaques collected at the time of carotid endarterectomy as part of an ongoing repository at the Mayo Clinic Rochester, approved by the Mayo Foundation Institutional Review Board. Written informed consent was obtained from all participants. As previously described (11,12), the decision to undertake surgical intervention followed clinical guidelines and included symptomatic and asymptomatic plaques. Demographic data, detailed clinical history, and imaging data were obtained for each patient by chart review with attention to cerebral ischemic events, cardiovascular risk factors, and medications. As part of the clinical evaluation and surgical planning, all patients at the Mayo Clinic underwent carotid artery imaging. The type of study (i.e., carotid ultrasound with Doppler, carotid computed tomographic angiography, or magnetic resonance angiography) was at the discretion of the providers and was conducted per routine clinical practice standards. The studies were read by board-certified radiologists, documented as clinical radiology reports, and reviewed for the diagnosis of specific plaque features such as ulceration, calcification, and hemorrhage.

ENZYME-LINKED IMMUNOSORBENT ASSAY. IL-1β and IL-1α in supernatant were measured using a standard commercial (DY200 for IL-1α and DY201 for IL-1β, R&D Systems, Minneapolis, Minnesota) and a high-sensitivity (HSLB00D for IL-1β, R&D Systems) enzyme-linked immunosorbent assay kit according to the manufacturer's instructions.

LESION COMPOSITION ANALYSIS, IMMUNOHISTOCHEMISTRY AND IMMUNOFLUORESCENT STAINING. Twenty-two carotid plaques were randomly selected from the BiKE study for lesion composition analysis. Macrophages and NLRP3 inflammasome were identified in consecutive sections by immunohistochemistry using primary antibodies to NLRP3 (AG-20B-0014, 1:200, AdipoGen Life Sciences, San Diego, California) and CD68 (HPA048982, Atlas Antibodies, Bromma, Sweden). The presence of iron was determined using Perls' Prussian blue stain as a sign of hemorrhage. Picrosirius red staining was used for the detection of collagen fibers and fibrous cap thickness. Toluidine blue staining and alizarin red staining were used to evaluate necrosis and calcium deposition, respectively. Quantification of staining was documented as threshold area divided by lesion area using QWin Standard Y 2.8 (Leica, Wetzlar, Germany) computerized analysis. The investigated endarterectomy samples were ranked

according to the results. Vulnerability index was defined by the ranks of CD68 and Perls' Prussian blue staining divided by the ranks of fibrous cap thickness.

Additionally, for immunofluorescent staining, sections of human carotid plaque and internal mammary artery were deparaffinized and rehydrated. Antigen retrieval was performed using Diva Decloaker (DV2004 MX, Biocare Medical, Pacheco, California) at 60°C overnight. The slides were then washed with PBS and blocked in avidin/biotin blocking kit (SP-2001, Vector Laboratories, Burlingame, California) for 30 min and then 5% normal horse serum in PBS with Tween 20 for 30 min. They were stained subsequently with primary antibodies diluted in 5% normal horse serum in PBS with Tween 20 and incubated at 4°C overnight, followed by incubation with a fluorochrome-conjugated secondary antibody (DI 2594, DI 1594, DI 2488, and DI 1488, 1:300, Vector Laboratories) in 5% normal horse serum in PBS with Tween 20 for 1 h. The following primary antibodies were used: NLRP3 (AG-20B-0014, 1:200), apoptosis-associated speck-like protein containing a CARD (ASC) (AG-25B-0006, 1:150, AdipoGen Life Sciences), CD68 (HPA048982, 1:400) and CD68 (NCL-L-CD68, 1:50, Leica Biosystems, Wetzlar, Germany). Immunofluorescent staining was analyzed using a laser scanning confocal microscope (TCP II, Leica). High-resolution images were taken under 40×/1.25 NA and 63×/1.4 NA oil-immersion objective lenses.

WESTERN BLOT ANALYSIS. Plaque-derived cell lysates and supernatants were used for Western blot analysis. The protein samples (200 μg/well from cell lysates and 15 μl from supernatants) were resolved on 15% sodium dodecyl sulfate polyacrylamide gel electrophoresis gels and transferred to polyvinylidene difluoride membrane using a wet-transfer system. Membranes were blocked in 10% wt/vol dried milk in TBST (50 mmol/l Tris/HCl [pH 7.6], 150 mmol/l NaCl, and 0.1% vol/vol Tween 20) for 1 h at room temperature. Membranes were incubated with primary antibodies diluted in 5% vol/vol bovine serum albumin in TBST at 4°C overnight and then with the appropriate horseradish peroxidase-conjugated secondary antibody diluted in 5% wt/vol dried milk in TBST for 1 h. Membranes were developed using ECL (Bio-Rad, Hercules, California) and stripped using ReBlot kit (Millipore, Billerica, Massachusetts) before being reprobed. Primary antibodies used were IL-β (#2021, 1:1,000, Cell Signaling Technology, Danvers, Massachusetts) and

FIGURE 1 Transcriptional Profiling of Inflammasome-Interleukin Pathways in Human Atherosclerotic Plaques

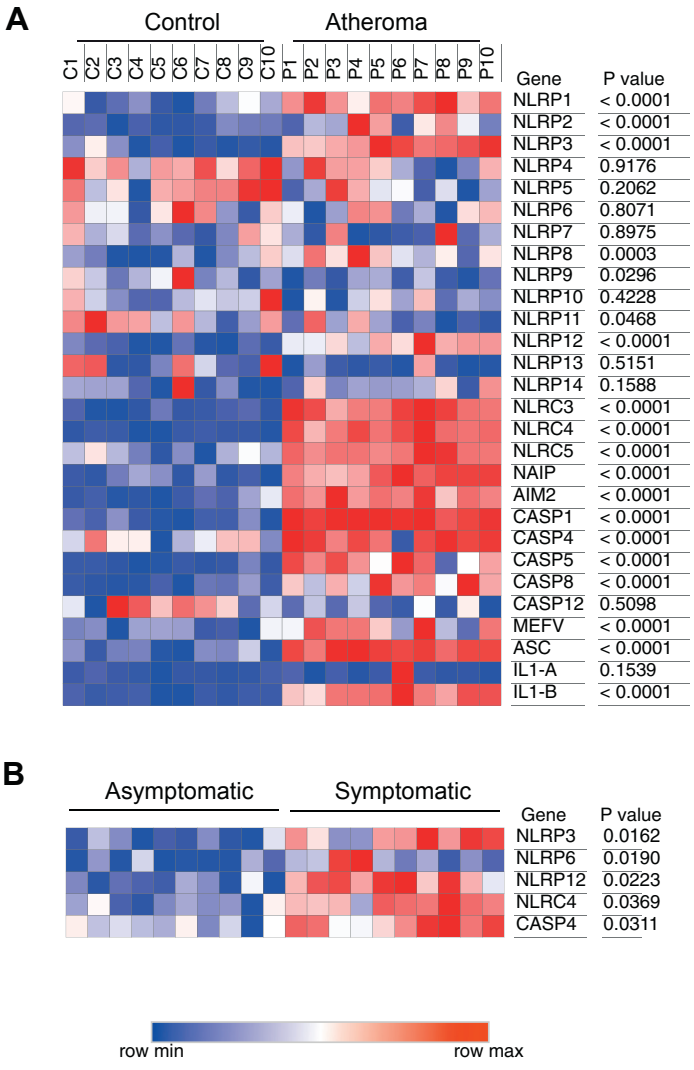

(A) Heat map representation of differentially expressed genes in inflammsome-interleukin-1 pathways in atherosclerotic plaques (atheroma, n = 125) obtained from patients undergoing carotid endarterectomy and in nondiseased arteries (control, n = 10) from organ donors. **(B)** Heat map representation of the top 5 differentially expressed inflammasome genes in atherosclerotic plaques from patients without clinical symptoms (asymptomatic, n = 40) and patients with clinical symptoms (symptomatic, n = 85). Gene expression was determined by ribonucleic acid microarray analysis. P values are based on Mann-Whitney *U* test. The scale bar shows color-coded differential expression, with **red** indicating higher levels of expression and **blue** indicating lower levels of expression. AIM2 = absent in melanoma 2; ASC = apoptosis-associated speck-like protein containing a CARD; CASP = caspase; IL = interleukin; NAIP = nucleotide-binding oligomerization domain, leucine-rich repeat and BIR domain-containing protein; MEFV = Mediterranean fever; NLRC = nucleotide-binding oligomerization domain, leucine-rich repeat and CARD domain-containing protein; NLRP = nucleotide-binding oligomerization domain, leucine-rich repeat and pyrin domain-containing protein.

FIGURE 2 Alternative Inflammasome Pathways in Atherosclerotic Lesions

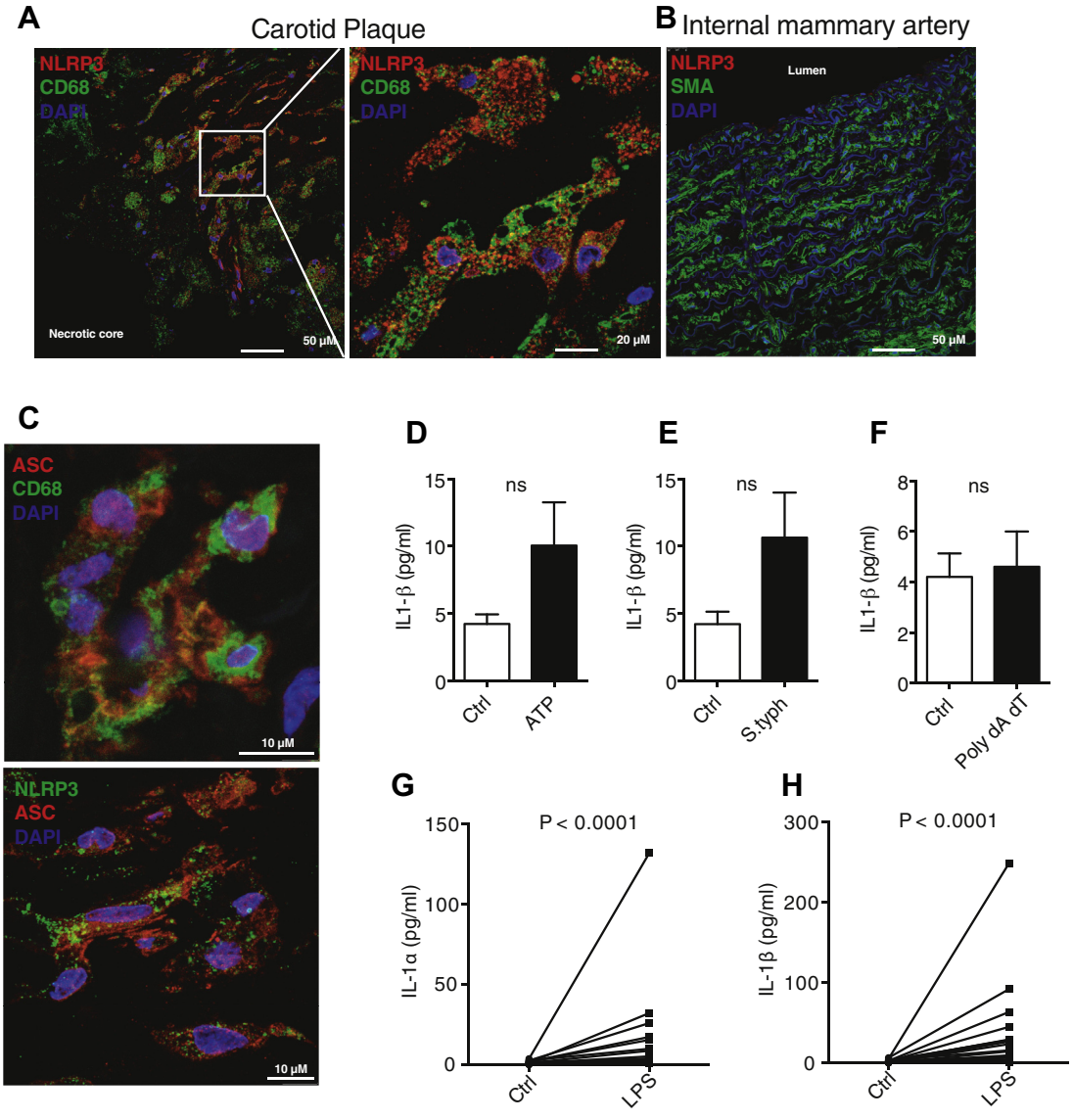

(A,B) Confocal microscopy of carotid plaque sections **(left)** stained for nucleotide-binding oligomerization domain, leucine-rich repeat and pyrin domain-containing protein (NLRP) 3 and CD68-positive macrophages **(left)** or internal mammary artery sections **(right)** stained for NLRP3 and SMC (SMA). Images are representative of carotid atherosclerotic plaques and internal mammary artery specimens. **(C)** Confocal microscopy of apoptosis-associated speck-like protein containing a CARD (ASC), NLRP3, and macrophages dual staining in adjacent sections of atherosclerotic plaque as shown in **B**. **(D to F)** Interleukin (IL)-1β production by atherosclerotic plaque samples in response to NLRP3 activators adenosine 5′-triphosphate disodium salt hydrate (5 mmol/l), nucleotide-binding oligomerization domain, leucine-rich repeat and CARD domain-containing protein (NLRC) 4 activator *Salmonella typhimurium* (S. typh) (10 μmol/l), or absent in melanoma 2 activator poly(deoxyadenylic-deoxythymidylic acid) (poly dA dT) (10 μg/ml). The concentration of IL-1β in the supernatant was quantified using enzyme-linked immunosorbent assay (ELISA). Data are shown as mean ± SEM; n = 3 to 7. ns, not significant (Mann-Whitney *U* test). **(G,H)** Release of IL-1 cytokines from atherosclerotic plaque samples upon lipopolysaccharide (LPS) challenge (100 ng/ml for 24 h). IL-1α (n = 16) and IL-1β (n = 24) concentrations in the supernatant were measured by ELISA. P values are based on Mann-Whitney *U* test. Ctrl = control; DAPI = 4′,6-diamidino-2-phenylindole.

GAPDH (ab181602, 1:20,000, Abcam, Cambridge, United Kingdom).

STATISTICAL ANALYSIS. Data are presented as mean ± SEM unless mentioned otherwise. Differences in mRNA abundances or IL-1 concentrations between groups were tested using the Mann-Whitney *U* test, Wilcoxon matched-pairs test, or Welch's *t* test, with p values as reported. Pearson correlation was applied for statistical analysis of the relationships between plaque IL-1 activity and clinical parameters. Associations between NLRP3 staining, plaque composition, and vulnerability index were assessed using Spearman's rank correlation coefficient test. A p value <0.05 was considered to indicate statistical significance.

RESULTS

SYMPTOMATIC ATHEROSCLEROTIC PLAQUES ARE ASSOCIATED WITH UP-REGULATION OF SELECTIVE INFLAMMASOME PATHWAYS. Analysis of the expression of inflammasome-related genes in the BiKE registry revealed significant changes in the inflammasome profile associated with atherosclerosis development, characterized by marked increases in canonical inflammasome (*NLRP1-3[13]*, *NLRP8-9*, *NLRP11-12*, nucleotide-binding oligomerization domain, leucine-rich repeat and CARD domain-containing protein [*NLRC3-5*], nucleotide-binding oligomerization domain, leucine-rich repeat and BIR domain-containing protein, *Pyrin*, and absent in melanoma 2) and noncanonical inflammasome components (*caspase-4*, *caspase-5*) compared with microscopically nonatherosclerotic iliac arterial specimens (Figure 1A). Moreover, although most inflammasome components were similar between symptomatic plaques and asymptomatic plaques, *NLRP6*, *NLRP12*, *NLRC4*, *NLRP3*, and *caspase-4* transcripts were distinctively enriched in symptomatic plaques (Figure 1B). These data highlight a correlation between the expression of multiple inflammasome elements, atherosclerosis, and plaque vulnerability.

ALTERNATIVE IL-1 SIGNALING PATHWAYS IN ATHEROSCLEROSIS. Given its significance for the generation of IL-1 in atherosclerosis (13), we further investigated the expression and activity of the NLRP3 inflammasome in human atherosclerosis. NLRP3 protein was detected ubiquitously in all advanced atherosclerotic lesions, primarily in lesional macrophages (Figure 2A) though rarely seen in microscopically nonatherosclerotic arteries (Figure 2B). This supports the notion that NLRP3 is negatively regulated by post-transcriptional modifications in healthy tissues at steady states (14). Besides NLRP3, ASC, the inflammasome adaptor protein, was also highly expressed in lesional macrophages (Figure 2C). However, the aggregate of NLRP3-ASC, indicative of the formation of activated NLRP3 inflammasomes, was rarely observed in atherosclerotic lesions (Figure 2C).

On the basis of the gene expression data shown in Figure 1, we postulated that there are likely additional inflammasome pathways with a functional role in atherosclerosis. Assessing IL-1β release from atheromatous tissues in response to the known canonical inflammasome activators, we found that IL-1β generation was increased, albeit not statistically significantly, upon exposure to the NLRP3 inflammasome activator ATP or the NLRC4 activator *S. typhimurium* (Figures 2D and 2E), but not the absent in melanoma 2 inflammasome activator poly(deoxyadenylic-deoxythymidylic acid) (Figure 2F). Alternatively, a burst in IL-1β production (38.9 ± 14.3 pg/ml) along with an equivalent quantity of IL-1α release (34.6 ± 16.5 pg/ml) was induced in 71% (17 of 24) and 41% (7 of 16) of plaques, respectively, after 24 h stimulation of atheromatous tissue with LPS, a defined noncanonical inflammasome stimulus (Figure 2E). Overall, 6 plaques (25%) exhibited a superior response to LPS, with an average IL-1β yield of ≥28.8 pg/ml, but 7 plaques (29%) produced minor or undetectable IL-1β (<3.9 pg/ml) in response to LPS. These data incline to the view that besides NLRP3, there are possibly additional inflammasome pathways, including noncanonical inflammasome pathways, with potential functional implications in atherosclerosis.

INCREASED IL-1β PRODUCTION IN PATIENTS WITH SUBOPTIMALLY CONTROLLED HYPERLIPIDEMIA. Modulation of immune and inflammation pathways is a central mechanism by which risk factors contribute to atherosclerosis (15). Yet whether and which cardiovascular risk factors affect IL-1 signaling in atherosclerotic plaques are unclear. Herein we analyzed the association between atheromatous tissue IL-1β production and age, sex, body mass index, serum levels of LDL cholesterol and triglycerides, hypertension, diabetes, and time interval from carotid endarterectomy and the latest ischemic cerebrovascular event. This revealed a connection

FIGURE 3 Uncontrolled Hypercholesterolemia Is Accompanied by Increased Interleukin-1β Production in Atherosclerotic Plaques

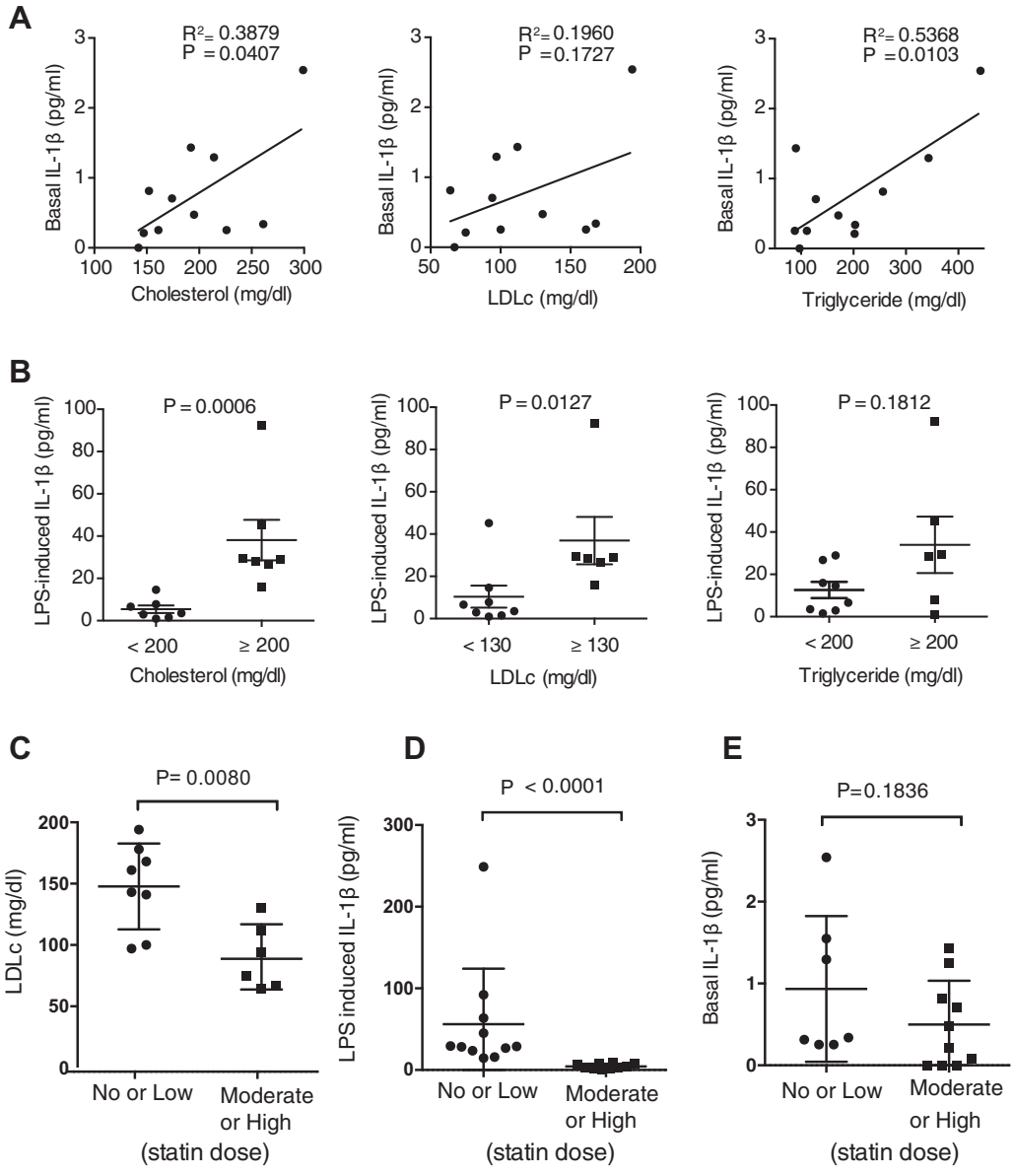

(A) Pearson correlation analysis between unstimulated interleukin (IL)-1β release from atherosclerotic plaque samples and serum levels of total cholesterol, low-density lipoprotein cholesterol (LDLc), and triglycerides (n = 11). **(B)** Analysis of lipopolysaccharide (LPS)–triggered IL-1β response of atherosclerotic plaque samples in relation to serum levels of total cholesterol, LDLc, and triglycerides. P values are based on Mann-Whitney *U* test. Data are shown as mean ± SEM; n = 14. **(C)** Blood LDLc levels in patients with indicated intensity of statin treatment. **(D)** LPS-induced IL-1β production by ex vivo cultured atheromatous tissue from patients with indicated intensity of statin treatment. **(E)** Baseline IL-1β production by ex vivo cultured atheromatous tissue from patients with indicated intensity of statin treatment. In **C to E**, data are shown as mean ± SEM; n = 14 to 24. The p values are based on Mann-Whitney *U* test.

between basal IL-1β production and serum total cholesterol and triglycerides levels (Figure 3A). Notably, the atheromatous tissue from patients with blood LDL cholesterol >130 mg/dl or total cholesterol ≥200 mg/dl yielded a 10-fold higher quantity of IL-1β than plaques from patients with lower blood LDL cholesterol or total cholesterol (Figure 3B).

FIGURE 4 Enhanced Interleukin-1β Signaling in Complex Atherosclerotic Plaques

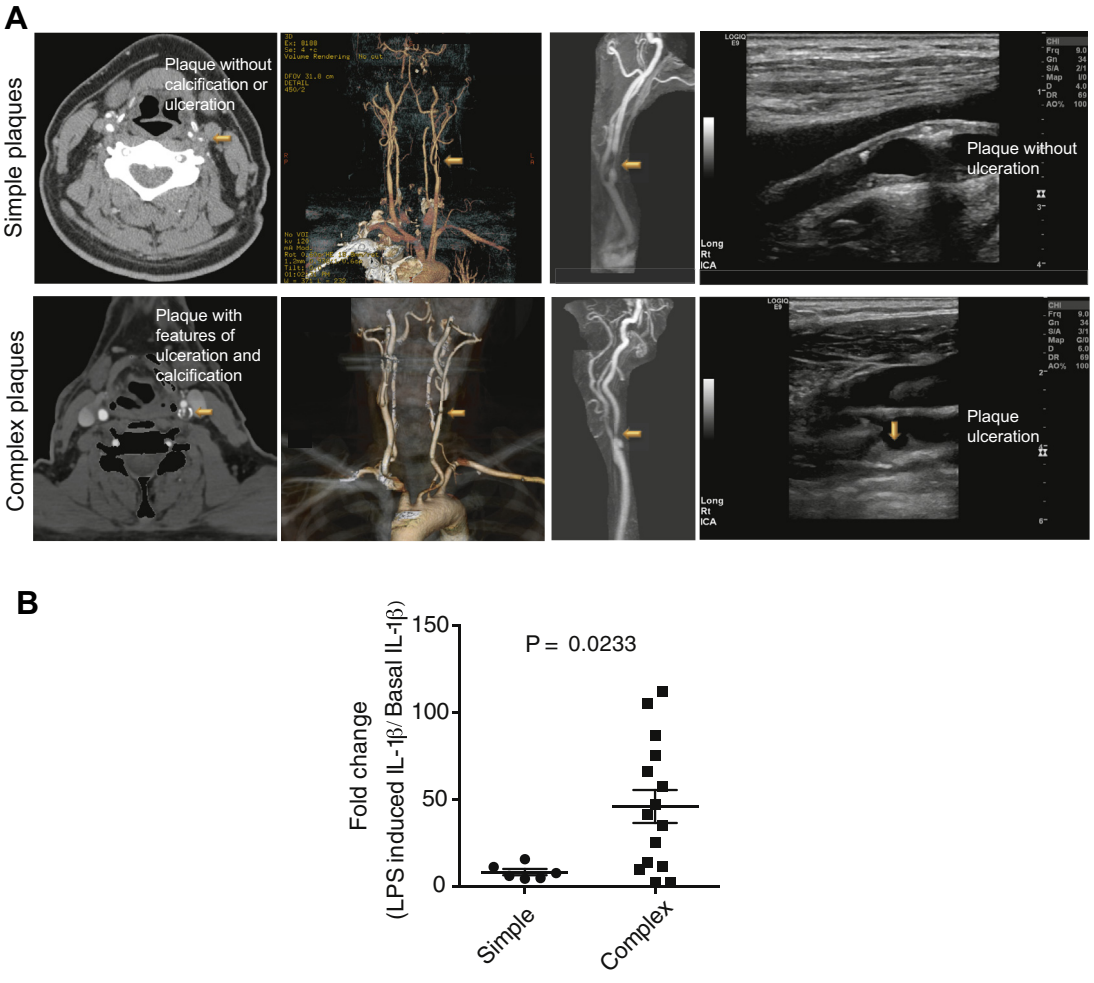

(A) Representative computed tomographic angiographic imaging **(left)**, magnetic resonance angiographic imaging **(middle)**, and ultrasound imaging **(right)** of simple **(top)** and complex **(bottom)** atherosclerotic plaques of human internal carotid arteries. **(B)** Lipopolysaccharide (LPS) (100 ng/ml)–induced interleukin (IL)-1β production relative to basal IL-1β production in atherosclerotic plaque samples isolated from simple (n = 6) and complex (n = 15) carotid atherosclerotic plaques. The concentration of IL-1β in the supernatant was determined using enzyme-linked immunosorbent assay. The p values are based on Wilcoxon matched-paired signed rank test.

We furthermore investigated plaque IL-1β generation in relation to blood cholesterol management. Analysis of blood LDL cholesterol levels in 21 patients and their statin therapy history showed that the average level of circulating LDL cholesterol was significantly higher in patients who received no or low-intensity statin therapy compared with patients who received moderate- or high-intensity stain therapy, on the basis of the American College of Cardiology/American Heart Association guideline (**Figure 3C**). Importantly, LPS-induced IL-1β generation was reduced in atheromatous tissues from patients on moderate- to high-intensity statin therapy (**Figure 3D**).

INCREASED IL-1β GENERATION IN COMPLEX PLAQUES. To investigate pathogenic activity of IL-1 in relation to plaque progression, we assessed the difference in IL-1β generation between atherosclerotic plaques with or without imaging signs of calcification, hemorrhage, or ulceration (16). Among the 21 consecutive Mayo Clinic patients who underwent carotid plaque imaging without exclusions

FIGURE 5 NLRP3 Expression Along the Progressive Stages of Atherosclerosis and Complex Plaques

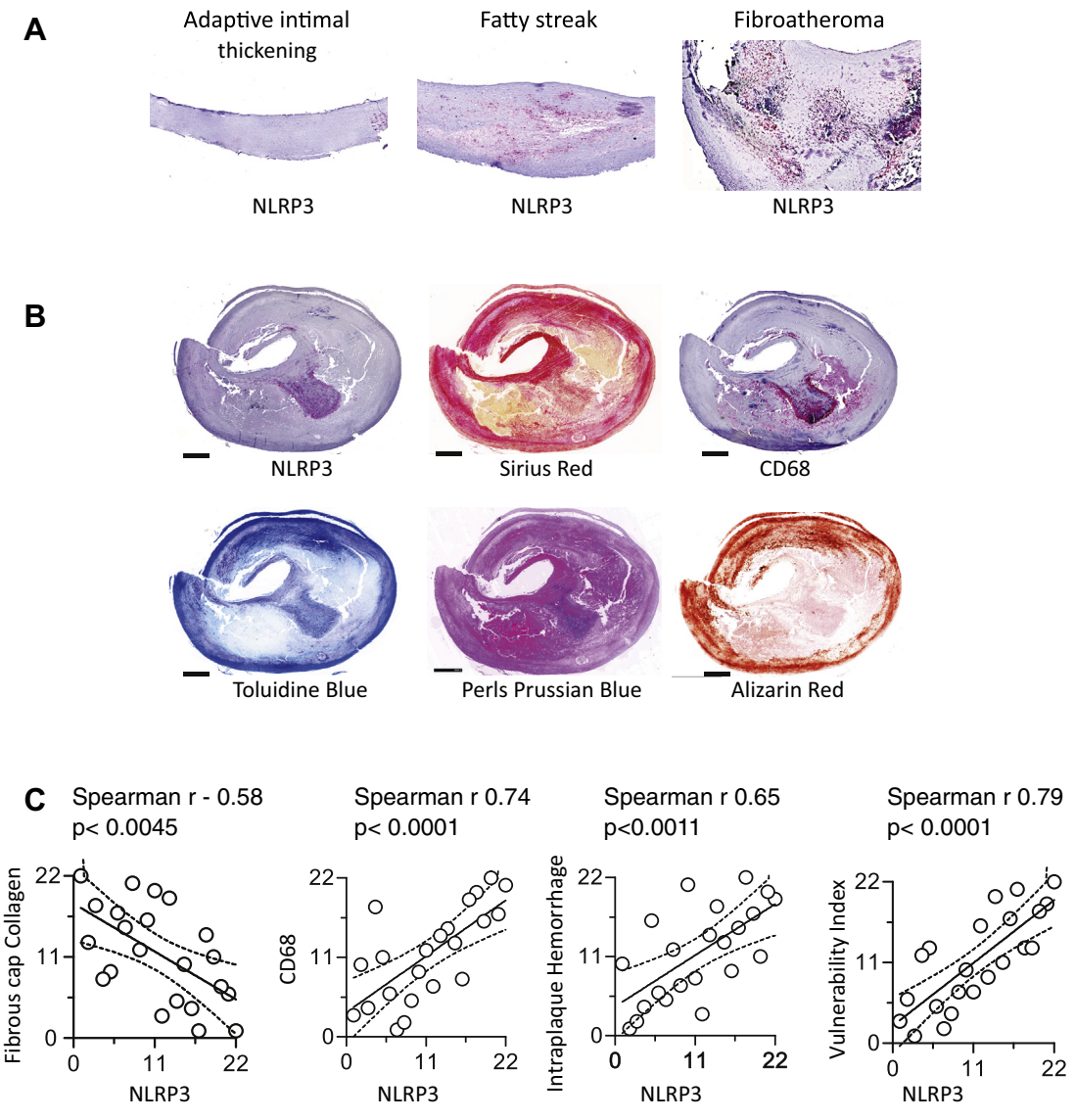

(A) Immunohistochemical characterization of nucleotide-binding oligomerization domain, leucine-rich repeat and pyrin domain–containing protein (NLRP) 3 expression and its correlation with the progression from adaptive intimal thickening to fatty streak and fibroatheroma in human carotid arteries. **(B)** Representative images of complex fibroatheromata in human carotid arteries stained for NLRP3 protein (NLRP3), fibrous cap collagen (Sirius red staining), macrophages (CD68), and intraplaque hemorrhage (Perl's Prussian blue staining). **(C)** Spearman rank correlation analysis of associations between lesional NLRP3 and fibrous cap collagen, macrophage content, intraplaque hemorrhage, and plaque vulnerability. Data are presented as ranks of corresponding measurement in numeric order (n = 22).

by either computed tomography, ultrasound, and/or magnetic resonance imaging, severe calcification, intraplaque hemorrhage, or ulceration, alone or combined, was reported in 15 (72%) cases, herein referred to as complex plaques (Figure 4A). Assessment of ex vivo cultured atheromatous tissues did not reveal statistically significant differences between simple and complex plaques in terms of basal IL-1β generation (data not shown). Nonetheless, the IL-1β yield in response to LPS was increased approximately 45-fold from baseline in tissues from complex plaques, compared with an 8-fold increase in tissues from simple plaques (Figure 4B).

UP-REGULATION OF NLRP3 INFLAMMASOME EXPRESSION IS A DISTINCTIVE CHARACTERISTIC OF PROGRESSIVE ATHEROSCLEROSIS. Given the role of NLRP3 observed in experimental atherosclerosis and enhanced IL-1 signaling in complex plaques, we further analyzed the relevance of NLRP3 inflammasome for plaque pathological alterations in humans. NLRP3 expression was noted first in fatty streaks and increased markedly in fibroatheroma (**Figure 5A**). In a series of 22 carotid plaques collected in the context of the BiKE study, we furthermore noted that NLRP3 inflammasome expression correlated positively with lesion macrophages and intraplaque iron content (a sign of plaque hemorrhage) and inversely with fibrous cap thickness (a sign of plaque stability) (**Figures 5B and 5C**). Overall, the analyses link the increased NLRP3 expression to pathological features of plaque vulnerability and complexity (**Figure 5C**).

CONCOMITANT RELEASE OF IL-1α AND IL-1β IN ATHEROSCLEROSIS. In contrast to IL-1α, the biology of IL-1β signaling in atherosclerosis remains elusive. Previous studies in mouse bone marrow-derived macrophages showed that activation of the inflammasome effector caspase-1 is implicated in the secretion of both IL-1α and IL-1β (17–19), yet whether a similar mechanism is implicated in IL-1α/β secretion in human atherosclerotic plaques remains understudied. Analyzing IL-1β production in the absence of extra stimuli, we unexpectedly found that atheromatous tissues produce not only IL-1β but also IL-1α constitutively (**Figure 6A**). Applying MCC950, an NLRP3 inhibitor (20), to atherosclerotic plaque–derived tissues, we corroborated whether the NLRP3 is required for IL-1α and IL-1β secretion in atherosclerotic lesions. We observed (**Figures 6B and 6C**) that exposure of human atherosclerotic plaque–derived tissue to MCC950 (at 0.1 μmol/l) significantly reduced both IL-1β and IL-1α release triggered by LPS (**Figure 6A**). Likewise, MCC950 at the same concentration was also capable of preventing basal as well as ATP-induced secretion of IL-1α and IL-1β by plaque-derived cells, composed of 30% to 40% macrophages, 10% to 20% smooth muscle cells, and 5% to 15% T cells according to a previous report (**Figures 6B and 6C**) (21). Similar to MCC950, IL-1α/β release under steady state conditions or in response to ATP was also impeded by Z-Val-Ala-Asp fluoromethyl ketone, a caspase-1 inhibitor (**Figures 6E and 6D**). These observations support the view that release of both cytokines, IL-1β and IL-1α, is likely determined by the NLRP3-caspase-1 pathway in atherosclerotic plaques.

DISCUSSION

The present study shows that: 1) NLRP3 expression increases with plaque progression and complexity; 2) NLRP3/caspase-1 inhibition blocks IL-1β and IL-1α release from atherosclerotic plaque–derived tissue and cells; 3) human atherosclerotic plaques produce IL-1β and IL-1α constitutively and with a several-fold increase upon stimulation with inflammasome activators; and 4) recruitable IL-1β and IL-1α release is higher in patients with suboptimally controlled hyperlipidemia, on no or low-intensity statin therapy, or with complex plaque imaging features. These findings confirm and extend prior experimental studies and lend translational support for optimal lipid control, high-intensity statin therapy, and anti-IL-1β therapies in patients with ASCVD, especially in those who had clinical events.

In a prior study, increased transcripts of NLRP3, ASC, caspase-1, and IL-1β and IL-18 were found in carotid atherosclerotic plaques (5). Herein we expanded the mRNA profiling studies with the generation of heat maps that more clearly show: 1) the profound differences between nondiseased and atherosclerotic vessels; 2) how many members of the inflammasome family are expressed in atherosclerotic plaques; and 3) how much "hotter" the expression is in symptomatic plaques in particular. Importantly, these genetic data provide a link between multiple inflammasome elements, atherosclerosis, and its activity. They furthermore suggest that apart from NLRP3, there are possibly additional inflammasome pathways relevant to IL-1 signaling in atherosclerosis. This is furthermore underscored by markedly elevated levels of NLRC4 in the plaque of symptomatic patients and plaque IL-1β production in response to external NLRC4 ligands. Additionally, increased expression of caspase-4 in atherosclerotic plaques and generation of IL-1β by plaque-derived tissue upon LPS stimulation point also into the direction of noncanonical inflammasome activation (5,22), an alternative mechanism that has been demonstrated for IL-1α secretion in murine macrophages in vitro but has not been shown in human atherosclerotic plaques (19).

The presence of both IL-1α and IL-1β was recently observed in human atherosclerotic plaques (23). Taking the advantage of ex vivo culture of

FIGURE 6 NLRP3 and Caspase-1-Dependent Generation of Interleukin-1α and Interleukin-1β in Atheroma

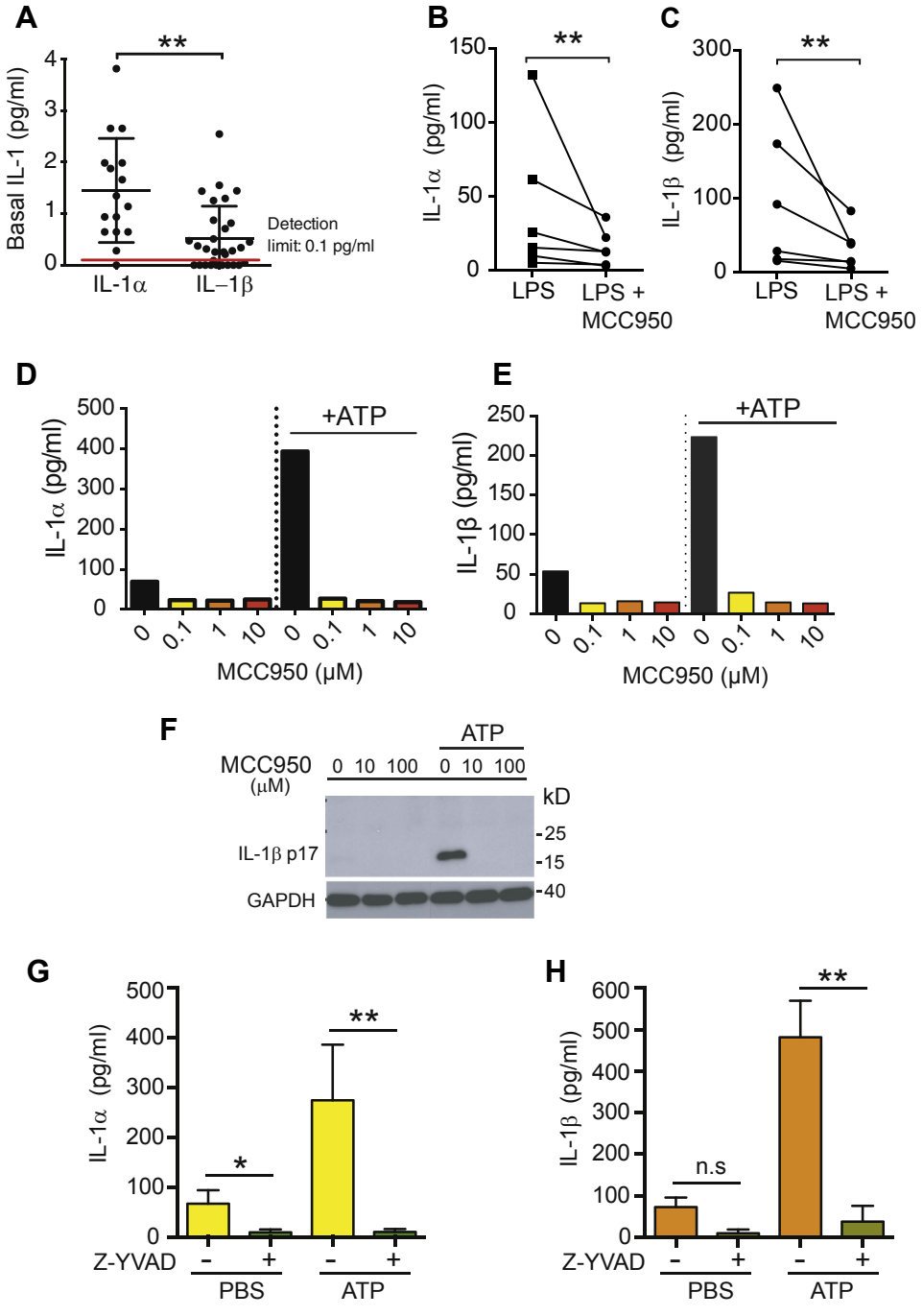

(A) Release of interleukin (IL)-1α and IL-1β from carotid atherosclerotic plaque samples cultured ex vivo for 20 h in the absence of external inflammasome stimuli. Supernatant concentrations of IL-1α (n = 16) and IL-1β (n = 24) were quantified using high-sensitivity enzyme-linked immunosorbent assay (ELISA). **(B,C)** ELISA assessment of lipopolysaccharide (LPS)-induced IL-1α and IL-1β release from carotid atherosclerotic plaque samples untreated or pre-treated with MCC950 (100 nmol/l) (n = 6); Wilcoxon matched-pairs test. **(D,E)** ELISA assessment of basal and adenosine 5′-triphosphate disodium salt hydrate (ATP)–induced IL-1α and IL-1β in the supernatant of ex vivo culture of carotid atherosclerotic cells with or without MCC950. Data are representative of 2 independent experiments. **(F)** Western blot analysis of basal and ATP-induced IL-1β release from atherosclerotic plaque–derived cells (5,000 cells/well) in the absence or presence of MCC950 (10 μmol/l). Results are representative of 2 independent experiments. **(G,H)** ELISA assessment of basal and ATP-induced IL-1α and IL-1β release from atherosclerotic plaque–derived cells (5,000 cells/well) in the absence or presence of caspase-1 inhibitor Z-Val-Ala-Asp fluoromethyl ketone (Z-YVAD). Data are shown as mean ± SEM; n = 3 to 10. Welch corrected *t* test. n.s, not significant; PBS = phosphate-buffered saline.

atherosclerotic plaque-derived tissue, our study provides further evidence that human atherosclerotic plaques secrete both IL-1 cytokines with similar kinetics under steady state conditions and in response to external stimuli. These independent observations suggest that both IL-1α and IL-1β may participate in atherosclerosis. In line with this notion is the observation that genetic deficiency of IL-1α, even if confined to bone marrow-derived cells, mitigates atherosclerotic burden in a mouse model. This protective effect was even more pronounced when combined with depletion of IL-1β (24). Thus, various lines of research point to the biological importance of both IL-1α and IL-1β for the atherosclerotic disease process. Given that atherosclerotic plaques retain a sufficient capacity of IL-1α production and functional similarities between the 2 cytokines, uncontrolled IL-1α generation can be as important as IL-1β in the pathogenesis of atherosclerosis.

Exploring the mechanisms contributing to IL-1α/β signaling in atherosclerotic lesions, we discovered that treatment of tissues or cells isolated from atheroma with the NLRP3-specific inhibitor MCC950 (20) or the caspase-1 inhibitor Z-Val-Ala-Asp fluoromethyl ketone inhibited the release of both IL-1α and IL-1β under ATP/LPS-stimulated and unstimulated baseline conditions. These findings lead to the hypothesis that NLRP3 inflammasome is a main determinant of IL-1β and IL-1α signaling in atherosclerosis. Mechanistically, ATP or LPS induce the processing of IL-1β and IL-1α by activation of caspase-1 via the NLRP3 inflammasome or noncanonical inflammasome pathways and the release of these ILs through gasdermin-D-formed pores (19,25,26). Alternatively, the NLRP3-caspase-1 pathway may have a dual mechanism of action, producing mature IL-1β and facilitating IL-1α/β secretion, suggesting that targeting NLRP3-caspase-1 may yield better outcomes than targeting the 2 IL-1 isoforms in separation. In keeping with an experimental in vivo study, noting a reduction in vascular inflammation and atherosclerotic lesion development by inhibition of the inflammasome with MCC950 (27), targeting the NLRP3 inflammasome may offer a new approach to mitigate IL-1-driven inflammatory responses in atherosclerosis.

Along these lines, the present results support CANTOS (Canakinumab Antiinflammatory Thrombosis Outcome Study) (1), which showed that the IL-1β-neutralizing antibody canakinumab reduced the primary combined endpoint of nonfatal myocardial infarction, nonfatal stroke, or cardiovascular death among patients with coronary artery disease and a history of myocardial infarction and elevated C-reactive protein levels despite aggressive secondary prevention measures. Finally, these data shed light on the link between an acutely and subacutely increased risk for acute ischemic events such as myocardial infarction and stroke in the setting of acute infections (28). The endogenous production of LPS under these circumstances may very well stimulate IL-1 production in human atherosclerotic plaques in vivo, with an increase in plaque inflammation and subsequent plaque destabilization. The convergence of these investigations underscores the significance of IL-1β-driven inflammatory responses in atherosclerosis.

An important observation of the present study is that IL-1β release kinetics relate to serum lipid levels. A linear correlation was seen between IL-1β production at baseline and total cholesterol and triglyceride levels. LPS-induced IL-1β release was significantly higher in patients with cholesterol levels >200 mg/dl and LDL levels >130 mg/dl. LDL cholesterol overload, oxidation of LDL, and fatty acids were shown before to induce a continuous state of intracellular stress with up-regulation of IL-1 and NLRP3 inflammasome expression in macrophages (4,29). However, the current analysis of the BiKE study, a large-scale mRNA transcriptional database of human carotid atherosclerotic plaques, did not substantiate a connection between elevated levels of systemic LDL cholesterol and the local inflammasome and IL-1 transcription in atherosclerotic plaque (data not shown). LDL cholesterol and oxidized LDL are implicated in training monocytes through epigenetic reprogramming to acquire a long-lasting proinflammatory phenotype with enhanced inflammasome activity (30). Alternatively, uncontrolled blood LDL cholesterol may lead to increased cholesterol crystal formation and noncrystalline cholesterol overload in atherosclerotic lesions, thus accounting for an increased risk of inflammasome activation and consequently IL-1 production (5). Such considerations lend support to the benefits of high-intensity lipid-lowering therapy. Indeed, in the present study, we did find that atherosclerotic plaque tissues from patients on no or low-intensity statin therapy mounted a much higher IL-1β production upon stimulation. Although it cannot be

excluded that non-lipid-lowering properties contributed to this observation, a correlation between LDL levels and statin therapy intensity was seen. In combination, these studies extend our understanding of the link between hyperlipidemia, inflammasome activity, and inflammation in atherosclerosis and support aggressive lipid-lowering therapy as an important translational aspect.

The present investigation also reveals marked heterogeneity in inflammasome activity among atherosclerotic plaques. Notably, complex lesions with imaging signs of hemorrhage, ulceration, or calcification mounted a 10-fold higher induction of IL-1β release than simple plaques. In keeping with increased expression of inflammasome components in symptomatic plaques, these data associate biologically active plaques with increased inflammasome activity. Indeed, up-regulation of the NLRP3 inflammasome in atherosclerotic plaques may relate to many aspects of disease pathogenesis such as vascular inflammation, intraplaque hemorrhage, plaque compositions, and vulnerability. In agreement with the present results, prior studies noted a correlation between elevated circulating levels of IL-1β, coronary calcium burden, and cardiac death (31).

CONCLUSIONS

The present study supports the concept that the NLRP3 inflammasome contributes to plaque IL-1α/β generation and provides biological insights into the clinical merit of anti-IL-1 signaling-directed and high-intensity lipid-lowering therapies in high-risk patients with atherosclerosis.

ADDRESS FOR CORRESPONDENCE: Dr. Joerg Herrmann, Department of Cardiovascular Diseases, Mayo Clinic, 200 1st Street, Southwest, Rochester, Minnesota 55905. E-mail: herrmann.joerg@mayo.edu. OR Dr. Zhong-qun Yan, Center for Molecular Medicine L8:03, Karolinska University Hospital, 171 76, Stockholm, Sweden. E-mail: zhong-qun.yan@ki.se.

PERSPECTIVES

COMPETENCY IN MEDICAL KNOWLEDGE: Hypercholesterolemia is the cardinal risk factor and inflammation the characteristic trait of atherosclerosis directing the clinical course. The 2018 American College of Cardiology/American Heart Association guidelines recommend high-intensity statin therapy and lower cholesterol goals for very high risk patients. The CANTOS trial indicated that IL-1β-directed therapy with a neutralizing antibody reduces recurrent ischemic events and cardiovascular death among patients with coronary artery disease and a history of myocardial infarction and elevated C-reactive protein levels despite aggressive secondary prevention measures. Herein we show that complex carotid artery plaques have a higher recruitable production of IL-1β. Similarly, plaques from patients on no or low-intensity statin therapy or with suboptimally controlled hyperlipidemia (LDL level >130 mg/dl) mount higher IL-1β release upon stimulation. Plaque generation of IL-1β is also paired with release of IL-1α and entails likely both the canonical and noncanonical inflammasome pathway. Overall the present study findings underscore a link between plaque inflammatory biological activity and hyperlipidemia as well as plaque complexity.

TRANSLATIONAL OUTLOOK: The results of the present study are supportive of the CANTOS trial by indicating that an IL-1β-directed approach would be most efficacious in patients with a vulnerable phenotype (complex plaques) and those with suboptimal secondary prevention measures. As indicated by the present findings, control of hypercholesterolemia and moderate- to high-intensity statin therapy translate into lower plaque interleukin-1 production and related inflammatory activity. Lipid-lowering and statin therapy intensification efforts should come first with additional anti-inflammatory therapies, especially those that specifically target the inflammasome-IL-1 axis, in very high risk patients as enrolled in the CANTOS trial. The present study lends support to biological plaque activity-directed treatment efforts and the testing thereof in future clinical trials.

REFERENCES

1. Ridker PM, Everett BM, Thuren T, et al. Antiinflammatory therapy with canakinumab for atherosclerotic disease. N Engl J Med 2017;377:1119–31.

2. Duewell P, Kono H, Rayner KJ, et al. NLRP3 inflammasomes are required for atherogenesis and activated by cholesterol crystals. Nature 2010; 464:1357–61.

3. Rajamaki K, Lappalainen J, Oorni K, et al. Cholesterol crystals activate the NLRP3 inflammasome in human macrophages: a novel link between cholesterol metabolism and inflammation. PLoS ONE 2010;5:e11765.

4. Sheedy FJ, Grebe A, Rayner KJ, et al. CD36 coordinates NLRP3 inflammasome activation by facilitating intracellular nucleation of

soluble ligands into particulate ligands in sterile inflammation. Nat Immunol 2013;14:812–20.

5. Paramel Varghese G, Folkersen L, Strawbridge RJ, et al. NLRP3 inflammasome expression and activation in human atherosclerosis. J Am Heart Assoc 2016;5:e003031.

6. Gaidt MM, Ebert TS, Chauhan D, et al. Human monocytes engage an alternative inflammasome pathway. Immunity 2016;44:833–46.

7. Folkersen L, van't Hooft F, Chernogubova E, et al. Association of genetic risk variants with expression of proximal genes identifies novel susceptibility genes for cardiovascular disease. Circ Cardiovasc Genet 2010;3:365–73.

8. Razuvaev A, Ekstrand J, Folkersen L, et al. Correlations between clinical variables and gene-expression profiles in carotid plaque instability. Eur J Vasc Endovasc Surg 2011;42:722–30.

9. Perisic L, Aldi S, Sun Y, et al. Gene expression signatures, pathways and networks in carotid atherosclerosis. J Intern Med 2016;279:293–308.

10. Ketelhuth DF, Rios FJ, Wang Y, et al. Identification of a danger-associated peptide from apolipoprotein B100 (ApoBDS-1) that triggers innate proatherogenic responses. Circulation 2011;124:2433–43.

11. Herrmann J, Mannheim D, Wohlert C, et al. Expression of lipoprotein-associated phospholipase A(2) in carotid artery plaques predicts long-term cardiac outcome. Eur Heart J 2009;30:2930–8.

12. Mannheim D, Herrmann J, Versari D, et al. Enhanced expression of Lp-PLA2 and lysophosphatidylcholine in symptomatic carotid atherosclerotic plaques. Stroke 2008;39:1448–55.

13. Vigano E, Diamond CE, Spreafico R, Balachander A, Sobota RM, Mortellaro A. Human caspase-4 and caspase-5 regulate the one-step non-canonical inflammasome activation in monocytes. Nat Commun 2015;6:8761.

14. Afonina IS, Zhong Z, Karin M, Beyaert R. Limiting inflammation-the negative regulation of NF-kappaB and the NLRP3 inflammasome. Nat Immunol 2017;18:861–9.

15. Hansson GK. Inflammation, atherosclerosis, and coronary artery disease. N Engl J Med 2005;352:1685–95.

16. Bentzon JF, Otsuka F, Virmani R, Falk E. Mechanisms of plaque formation and rupture. Circ Res 2014;114:1852–66.

17. Kuida K, Lippke JA, Ku G, et al. Altered cytokine export and apoptosis in mice deficient in interleukin-1 beta converting enzyme. Science 1995;267:2000–3.

18. Keller M, Ruegg A, Werner S, Beer HD. Active caspase-1 is a regulator of unconventional protein secretion. Cell 2008;132:818–31.

19. Gross O, Yazdi AS, Thomas CJ, et al. Inflammasome activators induce interleukin-1alpha secretion via distinct pathways with differential requirement for the protease function of caspase-1. Immunity 2012;36:388–400.

20. Coll RC, Robertson AA, Chae JJ, et al. A small-molecule inhibitor of the NLRP3 inflammasome for the treatment of inflammatory diseases. Nat Med 2015;21:248–55.

21. Monaco C, Andreakos E, Kiriakidis S, et al. Canonical pathway of nuclear factor kappa B activation selectively regulates proinflammatory and prothrombotic responses in human atherosclerosis. Proc Natl Acad Sci U S A 2004;101:5634–9.

22. Kayagaki N, Wong MT, Stowe IB, et al. Non-canonical inflammasome activation by intracellular LPS independent of TLR4. Science 2013;341:1246–9.

23. Beltrami-Moreira M, Vromman A, Sukhova GK, Folco EJ, Libby P. Redundancy of IL-1 isoform signaling and its implications for arterial remodeling. PLoS ONE 2016;11:e0152474.

24. Freigang S, Ampenberger F, Weiss A, et al. Fatty acid-induced mitochondrial uncoupling elicits inflammasome-independent IL-1alpha and sterile vascular inflammation in atherosclerosis. Nat Immunol 2013;14:1045–53.

25. Evavold CL, Ruan J, Tan Y, Xia S, Wu H, Kagan JC. The pore-forming protein gasdermin D regulates interleukin-1 secretion from living macrophages. Immunity 2018;48:35–44.e6.

26. Kayagaki N, Warming S, Lamkanfi M, et al. Non-canonical inflammasome activation targets caspase-11. Nature 2011;479:117–21.

27. van der Heijden T, Kritikou E, Venema W, et al. NLRP3 inflammasome inhibition by MCC950 reduces atherosclerotic lesion development in apolipoprotein E-deficient mice. Arterioscler Thromb Vasc Biol 2017;37:1457–61.

28. Smeeth L, Thomas S, Hall A, Hubbard R, Farrington P, Vallance P. Risk of myocardial infarction and stroke after acute infection or vaccination. N Engl J Med 2004;351:2611–8.

29. Dang EV, McDonald JG, Russell DW, Cyster JG. Oxysterol restraint of cholesterol synthesis prevents AIM2 inflammasome activation. Cell 2017;171:1057–71.e11.

30. Christ A, Gunther P, Lauterbach MAR, et al. Western diet triggers NLRP3-dependent innate immune reprogramming. Cell 2018;172:162–75.e14.

31. Ceneri N, Zhao L, Young BD, et al. Rac2 modulates atherosclerotic calcification by regulating macrophage interleukin-1beta production. Arterioscler Thromb Vasc Biol 2017;37:328–40.

KEY WORDS atherosclerosis, hypercholesterolemia, inflammasome, inflammation, interleukin-1

JACC: BASIC TO TRANSLATIONAL SCIENCE VOL. 4, NO. 3, 2019

PRECLINICAL RESEARCH

Prostacyclin Analogue–Loaded Nanoparticles Attenuate Myocardial Ischemia/Reperfusion Injury in Rats

Shin Yajima, MD, PhD,[a] Shigeru Miyagawa, MD, PhD,[a] Satsuki Fukushima, MD, PhD,[a] Yoshiki Sakai, BSc,[a] Hiroko Iseoka, PhD,[a] Akima Harada, BSc,[a] Kayako Isohashi, MD, PhD,[b] Genki Horitsugi, BSc,[b] Yuki Mori, PhD,[c] Motoko Shiozaki, PhD,[a] Hirotatsu Ohkawara, PhD,[a] Ryoto Sakaniwa, PhD,[d] Jun Hatazawa, MD, PhD,[b] Yoshichika Yoshioka, PhD,[c] Yoshiki Sawa, MD, PhD[a]

VISUAL ABSTRACT

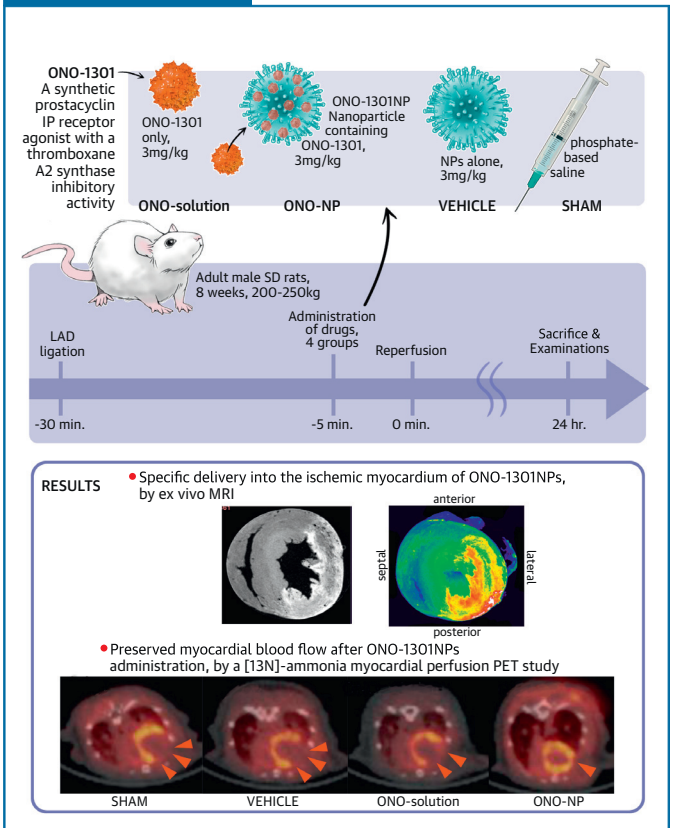

Yajima, S. et al. J Am Coll Cardiol Basic Trans Science. 2019;4(3):318–31.

HIGHLIGHTS

- **Intravenously injected ONO-1301–containing nanoparticles selectively accumulated in the ischemic border area of the myocardium.**
- **Prominent up-regulation occurred of proangiogenic cytokines such as vascular endothelial growth factor and angiopoietin-1 in the ischemic myocardium, which may have contributed to the preservation of the native vascular and capillary networks, thus preserving regional myocardial blood flow.**
- **Down-regulation of the proinflammatory cytokines interleukin-1β, interleukin-6, and tumor necrosis factor-α in the ischemic myocardium might have led to the attenuation of myocyte swelling and the suppression of the endothelial bleb formation, also contributing to the preservation of myocardial blood flow or the reduced infarct size.**

From the [a]Department of Cardiovascular Surgery, Osaka University Graduate School of Medicine, Osaka, Japan; [b]Department of Nuclear Medicine and Tracer Kinetics, Osaka University Graduate School of Medicine, Osaka, Japan; [c]Department of Biofunctional Imaging Laboratory, Immunology Frontier Research Center, Osaka University Graduate School of Medicine, Osaka, Japan; and the [d]Department of Public Health, Osaka University Graduate School of Medicine, Osaka, Japan. This work was supported by Grants-in-Aid for Scientific Research (KAKENHI), Tokyo, Japan (T16K106280). The authors have reported that they have no relationships relevant to the contents of this paper to disclose.

All authors attest they are in compliance with human studies committees and animal welfare regulations of the authors' institutions and Food and Drug Administration guidelines, including patient consent where appropriate. For more information, visit the *JACC: Basic to Translational Science* author instructions page.

Manuscript received April 2, 2018; revised manuscript received December 27, 2018, accepted December 27, 2018.

ISSN 2452-302X https://doi.org/10.1016/j.jacbts.2018.12.006

SUMMARY

Intravenously injected ONO-1301–containing nanoparticles (ONO-1301NPs), unlike an ONO-1301 solution, selectively accumulated in the ischemia/reperfusion (I/R)-injured myocardium of rats and contributed to the prolonged retention of ONO-1301 in the targeted myocardial tissue. In the ischemic area, proangiogenic cytokines were up-regulated and inflammatory cytokines were down-regulated upon ONO-1301NP administration. Consequently, ONO-1301NP-injected rats exhibited a smaller infarct size, better-preserved capillary networks, and a better-preserved myocardial blood flow at 24 h after I/R injury, compared with those in vehicle-injected or ONO-1301 solution–injected rats. ONO-1301NPs attenuate the myocardial I/R injury via proangiogenic and anti-inflammatory effects of the drug. (J Am Coll Cardiol Basic Trans Science 2019;4:318–31)

ABBREVIATIONS AND ACRONYMS

ANG = angiopoietin
EPR = enhanced permeability and retention
IL = interleukin
I/R = ischemia/reperfusion
MBF = myocardial blood flow
MRI = magnetic resonance imaging
NP = nanoparticle
PET = positron emission tomography
PMNL = polymorphonuclear leukocyte
VEGF = vascular endothelial growth factor

Myocardial ischemia/reperfusion (I/R) injury is a pivotal therapeutic target to optimize revascularization therapy for acute coronary syndrome (1). Although an array of basic studies have reported efficacious treatments targeting myocardial I/R injury (2–5), the therapeutic efficacy has not been established for any treatment in clinical settings (6–9). This critical gap between the basic and clinical findings may be explained by the narrow pharmacological therapeutic window of each treatment (10). Because myocardial I/R injury involves dynamic biological and physiological events regulated by serially invoked complex pathways, any simple treatments, targeting single cellular and/or molecular processes, would not modify this event in the therapeutic direction to a clinically beneficial extent.

A new drug, ONO-1301, is a synthetic prostacyclin IP receptor agonist lacking the typical prostanoid structures, which contributes to the biological and chemical stability of this compound, resulting in long-lasting prostacyclin activity in vivo (11,12). In addition, ONO-1301 has a 3-pyridine radical, which exerts thromboxane A_2 synthase inhibitory activity, inducing an intrinsic prostaglandin I2 synthesis-promoting effect to augment the IP receptor agonistic activity (13). Our laboratory and others have reported beneficial effects of a slow-releasing form of ONO-1301 for acute and chronic ischemic cardiac failure via its role as an inducer of protective cytokines (14–16). Indeed, it has been shown that ONO-1301 binds to IP receptors on endothelial cells, vascular smooth muscle cells, or fibroblasts to induce the release of protective cytokines such as vascular endothelial growth factor (VEGF), hepatocyte growth factor, or stromal cell-derived factor 1, contributing to the repair of an experimentally induced ischemic myocardium.

Drug targeting is more critical in myocardial I/R injury than in acute or chronic ischemic cardiac failure because multiple complex events are serially, dynamically, and multidirectionally provoked in the myocardium after reperfusion. In this regard, systemically injected lipid nanoparticles (NPs) reportedly accumulate in acutely damaged tissue, represented by I/R injury, via enhanced permeability and retention (EPR) effects (17,18). Importantly, the drug incorporated in NPs is selectively released into the target tissue (2,19). We herein hypothesized that NPs containing ONO-1301 (ONO-1301NPs) would accumulate in I/R-injured cardiac tissue and induce multiple protective cytokines, thereby contributing to the attenuation of myocardial I/R injury. Thus, the aim of the present study was to evaluate whether ONO-1301NPs attenuate myocardial I/R injury.

METHODS

PREPARATION OF ONO-1301NPS. NPs containing ONO-1301 were prepared as follows. Two types of lipids, 1,2-dierucoyl-sn-glycerol-3-phosphorylcholine (1.88 g, CAS No. 5177-95-4, Nippon Fine Chemical, Osaka, Japan) and *N*-(carbonyl-methoxypolyethyleneglycol 2000)-1,2 distearoyl-sn-glycero-3-phosphoethanolamine sodium salt (0.12 g, CAS No. 147867-65-0, Nippon Fine Chemical), were dissolved, together with ONO-1301 (100 mg, Ono Pharmaceuticals, Osaka, Japan), in 20 g of *t*-butanol at 70°C. The obtained solution was immediately frozen in dry ice/acetone, followed by freeze-drying for 17 h. The obtained powder was dispersed in phosphate-buffered saline in a warm bath (50°C) and sonicated until lumps disappeared. The solution was passed through a polycarbonate filter with pores of 400 nm in diameter and then through another filter, with

FIGURE 1 Characteristics of ONO-1301NPs

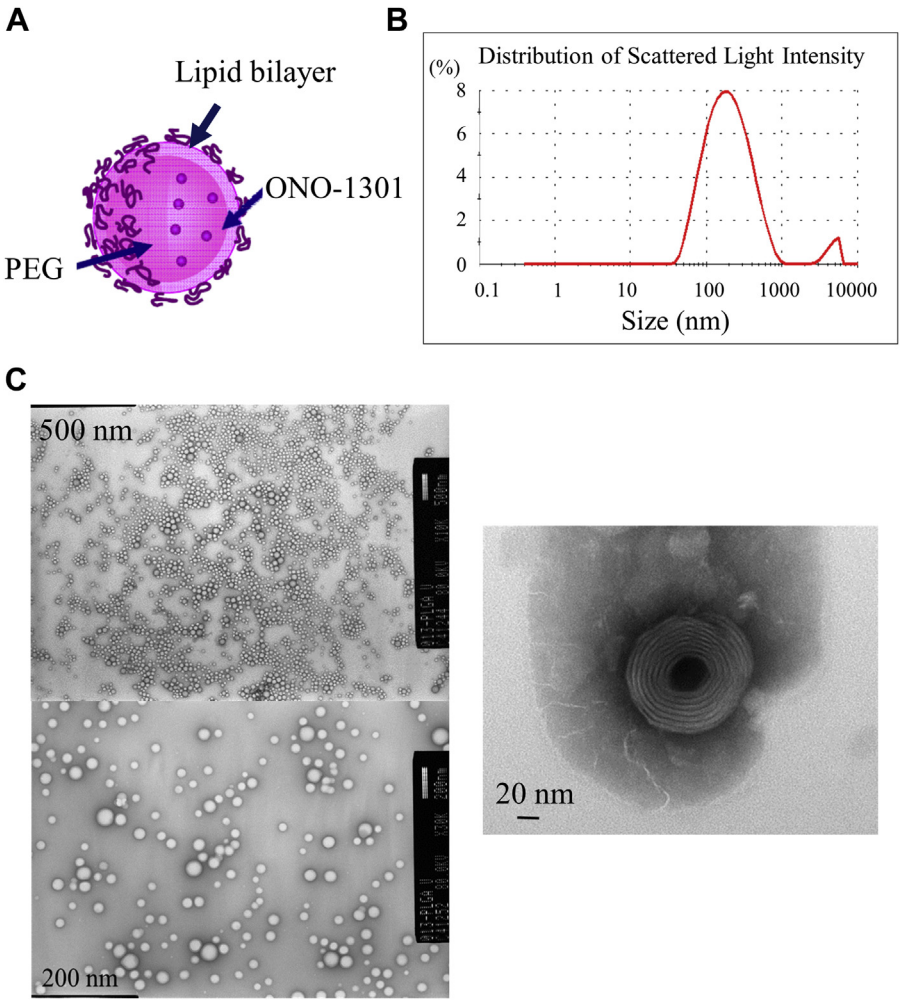

(A) Scheme of ONO-1301-containing nanoparticles (ONO-1301NPs). ONO-1301NPs are composed of a lipid bilayer with a polyethylene glycol (PEG) side chain on the surface and contain the ONO-1301 compound. **(B)** Details of ONO-1301NPs. Average particle diameter was obtained by the dynamic light scattering method. **(C)** Representative electron micrographic images of ONO-1301NPs. **Upper**: 10,000 × magnification; **Lower**: 30,000 magnification; **Right**: 50,000 × magnification.

pores of 200 nm in diameter, to obtain a translucent liposome fluid. The obtained solution was purified by ultrafiltration to prepare consistently nanosized and round-shaped ONO-1301NPs (Figure 1). ONO-1301NPs were prepared by mixing the drug and the lipid (1,2-dierucoyl-sn-glycerol-3-phosphorylcholine:*N*-(carbonyl-methoxypolyethyleneglycol 2000)-1,2 distearoyl-sn-glycero-3-phosphoethanolamine sodium salt = 94:6) in a drug-to-lipid ratio of 0.05. After encapsulation and ultrafiltration, the drug-to-lipid ratio determined by using high-performance liquid chromatography was 0.043, indicating that loading efficiency was 86%.

SURGERY AND GROUPING OF ANIMALS. The institutional ethics committee approved all experimental procedures. Animal care was conducted humanely in compliance with the principles of laboratory animal care.

Male Sprague-Dawley rats (200 to 250 g, Charles River Laboratories, Margate, United Kingdom) underwent left thoracotomy under general anesthesia with inhalation of isoflurane (2%, 0.2 ml/min); they

were then intubated and placed on a respirator during surgery to maintain ventilation. The myocardial I/R model was prepared as follows. The left anterior descending artery was ligated at approximately 2 mm below the atrioventricular groove for 30 min by using a 7-0 monofilament with a silicon tube (outside diameter: 0.7 mm) placed along the left anterior descending artery and then released for reperfusion (2). Five minutes before reperfusion, 5 ml/kg phosphate-buffered saline (sham group), 3 mg/kg nanoliposomes in 5 ml/kg phosphate-buffered saline (vehicle group), 3 mg/kg ONO-1301 in 5 ml/kg phosphate-buffered saline (ONO-solution group), and 3 mg/kg ONO-1301NPs in 5 ml/kg phosphate-buffered saline (ONO-NP group) were injected into the rats (Supplemental Figure 1A). In addition, nanosized liposomes with a fluorescently labeled reagent (cyanine 5.5, Katayama Chemical Co., Osaka, Japan) encapsulated were prepared in the same manner as ONO-1301NPs and injected intravenously 5 min before reperfusion into I/R model rats (n = 6) for confocal microscopic analysis. Moreover, a nanosized liposomal contrast agent (Gadolisome, 5 ml/kg; DS Pharma Biomedical, Osaka, Japan) or 5 ml/kg saline was intravenously injected 5 min before reperfusion into I/R model rats (n = 3 each) for ex vivo magnetic resonance imaging (MRI) analysis. In addition, the same amount of Gadolisome or saline was injected into normal rats (n = 2 each) for the control of the MRI study. The characteristics of NP preparations (empty, fluorescently labeled, and Gadolisome) are described in Supplemental Figure 2.

DEFINITION OF MYOCARDIAL AREA. Cardiac segmental analysis was performed according to the American Heart Association 17-segment model (20). The 17 segments were compiled into 3 territories according to the area of the ischemic insult: the infarct (1, 2, 7, 8, 13, and 14), border (3, 6, 9, 12, 15, and 16), and remote (4, 5, 10, and 11) areas (Supplemental Figure 1B).

OTHER METHODS. The methods of measurement of ONO-1301 concentrations in the plasma and heart, analysis of fluorescently labeled NPs, ex vivo MRI, [^{13}N]-ammonia positron emission tomography (PET), enzyme-linked immunosorbent assay, triphenyltetrazolium chloride–Evans blue staining, histology and immunohistolabeling, and real-time polymerase chain reaction are detailed in the Supplemental Methods.

STATISTICAL ANALYSIS. Continuous variables are presented as the mean ± SD. Statistical analyses were performed by using nonparametric methods because the sample sizes were too small to determine if a normal or a skewed distribution was followed. Intergroup differences were compared by using a Kruskal-Wallis analysis with a Mann-Whitney *U* test ad hoc analysis. A p value < 0.05 was considered statistically significant. All statistical analyses were performed with JMP version 12 software (SAS Institute, Inc., Cary, North Carolina).

RESULTS

STABILITY OF ONO-1301NPs IN ARTIFICIAL PLASMA. The stability of the ONO-1301NP preparation in artificial plasma (i.e., plasma that does not contain plasma components such as proteins and lipids) and lipase (which breaks down the ONO-1301/ONO-1301NP preparation) was investigated. Approximately 7% of free ONO-1301 was detected in artificial plasma 72 h after culture, whereas approximately 55% of free ONO-1301 was hydrolyzed by the lipoprotein lipase. However, separation of ONO-1301 due to ONO-1301NP breakdown could not be confirmed with phospholipase A2 processing even after 72 h. ONO-1301/ONO-1301NPs were hydrolyzed by the lipase in the plasma (mainly lipoprotein lipase), and then bare ONO-1301 was gradually separated. In addition, >50% of ONO-1301 was separated from ONO-1301NPs through hydrolysis by lipase after 72 h (Supplemental Figure 3).

PROLONGED RETENTION OF ONO-1301 IN THE PLASMA AND HEART AFTER NP INJECTION. ONO-1301 (ONO-solution group) or ONO-1301NPs (ONO-NP group) were injected intravenously into rats with myocardial I/R injury. Concentrations of ONO-1301 were measured in the plasma and heart according to liquid chromatography-tandem mass spectrometry analysis 8 and 24 h after the injection to explore targeted delivery of ONO-1301 incorporated into the liposome-based NPs. The results show that the plasma concentrations were not significantly different between the ONO-solution and ONO-NP groups at 8 h after the injection (ONO-solution: 10.0 ± 3.3 ng/ml; ONO-NP: 12.1 ± 4.2 ng/ml; p = 0.2611), whereas concentrations at 24 h were more prominently decreased in the ONO-solution group than in the ONO-NP group (ONO-solution: 0.6 ± 0.4 ng/ml; ONO-NP: 3.3 ± 3.1 ng/ml; p = 0.0016) (**Figure 2A**). The cardiac concentrations of ONO-1301 at 8 h were not significantly different between the 2 groups in the border area (ONO-solution: 4.3 ± 1.1 ng/g; ONO-NP: 6.1 ± 3.5 ng/g; p = 0.3703) and the remote area (ONO-solution: 2.9 ± 0.5 ng/g; ONO-NP: 3.2 ± 1.3 ng/g; p = 0.4292). Of note, the cardiac ONO-1301 concentrations were not significantly different at

FIGURE 2 Plasma and Cardiac Concentrations of ONO-1301 After Intravenous Injection

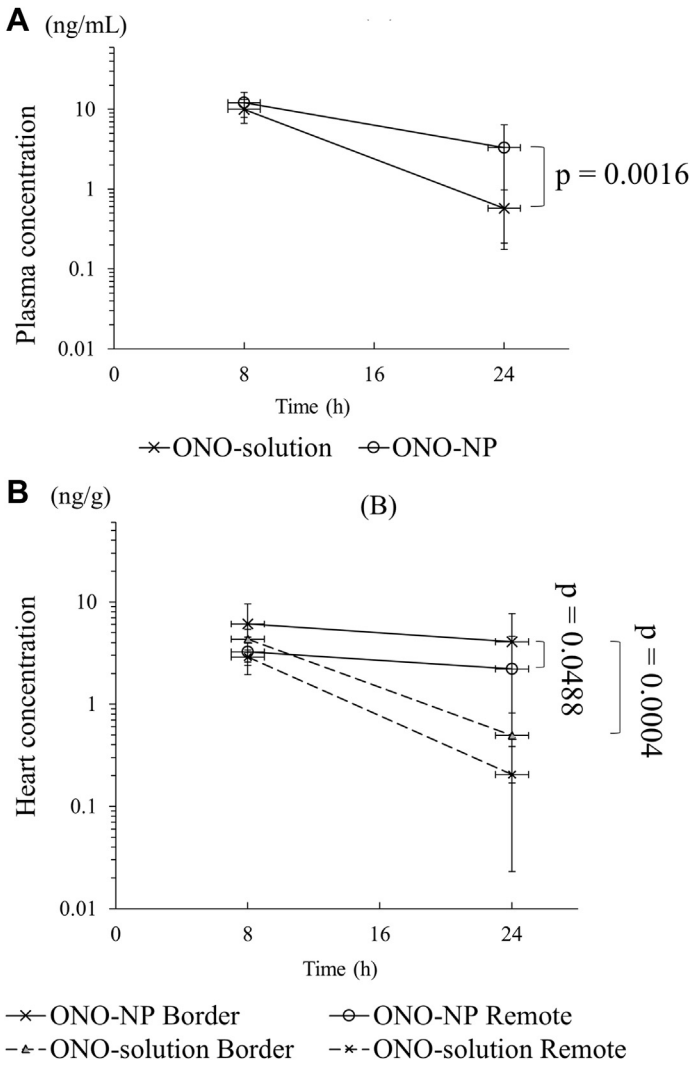

ONO-1301 concentrations **(A)** in the plasma and **(B)** in the heart. Injected ONO-1301NPs showed better migration properties than did an injected ONO-1301 solution, leading to a greater ONO-1301 concentration in the infarct border myocardium. NP = nanoparticle.

8 and 24 h in the border and remote areas in the ONO-NP group. In contrast, the cardiac ONO-1301 concentrations significantly decreased at 24 h in the border and remote areas in the ONO-solution group. The cardiac concentrations of ONO-1301 at 24 h were significantly greater in the ONO-NP group than in the ONO-solution group in the border (4.1 ± 3.6 ng/g vs. 0.5 ± 0.3 ng/g, respectively; p = 0.0004) and remote (2.2 ± 2.4 ng/g vs. 0.2 ± 0.2 ng/g; p = 0.0003) areas (Figure 2B). Furthermore, the concentration in the border area was still significantly greater than in the remote area (p = 0.0488). The half-life of ONO-1301NPs in the plasma was 13.2 h, whereas those in the border and remote areas were 23.8 and 20.5 h.

PREDOMINANT ACCUMULATION OF NPs IN THE BORDER AREA OF THE MYOCARDIUM. Fluorescently labeled NPs and Gadolisome were intravenously injected into myocardial I/R model rats to assess the distribution of NPs in cardiac tissue by using confocal microscopy and by ex vivo MRI, respectively. The results showed that the fluorescently labeled NPs were more abundantly present in the border area of the myocardium than in the remote area at 24 h after reperfusion (border: 615 ± 206 mm^2; remote: 56 ± 35 mm^2; p = 0.0039) (Figure 3A). The injected fluorescently labeled NPs were predominantly present in the interstitial space of the border and remote areas. Meanwhile, Gadolisome was abundantly detected in the infarct and infarct border myocardium but minimally detected in the remote myocardium and the normal heart (Figure 3B). On a three-dimensional, fast low-angle shot view, specific accumulation of Gadolisome was particularly obvious in the outer and inner layers, rather than in the mid-layers, of the infarct and border myocardium (Figure 3C).

UP-REGULATION OF THERAPEUTIC CYTOKINES IN THE HEART BY ONO-1301NP INJECTION. Gene expression of proangiogenic and inflammatory cytokines in the border area of the myocardium was assessed at 24 h after reperfusion by using real-time polymerase chain reaction. The results showed that the *Vegf* and angiopoietin-1 (*Ang-1*) genes were significantly up-regulated in the ONO-NP group compared with their expression in the other 3 groups (VEGF: vs. sham; p = 0.0024; vs. vehicle; p = 0.0194; vs. ONO-solution; p = 0.0051; ANG-1: vs. sham; p = 0.0024; vs. vehicle; p = 0.0006; vs. ONO-solution; p = 0.0014) (Figure 4A). In addition, the levels of gene expression for interleukin (IL)-1β, IL-6, and tumor necrosis factor-α were significantly lower in the ONO-NP group than in the other 3 groups (IL-1β: vs. sham; p = 0.0120; vs. vehicle; p = 0.0020; vs. ONO-solution; p = 0.0194; IL-6: vs. sham; p = 0.0226; vs. vehicle; p = 0.0029; vs. ONO-solution; p = 0.0166; tumor necrosis factor-α: vs. sham; p = 0.0020; vs. vehicle; p = 0.0024; vs. ONO-solution; p = 0.0464) (Figure 4B). There were no significant differences in the expression of these genes among the sham, vehicle, and ONO-solution groups.

PROTECTION OF CAPILLARIES IN THE BORDER AREA BY ONO-1301NP INJECTION. Pathological angiogenesis was assessed at the border area 24 h after the myocardial I/R injury. The residual capillary

FIGURE 3 Distribution of NPs in the Myocardium at 24 h After I/R Injury

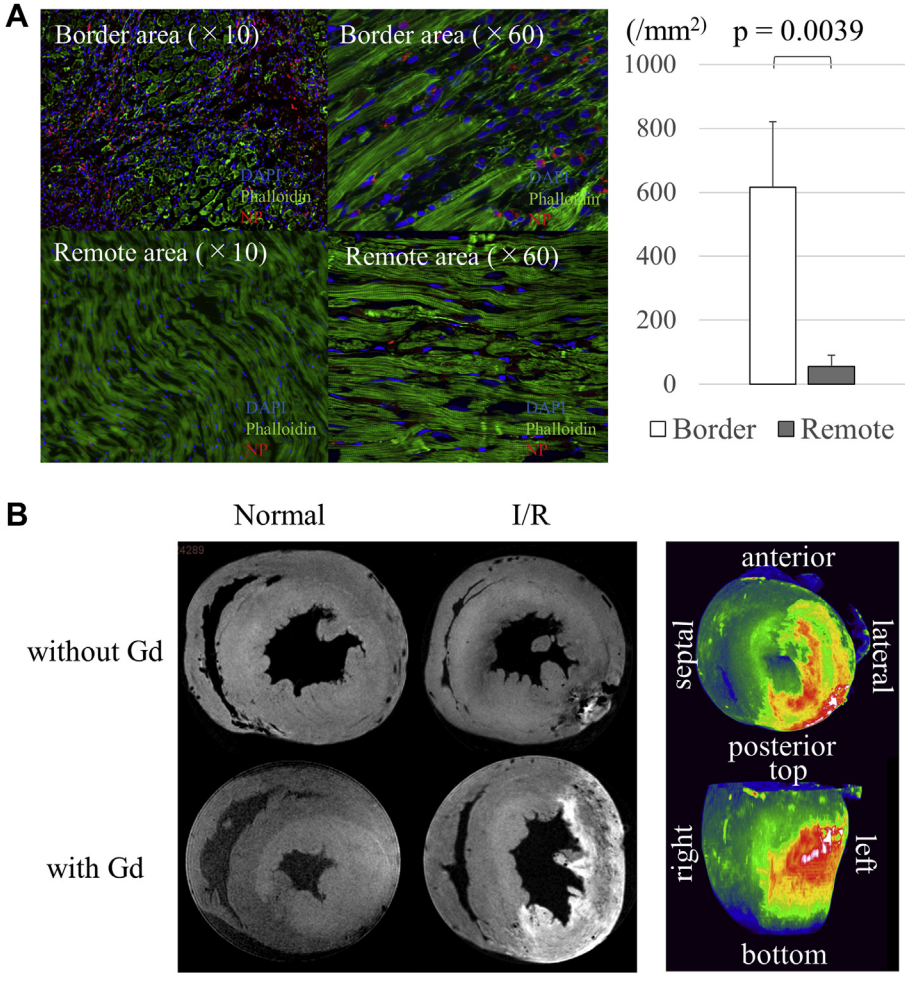

(A) Confocal microscopy showed predominant presence of fluorescently labeled liposomes in the border area rather than in the remote area. **(B)** Magnetic resonance imaging (11.7-T) displayed selective accumulation of gadolinium (Gd)-labeled liposomes in the ischemic area at 24 h after NP injection. I/R = ischemia/reperfusion; NP = nanoparticle.

network in the border area was semi-quantitatively assessed by using immunohistology for the von Willebrand factor. The results showed that the von Willebrand factor-positive capillary network was better preserved in the myocardial interstitium of the ONO-NP group than in the myocardial interstitium of the other groups (Figure 5A). The capillary density was significantly greater in the ONO-NP group (212 ± 54 mm^{-2}) than in the other groups (sham: 150 ± 36 mm^{-2}; p = 0.0124; vehicle: 117 ± 21 mm^{-2}; p = 0.0002; ONO-solution: 172 ± 25 mm^{-2}; p = 0.0397) (Figure 5B). The capillary area was significantly greater in the ONO-NP group (275 ± 111 μm^2) than in the other 3 groups (sham: 121 ± 34 μm^2; p = 0.0001; vehicle: 123 ± 26 μm^2; p = 0.0003; ONO-solution: 101 ± 52 μm; p = 0.0001) (Figure 5C).

ATTENUATION OF POLYMORPHONUCLEAR LEUKOCYTE INFILTRATION AND MYOCYTE SWELLING BY ONO-1301NP INJECTION. Infiltration of polymorphonuclear leukocytes (PMNLs) into the myocardium and the sizes of the cardiac myocytes were histologically assessed by hematoxylin/eosin and periodic acid-Schiff staining, respectively, 24 h after reperfusion to explore the distribution and degree of PMNL inflammation and myocyte swelling following I/R injury (Figure 6A). The results showed that PMNLs were markedly

FIGURE 4 Gene Expression in the Heart at 24 h After I/R Injury

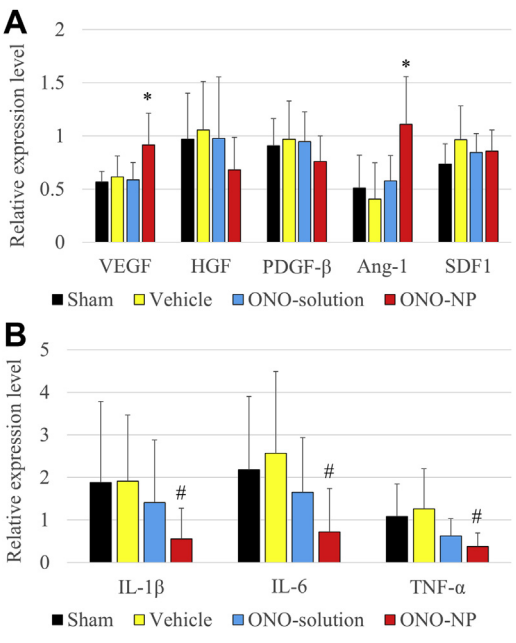

(A) Gene expression of the proangiogenic cytokines vascular endothelial growth factor (VEGF) and angiopoietin (ANG)-1 in the border area was significantly greater in the ONO-NP group than in the other 3 groups. **(B)** Gene expression of the inflammatory cytokines interleukin (IL)-1β, IL-6, and tumor necrosis factor (TNF)-α was significantly lower in the ONO-NP group than in the other 3 groups. *Significantly greater than in the sham, vehicle, and ONO-solution groups. #Significantly smaller than in the sham, vehicle, and ONO-solution groups. HGF = hepatocyte growth factor; PDGF = platelet-derived growth factor; SDF1 = stromal cell–derived factor 1; other abbreviations as in Figure 3.

accumulated in the infarct area in all groups but were rarely observed in the remote area in all groups. In contrast, in the border area, significantly fewer PMNLs were present in the ONO-NP group (1,677 ± 667 mm^{-2}) than in the other groups (sham: 6,923 ± 1,864 mm^{-2}; p = 0.0001; vehicle: 5,979 ± 2,002 mm^{-2}; p = 0.0002; ONO-solution: 5,295 ± 1,499 mm^{-2}; p < 0.0001) (Figure 6B). Meanwhile, the shape and size of myocytes were variable in the infarct area but uniform in the remote area in all groups. In contrast, in the border area, the size of myocytes was significantly smaller in the ONO-NP group (14.8 ± 0.9 μm) than in the other groups (sham: 17.7 ± 0.9 μm; p = 0.0001; vehicle: 18.9 ± 1.7 μm; p = 0.0001; ONO-solution: 14.8 ± 0.9 μm; p = 0.0001) (Figure 6C).

REDUCTION OF INFARCT SIZE BY ONO-1301NP INJECTION. The area at risk of infarction and the infarct area were determined at 24 h after reperfusion by using Evans blue and triphenyltetrazolium chloride staining (Figure 7A). The infarct size per area at risk was significantly smaller (p < 0.01) in the ONO-NP group (33 ± 15%) than in the other groups (sham: 55 ± 11%; p = 0.0149; vehicle: 60 ± 10%; p = 0.0046; ONO-solution: 53 ± 14%; p = 0.0343) (Figure 7B). Consistently, the plasma level of troponin I was significantly lower in the ONO-NP group (4.2 ± 3.9 ng/ml) than in the other groups (sham: 9.6 ± 4.6 ng/ml; p = 0.0074; vehicle: 9.3 ± 4.3%; p = 0.0126; ONO-solution: 9.4 ± 3.7%; p = 0.0054) (Figure 7C), as assessed by using an enzyme-linked immunosorbent assay.

TOTAL AND REGIONAL MYOCARDIAL BLOOD FLOW AFTER MYOCARDIAL I/R INJURY. The total and regional myocardial blood flow (MBF) was assessed 24 h after reperfusion according to a [^{13}N]-ammonia myocardial perfusion PET study (Figure 8A). The total MBF was significantly greater in the ONO-NP group (3.2 ± 0.5 ml/min/g) than in the sham and vehicle groups but not in the ONO-solution group (sham: 2.1 ± 0.6 ml/min/g; p = 0.0252; vehicle: 2.5 ± 0.1 ml/min/g; p = 0.0428; ONO-solution: 2.5 ± 0.5 ml/min/g; p = 0.0656) (Figure 8B).

In the sham, vehicle, and ONO-solution groups, regional MBF in the infarct region was significantly lower than that in the border and remote areas, whereas the former was not significantly different from the latter in the ONO-NP group. Consequently, regional MBF in the infarct area was markedly and significantly greater in the ONO-NP group (3.2 ± 0.5 ml/min/g) than in the other groups (sham: 1.8 ± 0.3 ml/min/g; p = 0.0142; vehicle: 2.1 ± 0.3 ml/min/g; p = 0.0142; ONO-solution: 2.1 ± 0.3 ml/min/g; p = 0.0082). In addition, in the border area, MBF was significantly greater (p = 0.0252) in the ONO-NP group than in the sham group (4.0 ± 0.5 vs. 2.7 ± 0.6 ml/min/g). In the remote area, MBF did not differ significantly among the 4 groups (Figure 8C).

DISCUSSION

OVERVIEW OF PHARMACOLOGICAL EFFECTS OF ONO-1301NPs. There are 2 potentially different mechanisms of ONO-1301NP: 1) activation of the prostacyclin IP receptor, which is expressed in a variety of cells in the myocardium and in the other organs/tissues; and 2) inhibitory effects on 3-pyridine radical-related thromboxane A_2 synthase, which allows bare ONO-1301 to be internalized within cells

FIGURE 5 Capillary Density and Area at 24 h After I/R Injury

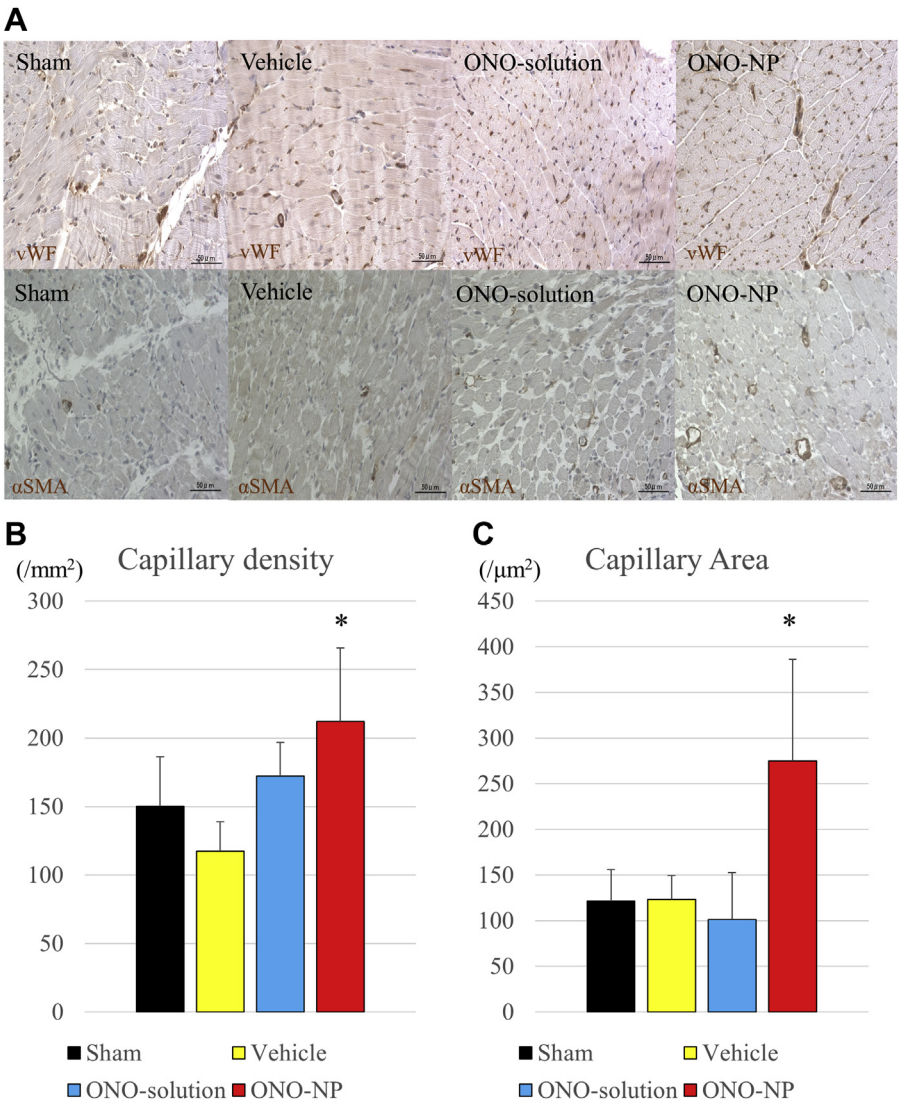

(A) Pathological angiogenesis at the infarct border. **(B)** The density of von Willebrand factor–positive capillaries and **(C)** the capillary area at the border were significantly greater in the ONO-NP group than in the other 3 groups. *Significantly greater than in the sham, vehicle, and ONO-solution groups. SMA = smooth muscle actin; vWF = von Willebrand factor; other abbreviations as in Figure 3.

in the myocardial tissue. We have considered that the IP receptor-related effect is the dominant mechanism of ONO-1301NP therapy, but the 3-pyridine radical-related effect cannot be overlooked. Prostacyclin IP receptor is up-regulated, in response to myocardial I/R, in the endothelial cells, vascular smooth muscle cells, or cardiac fibroblasts. This action causes the release of cytoprotective factors such as VEGF and inhibits proinflammatory factors such as IL-1β, tumor necrosis factor-α, or IL-6 over the 24 h after myocardial I/R.

Intravenously injected ONO-1301NPs selectively accumulated in the ischemic border area of the myocardium where microvasculature was impaired and exhibited enhanced permeability, as assessed by using MRI and confocal microscopy. As shown in the present study, NPs tended to remain in circulation, avoiding a pulmonary trap or renal excretion (17,21) and, subsequently, effectively accumulated in the ischemic myocardium, particularly in the infarct border area; these findings contrasted with the results obtained when a solution form was administered. This

FIGURE 6 PNML Accumulation and Myocyte Sizes at 24 h After I/R Injury

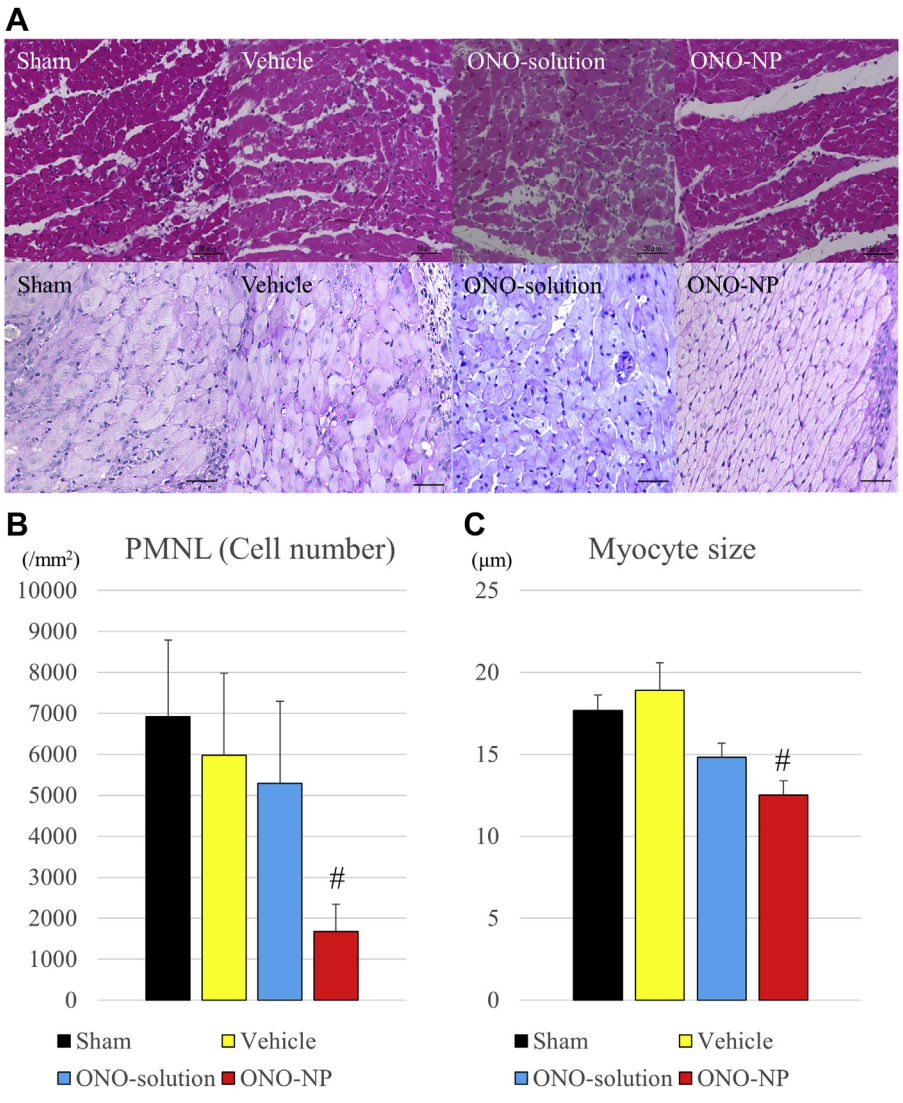

(A) Pathological angiogenesis and myocyte swelling at the infarct border. **(B)** Polymorphonuclear leukocyte (PNML) accumulation was significantly lower and **(C)** myocyte sizes at the border were significantly smaller in the ONO-NP group than in the other 3 groups. #Significantly smaller than in the sham, vehicle, and ONO-solution groups. Abbreviations as in Figure 3.

EPR effect resulted in prominent up-regulation of proangiogenic cytokines such as VEGF and ANG-1, which may have contributed to the preservation of the native vascular and capillary networks, thus preserving regional MBF in this group. Furthermore, down-regulation of the proinflammatory cytokines IL-1β, IL-6, and tumor necrosis factor-α in the border area might have led to the attenuation of myocyte swelling and the suppression of the endothelial bleb formation, also contributing to the preservation of MBF. In addition, the antiplatelet and vasodilatory effects of the prostacyclin analogue (22–24) could have prevented microvascular obstruction, although further studies are warranted to prove this hypothesis. Taken together, these multiple effects of targeted administration of ONO-1301 resulted in prominent cardioprotective effects in this study.

ADVANTAGE OF ONO-1301NPS OVER OTHER PROSTACYCLIN ANALOGUES. Other prostacyclin analogues such as epoprostenol, beraprost,

FIGURE 7 **Infarct Size at 24 h After I/R Injury**

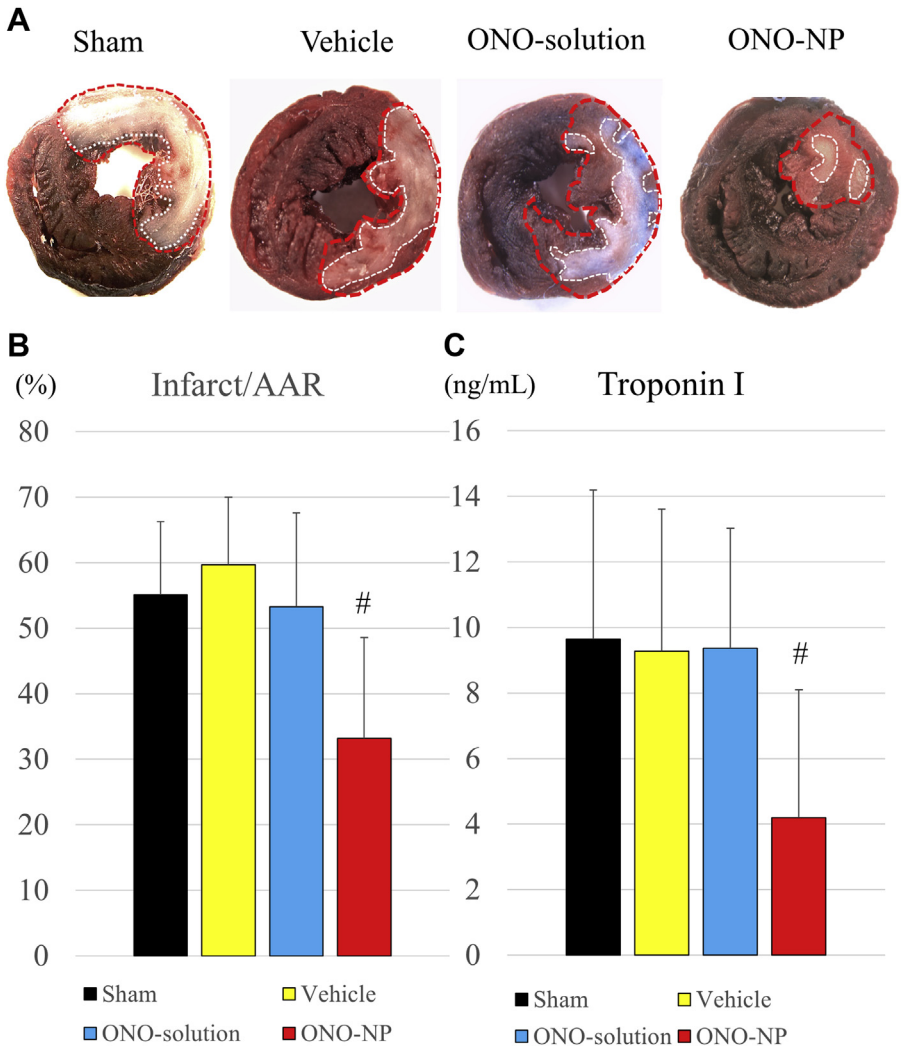

(A) Representative images of Evans blue and triphenyltetrazolium chloride staining of the heart in the 4 treatment groups. **(B)** The size of the area at risk of infarct was significantly smaller in the ONO-NP group than in the other 3 groups, as assessed by triphenyltetrazolium chloride staining. **(C)** The level of troponin I in the plasma was significantly lower in the ONO-NP group than in the other 3 groups, as assessed by enzyme-linked immunosorbent assay. #Significantly smaller than in the sham, vehicle, and ONO-solution groups. AAR = area at risk; other abbreviations as in Figure 3.

treprostinil, and iloprost have been reported to attenuate myocardial I/R injury via vasodilation, inhibition of platelet aggregation, or anti-inflammation (25,26). However, clinical applicability of these analogues is limited by adverse effects or drug tolerance, which is due to their short half-lives or the drug delivery systems used (26). It would be more suitable to administer these analogues intravenously immediately after the reperfusion, considering the nature of myocardial I/R injury. ONO-1301NPs have a much longer half-life (13.2 h in vivo) than that of the other prostacyclin analogues; therefore, ONO-1301NPs can be injected once a day, which may lead to the prevention of drug resistance. In addition, NPs containing cardioprotective agents have been shown to effectively operate in the damaged tissue, with minimal adverse effects, because of an EPR effect (2,19); ONO-1301NPs would thus be an ideal prostacyclin analogue for this pathology.

FIGURE 8 Total and Regional MBF at 24 h After I/R Injury

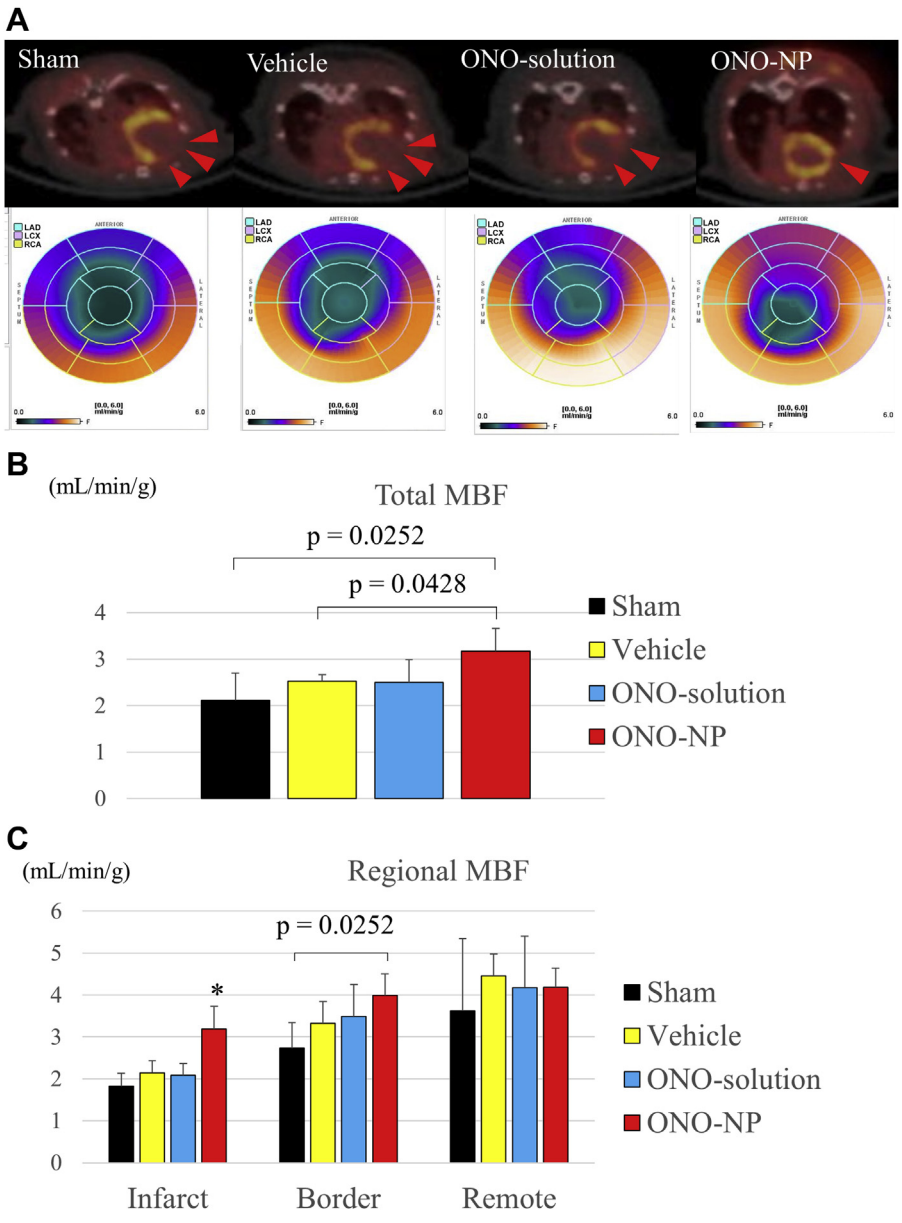

(A) Myocardial blood flow (MBF), assessed by a [^{13}N]-ammonia myocardial perfusion positron emission tomography (PET) study, was compared among the 4 treatment groups. **(B)** Total MBF was significantly greater in the ONO-NP group than in the other 3 groups. **(C)** MBF in the infarct and peri-infarct regions, but not in the remote regions, was significantly greater in the ONO-NP group than in the sham group. *Significantly greater than in the sham, vehicle, and ONO-solution groups. Abbreviations as in Figure 3.

ADVANTAGE OF ONO-1301NPs OVER ONO-1301 SOLUTION. In the present study, the therapeutic effects of the ONO-1301 solution were limited, whereas the same dose of ONO-1301NPs revealed proangiogenic and anti-inflammatory effects. In the plasma, the concentration of ONO-1301 was approximately 6-fold higher in the ONO-NP group than in the ONO-solution group at 24 h, even though no difference was observed at 8 h after myocardial I/R injury, demonstrating the superior stealth capability of NPs compared with that of the solution. Because of this characteristic, in addition to the EPR effect, the

ONO-1301 concentration in the border area of the I/R myocardium was approximately 8-fold higher in the ONO-NP group than in the ONO-solution group at 24 h after myocardial I/R injury, efficiently contributing to pharmacological effects. Injection of ONO-1301NPs revealed their better histological migration properties compared with those of the ONO-1301 solution, leading to a greater pharmacological efficacy in the reperfused ischemic myocardium. In addition, a protein corona effect (27,28) might contribute to the peculiar localization of NPs in the ischemic area; this topic was not investigated in the present study. We speculated that some ONO-1301NPs would be surrounded by a corona in circulation, which may interact specifically with the targeted cells and trigger an internalization process, whereas bare ONO-1301 may interact differently.

ANGIOGENIC AND ARTERIOGENIC EFFECTS OF ONO-1301NP INJECTION. The *Vegf* and *Ang-1* expression increased at 24 h after ONO-1301NP injection, possibly indicating that the myocardium was still ischemic, thus requiring angiogenesis and arteriogenesis. We consider that angiogenesis and arteriogenesis are still underway at this time point, when further development of the vascular network is needed in the border area. In contrast, in the other 3 groups, which exhibited lower levels of *Vegf* and *Ang-1* expression, angiogenic and arteriogenic activity in the myocardium may have ceased by this time point. Although the expression of hepatocyte growth factor and stromal cell-derived factor-1 did not differ among the 4 groups at 24 h after the injection, these factors might have been elevated early and then normalized by 24 h in the treatment groups. Because expression of proangiogenic factors occurs dynamically in response to an ischemic insult and any angiogenic treatments, the expression pattern may be variable, depending on the nature of the ischemic insult and treatment.

ANTI-INFLAMMATORY EFFECTS OF ONO-1301NP INJECTION. Prostacyclin is also known as a regulator of inflammation (26). The prostacyclin analogue iloprost has been reported to attenuate leukocyte adherence in both post-capillary and collecting intestinal venules and to improve the intestinal microvascular blood flow (29). In the present study, ONO-1301NP injection attenuated PMNL accumulation in intramyocardial arterioles of the reperfused myocardium, as assessed by histologic analysis. This and other anti-inflammatory effects, including a decrease in proinflammatory cytokines and suppression of myocardial enzymes, contribute to the attenuation of myocyte swelling, resulting in the relief of microvascular oppression and an increased MBF, particularly in the infarct border myocardium, as confirmed by the $[^{13}N]$-NH_3 PET study. Treatment by ONO-1301NPs attenuated myocardial I/R injury via cytoprotective and angiogenic effects, resulting in a smaller infarct size and better MBF. As a result, swelling of the cardiac myocytes was less severe in the ONO-NP group. Smaller cardiomyocyte size is therefore considered to be due to the indirect effects of ONO-NP. However, there may be a direct effect of the ONO-NP on the cardiac myocytes. Although the fluorescent-NP was not identified inside of the cardiac myocytes in this work as presented in **Figure 3**, the ONO-1301 molecule might be transferred into the cardiac myocytes, possibly via opsonization, and be ligated with the nuclear receptor of prostacyclin.

MBF INCREASE, PARTICULARLY IN THE INFARCT BORDER AREA, BY ONO-1301NP INJECTION. In the present study, MBF in the infarct area was significantly higher after injection of ONO-1301NPs than after injection of the 3 controls. This finding indicates a reduced myocardial infarct size and augmented MBF in the infarct border area but not an increased amount of viable myocardial tissue, containing abundant arterioles, in the infarct area. Variation in the infarct size would affect MBF in the infarct area because of the narrow border area.

STUDY LIMITATIONS. First, the lack of dose-dependent analysis may be a limitation of the study. The rationale to use 3 mg/kg ONO-1301 was based on preliminary experiments, which showed that 3 mg/kg was the maximum dose exhibiting linearity in plasma upon administration of 0.1, 0.3, 1.0, 3.0, and 10 mg/kg ONO-1301 solution to normal rats (Supplemental Table 1, Supplemental Figure 3). We therefore considered that 3 mg/kg was the optimum dose of ONO-1301. As a next step, further investigation is needed to explore the optimal dose and safety and to obtain a maximum benefit with minimum side effects in a large animal model. A second limitation of this study may be its relatively short observation period. Given that the method uses a single injection after myocardial I/R, 24 h was the optimal point to investigate the efficacy of ONO-1301NPs. Further investigation is needed to determine long-term effects, with the manner of drug administration adjusted. Third, evaluation of additional ischemic circulating markers such as the FABP3, which has been shown to provide faster stress-to-recovery response, would be necessary to better understand the mechanism of recovery.

CONCLUSIONS

We herein documented that intravenously injected ONO-1301NPs selectively accumulated in the I/R-injured myocardium, resulting in the prolonged retention of ONO-1301 in the targeted myocardial tissue of rats. Compared with the vehicle- or ONO-1301 solution-injected rats, the ONO-1301NP-injected rats showed a smaller infarct size, better-preserved capillary networks, and, importantly, a better-preserved MBF in the border area of the myocardium 24 h after I/R injury. Intravenously injected ONO-1301NPs selectively accumulated in the I/R area, protecting the myocardium from injury via proangiogenic and anti-inflammatory effects. This new drug may have the potential to bridge the gaps between basic and clinical research.

ACKNOWLEDGMENTS The authors thank Yuri Ide and the staff of the PET Molecular Imaging Center for their excellent technical assistance.

ADDRESS FOR CORRESPONDENCE: Dr. Yoshiki Sawa, Department of Cardiovascular Surgery, Osaka University Graduate School of Medicine, 2-2 Yamadaoka, Suita, Osaka 565-0871, Japan. E-mail: s-yajima@surg1.med.osaka-u.ac.jp.

PERSPECTIVES

COMPETENCY IN MEDICAL KNOWLEDGE: ONO-1301 is a synthetic prostacyclin IP receptor agonist with inhibitory activity for thromboxane A_2 synthase. ONO-1301 lacks the typical prostanoid structures, which contributes to its greater biological and chemical stability. In addition, ONO-1301 has been shown to be a multi-cytokine inducer, acting as a vasodilatory, proangiogenic, anti-inflammatory, and antifibrotic drug. Liposome-based biocompatible nanoparticles containing ONO-1301 may have an advantage over other existing prostacyclin analogues, considering the pathological nature of myocardial I/R injury and long-lasting prostacyclin activity of ONO-1301NPs, as well as their efficient drug delivery, with EPR.

TRANSLATIONAL OUTLOOK: Further investigation is needed to explore the optimal dose and safety of ONO-1301, with maximum pharmacological benefits and minimum adverse effects, and to establish a practical regimen for drug administration to achieve long-term effects.

REFERENCES

1. Yellon DM, Hausenloy DJ. Myocardial reperfusion injury. N Engl J Med 2007;357:1121–35.

2. Nakano Y, Matoba T, Tokutome M, et al. Nanoparticle-mediated delivery of irbesartan induces cardioprotection from myocardial ischemia-reperfusion injury by antagonizing monocyte-mediated inflammation. Sci Rep 2016;6:29601.

3. Fukushima S, Coppen SR, Varela-Carver A, et al. A novel strategy for myocardial protection by combined antibody therapy inhibiting both P-selectin and intercellular adhesion molecule-1 via retrograde intracoronary route. Circulation 2006;114:I251–6.

4. Hausenloy DJ, Maddock HL, Baxter GF, Yellon DM. Inhibiting mitochondrial permeability transition pore opening: a new paradigm for myocardial preconditioning? Cardiovasc Res 2002;55:534–43.

5. Gu J, Fan Y, Liu X, et al. SENP1 protects against myocardial ischaemia/reperfusion injury via a HIF1α-dependent pathway. Cardiovasc Res 2014;104:83–92.

6. Hausenloy DJ, Yellon DM. Ischaemic conditioning and reperfusion injury. Nat Rev Cardiol 2016;13:193–209.

7. Cung TT, Morel O, Cayla G, et al. Cyclosporine before PCI in patients with acute myocardial infarction. N Engl J Med 2015;373:1021–31.

8. Ross AM, Gibbons RJ, Stone GW, Kloner RA, Alexander RW. A randomized, double-blinded, placebo-controlled multicenter trial of adenosine as an adjunct to reperfusion in the treatment of acute myocardial infarction (AMISTAD-II). J Am Coll Cardiol 2005;45:1775–80.

9. Armstrong PW, Granger CB, Adams PX, et al. Pexelizumab for acute ST-elevation myocardial infarction in patients undergoing primary percutaneous coronary intervention: a randomized controlled trial. JAMA 2007;297:43–51.

10. Hausenloy DJ, Yellon DM. Myocardial ischemia-reperfusion injury: a neglected therapeutic target. J Clin Invest 2013;123:92–100.

11. Murakami S, Nagaya N, Itoh T, et al. Prostacyclin agonist with thromboxane synthase inhibitory activity (ONO-1301) attenuates bleomycin-induced pulmonary fibrosis in mice. Am J Physiol Lung Cell Mol Physiol 2006;290:L59–65.

12. Nakamura K, Sata M, Iwata H, et al. A synthetic small molecule, ONO-1301, enhances endogenous growth factor expression and augments angiogenesis in the ischaemic heart. Clin Sci (Lond) 2007;112:607–16.

13. Fukushima S, Miyagawa S, Sakai Y, Sawa Y. A sustained-release drug-delivery system of synthetic prostacyclin agonist, ONO-1301SR: a new reagent to enhance cardiac tissue salvage and/or regeneration in the damaged heart. Heart Fail Rev 2015;20:401–13.

14. Ishimaru K, Miyagawa S, Fukushima S, et al. Synthetic prostacyclin agonist, ONO1301, enhances endogenous myocardial repair in a hamster model of dilated cardiomyopathy: a promising regenerative therapy for the failing heart. J Thorac Cardiovasc Surg 2013;146:1516–25.

15. Imanishi Y, Miyagawa S, Fukushima S, et al. Sustained-release delivery of prostacyclin analogue enhances bone marrow-cell recruitment and yields functional benefits for acute myocardial infarction in mice. PLoS One 2013;8:e69302.

16. Shirasaka T, Miyagawa S, Fukushima S, et al. A slow-releasing form of prostacyclin agonist (ONO1301SR) enhances endogenous secretion of multiple cardiotherapeutic cytokines and improves cardiac function in a rapid-pacing-induced model of canine heart failure. J Thorac Cardiovasc Surg 2013;146:413–21.

17. Acharya S, Sahoo SK. PLGA nanoparticles containing various anticancer agents and tumour delivery by EPR effect. Adv Drug Deliv Rev 2011;63:170–83.

18. Matoba T, Egashira K. Nanoparticle-mediated drug delivery system for cardiovascular disease. Int Heart J 2014;55:281–6.

19. Takahama H, Minamino T, Asanuma H, et al. Prolonged targeting of ischemic/reperfused myocardium by liposomal adenosine augments cardioprotection in rats. J Am Coll Cardiol 2009;53:709–17.

20. Cerqueira MD, Weissman NJ, Dilsizian V, et al. Standardized myocardial segmentation and

nomenclature for tomographic imaging of the heart. A statement for healthcare professionals from the Cardiac Imaging Committee of the Council on Clinical Cardiology of the American Heart Association. Circulation 2002;105:539–42.

21. Markman JL, Rekechenetskiy A, Holler E, Ljubimova JY. Nanomedicine therapeutic approaches to overcome cancer drug resistance. Adv Drug Deliv Rev 2013;65:1866–79.

22. Camacho M, Rodriguez C, Guadall A, et al. Hypoxia upregulates PGI-synthase and increases PGI_2 release in human vascular cells exposed to inflammatory stimuli. J Lipid Res 2011;52:720–31.

23. Mohite A, Chillar A, So SP, Cervantes V, Ruan KH. Novel mechanism of the vascular protector prostacyclin: regulating microRNA expression. Biochemistry 2011;50:1691–9.

24. Aherne T, Price DC, Yee ES, Hsieh WR, Ebert PA. Prevention of ischemia-induced myocardial platelet deposition by exogenous prostacyclin. J Thorac Cardiovasc Surg 1986;92:99–104.

25. Chawengsub Y, Gauthier KM, Campbell WB. Role of arachidonic acid lipoxygenase metabolites in the regulation of vascular tone. Am J Physiol Heart Circ Physiol 2009;297:H495–507.

26. Dorris SL, Peebles RS Jr. PGI_2 as a regulator of inflammatory diseases. Mediators Inflamm 2012;2012:926968.

27. Dror Y, Sorkin R, Brand G, Boubriak O, Urban J, Klein J. The effect of the serum corona on interactions between a single nano-object and a living cell. Sci Rep 2017;7:45758.

28. Mahmoudi M, Lynch I, Ejtehadi MR, Monopoli MP, Bombelli FB, Laurent S. Protein-nanoparticle interactions: opportunities and challenges. Chemical Rev 2011;111:5610–37.

29. Lehmann C, Konig JP, Dettmann J, Birnbaum J, Kox WJ. Effects of iloprost, a stable prostacyclin analog, on intestinal leukocyte adherence and microvascular blood flow in rat experimental endotoxemia. Crit Care Med 2001;29:1412–6.

KEY WORDS ischemia/reperfusion injury, nanoparticles, ONO-1301, prostacyclin

APPENDIX For supplemental figures, table, and an expanded Methods section, please see the online version of this paper.

JACC: BASIC TO TRANSLATIONAL SCIENCE VOL. 4, NO. 3, 2019

PRECLINICAL RESEARCH

Cathepsin A Mediates Ventricular Remote Remodeling and Atrial Cardiomyopathy in Rats With Ventricular Ischemia/Reperfusion

Mathias Hohl, PhD,[a] Katharina Erb,[a] Lisa Lang,[a] Sven Ruf, PhD,[b] Thomas Hübschle, PhD,[b] Stefan Dhein, MD,[c] Wolfgang Linz, PhD,[b] Adrian D. Elliott, PhD,[d] Prashanthan Sanders, MBBS, PhD,[d] Olesja Zamyatkin,[a] Michael Böhm, MD,[a] Ulrich Schotten, MD, PhD,[e] Thorsten Sadowski, PhD,[b] Dominik Linz, MD, PhD[a,d]

VISUAL ABSTRACT

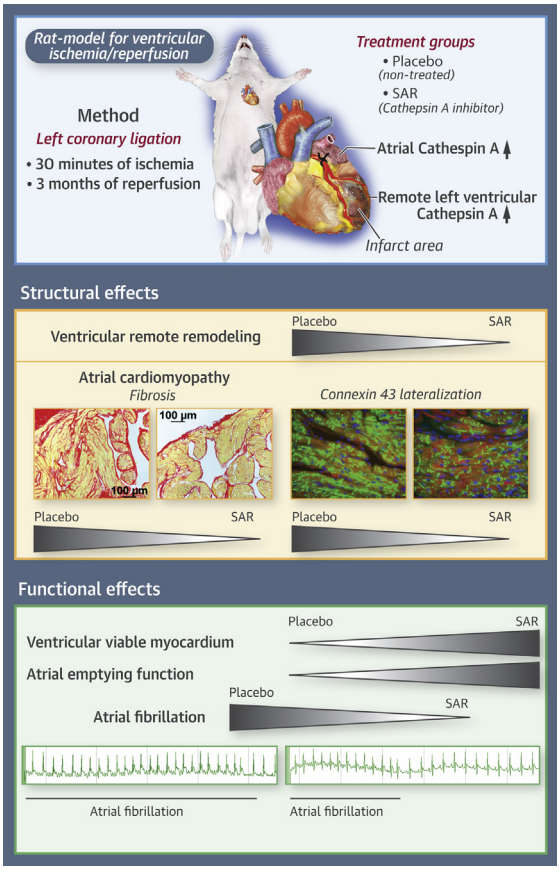

Hohl, M. et al. J Am Coll Cardiol Basic Trans Science. 2019;4(3):332–44.

HIGHLIGHTS

- **The role of the protease cathepsin A for the progression of left ventricular remote remodeling and atrial cardiomyopathy in ischemic cardiomyopathy is unknown.**
- **In rats with ventricular ischemia and reperfusion, cathepsin A is up-regulated in the left ventricular and atrial tissue remote from the infarcted area.**
- **Pharmacological inhibition of cathepsin A protease activity by SAR significantly reduces remote ventricular remodeling and atrial extracellular matrix remodeling, represented by fibrosis formation and connexin 43 lateralization.**
- **Prevention of ventricular remote remodeling and atrial cardiomyopathy by SAR increased ventricular viable myocardium and atrial emptying function reducing susceptibility to atrial fibrillation.**
- **Remote ventricular and atrial extracellular matrix remodeling may represent a promising target for pharmacological atrial fibrillation upstream therapy following myocardial infarction.**

ISSN 2452-302X https://doi.org/10.1016/j.jacbts.2019.01.008

SUMMARY

After myocardial infarction, remote ventricular remodeling and atrial cardiomyopathy progress despite successful revascularization. In a rat model of ventricular ischemia/reperfusion, pharmacological inhibition of the protease activity of cathepsin A initiated at the time point of reperfusion prevented extracellular matrix remodeling in the atrium and the ventricle remote from the infarcted area. This scenario was associated with preservation of more viable ventricular myocardium and the prevention of an arrhythmogenic and functional substrate for atrial fibrillation. Remote ventricular extracellular matrix remodeling and atrial cardiomyopathy may represent a promising target for pharmacological atrial fibrillation upstream therapy following myocardial infarction. (J Am Coll Cardiol Basic Trans Science 2019;4:332–44)

ABBREVIATIONS AND ACRONYMS

AF = atrial fibrillation

CatA = cathepsin A

Cx43 = connexin 43

ECM = extracellular matrix

ICM = ischemic cardiomyopathy

I/R = ischemia/reperfusion

LA = left atrial

LAD = left anterior descending coronary artery

LV = left ventricular

MRI = magnetic resonance imaging

mRNA = messenger ribonucleic acid

PL = permanent left anterior descending ligation

SAR = (S)-3-{[1-(2-Fluoro-phenyl)-5-methoxy-1H-pyrazole-3-carbonyl]-amino}-3-o-tolyl-propionic-acid

Long-term outcome after myocardial infarction is predicted by left ventricular (LV) dysfunction due to ischemic cardiomyopathy (ICM), which develops in ~40% of post-myocardial infarct patients (1). Current clinical practice is focused on maximizing myocardial salvage by coronary revascularization (2). However, LV remodeling due to structural and functional changes in the extracellular matrix (ECM) often progresses even following successful revascularization and is the most common reason for heart failure after myocardial infarction (3,4). Progressive ECM remodeling is characterized by scar formation and thinning of the infarcted ventricular wall as well as by maladaptive ECM alterations in the remote noninfarcted ventricular myocardium, which ultimately impairs LV function. The presence and amount of viable ventricular myocardium have been shown to determine the progression or potential regression of the ongoing LV remodeling process (5–9).

Importantly, ICM is not just associated with remote remodeling in the ventricle, but it may also contribute to the development of a progressive atrial cardiomyopathy (10) characterized by impaired atrial emptying function and increased risk of atrial fibrillation (AF) (11–13). It remains unclear whether atrial cardiomyopathy in ICM is solely a consequence of LV systolic dysfunction or whether it may represent the atrial manifestation of the cardiac structural remodeling process remote from the ventricular infarct region, which correlates clinically with the presence and amount of viable remote LV myocardium (5–8).

Cardiac ECM remodeling is characterized by changes in collagen composition, which contributes to interstitial fibrosis formation and impaired electrical and functional properties of the myocardium (14–16). The balance between ECM synthesis and degradation is of crucial relevance in maintaining cardiac structural integrity and is regulated by proteolysis as a key mechanism to control ECM function and turnover (16,17). A set of proteolytic enzymes, including cathepsins, degrade ECM components and target a broad range of intracellular and extracellular proteins. Cysteine proteases such as cathepsin B, K, L, and S

From the [a]Klinik für Innere Medizin III, Universität des Saarlandes, Homburg/Saar, Germany; [b]Sanofi-Aventis Deutschland GmbH, Frankfurt, Germany; [c]Herzzentrum Leipzig Abt. Herzchirurgie, Leipzig, Germany; [d]Centre for Heart Rhythm Disorders, South Australian Health and Medical Research Institute, Royal Adelaide Hospital, University of Adelaide, Adelaide, Australia; and the [e]Department of Physiology, University of Maastricht, Maastricht, the Netherlands. This research was supported by the German Research Foundation (DFG SFB/TRR219-M02/-S02). Ms. Lang received a scholarship by the "Stiftung Begabtenförderung berufliche Bildung (SBB) GmbH im Auftrag und mit Mitteln des Bundesministeriums für Bildung und Forschung." Drs. Sadowski, Hübschle, and Ruf are employees of Sanofi-Aventis Deutschland GmbH. Dr. Sanders is an advisory board member for Biosense-Webster, Medtronic, St. Jude Medical, Boston Scientific, and CathRx; has received lecture and/or consulting fees from Biosense-Webster, Medtronic, St. Jude Medical, and Boston Scientific; and is supported by a Practitioner Fellowship from the National Health and Medical Research Council of Australia and by the National Heart Foundation of Australia. Dr. Böhm has received funding from Amgen, Bayer, Servier, Medtronic, Boehringer Ingelheim, Vifor, and Bristol-Myers Squibb. Dr. Schotten has received funding from EP and YourRhythmics BV. All other authors have reported that they have no relationships relevant to the contents of this paper to disclose.

All authors attest they are in compliance with human studies committees and animal welfare regulations of the authors' institutions and U.S. Food and Drug Administration guidelines, including patient consent where appropriate. For more information, visit the *JACC: Basic to Translational Science* author instructions page.

Manuscript received September 10, 2018; revised manuscript received January 8, 2019, accepted January 11, 2019.

have been shown to play a pathophysiological role in myocardial infarction, congestive heart failure, and diabetes (17). The serine protease cathepsin A (CatA) is a multifunctional protein (18-20). Inside the lysosome, CatA exerts its catalytic function as a carboxypeptidase and protects beta-galactosidase and neuraminidase-1 from intralysosomal proteolysis by the formation of a lysosomal multienzyme complex (19). In addition, CatA is localized on the cell surface and is secreted into the extracellular space, where its proteolytic function has been suggested to be involved in ECM formation as well as degradation of different extracellular regulatory peptides (18-20). Recently, we showed that pharmacological inhibition of CatA activity prevented atrial fibrosis formation and reduces susceptibility to AF without significant effects on LV systolic function in an animal model of type 2 diabetes, suggesting a crucial role for CatA in ECM remodeling (21).

SEE PAGE 345

The cardiac regulation of CatA in ICM, its effect on viable LV myocardium after revascularization, and its role in the progression of ventricular and atrial cardiomyopathy as manifestations of remote remodeling remain unknown. Using a rat model for ICM induced by ventricular ischemia/reperfusion (I/R), we investigated the regulation of LV and left atrial (LA) CatA expression and the effect of pharmacological CatA inhibition on the induction of ICM and cardiac remodeling within and remote from the infarct area, including atrial cardiomyopathy. We compared the effect of pharmacological inhibition of CatA activity versus the effect of the angiotensin-converting enzyme inhibitor ramipril as an established drug for prevention of cardiac remodeling.

METHODS

For a more detailed description of all methods used see the Supplemental Methods.

HUMAN TISSUE. Human failing myocardium was obtained from patients with end-stage ICM who were scheduled for heart transplantation (n = 8). Eight donor hearts of patients with no signs of heart disease that could not be used for transplantation due to ABO-mismatch were used as nonfailing controls (n = 8). Information about clinical parameters and medication were not available. This investigation was reviewed by the regional ethics committee and conforms to the principles outlined in the Declaration of Helsinki.

ANIMAL MODELS. All animal studies were performed in accordance with the German law for the protection of animals. The investigation conforms to the guide for the Care and Use of Laboratory Animals published by the U.S. National Institutes of Health (eighth edition; revised 2011). All procedures were in accordance with current Sanofi-Aventis Laboratory Animal Science and Welfare guidelines. The study was approved by the regional animal ethics commission in Darmstadt, Germany. Ninety male Wistar rats (12 weeks old) were purchased from Harlan Winkelmann GmbH (Borchen, Germany), housed 3 per cage under standardized conditions (room temperature 24°C, relative humidity 55%, 12 h dark/light cycle) with free access to a standardized diet (#1320, Altromin, Lage, Germany) and tap drinking water.

PERMANENT LIGATION OF LEFT ANTERIOR DESCENDING CORONARY ARTERY IN RATS. Thirty male Wistar rats were anesthetized with 5% isoflurane in 95% oxygen followed by a deep anesthesia via intraperitoneal injection of ketamine hydrochloride (80 mg/kg body weight) and xylazine hydrochloride (6 mg/kg body weight). In 20 rats, the left anterior descending (LAD) coronary artery was permanently ligated; 10 sham-operated rats served as controls. Post-operative pain management was performed by using carprofen (5 mg/kg subcutaneously). After 8 weeks, rats were anesthetized (as discussed earlier), and the hearts were quickly removed. Additional details are provided in the Supplemental Methods.

Ventricular I/R was performed as previously described (22,23). Briefly, 60 male Wistar rats were anesthetized with 5% isoflurane in 95% oxygen followed by a deep anesthesia via intraperitoneal injection of ketamine hydrochloride (80 mg/kg body weight) and xylazine hydrochloride (6 mg/kg body weight). In 51 rats, myocardial ischemia was induced by temporary occlusion of the left coronary artery for 30 min followed by reperfusion upon release of the ligation. Nine rats underwent sham operation. Eight I/R-rats died during the 24-h post-operative period. The day after surgery, animals were randomized into 4 groups: sham-operated rats (I/R-Sham, n = 9), I/R-rats given placebo (I/R-Placebo, n = 15), ramipril-treated I/R-rats (I/R-Ramipril, n = 14), and CatA inhibitor [(S)-3-{[1-(2-Fluoro-phenyl)-5-methoxy-1H-pyrazole-3-carbonyl]-amino}-3-o-tolyl-propionic-acid (SAR)]-treated I/R-rats (I/R-SAR, n = 14). SAR, a new orally active CatA inhibitor, was administered daily via oral gavage (30 mg/kg per day) (22), and ramipril (1 mg/kg per day) (23) was administered in chow in accordance with the literature.

After 9 weeks of treatment, rats were anesthetized for magnetic resonance imaging (MRI) of the heart

with 1.5% to 2.5% isoflurane in an oxygen/nitrous oxide mixture (30%/70%) to determine LA emptying function at rest and global and regional LV function under basal and dobutamine stress conditions as previously described (21).

After 10 weeks of treatment, electrophysiological measurements were performed during general anesthesia by intraperitoneal injection of pentobarbital (100 mg/kg). Atrial electrophysiological measurements were performed in open-chest experiments to assess local conduction disturbances and susceptibility to AF by direct contact epicardial mapping (21). One I/R-Sham, four I/R-Placebo, and one I/R-SAR rat died during the open-chest experiments. Hearts were removed and quickly preserved for biochemical and histological analyses.

Additional details are provided in the Supplemental Methods.

BIOCHEMICAL AND HISTOLOGICAL ANALYSES. To visualize LA tissue fibrosis, cardiomyocyte diameter, and connexin 43 (Cx43), tissue preparation was performed as previously described (21), and 5-μm sections were either stained with Picro-Sirius Red (#13422.00500, Morphisto, Frankfurt am Main, Germany), hematoxylin and eosin (#2C-163, Waldeck, Münster, Germany), or anti-Cx43 (#MAB3068, Merck Millipore, Darmstadt, Germany). NIS-Elements BR 3.2 software (Nikon Instruments, Melville, New York) was used for the analysis. Gene expression analysis from human left ventricle, rat left ventricle, and rat LA tissue was performed by using TaqMan polymerase chain reaction. Western blot technique was used to determine protein expression. Additional details are provided in the Supplemental Methods.

STATISTICAL ANALYSIS. All data are expressed as mean ± SEM. An unpaired Student's *t*-test (2-tailed) was used for statistical analysis comparing 2 groups. For assessment of statistical significance between 4 groups, one-way analysis of variance followed by Tukey's multiple comparison test was applied. Statistical analysis was conducted by using Prism version 6.01 software (GraphPad Software, La Jolla, California). The p values that reached a value <0.0001 were reported as $p < 0.0001$. Additional details are provided in the Supplemental Methods.

RESULTS

EXPRESSION PATTERN OF CatA IN HUMAN ICM, IN RATS WITH PERMANENT LAD LIGATION, AND IN RATS WITH VENTRICULAR I/R. Human ICM. In LV samples of patients with heart failure and end-stage ICM, CatA gene and protein expression was enhanced compared with healthy nonfailing LV tissue ($p = 0.0271$ for messenger ribonucleic acid [mRNA] and $p = 0.0333$ for protein level) (**Figures 1A and 1B**). LV CatA up-regulation in ICM was associated with increased gene transcription of the heart failure marker atrial natriuretic peptide ($p = 0.0296$).

Rats with permanent LAD ligation. In a rat model with permanent LAD ligation (PL-rats), CatA protein abundance was significantly increased within the infarct area at 2 weeks (1.9-fold increase compared with sham control; $p = 0.0009$) and dropped back to control levels at 8 weeks. In contrast, CatA mRNA levels in the remote ventricular myocardium and in the LA myocardium were unchanged after 2 weeks but showed a significant increase at 8 weeks after PL (1.5-fold increase in left ventricle; $p = 0.0342$) and 1.8-fold increase in left atrium (compared with sham control; $p = 0.0086$), indicating a differential temporal and spatial pattern of CatA expression during PL (Supplemental Figure S1).

Rats with ventricular I/R. Given the late increase in CatA expression in the remote LV and LA myocardium at 8 weeks in PL-rats, we investigated the regulation of CatA expression in LV and LA myocardium in rats with 30 min of LAD ligation followed by 10 weeks of reperfusion (I/R); this animal model mimics the clinical situation of early revascularization after myocardial infarction and is suitable for investigating cardiac remote remodeling during ICM. In I/R-Placebo rats, mRNA levels of CatA were significantly increased in the remote left ventricle (1.7-fold; $p = 0.0072$) (**Figure 1C**) and left atrium (2.9-fold; $p = 0.0042$) (**Figure 1D**) compared with I/R-Sham rats; this finding was associated with increased gene transcription of atrial natriuretic peptide (vs. I/R-Sham, $p = 0.0008$).

LV STRUCTURE AND FUNCTION IN RATS WITH VENTRICULAR I/R. I/R-Placebo rats exhibited an increased heart-weight-to-body-weight ratio compared with I/R-Sham rats (0.29 ± 0.02 g/100 mg body weight vs. 0.24 ± 0.01 g/100 mg body weight; $p = 0.0360$). Treatment of I/R-rats with the CatA inhibitor SAR or ramipril did not significantly reduce the heart-weight-to-body-weight ratio (I/R-SAR 0.26 ± 0.01 g/100 mg body weight vs. I/R-Ramipril 0.27 ± 0.01 g/100 mg body weight) but reduced plasma brain natriuretic peptide levels (I/R-SAR 81 ± 4 pg/ml vs. I/R-Placebo 172 ± 31 pg/ml [$p = 0.0030$]; I/R-Ramipril 105 ± 9 pg/ml vs. I/R-Placebo, $p = 0.0455$).

Infarct size, determined at the midventricular level, was comparable between I/R-Placebo rats (15.1 ± 1.6% fibrotic wall surface/total wall surface), I/R-SAR (14.4 ± 1.9% fibrotic wall surface/total wall surface), and I/R-Ramipril (15.6 ± 1.5% fibrotic wall surface/total wall surface) rats (Supplemental Figure S2).

FIGURE 1 Differential Expression Pattern of CatA in Human ICM and in Rats With Permanent Ligation and in Rats With Ventricular I/R

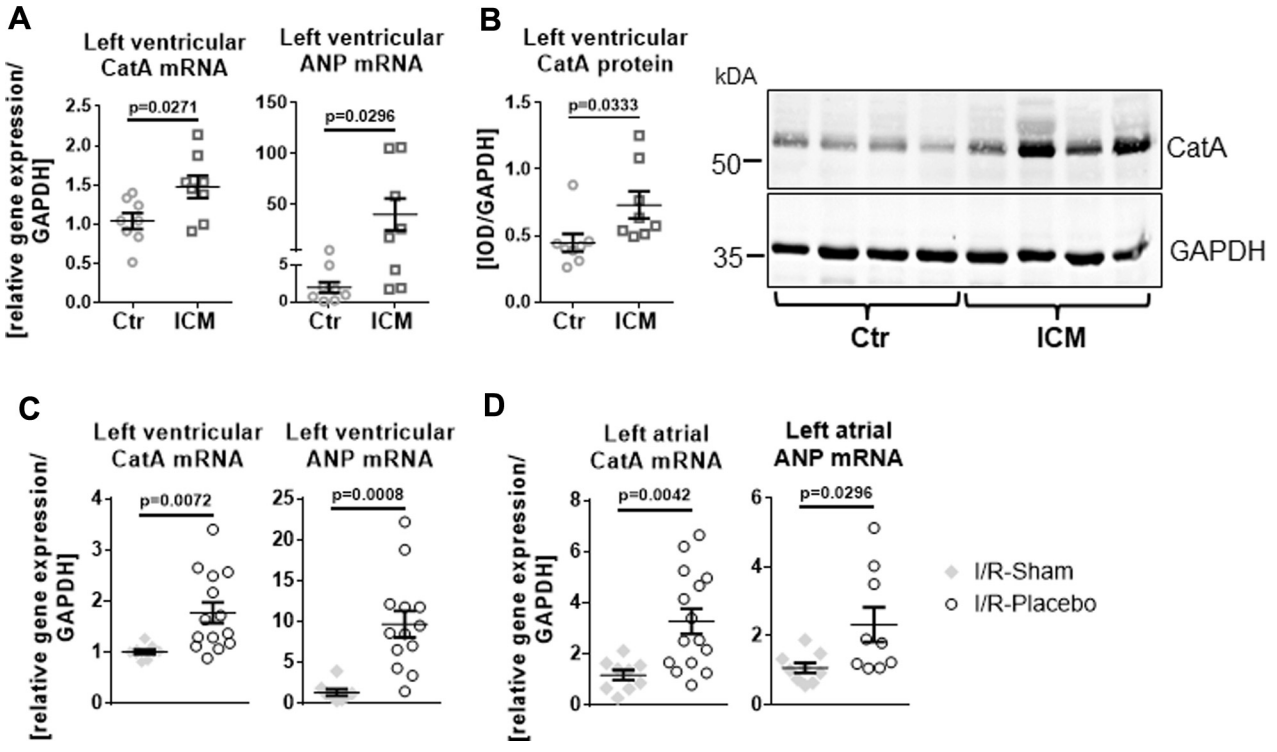

(A and B) Human ischemic cardiomyopathy (ICM). **(A)** Messenger ribonucleic acid (mRNA) expression of cathepsin A (CatA) and atrial natriuretic peptide (ANP) in left ventricular tissue from healthy nonfailing donor hearts (Ctr, n = 8) and from patients with end-stage ICM (n = 8). **(B)** Representative Western blot and quantification of CatA protein levels in the left ventricle of Ctr and ICM patients (n = 8 per group). **(C and D)** Rats with 30 min of ventricular ischemia followed by 10 weeks of reperfusion (ischemia/reperfusion [I/R]). **(C)** CatA and ANP mRNA content in the left ventricle (I/R-Sham, n = 9-8; I/R-Placebo, n = 14-13). **(D)** Left atrial tissue 10 weeks after I/R in sham-operated rats (I/R-Sham, n = 9) and rats receiving placebo (I/R-Placebo; n = 15-9). Values are mean ± SEM. GAPDH = glyceraldehyde 3-phosphate dehydrogenase; IOD = integrated optical density.

Global LV function. I/R-Placebo rats developed a significant impairment in LV function, indicated by a reduced ejection fraction and increased end-diastolic and end-systolic volume at rest. EF reduction was prevented by SAR but not by ramipril (Table 1). LV systolic function and cardiac output in I/R-Placebo rats did not improve during dobutamine perfusion. During dobutamine stress testing, I/R-SAR, but not I/R-Ramipril, rats exhibited higher ejection fraction and cardiac output. However, ramipril, but not SAR, significantly reduced LV end-systolic and end-diastolic mass compared with findings in I/R-Placebo rats at rest and during dobutamine stress testing.

Regional LV function. In I/R-Placebo rats, MRI analysis of slices selected from the midventricular level of each heart revealed impaired wall motion and nearly akinesia in the infarcted area, which did not improve significantly during dobutamine stress testing, indicative of dysfunctional nonviable myocardium (Figures 2A and 2B, lateral and anterior, infarct area). Wall motion of the noninfarcted remote area was reduced at rest but still responsive to dobutamine (Figures 2A and 2B, septal and posterior, remote area), indicating dysfunctional but viable residual remote ventricular myocardium. Ramipril preserved better wall motion in the lateral infarcted area under basal conditions, but both ramipril and SAR improved dobutamine response in this area (I/R-Ramipril rats vs. I/R-Placebo rats; p = 0.0331; I/R-SAR rats vs. I/R-Placebo rats; p = 0.0289) (Figure 2B, under dobutamine). However, SAR, but not ramipril, was able to preserve better wall motion in the noninfarcted remote area at rest, which significantly further improved during dobutamine stress testing, suggesting more viable remote myocardium (under dobutamine: I/R-SAR vs. Ramipril; p = 0.0380; I/R-SAR vs. placebo; p = 0.0203).

TABLE 1 Global Left Ventricular Function Determined by Using Magnetic Resonance Imaging in Rats

	Left Ventricle at Rest				Left Ventricle Under Dobutamine Stress			
	I/R-Sham (n = 9)	I/R-Placebo (n = 15)	I/R-Ramipril (n = 14)	I/R-SAR (n = 14)	I/R-Sham (n = 9)	I/R-Placebo (n = 15)	I/R-Ramipril (n = 14)	I/R-SAR (n = 14)
EF, %	59.4 ± 1.6	39.2 ± 2.1*	43.5 ± 3.2†	49.1 ± 3.0‡	73.8 ± 2.6	43.6 ± 3.1*	51.8 ± 4.8†	58.5 ± 4.0‡
CO, ml/min	126.6 ± 5.2	121.0 ± 3.4	111.2 ± 4.6§	129.8 ± 3.5	159.5 ± 7.2	133.6 ± 6.3‖	132.2 ± 6.6‖¶	158.3 ± 3.6‡
SV, μl	327.7 ± 17.9	325.3 ± 8.6	296.7 ± 10.3	333.5 ± 7.9	372.2 ± 18.0	330.2 ± 12.4	312.8 ± 13.1‖¶	370.0 ± 10.0
EDV, ml	0.55 ± 0.03	0.86 ± 0.05†	0.73 ± 0.06	0.70 ± 0.03	0.50 ± 0.02	0.80 ± 0.05†	0.67 ± 0.06	0.66 ± 0.04
ESV, ml	0.22 ± 0.01	0.53 ± 0.05#	0.43 ± 0.06‖	0.37 ± 0.04	0.13 ± 0.01	0.47 ± 0.05†	0.36 ± 0.07	0.29 ± 0.04
LVED mass, mg	487.1 ± 13.9	534.3 ± 17.7	451.1 ± 16.2**	503.6 ± 13.4	499.2 ± 8.8	528.3 ± 21.0	432.8 ± 17.5††¶	506.1 ± 13.9
LVES mass, mg	612.9 ± 14.7	646.9 ± 21.5	534.4 ± 20.4‖††§	622.3 ± 14.7	639.9 ± 12.7	642.2 ± 23.9	534.1 ± 25.4‖††§	646.5 ± 19.1
Heart rate, beats/min	389 ± 8	373 ± 7	375 ± 9	389 ± 3	427 ± 7	402 ± 8	421 ± 7	429 ± 5

Values are mean ± SEM. One-way analysis of variance followed by Tukey's multiple comparisons test was used. *p > 0.0001 vs. ischemia/reperfusion (I/R)-Sham. †p < 0.01 vs. I/R-Sham. ‡p < 0.05 vs. I/R-Placebo. §p < 0.01 vs. I/R-(S)-3-{[1-(2-Fluoro-phenyl)-5-methoxy-1H-pyrazole-3-carbonyl]-amino}-3-o-tolyl-propionic-acid (SAR). ‖p < 0.05 vs. I/R-Sham. ¶p < 0.05 vs. I/R-SAR. #p < 0.001 vs. I/R-Sham. **p < 0.01 vs. I/R-Placebo. ††p < 0.001 vs. I/R-Placebo.

CO = cardiac output; EDV = end-diastolic volume; EF = ejection fraction; ESV = end-systolic volume; LVED = left ventricular end-diastolic; LVES = left ventricular end-systolic; SV = stroke volume.

I/R-Placebo rats displayed a dramatic thinning of the infarcted myocardial wall (anterolateral) in the infarct area and a moderate thinning in the non-infarcted myocardial wall (posteroseptal) in the remote area, determined by MRI-derived systolic wall thickness at rest and during dobutamine stress testing (Figures 2C and 2D). Thinning of the infarcted myocardial wall was partially prevented by ramipril

FIGURE 2 Regional Left Ventricular Function

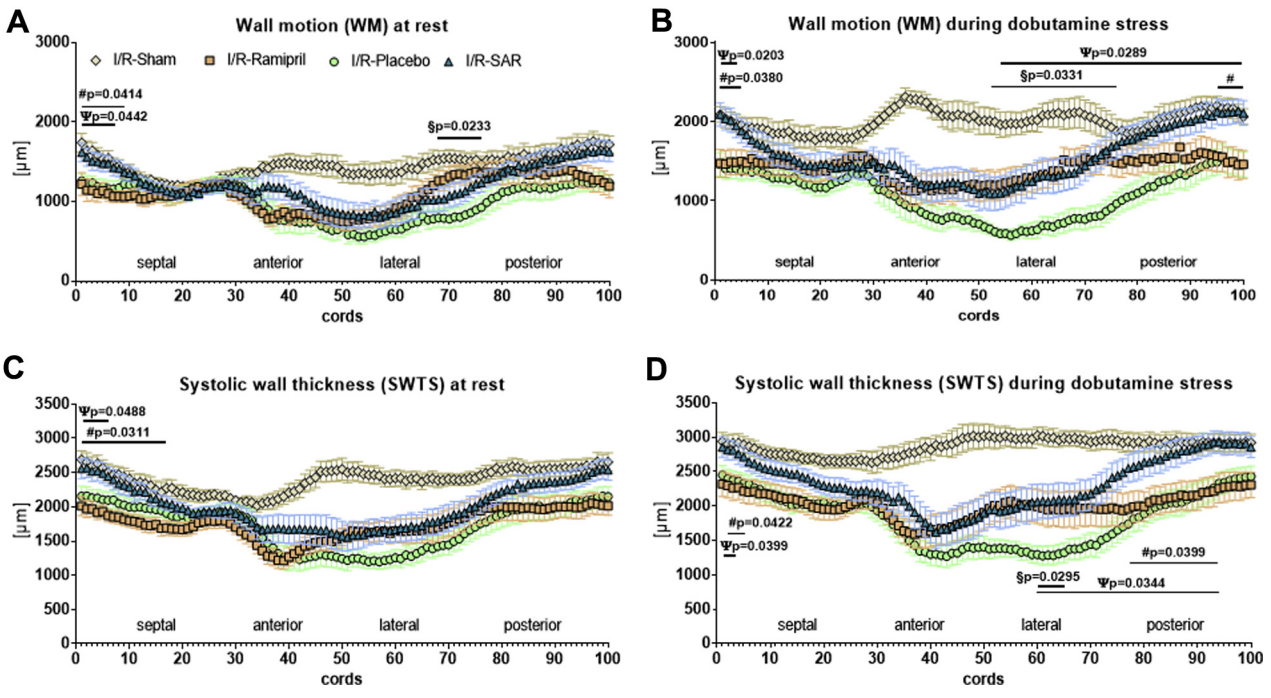

Using magnetic resonance imaging, 16 short-axis cine imaging slices of ischemia/reperfusion (I/R)-Sham (n = 9), I/R-rats given placebo (n = 15), and I/R-rats treated with ramipril (n = 14) or (S)-3-{[1-(2-Fluoro-phenyl)-5-methoxy-1H-pyrazole-3-carbonyl]-amino}-3-o-tolyl-propionic-acid (SAR; n = 14) were performed; slices were divided into 97 cords. **(A)** Every cord was analyzed for left ventricular wall motion (WM) at rest and **(B)** during dobutamine stress testing. Analysis of left ventricular systolic wall thickness (SWTS) for every cord **(C)** at rest and **(D)** during dobutamine stress testing. Values are mean ± SEM. #I/R-SAR vs. I/R-Ramipril. ψI/R-SAR vs. I/R-Placebo. §I/R-Ramipril vs. I/R-Placebo.

TABLE 2 Atrial Emptying Function Determined by Using Magnetic Resonance Imaging in Rats

	I/R-Sham (n = 9)	I/R-Placebo (n = 15)	I/R-Ramipril (n = 14)	I/R-SAR (n = 14)
LA diameter, cm	0.47 ± 0.01*	0.57 ± 0.02	0.52 ± 0.02*	0.54 ± 0.01
LA volume, maximum, ml	0.34 ± 0.04	0.48 ± 0.04	0.42 ± 0.03	0.41 ± 0.03
LA fractional shortening, %	20 ± 2†	16 ± 1	18 ± 2	22 ± 1†
Total percent emptying	50 ± 2†	37 ± 3	46 ± 3†	47 ± 2†
Active percent emptying	37 ± 4†	26 ± 3	33 ± 3†	34 ± 2†
Passive percent emptying	35 ± 6	24 ± 3	27 ± 1	28 ± 3

Values are mean ± SEM. *p < 0.05. †p < 0.01 vs. I/R-Placebo.
LA = left atrial; other abbreviations as in Table 1.

and SAR, whereas treatment with SAR proved to be more effective in preventing thinning of the non-infarcted myocardial wall in the remote area compared with ramipril.

Histological Picro-Sirius Red staining of the left ventricle confirmed thinning of the infarcted wall in I/R-Placebo rats (I/R-Sham 2.28 ± 0.11 mm vs. I/R-Placebo 1.78 ± 0.17 mm; p = 0.1348) (Supplemental Figures S3A and S3B). LV wall thinning was significantly attenuated in hearts from I/R-SAR rats (2.33 ± 0.13 mm) compared with I/R-Placebo rats (p = 0.0407) and considerably improved by ramipril (2.15 ± 0.15 mm vs. I/R-Placebo; p = 0.2604). LV septal wall thickness was unchanged in all groups (Supplemental Figure S3C). LV fibrosis formation was significantly increased upon I/R in rats receiving placebo (I/R-Sham 2.59 ± 0.46% vs. I/R-Placebo 23.62 ± 2.83%; p < 0.0001) and was not prevented by treatment with either ramipril (I/R-Ramipril 16.41 ± 3.34% vs. I/R-Sham; p = 0.0092; I/R-Ramipril vs. I/R-Placebo; p = 0.2195) or SAR (I/R-SAR 18.19 ± 2.29% vs. I/R-Sham; p = 0.0027; vs. I/R-Placebo; p = 0.4613) (Supplemental Figure S3D).

ATRIAL EMPTYING FUNCTION. In I/R-Placebo rats, LA diameter was significantly increased and LA fractional shortening was reduced compared with I/R-Sham rats (Table 2). LA emptying function as assessed by total percent emptying and active percent emptying was diminished in I/R-Placebo rats. Pharmacological inhibition of CatA activity by SAR did not affect LA dimensions in I/R-rats, and LA fractional shortening was significantly higher compared with I/R-Placebo rats. SAR preserved the LA emptying function in I/R-rats. Ramipril treatment reduced LA diameter in I/R-rats, but similar dimensions in I/R-Sham rats were not achieved. In I/R-Ramipril rats, LA fractional shortening and total percent emptying were only mildly depressed compared with I/R-Sham rats.

ATRIAL ELECTROPHYSIOLOGY. AF could be induced in 6 of 8 sham-operated rats and in all I/R-Placebo (11 of 11) rats by atrial burst stimulation (Figure 3A). Inducible AF duration was markedly increased in I/R-Placebo rats compared with I/R-Sham rats (I/R-Placebo 45.9 ± 19.1 s vs. I/R-Sham 1.4 ± 0.4 s; p = 0.0196). The percentage of areas of slow conduction during rapid pacing was significantly increased in I/R-Placebo rats compared with I/R-Sham rats (p < 0.0001) (Figure 3B). Total atrial activation time was significantly longer in I/R-Placebo rats compared with I/R-Sham rats (I/R-Placebo 15.2 ± 0.5 ms vs. I/R-Sham 11.5 ± 0.5 ms; p = 0.0006) (Figure 3C). The atrial effective refractory period did not differ between the groups (Figure 3D). In I/R-rats, SAR and ramipril reduced AF inducibility (I/R-SAR: 10 of 13; I/R-Ramipril: 11 of 14) and inducible AF duration (I/R-SAR: 3.7 ± 1.6 s; p = 0.0108; I/R-Ramipril: 3.8 ± 1.8 s; p = 0.0092) compared with I/R-Placebo rats. SAR and ramipril attenuated changes in total atrial activation time (I/R-SAR 12.9 ± 0.34 ms; p = 0.0302 vs. I/R-Placebo; I/R-Ramipril 11.9 ± 0.6 ms; p = 0.0012 vs. I/R-Placebo). Both ramipril and SAR in particular significantly reduced the percentage of areas of slow conduction.

FIGURE 3 Atrial Electrophysiological Measurements in I/R-Rats

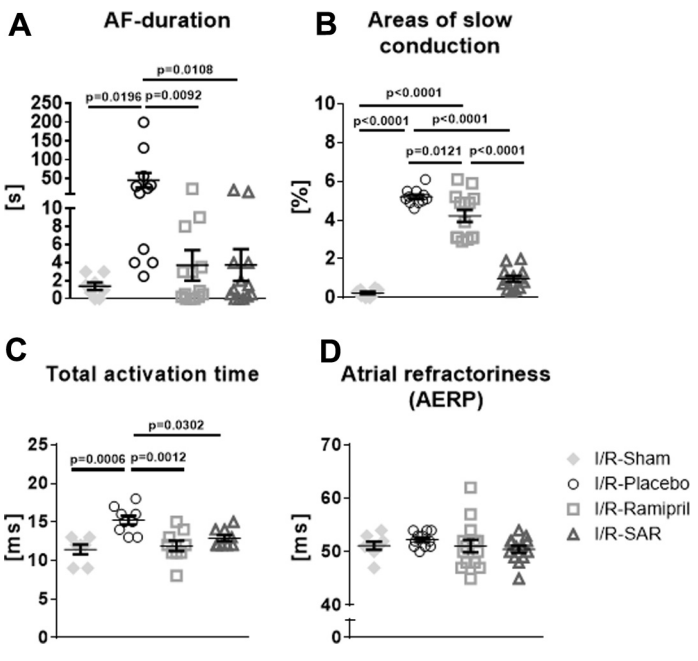

(A) Atrial fibrillation (AF) inducibility and duration induced by burst-stimulation in I/R-Sham (n = 8), I/R-rats given placebo (n = 11), and I/R-rats treated with ramipril (n = 14) or SAR (n = 13). **(B)** Areas of slow conduction. **(C)** Total atrial activation time (I/R-Sham, n = 7; I/R-Placebo, n = 9; I/R-Ramipril, n = 9; I/R-SAR, n = 9). **(D)** Left atrial effective refractory period (AERP) at a stimulation frequency of 400/min (basic cycle lengths: 150 ms). Values are mean ± SEM. Abbreviations as in Figures 1 and 2.

FIGURE 4 **Atrial Extracellular Matrix Remodeling**

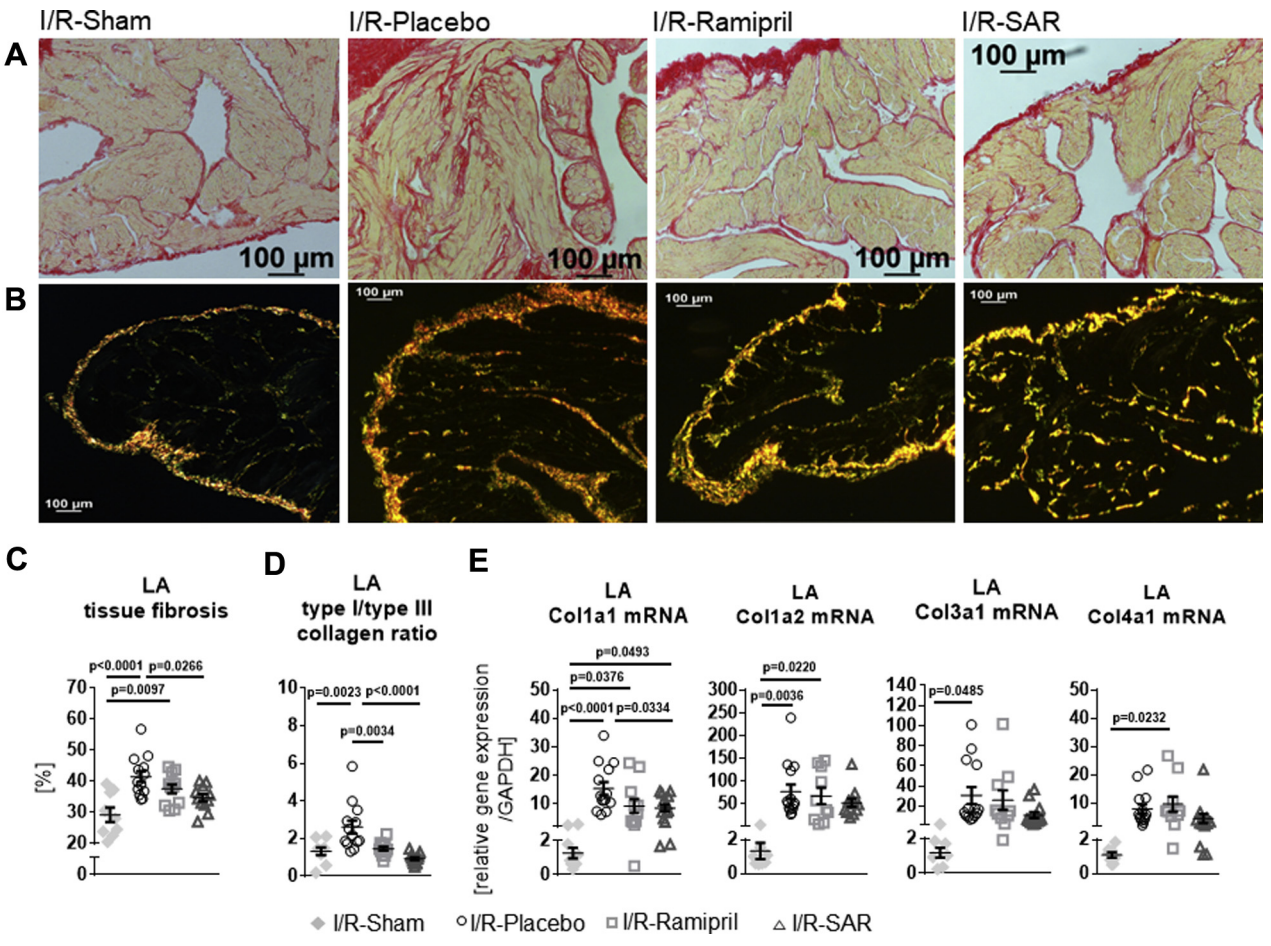

Representative histological images of **(A)** conventional total collagen (**red** fibers) and **(B)** polarized light microscopy (collagen type I [**red-yellow** fibers] and collagen type III [**green** fibers]) of Picro-Sirius Red–stained left atrial preparations in I/R-Sham (n = 9), I/R-rats given placebo (n = 13), and I/R-rats treated with ramipril (n = 12) or SAR (n = 11). **(C)** Quantification of left atrial (LA) fibrosis amount. **(D)** Collagen type I/type III ratio and **(E)** mRNA expression of collagen 1a (Col1a1), Col1a2, Col3a1, and Col4a1 normalized to expression of GAPDH in I/R-Sham (n = 9-7), I/R-Placebo (n = 14), I/R-Ramipril (n = 11-10), and I/R-SAR (n = 14-12). Values are mean ± SEM. Abbreviations as in Figures 1 and 2.

LA-ECM REMODELING. LA fibrosis. In Picro-Sirius Red–stained LA sections, the degree of atrial total collagen content was highly increased in I/R-Placebo rats compared with I/R-Sham rats (Figures 4A to 4D). Increased fibrosis formation in I/R-Placebo rats was associated with significantly enhanced mRNA expression of collagens 1a1, 1a2, and 3a1 and a distinct increase in collagen 4a1. Inhibition of CatA by SAR treatment significantly prevented accumulation of tissue fibrosis and significantly dampened collagen 1a1 mRNA expression (vs. I/R-Placebo; p = 0.0334). In contrast, ramipril did not significantly affect fibrosis formation or collagen mRNA levels (Figures 4C and 4E). Polarized light microscopy of Picro-Sirius Red–stained LA sections (Figure 4B) revealed an increase in the ratio of collagen type I (red-yellow fibers) to collagen type III (green fibers) in I/R-Placebo rats (vs. I/R-Sham; p = 0.0023). The collagen type I/type III ratio was normalized by both ramipril (vs. I/R-Placebo; p = 0.0034) and even more pronounced by SAR (vs. I/R-Placebo; p < 0.0001) (Figure 4D).

LA hypertrophy. LA weight-to-body-weight ratio and LA myocyte diameter are shown in Figures 5A to 5C. The LA weight-to-body-weight-ratio was significantly enhanced in I/R-rats given placebo (Figure 5B). Although ramipril had only a slight effect, SAR significantly lowered the LA weight-to-body-weight-ratio to the I/R-Sham level. Myocyte diameters were unchanged with placebo, SAR, and ramipril (Figure 5C). The LA mRNA level of hypertrophy

FIGURE 5 Atrial Hypertrophy

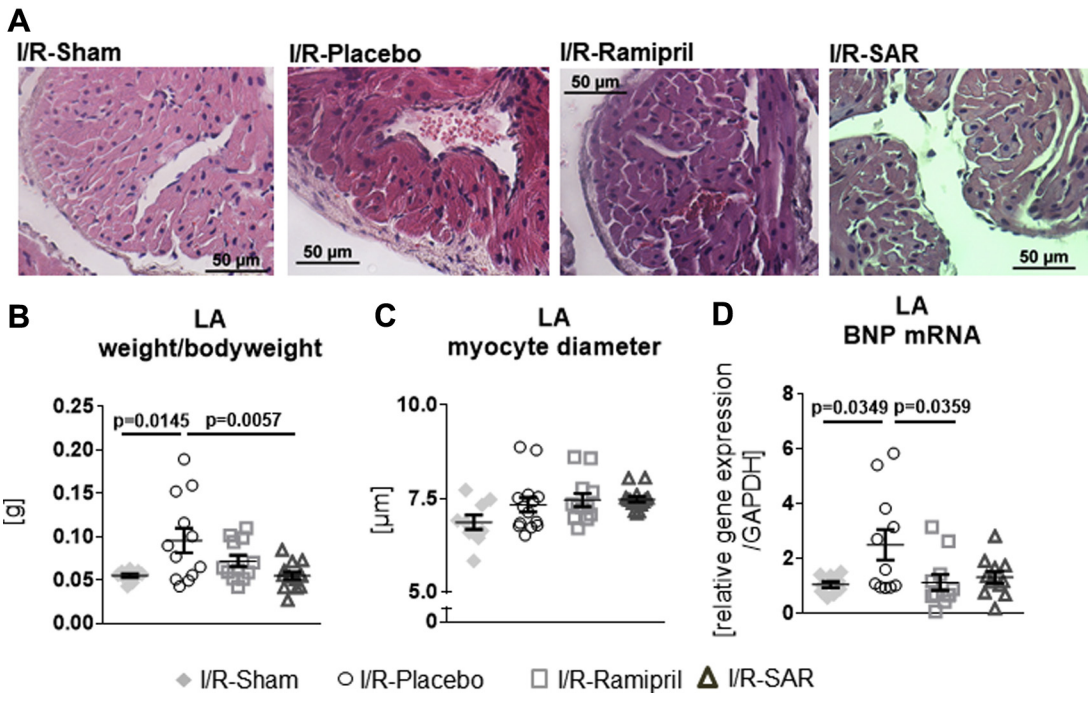

Representative histological images of **(A)** hematoxylin and eosin–stained LA tissue preparations in I/R-Sham rats, I/R-rats given placebo, and I/R-rats treated with ramipril or SAR. **(B)** Ratio of LA weight per 100 g body weight of I/R-Sham (n = 9), I/R-Placebo (n = 12), I/R-Ramipril (n = 12), and I/R-SAR (n = 13) rats. **(C)** Quantification of LA myocyte diameter and **(D)** brain natriuretic peptide (BNP) mRNA level in the left atrium in I/R-Sham (n = 9), I/R-rats given placebo (n = 11-12) and I/R-rats treated with ramipril (n = 11-12) or SAR (n = 11-14). Values are mean ± SEM. Abbreviations as in Figures 1, 2, and 4.

marker brain natriuretic peptide was significantly increased in I/R-Placebo rats (Figure 5D) and significantly lowered only by ramipril but not by SAR. In I/R-rats, neither treatment with SAR nor ramipril blunted the increased LA CatA gene expression (I/R-SAR 2.25 ± 0.43 relative gene expression/glyceraldehyde 3-phosphate dehydrogenase vs. I/R-Sham; p = 0.0427; I/R-Ramipril 4.33 ± 1.58 relative gene expression/glyceraldehyde 3-phosphate dehydrogenase vs. I/R-Sham; p = 0.0438).

LA spatial distribution of Cx43. In I/R-Sham rats, we found the typical intracellular distribution of Cx43, with a clear accentuation of Cx43 at the cell poles, and only sparse localization of Cx43 at the lateral sides of the cells (Figure 6). In I/R-Placebo rats, there was a significantly enhanced lateral and polar Cx43 immunostaining. Lateralization of Cx43 was significantly prevented by SAR (vs. I/R-Placebo; p = 0.0004), whereas polar Cx43 expression remained enhanced compared with control (vs. I/R-Sham; p = 0.0039). Ramipril did not significantly prevent Cx43 lateralization (vs. I/R-Sham; p = 0.0018), and polar Cx43 localization remained unchanged compared with I/R-Sham rats (p = 0.0697).

DISCUSSION

CatA expression is significantly increased in human failing ICM ventricular myocardium and in ventricular and atrial myocardium from rats with experimental ICM induced by permanent LAD ligation or ventricular I/R in rats. Herein, increased ventricular and atrial expression of CatA was accompanied by LV global systolic dysfunction and the development of remote atrial cardiomyopathy characterized by atrial ECM remodeling, impaired LA emptying function, conduction disturbances, and longer inducible AF duration. Pharmacological inhibition of CatA initiated at the time point of ventricular reperfusion did not significantly improve LV global systolic function at rest but preserved more viable LV myocardium and prevented the progression of atrial cardiomyopathy.

VENTRICULAR REMOTE REMODELING AND ATRIAL ARRHYTHMOGENIC SUBSTRATE IN I/R-RATS. Ventricular and atrial remodeling in rats with permanent LAD ligation has been previously described (12,13). To the best of our knowledge, the present analysis is the first detailed characterization of the development of ICM-induced ECM remodeling and arrhythmogenic and functional atrial cardiomyopathy in a heart failure rat model with ventricular I/R (22,23). Thirty minutes of myocardial ischemia induced by LAD ligation followed by 10 weeks of reperfusion led to global LV systolic dysfunction and impaired LV wall motion, with dysfunctional and nonviable myocardium in the infarct area and dysfunctional but partially viable myocardium in the LV remote noninfarcted myocardium. LV and LA CatA expression remote from the infarct area was increased at 10 weeks. This scenario was associated with the development of an atrial cardiomyopathy characterized by impaired atrial emptying function and increased AF susceptibility. The documented structural atrial changes, together with the disorganization of Cx43, resulted in the disruption of side-to-side electrical connections between muscle bundles, thereby contributing to the conduction abnormalities and increased susceptibility to AF observed in I/R-rats (24,25). Epicardial mapping of these structurally remodeled atria revealed longer total atrial activation times, larger areas of slower local atrial conduction, and an unchanged atrial effective refractory period. Overall, I/R-rats display characteristics consistent with changes observed in patients with ICM and various animal models for ICM-associated AF (26–29).

ROLE OF CatA FOR VENTRICULAR REMOTE REMODELING AND ATRIAL CARDIOMYOPATHY. In our rat model for ICM, pharmacological inhibition of CatA activity did not significantly improve LV global systolic function at rest; however, it did prevent wall thinning and preserve more viable myocardium in the LV infarct area and the LV noninfarcted remote myocardium without reducing LV fibrosis. In each of these parameters, SAR was more efficacious than ramipril.

We showed that this antiremodeling effect occurred not only in the ventricular infarct area and noninfarcted remote myocardium but also in the atrium. Inhibition of CatA activity hampered LA fibrosis formation and reduced gene expression of fibrillary collagen types I and III, which are known to be dysregulated in cardiac disease (14,30,31). In the heart, the predominant fibrillary collagens are the rigid type I (80%) and the elastic type III (11%), providing structure and elasticity to the ECM (14,31). The extent of this remodeling process is controlled by the balance between ECM synthesis and degradation, which is tightly regulated by proteolytic enzymes (e.g., cathepsins) as a key mechanism to control ECM function and turnover (16,17). Increased fibrosis formation directly influences architecture of the interstitial matrix, cell-to-cell coupling, cardiomyocyte excitability, and Cx43 distribution, impairing proper electrical conduction of the myocardium (15,32). In our rat model, I/R-Placebo rats exhibited increased atrial fibrosis formation and a higher collagen type I to type III ratio, providing the substrate for stiffer, less compliant atria. Attenuation of increased atrial

FIGURE 6 Atrial Cx43 Distribution

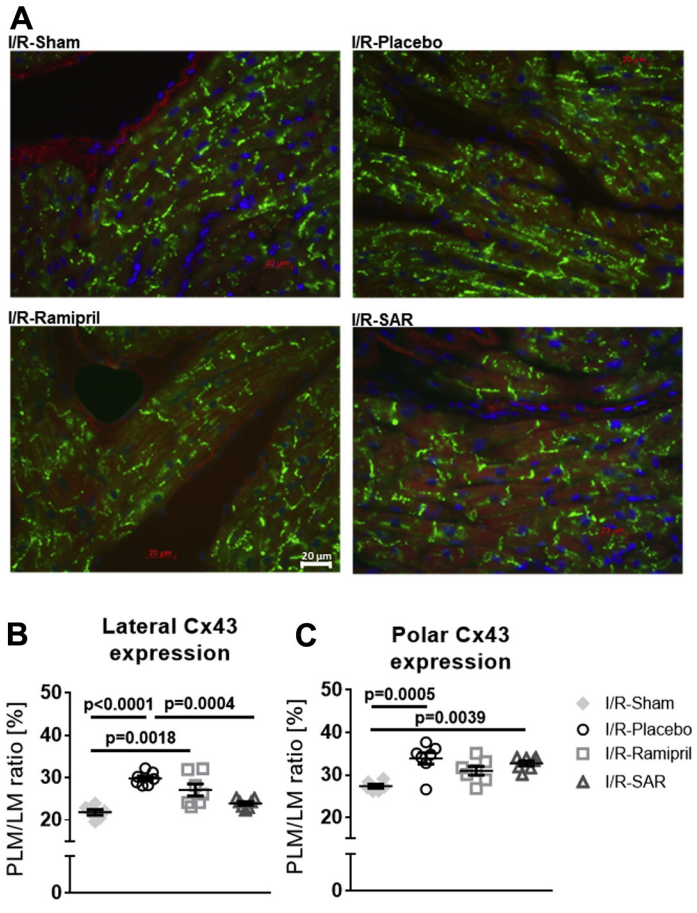

(A) Representative immunohistochemical staining for connexin 43 (Cx43) in left atrial tissue preparations in I/R-Sham (n = 6), I/R-rats given placebo (n = 7), and I/R-rats treated with ramipril (n = 7) or SAR (n = 7). **(B)** Quantification of Cx43-positively stained lateral and **(C)** polar cardiomyocyte membrane. Values are mean ± SEM. Other abbreviations as in Figure 1.

JACC: BASIC TO TRANSLATIONAL SCIENCE VOL. 4, NO. 3, 2019
JUNE 2019:332–44

fibrosis formation and normalization of the collagen type I to type III ratio by pharmacological CatA inhibition was associated with less lateralization of Cx43, preserving physiological coupling between the atrial bundles network and contributing to preserved atrial function and reduced AF susceptibility by fewer conduction disturbances. Importantly, the effect of SAR-mediated CatA inhibition on the development of atrial cardiomyopathy and atrial fibrosis in I/R-rats was more pronounced compared with ramipril, and it occurred independent of significant improvements in LV global systolic function or total LV fibrosis, suggesting prevention of atrial ECM remodeling beyond a simple consequence of improved LV function.

These findings support the concept that remote remodeling in ICM is not restricted to the non-infarcted ventricular myocardium (3-6) but also manifests in the atrium and is critically mediated by ECM proteinases such as CatA. This theory is in line with our previous studies, showing that cardiomyocyte-specific overexpression of CatA in mice mediated AF susceptibility and initiates the development of structural remodeling in the atrium, even in the absence of ventricular dysfunction of other stressors (21). A previous proteomic analysis performed in mice with permanent LAD ligation found that pharmacological inhibition of CatA activity partially restored the infarction-induced alterations of proteins associated with ECM remodeling (33). Our study extended these findings by showing the cardiac functional and structural changes of CatA inhibition in rats with I/R. These changes translate the biochemical beneficial effects of CatA inhibition into a common clinical scenario of early reperfusion following myocardial infarction by using clinically relevant functional imaging techniques and in vivo electrophysiological measures of LV and LA function.

SAR exhibits high cell permeability (20). Pharmacological inhibition of CatA by SAR may therefore display its beneficial effects by inhibition of both intracellular and extracellular CatA. Due to the design of this in vivo study, which mainly focused on the effect of SAR on clinically relevant measures of ventricular and atrial remodeling and function, the mechanism by which SAR prevented cardiac remodeling could not be identified. Further biochemical studies are warranted to identify potential intracellular and extracellular target proteins of CatA to explain the mechanisms underlying the benefit of pharmacological CatA inhibition on ECM remodeling in the heart.

STUDY LIMITATIONS. Although we found strong indications for the development of an arrhythmogenic substrate in the atrium, we observed no spontaneous, nonsustained episodes of AF in these study rats, probably due to the small size of the atrium. The determination of atrial activation times by using conventional contact mapping procedures in small animals has several technical limitations, including spatial and time resolution disparities. Due to the tissue size of the small rat atria, we had to focus on detailed histological and biochemical analyses but could not identify the underlying cellular mechanisms by which pharmacological CatA inhibition attenuates the development of an arrhythmogenic substrate. We did not investigate whether a combination of ramipril and SAR would show synergistic effects and whether the agents tested are able to reverse pre-existing structural and functional atrial remodeling. These findings would be of clinical relevance, because upstream therapy to prevent development of the AF substrate cannot be started early enough. We performed LAD ligation distal to possible atrial branches. Therefore, ischemic effects on atrial myocardium, which have been described following ligation of the right coronary artery or the left circumflex artery, should be limited (34,35).

CONCLUSIONS

Cardiac CatA gene expression was significantly increased in human ICM and experimental ICM in various rat models. Ventricular I/R in rats was associated with reduced LV global systolic function and the development of atrial cardiomyopathy. Pharmacological CatA inhibition initiated at the time point of reperfusion preserved more viable LV myocardium and prevented ECM remodeling and the development of an arrhythmogenic and functional substrate for AF, independent of preserved LV function at rest. Whether preservation of LV viable myocardium, in the absence of improved LV systolic function, helps prevent atrial cardiomyopathy in the setting of ICM and whether LV viable myocardium represents a more suitable metric than LV systolic function and LV fibrosis for the assessment of remote remodeling to guide AF upstream therapy warrant further study (36).

ADDRESS FOR CORRESPONDENCE: Dr. Dominik Linz, Centre for Heart Rhythm Disorders, Department of Cardiology, Royal Adelaide Hospital, University of Adelaide, North Terrace, Adelaide 5000, Australia. E-mail: dominik.linz@adelaide.edu.au.

PERSPECTIVES

COMPETENCY IN MEDICAL KNOWLEDGE: Herein we report that a pharmacological intervention, which preserves more viable ventricular myocardium in ICM with no significant improvements in LV global systolic function, goes hand in hand with a prevention of atrial cardiomyopathy. This observation suggests that atrial cardiomyopathy most likely represents the manifestation of global remote ECM remodeling in ICM and is not simply the result of ICM-related reduction in LV systolic function. Ventricular adverse remodeling and the amount of viable myocardium are powerful predictors for the development of chronic heart failure after myocardial infarction and therefore remain an important pharmacological treatment target, even independent from crude global parameters such as LV systolic function in heart failure.

TRANSLATIONAL OUTLOOK: Further clinical studies are warranted to test whether preservation of LV viable myocardium, even without improvements in LV global systolic function, translates into prevention of atrial cardiomyopathy in the setting of ICM and whether LV viable myocardium represents a better metric than LV global systolic function to guide AF upstream therapy. In this context, the CatA inhibitor SAR has already shown a favorable safety profile in early Phase I studies in healthy young and elderly human subjects alike.

REFERENCES

1. Køber L, Torp-Pedersen C, Carlsen JE, et al. A clinical trial of the angiotensin-converting-enzyme inhibitor trandolapril in patients with left ventricular dysfunction after myocardial infarction. Trandolapril Cardiac Evaluation (TRACE) Study Group. N Engl J Med 1995;333:1670–6.

2. Neumann FJ, Sousa-Uva M, Ahlsson A, et al. 2018 ESC/EACTS guidelines on myocardial revascularization. Eur Heart J 2019;40:87–165.

3. Carberry J, Carrick D, Haig C, et al. Remote zone extracellular volume and left ventricular remodeling in survivors of ST-elevation myocardial infarction. Hypertension 2016;68:385–91.

4. Wilson EM, Moainie SL, Baskin JM, et al. Region- and type-specific induction of matrix metalloproteinases in post-myocardial infarction remodeling. Circulation 2003;107:2857–63.

5. Wijns W, Vatner SF, Camici PG. Hibernating myocardium. N Engl J Med 1998;339:173–81.

6. Bax JJ, Poldermans D, Elhendy A, et al. Improvement of left ventricular ejection fraction, heart failure symptoms and prognosis after revascularization in patients with chronic coronary artery disease and viable myocardium detected by dobutamine stress echocardiography. J Am Coll Cardiol 1999;34:163–9.

7. Meluzín J, Cerný J, Frélich M, et al. Prognostic value of the amount of dysfunctional but viable myocardium in revascularized patients with coronary artery disease and left ventricular dysfunction. Investigators of this Multicenter Study. J Am Coll Cardiol 1998;32:912–20.

8. Pagley PR, Beller GA, Watson DD, Gimple LW, Ragosta M. Improved outcome after coronary bypass surgery in patients with ischemic cardiomyopathy and residual myocardial viability. Circulation 1997;96:793–800.

9. Rizzello V, Poldermans D, Boersma E, et al. Opposite patterns of left ventricular remodeling after coronary revascularization in patients with ischemic cardiomyopathy: role of myocardial viability. Circulation 2004;110:2383–8.

10. Pedersen OD, Søndergaard P, Nielsen T, et al. Atrial fibrillation, ischaemic heart disease, and the risk of death in patients with heart failure. Eur Heart J 2006;27:2866–70.

11. Lubitz SA, Benjamin EJ, Ellinor PT. Atrial fibrillation in congestive heart failure. Heart Fail Clin 2010;6:187–200.

12. Cardin S, Guasch E, Luo X, et al. Role for MicroRNA-21 in atrial profibrillatory fibrotic remodeling associated with experimental post-infarction heart failure. Circ Arrhythm Electrophysiol 2012;5:1027–35.

13. Jumeau C, Rupin A, Chieng-Yane P, et al. Direct thrombin inhibitors prevent left atria remodeling associated with heart failure in rats. J Am Coll Cardiol Basic Trans Science 2016;1:328–39.

14. Weber KT. Cardiac interstitium in health and disease: the fibrillar collagen network. J Am Coll Cardiol 1989;13:1637–52.

15. De Jong S, van Veen TA, van Rijen HV, de Bakker JM. Fibrosis and cardiac arrhythmias. J Cardiovasc Pharmacol 2011;57:630–8.

16. Müller AL, Dhalla NS. Role of various proteases in cardiac remodeling and progression of heart failure. Heart Fail Rev 2012;17:395–409.

17. Cheng XW, Shi GP, Kuzuya M, Sasaki T, Okumura K, Murohara T. Role for cysteine protease cathepsins in heart disease: focus on biology and mechanisms with clinical implication. Circulation 2012;125:1551–62.

18. Ruf S, Buning C, Schreuder H, et al. Inhibition of CatA: an emerging strategy for the treatment of heart failure. Future Med Chem 2013;5:399–409.

19. Hiraiwa M. Cathepsin A/protective protein: an unusual lysosomal multifunctional protein. Cell Mol Life Sci 1999;56:894–907.

20. Seyrantepe V, Hinek A, Peng J, et al. Enzymatic activity of lysosomal carboxypeptidase (cathepsin) A is required for proper elastic fiber formation and inactivation of endothelin-1. Circulation 2008;117:1973–81.

21. Linz D, Hohl M, Dhein S, et al. Cathepsin A mediates susceptibility to atrial tachyarrhythmia and impairment of atrial emptying function in Zucker diabetic fatty rats. Cardiovasc Res 2016;110:371–80.

22. Ruf S, Buning C, Schreuder H, et al. Novel β-amino acid derivatives as inhibitors of cathepsin A. J Med Chem 2012;55:7636–49.

23. Wohlfart P, Linz W, Hübschle T, et al. Cardioprotective effects of lixisenatide in rat myocardial ischemia-reperfusion injury studies. J Transl Med 2013;11:84.

24. Wakili R, Voigt N, Kääb S, Dobrev D, Nattel S. Recent advances in the molecular pathophysiology of atrial fibrillation. J Clin Invest 2011;121:2955–68.

25. Schotten U, Verheule S, Kirchhof P, Goette A. Pathophysiological mechanisms of atrial fibrillation: a translational appraisal. Physiol Rev 2011;91:265–325.

26. Shi Y, Ducharme A, Li D, Gaspo R, Nattel S, Tardif JC. Remodeling of atrial dimensions and emptying function in canine models of atrial fibrillation. Cardiovasc Res 2001;52:217–25.

27. Li D, Fareh S, Leung TK, Nattel S. Promotion of atrial fibrillation by heart failure in dogs: atrial remodeling of a different sort. Circulation 1999;100:87–95.

28. Lau DH, Psaltis PJ, Mackenzie L, et al. Atrial remodeling in an ovine model of anthracycline-induced nonischemic cardiomyopathy: remodeling of the same sort. J Cardiovasc Electrophysiol 2011;22:175–82.

29. Sanders P, Morton JB, Davidson NC, et al. Electrical remodeling of the atria in congestive heart failure: electrophysiological and electroanatomic mapping in humans. Circulation 2003;108:1461–8.

30. Boixel C, Fontaine V, Rucker-Martin C, et al. Fibrosis of the left atria during progression of heart failure is associated with increased matrix metalloproteinases in the rat. J Am Coll Cardiol 2003;42:336–44.

31. Li L, Zhao Q, Kong W. Extracellular matrix remodeling and cardiac fibrosis. Matrix Biol 2018; 68–69:490–506.

32. Jansen JA, van Veen TA, de Jong S, et al. Reduced Cx43 expression triggers increased fibrosis due to enhanced fibroblast activity. Circ Arrhythm Electrophysiol 2012;5:380–90.

33. Petrera A, Gassenhuber J, Ruf S, et al. Cathepsin A inhibition attenuates myocardial infarction-induced heart failure on the functional and proteomic levels. J Transl Med 2016;14:153.

34. Nishida K, Qi XY, Wakili R, et al. Mechanisms of atrial tachyarrhythmias associated with coronary artery occlusion in a chronic canine model. Circulation 2011;123:137–46.

35. Alasady M, Shipp NJ, Brooks AG, et al. Myocardial infarction and atrial fibrillation: importance of atrial ischemia. Circ Arrhythm Electrophysiol 2013;6:738–45.

36. Tillner J, Lehmann A, Paehler T, et al. Tolerability, safety, and pharmacokinetics of the novel cathepsin A inhibitor SAR164653 in healthy subjects. Clin Pharmacol Drug Dev 2016; 5:57–68.

KEY WORDS atrial cardiomyopathy, atrial fibrillation, ischemia/reperfusion, myocardial infarction, remote remodeling

APPENDIX For an expanded Methods section and supplemental figures, please see the online version of this paper.

JACC: BASIC TO TRANSLATIONAL SCIENCE VOL. 4, NO. 3, 2019

EDITORIAL COMMENT

Cathepsin A Inhibitors to Treat Heart Disease

Much Potential, Many Questions*

Randy T. Cowling, PhD

Cathepsin A is a ubiquitously expressed, multifunctional lysosomal protein. In the lysosome, it binds to neuraminidase and β-galactosidase to activate the former and stabilize the latter, functions that led to the term "lysosomal protective protein." It also possesses serine carboxypeptidase activity at acidic pH as well as deamidase and esterase activities at neutral pH. Mutations that disrupt its "protective" functions are known to cause the lysosomal storage disease, galactosialidosis, in humans (summarized by Hiraiwa [1]). However, its enzymatic activity has garnered the most attention in recent years. Although localized to lysosomes intracellularly, cathepsin A can also be secreted. Extracellularly, it is capable of degrading many bioactive peptides that function in the cardiovascular system, including endothelin-1, bradykinin, and angiotensin I. Because the enzymatic activity of cathepsin A can be targeted separately from its "protective" functions (2), there has been interest for at least a decade in clinically targeting cathepsin A in patients with cardiovascular disease, and novel β-amino acid inhibitors were synthesized for this purpose (3).

In the paper by Hohl et al. (4) in this issue of *JACC: Basic to Translational Science*, the investigators examine the effect of 1 of these inhibitors, SAR164653 ((S)-3-{[1-(2-fluoro-phenyl)-5-methoxy-1H-pyrazole-3-carbonyl]-amino}-3-o-tolyl-propionic-acid), in ischemic cardiomyopathy. Analysis of left ventricle specimens of patients with end-stage ischemic cardiomyopathy revealed significant increases in cathepsin A mRNA and protein levels (~50% increase over tissue from healthy donor hearts), although details of these patients were not available. Using a rat model of myocardial infarction, cathepsin A mRNA levels in the remote left ventricular myocardium and left atrial myocardium were significantly increased 8 weeks after left anterior descending artery ligation (1.5- and 1.8-fold, respectively). Using an ischemia/reperfusion rat model (30-min ischemia followed by 10-week reperfusion), these increases were 1.7- and 2.9-fold, respectively. The up-regulated cathepsin A levels were associated with increased atrial natriuretic peptide mRNA levels. Treatment of the ischemia/reperfusion rats with SAR164653 had no effect on infarct size or normalized heart weight, but did improve ejection fraction and reduce plasma brain natriuretic peptide levels. Magnetic resonance imaging analysis revealed better contractility in the SAR164653-treated rats than in the placebo-treated rats, which seemed to be caused by preservation of remote myocardium with SAR164653 treatment (i.e., there was better wall motion in these areas).

SEE PAGE 332

Regarding the left atrium, SAR164653 did not affect chamber dimensions in the ischemia/reperfusion rats, but fractional shortening was significantly higher compared with that of the placebo-treated controls. With respect to left atrial remodeling at 10 weeks,

*Editorials published in *JACC: Basic to Translational Science* reflect the views of the authors and do not necessarily represent the views of *JACC: Basic to Translational Science* or the American College of Cardiology.

From Department of Medicine, Division of Cardiovascular Medicine, University of California-San Diego, La Jolla, California. Dr. Cowling is currently funded by National Institutes of Health grant HL141361.
The authors attest they are in compliance with human studies committees and animal welfare regulations of the authors' institutions and Food and Drug Administration guidelines, including patient consent where appropriate. For more information, visit the *JACC: Basic to Translational Science* author instructions page.

ISSN 2452-302X https://doi.org/10.1016/j.jacbts.2019.05.004

JACC: BASIC TO TRANSLATIONAL SCIENCE VOL. 4, NO. 3, 2019
JUNE 2019:345–7

fibrosis was increased, accompanied by increased procollagen mRNA levels and an increased collagen I/collagen III ratio; SAR164653 treatment significantly reduced the fibrosis, collagen ratio, and Col1A1 mRNA levels. Polar and lateral connexin 43 expression was increased in the left atria of the ischemia/reperfusion rats, and SAR164653 treatment significantly reduced lateralization of the connexin 43. In the left atrium post-ischemia/reperfusion, the duration of atrial fibrillation, total activation time, and areas of slow conduction increased, and all of these values were significantly reduced by SAR164653 treatment. As a comparison, treatment with the angiotensin-converting enzyme (ACE) inhibitor ramipril produced similar results as those with SAR164653, although, overall, the latter was more efficacious. As a notable exception, echocardiographic estimations of left ventricular mass suggested that SAR164653 was less effective at reducing post-ischemic hypertrophy than ramipril (although direct measures of left ventricular cardiomyocyte size were not shown).

Hohl et al. (4) have certainly shown an association of cathepsin A levels with dilated cardiomyopathy, and SAR164653 was able to improve cardiac structural/functional parameters post-infarct in the rat models. Targeting cathepsin A holds a lot of promise in this regard, especially the attenuation of atrial and remote site remodeling that can lead to heart failure progression. However, many questions remain unanswered, and 2 are critical in order to move this from the bench to the bedside: 1) What is the mechanism?; and 2) What will this mean for patients and potential therapies? Regarding the mechanism(s) of activity, the investigators (or a subset of them) have studied the effect of SAR164653 in rat experimental infarct models (the focus of this editorial), a rat model of type 2 diabetes (5), and a mouse model of myocardial infarction (6). All of these studies have shown significant improvements or trends toward improvement with SAR164653 treatment, yet no mechanism has been determined. Together, cathepsin A, neuraminidase, and an enzymatically inactive splice variant of β-galactosidase form the cell-surface elastin receptor, and inhibition of cathepsin A catalytic activity has been shown to lead to reduced elastic fibers in the lungs, skin, and aortic adventitia of mice (2). However, how this is related to tissue remodeling and fibrosis in the heart is unclear. Mechanistically, the authors appear to be favoring the tissue-specific stabilization of protective bioactive peptides, such as bradykinin, which is a reasonable hypothesis. However, tissue-specific stabilization of endothelin-1 may also occur and could be detrimental, as it could lead to vasoconstriction, prolonged inflammation, and fibrosis (7,8). For these reasons, determining tissue-specific mechanisms of the efficacy of cathepsin A inhibitors is crucial for future translational studies.

Finally, what does this mean for patients and potential therapies? The trajectory of SAR164653 in this regard is unclear at the moment. Sanofi was originally going to use this compound to treat cardiovascular-related complications in diabetic patients, but abandoned this in 2013 in order to evaluate the compound in pulmonary hypertension (9). A phase I trial was conducted in the United Kingdom (no later than 2014) on 45 healthy subjects (20 to 82 years of age), and no adverse effects were noted over 14 days up to the maximum dose of 800 mg daily (10). However, to the best of my knowledge, there have been no further updates on relevant clinical trials. Although tissue expression levels can vary, the rather ubiquitous expression of cathepsin A emphasizes the importance of long-term safety studies in human patients. The outcomes can be hard to predict and need to be assessed empirically. However, a lessen can be garnered from the positive outcomes on morbidity and mortality of the combined neutral endopeptidase (neprilysin) inhibitor and angiotensin receptor blocker, sacubitril/valsartan, in heart failure with reduced ejection fraction (i.e., the PARADIGM-HF [Prospective Comparison of ARNI With ACEI to Determine Impact on Global Mortality and Morbidity in Heart Failure] trial) (11). The trials and tribulations of this treatment strategy, from the efficacy failures of neprilysin inhibitors (e.g., ecadotril) to the unacceptably high angioedema associated with neprilysin/ACE dual inhibition (with omapatrilat) to the eventual success of switching from ACE inhibitor to angiotensin receptor blocker in order to target the renin-angiotensin system, have been summarized very thoroughly in Eugene Braunwald's 2015 review (12). The important message here is that scientific and medical advances rarely take a linear path, with some successes and many more failures. However, even in the failures, there can be something of value, some knowledge to be gained, albeit sometimes not what was originally intended. I am unsure of what is to come of cathepsin A inhibition to treat cardiovascular disease, but I am positive that much will be learned in the process. The current study by Hohl et al. (4) is an important step in that direction.

ADDRESS FOR CORRESPONDENCE: Dr. Randy T. Cowling, Department of Medicine, Division of Cardiovascular Medicine, University of California San Diego, 9500 Gilman Drive, Mail code 0663, La Jolla, California 92093-0663. E-mail: rcowling@ucsd.edu.

REFERENCES

1. Hiraiwa M. Cathepsin A/protective protein: an unusual lysosomal multifunctional protein. Cell Mol Life Sci 1999;56:894–907.

2. Seyrantepe V, Hinek A, Peng J, et al. Enzymatic activity of lysosomal carboxypeptidase (cathepsin) A is required for proper elastic fiber formation and inactivation of endothelin-1. Circulation 2008;117:1973–81.

3. Ruf S, Buning C, Schreuder H, et al. Novel beta-amino acid derivatives as inhibitors of cathepsin A. J Med Chem 2012;55:7636–49.

4. Hohl M, Erb K, Lang L, et al. Cathepsin A mediates ventricular remote remodeling and atrial cardiomyopathy in rats with ventricular ischemia/reperfusion. J Am Coll Cardiol Basic Trans Science 2019;4:332–44.

5. Linz D, Hohl M, Dhein S, et al. Cathepsin A mediates susceptibility to atrial tachyarrhythmia and impairment of atrial emptying function in Zucker diabetic fatty rats. Cardiovasc Res 2016;110:371–80.

6. Petrera A, Gassenhuber J, Ruf S, et al. Cathepsin A inhibition attenuates myocardial infarction-induced heart failure on the functional and proteomic levels. J Transl Med 2016;14:153.

7. Zolk O, Bohm M. The role of the cardiac endothelin system in heart failure. Nephrol Dial Transplant 2000;15:758–60.

8. Bugiani M, Kevelam SH, Bakels HS, et al. Cathepsin A-related arteriopathy with strokes and leukoencephalopathy (CARASAL). Neurology 2016;87:1777–86.

9. Sanofi. Q1 2013 business EPS[(1)] impacted by exclusivity losses in prior year - Growth platforms[(2)] sales increased 8.6%[(3)]. 2013. Available at: https://www.sanofi.com/-/media/Project/One-Sanofi-Web/Websites/Global/Sanofi-COM/Home/events/2013_1stQR/docs/20130502_Q1RESULTS_en.pdf. Accessed May 2, 2019.

10. Tillner J, Lehmann A, Paehler T, et al. Tolerability, safety, and pharmacokinetics of the novel cathepsin A inhibitor SAR164653 in healthy subjects. Clin Pharmacol Drug Dev 2016;5:57–68.

11. McMurray JJ, Packer M, Desai AS, et al. Angiotensin-neprilysin inhibition versus enalapril in heart failure. N Engl J Med 2014;371:993–1004.

12. Braunwald E. The path to an angiotensin receptor antagonist-neprilysin inhibitor in the treatment of heart failure. J Am Coll Cardiol 2015;65:1029–41.

KEY WORDS atrium, bioactive peptide, cardiac remodeling, CTSA, fibrosis

JACC: BASIC TO TRANSLATIONAL SCIENCE VOL. 4, NO. 3, 2019

PRECLINICAL RESEARCH

Administration of a TLR9 Inhibitor Attenuates the Development and Progression of Heart Failure in Mice

Hiromichi Ueda, MD,[a] Osamu Yamaguchi, MD, PhD,[a] Manabu Taneike, MD, PhD,[a] Yasuhiro Akazawa, MD,[a] Haruko Wada-Kobayashi, MD,[a] Ryuta Sugihara, MD,[a] Hiroki Yorifuji, MD,[a] Hiroyuki Nakayama, MD, PhD,[b] Shigemiki Omiya, MD, PhD,[c] Tomokazu Murakawa, MD, PhD,[c] Yasushi Sakata, MD, PhD,[a] Kinya Otsu, MD, PhD[c]

VISUAL ABSTRACT

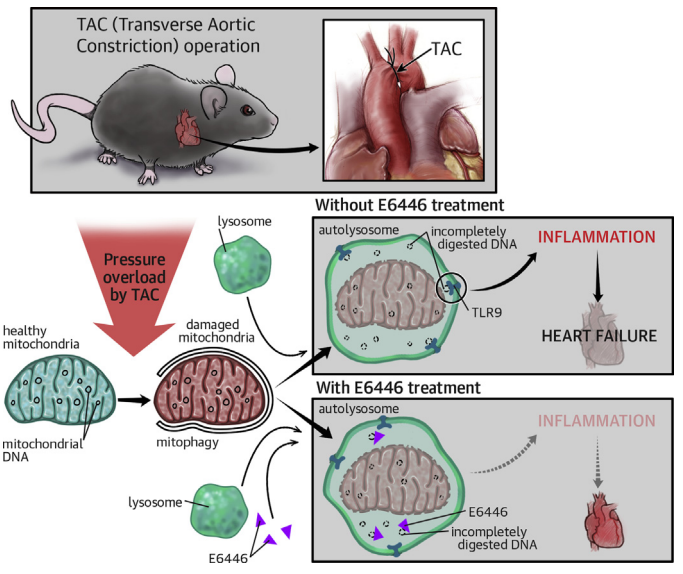

Ueda, H. et al. J Am Coll Cardiol Basic Trans Science. 2019;4(3):348-63.

HIGHLIGHTS

- **Under pressure overload, mitochondrial deoxyribonucleic acid containing the unmethylated cytidine-phosphate-guanosine motif is accumulated in cardiomyocytes and stimulates Toll-like receptor 9, resulting in inflammation and heart failure.**
- **Treatment with E6446, (6-[3-(pyrrolidin-1-yl)propoxy)-2-(4-(3-(pyrrolidin-1-yl) propoxy)phenyl]benzo[d]oxazole), a specific Toll-like receptor 9 inhibitor, prevented the development and slowed the progression of left ventricular dilatation and cardiac dysfunction in mice after pressure overload.**
- **E6446 attenuated the inflammatory responses in the pressure-overloaded mouse heart, even though the accumulation of mitochondrial deoxyribonucleic acid in cardiomyocytes was observed.**
- **E6446 could be a new therapeutic agent against heart failure.**

From the [a]Department of Cardiovascular Medicine, Graduate School of Medicine, Osaka University, Suita, Osaka, Japan; [b]Laboratory of Clinical Science and Biomedicine, Graduate School of Pharmaceutical Sciences, Osaka University, Suita, Osaka, Japan; and the [c]School of Cardiovascular Medicine and Sciences, King's College London British Heart Foundation Centre of Excellence, London, United Kingdom. This research was supported by the British Heart Foundation (CH/11/3/29051 and RG/16/15/32294), Fondation Leducq (RA15CVD04), and JSPS KAKENHI (18H02807), to Dr. Otsu. The authors have reported that they have no relationships relevant to the contents of this paper to disclose.

All authors attest they are in compliance with human studies committees and animal welfare regulations of the authors' institutions and Food and Drug Administration guidelines, including patient consent where appropriate. For more information, visit the *JACC: Basic to Translational Science* author instructions page.

Manuscript received October 3, 2018; revised manuscript received January 10, 2019, accepted January 11, 2019.

ISSN 2452-302X https://doi.org/10.1016/j.jacbts.2019.01.002

SUMMARY

Mitochondrial deoxyribonucleic acid, containing the unmethylated cytidine-phosphate-guanosine motif, stimulates Toll-like receptor 9 to induce inflammation and heart failure. A small chemical, E6446 [(6-[3-(pyrrolidin-1-yl)propoxy)-2-(4-(3-(pyrrolidin-1-yl)propoxy)phenyl]benzo[d]oxazole)], is a specific Toll-like receptor 9 inhibitor in cardiomyocytes. In this study, we showed that E6446 exerts beneficial effects for the prevention and treatment of pressure overload-induced heart failure in mice. When administered before the operation and chronically thereafter, E6446 prevented the development of left ventricular dilatation as well as cardiac dysfunction, fibrosis, and inflammation. Furthermore, when administered after the manifestation of cardiac dysfunction, E6446 slowed progression of cardiac remodeling. Thus, the inhibitor may be a novel therapeutic agent for treating patients with heart failure. (J Am Coll Cardiol Basic Trans Science 2019;4:348–63)

ABBREVIATIONS AND ACRONYMS

CCCP = carbonyl cyanide *m*-chlorophenyl hydrazine

CpG = cytidine-phosphate-guanosine

CpG ODN = unmethylated cytidine-phosphate-guanosine containing oligodeoxynucleotide

DNA = deoxyribonucleic acid

E6446 = (6-[3-(pyrrolidin-1-yl)propoxy)-2-(4-(3-(pyrrolidin-1-yl)propoxy)phenyl]benzo[d]oxazole)

EdU = 5-ethynyl-2′-deoxyuridine

IL = interleukin

IVSd = end-diastolic interventricular septal wall thickness

LAMP = lysosome-associated membrane protein

LC = microtubule-associated protein light chain

LPS = lipopolysaccharide

LV = left ventricular

mRNA = messenger ribonucleic acid

TAC = transverse aortic constriction

TLR = Toll-like receptor

TNF = tumor necrosis factor

Heart failure is a complex disease associated with high levels of morbidity and mortality and marked reductions in quality of life. Previous extensive studies on heart failure have reported an important role for proinflammatory cytokines in its pathogenesis (1). Circulating levels of proinflammatory cytokines, including tumor necrosis factor (TNF)-α, are related to the severity and prognosis of the disease. However, the targeted anti-TNF-α approaches were neutral with respect to the primary endpoints of the trial or resulted in worsening heart failure or death (2,3). In addition to TNF-α, the pro-inflammatory cytokines that are elaborated in heart failure include other members of the TNF superfamily, members of the interleukin-1 family, and interleukin (IL)-6 (1). Recognizing the molecular mechanism underlying the developing inflammation in heart failure is essential for developing strategies to control disease progression, including therapeutic drugs.

Mitochondrial deoxyribonucleic acid (DNA) contains the unmethylated cytidine-phosphate-guanosine (CpG) motif, which stimulates Toll-like receptor (TLR) 9 to induce inflammation (4,5). Mitochondria damaged by external hemodynamic stress are degraded by the autophagy/lysosome system in cardiomyocytes (6). Insufficient degradation of mitochondrial DNA mediated through autophagy in pressure-overloaded mouse hearts leads to its binding to TLR9 to induce inflammation and heart failure (7). In failing mouse hearts, mitochondrial DNA is located in autolysosomes. Furthermore, TLR9 ablation in pressure-overloaded mice attenuated the development of inflammation and heart failure. Thus, interference with TLR9 function by small molecules is likely to produce a better clinical outcome by preventing its aberrant inflammatory responses.

E6446 (6-[3-(pyrrolidin-1-yl)propoxy)-2-(4-(3-(pyrrolidin-1-yl)propoxy)phenyl]benzo[d]oxazole), is a synthetic antagonist of nucleic acid-sensing TLRs and is orally bioactive (8,9). In vitro, E6446 specifically inhibits the activation of TLR9 (8). Others have reported that the compound inhibits TLR9 but also TLR7 in a ligand-dependent manner (9). When E6446 is administered to mice, it suppresses inflammatory responses to challenge doses of unmethylated CpG containing oligodeoxynucleotide (CpG ODN) (8,9). When E6446 is administered chronically in mouse cerebral malaria and spontaneous lupus models, the compound inhibits cytokine production with prevention of signs of cerebral malaria and circulating antinuclear antibodies, respectively.

In the present study, the efficacy of oral treatment with E6446 was evaluated on mouse pressure overload-induced heart failure models. Our results indicate that E6446 exerts beneficial effects for the prevention and treatment of heart failure in mice and might be a novel therapeutic agent for treating patients with heart failure.

METHODS

CELL CULTURE. Adult cardiomyocytes were isolated from 10- to 12-week-old C57BL/6J male mice (CLEA Japan, Inc., Tokyo, Japan) by using a Langendorff system and were then cultured (7).

RIBONUCLEIC ACID ANALYSIS. Total ribonucleic acid (RNA) was extracted from the left ventricle or cultured cardiomyocytes by using the TRIzol reagent (Thermo Fisher Scientific, Waltham, Massachusetts) and reverse transcribed by using TaqMan Reverse Transcription Reagents (Thermo Fisher Scientific) (7).

TABLE 1 Echocardiographic Parameters of All Mice Subjected to TAC Operation for 2 Weeks

	Baseline (n = 30)	TAC for 2 Weeks (n = 30)
LVDd, mm	2.31 ± 0.02	2.77 ± 0.03*
LVDs, mm	0.88 ± 0.01	1.45 ± 0.03*
LVFS, %	62.0 ± 0.40	47.8 ± 0.71*
IVSd, mm	0.92 ± 0.00	1.04 ± 0.01*
LVPWd, mm	0.86 ± 0.01	1.02 ± 0.01*
Heart rate, beats/min	696 ± 3.4	685 ± 4.3
LV mass, mg	58.7 ± 0.7	96.6 ± 2.1*

The echocardiographic parameters of the mice were obtained 2 weeks after the operation. Values are mean ± SE. *p < 0.05 vs. baseline.

IVSd = end-diastolic interventricular septal wall thickness; LV = left ventricular; LVDd = end-diastolic left ventricular internal dimension; LVDs = end-systolic left ventricular internal dimension; LVFS = left ventricular fractional shortening; LVPWd = end-diastolic left ventricular posterior wall thickness; TAC = transverse aortic constriction.

Real-time quantitative polymerase chain reaction was performed by using the Platinum Quantitative PCR SuperMix-UDG (Thermo Fisher Scientific). Relative levels of gene expression were normalized to the *Gapdh* messenger RNA (mRNA) expression. The primers (Thermo Fisher Scientific: Assay identity) used were as follows: *Nppa*, Mm01255747_g1; *Nppb*, Mm00435304_g1; *Col1a2*, Mm01165107_m1; *Col3a1*, Mm00802331_m1; *Gapdh*, 4352339E; *Il6*, Mm99999064_m1; *Il1b*, Mm01336189_m1; and *Tnfa*, Mm00443260_g1.

IMMUNOFLUORESCENCE MICROSCOPY. Adult mouse cardiomyocytes on laminin-coated glass-based dishes (IWAKI Cell Biology, Bio-REV Pte. Ltd., Singapore) were incubated with 100 nmol/l carbonyl cyanide *m*-chlorophenyl hydrazine (CCCP) for 6 h. To estimate mitochondrial membrane potential, the cells were treated with 10 nmol/l of tetramethylrhodamine ethyl ester (Molecular Probes, Eugene, Oregon) for 30 min. To visualize DNA and autophagosomes, the cells were incubated in three-dimensional gel with Cellmatrix I-A (Nitta Gelatin Inc., Osaka, Japan) and fixed with methanol at −30°C for 15 min. The cells were incubated with anti-microtubule-associated protein light chain (LC) 3B antibody (Cell Signaling Technology, Danvers, Massachusetts) overnight at 4°C, followed by staining with anti-rabbit Alexa 568 secondary antibody (Abcam, Cambridge, United Kingdom) overnight. The cells were incubated with 100-fold diluted PicoGreen (Thermo Fisher Scientific) for 30 min before confocal microscopic analysis using an FV-1000D microscope (Olympus, Tokyo, Japan) (7).

ANIMAL STUDY. The investigation conforms to the Position of the American Heart Association on Research Animal Use adopted by the American Heart Association on November 11, 1984. All in vivo and in vitro experimental protocols were conducted under the supervision of the Animal Research Committee of Osaka University and in accordance with the Guidelines for Animal Experiments of Osaka University and the Japanese Animal Protection and Management Law.

The 10- to 12-week-old male C57BL/6J mice were subjected to transverse aortic constriction (TAC) surgery (10). Sham-operated animals underwent the same operation without aortic constriction. Blood pressure was measured noninvasively on mice anesthetized with 2.5% tribromoethanol by using a pressure monitor (Model MK-2000, Muromachi Kikai Co., Ltd., Tokyo, Japan). The pressure gradient across TAC was estimated by the difference in blood pressure between both arms by using a pressure monitor. Ultrasonography (Sonos 5500, equipped with a 15-MHz linear probe, Philips Medical Systems, Cambridge, Massachusetts) was used for assessing left ventricular (LV) size and function on conscious mice.

DRUG AND TREATMENT. E6446 (Eisai, Inc., Andover, Massachusetts) was dissolved in dimethyl sulfoxide (final 0.04% v/v) for experiments. Isolated cardiomyocytes were pretreated with E6446 (0 to 10 μmol/l) for 1 h, followed by treatment with 1 μg/ml of lipopolysaccharide (LPS) (FUJIFILM WAKO Pure Chemical Co., Osaka, Japan), 2 mmol/l of loxoribine (InvivoGen, San Diego, California), or 5 μmol/l of type B CpG ODN (ODN1668, InvivoGen) for 6 h. To examine the effect of E6446 on the level of cytokine mRNAs, cardiomyocytes were pretreated with 10 μmol/l of E6446 for 1 h, followed by treatment with 100 nmol/l of CCCP for 6 h.

For the in vivo ODN1668 challenge experiments with E6446, the mice were orally administered E6446 at a dose of 1.5 mg/200 μl per mouse using animal feeding needles (Natsume Seisakusho Co., Ltd., Tokyo, Japan). One, two, or 3 days later, the mice were injected intraperitoneally with 60 μg/mouse of ODN1668 2 h before sacrifice, following intraperitoneal injection of 20 mg/mouse of D-galactosamine (MilliporeSigma, Burlington, Massachusetts) for 30 min. In the prevention study, E6446 administration was started 2 days before the operation. Mice were administered E6446 orally at a dose of 1.5 mg/mouse or its vehicle (saline) as a control every 2 days. In the treatment study, 30 mice were subjected to TAC operation for 2 weeks. Ten mice with fractional shortening >50% were excluded from the study. The remaining 20 mice were randomized to the saline- and E6446-treated groups and then orally administered saline or E6446 (1.5 mg/mouse) every 2 days (Table 1).

FIGURE 1 **Selectivity of E6446**

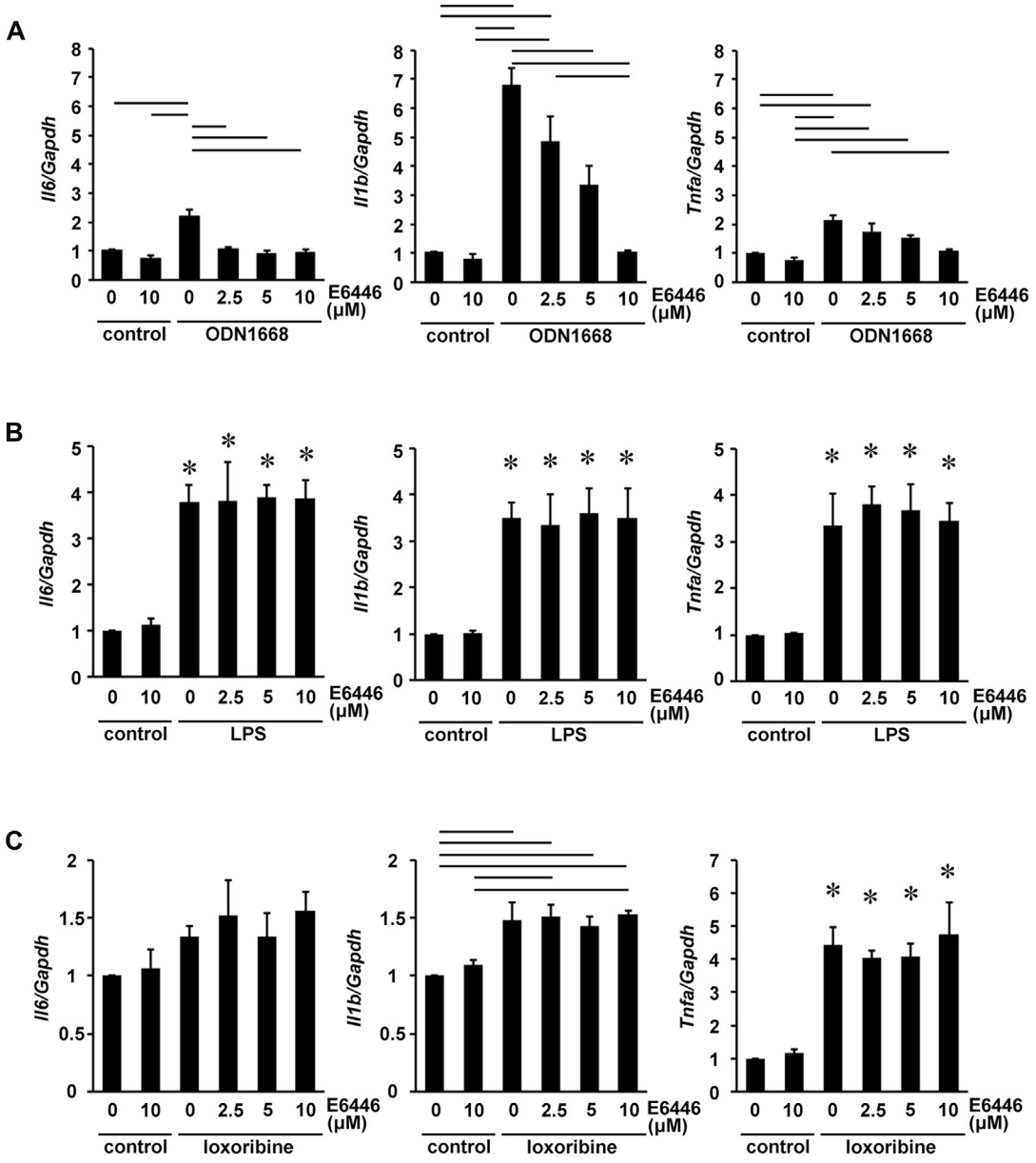

The expression level of cytokine messenger ribonucleic acid in cardiomyocytes with increasing concentrations of E6446, (6-[3-(pyrrolidin-1-yl)propoxy)-2-(4-(3-(pyrrolidin-1-yl)propoxy)phenyl]benzo[d]oxazole) (n = 3). Cardiomyocytes were treated with 0 to 10 μmol/l of E6446 for 1 h, followed by **(A)** 5 μmol/l ODN1668, **(B)** 1 μg/ml of lipopolysaccharide (LPS), or **(C)** 2 mmol/l of loxoribine for 6 h. Control groups were treated with vehicle. Data were normalized to the content of *Gapdh* messenger ribonucleic acid. Values are mean ± SE. **Bars in graphs** indicate $p < 0.05$. *$p < 0.05$ versus both control groups.

A blood sample was taken from the right ventricle. IL-6, IL-1B, and TNF-α serum levels were measured with an enzyme-linked immunoadsorbent assay kit (Thermo Fisher Scientific for IL-6 and IL-1B, R and D Systems [Minneapolis, Minnesota] for TNF-α).

HISTOLOGICAL ANALYSIS. Heart samples were fixed in buffered 4% paraformaldehyde solution and embedded in paraffin (10). Fibrosis fraction was quantified by using ImageJ software (National Institutes of Health, Bethesda, Maryland) and

FIGURE 2 Effect of E6446 on Mitochondrial Damage-Induced Cytokine Messenger Ribonucleic Acid Production in Isolated Adult Mouse Cardiomyocytes

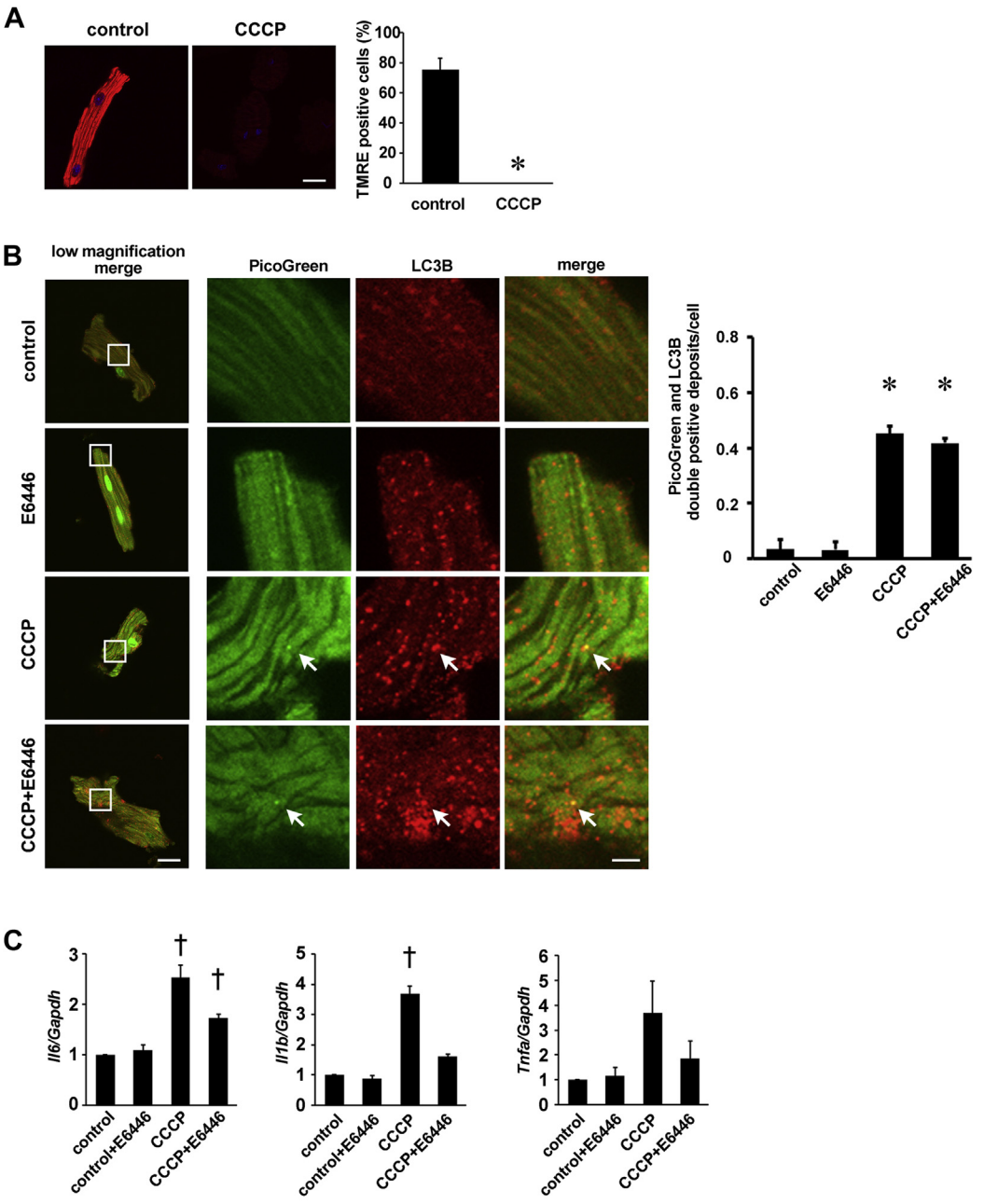

(A) Disruption of mitochondrial membrane potential by carbonyl cyanide *m*-chlorophenyl hydrazine (CCCP). Isolated cardiomyocytes were incubated with 100 nmol/l CCCP for 6 h and stained with tetramethylrhodamine ethyl ester (TMRE). Scale bar, 20 μm. The **right graph** shows the proportion of TMRE-positive cells. **(B)** Double staining of E6446-treated cardiomyocytes stimulated with CCCP using PicoGreen **(green)** and anti-microtubule-associated protein light chain (LC) 3B antibody **(red)**. Low-magnified images are shown in the **left panels**. Scale bar, 20 μm. Higher magnified images of the squared areas are shown in the **right panels**. Scale bar, 5 μm. **Arrows** indicate PicoGreen and LC3B merged deposits. The **right graph** shows the number of PicoGreen and LC3B double-positive deposits per cell. Ten or more cells were analyzed for each experiment. **(C)** Inhibition of cytokine messenger ribonucleic acid expression in CCCP-stimulated cardiomyocytes by E6446. Cardiomyocytes were treated with 10 μmol/l E6446 for 1 h, followed by 100 nmol/l CCCP for 6 h. Values are mean ± SE ($n = 3$). *$p < 0.05$ versus corresponding controls. †$p < 0.05$ versus all other groups. Abbreviation as in Figure 1.

FIGURE 3 Determination of the Experimental Conditions for E6446 Administration

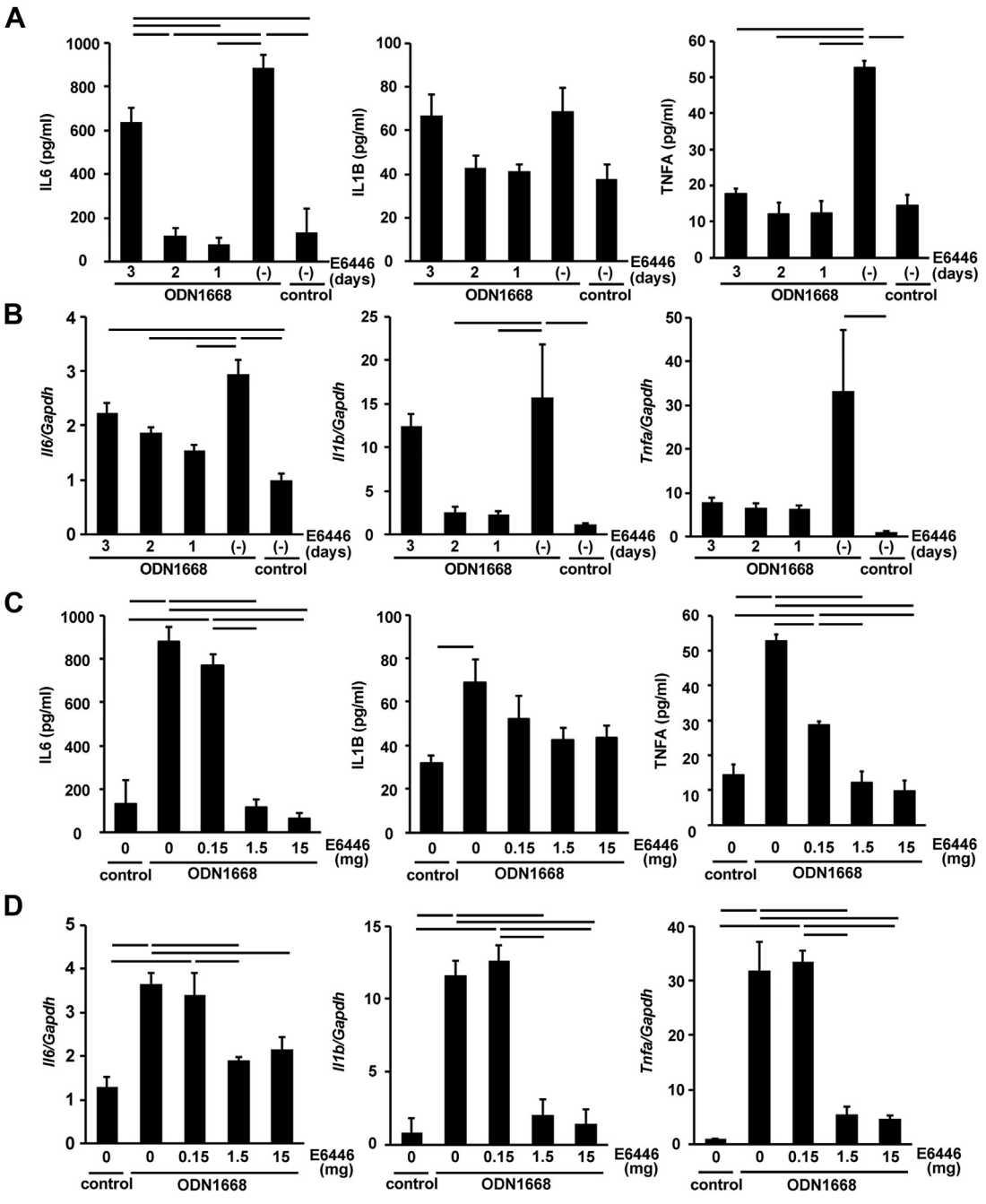

The time dependence of **(A)** cytokine protein and **(B)** messenger ribonucleic acid (mRNA) expression in the heart after injection with ODN1668. Mice (body weight 24.4 to 25.8 g) were pretreated with oral administration of 1.5 mg/mouse (60 mg/kg) of E6446 1, 2, or 3 days before intraperitoneal injection with 60 μg/mouse of ODN1668. Two hours after ODN1668 injection, mice were sacrificed for analysis (see Figure 9A). Dose dependency in the inhibition of **(C)** cytokine protein and **(D)** mRNA expression after ODN1668 injection with increasing concentrations of E6446. Two days after oral administration with the indicated dose of E6446, mice were administered an intraperitoneal injection of 60 μg/mouse of ODN1668. Two hours later, mice were sacrificed for analysis (see Figure 9B). Data were normalized to the content of *Gapdh* mRNA in **B and D**. Values are mean ± SE (n = 3). Bars in graphs indicate $p < 0.05$. IL = interleukin; TNF = tumor necrosis factor; other abbreviation as in Figure 1.

FIGURE 4 Improvement of Echocardiographic Parameters by Treatment With E6446 Initiated Before TAC

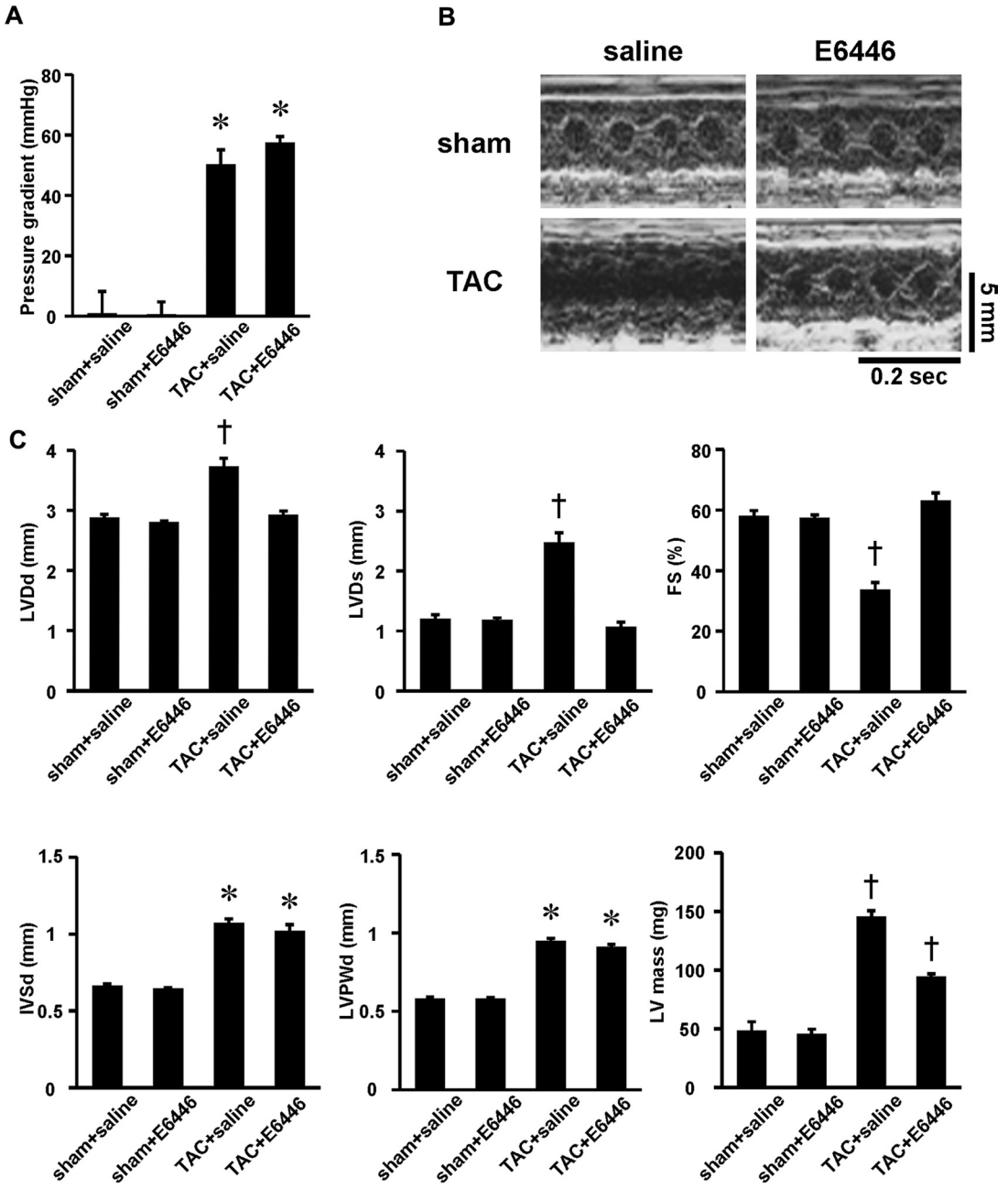

The oral administration of E6446 (1.5 mg/mouse) was performed every 2 days from 2 days before transverse aortic constriction (TAC) (see Figure 10A). **(A)** Pressure gradient across TAC estimated by using a pressure monitor 1 week after operation. **(B)** Representative images of transthoracic M-mode echocardiographic tracing. Scale bars, 0.2 s and 5 mm, respectively. **(C)** Echocardiographic parameters of the mice treated with E6446 4 weeks after TAC (n = 4 in sham groups, n = 5 in TAC groups). Values are mean ± SE. *p < 0.05 versus sham-operated groups. †p < 0.05 versus all other groups. FC = fractional shortening; IVSd = end-diastolic interventricular septal wall thickness; LV = left ventricular; LVDd = end-diastolic left ventricular internal dimension; LVDs = end-systolic left ventricular internal dimension; LVPWd = end-diastolic left ventricular posterior wall thickness; other abbreviation as in Figure 1.

FIGURE 5 Improvement of Cardiac Phenotypes by Treatment With E6446 Initiated Before TAC

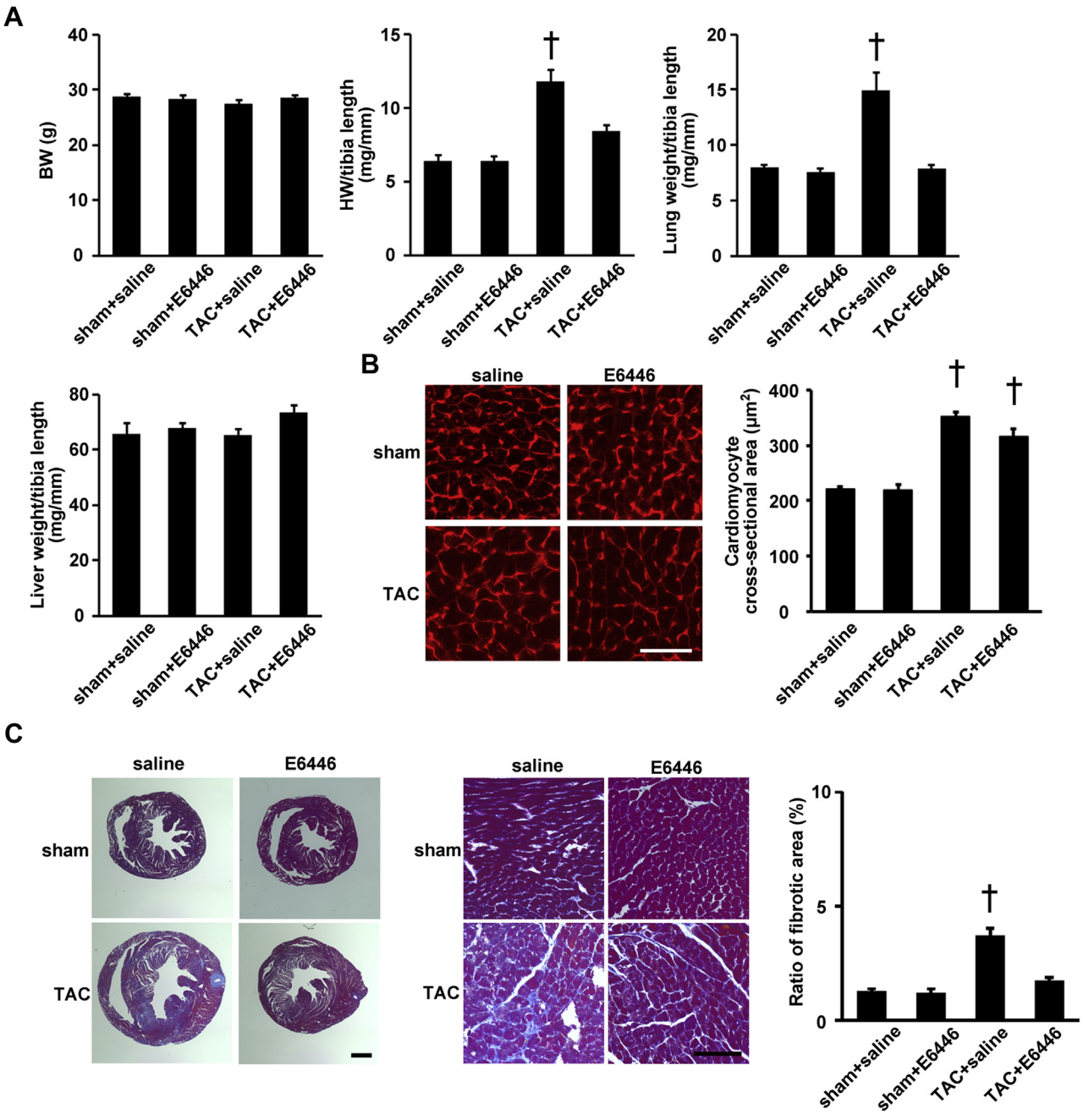

The treatment with E6446 was performed every 2 days from 2 days before TAC. The mice were analyzed 4 weeks after the operation (see Figure 10A). **(A)** Physiological parameters of the mice treated with E6446 (n = 4 in sham groups, n = 5 in TAC groups). **(B)** The representative images of WGA-Alexa 555–stained heart sections. Scale bar, 50 μm. The **right graph** shows the cross-sectional area of cardiomyocytes. **(C)** Azan-Mallory–stained heart sections. **Left and middle panels** show the whole heart and magnified sections, respectively. Scale bars, 1 mm **(left panels)** and 100 μm **(middle panels)**. The **right graph** shows the ratio of the fibrotic area in the heart. n = 3 in sham-operated groups, n = 5 in TAC-operated saline-treated group, n = 4 in TAC-operated E6446-treated group in **B and C**. Values are mean ± SE. †p < 0.05 versus all other groups. BW = body weight; HW = heart weight; other abbreviations as in Figures 1 and 4.

FIGURE 6 Effects of E6446 on mRNA Expressions

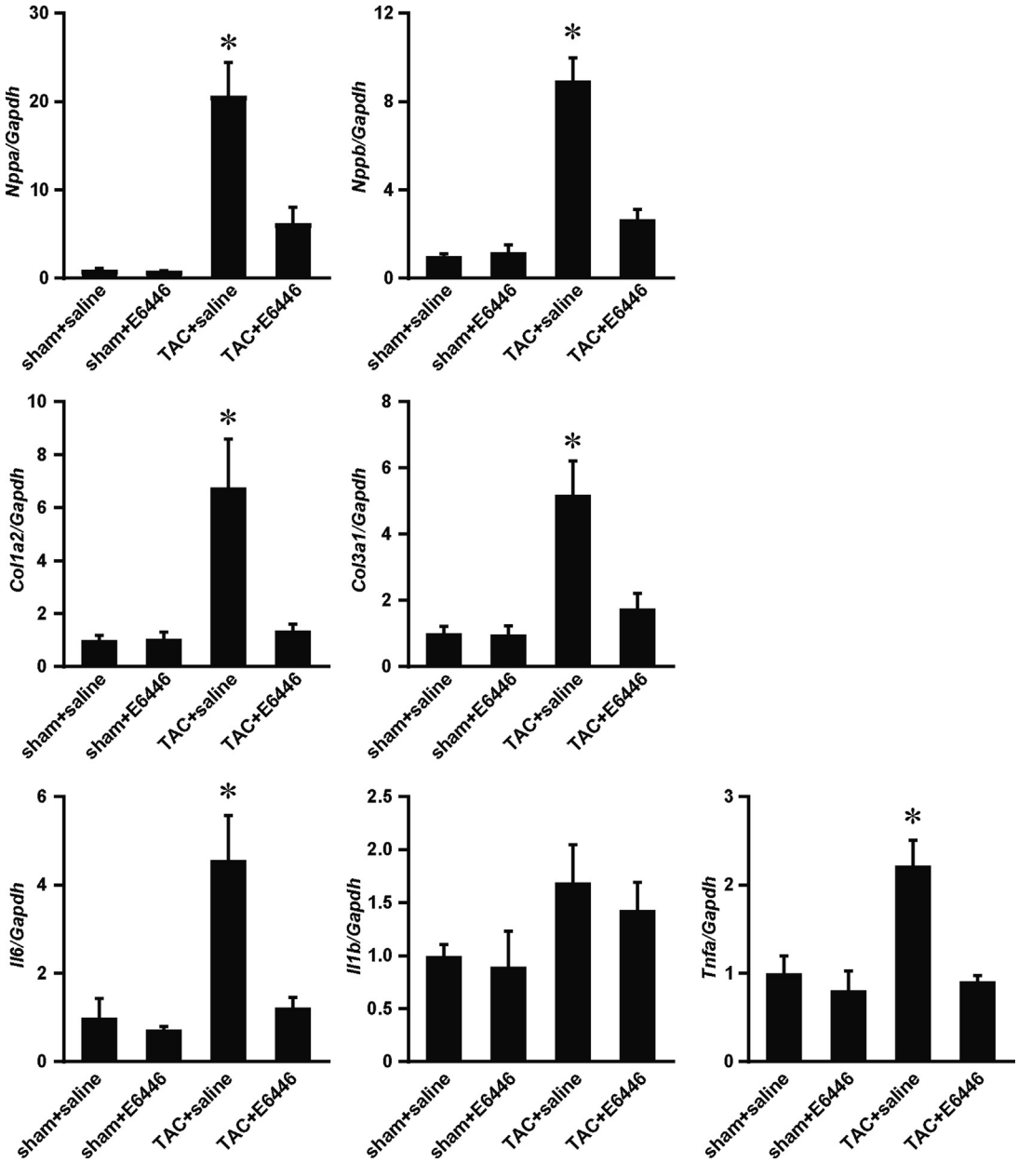

The treatment with E6446 was performed every 2 days from 2 days before TAC. The mice were analyzed 4 weeks after the operation (see Figure 10A). Data were normalized to the content of *Gapdh* mRNA. Values are mean ± SE (n = 4 in sham groups, n = 5 in TAC groups). *p < 0.05 versus all other groups. Abbreviations as in Figures 1, 3, and 4.

expressed as a proportion of the ventricles. For immunohistochemical analysis, frozen heart sections 5-μm thick were fixed in buffered paraformaldehyde and stained with anti-mouse CD45 (R and D Systems), CD68 (Bio-Rad, Hercules, California), Ly6G/C (BD Pharmingen, BD Biosciences, San Jose, California), CD3 (Abcam), and lysosome-associated membrane protein (LAMP) 2a (Thermo Fisher Scientific) antibodies. To measure the cardiomyocyte cross-sectional area, the frozen heart sections were stained with WGA-Alexa 555 (Thermo Fisher Scientific) for 1 h. The cardiomyocyte cross-sectional area was measured by tracing the outline of >100 cardiomyocytes in each section by using ImageJ software. For detection of

FIGURE 7 Attenuation of Inflammatory Responses With Treatment With E6446 Initiated Before TAC

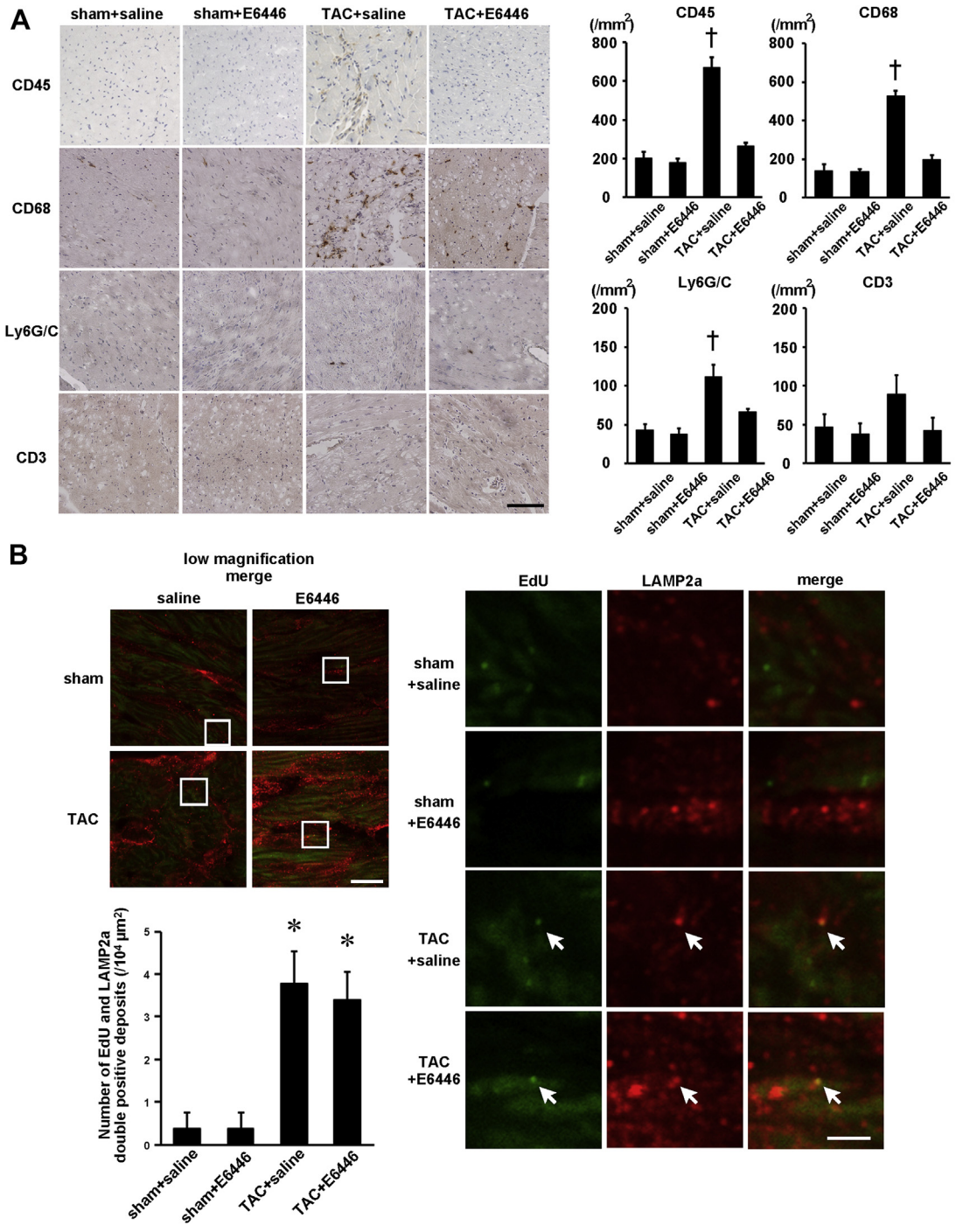

The treatment with E6446 was performed every 2 days from 2 days before TAC. The mice were analyzed 4 weeks after the operation (see Figure 10A). **(A)** Immunohistochemical analysis of the heart. Scale bar, 100 μm. The **right graphs** show the quantitative data for numbers of infiltrated inflammatory cells. **(B)** Deposition of mitochondrial deoxyribonucleic acid in lysosomes. Double staining of the heart sections with 5-ethynyl-2′-deoxyuridine (EdU) **(green)** and anti-lysosome-associated membrane protein (LAMP) 2a antibody **(red)**. Low-magnified images are shown in **left panels**. Scale bar, 10 μm. Higher magnified images of the squared areas are shown in **right panels**. Scale bar, 2 μm. **Arrows** indicate EdU and LAMP2a merged deposits. The **left graph** shows the number of EdU- and LAMP2a double-positive deposits. n = 3. Values are mean ± SE. *p < 0.05 versus sham-operated groups. †p < 0.05 versus all other groups. Abbreviations as in Figures 1 and 4.

FIGURE 8 Improvement of Echocardiographic Parameters and Lung Congestion After Treatment With E6446 Initiated After TAC

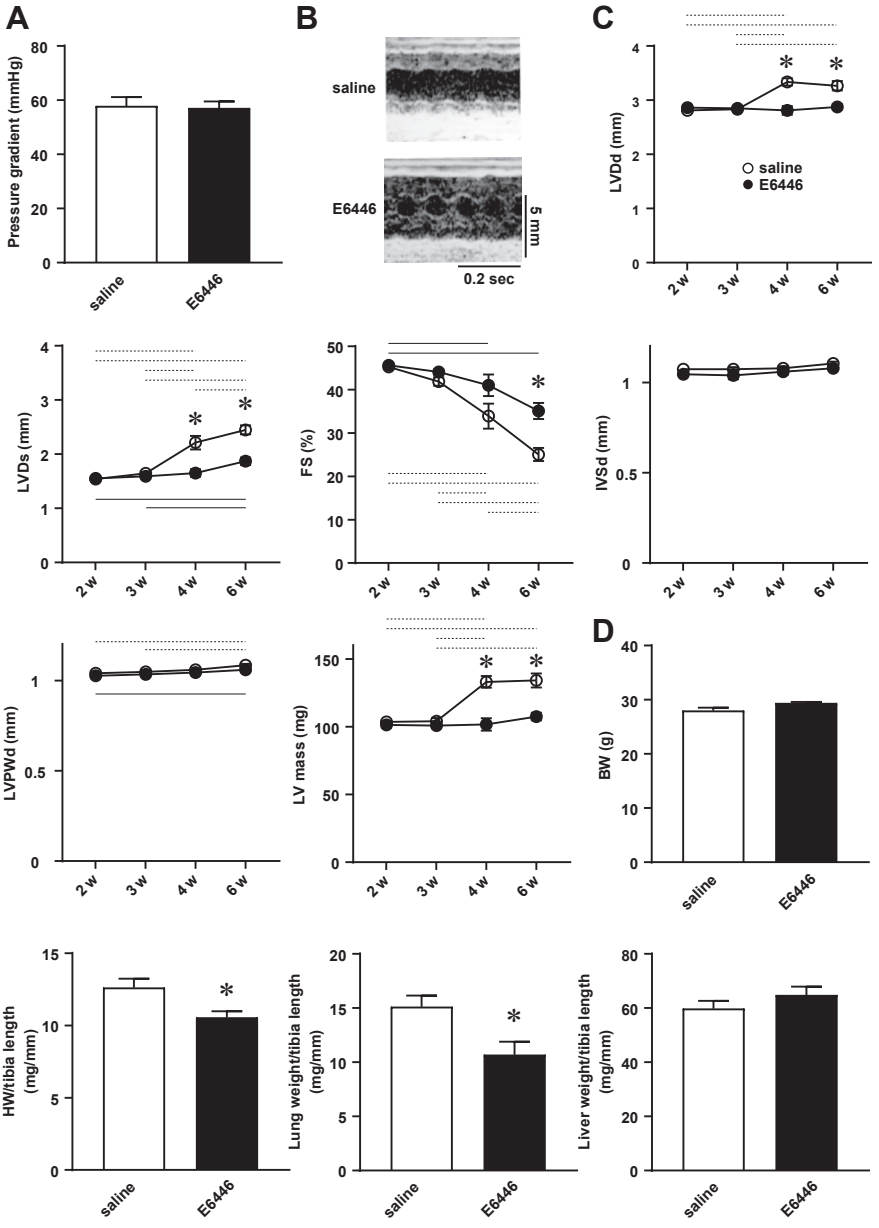

Two weeks after TAC, treatment with E6446 was performed every 2 days (see Figure 10B). Values are mean ± SE (n = 10). **(A)** Pressure gradient across TAC estimated by using a pressure monitor 1 week after operation. **(B)** Representative images of transthoracic M-mode echocardiographic tracing. Scale bars, 0.2 s and 5 mm, respectively. **(C)** Echocardiographic parameters. The parameters were examined for 6 weeks after TAC. **Open and closed circles** indicate saline-treated control groups and E6446-treated groups, respectively. The data were analyzed by using 2-way repeated measure analysis of variance followed by Tukey's post hoc test. *$p < 0.05$ between the 2 groups at the corresponding time point. **Dotted lines** indicate $p < 0.05$ between the 2 saline-treated control groups at different time points. **Solid lines** indicate $p < 0.05$ between the 2 E6446-treated groups at different time points. **(D)** Physiological parameters 6 weeks after the operation. *$p < 0.05$ versus saline-treated control group. Abbreviations as in Figures 1, 4, and 5.

mitochondrial DNA, mice were intraperitoneally injected with 5 mg of 5-ethynyl-2′-deoxyuridine (EdU) (Invitrogen) 1 day before sacrifice. EdU was detected by using a Click-iT EdU Alexa Fluor 488 Imaging Kit (Thermo Fisher Scientific) (7). EdU- and LAMP2a double-positive deposits were counted in 5 different areas per section in each mouse.

STATISTICAL ANALYSIS. Results are shown as mean ± SE. GraphPad Prism version 7.04 (GraphPad Software, La Jolla, California) was used for statistical analysis. A Student's *t*-test was used for a 2-group comparison; a 1-way analysis of variance followed by Tukey's post hoc test or 2-way repeated measure analysis of variance followed by Tukey's post hoc test were used for multiple comparisons. Significant differences were defined as $p < 0.05$.

TABLE 2 Echocardiographic Parameters of Mice Included in the E6646 Treatment Study 2 Weeks After TAC Operation

	Baseline		2 Weeks After TAC	
	Saline (n = 10)	E6446 (n = 10)	Saline (n = 10)	E6446 (n = 10)
LVDd, mm	2.30 ± 0.03	2.27 ± 0.03	2.81 ± 0.03*	2.86 ± 0.03*
LVDs, mm	0.88 ± 0.02	0.86 ± 0.02	1.54 ± 0.03*	1.55 ± 0.02*
LVFS, %	61.5 ± 0.71	62.3 ± 0.79	45.2 ± 0.77*	45.6 ± 0.43*
IVSd, mm	0.92 ± 0.01	0.92 ± 0.01	1.07 ± 0.01*	1.05 ± 0.01*
LVPWd, mm	0.86 ± 0.02	0.87 ± 0.01	1.04 ± 0.01*	1.03 ± 0.01*
Heart rate, beats/min	692 ± 3.9	695 ± 6.5	689 ± 7.2	672 ± 7.5
LV mass, mg	58.2 ± 1.4	58.9 ± 1.1	103.5 ± 3.1*	101.4 ± 2.1*

Values are mean ± SE. Thirty mice were subjected to TAC operation for 2 weeks. Ten mice with fractional shortening >50% were excluded from the study. The remaining 20 mice were randomized to the saline- and E6446-treated groups. The parameters of the mice were obtained 2 weeks after the operation by using echocardiography. *$p < 0.05$ vs. corresponding control at baseline.

Abbreviations as in Table 1.

RESULTS

EFFECT OF E6446 ON CYTOKINE mRNA PRODUCTION IN ISOLATED CARDIOMYOCYTES. Isolated cardiomyocytes were stimulated by a TLR9 ligand (e.g., ODN1668), a TLR4 ligand (e.g., LPS), or a TLR7 ligand (e.g., loxoribine) in the presence of increasing concentrations of E6446 (11,12). ODN1668 significantly increased the expression levels of *Il6*, IL-1B (*Il1b*), and *Tnfa* mRNAs (Figure 1A). Incubation of cardiomyocytes with E6446 significantly reduced the induction of *Il6*, *Il1b,* and *Tnfa* mRNAs in response to ODN1668. LPS significantly increased the expression levels of *Il6*, *Il1b,* and *Tnfa* mRNAs, whereas loxoribine significantly increased the expression levels of *Il1b* and *Tnfa* mRNAs but not *Il6* mRNA (Figures 1B and 1C). E6446 had no effect on the induction of the cytokine mRNAs induced by LPS or loxoribine.

Incubation of cardiomyocytes with CCCP diminished mitochondrial membrane potential (Figure 2A). Cardiomyocytes were stained with PicoGreen, a highly sensitive marker for DNA, and anti-LC3B antibody, a marker for autophagosomes. CCCP increased the number of PicoGreen and LC3B double-positive deposits, suggesting accumulation of DNA in autophagosomes or autolysosomes (Figure 2B). Incubation of cardiomyocytes with CCCP increased the levels of *Il6* and *Il1b* mRNAs (Figure 2C). E6446 had no effect on the number of PicoGreen and LC3B double-positive deposits, but it significantly reduced *Il6* and *Il1b* mRNA expression in CCCP-treated cardiomyocytes.

IN VIVO ADMINISTRATION OF E6446. To examine the in vivo efficacy of E6446 on inhibition of TLR9 and determine the experimental conditions for its administration in mice, 1.5 mg/mouse (60 mg/kg) of E6446 was orally administered to mice 3, 2, or 1 day before intraperitoneal injection of ODN1668. Two hours after the mice were administered ODN, the treated mice produced a higher level of IL-6 than control mice (Figure 3A). When E6446 was administered 2 or 1 day before ODN1668 injection, IL-6 levels were lower than the E6446-nontreated ODN1668-injected group and showed no significant difference compared with the control group without ODN1668 injection. When E6446 was administered 3 days before ODN1668 injection, the level of IL-6 did not differ from that in the nontreated group. To confirm the protein data, mRNA levels in the heart were measured (Figure 3B). The level of *Il6* mRNA in ODN1668-injected mouse hearts was higher than that in control hearts. When E6446 was administered 2 or 1 day before ODN1668 injection, *Il6* mRNA levels were lower than the E6446-nontreated ODN1668-injected group. When E6446 was administered 3 days before ODN1668 injection, the level of *Il6* mRNA differed from the control group but not from other ODN1668-injected groups. The level of *Il1b* mRNA in the E6446-nontreated ODN1668-injected mouse hearts was higher than that in the control hearts and showed a significant difference from that treated with E6446 1 and 2 days but not 3 days before ODN1668 injection; the levels of IL-1B protein were not significantly different among groups. The level of TNF-α in the ODN1668-injected mouse group was higher than that in the nontreated control group and in all the E6446-treated ODN1668-injected groups. The level of *Tnfa* mRNA in E6446-nontreated ODN1668-injected mouse hearts was higher than that in control hearts but showed no difference from all other groups. Thus, the inhibitory effect of E6446 on the induction of cytokines lasted over a period of 2 days, providing a rationale for every-other-day dosing.

The dose of E6446 necessary to inhibit the induction of cytokines was next examined. The serum level

FIGURE 9 Schematic Protocol to Determine the Experimental Conditions for E6446 Administration

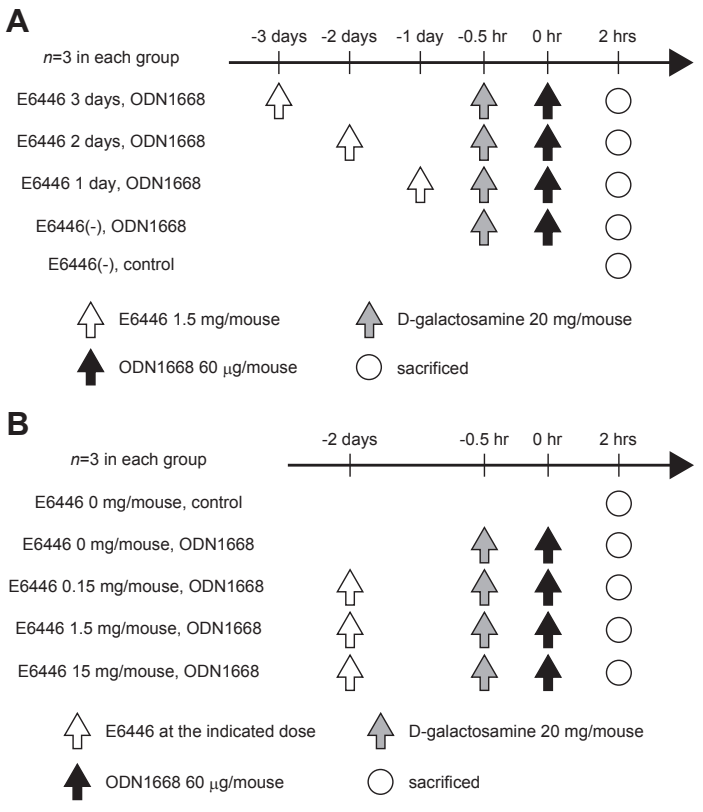

(A) Schematic protocol to examine the time dependence of cytokine protein and mRNA expression in the heart after injection with ODN1668 (n = 3 for each group). Mice were pretreated with E6446 1.5 mg/mouse for 1, 2, or 4 days before injection of 60 μg/mouse of ODN1668. Two hours after ODN1668 injection, mice were sacrificed for analysis, following treatment with D-galactosamine. **(B)** Schematic protocol to examine dose dependency in the inhibition of cytokine expression after ODN1668 injection with increasing concentrations of E6446 (n = 3 for each group). Two days after administration with the indicated dose of E6446, mice received 60 μg/mouse of ODN1668, following D-galactosamine injection. Two h later, mice were sacrificed for analysis. Abbreviations as in Figures 1 and 3.

of IL-6 and TNF-α protein in mice treated with 1.5 or 15 mg/mouse of E6446 was lower than that in nontreated mice or in mice treated with 0.15 mg/mouse of E6446 but did not differ from that in control mice (Figure 3C). ODN1668 injection increased serum levels of IL-1B protein. E6446 administration produced no significant inhibitory effect on the increase of IL-1B protein. The levels of *Il6*, *Il1b*, and *Tnfa* mRNAs in hearts treated with 1.5 or 15 mg/mouse were significantly lower than those in the hearts of nontreated mice (Figure 3D). Thus, 1.5 mg/mouse of E6446 was administered every 2 days in the following experiments.

PREVENTION OF THE DEVELOPMENT OF HEART FAILURE BY E6446. To investigate the efficacy of E6446 on the development of heart failure, mice orally received E6446 or saline 2 days before TAC and every 2 days for 4 weeks thereafter. There was no significant difference in pressure gradient across TAC between the E6446- and saline-treated groups 1 week after TAC (Figure 4A). Four weeks after TAC, saline-treated mice exhibited larger end-diastolic LV internal dimensions and end-systolic LV internal dimensions and lower fractional shortening than those in the sham-operated saline-treated group (Figures 4B and 4C). E6446 treatment significantly reduced LV chamber size and improved cardiac function in TAC-operated mice. TAC increased end-diastolic interventricular septal wall thickness (IVSd) and end-diastolic LV posterior wall thickness in saline- and E6446-treated mice. However, there were no significant differences in IVSd and end-diastolic LV posterior wall thickness between saline- and E6446-treated mice. LV mass was increased by TAC, and E6446 treatment attenuated the increase in LV mass in TAC-operated mice.

There was no significant difference in body weight between the 4 groups (Figure 5A). TAC-operated saline-treated mice exhibited increases in the heart weight-to-tibia length ratio and the lung weight-to-tibia length ratio. E6446 significantly attenuated cardiac hypertrophy and lung congestion. TAC increased the cross-sectional area of cardiomyocytes in saline-treated mice, and the increase was significantly attenuated by E6446 treatment (Figure 5B). *Nppa* and *Nppb* mRNAs increased in TAC-operated saline-treated mice. E6446 attenuated the increases induced by TAC (Figure 6). TAC-operated saline-treated mice exhibited cardiac fibrosis, which was diminished in E6446-treated mice (Figure 5C). The mRNA levels of *Col1a2* and *Col3a1* increased in TAC-operated saline-treated mice. E6446 attenuated the increase in the mRNAs.

ATTENUATION OF INFLAMMATION IN PRESSURE-OVERLOADED HEARTS BY E6446. TAC-operated saline-treated mice showed infiltration of $CD45^+$ cells, including $CD68^+$ macrophages in the heart, which was inhibited by treatment with E6446 (Figure 7A). Although increases in the mRNA expressions of *Il6* and *Tnfa* were detected in saline-treated TAC-operated mice, E6446 attenuated the induction of the mRNAs (Figure 6).

To label mitochondrial DNA, mice were injected with EdU 1 day before sacrifice. EdU specifically binds to mitochondrial DNA during active DNA synthesis in nondividing cardiomyocytes (7). LAMP2a is a marker for lysosomes. In TAC-operated saline- and

E6446-treated hearts, EdU and LAMP2a double-positive deposits were observed (Figure 7B). There was no significant difference in the number of the double-positive deposits between TAC-operated saline- and E6446-treated hearts.

SLOWING THE PROGRESSION OF HEART FAILURE BY E6446. Finally, the effect of E6446 on the progression of an already established disease was examined. Mice were subjected to TAC operation (Figure 8A) and divided into 2 groups 2 weeks later. There were no significant differences in echocardiographic parameters between the 2 groups, which already exhibited chamber dilatation and cardiac dysfunction (Table 2). The mice were then administered E6446 or saline every 2 days for 4 weeks. LV chamber dilatation and cardiac dysfunction progressively worsened with time in both groups (Figures 8B and 8C). End-diastolic LV internal dimensions, end-systolic LV internal dimensions, and LV mass showed no significant difference between saline- and E6446-treated TAC-operated mice until 3 weeks after TAC. However, the parameters were significantly smaller in E6446-treated mice than those in saline-treated mice 4 and 6 weeks after the operation. Fractional shortening was significantly higher in E6446-treated mice than that in saline-treated mice 6 weeks after TAC. There were no significant differences in IVSd and end-diastolic LV posterior wall thickness between the 2 groups at any time point. The heart weight-to-tibia length and lung weight-to-tibia length ratios were significantly reduced by E6446 treatment (Figure 8D). Schematic protocols to examine the effect of treatment of E6446 on cardiac phenotypes are described in Figures 9 and 10.

FIGURE 10 Schematic Protocols to Examine the Effect of E6446 on TAC-Induced Heart Failure

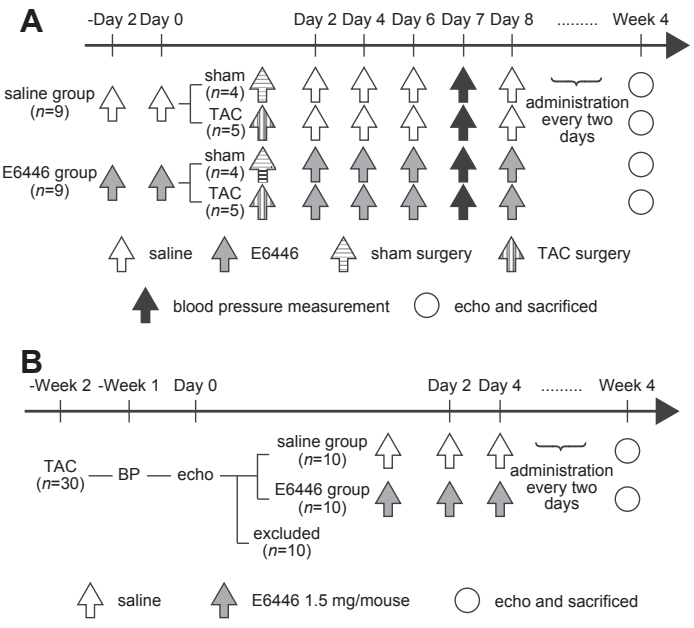

(A) Schematic protocol to examine the effect of treatment with E6446 initiated before TAC on cardiac phenotypes. E6446 (1.5 mg/mouse) (n = 9) or saline (n = 9) was administered every 2 days from 2 days before TAC. Blood pressure was measured 7 days after TAC. Four weeks after TAC, mice were subjected to echocardiographic analysis and sacrificed. **(B)** Schematic protocol to examine the effect of treatment with E6446 initiated after TAC on cardiac phenotypes. Thirty mice were subjected to TAC operation for 2 weeks. Ten mice with fractional shortening >50% were excluded from the study. The remaining 20 mice were randomized to the saline- and E6446-treated groups and then administered saline or E6446 (1.5 mg/mouse) every 2 days. Six weeks after TAC, mice were subjected to echocardiographic analysis and sacrificed. Abbreviations as in Figures 1 and 4.

DISCUSSION

The present study showed that E6446 prevents the development of pressure overload-induced heart failure when administered before the cardiac event and also suppresses the progression of heart failure when started after cardiac dysfunction manifested. We have reported that TLR9 is essential in producing inflammatory cytokines in failing hearts (7). TLRs are essential in driving the recruitment of inflammatory cells and production of cytokines during cardiac remodeling (13). E6446 prevents cellular events activated by TLR9, exerting broader inhibitory effects on inflammatory cytokine production, and thus the treatment of heart failure with the inhibitor has an advantage over the therapy neutralizing only 1 cytokine. The near-complete rescue of TAC-induced LV dilatation and dysfunction by E6446 pretreatment suggests that the TLR9-signaling pathway is the dominant pathway for inducing adverse ventricular remodeling, with a limited role for other pathways such as nucleotide-binding domain leucine-rich repeat containing protein 3 (NLRP3) and cyclic GMP-AMP synthase (cGAS)-stimulator of interferon genes (STING) activation by mitochondrial DNA released in the cytosol in the setting of mitophagy dysfunction (14).

In human peripheral blood mononuclear cells or mouse spleen cells, E6446 diminished IL-6 production in response to CpG ODN (8). A 100-fold higher concentration of E6446 inhibited cytokine production in response to the imidazoquinoline compound R848, which is a TLR7/8 agonist (15). When C57BL/6 mice were orally treated with E6446, E6446 completely inhibited CpG ODN-induced IL-6 production in sera but not R848- and LPS-mediated cytokine production (8). Consistent with these results, our findings indicate that E6446 specifically

inhibited the expression of inflammatory cytokines through a TLR9-dependent pathway but not TLR4- or TLR7-dependent pathways in adult cardiomyocytes. Thus, E6446 has high specificity to TLR9. In mouse bone marrow-derived dendritic cells, E6446 potently inhibited IL-6 production induced by CpG ODN but not by TLR3 ligands (9). However, E6446 was a potent inhibitor of IL-6 induction by single-stranded RNA, a TLR7/8 agonist, but a relatively poor inhibitor of IL-6 induction by R848, suggesting that the ability of E6446 to suppress TLR7/8 might be ligand dependent. Based on our data showing the importance of TLR9 signaling in the development of inflammation and heart failure and its specificity to TLR9 in cardiomyocytes, the cardioprotective action of E6446 is TLR9 mediated. However, we cannot exclude the possibility that TLR7/8 is involved in the effect of E6446 on the development of heart failure.

E6446 inhibits in vitro DNA–TLR9 interaction via an association with DNA but not with TLR9 (9). Furthermore, E6446 accumulates in the intracellular acidic compartment. Mitochondrial DNA is accumulated in autolysosome and coexists with TLR9 in failing hearts (7). DNase II activity was up-regulated in hypertrophied hearts but not in failing hearts. The incomplete digestion of mitochondrial DNA would be due to the loss of up-regulation of DNase II activity. Mitophagy impairment occurs in the TAC-induced mouse heart failure model (16). Thus, it is also possible that impairment of mitophagy or lysosomal permeabilization or lysosomal dysfunction might result in the accumulation of mitochondrial DNA in autolysosome. Our data in this study showed that there was no significant difference in the number of EdU and LAMP2a double-positive deposits between TAC-operated saline- and E6446-treated hearts. This outcome suggests that E6446 has no effect on mitochondrial DNA accumulation in autolysosomes. Thus, we can assume that the E6446 administered accumulates in lysosomes in the cardiomyocytes and interacts with mitochondrial DNA. When E6446 was orally administered to mice before TAC, E6446 inhibited TLR9 signaling by interfering with the mitochondrial DNA–TLR9 interaction and subsequent development of inflammation and heart failure.

We showed that *Tlr9*$^{-/-}$ mice are more resistant to pressure overload than control mice, and inhibitory ODN to TLR9 (ODN2088) improved survival in TAC-operated wild-type mice when administered before TAC (7). However, administration of a drug before cardiac events is not clinically relevant. The results indicate that E6446 can slow the development of heart failure even after cardiac dysfunction manifested. Thus, E6446 or other immunomodulatory therapy can be used to prevent or delay pressure overload-induced heart failure.

STUDY LIMITATIONS. This study shows the therapeutic effects of a TLR9 inhibitor, E6446, on mouse pressure-overload heart failure model. Obviously, further studies are necessary to translate the findings into human heart failure therapy. TAC-induced mouse model does not fully represent the complex features of clinical heart failure. To establish the clinical feasibility of E6446 treatment for heart failure, the effects of E6446 on different heart failure models have to be examined, such as myocardial infarction. In addition, we used young healthy mice in this study. However, in most patients, and particularly in elderly patients, heart failure is accompanied by a range of comorbidities, such as hypertension, diabetes mellitus, renal dysfunction and hyperlipidemia. Such factors may influence on the cardioprotective effect of E6446 in heart failure. Thus, further investigation using various disease models is required to clarify the clinical target of E6446 treatment. Furthermore, it will be important to validate the findings in large animal models and ultimately in human patients. It remains unclear whether mitochondrial DNA is accumulated in autolysosomes and mitochondrial DNA-TLR9 axis is involved in the genesis of inflammation in human failing hearts.

CONCLUSIONS

Heart failure is the result of various cardiac diseases such as myocardial infarction, high blood pressure, cardiomyopathy, valvular diseases, arrhythmia, and congenital heart diseases. Elevated levels of inflammatory mediators have been identified in patients with heart failure, including heart failure with reduced and preserved ejection fraction, as well as short-term decompensated heart failure (1). Thus, investigation of the involvement of the TLR9-signaling pathway in other mouse or larger animal heart failure models and various types of human heart failure is warranted. We ultimately will be able to identify subsets of patients with heart failure who will benefit from inhibition of TLR9 signaling.

ACKNOWLEDGMENTS The authors thank Eisai Inc. for the generous gift of E6446, and Ms. Yuri Kiura for technical assistance.

ADDRESS FOR CORRESPONDENCE: Dr. Kinya Otsu, School of Cardiovascular Medicine and Sciences, King's College London British Heart Foundation Centre of Excellence, 125 Coldharbour Lane, London SE5 9NU, United Kingdom. E-mail: kinya.otsu@kcl.ac.uk.

PERSPECTIVES

COMPETENCY IN MEDICAL KNOWLEDGE: Heart failure is a major health threat in the developed countries with high morbidity and mortality. Novel and effective therapeutic agents against heart failure need to be developed. Inflammation and proinflammatory cytokines play an important role in the pathogenesis of heart failure. Inflammatory mediators can be therapeutic targets in heart failure.

TRANSLATIONAL OUTLOOK: A TLR9 inhibitor, E6446, exerted a beneficial effect on attenuating the development or progression of heart failure in a pressure overload–induced mouse model. E6446 treatment has an advantage over targeted anticytokine approaches using biological response modifiers, because it modulates a broad spectrum of inflammatory mediators. Thus, it may be a new promising therapeutic agent for human heart failure.

REFERENCES

1. Mann DL. Innate immunity and the failing heart: the cytokine hypothesis revisited. Circ Res 2015;116:1254–68.

2. Chung ES, Packer M, Lo KH, Fasanmade AA, Willerson JT. Randomized, double-blind, placebo-controlled, pilot trial of infliximab, a chimeric monoclonal antibody to tumor necrosis factor-alpha, in patients with moderate-to-severe heart failure: results of the anti-TNF Therapy Against Congestive Heart Failure (ATTACH) trial. Circulation 2003;107:3133–40.

3. Mann DL, McMurray JJ, Packer M, et al. Targeted anticytokine therapy in patients with chronic heart failure: results of the Randomized Etanercept Worldwide Evaluation (RENEWAL). Circulation 2004;109:1594–602.

4. Deng GM, Nilsson IM, Verdrengh M, Collins LV, Tarkowski A. Intra-articularly localized bacterial DNA containing CpG motifs induces arthritis. Nat Med 1999;5:702–5.

5. Hemmi H, Takeuchi O, Kawai T, et al. A Toll-like receptor recognizes bacterial DNA. Nature 2000;408:740–5.

6. Saito T, Sadoshima J. The molecular mechanisms of mitochondrial autophagy/mitophagy in the heart. Circ Res 2015;116:1477–90.

7. Oka T, Hikoso S, Yamaguchi O, et al. Mitochondrial DNA that escapes from autophagy causes inflammation and heart failure. Nature 2012;485:251–5.

8. Franklin BS, Ishizaka ST, Lamphier M, et al. Therapeutical targeting of nucleic acid-sensing Toll-like receptors prevents experimental cerebral malaria. Proc Natl Acad Sci U S A 2011;108:3689–94.

9. Lamphier M, Zheng W, Latz E, et al. Novel small molecule inhibitors of TLR7 and TLR9: mechanism of action and efficacy in vivo. Mol Pharmacol 2014;85:429–40.

10. Nakai A, Yamaguchi O, Takeda T, et al. The role of autophagy in cardiomyocytes in the basal state and in response to hemodynamic stress. Nat Med 2007;13:619–24.

11. Hoshino K, Takeuchi O, Kawai T, et al. Cutting edge: Toll-like receptor 4 (TLR4)-deficient mice are hyporesponsive to lipopolysaccharide: evidence for TLR4 as the lps gene product. J Immunol 1999;162:3749–52.

12. Florian H, Parviz AN, Hiroaki H, et al. The Toll-like receptor 7 (TLR7)-specific stimulus loxoribine uncovers a strong relationship within the TLR7, 8 and 9 subfamily. Eur J Immunol 2003;33:2987–97.

13. Mann DL. Inflammatory mediators and the failing heart: past, present, and the foreseeable future. Circ Res 2002;91:988–98.

14. Nakayama H, Otsu K. Mitochondrial DNA as an inflammatory mediator in cardiovascular diseases. Biochem J 2018;475:839–52.

15. Jurk M, Heil F, Vollmer J, et al. Human TLR7 or TLR8 independently confer responsiveness to the antiviral compound R-848. Nat Immunol 2002;3:499.

16. Shirakabe A, Zhai P, Ikeda Y, et al. Drp1-dependent mitochondrial autophagy plays a protective role against pressure overload-induced mitochondrial dysfunction and heart failure. Circulation 2016;133:1249–63.

KEY WORDS heart failure, mitochondria, pressure overload, Toll-like receptor 9

JACC: BASIC TO TRANSLATIONAL SCIENCE VOL. 4, NO. 3, 2019

PRECLINICAL RESEARCH

Successful Reconstruction of the Right Ventricular Outflow Tract by Implantation of Thymus Stem Cell Engineered Graft in Growing Swine

Ambra Albertario, PhD, Megan M. Swim, PhD, Eltayeb Mohamed Ahmed, MCh, Dominga Iacobazzi, PhD, Michael Yeong, MBBS, Paolo Madeddu, MD, Mohamed T. Ghorbel, PhD,* Massimo Caputo, MD*

VISUAL ABSTRACT

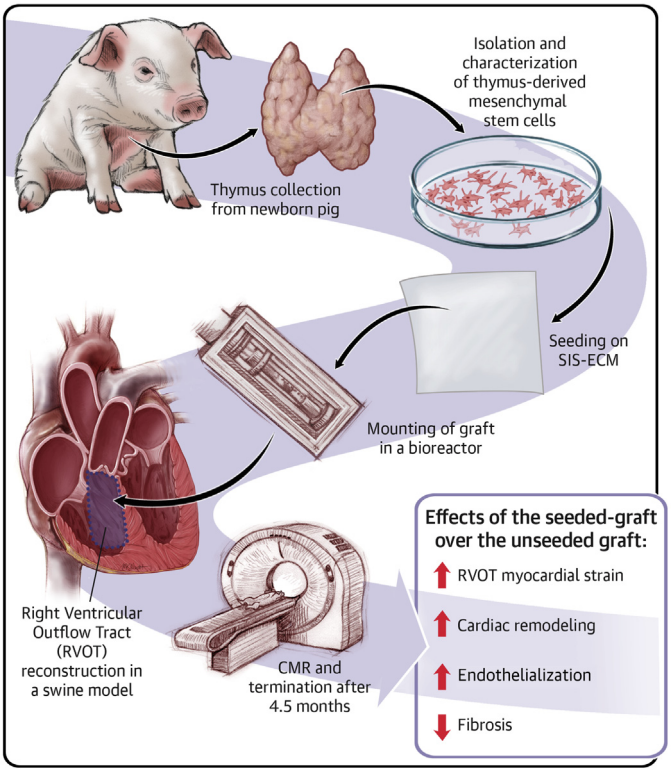

Albertario, A. et al. J Am Coll Cardiol Basic Trans Science. 2019;4(3):364–84.

HIGHLIGHTS

- **T-MSCs were isolated from the thymus gland of new born pigs, expanded, characterized and seeded onto a commercially available scaffold.**
- **The seeded-grafts were cultured within a bioreactor and then used to reconstruct the RVOT of a growing swine model.**
- **Pigs were followed up for 4.5 months; then scanned with a cardiac magnetic resonance and terminated to harvest the implants.**
- **By comparing the outcome of the seeded-grafts to the unseeded-ones used as control, we observed a reduced fibrosis and an improved RVOT strain, cardiac remodeling and endothelialization.**

From the University of Bristol, Bristol Heart Institute, Bristol, United Kingdom. *Drs. Ghorbel and Caputo contributed equally to this paper and are joint senior authors. This study was supported by grants from the Sir Jules Thorn Charitable Trust (Drs. Caputo and Madeddu), the Enid Linder Foundation (Drs. Caputo and Ghorbel), the British Heart Foundation (Dr. Caputo), the National Institute for Health Research Bristol Biomedical Research Unit in Cardiovascular Medicine (Dr. Caputo), and the Medical Research Council (Drs. Madeddu, Caputo, and Ghorbel). All other authors have reported that they have no relationships relevant to the contents of this paper to disclose.

All authors attest they are in compliance with human studies committees and animal welfare regulations of the authors' institutions and U.S. Food and Drug Administration guidelines, including patient consent where appropriate. For more information, visit the *JACC: Basic to Translational Science* author instructions page.

Manuscript received September 17, 2018; revised manuscript received January 29, 2019, accepted February 2, 2019.

ISSN 2452-302X https://doi.org/10.1016/j.jacbts.2019.02.001

SUMMARY

Graft cellularization holds great promise in overcoming the limitations associated with prosthetic materials currently used in corrective cardiac surgery. In this study, the authors evaluated the advantages of graft cellularization for right ventricular outflow tract reconstruction in a novel porcine model. After 4.5 months from implantation, improved myocardial strain, better endothelialization and cardiomyocyte incorporation, and reduced fibrosis were observed in the cellularized grafts compared with the acellular grafts. To the authors' knowledge, this is the first demonstration of successful right ventricular outflow tract correction using bioengineered grafts in a large animal model. (J Am Coll Cardiol Basic Trans Science 2019;4:364–84)

Cardiac tissue engineering holds great promise for definitive correction of congenital heart disease. By seeding cells on a biodegradable scaffold, this approach is aimed at developing a viable graft capable of growing and remodeling in parallel with the recipient's organ. Once implanted in vivo, an ideal biofunctional graft is remodeled and eventually replaced by the host's own extracellular matrix (1). Several cell types have been used for cardiac tissue engineering, including mesenchymal stem cells (MSCs) (2), induced pluripotent stem cells (3), endothelial cells (ECs) (4), and pericytes (5). In particular, MSCs are a preferred choice because of their immune-privileged nature, multilineage differentiation potential, and ability to promote tissue healing by paracrine mechanisms (6,7). Furthermore, MSCs can be isolated from various tissues and organs, including bone marrow, umbilical cord, adipose tissue, and thymus (8,9). Infants who undergo palliative cardiac surgery for tetralogy of Fallot often have the thymus removed to facilitate access to the heart. Hence, the explanted gland represents a convenient source of autologous MSCs for use during definitive correction of congenital cardiac defects.

To date, cardiac tissue engineering has been applied principally to the reconstruction of pulmonary arteries or valves, whereas problems associated with the right ventricular outflow tract (RVOT) remain an unmet clinical need. In fact, surgical correction of RVOT obstruction is reportedly associated with the development of aneurysmal or akinetic regions and an arrhythmogenic substrate (10). These complications have long-term consequences for outcomes in patients with tetralogy of Fallot (11).

In this paper, we report a controlled, randomized study in growing female piglets, comparing the feasibility, safety, and efficacy of RVOT reconstruction using a graft made of small intestinal submucosa-derived extracellular matrix (SIS-ECM) or the same graft engineered using porcine thymus-derived MSCs (T-MSCs).

METHODS

ANIMALS. Animals were treated in accordance with the Guide for the Care and Use of Laboratory Animals published by the National Institutes of Health in 1996 and conforming to the Animals (Scientific Procedures) Act of 1986. In vivo graft implantation was carried out under United Kingdom Home Office project license PPL 30/3019.

ISOLATION AND EXPANSION OF T-MSCs. T-MSCs were isolated from newborn female piglets as previously described (2). Briefly, cells were mechanically and enzymatically digested with collagenase I for 2 h at 37°C. The isolated cells were selected by adherence to plastic and expanded until passages 3 to 5.

NEONATAL RAT CARDIOMYOCYTE ISOLATION. Cardiomyocytes (CMs) were isolated from 1- to 3-day-old Wistar rats (Charles River Laboratories, Wilmington, Massachusetts). Three litters of neonatal rats were killed by means of decapitation, according to schedule 1 of the Animals (Scientific Procedures) Act. The hearts were washed with 1% penicillin/streptomycin (P/S) (Life Technologies, Carlsbad, California) phosphate-buffered saline (PBS) (Life Technologies), minced into thin pieces, and dissociated with 0.05% trypsin and 0.02% ethylenediaminetetraacetic acid in PBS for 15 min at 37°C. Cell suspension was filtered using a 70-μm nylon mesh, and enzyme activity was stopped with fetal bovine serum (FBS; Thermo Fisher Scientific, Waltham, Massachusetts). A second digestion was performed with 0.1% trypsin and 0.02% ethylenediaminetetraacetic acid in PBS for 15 min at 37°C, after which the cell fraction was filtered and the enzyme blocked with FBS. This procedure was repeated 3 more times. Then the cell fractions were

ABBREVIATIONS AND ACRONYMS

CM = cardiomyocyte

cMYH = cardiac myosin heavy chain

Cx-43 = connexin-43

DMEM = Dulbecco's modified Eagle's medium

EC = endothelial cell

FBS = fetal bovine serum

IL = interleukin

IsoB4 = isolectin B4

MSC = mesenchymal stem cell

PBS = phosphate-buffered saline

PS = penicillin/streptomycin

RT = room temperature

RV = right ventricular

RVOT = right ventricular outflow tract

RVOT-MS = fractional area of change in the right ventricular outflow tract

SIS-ECM = small intestinal submucosa-derived extracellular matrix

T-MSC = thymus-derived mesenchymal stem cell

VMSC = vascular smooth muscle cell

TABLE 1 Antibodies for Immunohistochemistry

Primary Antibody	Primary Antibody Dilution	Manufacturer	Secondary Antibody	Secondary Antibody Dilution	Manufacturer
Mouse anti-alpha-sarcomeric actinin	1:100	Abcam	Goat antimouse-Alexa Fluor 488	1:400	Abcam
Mouse anti-alpha-smooth muscle actin	1:200	Abcam	Goat antimouse-Alexa Fluor 488	1:400	Abcam
Mouse anti-cardiac myosin heavy chain	1:150	Thermo Fisher Scientific	Goat antimouse-Alexa Fluor 488	1:400	Abcam
Rabbit anti-connexin-43	1:100	Santa Cruz Biotechnology	Goat antirabbit-Alexa Fluor 546	1:400	Abcam
Mouse anti-discoidin domain receptor 2	1:100	Santa Cruz Biotechnology	Goat antimouse-Alexa Fluor 488	1:400	Abcam
Isolectin B4-biotin	1:100	Life Technologies	Streptavidin-Alexa Fluor 488	1:200	Life Technologies
Rabbit anti-Ki67	1:200	Abcam	Goat antirabbit-Alexa Fluor 546	1:400	Abcam
Mouse anti-metalloproteinase 1	1:200	Abcam	Goat antimouse-Alexa Fluor 488	1:400	Abcam
Mouse anti-smooth muscle myosin heavy chain	1:100	Dako	Goat antimouse-Cy3	1:300	Jackson ImmunoResearch Laboratories

Primary antibodies used for immunofluorescent staining and respective secondary antibodies used for detection.

pooled together and centrifuged for 5 min at 100*g*. The resulting pellet was resuspended in low-glucose Dulbecco's modified Eagle's medium (DMEM; Life Technologies), seeded onto a T75 flask and incubated for 1 h in a humidified chamber at 37°C in 5% CO_2 (incubator) to allow as many fibroblasts as possible to attach to the plastic. The cell suspension was then harvested, centrifuged, and resuspended into 1% FBS and 1% P/S DMEM:M199 medium (Thermo Fisher Scientific) in a ratio of 1:1 and seeded onto previously coated plates with 0.1% gelatin (Sigma-Aldrich, St. Louis, Missouri).

FLOW CYTOMETRY. Fluorescence-activated cell sorting analysis was used to determine cell surface marker expression. The protocol was performed as described by Iacobazzi et al. (2). The following primary antibodies were used: 1:10 CD31-PE (Bio-Rad, Hercules, California), 1:600 CD44-APC (Thermo Fisher Scientific), 1:25 CD45-FITC (Bio-Rad), 1:10 CD73-APC (R and D Systems, Minneapolis, Minnesota), 1:20 CD90-PE (BioLegend, San Diego, California), and 1:5 CD105-PE (LSBio, Seattle, Washington). Analysis was performed on a NovoCyte flow cytometer (ACEA Bioscience, San Diego, California) using NovoExpress (ACEA Bioscience) for data collection and FlowJo (TreeStar, Ashland, Ohio) for analysis.

IN VITRO MULTILINEAGE DIFFERENTIATION. Multilineage differentiation into osteocytes, adipocytes, and chondrocytes was performed with MSCs at passages between 3 and 5. Cells were cultured in alpha-MEM medium with specific StemXVivo supplement kits (R and D Systems) for different time points. Osteogenic differentiation was assessed after 3 weeks of culture using alizarin red (Sigma-Aldrich) to detect calcium deposition. Oil red O staining (Sigma-Aldrich) was used to detect lipid accumulation of cells undergoing 2 weeks of adipogenic differentiation. Alcian blue staining (Sigma-Aldrich) was used to determine chondrogenic cartilage formation after 3 weeks of cell culture.

SIS-ECM CELLULARIZATION. Pieces of SIS-ECM (CorMatrix Cardiovascular, Roswell, Georgia) approximately 7 cm^2 were soaked in DMEM for 24 h in a 1% agarose (Sigma-Aldrich) coated plate. The scaffold was then seeded with P3 swine T-MSCs at a density of 5×10^5 cells/cm^2 and cultured in growing medium for 1 week under static conditions in an incubator. The graft was then stitched to the rotating arm of a InBreath bioreactor (Harvard Apparatus, Cambridge, Massachusetts) and stitched back to itself as to fashion a conduit shape with the cells facing the outer side of the scaffold. The bioreactor chamber was filled with growing medium and connected to a motor platform placed at 37°C in a CO_2 incubator. The rotation was initially set at 0.5 rpm and slowly increased within 24 h to the final speed of 2 rpm, which was maintained for 1 week.

CELL VIABILITY. To determine cell viability on the engineered scaffolds, a Live/Dead Viability/Cytotoxicity Kit for mammalian cells (Thermo Fisher Scientific) was used according to the manufacturer's instructions. Fluorescence imaging was carried out using a Zeiss Axio Observer.Z1 with Zen Blue software (Carl Zeiss, Oberkochen, Germany).

MECHANICAL TESTING. Unseeded and seeded SIS-ECM pieces were analyzed for mechanical properties using an Instron 3343B machine (Instron, Norwood, Massachusetts) with pneumatic grips and a 100-N load cell. Crosshead speed was set at 10 mm/min. Samples were measured for tensile stress at maximum load and Young's modulus using Bluehill software (Instron).

SCANNING ELECTRON MICROSCOPY. Samples were fixed, washed, and completely dehydrated as previously described (2). Surface topography was imaged using a Quanta 200 FEI field emission scanning electron microscope (Thermo Fisher Scientific).

FIGURE 1 Phenotypic and Functional Characterization of Thymus-Derived Mesenchymal Stem Cells

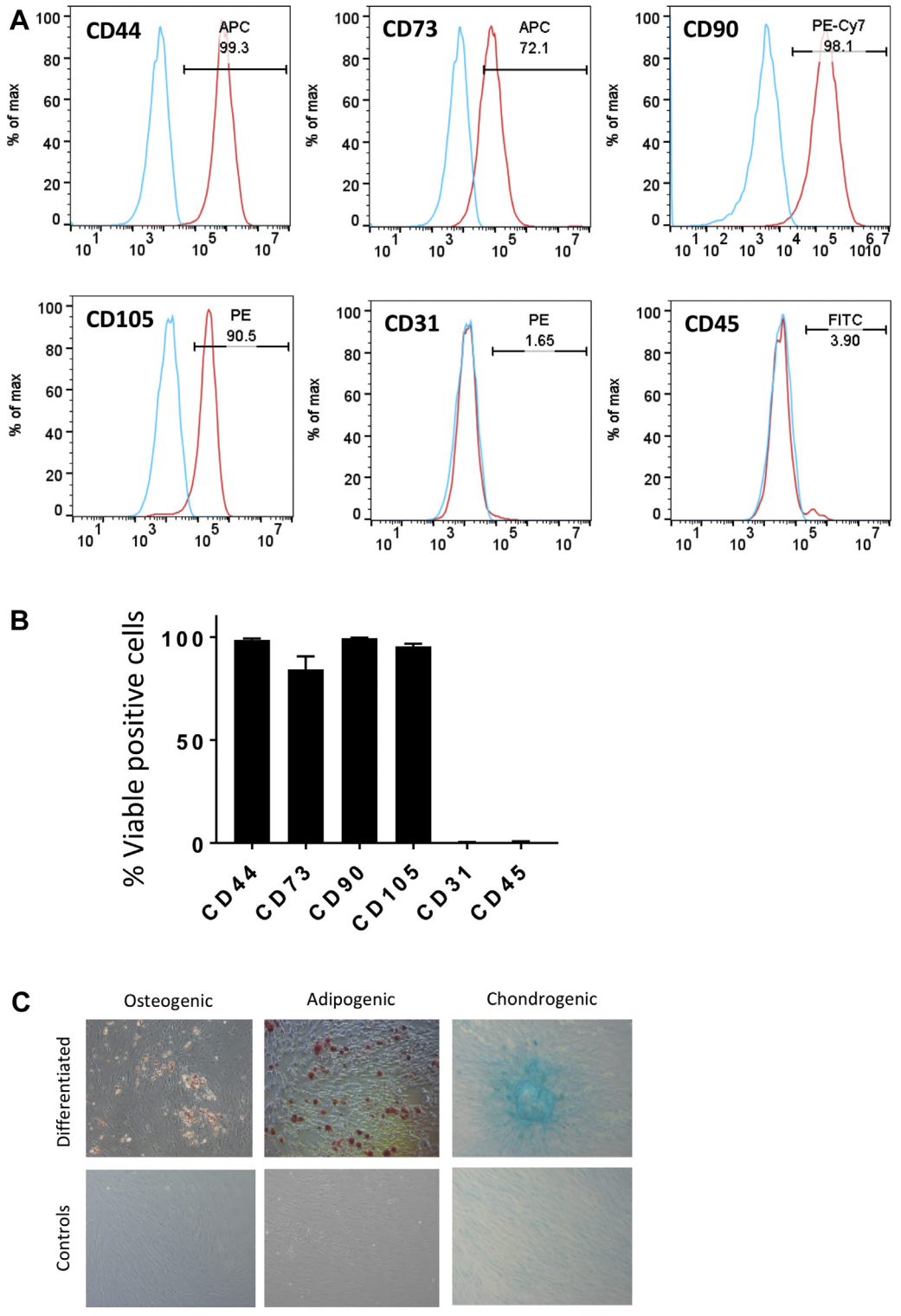

(A) Flow cytometry representative histograms illustrate the expression of CD44, CD73, CD90, and CD105 and lack of endothelial and hematopoietic markers on thymus-derived mesenchymal stem cells. **(B)** Bar chart showing the proportion of viable cells positive to the investigated markers (n = 4; mean ± SE). **(C)** Multilineage differentiation of the cells into osteocytes, adipocytes. Nontreated cells were used as negative controls.

FIGURE 2 Biological and Mechanical Assessment of the Unseeded and Cell-Seeded Grafts

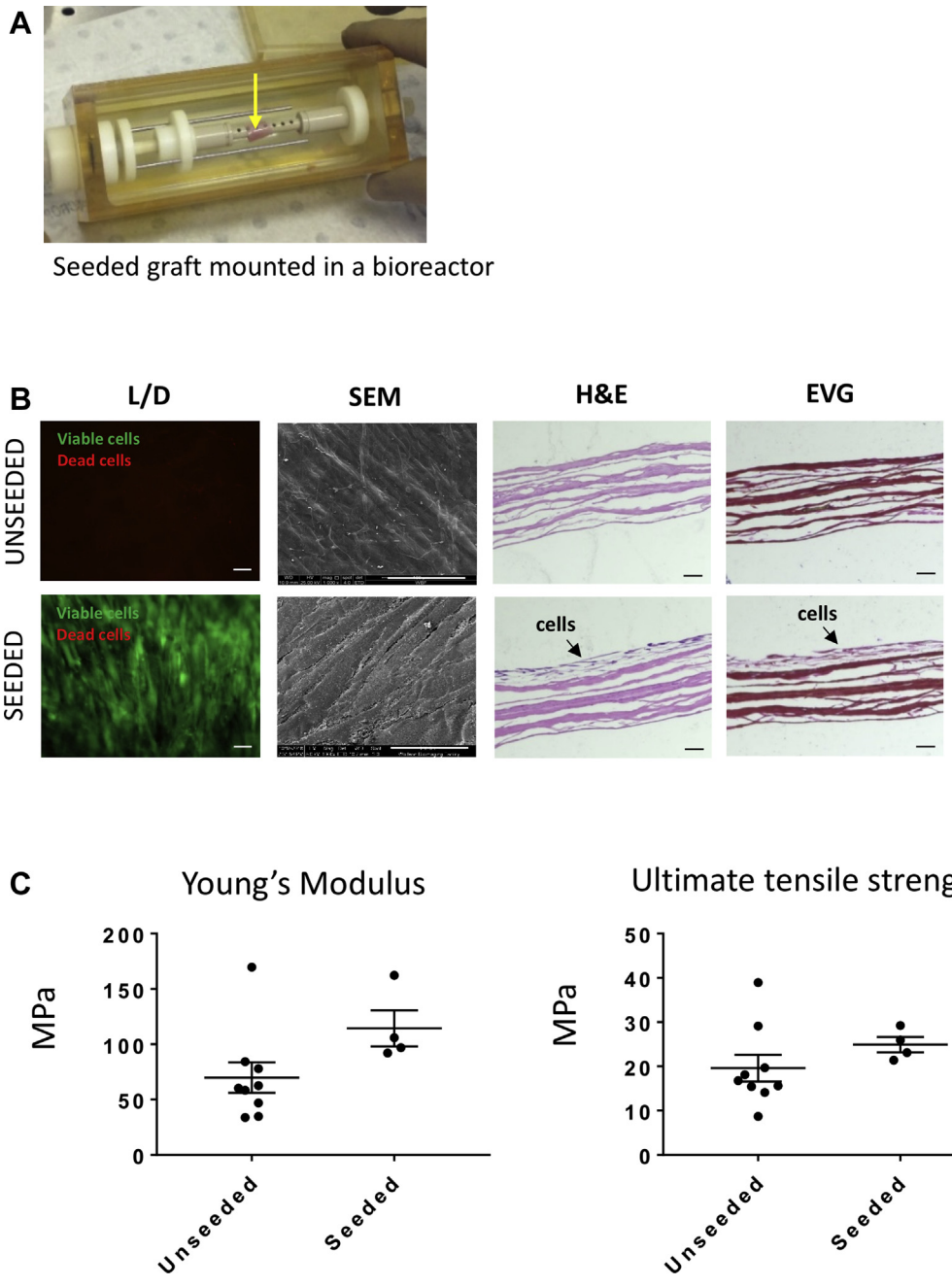

(A) Seeded graft **(arrow)** is mounted and cultured in a bioreactor. **(B)** Viable (L) and dead (D) cells attached to the seeded scaffold. Scanning electron microscopic (SEM) images illustrate the topography of the unseeded graft and a confluent layer of oriented cells growing on the seeded sample. Scale bars, 100 μm. Hematoxylin and eosin (H and E) staining shows lack of nuclei in the unseeded scaffold and a multilayer of cells in the seeded graft. Elastic van Gieson (EVG) staining confirmed the capacity of the seeded cells to produce their own extracellular matrix. Scale bars, 50 μm. **(C)** Young's modulus and ultimate tensile strength of the unseeded and seeded grafts showed no significant differences between the 2 groups ($n = 4$; mean ± SE).

FIGURE 3 **in Vivo Right Ventricular Outflow Tract Reconstruction and Operated Animals Follow-Up**

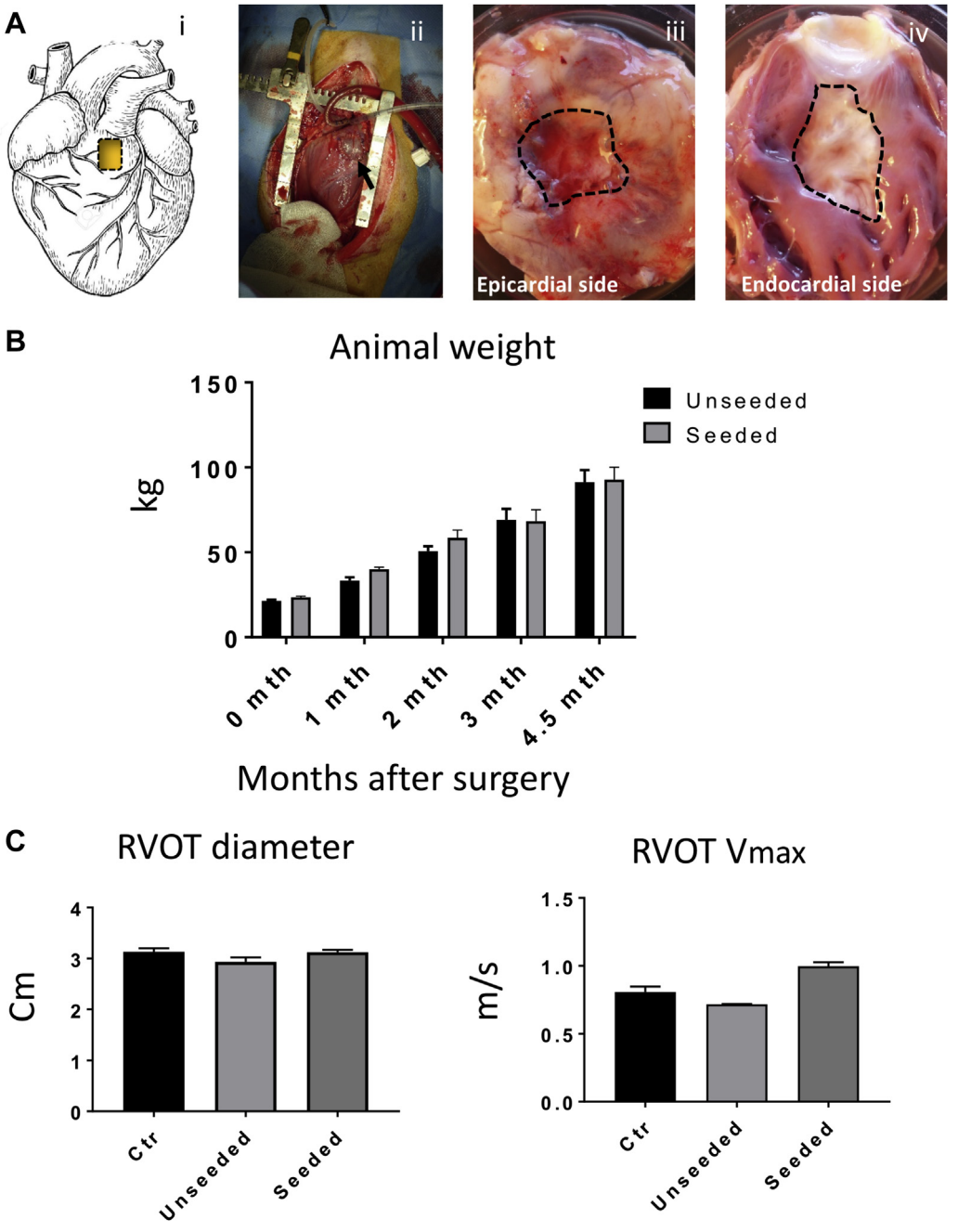

(A) Cartoon **(i)** and macroscopic image **(ii)** showing the site of the implant on the right ventricular outflow tract (RVOT). Gross analysis of the explants after 4.5 months in vivo shows the epicardial **(iii)** and endocardial **(iv)** sides of the graft **(dotted line)**. **(B)** The operated pigs increased their body weight at a normal rate. **(C)** Doppler echocardiographic measurements of the right ventricle immediately before termination demonstrate comparable RVOT diameter and maximum velocity (Vmax) in the operated animals and unoperated control (Ctr) pigs. **(D)** Representative cardiac magnetic resonance images of right ventricular diastolic and systolic area (encircled in **green**) before surgery and 4.5 months thereafter. The patches could be visualized as a small bump protruding from the right ventricle **(arrows)**. **(E)** RVOT myocardial strain measured at termination was greater in the animals implanted with seeded grafts. See Supplemental Video 1.

Continued on the next page

FIGURE 3 Continued

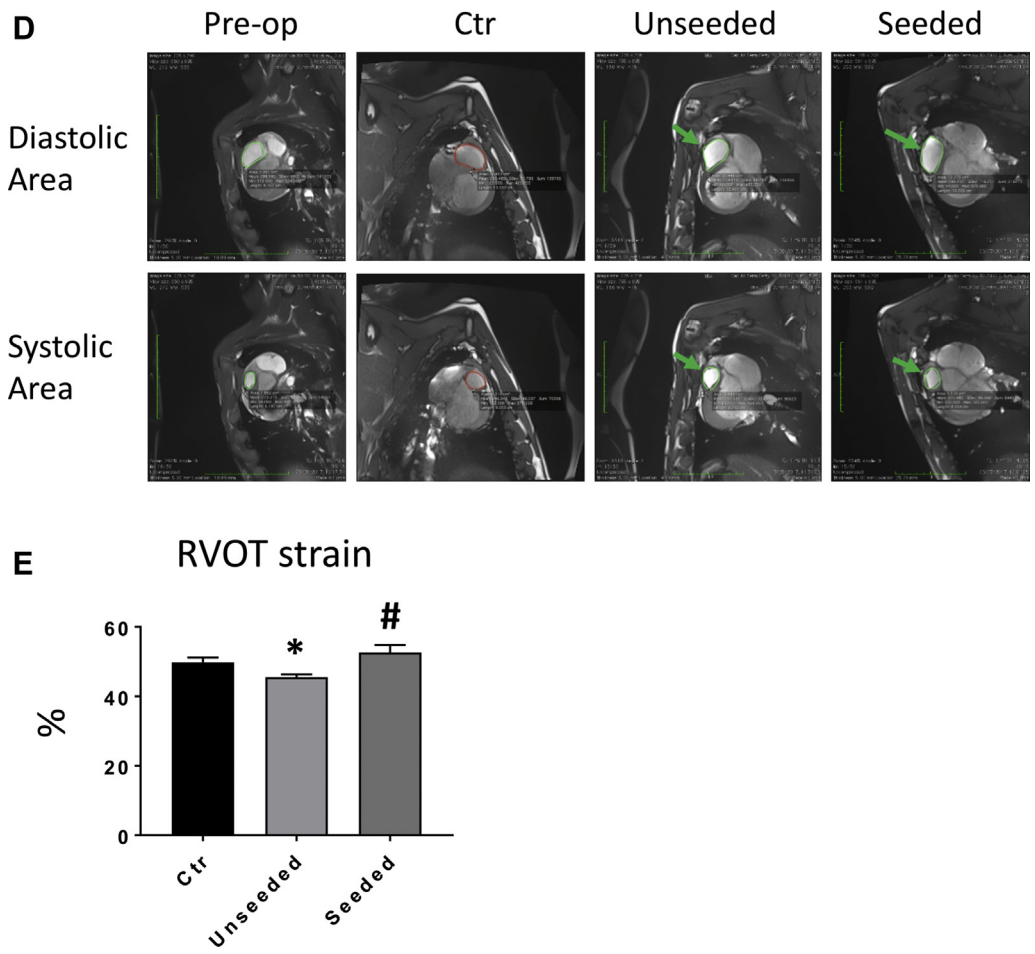

For cell confluence quantification, ImageJ (National Institutes of Health, Bethesda, Maryland) was used on 1,000× images to measure the gaps between cells. This area was converted into a proportion and expressed as confluence rather then emptiness.

IN VIVO STUDIES. A total of 13 female Landrace piglets weighing 20 to 25 kg underwent cardiac surgery. Four additional unoperated pigs weighing approximately 90 kg were used as internal controls. All surgical procedures were performed under general anesthesia (ketamine, midazolam, dexmedetomidine, and isoflurane) and neuromuscular blockade (pancuronium bromide). The heart was exposed through a median sternotomy, and cardiopulmonary bypass was established by cannulating the inferior and superior vena cavae and the ascending aorta. An incision approximately 4 cm in length was made over the RVOT and below the pulmonary valve annulus, leaving the valve intact. The cut created was then patched with either regular SIS-ECM or T-MSC-seeded SIS-ECM. The latter was implanted with seeded cells facing the inner side of the heart. Ten swine were randomized to treatment according to a controlled study design. Details of the operation are reported in Supplemental Video 1. Animals were allowed to recover under continuous post-operative monitoring for the initial 24 to 48 h. Analgesic agents (paracetamol, morphine) and an antibiotic agent (cefuroxime) were administered regularly during this period.

DOPPLER ECHOCARDIOGRAPHY. A 2-dimensional echocardiographic assessment was performed under general anesthesia using a 2-dimensional system (VividQ, GE Healthcare, Little Chalfont, United Kingdom) before graft implantation and 1, 2, 3, and 4.5 months thereafter.

CARDIAC MAGNETIC RESONANCE. Cardiac magnetic resonance was performed under anesthesia using a 3-T scanner (Siemens Healthcare, Erlangen, Germany). Dedicated long-axis and short-axis cine imaging of the RVOT was performed using steady-state free

precession sequences. Biomechanical properties in the RVOT were investigated by measuring the fractional area of change in the RVOT (RVOT-MS) defined as follows: RVOT MS = [RVOT short-axis area (diastole) − RVOT short-axis area (systole)]/RVOT short-axis area (diastole).

IN VIVO ENDPOINTS. The average in vivo follow-up of 10 of the operated animals was 145 ± 14 days, corresponding to approximately 4.5 months. The remaining 3 animals, all of them implanted with T-MSC SIS-ECM, were terminated 24 h, 1 week, and 2 weeks after implantation to determine the persistence of seeded cells in the graft post-surgery. Euthanasia was performed with an intravenous injection of 150 mg/kg of pentobarbital sodium.

HISTOLOGY. Explanted samples were washed in PBS and fixed overnight with 4% paraformaldehyde at 4°C. Fixed tissues were processed in a Thermo Excelsior AS (Thermo Fisher Scientific) and embedded with a Thermo HistoStar (Thermo Fisher Scientific) machine. Five-micrometer-thick sections were cut using a Shandon Finesse 325 microtome (Thermo Fisher Scientific). Hematoxylin and eosin, elastic van Gieson, and Masson's trichrome staining was performed either manually or using a Shandon Varistain 24-4 (Thermo Fisher Scientific) automated machine. Von Kossa staining was carried out using a Silver plating kit (In Vitro Diagnostic Medical Device, Darmstadt, Germany) for the detection of microcalcification. Fibrosis was evaluated by measuring the collagen content of the explants in the Masson's trichrome staining. Results were expressed as proportion of area occupied by collagen within the graft tissue.

FLUORESCENT IMMUNOHISTOCHEMISTRY. Paraffin-embedded sections were deparaffinized by 2 changes of clearene and rehydrated through an alcohol gradient. A heated antigen retrieval with 10 mmol/l citrate buffer (pH 6.0) was performed. Samples were blocked with 10% goat serum (Sigma-Aldrich) in PBS for 30 min at room temperature (RT) and incubated with the unconjugated primary antibodies overnight at 4°C. A list of the primary and secondary antibodies is provided in Table 1. Fluorophore-conjugated secondary antibodies were incubated on the sections for 1 h at RT in the dark. Nuclei were counterstained with 4′,6-diamidino-2-phenylindole (1:1,000, Sigma-Aldrich) for 10 min at RT. Slides were mounted with Vectashield Hardset Mounting Medium (Vector Laboratories, Burlingame, California). Images were taken using a Zeiss Observer.Z1 fluorescent microscope.

For microvasculature quantification, 10 random fields per section of the explanted grafts were analyzed under 20× magnification of a fluorescent microscope. Arterioles were quantified by counting the number of α-smooth muscle actin-positive vessels costained with isolectin B4 (IsoB4). Moreover, the number of α-smooth muscle actin-negative, IsoB4-positive vessels was counted to determine the number of capillaries developed in the healing cardiac tissue. The average number of arterioles and capillaries was then divided by the total acquired section area to calculate vascular density.

The graft regions composed of myocyte pockets were identified immunohistochemically using cardiac myosin heavy chain (cMYH) expression. Under a 20× magnification lens, 10 to 20 images were captured to cover all the cMYH-positive areas that developed in the newly formed tissue. Following identification of the regions containing CMs, ImageJ software was used to quantify the remodeling of the tissue sections. The images were split into individual channels. The ImageJ function threshold was applied in the channel of interest to convert each image to a binary version, where pixels were classified as representing either a

TABLE 2 Doppler Echocardiographic Measurements

	Pre-Operative	Control	Post-Operative Unseeded	Post-Operative Seeded
IVSd (cm)	1.12 ± 0.48	1.30 ± 0.10	1.40 ± 0.17	1.35 ± 0.16
IVSs (cm)	0.89 ± 0.08	2.10 ± 0.10	1.60 ± 0.17	2.00 ± 0.22
LVIDd (cm)	2.82 ± 0.12	3.40 ± 0.23	3.43 ± 0.46	3.72 ± 0.14
LVIDs (cm)	1.96 ± 0.13	1.75 ± 0.27	1.70 ± 0.44	2.10 ± 0.07
LVPWd (cm)	0.85 ± 0.06	1.20 ± 0.11	1.36 ± 0.20	1.62 ± 0.11
LVPWs (cm)	1.37 ± 0.10	2.25 ± 0.15	2.16 ± 0.03	2.15 ± 0.12
EDV (ml)	31 ± 3	49 ± 8	50 ± 15	59 ± 5
ESV (ml)	12 ± 2	11 ± 3	10 ± 6	14 ± 1
EF (%)	60 ± 5	80 ± 6	83 ± 6	76 ± 4
SV (ml)	18 ± 2	39 ± 6	40 ± 10	46 ± 6
FS (%)	31.3 ± 3.1	50.0 ± 6.6	51.3 ± 5.6	44.0 ± 3.9
RV FAC (%)	48.97 ± 5.41	50.80 ± 2.88	49.16 ± 2.89	47.11 ± 3.5

Values are mean ± SE. Left ventricular and RV function measured using electrocardiography before surgery and 4.5 months thereafter. Unoperated adult pigs were used as control subjects.

EDV = end-diastolic volume; EF = ejection fraction; ESV = end-systolic volume; FAC = fractional area change; FS = fractional shortening; IVSd = intraventricular septum in diastole; IVSs = interventricular septum in systole; LVIDd = left ventricular internal diameter in diastole; LVIDs = left ventricular internal diameter in systole; LVPWd = left ventricular posterior wall diastole; LVPWs = left ventricular posterior wall systole; RV = right ventricular; SV = stroke volume.

TABLE 3 Cardiac Magnetic Resonance Imaging Measurements

	Pre-Operative	Unoperated Controls	Post-Operative Unseeded	Post-Operative Seeded
Diastolic area (cm^2)	3.91 ± 0.25	11.98 ± 0.56	11.87 ± 0.73	12.01 ± 0.10
Systolic area (cm^2)	1.96 ± 0.22	6.03 ± 0.40	6.48 ± 0.45	5.68 ± 0.21
Strain (%)	51 ± 3	50 ± 1.08	45.50 ± 0.84*	52.63 ± 2.17*

Values are mean ± SE. Diastolic and systolic area and right ventricular outflow tract strain as assessed using cardiac cardiac magnetic resonance before surgery (pre-operative) and 4.5 months thereafter (unseeded and seeded animals). Unoperated adult pigs were used as control subjects. *$p < 0.05$ when comparing unseeded control animals vs. unoperated control animals, and seeded vs. unseeded animals.

FIGURE 4 Examination of the Explanted Grafts

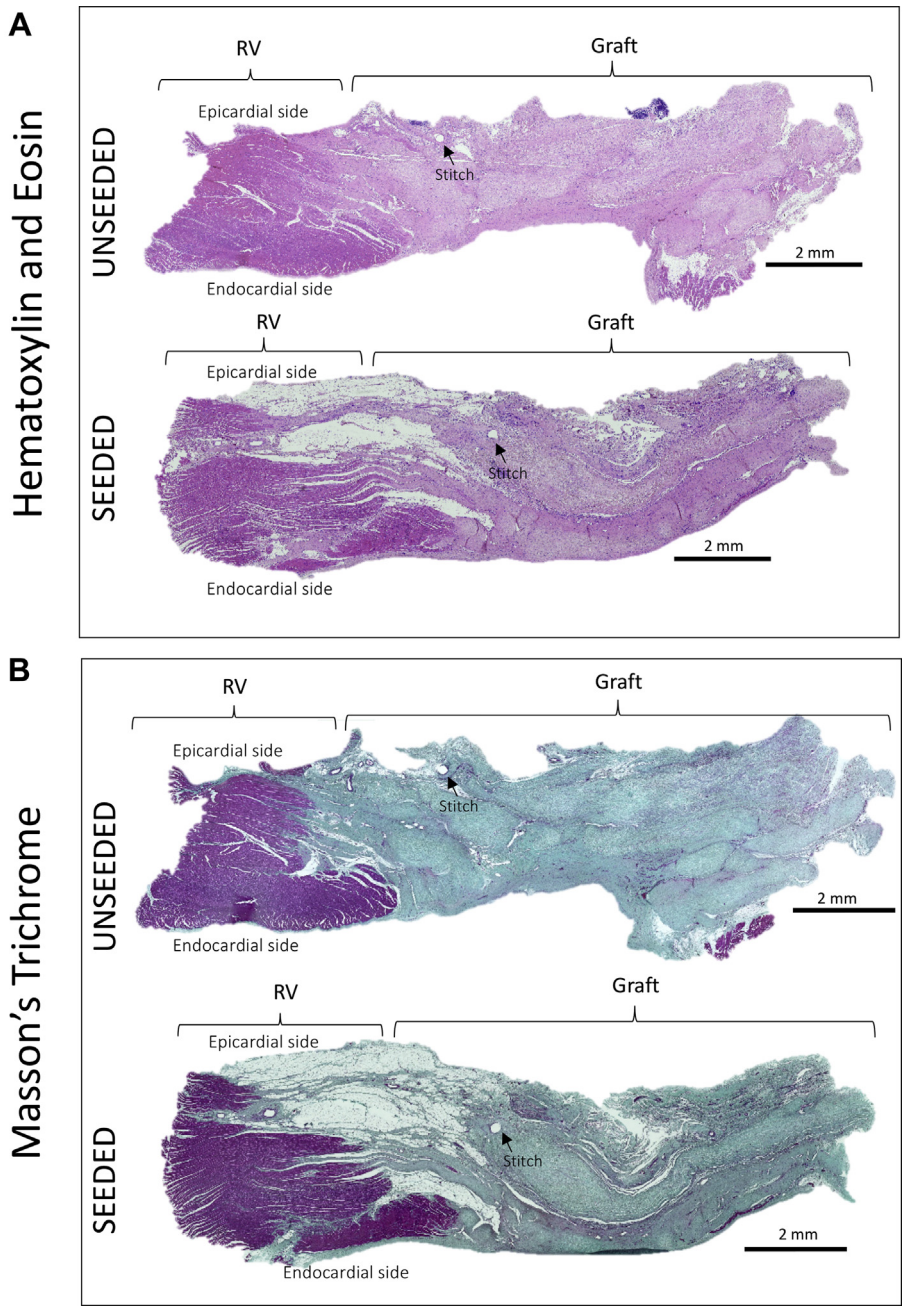

(A,B) Hematoxylin and eosin (H and E) and Masson's trichrome staining of the explants illustrates the collagen-rich grafts well integrated with the right ventricle (RV). **(C)** Higher magnification images of the samples. H and E staining shows little remains of the scaffold **(arrows)** 4.5 months after implantation **(i,v)**. Masson's trichrome staining demonstrates the presence of new muscle tissue **(arrows)** generated from the implanted grafts **(ii,vi)**. Elastic van Gieson staining illustrates an elastin-rich endothelium laying the inner side of the explants **(iii,vii)**. No calcification was detected as shown by von Kossa stain **(iv,viii)**. **(D)** More abundance of collagen was detected in the unseeded samples in comparison with the seeded group. **(E)** Immunostaining for matrix metalloproteinase 1 (MMP1) confirmed that the extracellular matrix was undergoing remodeling processes, and no differences were observed between the 2 groups. **(F)** Immunostaining and quantification of the fibrotic marker discoidin domain-containing receptor 2 (DDR2) (**green** fluorescence) showed more fibrosis in the unseeded explants compared with the seeded ones. **(G)** Cells expressing cardiac myosin heavy chain (cMYH) were present in explants from both groups, though more abundant in the seeded one. In addition, only the seeded graft contained cells double positive for cMYH and connexin-43 (Cx-43). Scale bars, 50 μm. Dapi = 4′,6-diamidino-2-phenylindole; Iso = isolectin B4.

Continued on the next page

FIGURE 4 Continued

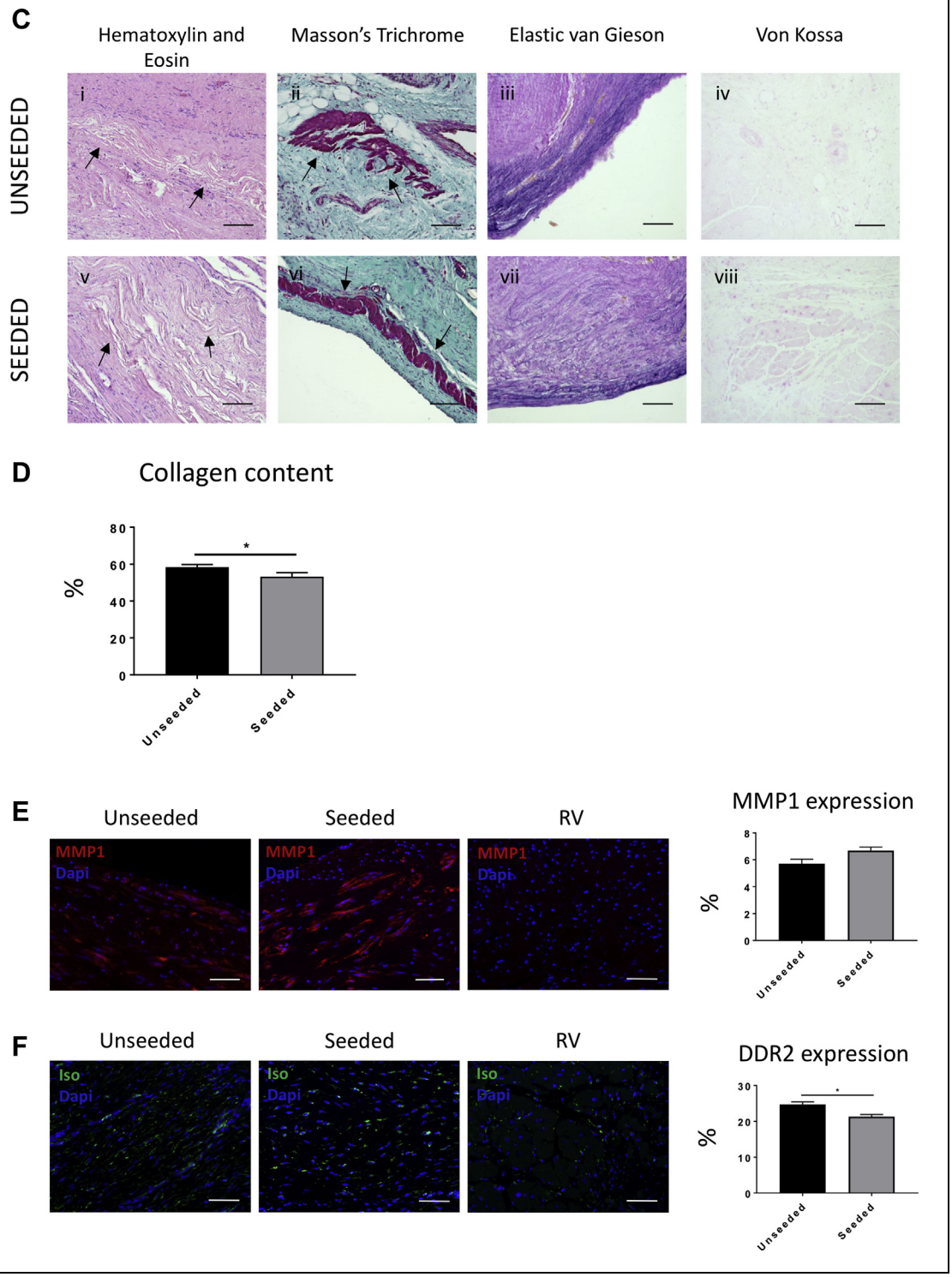

Continued on the next page

FIGURE 4 Continued

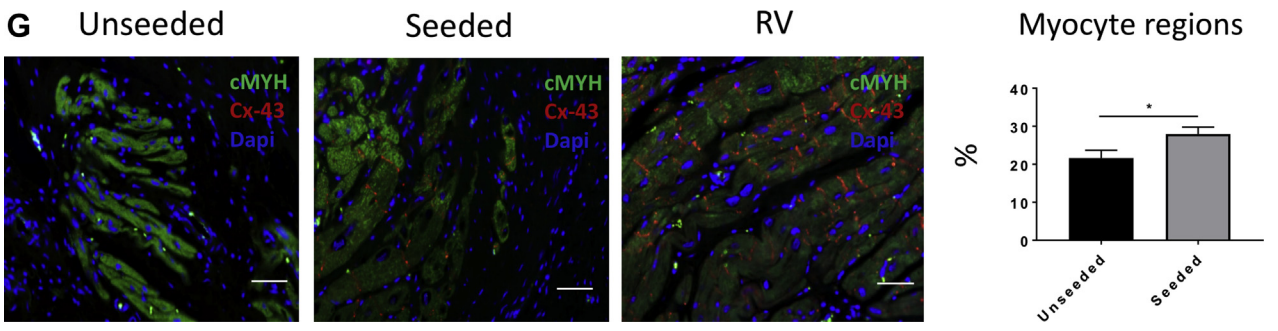

region of myocytes or a region not containing myocytes. The pixels representing myocyte regions were quantified, pooled together, and converted into square millimeters. The myocyte area was then divided by the total area of the newly formed tissue. Similarly, the expression of the remodeling marker matrix metalloproteinase 1, the fibrotic protein discoidin domain-containing receptor 2, and the proliferation marker Ki67 were quantified using the same analytic method. Moreover, the isolectin-stained samples were used to measure the thickness of the endocardium that developed in the graft tissue of the seeded and unseeded patches after 4.5 months in vivo. The endocardium thickness of the native tissue was used as a positive control.

FLUORESCENT IN SITU HYBRIDIZATION. Paraffin-embedded tissues were deparaffinized, rehydrated, and allowed to air-dry. Slides were incubated with 30% sodium bisulfite (Sigma-Aldrich) for 20 min at 37°C and washed with 2× SSC (Thermo Fisher Scientific). Samples were incubated with a proteinase K (Qiagen, Hilden, Germany) solution for 15 min at 45°C and then washed with 2× SSC. Slides were rehydrated through an alcohol gradient and allowed to air-dry. The Y-chromosome probe mixture (Chrombios, Nussdorf AM Inn, Germany) was added to the samples. The slides were placed on a hotplate for 10 min at 80°C and then transferred overnight to a humidified chamber at 37°C. At the end of the hybridization, the samples were washed with 0.4× SSC at 73°C and with 2× SSC at RT. Nuclei were counterstained with 4′,6-diamidino-2-phenylindole (1:1,000) and mounted with Vectashield Hardset Mounting Medium. Fluorescent in situ hybridization was performed on the seeded grafts before in vivo implantation and on seeded grafts explanted after 24 h, 1 week, 2 weeks, and 4.5 months. The number of cells expressing the Y chromosome was measured in the seeded grafts before implantation and after the defined time points. Results were expressed as density of Y chromosome-positive cells per square millimeter.

EFFECTS OF T-MSCs ON CMs. The in vitro proliferation and apoptosis of P0 rat CMs primary culture were measured respectively with Cell Proliferation ELISA, BrdU (Roche, Basel, Switzerland) and Caspase-Glo 3/7 Assay (Promega, Madison, Wisconsin). The CMs were either cultured with the T-MSC-conditioned medium or cocultured with the T-MSCs. Three independent experiments were carried out. The conditioned medium was freshly harvested from passage 2 and 3 T-MSCs, centrifuged, mixed with 1% FBS and 1% P/S M199 at a ratio of 1:1, and added to the CMs. Regarding the coculture condition, P0 primary culture of rat CMs was seeded in 96-well plates, onto which cell culture inserts (CellCrown inserts, Sigma-Aldrich) were placed and seeded with T-MSCs. CMs cultured with 1% FBS and 1% P/S DMEM:M199 (1:1) were used as a negative control. Twenty-four hours after seeding, bromodeoxyuridine was added to the cells to assess proliferation. Cells were incubated for 24 h at 37°C in a CO_2 incubator, and the enzyme-linked immunosorbent assay kit was used according to the manufacturer's instructions. Absorbance was measured at 450 nm using a microplate photometer (Opsys MR, Dynex Technologies, Chantilly, Virginia). Apoptosis was measured 48 h after seeding. Caspase reagent was incubated with the cells for 45 min at RT. The resulting luminescence was detected at 485 nm by using a microplate luminometer (GloMax, Promega).

A migration assay was performed on CMs to investigate the effect of the T-MSCs on the migration potential of the cardiac cells. CMs were either cultured with the T-MSC-conditioned medium or cocultured with the stem cells in a 24-well plate. After confluence was reached, the cell monolayer was scratched with a P200 tip at the center of the well. Then the cells were washed and 2 mmol/l

FIGURE 5 Evaluation of the Endothelialization and Vascularization of the Explants

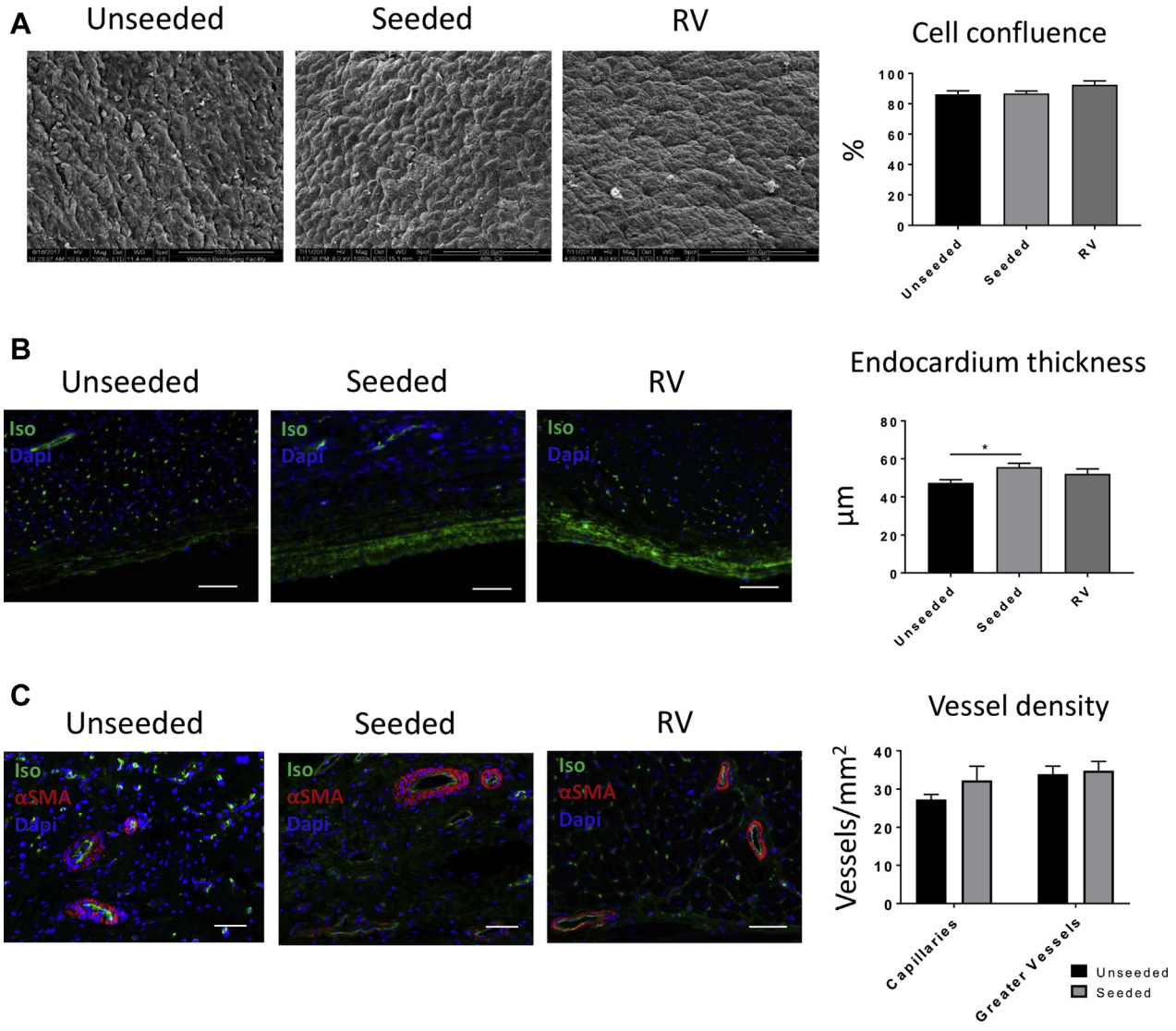

(A) Scanning electron microscopic images show that the topography of the endocardial surface of the explants is composed of aligned and compacted cells. Similar cell confluency to the native tissue was detected in the unseeded and seeded patches. **(B)** By measuring the thickness of the endocardium of the sections stained for isolectin B4 (Iso), we observed that the seeded group developed a thicker layer than the unseeded group **(C)**. The explanted grafts generated a fine and rich vascularization shown by isolectin B4 and alpha-smooth muscle actin (αSMA) staining. However, no differences were observed between the 2 groups in terms of capillaries and arteriole density. Scale bars, 50 µm. Dapi = 4′,6-diamidino-2-phenylindole; RV = right ventricle.

hydroxyurea (Sigma-Aldrich) was added to the media. Images were taken using a bright-field microscope at 4×. The proportion of gap closure was measured using ImageJ to calculate the area of the wound at the time of the scratch and 14 h later. Each experiment was performed in triplicate and repeated 3 times.

Released cytokines and growth factors were analyzed in the secretome of T-MSCs. A customized cytokine/chemokine multiplex kit (Millipore, Burlington, Massachusetts) composed of magnetic beads for the detection of interleukin (IL)-1ra, IL-2, IL-6, IL-8, interferon-γ, and tumor necrosis factor-α was used according to the manufacturer's instructions. The analysis was limited to 6 analytes because of the low availability of porcine antibodies. Reading was performed using a Luminex MAGPIX instrument (Luminex, Austin, Texas). Standard culture medium was used as control for data normalization.

FIGURE 6 Y Chromosome Fluorescent in Situ Hybridization of the Explanted Grafts

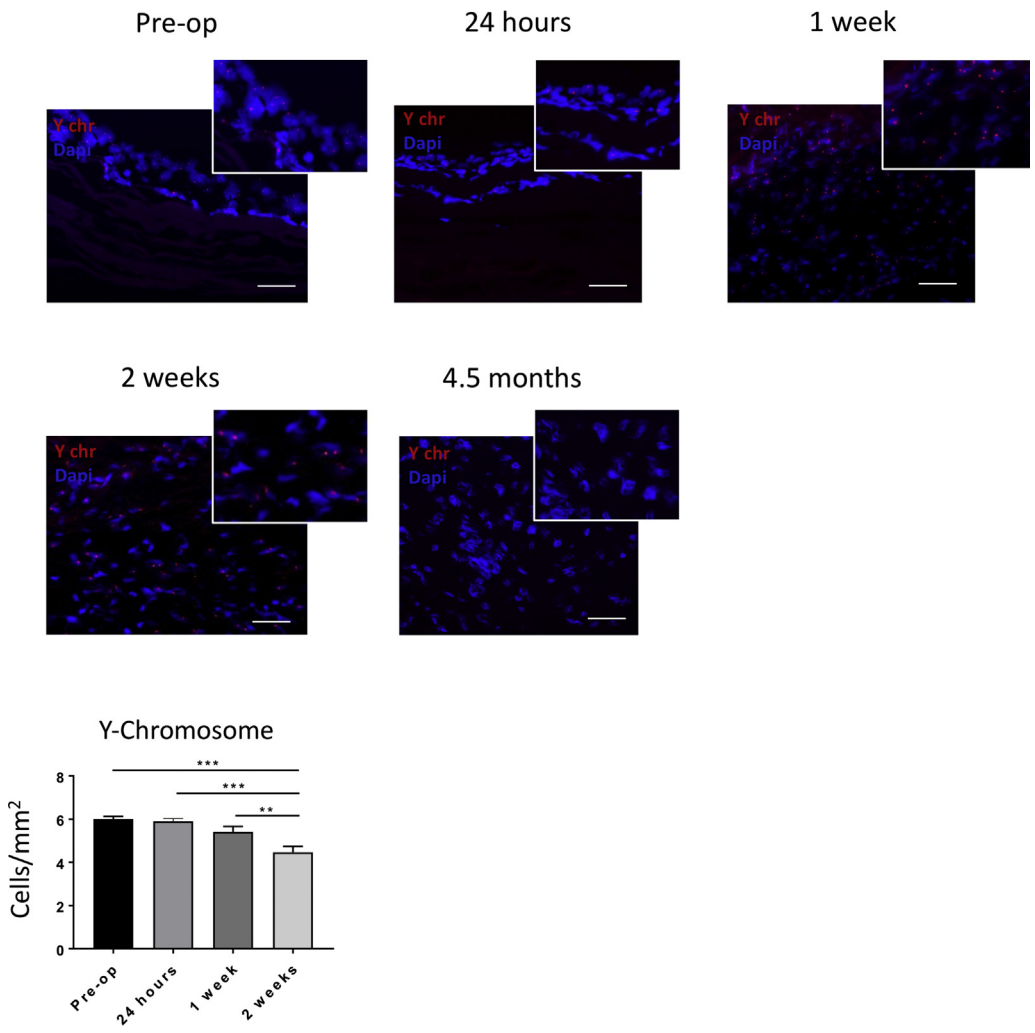

The male seeded cells (Y chromosome [Y chr] positive) were detected over the scaffold before implantation and after 24 h, 1 week, and 2 weeks. The number of seeded cells decreased with time in vivo. No seeded cells were observed at 4.5 months. Scale bars, 50 μm. Dapi = 4′,6-diamidino-2-phenylindole.

STATISTICAL ANALYSIS. Data are expressed as mean ± SEM. Statistical analysis was carried out using the Student's t-test to determine the difference between 2 groups. Alternatively, 1-way analysis of variance followed by Tukey post hoc testing was applied to analyze the differences among multiple groups. Results were considered statistically significant at $p < 0.05$.

RESULTS

CHARACTERIZATION OF T-MSCs. Adherent cells from the swine thymus gland exhibited the typical spindle-shape morphology. Flow cytometry of 4 cell lines showed abundant expression of the mesenchymal markers CD44, CD73, CD90, and CD105 and negativity for CD31 and CD45 (Figures 1A and 1B). Furthermore, we confirmed the ability of T-MSCs to differentiate into mesenchymal lineages (Figure 1C).

CHARACTERIZATION OF T-MSC-ENGINEERED SIS-ECM SCAFFOLDS. The T-MSCs seeded on the SIS-ECM scaffold were grown for 1 week under static condition and then 1 week under dynamic condition in a bioreactor (Figure 2A). T-MSCs were viable within the scaffold at 2 weeks from seeding, with only a few dead cells being observed (4.0 ± 0.6% of total cell counts) (Figure 2B). They were stratified on the

FIGURE 7 Evaluation of Proliferating Cells in Vivo

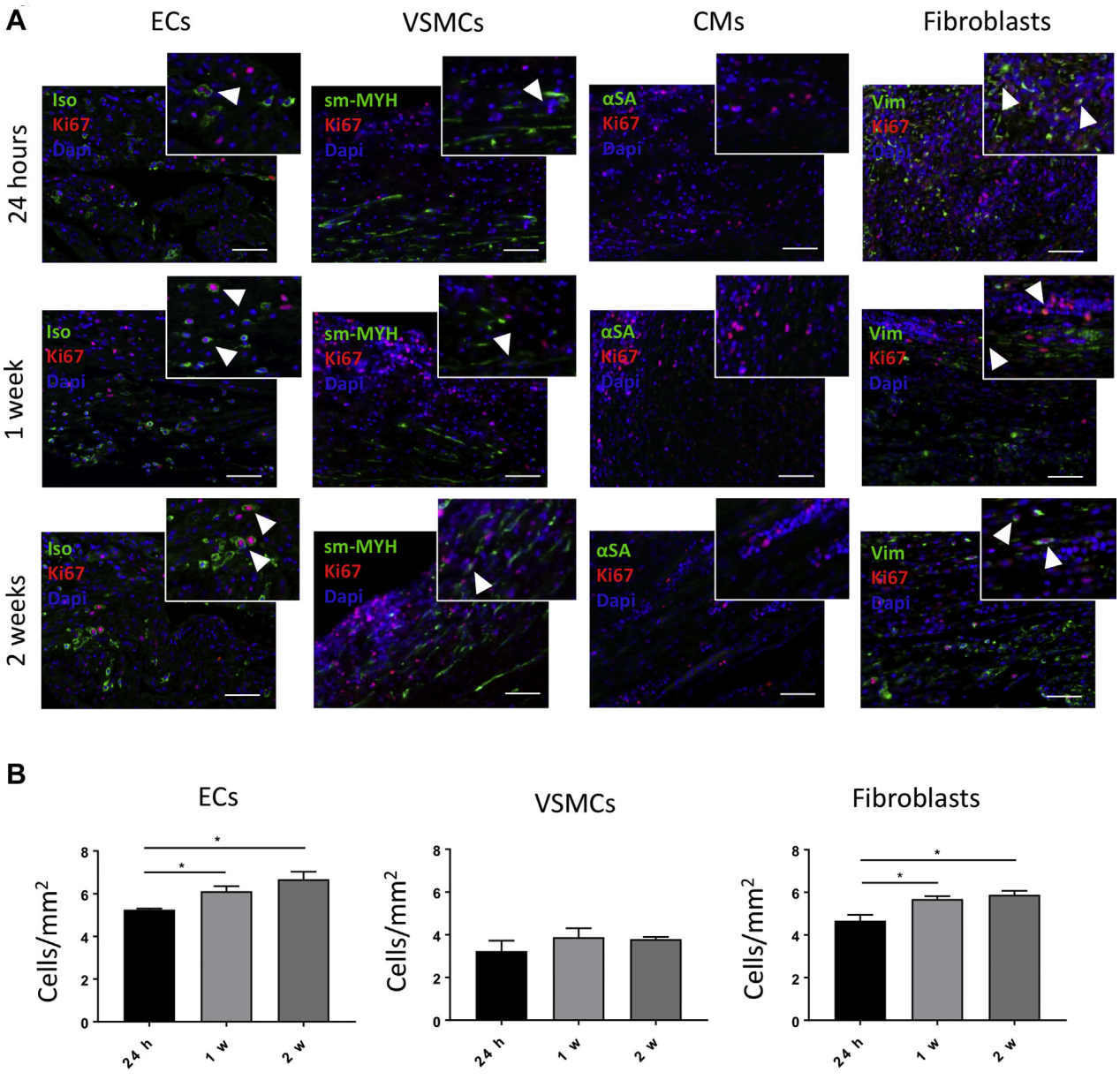

(A) Immunostaining for Ki67 and isolectin B4 (Iso), smooth muscle myosin heavy chain (sm-MYH), α-sarcomeric actinin (αSA), and vimentin (Vim) in the seeded grafts explanted at 24 h, 1 week, and 2 weeks. Coexpression of Ki67 with Iso and Vim suggests that the proliferating cells at early stages consist of endothelial cells (ECs) and fibroblasts. Scale bars, 50 μm. **(B)** The numbers of proliferating ECs and fibroblasts increase after 1 week in vivo, with the fibroblasts showing an increased proliferation also after 2 weeks. **(C)** Double staining for Ki67 and Iso, sm-MYH, αSA, and Vim in the unseeded and seeded grafts explanted at 4.5 months. Cells coexpressing Ki67 with Iso, sm-MYH, and Vim were detected in the grafts, suggesting that the proliferating cells are ECs, vascular smooth muscle cells (VSMCs), and fibroblasts. Scale bars, 50 μm. **(D)** The number of Ki67-positive cells seemed to be the same between the unseeded and seeded groups 4.5 months after implantation.

Continued on the next page

surface of the scaffold (hematoxylin and eosin staining) and interposed with newly formed collagen (elastic van Gieson staining). Scanning electron microscopy confirmed the presence of a confluent and oriented layer of cells on the surface of the SIS-ECM scaffold.

Next, we compared the mechanical characteristics of the unseeded and T-MSC-seeded scaffolds. No

FIGURE 7 Continued

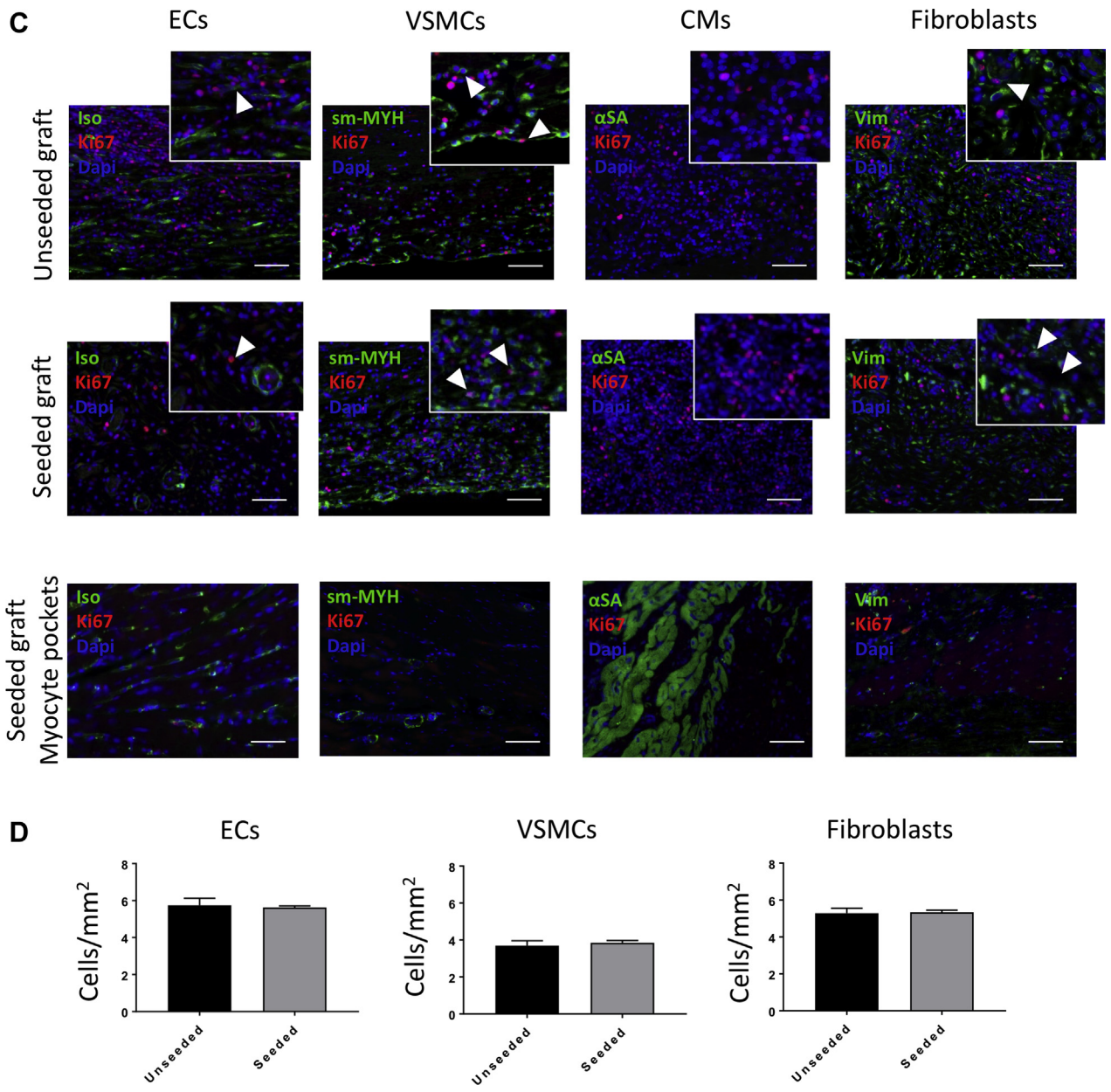

difference between groups was observed with regard to stiffness or tensile stress at maximum load ($p = 0.1075$ and $p = 0.2890$, respectively) (Figure 2C).

FEASIBILITY AND SAFETY OF T-MSC-ENGINEERED GRAFTS IMPLANTATION. Figure 3A illustrates the topography (i) and operative characteristics of the RVOT lesion (ii-iv). All operated animals survived the surgical procedure and recovered well, with no loss during follow-up and similar body weight gain (Figure 3B). At termination, body weight was similar to that of unoperated swine of the same age (91 ± 6 kg and 93 ± 7 kg, respectively, in the unseeded and seeded groups vs. 90 ± 1 kg in control groups). Echocardiography showed similar values of RVOT diameters (control subject vs. unseeded; $p = 0.1726$; control subject vs. seeded; $p = 0.995$), left ventricular contractile function, and left ventricular volumes among unoperated, unseeded, and T-MSC-seeded groups (Figure 3C, Table 2). Likewise, Doppler analysis demonstrated no change in maximum RVOT velocity between the control subject and operated animals (control subject vs. unseeded; $p = 0.1569$; control

FIGURE 8 **in Vitro Assessment of the Paracrine Effect of the Thymus-Derived Mesenchymal Stem Cells**

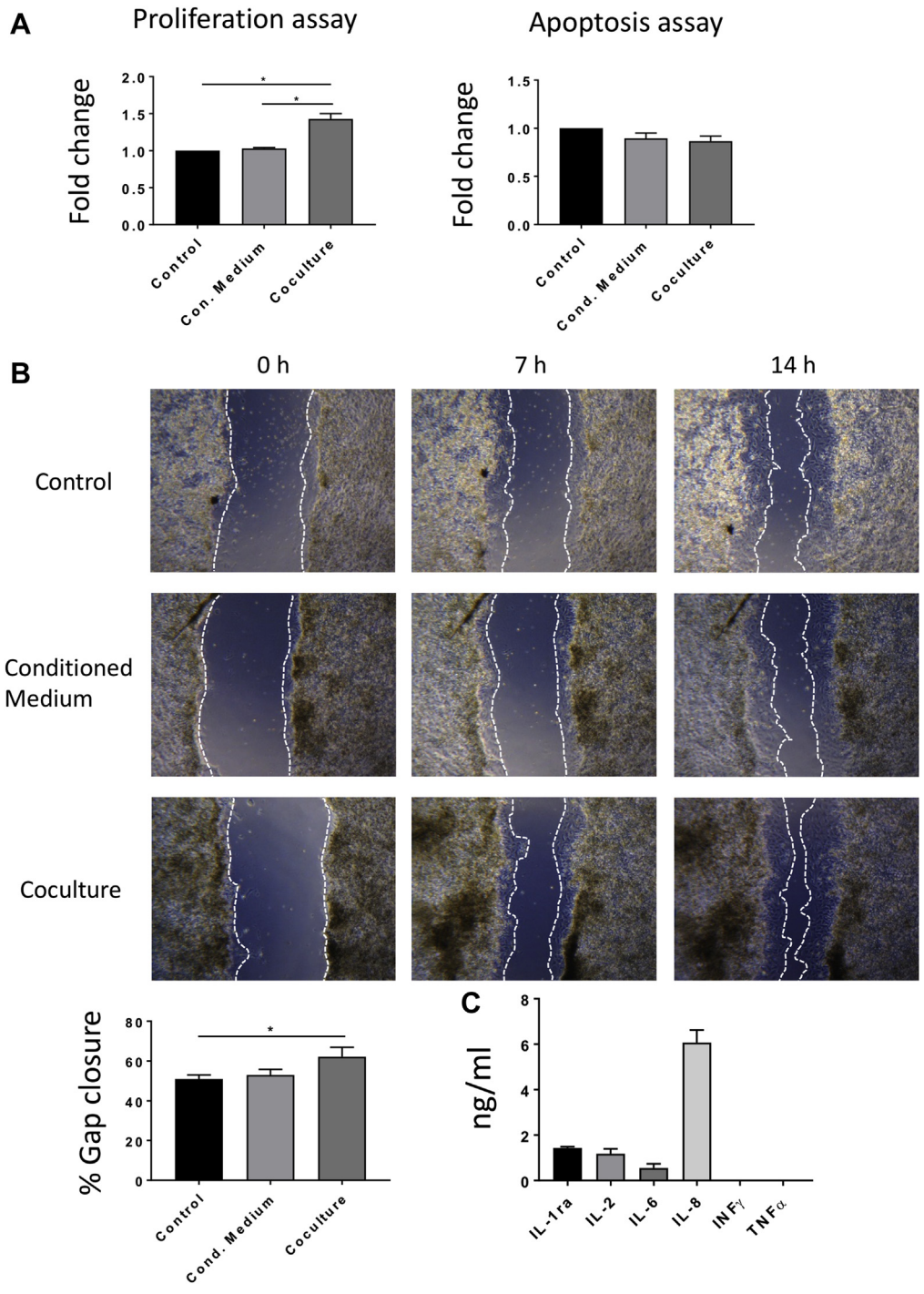

(A) Evaluation of the proliferation and apoptosis of rat cardiomyocytes (rCMs) cultured in the presence of thymus-derived mesenchymal stem cells (T-MSCs) or with their conditioned medium showed that the presence of the stem cells stimulates the proliferation of the cardiomyocytes (CMs), without affecting apoptosis ($n = 3$). **(B)** A migration assay of the rCMs either cultured with the conditioned medium or cocultured with the T-MSCs demonstrated that the stem cells can promote the migration of the CMs. The proportion of gap closure 14 h following the scratch was greater in the cocultured condition compared with the control. **(C)** Analysis of the cytokines and growth factors released by the T-MSCs showed secretion of interleukin (IL)-1ra, IL-2, and IL-6 and a high level of IL-8. Absence of interferon (INF)-γ and tumor necrosis factor (TNF)-α was observed in the porcine T-MSC (pT-MSC)-conditioned medium.

subject vs. seeded; p = 0.052) (Figure 3C). Similarly, the proportion of right ventricular (RV) fractional area change did not differ between groups and was within clinical reference range (32% to 60%) of normal RV function (Table 2).

IMPLANTATION OF T-MSC-ENGINEERED GRAFTS IMPROVES RVOT CONTRACTILITY COMPARED WITH UNSEEDED GRAFTS. Cardiac cardiac magnetic resonance assessments of RVOT motion and deformation were carried out before surgery and at termination, using unoperated adult pigs as control subjects for the latter time point (Figure 3D). Basal RVOT-MS values did not differ between the study groups, thus excluding a chance of imbalance that may influence outcome, and were therefore cumulated (Table 3). At the final measurement, unseeded animals showed reduced RVOT-MS compared with unoperated control subjects (p < 0.05), with this gap being totally abrogated in the T-MSC-seeded group (control subject vs. unseeded; p = 0.1835; control subject vs. seeded; p = 0.0432; unseeded vs. seeded; p = 0.0408) (Figure 3E). The RVOT-MS increase observed in the seeded group was the consequence of a reduction of the systolic area, whereas diastolic area did not differ between the 2 groups (Table 3).

IN VIVO INTEGRATION AND REMODELING OF T-MSC-ENGINEERED GRAFTS WITHIN THE HOST CARDIAC TISSUE. The results of cardiac cardiac magnetic resonance suggest that T-MSCs can confer the implanted scaffold with the capacity to preserve RVOT contractility. Therefore, we investigated the mechanisms responsible for this beneficial effect. At macroscopic inspection, explanted RVOTs presented a smooth luminal surface with no sign of tissue degradation in both groups. Hematoxylin and eosin staining showed in vivo integration of the grafts within the neighboring myocardium (Figure 4A). The newly formed tissue within the implants was composed mainly of collagenous fibers, as shown by Masson's trichrome (Figure 4B) and elastic van Gieson (Supplemental Figure 1) staining. A close inspection revealed only few discernible remnants of the SIS-ECM scaffold (Figure 4C), suggesting that the implanted graft underwent remodeling and new tissue formation. Moreover, von Kossa staining showed no calcification in the explanted cell-seeded or unseeded grafts (Figure 4C, Supplemental Figure 2). Interestingly, the amount of collagen developed in the cell-seeded explants was significantly lower compared with the unseeded explants (53.31 ± 2.07% and 58.45 ± 1.36% of total section area, respectively; p = 0.0429) (Figure 4D). Immunostaining and quantification of the remodeling marker matrix metalloproteinase 1 demonstrated similar expression in the unseeded and seeded groups (5.91 ± 0.32% and 6.67 ± 0.25%, respectively; p = 0.0516) (Figure 4E). Moreover, discoidin domain-containing receptor 2 was significantly down-regulated in the cell-seeded compared with the unseeded group (22.5 ± 0.64% vs. 24.7 ± 0.73%, respectively; p = 0.0422) (Figure 4F), which, together with the data of collagen content, suggests an antifibrotic effect that was exerted by T-MSCs. The control RV tissue distant from the implant was negative for the matrix metalloproteinase 1 and discoidin domain-containing receptor 2 markers.

Immunostaining for the cardiac marker cMYH confirmed the presence of myocyte-like clusters dispersed within the explants of both unseeded and cell-seeded groups (Figure 4G). Interestingly, the area of the explant occupied by these myocyte-like islets was greater in the cell-seeded group (p = 0.0462). Moreover, seeded grafts contained myocytes that coexpress cMYH and the ventricular gap junction protein connexin-43 (Cx-43), whereas these double-positive myocytes were absent in unseeded grafts. Scanning electron microscopy of the endocardial side of the explanted grafts showed that both the unseeded and seeded patches developed a compact cell layer, resembling the topography of the native tissue (cell confluence 86.12 ± 2.39%, 86.77 ± 1.62%, and 92.54 ± 2.36%, respectively; unseeded vs. seeded; p = 0.9702; unseeded vs. RV; p = 0.1598; seeded vs. RV; p = 0.2045) (Figure 5A). Immunostaining with IsoB4 demonstrated that the seeded grafts developed a thicker layer of ECs compared with unseeded group (53.54 ± 2.04 and 46.45 ± 1.81 μm, respectively; unseeded vs. seeded; p = 0.0291; unseeded vs. RV; p = 0.2793; seeded vs. RV; p = 0.4611) (Figure 5B).

Fluorescent microscopy identified capillaries and arterioles within the grafts, although the former were less abundant than in control RV myocardium, suggesting that graft arteriogenesis prevailed on capillarization in the healing process of tissue (Figure 5C).

3The improved physiological remodeling in the cell-seeded group prompted us to examine the fate of the implanted male donor cells into the female recipients using fluorescent in situ hybridization analysis of Y chromosome in the explanted grafts. Cells expressing the Y chromosome were detected in grafts explanted 24 h, 1 week, and 2 weeks post-implantation (Figure 6). We observed a progressive decline in the abundance of cells expressing the Y chromosome, but positive cells were still present at 2 weeks after implantation (pre-operative vs. 24 h; p = 0.9842; pre-operative vs. 1 week, p = 0.2040; pre-operative vs. 2 weeks; p < 0.0001; 24 h vs. 1 week; p = 0.03695; 24 h vs. 2 weeks; p < 0.001; 1 week vs. 2 weeks; p = 0.009). In contrast, no Y chromosome-positive cells were

detected at 4.5 months. Therefore, it is most likely that CMs and ECs found in the explanted grafts derive from the recipient rather than from donor T-MSCs.

Next, we measured cell proliferation in grafts explanted at 24 h, 1 week, 2 weeks, and 4.5 months by immunostaining for Ki67, in combination with IsoB4, smooth muscle myosin heavy chain, α-sarcomeric actinin, and vimentin to detect, respectively, proliferating ECs, vascular smooth muscle cells (VSMCs), CMs, and fibroblasts (Figure 7). Some Ki67-positive ECs and fibroblast-like cells were observed in the seeded grafts explanted after 24 h, 1 week, and 2 weeks, whereas neither VSMCs nor CMs were positive for Ki67 (Figure 7A). The number of proliferating ECs increased after 1 week; likewise fibroblasts showed greater proliferation at 1 and 2 weeks compared with 24 h (ECs: 24 h vs. 1 week; $p = 0.0411$; 24 h vs. 2 weeks; $p = 0.0141$; 1 week vs. 2 weeks; $p = 0.3021$; VSMCs: 24 h vs. 1 week; $p = 0.4812$; 24 h vs. 2 weeks, $p = 0.5724$; 1 week vs. 2 weeks; $p = 0.9839$; fibroblasts: 24 h vs. 1 week; $p = 0.0284$; 24 h vs. 2 weeks; $p = 0.0126$; 1 week vs. 2 weeks; $p = 0.7590$) (Figure 7B). Additionally, we analyzed the proliferating cells in the seeded and unseeded grafts explanted after 4.5 months (Figure 7C). Ki67-positive ECs, VSMCs, and fibroblasts were detected at this time point within the grafts, but no proliferating cells were found in the myocyte pockets, and no differences were observed regarding the number of proliferating ECs, VSMCs, and fibroblasts (ECs: unseeded vs. seeded; $p = 0.7649$; VSMCs: unseeded vs. seeded; $p = 0.6262$; fibroblasts: unseeded vs. seeded; $p = 0.8648$) (Figure 7D).

EVALUATION OF THE PARACRINE EFFECT OF THE T-MSCs ON THE CMs IN VITRO. To assess the paracrine properties of T-MSCs, we measured the proliferation and apoptosis of CMs in the presence of T-MSCs or their conditioned medium (Figure 8A). Results showed stimulation of CM proliferation by T-MSCs in a coculture system ($p = 0.0489$ vs. control), whereas the T-MSC-conditioned medium was ineffective ($p = 0.9901$ vs. control). T-MSCs or their conditioned medium did not affect CM apoptosis (control vs, conditioned medium; $p = 0.2588$; control vs. coculture; $p = 0.1244$). Therefore, continuous production of paracrine factors by T-MSCs is indispensable for induction of CM expansion in vitro. Similarly, a migration assay of the CMs either cultured with the T-MSC-conditioned medium or cocultured with the T-MSCs confirmed that the stem cells have the potential to trigger the migration of CMs in vitro (Figure 8B). Fourteen hours after the scratch was made, the proportion of gap closure in the coculture system was higher compared with the control subject (62.18 ± 4.69% and 51.06 ± 2.01%, respectively; $p = 0.0487$ vs. control subject).

A multiplex analysis of the cytokines produced by the T-MSCs showed that high levels of the proangiogenic factor IL-8 are secreted by the MSCs in vitro (Figure 8C). Relatively low levels of inflammatory IL-2 and IL-6 and the anti-inflammatory cytokine IL-1ra were detected, whereas complete absence of proinflammatory interferon-γ and tumor necrosis factor-α was revealed.

DISCUSSION

Because of their similarities to humans and rapid growing rate, pigs are valuable animal models for preclinical assessment of cardiac tissue engineering (12,13). The present study confirms the feasibility and safety of RVOT reconstruction using a SIS-ECM graft in growing piglets. In addition, we report for the first time that the addition of allogeneic T-MSCs to the SIS-ECM can upgrade the scaffold, converting it into a living tissue, capable of remodeling and improving RVOT contractility. Immunostaining of the explants showed similar neovascularization but a lower degree of fibrosis and a greater abundance of mature myocytes in the group implanted with seeded grafts. Moreover, scanning electron microscopy and immunohistochemistry analysis demonstrated a more organized endothelialization of the T-MSC-engineered grafts.

Very few studies have focused on reconstruction of the RVOT in animal models. Tanaka et al. (14) implanted a SIS-ECM graft allowing the controlled release of basic fibroblast growth factor in an RVOT porcine model. They reported the occurrence of regional myocardial remodeling and increased tissue viability within the patch. However, there was no improvement in the RVOT strain. Thus, our SIS-ECM cellularization approach seems to have a significant functional advantage over basic fibroblast growth factor treatment of SIS-ECM. In another study, induced pluripotent stem cells were used to engineer a synthetic scaffold that was implanted in the RVOT of a rat model (3). Host CM regeneration was observed in the cell-seeded group.

SIS-ECM material has been widely used in cardiovascular surgery since 2006. Early results suggested a therapeutic potential for correction of congenital heart defects (1,15). However, more recent data have demonstrated less favorable clinical outcomes. For instance, Woo et al. (16) showed a relatively high degree of chronic inflammation and fibrosis and poor graft recellularization and integration with the surrounding tissue in SIS-ECM specimens explanted from pediatric patients who underwent corrective

heart surgery. Similar concerns were raised by studies using SIS-ECM for valve repair in children. An intense inflammatory response was observed in the surrounding tissue, and little or no remodeling was detected 9 months after implantation (17).

Our group recently showed that T-MSCs isolated from human donors are capable to engraft and proliferate onto the SIS-ECM (2). We have now established the isolation and expansion of porcine T-MSC lines suitable for use in an allogeneic or autologous setting. The porcine T-MSCs displayed plastic adherence, a high rate of growth, high expression of the typical mesenchymal markers, and trilineage differentiation capacity into osteocytes, adipocytes, and chondrocytes (18). Hence, our results indicate that the isolation of MSCs from the porcine thymus is feasible and provides a homogenous cell population. Successful seeding of the T-MSCs on the SIS-ECM allowed the generation of an engineered patch composed of a multilayer of oriented cells growing on the surface of the scaffold. Mechanical testing of the construct showed that T-MSC incorporation is not detrimental to the graft physical properties. Furthermore, Y chromosome fluorescent in situ hybridization staining on seeded grafts explanted 24 h, 1 week, and 2 weeks post-operatively indicated that the donor cells engrafted into the SIS-ECM. However, Y chromosome staining on the 4.5-month explant demonstrated no trace of the implanted cells. This implies that the effects exerted by the cells on the surrounding tissue are due mainly to a paracrine stimulation that must have happened relatively soon after implantation. In line with our results, Sugiura et al. (3) showed that the seeded cells disappeared from the graft 4 weeks after implantation. Nonetheless, their early presence in vivo was sufficient to favor the regeneration of cardiac tissue.

The analysis of graft remodeling provided a possible interpretation for the improvement of RVOT contractility. The reduction of fibrosis associated with an increase in CMs' number may have contributed to rescue RVOT strain in animals implanted with T-MSC-seeded grafts. We excluded the possibility that the CMs colonizing the graft derived from the donor cells, as none were found to be positive for the Y chromosome at the latest time point. Migration or proliferation of CMs from the neighboring myocardium could have contributed to the muscularization of the graft. In vitro studies showed that T-MSCs have the potential to stimulate the proliferation and migration of neonatal CMs. However, in agreement with the notion that adult CMs are terminally differentiated, we did not find any sign of CM proliferation in the explanted grafts, the only Ki67-positive cells being vascular and stromal cells. Therefore, CM migration remains the most likely explanation for graft muscularization in vivo. Furthermore, only seeded grafts induced the colonization of CMs coexpressing cMYH and Cx-43, while unseeded grafts were unable to maintain normal RVOT strain and contained cMYH cells negative for Cx-43. This marker has been associated with preserved CM functionalities. For instance, early-stage compensated left ventricular hypertrophy is characterized by increased Cx-43 immunofluorescent signal per myocyte volume and extensive Cx-43 lateral labeling, whereas Cx-43 becomes down-regulated in the decompensated stage of cardiac hypertrophy (19). Gap junctional coupling is important for functional integration of transplanted cells with host myocardium (20). Furthermore, noncanonical functions of Cx-43 include the control of sodium channels with important repercussions on the propagation of electric activity in the heart (21).

Graft cellularization resulted in a more organized endothelialization of the endocardial side of the graft but did not improve revascularization at capillary or arteriole level. Interestingly, arteriogenesis was not associated with a robust capillarization of the graft. Hence, it would be important to determine in the future whether stimulation of angiogenesis could further improve RVOT functionalization.

CONCLUSIONS

Our study indicates that functionalization of the graft with T-MSCs may obviate the contractility and endothelialization problems reported after surgical correction of the RVOT (10). The addition of T-MSCs to the SIS-ECM converted it into a living tissue, capable of preventing the formation of an akinetic RVOT area. Akinetic regions developed in the RVOT have been associated with myocardial scarring, fibrosis, and electromechanical delay (22). Furthermore, abnormal fibrous tissue deposition and adipose tissue substitution can develop around the surgical scar and can eventually lead to electric instability, re-entrant arrhythmias, and even sudden cardiac death (23,24). We did not perform electrophysiological studies; thus, we can only infer the absence of life-threatening arrhythmias from the fact that no fatality was observed. Another limitation of the study was the absence of a sham-operated group to assess unspecific background effect of surgery on the heart. However, the main comparator was the group of pigs with grafts that were not seeded with stem cells.

Most of the grafts currently used in cardiac surgery are either synthetic or fixed materials. These materials

have not been proved to be particularly effective during long-term follow-up, leading to lack of contractility and mismatched mechanical properties, which might contribute to the risk for sudden death (25,26). Our feasibility, safety, and efficacy in vivo study has shown that seeding SIS-ECM with T-MSCs overcomes some of the known limitations of current prosthetic material. These results may pave the way to new modalities for effective surgical restoration of RV function in patients with tetralogy of Fallot.

ACKNOWLEDGMENTS The authors are grateful to all staff members of the University of Bristol Large Animal Surgical Facility.

ADDRESS FOR CORRESPONDENCE: Prof. Massimo Caputo, and Dr Mohamed Ghorbel, University of Bristol, Bristol Heart Institute, Research Level 7, BRI, Upper Maudlin Street, Bristol BS2 8HW, United Kingdom. E-mail: m.caputo@bristol.ac.uk OR m.ghorbel@bristol.ac.uk.

PERSPECTIVES

COMPETENCY IN MEDICAL KNOWLEDGE: Our study demonstrates for the first time in a clinically relevant, randomized, large animal study the importance of using autologous stem cell tissue engineered patches for reconstruction of the RVOT.

TRANSLATIONAL OUTLOOK: The translation of this work into a clinical safety and efficacy study in patients with tetralogy of Fallot can open the way to the application of personalized grafts for reconstructive surgery in congenital heart disease, which can grow and remodel in vivo and therefore avoid the life-threatening complications seen in these complex patients. Our main challenges will be to transfer the production of our tissue-engineered grafts into clinically upgraded facilities and to identify funding for this very new and exciting "personalized" approach for neonates and infants born with congenital heart disease.

REFERENCES

1. Scholl FG, Boucek MM, Chan KC, Valdes-Cruz L, Perryman R. Preliminary experience with cardiac reconstruction using decellularized porcine extracellular matrix scaffold: human applications in congenital heart disease. World J Pediatr Congenit Heart Surg 2010;1:132–6.

2. Iacobazzi D, Swim MM, Albertario A, Caputo M, Ghorbel MT. Thymus-derived mesenchymal stem cells for tissue engineering clinical-grade cardiovascular grafts. Tissue Eng Part A 2018;24:794–808.

3. Sugiura T, Hibino N, Breuer CK, Shinoka T. Tissue-engineered cardiac patch seeded with human induced pluripotent stem cell derived cardiomyocytes promoted the regeneration of host cardiomyocytes in a rat model. J Cardiothorac Surg 2016;11:163.

4. Dohmen PM, da Costa F, Yoshi S, et al. Histological evaluation of tissue-engineered heart valves implanted in the juvenile sheep model: is there a need for in-vitro seeding? J Heart Valve Dis 2006;15:823–9.

5. He W, Nieponice A, Soletti L, et al. Pericyte-based human tissue engineered vascular grafts. Biomaterials 2010;31:8235–44.

6. Gonzales C, Pedrazzini T. Progenitor cell therapy for heart disease. Exp Cell Res 2009;315:3077–85.

7. Pittenger MF, Mackay AM, Beck SC, et al. Multilineage potential of adult human mesenchymal stem cells. Science 1999;284:143–7.

8. Iacono E, Brunori L, Pirrone A, et al. Isolation, characterization and differentiation of mesenchymal stem cells from amniotic fluid, umbilical cord blood and Wharton's jelly in the horse. Reproduction 2012;143:455–68.

9. Secunda R, Vennila R, Mohanashankar AM, Rajasundari M, Jeswanth S, Surendran R. Isolation, expansion and characterisation of mesenchymal stem cells from human bone marrow, adipose tissue, umbilical cord blood and matrix: a comparative study. Cytotechnology 2015;67:793–807.

10. Udink ten Cate FE, Sreeram N, Brockmeier K. The pathophysiologic aspects and clinical implications of electrocardiographic parameters of ventricular conduction delay in repaired tetralogy of Fallot. J Electrocardiol 2014;47:618–24.

11. Davlouros PA, Kilner PJ, Hornung TS, et al. Right ventricular function in adults with repaired tetralogy of Fallot assessed with cardiovascular magnetic resonance imaging: detrimental role of right ventricular outflow aneurysms or akinesia and adverse right-to-left ventricular interaction. J Am Coll Cardiol 2002;40:2044–52.

12. Mosala Nezhad Z, Poncelet A, de Kerchove L, et al. CorMatrix valved conduit in a porcine model: long-term remodelling and biomechanical characterization. Interact Cardiovasc Thorac Surg 2017;24:90–8.

13. Iop L, Bonetti A, Naso F, et al. Decellularized allogeneic heart valves demonstrate self-regeneration potential after a long-term preclinical evaluation. PLoS ONE 2014;9:e99593.

14. Tanaka A, Kawaji K, Patel AR, et al. In situ constructive myocardial remodeling of extracellular matrix patch enhanced with controlled growth factor release. J Thorac Cardiov Sur 2015;150:1280–90.

15. Quarti A, Nardone S, Colaneri M, Santoro G, Pozzi M. Preliminary experience in the use of an extracellular matrix to repair congenital heart diseases. Interact Cardiov Th 2011;13:569–72.

16. Woo JS, Fishbein MC, Reemtsen B. Histologic examination of decellularized porcine intestinal submucosa extracellular matrix (CorMatrix) in pediatric congenital heart surgery. Cardiovasc Pathol 2016;25:12–7.

17. Zaidi AH, Nathan M, Emani S, et al. Preliminary experience with porcine intestinal submucosa (CorMatrix) for valve reconstruction in congenital heart disease: histologic evaluation of explanted valves. J Thorac Cardiovasc Surg 2014;148:2216–4, 2225.e1.

18. Dominici M, Le Blanc K, Mueller I, et al. Minimal criteria for defining multipotent mesenchymal stromal cells. The International Society for Cellular Therapy position statement. Cytotherapy 2006;8:315–7.

19. Kostin S, Dammer S, Hein S, Klovekorn WP, Bauer EP, Schaper J. Connexin 43 expression and distribution in compensated and decompensated cardiac hypertrophy in patients with aortic stenosis. Cardiovasc Res 2004;62:426–36.

20. Ramkisoensing AA, Pijnappels DA, Swildens J, et al. Gap junctional coupling with cardiomyocytes is necessary but not sufficient for cardiomyogenic differentiation of cocultured human mesenchymal stem cells. Stem Cells 2012;30:1236–45.

21. Agullo-Pascual E, Delmar M. The noncanonical functions of Cx43 in the heart. J Membr Biol 2012;245:477–82.

22. Bonello B, Kempny A, Uebing A, et al. Right atrial area and right ventricular outflow tract akinetic length predict sustained tachyarrhythmia in repaired tetralogy of Fallot. Int J Cardiol 2013;168:3280–6.

23. Silka MJ, Hardy BG, Menashe VD, Morris CD. A population-based prospective evaluation of risk of sudden cardiac death after operation for common congenital heart defects. J Am Coll Cardiol 1998;32:245–51.

24. Misaki T, Tsubota M, Watanabe G, et al. Surgical treatment of ventricular tachycardia after surgical repair of tetralogy of Fallot. Relation between intraoperative mapping and histological findings. Circulation 1994;90:264–71.

25. Tweddell JS, Pelech AN, Frommelt PC, et al. Factors affecting longevity of homograft valves used in right ventricular outflow tract reconstruction for congenital heart disease. Circulation 2000;102:III130–5.

26. Allen BS, El-Zein C, Cuneo B, Cava JP, Barth MJ, Ilbawi MN. Pericardial tissue valves and Gore-Tex conduits as an alternative for right ventricular outflow tract replacement in children. Ann Thorac Surg 2002;74:771–7.

KEY WORDS congenital heart disease, reconstruction, right ventricular outflow swine model, tissue engineering, tract stem cells

APPENDIX For supplemental figures and a video, please see the online version of this paper.

JACC: BASIC TO TRANSLATIONAL SCIENCE VOL. 4, NO. 3, 2019

PRECLINICAL RESEARCH

Malonyl CoA Decarboxylase Inhibition Improves Cardiac Function Post-Myocardial Infarction

Wei Wang, MD, PhD,[a,b,*] Liyan Zhang, PhD,[a,*] Pavan K. Battiprolu, PhD,[c] Arata Fukushima, MD, PhD,[a] Khanh Nguyen, BS,[c] Kenneth Milner, BS,[a] Abhishek Gupta, PhD,[a] Tariq Altamimi, PhD,[a] Nikole Byrne, BS,[a] Jun Mori, MD, PhD,[a] Osama Abo Alrob, PhD,[a] Cory Wagg,[a] Natasha Fillmore, PhD,[a] Shao-hua Wang, MD, PhD,[b] Dongming M. Liu, BS,[c] Angela Fu, BS,[c] Jenny Yinglin Lu, BS,[c] Mary Chaves, MS,[c] Alykhan Motani, PhD,[c] John R. Ussher, PhD,[d] Jeff D. Reagan, PhD,[c] Jason R.B. Dyck, PhD,[a] Gary D. Lopaschuk, PhD[a]

VISUAL ABSTRACT

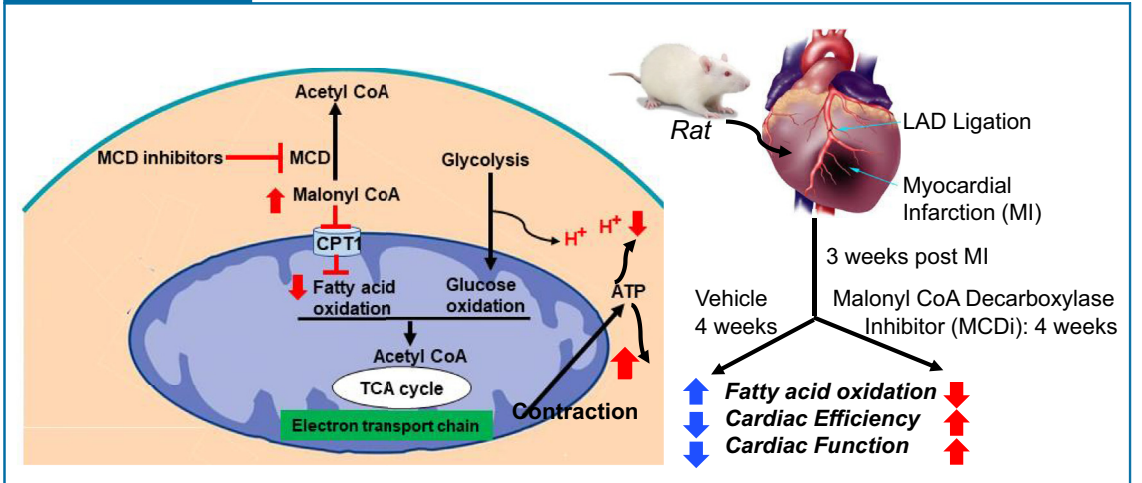

Wang, W. et al. J Am Coll Cardiol Basic Trans Science. 2019;4(3):385-400.

HIGHLIGHTS

- **MCD inhibition decreases fatty acid oxidation via increasing malonyl coenzyme A levels to prevent fatty acid uptake into mitochondria in the failing hearts induced by coronary artery ligation.**
- **Downregulating fatty acid oxidation by MCD inhibition occurrs in conjuction with a decrease in glycolysis and in proton production while an increase in triacylglycerol biosynthesis.**
- **MCD inhibition enhances antioxidative capacity through increasing mitochondrial superoxide dismutase activity via reducing its acetylation.**

From the [a]Cardiovascular Research Centre, Department of Pediatrics, University of Alberta, Edmonton, Alberta, Canada; [b]Department of Cardiac Surgery, University of Alberta, Edmonton, Alberta, Canada; [c]Amgen, San Francisco, California; and the [d]Faculty of Pharmacy and Pharmaceutical Sciences, University of Alberta, Edmonton, Alberta, Canada. *Drs. Wang and Zhang contributed equally to this work and are joint first authors. Drs. Nguyen, Fu, Motani, and Reagan are employees/shareholders of Amgen, Inc. Dr. Lupaschuk has received grants from the Canadian Institutes of Health Research; is an Alberta Heritage Foundation for Medical Research Medical Scientist; and is a shareholder in Metabolic Modulators Research Ltd. All other authors have reported that they have no relationships relevant to the contents of this paper to disclose.

All authors attest they are in compliance with human studies committees and animal welfare regulations of the authors' institutions and U.S. Food and Drug Administration guidelines, including patient consent where appropriate. For more information, visit the *JACC: Basic to Translational Science* author instructions page.

Manuscript received November 13, 2018; revised manuscript received February 4, 2019, accepted February 11, 2019.

ISSN 2452-302X https://doi.org/10.1016/j.jacbts.2019.02.003

ABBREVIATIONS AND ACRONYMS

ATGL = adipose triglyceride lipase

CPT1 = carnitine palmitoyltransferase 1

EF = ejection fraction

FOXO3 = forkhead box O3

MCD = malonyl coenzyme A decarboxylase

MI = myocardial infarction

SERCA2 = sarco(endo)plasmic reticulum Ca^{2+}-ATPase 2

SOD = superoxide dismutase

SPT = serine palmitoyltransferase

TAG = triacylglycerol

Trx = thioredoxin

SUMMARY

Alterations in cardiac energy metabolism after a myocardial infarction contribute to the severity of heart failure (HF). Although fatty acid oxidation can be impaired in HF, it is unclear if stimulating fatty acid oxidation is a desirable approach to treat HF. Both immediate and chronic malonyl coenzyme A decarboxylase inhibition, which decreases fatty acid oxidation, improved cardiac function through enhancing cardiac efficiency in a post-myocardial infarction rat that underwent permanent left anterior descending coronary artery ligation. The beneficial effects of MCD inhibition were attributed to a decrease in proton production due to an improved coupling between glycolysis and glucose oxidation. (J Am Coll Cardiol Basic Trans Science 2019;4:385–400)

Ischemic heart disease and heart failure (HF) are the major causes of death worldwide. As such, there is an urgent need for novel therapeutic approaches that focus on different mechanisms to improve outcomes of patients suffering from ischemic heart disease and HF. Adverse remodeling of the myocardium after a myocardial infarction (MI) contributes to the severity of HF (1), which includes alterations in myocardial energy metabolism (1,2). Whereas it is generally accepted that mitochondrial oxidative metabolism is compromised in the failing heart (3), there is less agreement as to whether the heart switches energy substrate preference in the failing heart (3). Impaired mitochondrial oxidative metabolism in the failing heart can decrease not only fatty acid oxidation, but also glucose oxidation (2,4,5). This is accompanied by an increase in glycolysis as the remodeled heart attempts to compensate for the decrease in mitochondrial energy production (2). This can result in an uncoupling between glycolysis and glucose oxidation, which accelerates proton production. As a result, energy has to be used for correcting acidosis-induced dysregulation of ion homeostasis (including Na^+ and Ca^{2+} overload) rather than supporting mechanical function, which ultimately decreases cardiac mechanical efficiency (2,6,7).

SEE PAGE 401

Although fatty acid oxidation can be impaired in HF (due to a decrease in mitochondrial oxidative capacity) it is unclear if stimulating fatty acid oxidation is a desirable approach to treat HF. Increasing fatty acid oxidation by cardiac-specific overexpression of peroxisome proliferator-activated receptor α results in the development of cardiomyopathy (8). Administration of peroxisome proliferator-activated receptor α agonists to isolated perfused hearts also decreases cardiac efficiency (9). In contrast, cardiac-specific deletion of acetyl CoA carboxylase 2, which lowers malonyl CoA, accelerates fatty acid oxidation, and improves cardiac function in mice subjected to transverse aortic constriction (10). However, this approach also markedly improves the coupling of glycolysis to glucose oxidation, resulting in a decreased lactate production. Improved coupling of glycolysis to glucose oxidation has been shown to be beneficial in reducing the symptoms of myocardial ischemia (2,6,7,11,12). This can be achieved by inhibiting fatty acid oxidation, which increases glucose oxidation, thereby improving the coupling of glycolysis to glucose oxidation (13). This approach benefits cardiac function (6,11,14) and reduces infarct size (6) in the immediate post-ischemic period.

Malonyl CoA is a key regulator of fatty acid oxidation, which inhibits carnitine palmitoyltransferase 1 (CPT1) and prevents the mitochondrial uptake of fatty acids. Myocardial malonyl CoA levels can be increased by inhibiting malonyl CoA decarboxylase (MCD), the enzyme responsible for malonyl CoA degradation (11,12). Deletion of MCD ($MCD^{-/-}$) protects the hearts from ischemia/reperfusion injury and decreases infarct size (6), which is associated with an increase in malonyl CoA levels, a decrease in fatty acid oxidation, and an increase in glucose oxidation (6,12). Similar findings have been recapitulated following immediate pharmacological inhibition of MCD in an experimental model of ex vivo ischemia/reperfusion injury in the heart (11,15).

The objective of this study was to determine whether immediate or chronic inhibition of cardiac fatty acid oxidation by pharmacological inhibiting MCD in MI rats, induced by a permanent left anterior descending coronary artery ligation, could decrease the severity of HF post-MI.

METHODS

ANIMAL CARE. All protocols performed on male Sprague-Dawley rats (200 to 300 g, Charles River,

Wilmington, Massachusetts) were reviewed and approved by the Animal Care and Use Committee at University of Alberta, or by Amgen's Internal Animal Care and Use Committee. All animal experiments were performed in accordance with the guidelines of Canadian Council of Animal Care.

IMMEDIATE EFFECT OF MCD INHIBITION ON HEMODYNAMIC ANALYSIS, CARDIAC MALONYL CoA LEVELS, AND EXERCISE CAPACITY TESTING. A series of male Sprague-Dawley rats (n = 25) underwent a sham (n = 8) or an MI (n = 17) (6,16) procedure. At 9 weeks post-MI, rats were subjected to transthoracic echocardiogram for invasive hemodynamic analysis with a 120-min short-term intravenous stepped-dose infusion of the MCD inhibitor (CBM-3001106, obtained from Metabolic Modulators Research Ltd., Edmonton, AB, Canada) to assess the cardiac function. Then the hearts were isolated for assessing the levels of malonyl CoA. To measure the exercise capacity, rats were randomized (sham, n = 6; MI, n = 7) to a graded exercise test that was performed at a 5% incline, beginning with 10 m/min for 1 min, 11 m/min for 1 min, 12 m/min for 1 min, 13 m/min for 2 min, 15 m/min for 5 min, 17 m/min for 5 min, and 20 m/min until exhaustion (17). A rat was deemed to be fatigued when it was no longer able to run on the treadmill, as judged by rat spending >50% of time or >30 consecutive seconds on the platform and resistant to prodding by the air puff.

IMMEDIATE EFFECT OF MALONYL CoA ON INHIBITING FATTY ACID OXIDATION IN LIVER AND HEART MITOCHONDRIA. The dose-dependent effect of malonyl CoA on inhibiting fatty acid oxidation in liver (n = 12) and heart (n = 6) was discovered in vitro by using freshly isolated mitochondria from the tissue homogenate centrifuged at 27,000 × g for 10 min. The pellet was re-suspended in a A buffer containing 70 mmol/l sucrose, 210 mmol/l mannitol, 5 mmol/l 4-(2-Hydroxyethyl)piperazine-1-ethanesulfonic acid, N-(2-Hydroxyethyl)piperazine-N′-(2-ethanesulfonic acid) (HEPES), 1 mmol/l ethylene glycol-bis(β-aminoethyl ether)-N,N,N′,N′-tetraacetic acid (EGTA), and 0.5% (w/v) fatty acid-free bovine serum albumin (BSA) (pH 7.2) and centrifuged at 10,000 × g. The resulting pellets were re-suspended in the ice-cold A buffer without BSA, from which, 1.5 μg of protein were used for recording fatty acid oxidation as a rate of oxygen consumption by using a Seahorse XF96 Extracellular Flux Analyzer (Seahorse Bioscience, North Billerica, Massachusetts). The substrates consist of either 10 mmol/l pyruvate/2 mmol/l malate or 160 μmol/l palmitoyl CoA/0.5 mmol/l carnitine/0.2 mmol/l malate. Malonyl CoA was added to a final concentration of either 100 μmol/l, 10 μmol/l, 1 μmol/l, 100 nmol/l, or 0 nmol/l. Following this, adenosine diphosphate was added to a final concentration of 6 mmol/l, followed by oligomycin (2 μmol/l final) and carbonyl cyanide 4-(trifluoromethoxy)-phenylhydrazone (4 μmol/l final).

MALONYL CoA CONTENT ASSESSMENT. This was performed via high-performance liquid chromatography (6,18). To optimize the dosage of MCD inhibitor on altering malonyl CoA levels, the male rats (n = 32) were administrated with different oral doses of MCD inhibitor (0, 1, 3, 10, 20, 50, 100 mg/kg BW (body weight), n = 4 to 5/group). The hearts and gastrocnemius muscle were isolated at 12 h post-treatment for assessing the levels of malonyl CoA.

CHRONIC INTERVENTIONS OF MI MODEL AND INFARCT SIZE ASSESSMENT. Sham (n = 16) and post-MI rats (n = 31) were randomized into 5 groups: 1) sham + vehicle (ethanol + DMSO + Cremophor + H_2O); 2) sham + high-dose MCD inhibitor (100 mg/kg/day); 3) MI + vehicle; 4) MI + low-dose MCD inhibitor (50 mg/kg/day); and 5) MI + high-dose MCD inhibitor (100 mg/kg/day), for daily oral gavage for a 4-week period. The infarct size was assessed by cutting the frozen hearts (n = 7 to 8/group) into ~10 μm slices followed by incubation in 1% triphenyltetrazolium chloride for 10 min at 37°C as described previously (6).

ASSESSMENT OF IN VIVO CARDIAC FUNCTION. At 3 weeks post-MI and 4 weeks post-treatment (7 weeks post-MI), rats were subjected to an ultrasound echocardiography using a VisualSonics Vevo 2100 machine (VisualSonics Inc, Canada) to assess in vivo left ventricular ejection fraction (%EF). Parasternal long axis and short axis views were performed in both systole and diastole from the base to apex. The Simpson method was used for the data analysis (19).

ASSESSMENT OF EX VIVO CARDIAC FUNCTION AND ENERGY METABOLISM BY HEART PERFUSION. At the end of the 7-week study period, heart perfusions were performed with oxygenated Krebs-Henseleit solution, consisting of either 0.8 mmol/l palmitate bound to 3% fatty acid-free BSA, 5 mmol/l [5-^{3}H/U-^{14}C]glucose for glycolysis and glucose oxidation measurements, or with 0.8 mmol/l [9,10-^{3}H] palmitate bound to 3% fatty acid-free bovine serum albumin, and 5 mmol/l glucose for fatty acid oxidation measurements (16). Hearts were perfused aerobically for 30 min without insulin and an additional 30 min with insulin (100 μU/ml), then were snap frozen for later biochemical analysis.

CALCULATIONS OF PROTON PRODUCTION RATES, ADENOSINE TRIPHOSPHATE PRODUCTION RATE, CARDIAC WORK. Proton production rates were

calculated following the equation: 2 × (glycolysis rates − glucose oxidation rates) (16). Adenosine triphosphate (ATP) production rates were calculated based on ATP production from each substrate (104 for palmitate oxidation, 29 for glucose oxidation, and 2 for glycolysis) (18). Cardiac work (unit as Joules/min/g dry weight) was calculated following the equation: cardiac output × (peak systolic pressure − preload pressure) × 0.1332 × 10^{-3}/3,600/heart dry mass. The preload pressure is determined by the flow to the atria, which is controlled by the height of the oxygenator above the perfused heart with a value of 11.5 mm Hg. The cardiac efficiency was calculated as: cardiac work/total ATP production rates (18).

MEASUREMENT OF TRIACYLGLYCEROL AND THE INCORPORATION OF ^{3}H-PALMITATE INTO TRIACYLGLYCEROL. Triacylglycerol (TAG) content was assessed in the set of hearts perfused with [9,10-^{3}H]palmitate in the perfusate (n = 6 to 7/group) as described previously (16) by colorimetric assay kit (Wako Pure Chemical Industries, Richmond, Virginia), while another potion of the lipid extraction was counted with scintillation fluid to measure the incorporation of [9,10-^{3}H]palmitate into TAG based on the specific activity of [9,10-^{3}H]palmitate from the perfusate.

MEASUREMENT OF GLYCOGEN AND THE INCORPORATION OF GLYCOGEN FROM ^{3}H-GLUCOSE. Glycogen was assessed in the set of hearts perfused with [5-^{3}H]glucose (n = 6 to 9/group) via measurement of glucose content by using glucose assay kit (Sigma), as described previously (16).

DETECTION OF LACTATE DEHYDROGENASE ISOENZYMES. Heart proteins (20 μg/well) were electrophoresed on 6% native gel at 4°C as described previously (20), and followed by western blot to detect isoforms of lactate dehydrogenase (LDH), of which the densitometry were analyzed using Image J-win64 software.

MEASUREMENT OF ENZYME ACTIVITIES. Citrate synthase activity (n = 7 to 8/group) was measured based on continuous kinetic changes of absorbance at 412 nm over 2 to 5 min by recording the reduction of dithiobis-nitrobenzoic acid. Complex I activity (n = 7 to 8/group) was measured by recording the reduction of 2,6-dichloroindophenol at 600 nm (21). Cytosolic glycerol-3-phosphate acyltransferase activity (n = 6/group) was measure by using cytosolic fractions of heart samples in the assay buffer containing 1 mmol/l glycerol-3-phosphate, 0.1 mmol/l palmitoyl CoA, and 0.1 mmol/l 5,5′-dithio-bis-2-nitrobenzoic acid at 412 nm (22). Superoxide dismutase 2 (SOD2) activity (n = 7 to 8/group) was measured in the presence of 1 mmol/l KCN potassium cyanide (to inhibit Cu/ZnSOD activity) at 450 nm by using water soluble tetrazolium salt-1 (WST-1) that produces a water-soluble formazan dye upon reduction with superoxide anion (23).

FRACTIONATION OF NUCLEAR OR CYTOSOLIC PROTEINS. Frozen heart tissues were homogenized in a buffer containing 10 mmol/l HEPES (pH 7.9), 1.5 mmol/l MgCl2, 10 mmol/l KCl, and 0.05% NP40 with cocktail of protease inhibitor and 2 mmol/l DTT. The resulting pellets, after the centrifugation at 1,000 × g for 15 min at 4°C, were resuspended for nuclear protein assays. The resulted supernatant was subjected to centrifugation at 10,000 × g for 60 min at 4°C to obtain the supernatant as cytosolic protein fraction.

WESTERN BLOTTING AND IMMUNOPRECIPITATION. The following antibodies were used: adipose triglyceride lipase (ATGL), lamin A and thioredoxin-1 (Cell Signaling Technology); sarco(endo)plasmic reticulum Ca^{2+}-ATPase 2 (SERCA2, Pierce); CD36 and forkhead box O3 (FOXO3), SIRT3, and LDH (Abcam). Serine palmitoyltransferase (SPT1) (Santa Cruz Biotechnology). To detect acetylation of mitochondrial SOD2, 500 μg of the total heart lysates were used for incubation with 10 μl acetyl-lysine antibodies (Millipore) and protein A/G-agarose beads (Santa Cruz Biotechnology) overnight at 4°C followed by incubation with the antibody against SOD2. To determine the interaction of MCD with SOD2 (Millipore), the heart lysates were immunoprecipitated with MCD antibody or with mitochondrial SOD2 antibody, then western blots were performed to detect SOD2 or MCD from the respective membranes. Positive control was the same sample(s) used for immunocapture without incubation of antibody. The negative control was the antibody (immunoglobulin G) used for immune-capture without incubation of the respective samples. Bound antibody was visualized by incubation with enhanced chemiluminescent substrate. ImageJ-win64 (by Johannes Schindelin, Albert Cardona, Mark Longair, Benjamin Schmid, and others) was used for evaluation of each band (n = 4 to 5/group, except n = 3/group for immunoprecipitation).

STATISTICAL ANALYSIS. Values represent the mean ± SD. Samples sizes are indicated in the table and figure legends. The significance of differences for multiple comparisons in **Figures 1D, 2B, 2F to 2K, and 3 to 5** was analyzed by 1-way analysis of variance (ANOVA). If ANOVA revealed differences, selected datasets were compared by Bonferroni's multiple comparison test. The significance of differences for the effect of MCD inhibition on time-dependent changes of cardiac function in **Figures 1F to 1H, 1J to 1L, and 6** was analyzed by 2-way ANOVA. The significance

of differences between 2 groups was estimated by unpaired, 2-tailed Student's *t* test where appropriate. Differences were considered significant at $p < 0.05$.

RESULTS

IMMEDIATE MCD INHIBITION INCREASES MALONYL CoA LEVELS AND INHIBITS FATTY ACID OXIDATION AND STIMULATES GLUCOSE OXIDATION IN NORMAL RAT HEARTS AND IMPROVES CARDIAC FUNCTION IN FAILING HEARTS. The direct effects of the MCD inhibitor CBM-3001106 on fatty acid and glucose oxidation were initially examined in isolated working rat hearts. A dose of 1 μmol/l CBM-3001106 added to the hearts resulted in a decrease in fatty acid oxidation rates (Figure 1A) and a significant increase in glucose oxidation rates (Figure 1B) without affecting ex vivo cardiac function (data not shown). This was accompanied by a significant increase in cardiac malonyl CoA levels (Figure 1C). Twelve hours after oral administration a single dose of either 50 or 100 mg/kg of CBM-3001106 to rats, a significant increase in cardiac malonyl CoA levels was also evident (Figure 1D). Malonyl CoA showed a dose-dependent inhibition of fatty acid oxidation as reflected by a decrease in oxygen consumption rates (Figure 1E). However, the concentration that inhibits 50% was 900 nmol/l in heart mitochondria and greater than 100 μmol/l in liver mitochondria (Figure 1E), supporting the concept that malonyl CoA has a higher binding affinity to CPT1 in heart than in liver (24).

To investigate if Immediate inhibition of MCD could improve cardiac function in failing hearts, invasive hemodynamics was used to assess cardiac function following a 120 min, immediate intravenous stepped-dose infusion of CBM-3001106 to 9-week post-MI rats. MI-rats exhibited a significant decrease in %EF, stroke volume, and exercise capacity, whereas an increase in left atria diameter was seen (Table 1). Immediate exposures of CBM-3001106 to the post-MI hearts dose-dependently increased %EF (Figure 1F) and stroke volume (Figure 1G), whereas there was decreased peak elastance (Figure 1H), which was accompanied by an increase in malonyl CoA levels (Figure 1I). In contrast, Immediate exposure to CBM-3001106 had no effects on these factors in sham hearts (Figures 1J to 1L), neither had effect on maximal/minimal rate of rise of left ventricular pressure (dp/dt max/min), and systolic/diastolic duration in either sham (Figures 6A, 6C, 6E, and 6G) or post-MI hearts (Figures 6B, 6D, 6F, and 6H). The minimally effective concentration to improve cardiac function was 10 μmol/l in the sham group (Figure 6I), but required a lower concentration (4 μmol/l) in the MI group (Figure 6J).

CHRONIC MCD INHIBITION IMPROVES CARDIAC FUNCTION IN FAILING HEARTS. To determine if chronic MCD inhibition was beneficial in failing hearts, rats were treated orally for a 4-week period with a high or low dose of CBM-3001106, starting at 3 weeks post-MI surgery (Figure 2A). Before treatment, the decrease in %EF was similar among all post-MI groups compared to sham (Figure 2B). However, over the subsequent 4-week treatment period a significant increase in %EF was evident in the MI + high-dose group (Figures 2B to 2E), which was further supported by comparing individual %EF value in the post-MI rats between the pre-treatment and post-treatment periods (Figure 2E). In contrast, %EF continued to decline in the majority of the vehicle-treated post-MI rats (Figure 2C).

To further illustrate the chronic effect of MCD inhibition on cardiac function, ex vivo cardiac function was assessed in isolated working hearts at the end of the 4-week treatment period (Figure 3F). Cardiac work was similar between the sham groups (Table 2), but was reduced in the MI + vehicle group (Figure 2F). The reduction in cardiac work was significantly restored by both the low- and high-dose MCD inhibition (Figure 2F), regardless of the presence or absence of insulin (Table 3). The restoration of function was accompanied by an increase in the protein expression of SERCA2 (Figure 2G) without affecting heart weight (Figure 2H), and the size of the left ventricular infarct scar tissues (Figure 2I), confirming that the beneficial effect of MCD inhibition on cardiac function was not due to the differences in the severity of the infarct among the groups.

The efficacy of in vivo MCD inhibitor in increasing tissue malonyl CoA levels was evident not only in ex vivo perfused hearts (Figure 2J), but also in gastrocnemius muscle (Figure 2K) from post-MI rats after the high- and low-dose MCD inhibitor treatment.

CHRONIC MCD INHIBITION ENHANCES CARDIAC EFFICIENCY BY ALTERING ENERGY METABOLISM IN FAILING HEARTS. To understand the mechanisms underlying chronic MCD inhibition-mediated improvement of cardiac function, the energy metabolism rates in the perfused hearts were assessed. Since cardiac insulin resistance has been suggested to be a contributor to HF (5,18), the heart perfusions were performed with and without insulin to check if cardiac insulin sensitivity was altered in post-MI hearts. Absolute fatty acid oxidation rates were similar among the groups regardless of the absence or the presence of insulin (Table 3). Because cardiac

FIGURE 1 Acute Effects of CoA Decarboxylase Inhibition on Cardiac Energy Metabolism and Malonyl CoA Levels in Normal Rat Hearts and on Cardiac Function in Post-Myocardial Infarction Failing Rat Hearts

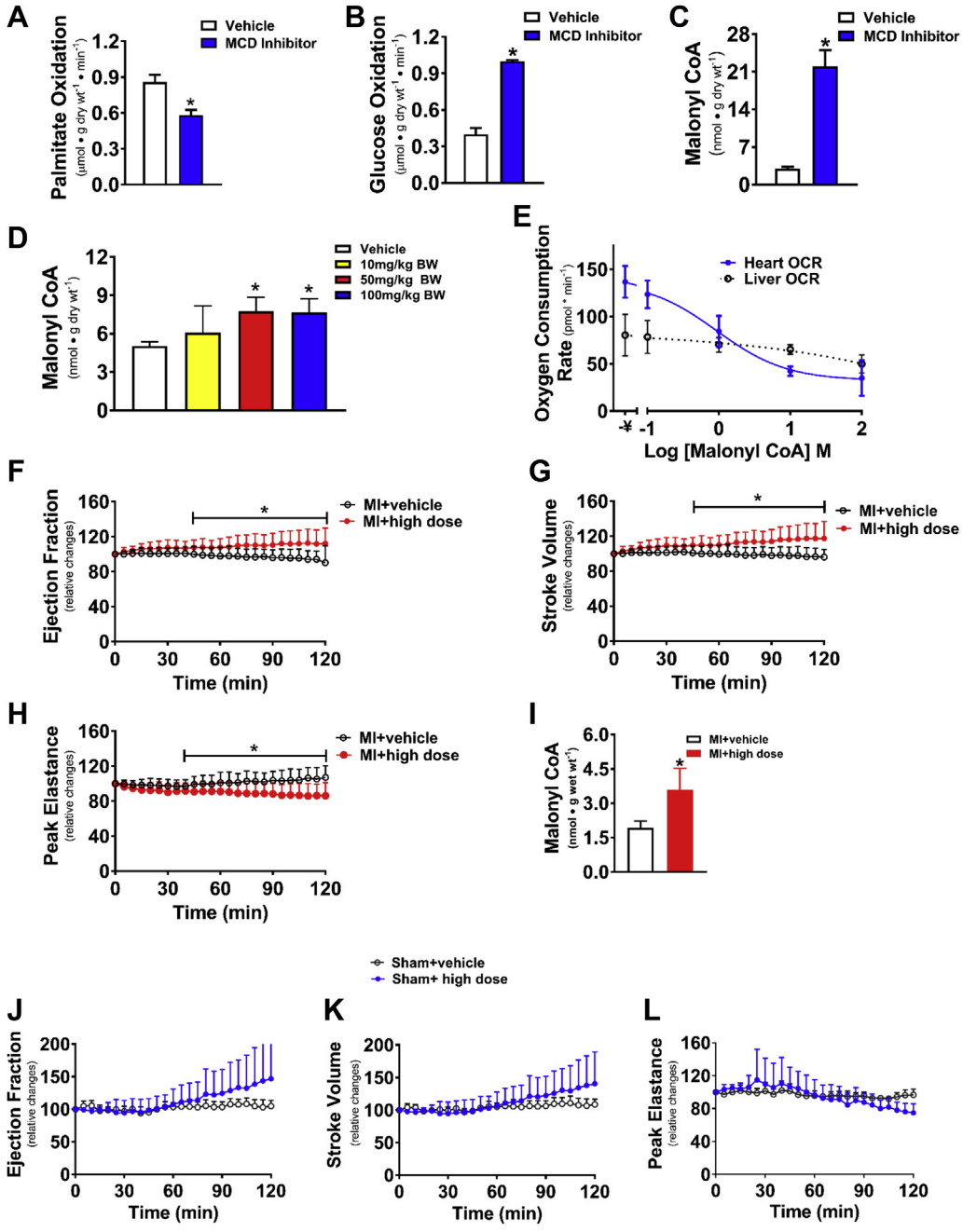

Effects of 1 μmol/l CBM-300116 on rates of palmitate oxidation **(A),** glucose oxidation **(B),** and levels of malonyl CoA **(C)** in perfused hearts (n = 5). Dose-dependent changes in cardiac malonyl CoA content (n = 4 to 5/group) 12-h post-malonyl CoA decarboxylase (MCD) inhibition **(D).** Differential effect of malonyl CoA on inhibiting fatty acid oxidation in heart (n = 6/group) and liver mitochondria (n = 12/group) **(E).** Invasive hemodynamic analysis in failing and sham rat hearts with a 120-min acute intravenous stepped-dose infusion of the MCD inhibitor, including relative changes from the baseline of systolic function in percent ejection fraction (EF) **(F and J),** of stroke volume **(G and K),** and of peak elastance **(H and L)** as well as the malonyl CoA content in myocardial infarction (MI) hearts **(I)** (n = 7 to 8/group). Values represent the mean ± SD. *p < 0.05, significantly different from the vehicle group. BW = body weight; CoA = Malonyl Coenzyme A; OCR = oxygen consumption rate.

FIGURE 2 Effect of Chronic MCD Inhibition on In Vivo and Ex Vivo Cardiac Function in Failing Rat Hearts

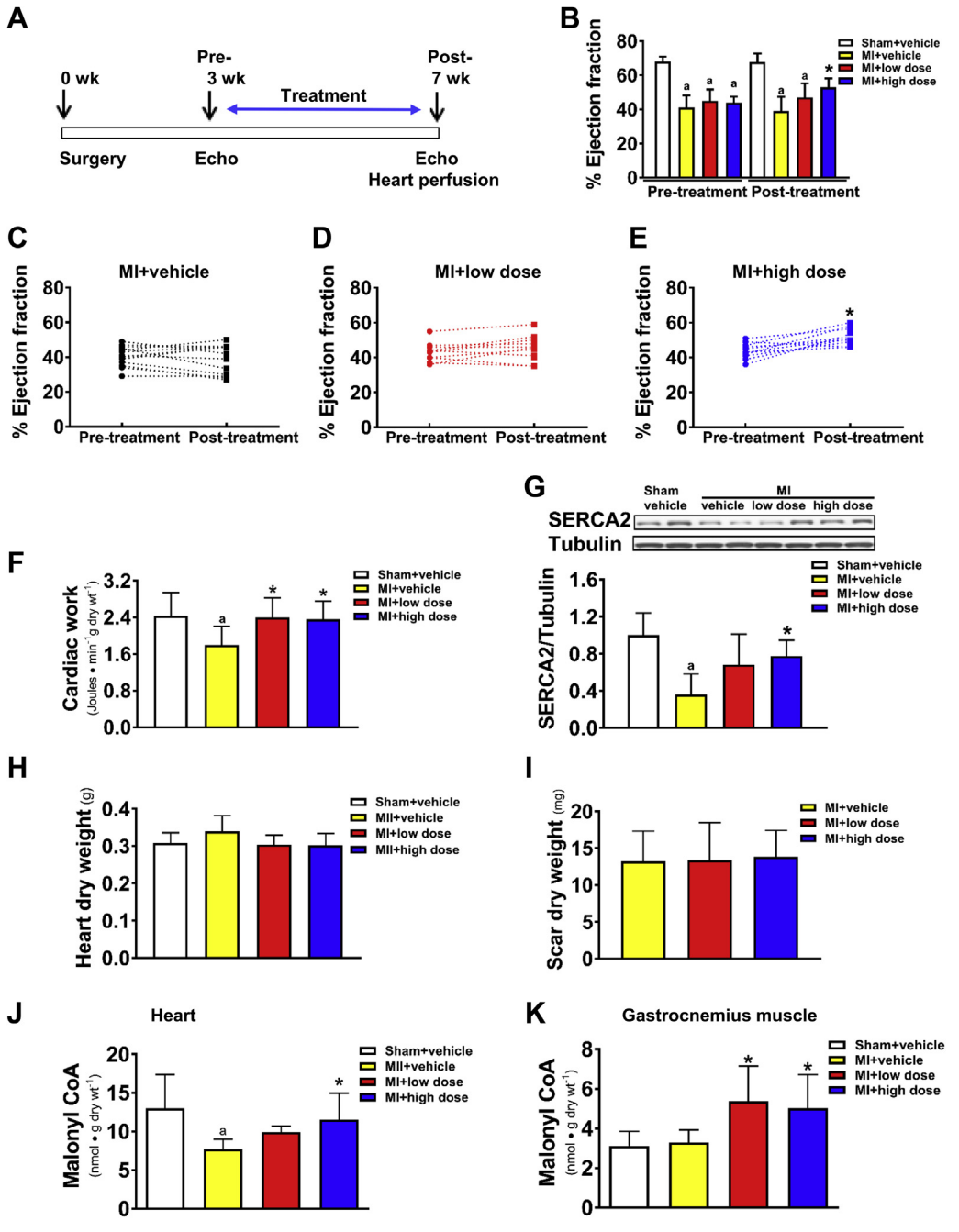

Schematic drawing of the experimental timeline **(A).** Rats were subjected to a permanent left anterior descending artery ligation to product an MI. Three-weeks post-MI, rats were treated with 50 mg/kg/day (low dose) or 100 mg/kg/day (high dose) of CBM-3001106 for an additional 4 weeks. Alterations of %EF pre- and post-MCD inhibition **(B).** Alterations of %EF in the individual MI rats pre- and post-MCD inhibition **(C to E).** Cardiac work in perfused working hearts **(F).** Representative blots of SERCA2 and densitometric analyses **(G).** Heart dry weight **(H).** Scar dry weight **(I).** Malonyl CoA content in perfused hearts **(J)** and in gastrocnemius muscle **(K).** Values represent the mean ± SD (n = 5 to 11/group). $^{a}p < 0.05$ or $^{*}p < 0.05$, significantly different from sham + vehicle or MI + vehicle group, respectively. Abbreviations as in Figure 1.

FIGURE 3 Effect of Chronic MCD Inhibition on Cardiac Energy Metabolism in Failing Rat Hearts

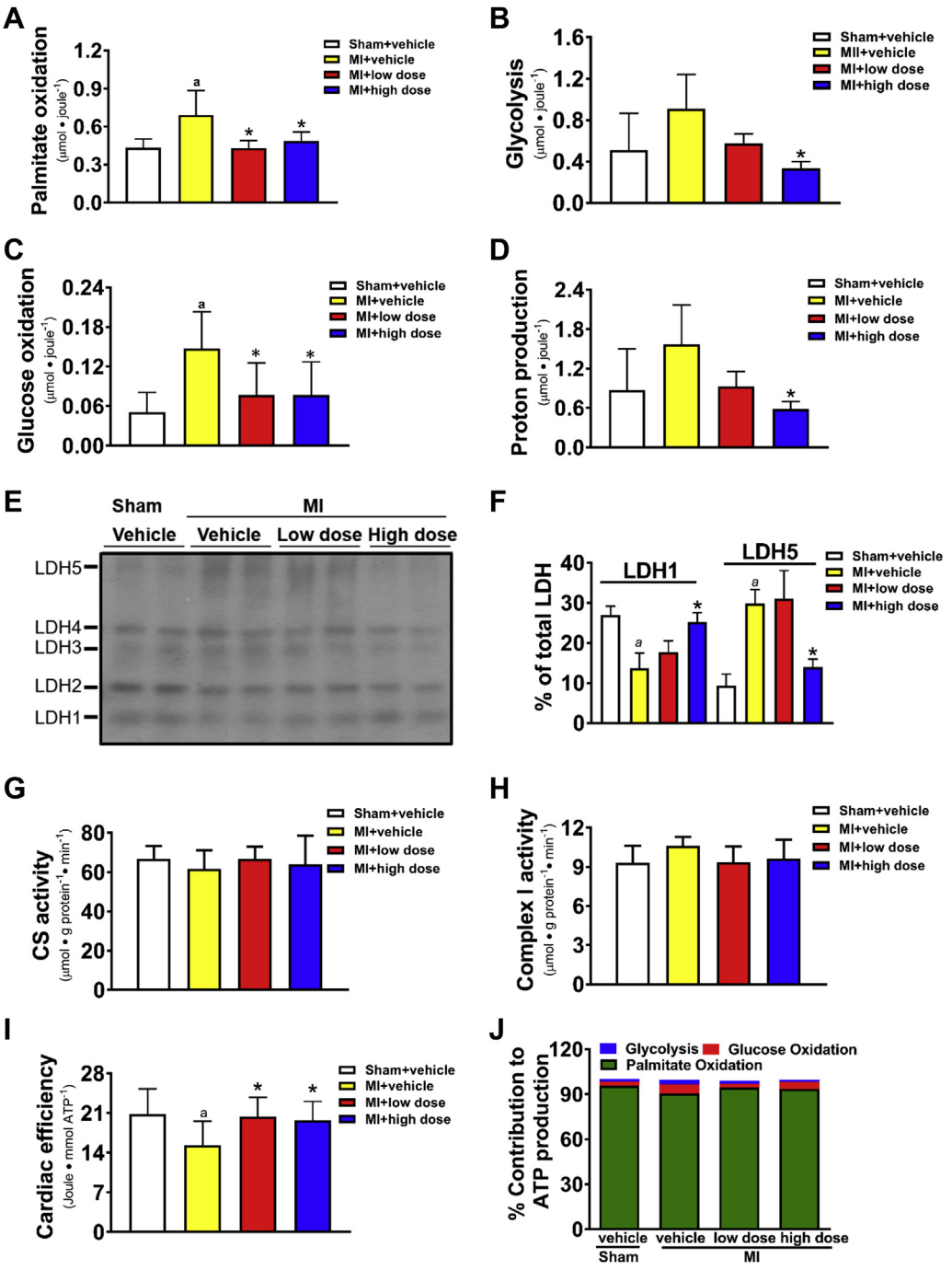

Post-MI rats were treated with 50 mg/kg/day (low dose) or 100 mg/kg/day (high dose) of CBM-3001106 for 4 weeks, followed by isolated working heart perfusions. Rates of palmitate oxidation per cardiac work **(A).** Rates of glycolysis per cardiac work **(B).** Rates of glucose oxidation per cardiac work **(C).** Rates of proton production **(D).** Expression of lactic acid dehydrogenase (LDH) isoenzymes **(E)** and % of LDH1 and LDH5 in total LDH **(F).** Citrate synthase activity **(G).** Mitochondrial complex I activity **(H).** Cardiac efficiency **(I).** Percent contribution of adenosine triphosphate (ATP) production from individual substrate **(J).** Values represent the mean ± SD (n = 3 to 10). $^{a}p < 0.05$ or $^{*}p < 0.05$, significantly different from sham + vehicle or MI + vehicle group, respectively. CS = citrate synthase; other abbreviations as in Figure 1.

FIGURE 4 Effect of Chronic MCD Inhibition on Status of Myocardial Triacylglycerol, on Serine Palmitoyltransferase 1 Protein Expression, and Alterations of Glycogen

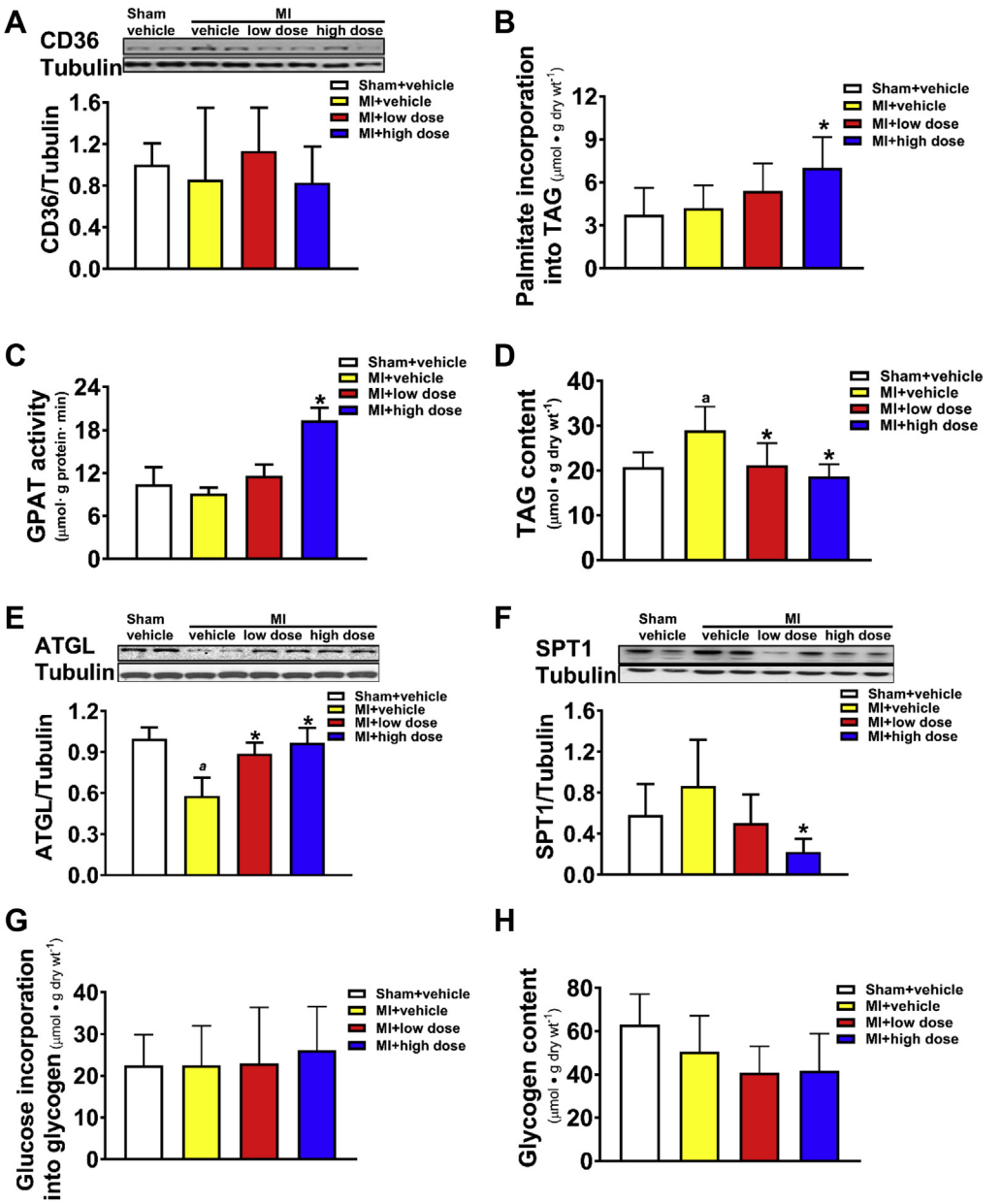

Post-MI rats were treated with 50 mg/kg/day (low dose) or 100 mg/kg/day (high dose) of CBM-3001106 for 4 weeks. Protein expression of CD36 **(A).** Incorporation of [^{3}H]-palmitate into triacylglycerol (TAG) during the 1-h perfusion **(B).** Cytosolic GPAT activity **(C).** Myocardial TAG content **(D).** Protein expression of ATGL **(E),** and of SPT1 **(F).** Glucose incorporation into glycogen **(G).** Glycogen content **(H).** Values represent the mean ± SD (n = 4 to 7). ^{a}p < 0.05 or *p < 0.05, significantly different from sham + vehicle or MI + vehicle group, respectively. ATGL = adipose triglyceride lipase; GPAT = Glycerol-3-phosphate acyltransferase; SPT1 = serine palmitoyltransferase 1; other abbreviations as in Figure 1.

work is a major determinant of cardiac mitochondrial oxidative metabolism (2,25), we normalized the energy metabolic rates by cardiac work. The increases in fatty acid oxidation rates (Figure 3A), in glycolysis rates (Figure 3B) and in glucose oxidation rates (Figure 3C) were prevented in post-MI hearts by MCD inhibition. Absolute rates of glycolysis and glucose oxidation tended to increase in the MI + vehicle

FIGURE 5 Effect of Chronic MCD Inhibition on Anti-Oxidants Expression and Interaction of MCD With Superoxide Dismutase 2

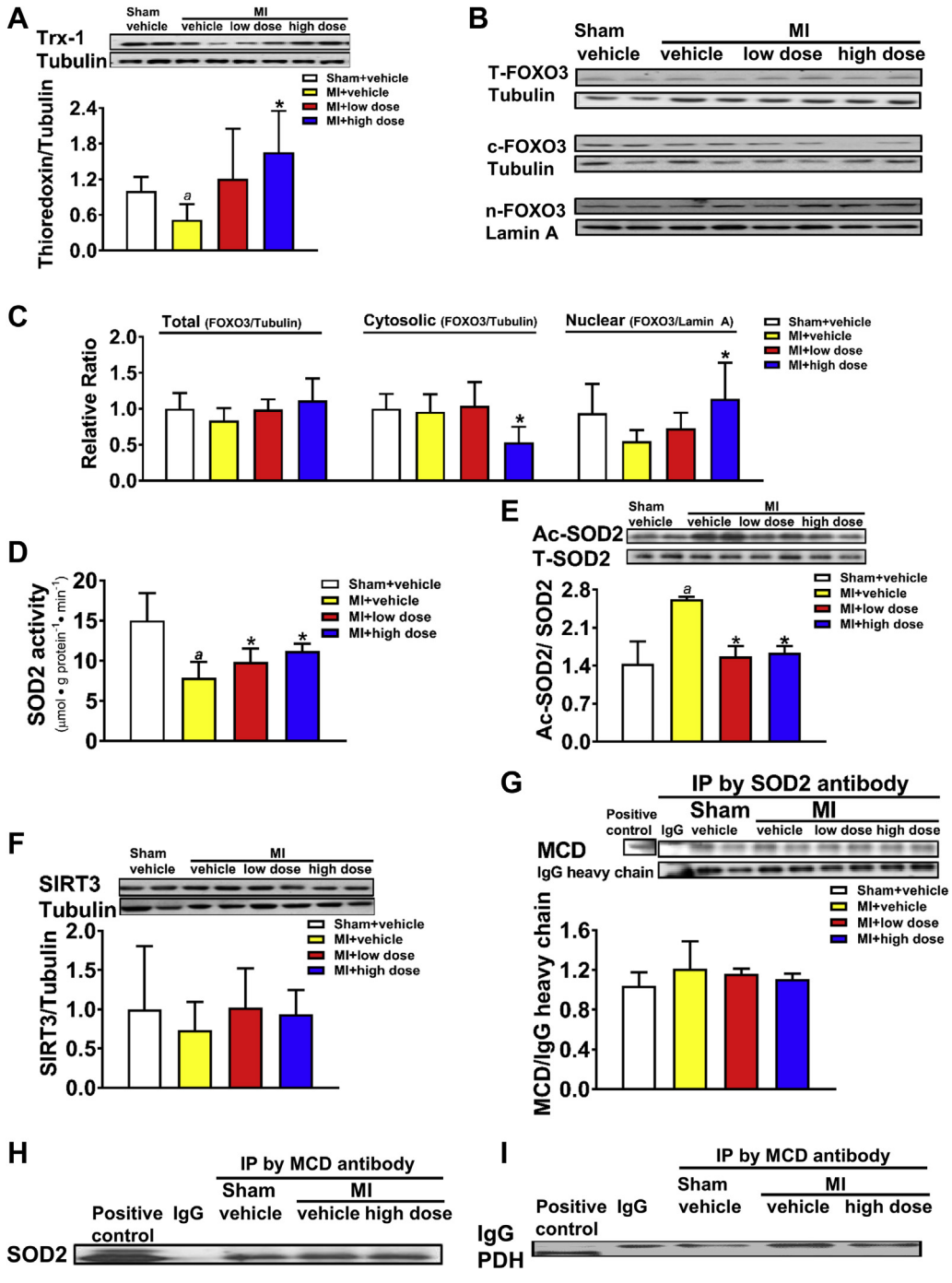

Post-MI rats were treated with 50 mg/kg/day (low dose) or 100 mg/kg/day (high dose) of CBM-3001106 for 4 weeks. Protein expression of thioredoxin-1 (Trx-1) **(A).** Protein expression of total forkhead box O3 (T-FOXO3), cytosolic FOXO3 (c-FOXO3) and nuclear FOXO3 (n-FOXO3) **(B),** as well as the densitometric analyses **(C).** Superoxide dismutase 2 (SOD2) activity **(D).** Acetylated SOD2 (Ac-SOD2) **(E).** Protein expression of SIRT3 **(F).** MCD-SOD2 interaction **(G,H).** Negative interaction of MCD-PDH **(I).** Values represent the mean ± SD (n = 3 to 7). [a]$p < 0.05$ or *$p < 0.05$, significantly different from sham + vehicle or MI + vehicle group, respectively. IgG = immunoglobulin G; Ip = immunoprecipitation; PDH = pyruvate dehydrogenase; SIRT3 = Sirtuin-3; other abbreviations as in Figure 1.

FIGURE 6 Effect of Acute MCD Inhibition on Invasive Hemodynamic Analysis in Failing and Sham Rat Hearts and the Minimally Effective Concentration to Improve Cardiac Function

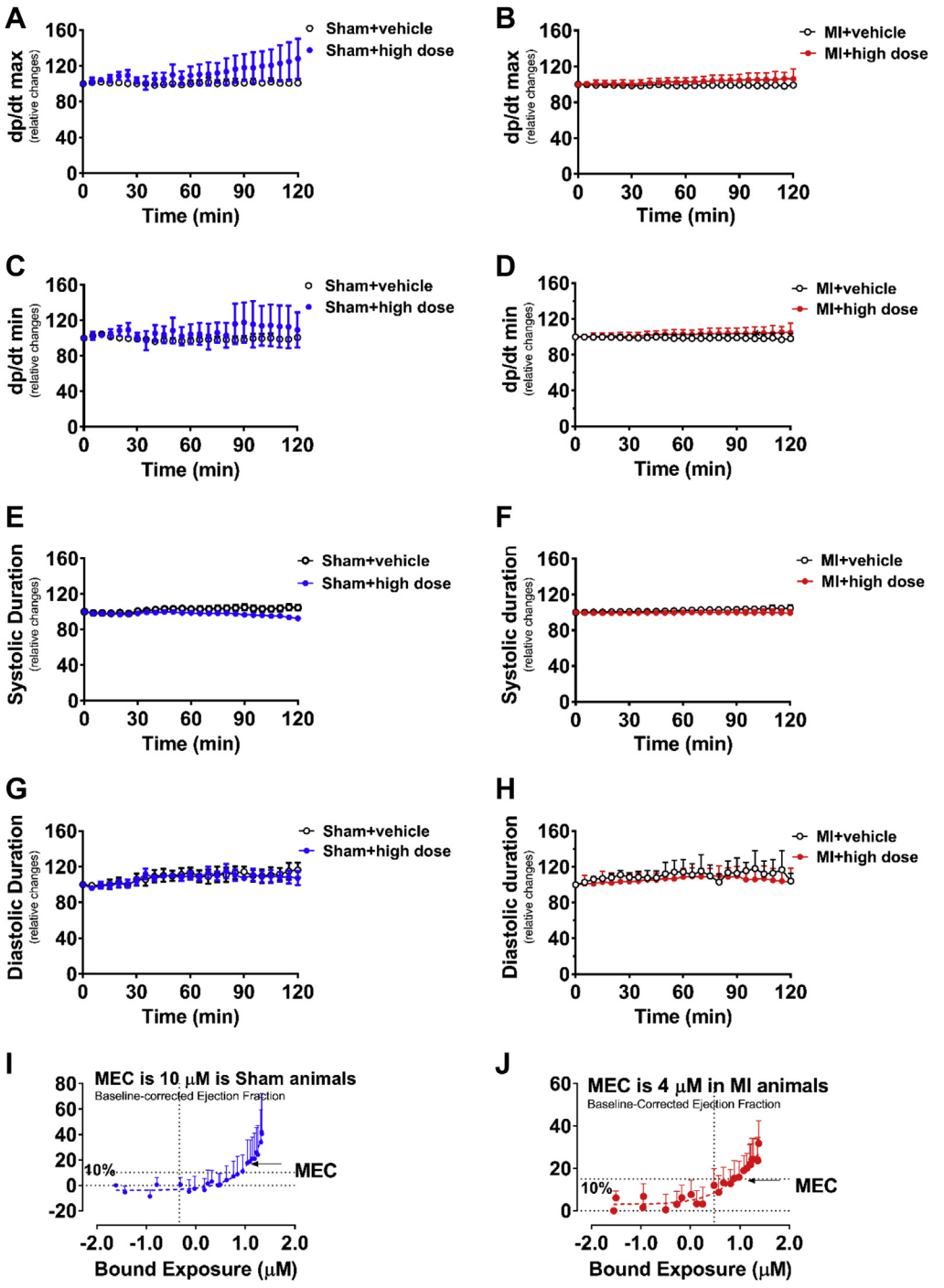

Invasive hemodynamic analysis in failing and sham rat hearts with a 120-min acute intravenous stepped-dose infusion of the MCD inhibitor, including relative changes of dp/dt max **(A,B)** and dp/dt min **(C,D),** relative changes of systolic duration **(E,F),** diastolic duration **(G,H),** as well as the minimal effective concentration (MEC) to improve cardiac function **(I,J).** Values represent the mean ± SD (n = 8 to 17). dp/dt max/min = maximal/minimal rate of rise of left ventricular pressure; other abbreviations as in Figure 1.

TABLE 1 Alterations in Cardiac Function and Exercise Capacity in Sprague Dawley Rats That Underwent Either a Sham or a Coronary Artery Ligation Procedure (Myocardial Infarction) for 9 Weeks

	Sham	MI
Cardiac function	8	17
Heart rate (beats/min)	357.3 ± 13.8	364.7 ± 22.5
Ejection fraction %	65.9 ± 5.7	41.6 ± 8.9*
Stroke volume (μl)	300.5 ± 47.4	216.2 ± 44.3*
Left atria diameter (mm)	4.4 ± 0.5	5.7 ± 0.7*
Exercise capacity	6	7
Body weight (g)	479.8 ± 63.5	507.1 ± 56.9
Running speed ($m \cdot min^{-1}$)	18.3 ± 2.0	12.2 ± 5.2*
Running distance (m)	271.2 ± 145.2	169.2 ± 67.5*

Values are n or mean ± SD. *$p < 0.05$, significantly different from sham + vehicle.

group when compared to sham (Table 3), which resulted in an increased proton production in MI + vehicle group (Figure 3D), whereas the increase was prevented in MI + high-dose group (Figure 3D).

An increase in the expression of M subunit of LDH has been shown to be an indication of an increased glycolytic capacity (26). Five isoenzymes of LDH were observed in hearts (Figure 3E). An increase in the expression of LDH5, the M4 isoenzyme, was evident in the post-MI hearts relative to sham (Figure 3F), whereas MCD inhibition reduced LDH5 but increased LDH1 (Figure 3F), the H4 isoenzyme, in post-MI hearts.

ATP production rates (Table 3) were unchanged among all the groups, as were citrate synthase activity (Figure 3G) and mitochondrial complex I activity (Figure 3H). However, a reduced cardiac efficiency was observed in the MI + vehicle group relative to the sham group (Figure 3I), whereas the reduction was restored by MCD inhibition (Figure 3I). Despite the concept that the failing heart switches from fatty acid to glucose metabolism (2), overall, fatty acid oxidation remained the predominant source of ATP production in the post-MI hearts (Figure 3J).

CHRONIC MCD INHIBITION ENHANCES INCORPORATION OF [^{3}H]-PALMITATE INTO TAG WHILE REDUCING MYOCARDIAL TAG CONTENT AND BIOSYNTHESIS OF CERAMIDE IN POST-MI HEARTS. Inhibiting MCD could divert palmitate into TAG synthesis as an effect of decreasing fatty acid oxidation. Although protein expression of CD36, a major enzyme involved in plasma fatty acid uptake, was unaltered (Figure 4A), the incorporation of ^{3}H-palmitate into TAG (Figure 4B) was increased in the MCD inhibition groups relative to the MI + vehicle group. This increase was mirrored by the activity of cytosolic glycerol phosphate acyltransferase (Figure 4C), the rate-limiting enzyme for de novo TAG synthesis. However, despite this, myocardial TAG content was decreased by MCD inhibition (Figure 4D), accompanied by an upregulation of ATGL, a major enzyme involved in TAG lipolysis (Figure 4E), while downregulating SPT1 (Figure 4F), a key enzyme for ceramide biosynthesis that has been suggested to be a contributor of cardiac dysfunction (27). Unlike myocardial lipids, neither the incorporation of radiolabeled glucose into glycogen (Figure 4G), nor total glycogen content was altered among any of the groups (Figure 4H).

CHRONIC MCD INHIBITION INCREASES ANTIOXIDATIVE CAPACITY IN POST-MI HEARTS. As MCD inhibition-mediated improvement of cardiac dysfunction was accompanied by the alterations in lipid biosynthesis, we determined if any alteration in myocardial antioxidative capacity, which is associated with pathophysiology of HF in humans (28), also occurred concurrently. The protein expression of cardiac thioredoxin-1 (Trx-1), 1 of the molecules with a high antioxidative action in cytosol, was significantly reduced in the MI + vehicle group relative to sham, whereas the reduction was restored in the MI + MCD inhibitor high-dose group (Figure 5A). FOXO3 is known to bind to the Trx-1 promoter, thereby upregulating expression of Trx-1 (29). The total protein expression of cardiac FOXO3 was unaltered among the groups (Figures 5B to 5C). However, the cytosolic expression of FOXO3 was significantly reduced, concomitant with an increased nuclear expression of FOXO3, in the MI + high-dose group relative to the MI + vehicle group (Figures 5B to 5C), implicating an association between upregulation of myocardial Trx-1 and nuclear translocation of FOXO3 in the MI + high-dose group.

In addition, SOD2, a mitochondrial antioxidant, was less active in the post-MI hearts, but the activity was enhanced by MCD inhibition (Figure 5D). Alterations in SOD2 activity were inversely reflected by the acetylation of SOD2 (Figure 5E). Neither protein expression of SIRT3 (Figure 5F), a mitochondrial deacetylase (30), nor GCN5L1, a mitochondrial acetylase, was altered among the groups (data not shown). MCD has been suggested to exhibit acetyltransferase activity (31); therefore, we investigated if acetylation of SOD2 was associated with MCD through a direct interaction. Immunoprecipitation of the heart lysates revealed that SOD2 was captured by the MCD antibody (Figure 5G), and vice versa (Figure 5H), suggestive of an association between MCD and SOD2. In contrast, pyruvate dehydrogenase, a key mitochondrial enzyme modulating glucose oxidation (6), was

unable to be captured by MCD antibody in the same heart lysates (Figure 5I).

DISCUSSION

This study shows several important novel findings. 1) Inhibition of MCD is able to reverse pre-existing HF as the MCD inhibitor was added after HF had already occurred in the post-MI rat (Figures 1F to 1H and 2B). Pharmacological inhibiting MCD in post-MI rats decreases the severity of pre-existing HF post-MI, which is relevant and practical to clinic treatment for HF patients. In the previous studies with MCD-deficient mice it was not possible to separate possible beneficial effects of MCD inhibition during the infarct development from preventing adverse remodeling of the post-MI heart. 2) MCD inhibition is able to immediately improve cardiac function in the failing heart (Figures 1F to 1H), suggesting that optimizing cardiac energy metabolism can acutely improve heart function in the failing heart. 3) Both immediate and chronic inhibition of MCD improves cardiac contractility in the failing hearts, which is associated with an increase in malonyl CoA content in the post-MI hearts, resulting in a decreased cardiac fatty acid oxidation rate. 4) MCD inhibition improves cardiac efficiency that is associated with a reduced proton production through increasing LDH1 expression while decreasing LDH5 expression, thereby ameliorating coupling of glycolysis with glucose oxidation. 5) MCD inhibition can enhance cardiac antioxidant capacity through increasing SOD2 activity by reducing its acetylation. As a result, our data suggest a mechanism that failing heart is metabolically inefficient at using energy, while inhibiting MCD reprograms fuel use prevents proton production that improves cardiac efficiency in the post-MI heart. Thus, inhibiting fatty acid oxidation may be a promising therapeutic approach to treat HF.

It is generally assumed that the heart switches from fatty acid to glucose metabolism in the failing heart (2). If this was the case, it would not appear logical to inhibit fatty acid oxidation as an approach for improving cardiac energetics in the failing heart. It has been proposed by Kolowicz et al. (10) that stimulating fatty acid oxidation may be beneficial in the failing heart. However, it is probably more accurate to suggest that mitochondrial oxidative metabolism decreases in the HF, with a switch in energy metabolism towards glycolysis in HF (2).

Glycolysis is a source of lactate and protons especially when glucose oxidation is impaired (2,22). The clearance of protons is rapid. However, this still decreases the cardiac efficiency because of the association with the influx of Na^+, which can subsequently lead to accumulation of intracellular Ca^{2+}. As a result, a significant amount of cardiac ATP is shunted away from providing energy for contraction to re-establishing normal Na^+ and Ca^{2+} ionic homeostasis (7,32). The assessment of proton production rates in the current study is a technical limitation, which is not a direct measurement but a calculation from the rates of glycolysis and glucose oxidation. Our previous studies have shown that the calculated proton production from glycolysis and glucose oxidation is inversely correlated to intracellular pH, measured by using ^{31}-P-NMR spectroscopy, and to cardiac efficiency in post-ischemic hearts (7), whereas cardiac efficiency is improved in post-ischemic hearts by altering both the source and fate of proton (7,32). Kolowicz et al. (10) also observed an improved coupling of glucose metabolism with a decreased lactate production in mice with cardiac-specific deletion of acetyl CoA carboxylase 2. We further extended our understanding towards the mechanisms underlying MCD inhibition-mediated coupling of glucose metabolism and found an increased expression of LDH1 with a decreased expression of LDH5 in MI hearts post-MCD inhibition.

TABLE 2 Effect of Chronic Malonyl Coenzyme A Decarboxylase Inhibition on Ex Vivo Cardiac Function

	Sham + ve (n = 10)	Sham + High (n = 6)	MI + ve (n = 11)	MI + Low (n = 10)	MI + High (n = 10)
Heart rate (beats/min)					
− Insulin	264 ± 25	269 ± 15	255 ± 51	265 ± 15	264 ± 26
+ Insulin	288 ± 19	281 ± 13	266 ± 50	284 ± 26	289 ± 31
Peak systolic pressure (mm Hg)					
− Insulin	108 ± 7	112 ± 6	102 ± 9	106 ± 5	107 ± 4
+ Insulin	104 ± 7	108 ± 5	101 ± 8	103 ± 5	103 ± 5
Developed pressure (mm Hg)					
− Insulin	42 ± 8	50 ± 10	37 ± 9	40 ± 8	38 ± 6
+ Insulin	37 ± 3	44 ± 8	35 ± 10	35 ± 8	33 ± 6
Cardiac output (ml · min^{-1})					
− Insulin	47 ± 11	50 ± 6	41 ± 9	44 ± 5	41 ± 9
+ Insulin	49 ± 10	52 ± 7	39 ± 10	46 ± 6	43 ± 10
Aortic outflow (ml · min^{-1})					
− Insulin	22 ± 8	24 ± 6	15 ± 7	21 ± 6	19 ± 7
+ Insulin	24 ± 6	25 ± 7	15 ± 6	20 ± 6	18 ± 7
Coronary flow (ml · min^{-1})					
− Insulin	26 ± 8	26 ± 6	22 ± 6	24 ± 6	23 ± 8
+ Insulin	25 ± 7	27 ± 7	23 ± 6	26 ± 6	25 ± 9
Cardiac work (J· min^{-1}· g dry wt^{-1})					
− Insulin	2.4 ± 0.5	3.1 ± 0.9	1.7 ± 0.4*	2.4 ± 0.4†	2.4 ± 0.4†
+ Insulin	2.5 ± 0.1	3.1 ± 0.8	1.8 ± 0.4*	2.5 ± 0.5†	2.3 ± 0.4†

Values are mean ± SD. Sham or post-MI rats were treated with either vehicle (ve), 50 mg/kg/day (low = low dose) or 100 mg/kg/day (high = high dose) of CBM-3001106 for 4 weeks, following which isolated working heart perfusions were performed for 30 min in the absence of insulin, and then 30 min in the presence of 100 μU/ml insulin. *$p < 0.05$ or †$p < 0.05$, significantly different from sham + vehicle or MI + vehicle group, respectively.
MI = myocardial infarction.

TABLE 3 Effect of Chronic Malonyl Coenzyme A Decarboxylase Inhibition on Cardiac Energy Metabolism

	Sham + ve	Sham + High	MI + ve	MI + Low	MI + High
Glucose oxidation: μmol · g dry wt^{-1} · min^{-1}					
− Insulin	0.1 ± 0.05	0.1 ± 0.02	0.2 ± 0.06	0.2 ±0.1	0.2 ± 0.1
+ Insulin	0.3 ± 0.2	0.1 ± 0.04	0.5 ± 0.2	0.4 ± 0.2	0.4 ± 0.2
n	10	6	11	10	10
Glycolysis: μmol · g dry wt^{-1} · min^{-1}					
− Insulin	1.0 ± 0.5	1.0 ± 0.8	1.9 ± 0.7	1.3 ± 0.1	0.9 ± 0.3
+ Insulin	1.3 ± 0.7	0.9 ± 0.5	2.0 ± 0.5	2.0 ± 0.8	1.6 ± 0.4
n	3	3	5	4	3
Palmitate oxidation: μmol · g dry wt^{-1} · min^{-1}					
− Insulin	1.1 ± 0.2	1.0 ± 0.1	1.0 ± 0.2	1.1 ± 0.2	1.1 ± 0.2
+ Insulin	1.0 ± 0.2	0.9 ± 0.1	1.0 ± 0.1	1.1 ± 0.2	1.1 ± 0.4
n	7	3	6	6	7
Proton production: μmol · g dry wt^{-1} · min^{-1}					
− Insulin	1.7 ± 0.8	1.9 ± 1.5	3.1 ± 1.3	2.0 ± 0.2	1.5 ± 0.4
+ Insulin	2.0 ± 1.1	1.4 ± 1.0	3.2 ± 1.1	3.1 ± 1.2	2.5 ± 0.6
n	3	3	5	4	3
ATP production: μmol · g dry wt^{-1} · min^{-1}					
− Insulin	118 ± 16	104 ± 6	119 ± 18	118 ± 12	120 ± 14
+ Insulin	113 ± 20	102 ± 9	127 ± 11	129 ± 15	133 ± 35
n	10	6	11	10	10

Values are n or mean ± SD. Sham or post-MI rats were treated with either vehicle (ve), 50 mg/kg/day (low = low dose) or 100 mg/kg/day (high = high dose) of CBM-3001106 for 4 weeks, following which isolated working heart perfusions were performed for 30 min in the absence of insulin, and then 30 min in the presence of 100 μU/ml insulin.

ATp = adenosine triphosphate; MI = myocardial infarction.

An increase in M subunit of LDH is an indicator of increased glycolytic capacity (26). An increase in LDH5 and a decrease in LDH1 isoenzyme expression was seen in myocardium from patients with chronic HF, in which a shift of LDH pattern towards an increase in LDH1 paralleled by a decrease in LDH5 was observed after treatment with the angiotensin-converting enzyme inhibitor (33). Therefore, we propose that the alteration of LDH isoenzymes in MI hearts post-MCD inhibition may increase to the conversion of lactate to pyruvate, thereby reducing glycolysis to improve the coupling of glucose metabolism. Thus, monitoring of cardiac LDH enzymatic adaptation may be of clinical interest (34).

Decreased mitochondrial fatty acid oxidation with MCD inhibition has the potential to shunt fatty acids towards TAG. However, instead of increasing TAG levels, the decrease in TAG level and an increased ATGL expression were observed concomitant with a reduction of SPT1 in MI hearts post-MCD inhibition, suggesting a reduction of ceramide biosynthesis occurred in conjunction with an increased TAG turnover by MCD inhibition. Tian et al. (35) have recently shown that elevated rates of TAG turnover due to cardiac-specific overexpression of DGAT1 Diacylglycerol O-Acyltransferase 1 are associated with improved functional recovery from ischemic stress, in part, by sequestering fatty acids into the TAG pool and reducing the accumulation of ceramides (35). In addition, among the lipids, ceramide, as a potent massager molecule to induce oxidative stress, is associated with pathophysiology of HF in humans (28). Our data also suggest that MCD inhibition enhances antioxidative capacity through at least 2 pathways via FOXO3/Trx-1 axis and acetylation/SOD2 axis. The mechanisms for down-regulating Trx-1 in the post-MI heart are unclear, but degradation of Trx-1, 1 of the mechanisms induced by oxidative stress (36), needs further studies. Deacetylation of SOD2 was also observed in gastrocnemius muscle from aged $MCD^{-/-}$ mice, in which reduction of oxidative stress was evident (37). MCD has been suggested to function as an acetyltransferase (31). At this point it remains unclear whether the deacetylation of SOD2 following MCD inhibition is due to a reduced acetyltransferase activity of MCD as our findings do not confirm whether MCD acts as an acetylase or simply controls protein acetylation via controlling acetyl CoA content. Thus, the dynamic nature of endogenous cardiac ceramide and TAG may indicate a novel role of enhanced intracellular lipids metabolism as a result of MCD inhibition in preventing cardiac oxidative stress in post-MI hearts.

The use of MCD inhibitors in vivo has to consider issues such as the potential for liver steatosis due to redirecting lipids towards TAG synthesis. However, we observed that hepatic TAG content was similar among the MI groups (data not shown), which may be

due to a fact that malonyl CoA is more sensitive in inhibiting fatty acid oxidation in heart versus liver mitochondria (**Figure 1E**). In addition, aged MCD$^{-/-}$ mice, despite elevated hepatic TAG levels, displayed a significant increase in life span of ~30% than the wild-type littermates (37).

Infarct size is a key determinant of the outcome of an acute MI (38). It was therefore important to rule out that any of the beneficial effects of MCD inhibition post-MI were occurring secondary to a reduction in infarct size. This possibility is unlikely because rats were subjected to a permanent MI and MCD inhibition was not initiated until 3 weeks post-MI, and the scar sizes were similar among the post-MI groups. This is of potential important clinical importance, considering many patients who suffer from chronic HF have permanent myocardial infarcts/scars that cannot be revascularized or repaired. Thus, the cardioprotective effects of MCD inhibition may not only enhance coronary revascularization therapy in patients with acute MI, but may also be useful as long-term therapy to prevent the transition to HF.

STUDY LIMITATIONS. In this study, MCD inhibition of fatty acid oxidation was primarily observed when fatty acid oxidation rates were normalized for cardiac work, with absolute fatty acid oxidation rates being similar among the groups. This normalization of fatty acid oxidation rates was performed to account for the dramatic changes in cardiac work, which is a major determinant of cardiac mitochondrial oxidative metabolism (2,25). However, it must be recognized that the possibility exists that the absence of change in absolute metabolic fatty acid oxidation rates following chronic MCD inhibitor treatment could suggest that the underlying mechanisms may not be dependent on changes in metabolic pathways. A second limitation concerns the mechanisms underlying the effect of MCD inhibition on cardiac function. Emerging evidence has shown that downregulating malic enzyme 1 expression in failing hearts induces favorable shifts in not only improving coupling between glycolysis and glucose oxidation, but also improving redox state and contractile function (39). As MCD inhibition enhances the antioxidative capacity in MI hearts in conjunction with the improved uncoupling of glycolysis and glucose oxidation, whether this is achieved by preserving nicotinamide adenine dinucleotide phosphate through reducing malic enzyme 1 thereby mediating coupling of glycolysis and glucose oxidation, needs further investigation. We are unable to discern whether the MCD inhibition-mediated functional benefits are a direct result of either restoration of cellular redox state due to a better coupling between glycolysis and glucose oxidation for preserving nicotinamide adenine dinucleotide phosphate and enhancing antioxidative capacity, or induction of the more efficient oxidation of glucose to reduce protons thereby altering calcium dynamics, or the consequence of multiple metabolic responses.

In conclusion, chronic MCD inhibition reverses cardiac dysfunction in rats with established HF by improving cardiac energy inefficiency due to optimizing cardiac energy metabolism. MCD inhibition might be a novel potential therapy for treating post-MI heart disease. Certainly, establishing efficacy and safety in large animal models would be essential before the MCD inhibitor would be introduced into clinical studies.

ADDRESS FOR CORRESPONDENCE: Dr. Gary Lopaschuk, Cardiovascular Research Centre, Department of Pediatrics, University of Alberta, 423 Heritage Medical Research Center, University of Alberta, Edmonton T6G 2S2, Canada. E-mail: gary.lopaschuk@ualberta.ca.

PERSPECTIVES

COMPETENCY IN MEDICAL KNOWLEDGE: Cardiac energetics is compromised in the human failing heart, due both to a decrease in energy production and a decrease in cardiac efficiency. Inhibition of fatty acid oxidation with MCD inhibition improves cardiac efficiency in the failing heart, which is associated with an improvement of cardiac function. As a result, MCD inhibition is a potentially promising approach to decrease the severity of HF.

TRANSLATIONAL OUTLOOK: Therapeutic strategies that involve the inhibition of cardiac fatty acid oxidation have been shown to be clinically beneficial in the setting of ischemic heart disease and heart failure. This includes the use of CPT1 inhibitors and direct fatty acid ß-oxidation inhibitors. The strategy of increasing malonyl CoA levels, which inhibits CPT1, by inhibiting MCD is another novel approach to inhibiting fatty acid oxidation in the heart. From a clinical viewpoint, oral delivery of MCD inhibitors for the treatment of ischemic heart disease would be practical. We have shown previously that this did not affect peripheral tissue metabolism because there was no insulin resistance observed in skeletal muscle, and no TAG accumulation in liver. In addition, MCD inhibition-mediated improvement of cardiac efficiency was independent of the scar size, suggesting that the cardioprotective effects of MCD inhibition may occur by directly optimizing energy metabolism in the remodeled post-MI myocardium.

REFERENCES

1. Heusch G, Libby P, Gersh B, et al. Cardiovascular remodelling in coronary artery disease and heart failure. Lancet 2014;383:1933–43.

2. Lopaschuk GD, Ussher JR, Folmes CD, Jaswal JS, Stanley WC. Myocardial fatty acid metabolism in health and disease. Physiol Rev 2010;90:207–58.

3. Huss JM, Kelly DP. Mitochondrial energy metabolism in heart failure: a question of balance. J Clin Invest 2005;115:547–55.

4. Mori J, Basu R, McLean BA, et al. Agonist-induced hypertrophy and diastolic dysfunction are associated with selective reduction in glucose oxidation: a metabolic contribution to heart failure with normal ejection fraction. Circ Heart Fail 2012;5:493–503.

5. Zhabyeyev P, Gandhi M, Mori J, et al. Pressure-overload-induced heart failure induces a selective reduction in glucose oxidation at physiological afterload. Cardiovasc Res 2013;97:676–85.

6. Ussher JR, Wang W, Gandhi M, et al. Stimulation of glucose oxidation protects against acute myocardial infarction and reperfusion injury. Cardiovasc Res 2012;94:359–69.

7. Liu Q, Docherty JC, Rendell JC, Clanachan AS, Lopaschuk GD. High levels of fatty acids delay the recovery of intracellular pH and cardiac efficiency in post-ischemic hearts by inhibiting glucose oxidation. J Am Coll Cardiol 2002;39:718–25.

8. Finck BN, Lehman JJ, Leone TC, et al. The cardiac phenotype induced by PPARalpha overexpression mimics that caused by diabetes mellitus. J Clin Invest 2002;109:121–30.

9. Hafstad AD, Khalid AM, Hagve M, et al. Cardiac peroxisome proliferator-activated receptor-alpha activation causes increased fatty acid oxidation, reducing efficiency and post-ischaemic functional loss. Cardiovasc Res 2009;83:519–26.

10. Kolwicz SC Jr., Olson DP, Marney LC, Garcia-Menendez L, Synovec RE, Tian R. Cardiac-specific deletion of acetyl CoA carboxylase 2 prevents metabolic remodeling during pressure-overload hypertrophy. Circ Res 2012;111:728–38.

11. Dyck JR, Cheng JF, Stanley WC, et al. Malonyl coenzyme a decarboxylase inhibition protects the ischemic heart by inhibiting fatty acid oxidation and stimulating glucose oxidation. Circ Res 2004;94:e78–84.

12. Dyck JR, Hopkins TA, Bonnet S, et al. Absence of malonyl coenzyme A decarboxylase in mice increases cardiac glucose oxidation and protects the heart from ischemic injury. Circulation 2006;114:1721–8.

13. Randle PJ, Sugden PH, Kerbey AL, Radcliffe PM, Hutson NJ. Regulation of pyruvate oxidation and the conservation of glucose. Biochem Soc Symp 1978:47–67.

14. Stanley WC, Morgan EE, Huang H, et al. Malonyl-CoA decarboxylase inhibition suppresses fatty acid oxidation and reduces lactate production during demand-induced ischemia. Am J Physiol Heart Circ Physiol 2005;289:H2304–9.

15. Wu H, Zhu Q, Cai M, et al. Effect of inhibiting malonyl-CoA decarboxylase on cardiac remodeling after myocardial infarction in rats. Cardiology 2014;127:236–44.

16. Masoud WG, Ussher JR, Wang W, et al. Failing mouse hearts utilize energy inefficiently and benefit from improved coupling of glycolysis and glucose oxidation. Cardiovasc Res 2014;101:30–8.

17. Dolinsky VW, Jones KE, Sidhu RS, et al. Improvements in skeletal muscle strength and cardiac function induced by resveratrol during exercise training contribute to enhanced exercise performance in rats. J Physiol 2012;590:2783–99.

18. Zhang L, Jaswal JS, Ussher JR, et al. Cardiac insulin-resistance and decreased mitochondrial energy production precede the development of systolic heart failure after pressure-overload hypertrophy. Circ Heart Fail 2013;6:1039–48.

19. Picard MH, Popp RL, Weyman AE. Assessment of left ventricular function by echocardiography: a technique in evolution. J Am Soc Echocardiogr 2008;21:14–21.

20. Singh TD, Barbhuiya MA, Gupta S, et al. Quantitative assessment of expression of lactate dehydrogenase and its isoforms 3 and 4 may serve as useful indicators of progression of gallbladder cancer: a pilot study. Indian J Clin Biochem: IJCB 2011;26:146–53.

21. Janssen AJ, Trijbels FJ, Sengers RC, et al. Spectrophotometric assay for complex I of the respiratory chain in tissue samples and cultured fibroblasts. Clin Chem 2007;53:729–34.

22. Krishnan J, Suter M, Windak R, et al. Activation of a HIF1alpha-PPARgamma axis underlies the integration of glycolytic and lipid anabolic pathways in pathologic cardiac hypertrophy. Cell Metab 2009;9:512–24.

23. Peskin AV, Winterbourn CC. A microtiter plate assay for superoxide dismutase using a water-soluble tetrazolium salt (WST-1). Clinica Chimica Acta 2000;293:157–66.

24. Bird MI, Saggerson ED. Binding of malonyl-CoA to isolated mitochondria. Evidence for high- and low-affinity sites in liver and heart and relationship to inhibition of carnitine palmitoyltransferase activity. Biochem J 1984;222:639–47.

25. Heineman FW, Balaban RS. Control of mitochondrial respiration in the heart in vivo. Annu Rev Physiol 1990;52:523–42.

26. Cahn RDZE, Kaplan NO, Levine L. Nature and development of lactic dehydrogenases: the 2 major types of this enzyme form molecular hybrids which change in makeup during development. Science 1962;136:962–9.

27. Perman JC, Bostrom P, Lindbom M, et al. The VLDL receptor promotes lipotoxicity and increases mortality in mice following an acute myocardial infarction. J Clin Invest 2011;121:2625–40.

28. Myoishi M, Hao H, Minamino T, et al. Increased endoplasmic reticulum stress in atherosclerotic plaques associated with acute coronary syndrome. Circulation 2007;116:1226–33.

29. Li XN, Song J, Zhang L, et al. Activation of the AMPK-FOXO3 pathway reduces fatty acid-induced increase in intracellular reactive oxygen species by upregulating thioredoxin. Diabetes 2009;58:2246–57.

30. Qiu X, Brown K, Hirschey MD, Verdin E, Chen D. Calorie restriction reduces oxidative stress by SIRT3-mediated SOD2 activation. Cell Metab 2010;12:662–7.

31. Aparicio D, Perez-Luque R, Carpena X, et al. Structural asymmetry and disulfide bridges among subunits modulate the activity of human malonyl-CoA decarboxylase. J Biol Chem 2013;288:11907–19.

32. Liu B, Clanachan AS, Schulz R, Lopaschuk GD. Cardiac efficiency is improved after ischemia by altering both the source and fate of protons. Circ Res 1996;79:940–8.

33. Schultheiss HP. Effect on the myocardial energy metabolism of angiotensin-converting enzyme inhibition in chronic heart failure. Am J Cardiol 1990;65:74–81.

34. Lin L, Sylven C, Astrom H, Liska J, Ljungquist A, Jansson E. Myocardial lactate dehydrogenase and its isoenzyme activities in transplanted human hearts. Scand J Thorac and Cardiovasc Surg 1991;25:51–5.

35. Kolwicz SC Jr., Liu L, Goldberg IJ, Tian R. Enhancing cardiac triacylglycerol metabolism improves recovery from ischemic stress. Diabetes 2015;64:2817–27.

36. Kato T, Niizuma S, Inuzuka Y, et al. Analysis of metabolic remodeling in compensated left ventricular hypertrophy and heart failure. Circ Heart Fail 2010;3:420–30.

37. Ussher JR, Fillmore N, Keung W, et al. Genetic and pharmacological inhibition of malonyl CoA decarboxylase does not exacerbate age-related insulin resistance in mice. Diabetes 2016;65:1–9.

38. Bosch X, Theroux P. Left ventricular ejection fraction to predict early mortality in patients with non-ST-segment elevation acute coronary syndromes. Am Heart J 2005;150:215–20.

39. Lahey R, Carley AN, Wang X, et al. Enhanced redox state and efficiency of glucose oxidation with miR based suppression of maladaptive NADPH-dependent malic enzyme 1 expression in hypertrophied hearts. Circ Res 2018;122:836–45.

KEY WORDS fatty acid oxidation, heart failure, glucose oxidation, uncoupling of glycolysis

JACC: BASIC TO TRANSLATIONAL SCIENCE VOL. 4, NO. 3, 2019

EDITORIAL COMMENT

Metabolic Coupling as a Therapeutic Strategy for Heart Failure*

Martin E. Young, DPHIL

The heart is a metabolic omnivore that requires use of a plethora of substrates, not only to meet energetic demands for continual contraction, but also to provide necessary building blocks for turnover of cellular constituents and synthesis of metabolically derived signaling species (1). A key concept for cardiac metabolism centers around the need for homeostasis (i.e., maintenance of processes within a discrete physiological range) in the face of perpetual fluctuations in environmental stimuli and/or stresses. This is achieved through metabolic flexibility, which in essence affords a buffering capacity. A simple example involves perturbations that occur over the course of the day; sleep and/or wake and fasting and/or feeding cycles result in daily fluctuations in energetic demand and nutrient availability, as well as a host of additional neurohumoral factors that are met by reciprocal oscillations in cardiac metabolism (2). During cardiac disease states, the heart is often described as metabolically inflexible, typically being suspended at extremities (i.e., chronic activation or repression, depending upon the pathology and metabolic parameter), coupled with an inability to appropriately respond to physiological challenges (3). This is exemplified by heart failure. The failing human heart has been described as an engine without fuel, due to severe metabolic impairments and an inability to generate sufficient adenosine triphosphate (ATP) for maintenance of contractile performance (4). Dysfunction of mitochondria (the primary site of ATP synthesis via oxidative phosphorylation) appears to be central to this pathology (4). Consistent with this idea, numerous studies suggest that myocardial oxidation of both glucose and fatty acids (major substrates for the heart) are reduced during heart failure. This is despite observations that circulating levels of these substrates are often elevated (5), which potentially leads to an imbalance between carbon availability and use. Glucose serves as a good example. During heart failure, diminished glucose oxidation occurs concomitantly with accelerated glucose uptake and glycolytic flux (4,5). This uncoupling of glycolysis from glucose oxidation is associated with accumulation of lactate and protons; the latter decreases cardiac efficiency, in part, through augmented ATP-dependent ion homeostasis required for proton extrusion from the cardiomyocyte (6). Uncoupling of glycolysis from glucose oxidation has been reported during other pathological states, including diabetes mellitus and acute ischemia and/or reperfusion (7,8).

SEE PAGE 385

Multiple groups have reasoned that targeting metabolic derangements during heart failure has the therapeutic potential to improve cardiac function. The uncoupling of glycolysis and glucose oxidation was targeted in the study by Wang et al. (9) in this issue of *JACC: Basic to Translational Science*. More specifically, these investigators hypothesized that pharmacological inhibition of malonyl-CoA decarboxylase (MCD) would decrease the severity of heart failure in a rat model of myocardial infarction (permanent ligation of the left anterior descending artery). MCD is most commonly known for regulation of fatty acid oxidation; by catabolizing malonyl-CoA (an

*Editorials published in *JACC: Basic to Translational Science* reflect the views of the authors and do not necessarily represent the views of JACC or the American College of Cardiology.

From the Division of Cardiovascular Disease, Department of Medicine, University of Alabama at Birmingham, Birmingham, Alabama. This work was supported by the National Heart, Lung, and Blood Institute (HL123574, HL122975, HL142216).

The author attest he is in compliance with human studies committees and animal welfare regulations of the authors' institutions and Food and Drug Administration guidelines, including patient consent where appropriate. For more information, visit the *JACC: Basic to Translational Science* author instructions page.

ISSN 2452-302X https://doi.org/10.1016/j.jacbts.2019.05.001

established endogenous inhibitor of the mitochondrial carnitine shuttle, a process critical for fatty acid uptake into the mitochondrial matrix), MCD promotes fatty acid oxidation (FAO) (10). Accordingly, MCD inhibition is predicted to increase malonyl-CoA levels, thus inhibiting FAO. Initially, it may appear counterintuitive to selectively inhibit FAO in the failing myocardium, because this process is apparently diminished already. However, due to the interrelationship between FAO and glucose oxidation [initially described by Randle et al.(11)], inhibition of FAO invariably promotes glucose oxidation (thereby augmenting coupling with glycolysis). As a proof of concept, Wang et al. (9) reported that a pharmacological inhibitor of MCD (CBM-3001106) acutely (<1 h) increased cardiac malonyl-CoA levels, in parallel with attenuated FAO and concomitant glucose oxidation augmentation (in ex vivo perfused working rat hearts). The investigators also observed an improvement in cardiac function in vivo (echocardiographic parameters, such as ejection fraction and fractional shortening) when rats with heart failure were treated with the MCD inhibitor either acutely (2 h) or for the long term (4 weeks). Moreover, improvements in cardiac function following 4 weeks of MCD inhibition persisted in ex vivo working heart perfusions. The latter studies also revealed a dramatic reduction in glycolytic flux in rats with heart failure treated with the MCD inhibitor (translating to a significant reduction in calculated proton production) and improved cardiac efficiency. Adverse remodeling markers were also attenuated in rats with heart failure following long-term MCD inhibitor treatment (in the absence of differences in infarct size). This included normalization of sarcoplasmic/endoplasmic reticulum Ca (2+) ATPase 2a (SERCA2a) levels and lactate dehydrogenase (LDH) isoform switching. Additional parameters were assessed, including forkhead box O3 (FOXO3) nucleo-cytoplasmic distribution and superoxide dismutase 2 (SOD2) acetylation, both of which were normalized in the failing heart by MCD inhibition. Collectively, these observations suggested that MCD (and presumably, FAO) inhibition reversed adverse remodeling of the failing myocardium, potentially through improved coupling of glycolysis with glucose oxidation.

Metabolic modulation as a heart failure therapy is an attractive concept. In addition to extensive evidence that perturbed myocardial metabolism plays a causal role in adverse remodeling during heart failure, various cardiometabolic disease states are significant contributors to the etiology of heart failure. These include obesity and diabetes mellitus. Moreover, heart failure profoundly disrupts systemic metabolism, in a manner similar to cachexic states (e.g., skeletal muscle loss, lipolysis, insulin resistance). Heart failure–induced perturbations in systemic metabolism likely worsen myocardial contractility and outcomes (i.e., a viscous feed-forward cycle develops). Pharmacological inhibition of FAO as a therapeutic for cardiometabolic diseases and/or heart failure has been proposed previously. Both inhibitors of carnitine acyl-transferase I (CPTI) (the carnitine shuttle component inhibited by malonyl-CoA; CPTI inhibitors include oxfenicine, perhexiline, and etomoxir) and β-oxidation enzymes (e.g., trimetazidine inhibits 3-ketoacyl thiolase) have reported beneficial effects in preclinical models of heart failure, as well as in humans (12). For example, oxfenicine attenuated heart failure progression in a dog model (13), whereas perhexiline was shown to improve ejection fraction in patients with heart failure (14). However, some CPT1 inhibitors might have detrimental side effects. For example, although etomoxir initially appeared to confer contractile function improvements in patients with heart failure (15), clinical trials were halted due to hepatotoxicity (16). This led to concerns that CPTI inhibition in the liver may promote nonalcoholic hepatic steatosis (NASH). Wang et al. (9) proposed that one advantage of targeting MCD was that the liver isoform of CPT1 was less sensitive to malonyl-CoA–mediated inhibition, relative to the muscle isoform. However, whether prolonged MCD inhibition, particularly during dyslipidemic states (e.g., obesity, diabetes), leads to NASH is a distinct possibility. Germline MCD knockout mice developed triglyceride accumulation in the liver with age (17).

In addition to an uncoupling between glycolysis and glucose oxidation, heart failure is also characterized by an uncoupling between substrate availability and use. Circulating levels of glucose, fatty acids, ketone bodies, and amino acids (notably branched chain amino acids [BCAAs]) are typically elevated during heart failure, concomitant with decreased myocardial oxidative metabolism (5). This mismatch has the potential of precipitating contractile dysfunction. Putative glucose- and lipid-dependent mechanisms have been studied extensively, including imbalances in signaling metabolites (e.g., ceramide, diacylglycerol), redox status (e.g., NAD(P)+/NAD(P)H ratios), and post-translational modifications (e.g., protein palmitoylation and/or O-GlcNAcylation) (5). Recently, impaired ketone body and BCAA oxidation has been reported in the failing myocardium (18–20); accumulation of metabolites in these catabolic pathways adversely affects cellular signaling, protein acetylation, and mitochondrial function. In light of these findings, the failing

myocardium has been described as a broken engine flooded with fuel (5). How might MCD (and therefore, FAO) inhibition help resolve this mismatch? Two main possibilities exist. First, inhibition of FAO in tissues such as skeletal muscle and the liver would likely lower circulating glucose (through increased skeletal muscle glucose use and reduced hepatic gluconeogenesis; etomoxir was initially developed as a glucose-lowering agent), BCAAs (through increased oxidation in both muscle and liver), and ketone bodies (through decreased hepatic acetyl-CoA availability for ketogenesis) levels. Second, FAO inhibition in the heart would increase myocardial glucose, ketone body, and BCAA oxidation. Together, a balance between availability and oxidation would be reestablished for these substrates. The study by Wang et al. (9) provides indirect evidence of this concept, at the level of protein acetylation. Elevated SOD2 acetylation in the failing heart is normalized by MCD inhibition. Moreover, nuclear translocation of FOXO3 following MCD inhibition is consistent with reduced acetylation [as acetylation sequesters FOXO3 in the cytosol (21)]. These observations raise the possibility that, in addition to improving the coupling between glycolysis and glucose oxidation, MCD inhibition may improve coupling between substrate availability and oxidation, thereby reducing excess acetyl-CoA (and subsequent use for protein acetylation). However, MCD inhibition would not normalize the balance between lipid availability and oxidation, an issue that may become more problematic in dyslipidemic states.

In summary, Wang et al. (9) have revealed MCD inhibition as a promising therapeutic target for heart failure. Improved cardiac function and efficiency following MCD inhibition (in a rat model of myocardial infarction–induced heart failure) was associated with reduced myocardial glycolytic flux (and presumably, proton accumulation). The investigators postulated that benefits of MCD inhibition were primarily through coupling of glycolysis with glucose oxidation. The relative contribution of other metabolism-related mechanisms (e.g., coupling between substrate availability and oxidation) requires further elucidation.

ADDRESS FOR CORRESPONDENCE: Dr. Martin E. Young, Division of Cardiovascular Diseases, Department of Medicine, University of Alabama at Birmingham, 703 19th Street South, ZRB 308, Birmingham, Alabama 35294. E-mail: meyoung@uab.edu.

REFERENCES

1. Taegtmeyer H, Lubrano G. Rethinking cardiac metabolism: metabolic cycles to refuel and rebuild the failing heart. F1000Prime Rep 2014;6:90.

2. Young ME. Temporal partitioning of cardiac metabolism by the cardiomyocyte circadian clock. Exp Physiol 2016;101:1035–9.

3. Taegtmeyer H, Golfman L, Sharma S, Razeghi P, van Arsdall M. Linking gene expression to function: metabolic flexibility in the normal and diseased heart. Ann N Y Acad Sci 2004;1015:202–13.

4. Neubauer S. The failing heart-an engine out of fuel. N Engl J Med 2007;356:1140–51.

5. Wende AR, Brahma MK, McGinnis GR, Young ME. Metabolic origins of heart failure. J Am Coll Cardiol Basic Transl Sci 2017;2:297–310.

6. Liu Q, Docherty JC, Rendell JC, Clanachan AS, Lopaschuk GD. High levels of fatty acids delay the recovery of intracellular pH and cardiac efficiency in post-ischemic hearts by inhibiting glucose oxidation. J Am Coll Cardiol 2002;39:718–25.

7. Lopaschuk GD, Ussher JR, Folmes CD, Jaswal JS, Stanley WC. Myocardial fatty acid metabolism in health and disease. Physiol Rev 2010;90:207–58.

8. Fillmore N, Mori J, Lopaschuk GD. Mitochondrial fatty acid oxidation alterations in heart failure, ischaemic heart disease and diabetic cardiomyopathy. Br J Pharmacol 2014;171:2080–90.

9. Wang W, Zhang L, Battiprolu PK, et al. Malonyl CoA decarboxylase inhibition improves cardiac function post myocardial infarction. J Am Coll Cardiol Basic Transl Sci 2019;4:385–400.

10. Fillmore N, Lopaschuk GD. Malonyl coA: a promising target for the treatment of cardiac disease. IUBMB Life 2014;66:139–46.

11. Randle PJ, Garland PB, Hales CN, Newsholme EA. The glucose fatty-acid cycle. Its role in insulin sensitivity and the metabolic disturbances of diabetes mellitus. Lancet 1963;1:785–9.

12. Lionetti V, Stanley WC, Recchia FA. Modulating fatty acid oxidation in heart failure. Cardiovasc Res 2011;90:202–9.

13. Lionetti V, Linke A, Chandler MP, et al. Carnitine palmitoyl transferase-I inhibition prevents ventricular remodeling and delays decompensation in pacing-induced heart failure. Cardiovasc Res 2005;66:454–61.

14. Lee L, Campbell R, Scheuermann-Freestone M, et al. Metabolic modulation with perhexiline in chronic heart failure: a randomized, controlled trial of short-term use of a novel treatment. Circulation 2005;112:3280–8.

15. Bristow M. Etomoxir: a new approach to treatment of chronic heart failure. Lancet 2000;356:1621–2.

16. Holubarsch CJ, Rohrbach M, Karrasch M, et al. A double-blind randomized multicentre clinical trial to evaluate the efficacy and safety of two doses of etomoxir in comparison with placebo in patients with moderate congestive heart failure: the ERGO (Etomoxir for the Recovery of Glucose Oxidation) study. Clin Sci (Lond) 2007;113:205–12.

17. Ussher JR, Fillmore N, Keung W, et al. Genetic and pharmacological inhibition of malonyl CoA decarboxylase does not exacerbate age-related insulin resistance in mice. Diabetes 2016;65:1883–91.

18. Aubert G, Martin OJ, Horton JL, et al. The failing heart relies on ketone bodies as a fuel. Circulation 2016;133:698–705.

19. Bedi KC Jr., Snyder NW, Brandimarto J, et al. Evidence for intramyocardial disruption of lipid metabolism and increased myocardial ketone utilization in advanced human heart failure. Circulation 2016;133:706–16.

20. Sun H, Olson KC, Gao C, et al. Catabolic defect of branched-chain amino acids promotes heart failure. Circulation 2016;133:2038–49.

21. Senf SM, Sandesara PB, Reed SA, Judge AR. p300 Acetyltransferase activity differentially regulates the localization and activity of the FOXO homologues in skeletal muscle. Am J Physiol Cell Physiol 2011;300:C1490–501.

KEY WORDS cardiac metabolism, heart failure, malonyl-coA decarboxylase

JACC: BASIC TO TRANSLATIONAL SCIENCE VOL. 4, NO. 3, 2019

PRECLINICAL RESEARCH

Western Diet-Fed, Aortic-Banded Ossabaw Swine

A Preclinical Model of Cardio-Metabolic Heart Failure

T. Dylan Olver, PhD,[a,*] Jenna C. Edwards, BS,[a,*] Thomas J. Jurrissen, BS,[b] Adam B. Veteto, MS,[c] John L. Jones, MS,[c] Chen Gao, BS,[d] Christoph Rau, PhD,[d] Chad M. Warren, MS,[e] Paula J. Klutho, PhD,[f] Linda Alex, PhD,[f] Stephanie C. Ferreira-Nichols, BS,[f] Jan R. Ivey, BS,[a] Pamela K. Thorne, MS,[a] Kerry S. McDonald, PhD,[c] Maike Krenz, MD,[c,f] Christopher P. Baines, PhD,[a,c,f] R. John Solaro, PhD,[e] Yibin Wang, PhD,[d] David A. Ford, PhD,[g] Timothy L. Domeier, PhD,[c,†] Jaume Padilla, PhD,[b,f,i,†] R. Scott Rector, PhD,[b,h,j,†] Craig A. Emter, PhD[a,†]

VISUAL ABSTRACT

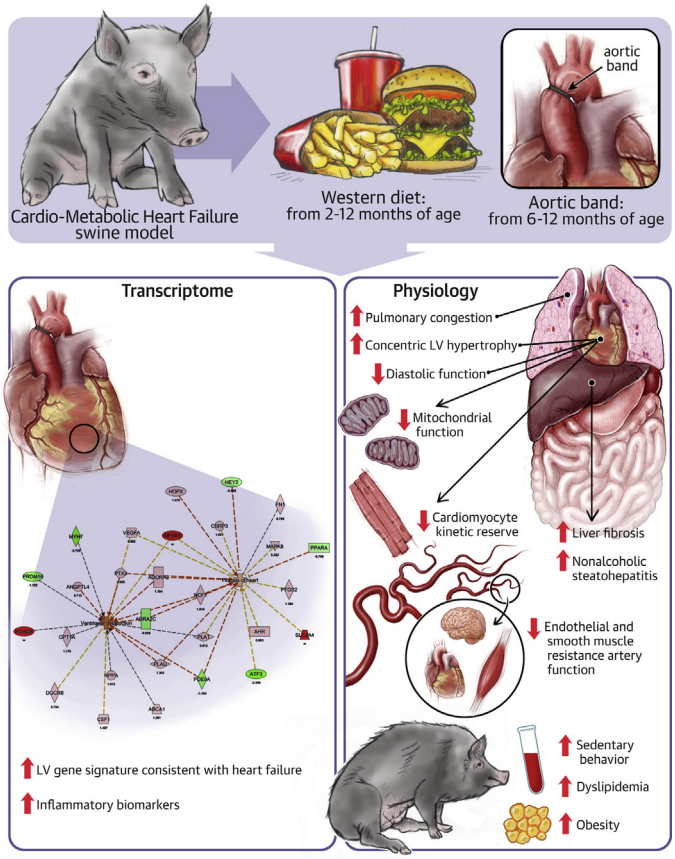

Olver, T.D. et al. J Am Coll Cardiol Basic Trans Science. 2019;4(3):404–21.

HIGHLIGHTS

- **The combination of a Western-diet and aortic banding results in a cardio-metabolic heart failure phenotype in Ossabaw swine.**
- **Ossabaw swine with cardio-metabolic heart failure display cardiac dysfunction at the whole heart and cellular levels.**
- **The left ventricle transcriptome showed gene signatures consistent with pro-inflammatory heart failure.**
- **Cardio-metabolic heart failure was coupled with microvascular dysfunction in the heart, skeletal muscle, and brain.**
- **Ossabaw swine with cardio-metabolic heart failure are sedentary and obese with liver dysfunction.**

From the [a]Department of Biomedical Science, University of Missouri-Columbia, Columbia, Missouri; [b]Department of Nutrition and Exercise Physiology, University of Missouri-Columbia, Columbia, Missouri; [c]Department of Medical Pharmacology and Physiology, University of Missouri-Columbia, Columbia, Missouri; [d]David Geffen School of Medicine, University of California, Los Angeles,

ISSN 2452-302X https://doi.org/10.1016/j.jacbts.2019.02.004

SUMMARY

The development of new treatments for heart failure lack animal models that encompass the increasingly heterogeneous disease profile of this patient population. This report provides evidence supporting the hypothesis that Western Diet–fed, aortic-banded Ossabaw swine display an integrated physiological, morphological, and genetic phenotype evocative of cardio-metabolic heart failure. This new preclinical animal model displays a distinctive constellation of findings that are conceivably useful to extending the understanding of how pre-existing cardio-metabolic syndrome can contribute to developing HF.

ABBREVIATIONS AND ACRONYMS

AB = aortic-banded
CON = control
EDPVR = end-diastolic pressure–volume relationship
EF = ejection fraction
HF = heart failure
HFpEF = heart failure with preserved ejection fraction
HFrEF = heart failure with reduced ejection fraction
IL1RL1 = interleukin 1 receptor-like 1
LV = left ventricle
NF = nuclear factor
PTX3 = pentraxin-3
WD = Western Diet

Heart failure (HF) is currently among the most challenging issues facing the treatment of cardiovascular disease. Of the approximately 6 million patients with HF in the United States, there is an approximately equal diagnosis of HF with reduced ejection fraction (HFrEF) and HF with preserved ejection fraction (HFpEF) (1-5). The disease profile of HF patients is becoming more heterogeneous, often displaying various combinations of numerous comorbidities, including obesity, metabolic syndrome, diabetes, and hypertension. Although the prevalence of HF is expected to increase during the next 15 years, traditional treatments for HF have remained largely unchanged over the last 20 years. Furthermore, HFpEF patients are largely unresponsive to standardized therapeutic approaches proven effective for HFrEF (1,2,6-9). Thus, new therapeutic targets for HF patients are desperately needed.

The development of effective treatments for HF patients may be limited by a lack of translational animal models that encompass the wide ranging pathology of an ever-increasing population of HF patients with pre-existing cardio-metabolic syndrome. Recently, attention has focused on the role of increased systemic inflammation that results from common risk factors for developing HF. This has prompted discussion regarding the need to develop preclinical animal models that include comorbidities in parallel with a HF phenotype. A number of syndromes may predispose patients to HF, including metabolic disease (e.g., obesity, insulin resistance), hypertension, renal disease, and coronary artery disease. Impairment in multiple organ systems, including both central (cardiac morphology, coronary vasculature, both systolic and diastolic function, cardiac reserve) and peripheral (pulmonary, renal, hepatic, immune, skeletal muscle, cerebral, and associated vascular beds) components, has been highlighted as a critical risk factor predisposing patients to HF. Comprehensive

Los Angeles, California; [e]Department of Physiology and Biophysics, Center for Cardiovascular Research, University of Illinois at Chicago, Chicago, Illinois; [f]Dalton Cardiovascular Research Center, University of Missouri-Columbia, Columbia, Missouri; [g]Department of Biochemistry and Molecular Biology and Center for Cardiovascular Research, Saint Louis University- School of Medicine, St. Louis, Missouri; [h]Department of Medicine - University of Missouri-Columbia, Columbia, Missouri; [i]Department of Child Health, University of Missouri-Columbia, Columbia, Missouri; and the [j]Research Service, Harry S Truman Memorial VA Hospital, University of Missouri-Columbia, Columbia, Missouri. *Dr. Oliver and Ms. Edwards contributed equally to this work and are joint first authors. †Drs. Domeier, Padilla, Rector, and Emter contributed equally to this work and are joint senior authors. This study was supported by a University of Missouri Research Board Grant (principal investigators [PIs]: Drs. Emter and Rector); National Institutes of Health (NIH) Grant RO1 HL112998 (PI: Dr. Emter); VA-Merit Grant I01BX003271-01 (PI: Dr. Rector); NIH Grant K01 HL125503 (PI: Dr. Padilla); NIH Grant K01 AG041208 and R01 HL136292 (PI: Dr. Domeier); American Heart Association postdoctoral fellowship 16POST27760052 (PI: Dr. Olver); NIH Grant R01 HL094404 (PI: Dr. Baines); NIH Grant R01 GM115552 (PI: Dr. Ford); NIH Grants R01 HL122737, NIH R01 HL123295, and NIH HL129639 (PI: Dr. Wang); American Heart Association postdoctoral fellowship 17POST33661136 (PI: Dr. Gao); NIH Grant R01 HL116525 (PI: Krenz); and NIH Grant PO1 HL62426 (Project 1, Dr. Solaro; Core C: Dr. Warren). The authors acknowledge NIH grants RR013223 and HL062552 to M. Sturek and the CMP of IUSM and Purdue University, and NIH grant U42 OD011140 to R. Prather and the National Swine Resource and Research Center at the University of Missouri-Columbia for the Ossabaw swine. Dr. Solaro has served on the Scientific Advisory Board and been a consultant for Cytokinetics; and has a fee-for-service agreement with Pfizer. Dr. Wang has been a consultant for REMD Biotherapeutics. All other authors have reported that they have no relationships relevant to the contents of this paper to disclose. All authors attest they are in compliance with human studies committees and animal welfare regulations of the authors' institutions and Food and Drug Administration guidelines, including patient consent where appropriate. For more information, visit the *JACC: Basic to Translational Science* author instructions page.

Manuscript received January 17, 2019; revised manuscript received February 13, 2019, accepted February 21, 2019.

TABLE 1 Postmortem Analysis of Heart and Lung Morphology, and Pressure–Volume Assessment of Resting Systolic and Diastolic LV Function

Gross Morphology	CON (n = 5)	WD-AB (n = 5)	*t*-Test (p Value)
Body surface area (m^2)	1.10 ± 0.01	1.51 ± 0.04*	<0.0001
Tibia length (cm)	16.6 ± 0.2	16.6 ± 0.1	0.93
Lung weight (g)	236 ± 11	294 ± 12†	0.01
Heart weight (g)	157 ± 4	229 ± 6*	<0.0001
LV+S weight (g)	107 ± 2	150 ± 4*	<0.0001
RV weight (g)	28 ± 2	46 ± 2‡	<0.001
Atria weight (g)	21 ± 2	33 ± 1‡	<0.001
LV Function: Pressure-Volume and Echocardiography	**CON (n = 4 to 5)**	**WD-AB (n = 4 to 5)**	***t*-Test (p Value)**
Systolic function			
HR (beats/min)	94 ± 17	80 ± 8	0.49
LVESV (ml)	48 ± 6	33 ± 9	0.21
LVESP (mm Hg)	94 ± 12	102 ± 6	0.54
LVEF (%)	52 ± 3	63 ± 5	0.12
LV SV (ml)	50 ± 2	51 ± 5	0.83
LV SVI (ml/m^2)	46 ± 1	34 ± 4§	<0.05
ESPVR (mm Hg/ml)	11 ± 5	23 ± 7	0.21
PRSW (mm Hg)	65 ± 10	91 ± 8	0.09
Diastolic function			
LVEDV (ml)	98 ± 6	84 ± 12	0.34
LVEDP (mm Hg)	10 ± 1	8 ± 2	0.22
EDPVR (mm Hg/ml)	0.015 ± 0.003	0.040 ± 0.010§	<0.05
LV untwisting: apical early diastolic rotation rate (°/s)	112 ± 6	94 ± 4§	<0.05
LV global longitudinal late diastolic strain rate (1/s)	1.1 ± 0.1	1.8 ± 0.1*	<0.0001

Values are mean ± SE. *p < 0.0001. †p < 0.01. ‡p < 0.001. §p < 0.05; for significantly different versus control (CON).

Atria = right + left atria; EDPVR = end-diastolic pressure–volume relationship; ESPVR = end-systolic pressure–volume relationship; HR = heart rate; LV = left ventricular; LVEDP = LV end-diastolic pressure; LVEDV = LV end-diastolic volume; LVEF = LV ejection fraction; LVESP = LV end-systolic pressure; LVESV = LV end-systolic volume; LV+S = LV + septum; LV SV = LV stroke volume; LV SVI = LV stroke volume index; PRSW = preload recruitable stroke work; RV = right ventricle; WD-AB = Western diet, aortic banded.

characterization of animal models of experimental HF that include multisystem contributions to the overall pathology are therefore critical to advancing the understanding of a growing population of HF patients with multiple pre-existing comorbidities.

SEE PAGE 422

A number of previous reports from our laboratory (and others) showed that Ossabaw swine, a unique translational large animal model genetically predisposed to obesity and metabolic derangement, do not develop HF from dietary intervention alone (10-17). Furthermore, our laboratory previously published numerous studies that examined the impact of aortic banding alone (in the absence of comorbidities) on developing disease in a separate preclinical swine model of HF (18-27). Thus, the primary goal of this study was to develop a swine model of experimental cardio-metabolic HF. Specifically, our aim was to determine whether the combination of dietary and pressure-overload interventions would produce a cardio-metabolic HF phenotype. We hypothesized Western Diet (WD)–fed Ossabaw swine subject to chronic cardiac pressure overload by aortic banding would display physiological, morphological, and genetic phenotypes relevant to patients with pre-existing metabolic derangement who are at risk of developing HF. We provide detailed integrated analyses that demonstrate the potential relevance of this preclinical swine model for cardio-metabolic HF (28,29).

METHODS

EXPERIMENTAL DESIGN. Two-month-old, intact female Ossabaw swine (15 to 20 kg, Ossabaw pigs were generously provided by: 1) Michael Sturek, PhD, in the Ossabaw Swine Resource, Comparative Medicine Program at Purdue University and Indiana University School of Medicine; and 2) Randall Prather, PhD, and Eric M. Walters, PhD, in the National Swine Resource and Research Center at the University of Missouri-Columbia), were assigned into 2 groups: nonsham sedentary control (CON) (n = 5) and WD-fed aortic-banded (WD-AB) with HF (n = 7). Two animals were lost in the WD-AB group as a result of not surviving the aortic banding surgery at 6 months of age; both animals weighed >50 kg at the time of surgery. We believe this issue can be remedied through weight control in the initial phases of obesity development, given all WD-AB animals in the current study under this specific weight threshold survived without surgical complications following thoracotomy. A third animal was lost to sudden cardiac death 1 week before terminal experiments were scheduled in the WD-AB group. Necrospy of this animal revealed complications due to renal infarction, pulmonary and hepatic congestion, and a systemic inflammatory process. Ultimately, outcome measures in the WD-AB group were assessed in 4 to 5 animals.

The CON group ingested a standard chow diet (5L80, Lab Diet; 3.03 $kcal/g^{-1}$; carbohydrate: 71%; protein: 18.5%, and fat: 10.5%; 500 g/day), whereas the WD-AB group was fed a WD (1,000 g/day) high in fat, high-fructose corn syrup, and cholesterol (5B4L, Laboratory Diet; 4.14 $kcal/g^{-1}$; carbohydrate: 40.8% [17.8% of total calories from high-fructose corn syrup]; protein: 16.2%; fat: 43%, 2% cholesterol wt/wt) as previously reported (13-17). At 6 months of age, aortic banding was used to induce HF as previously described (19-23,25-27). A trans-stenotic systolic gradient of approximately 70 mm Hg (72 ± 2 mm Hg) was achieved under anesthesia using phenylephrine (intravenously 1 to 3 μg/kg/min) to maintain a distal

TABLE 2 Serial Echocardiographic Assessment of LV Morphology

	CON (n = 5)			WD-AB (n = 5)			
	Age 6 months	Age 8 months	Age 12 months	Pre-AB Age 6 months	Post-AB Age 8 months	Post-AB Age 12 months	RM ANOVA
Body weight (kg)	31 ± 2	36 ± 2	46 ± 1†††	45 ± 2***	56 ± 3***†††	76 ± 3***†††	ME group##
LVIDd (mm)	40 ± 1	41 ± 1	45 ± 1†	37 ± 1	42 ± 1†	46 ± 2††	ME time##
LVIDs (mm)	24 ± 1	25 ± 1	26 ± 1	23 ± 1	21 ± 1	23 ± 2	p = 0.33
LV WTd (mm)	6.2 ± 0.5	6.4 ± 0.2	5.7 ± 0.3	6.6 ± 0.2	9.8 ± 0.3***††	9.7 ± 0.5***††	Interaction‡
LV WTs (mm)	10.0 ± 0.5	11.0 ± 0.3	11.3 ± 0.4	11.8 ± 0.3**	14.8 ± 0.3***††	16.1 ± 0.4***††	Interaction§

Values are mean ± SE. Statistics: Post hoc versus CON at the same time point (**p < 0.01; ***p < 0.001); main effect (ME) (##p < 0.0001); interaction effect = group × time (§ p <0.01, ‡p < 0.001); †post hoc within same group versus 6-month time point (†p < 0.01; †† p < 0.001; p < 0.0001).

LVIDd = left ventricular internal diastolic dimension; LVIDs = left ventricular internal systolic dimension; LV WTd = left ventricular diastolic wall thickness; LV WTs = left ventricular systolic wall thickness; RM ANOVA, repeated measure analysis of variance.

peripheral vascular mean aortic pressure of approximately 90 mm Hg (87 ± 2 mm Hg) at a heart rate of 85 beats/min (84 ± 3 beats/min). In total, Ossabaw swine in the WD-AB group were subjected to 10 months of WD and 6 months of chronic cardiac pressure overload. Body surface area was calculated as previously published for swine (30,31). Animals were fed once per day, and water was provided ad libitum. All animal protocols were in accordance with the Principles for the Utilization and Care of Vertebrate Animals Used in Testing Research and Training and approved by the University of Missouri Animal Care and Use Committee.

STATISTICAL ANALYSIS. Data analyses were performed using SPSS (version 19.0, IBM, Armonk, New York) or SigmaStat (version 3.5, Systat Software, San Diego, California). Linear regression was used to examine the relationship between inflammatory biomarkers and diastolic function. Group comparisons were made using a Student's *t*-test (32). Group comparisons for in vitro vascular function and serial ultrasound morphological experiments were made using a repeated-measures analysis of variance (group × dose and group × time, respectively). Group differences revealed by analysis of variance were found using Student Newman-Keuls post hoc analysis. Interobserver variability for ultrasound measures was evaluated using the intraclass correlation coefficient in a 2-way random model (<0.40: poor agreement; 0.40 to 0.75: good agreement; >0.75: excellent agreement) (33). Power analyses were conducted to determine the appropriate number of pigs to detect differences between groups as recommended by Kim and Seo (34) using the Sealed Envelope Power Calculator (https://www.sealedenvelope.com/power/continuous-superiority). For input, we used published end-diastolic pressure–volume relationship (EDPVR) data reported in 6 CON and 7 AB pigs (20) because of the well-established development of diastolic dysfunction in patients with metabolic syndrome and the reputation of EDPVR as a gold standard for measuring diastolic function. Significance level was set to 5%, power to 80%, mean outcome in control group = 0.011, mean outcome in experimental group = 0.021, and standard deviation = 0.004 (20). This power analysis indicated 4 swine per group would be sufficient. All data are presented

TABLE 3 Ingenuity Pathway and Gene Ontology Analyses of Induced Heart Failure-Related Gene Pathways Expressed between CON and WD-AB Left Ventricle

Ingenuity Pathway Analysis, Top Toxicology Lists		
Name		**p Value**
Cardiac hypertrophy		<0.0001
Increases renal damage		<0.0001
Renal necrosis/cell death		<0.0001
Cardiac fibrosis		<0.0001
Liver proliferation		<0.0001
Name	**Matched Gene Symbols**	**p Value**
Gene ontology, signaling pathways: heart failure		
Cardiomyocyte differentiation through BMP receptors	MYH7, MYH7B, NPPA, NPPB, BMP4, BMP5	<0.0001
Hypertrophy model	EIF4E, IL1R1, IFRD1, ATF3, VEGFA	<0.001
Gene ontology, function-based analysis phenotype: heart failure		
Cardiac fibrosis	ACKR3, AHR, HEY2, PPARA, HOPX, PTGS2, THBS4, CSRP3, MAPK8, PDL	<0.001
Gene ontology, diseases: heart failure		
Myocardial infarction	ABCA1, ALDH2, CCL2, CIITA, F13A1, HMGCR, LDLR, NPPA, NPPB, PLAT, PROCR, PTGS2, SELP, THBS4, TLR4, TNNT1, VEGFA	<0.0001
Dilated cardiomyopathy	ADRA2C, ANKRD2, CCL2, CSRP3, KCNIP2, LAMA2, MYH7, NPPA, NPPB, PDLIM3, PGM1, SUN2, TNNI1, TNNT1, VCAM1	<0.0001
Pulmonary fibrosis	CCL2, CD24, CTGF, CXCL8, MMP11, RGS1, SLN, UBD, VCAM1	<0.01
Left ventricular noncompaction	CSRP3, MYH7, MYH7B, PRDM16, YWHAE	<0.01
Pulmonary hypertension	ADORA3, BMP4, NPPA, NPPB, PDE4A, PLAT, VEGFA	<0.01
Heart disease	C3, HMGCR, MYH7, NPPA, NPPB, PPARA	<0.05
Atrial fibrillation	NPPA, NPPB, PLAT, SCN3B, SELP	<0.05
Hypertrophic cardiomyopathy	CSRP3, MYH7, NPPB, TNNT1	<0.05

BMP = bone morphogenic protein; other abbreviations as in Table 1.

FIGURE 1 Representative P-V Loops

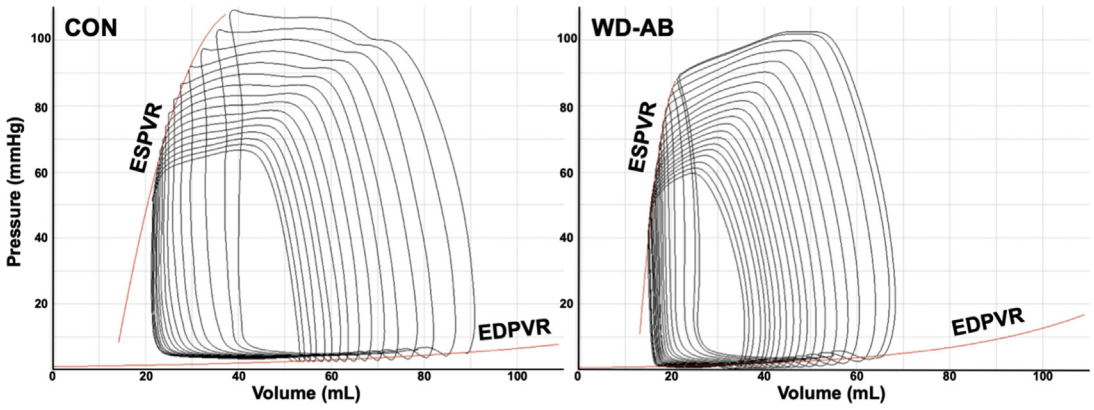

Representative pressure–volume (P-V) loops at rest from individual control (CON) and Western diet, aortic-banded (WD-AB) animals. EDPVR = end-diastolic P-V relationship; ESPVR = end-systolic P-V relationship.

as means ± SE, and significance was reported at $p < 0.10$ and $p < 0.05$ levels (35,36).

See Supplemental Material for a comprehensive account of all Methods utilized in the current study (Supplemental Tables 1 to 3, Supplemental Figures 1 to 8, and Supplemental References).

RESULTS

CARDIAC REMODELING AND FUNCTION. **Tables 1 to 3 and Figures 1 to 4** provide evidence supporting functional, structural, and genetic characteristics consistent with HF in the WD-AB group using echocardiographic, pressure–volume, post-mortem morphology, and RNA-seq techniques. Considering 1 independent variable was diet, tibia length was examined to determine if normalization of the morphometric data was necessary (37,38). Tibia length was the same between groups, indicating that differences in body weight and body surface area between groups were observed in animals with similar age-related growth (**Table 1**). Because there were no significant differences in tibia length, absolute heart and lung weights were used for group morphological analyses (39). WD-AB animals displayed increased lung weight compared with the CON group, with no differences in resting ejection fraction (EF) (**Table 1**). Significant concentric left ventricular (LV) hypertrophy was present in WD-AB animals, as indicated by an increase in global hypertrophy (LV, right ventricle, and atria) (**Table 1**) and increased LV diastolic wall thickness 2 and 6 months post-aortic banding that was dependent on the group at 8 and 12 months of age, respectively (**Table 2**) (group × time interaction; representative ultrasound images are shown in Supplemental Figures 1A and 1B). There were no differences in LV internal diastolic dimension or end-diastolic volume between groups (**Tables 1 and 2**). Analysis of aortic hemodynamics (proximal to the AB in the WD-AB group) (Supplemental Table 1) indicated WD-AB animals faced a greater afterload compared with CON animals, which was evident 6 months post-aortic banding as significant increases in both aortic systolic blood pressure and pulse pressure.

Additional analysis of LV function resulted in paradoxical findings with respect to systolic function. Stroke volume (**Table 1**) and torsion (Supplemental Figure 1D) relative to cardiac remodeling were similar between groups. There was a trend toward increased LV contractility (measured as preload recruitable stroke work, shown by our laboratory and others in AB swine) (20,23,24,40) in the WD-AB group, which was observed in parallel with a decreased stroke volume index (**Table 1**). **Figure 2** outlines the potential contributions of individual cardiomyocyte function to whole heart cardiac dysfunction (representative traces of calcium transients and sarcomere length are presented in Supplemental Figures 2A and 2B). Diastolic and systolic calcium and sarcomere length (Supplemental Figures 2C and 2D), as well as calcium transient and shortening amplitudes (Supplemental Figures 2E and 2F), were comparable between the CON and WD-AB groups under both baseline and dobutamine (1 μM) experimental conditions, which was consistent with preserved systolic function at the whole organ level. However, differences among groups were apparent in

FIGURE 2 **Ossabaw Swine Fed A WD With Chronic Pressure Overload-Induced HF Show Impaired Individual Cardiomyocyte Function**

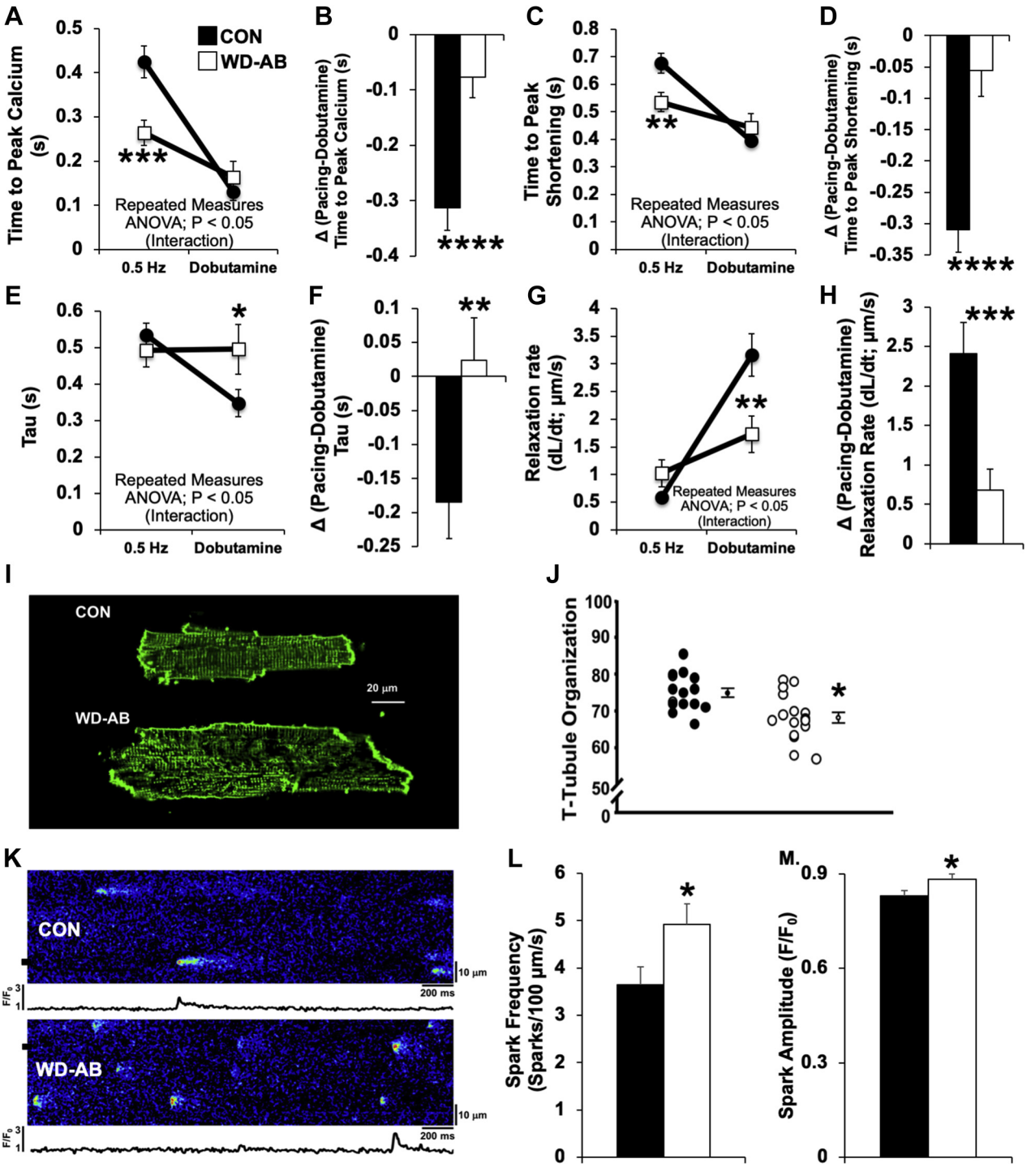

(A) Systolic cardiomyocyte calcium and **(C)** shortening kinetics are faster under baseline pacing conditions in the WD-AB group, but **(B and D)** lack β-adrenergic reserve in response to dobutamine. **(E and F)** Diastolic calcium reuptake (tau) and **(G and H)** relaxation rate kinetic reserve following exposure to dobutamine is impaired in WD-AB cardiomyocytes. **(I)** Representative cardiomyocyte images show **(J)** cardiomyocyte t-tubule disorganization in WD-AB animals. **(K)** Representative line scans illustrate spontaneous ryanodine receptor-mediated calcium **(L)** spark frequency and **(M)** amplitude were increased in the WD-AB group. *t-test versus CON (*$p < 0.05$; **$p < 0.01$; ***$p < 0.001$; ****$p < 0.0001$). n = 4 animals, 25 to 27 cells in the CON group; n = 4 animals, 23 to 25 cells in the WD-AB group. ANOVA = analysis of variance; HF = heart failure; other abbreviations as in Figure 1.

FIGURE 3 Isolated Mitochondrial Function Is Compromised in Ossabaw Swine Fed a WD With Chronic Pressure Overload-Induced HF and Associated With Decreased L_4CL

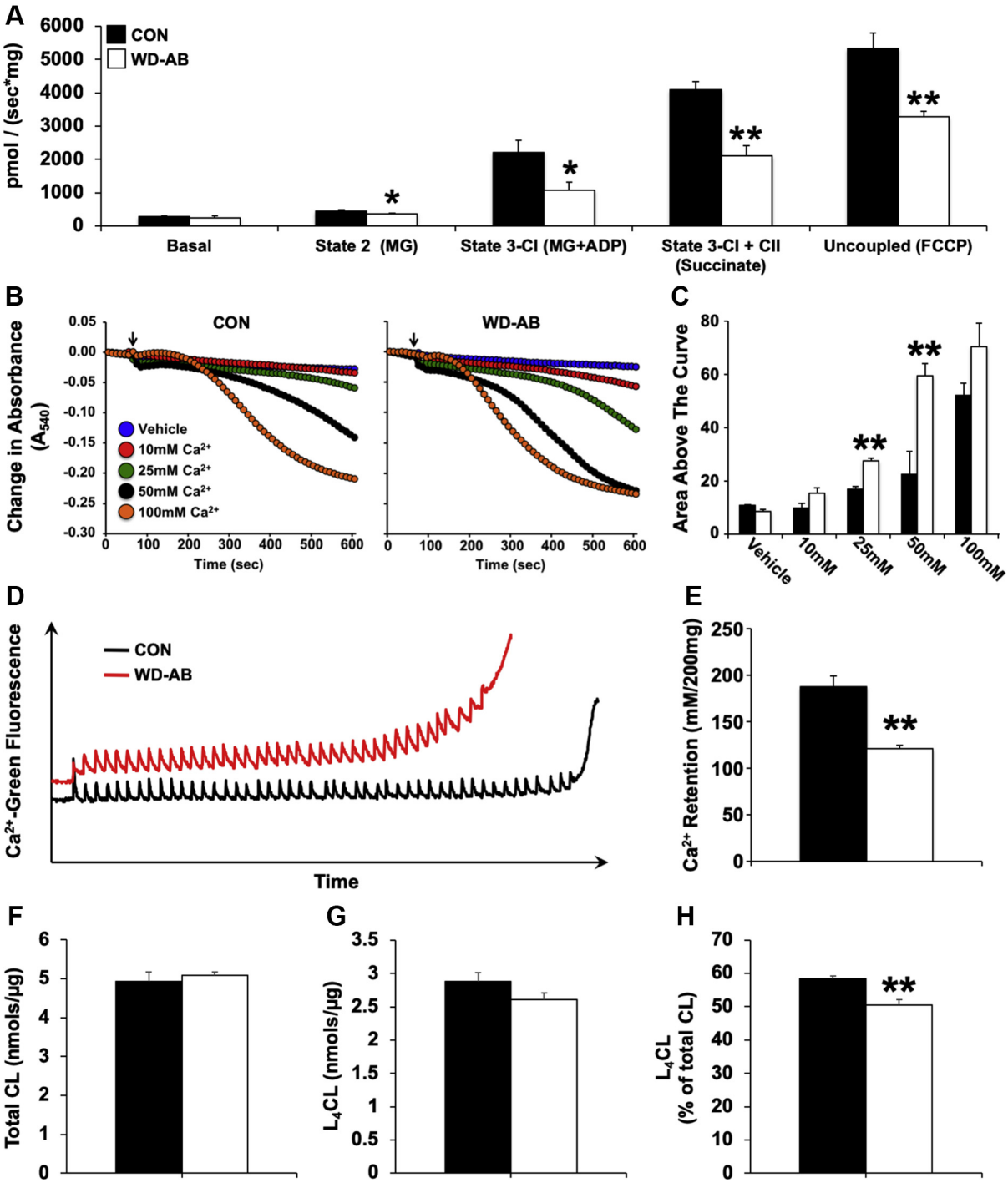

(A) Mitochondrial dysfunction evident as impaired complex 1 and 2-dependent respiration and functional uncoupling of the respiratory chain and adenosine triphosphate synthesis. **(B to E)** Susceptibility to calcium (Ca^{2+})-induced mitochondrial permeability transition (an early indicator of mitochondrial dysfunction) was increased in the WD-AB group. **(B and C)** Quantification of the area above the curve of the Ca^{2+}-induced swelling traces was increased in WD-AB animals. **(D and E)** Conversely, Ca^{2+}-retention capacity was decreased in the WD-AB group. **(F to H)** The composition of **(G)** tetralinoleoyl cardiolipin (L_4CL) to **(F)** total cardiolipin levels was **(H)** decreased in WD-AB animals. *t-test versus CON (*$p < 0.05$; ** $p < 0.01$). $n = 4$ for CON and WD-AB groups. ADP = adenosine diphosphate; MG = malate/glutamate; other abbreviations as in Figures 1 and 2.

FIGURE 4 Ossabaw Swine Fed a WD With Chronic Pressure Overload-Induced HF Exhibit Distinct Molecular Signatures Indicative of LV Pathological Remodeling

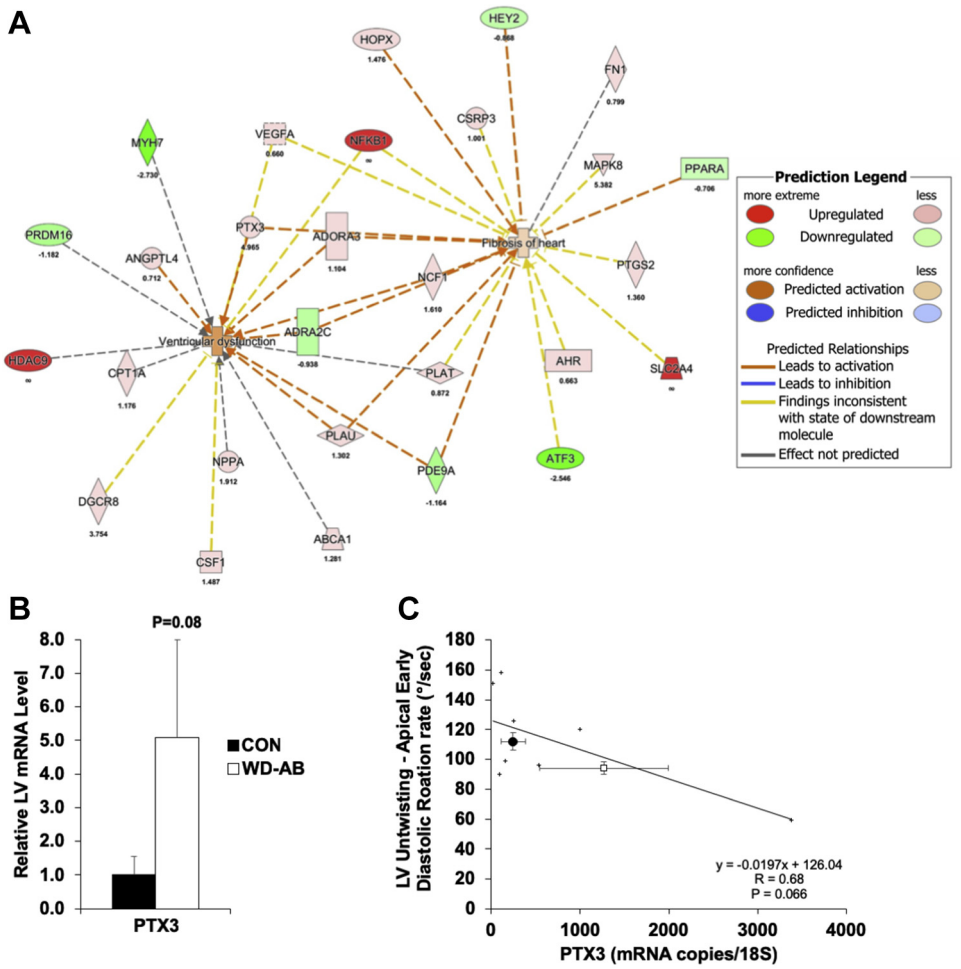

(A) Left ventricular (LV) gene interactions between significant cardiac hypertrophy and cardiac fibrosis networks revealed by ingenuity pathway analysis between CON and WD-AB animals. **(B)** Pentraxin-3 (PTX3) mRNA level is increased in the WD-AB group and **(C)** negatively correlated with LV untwisting. WD-AB animals show a right and downward shift along this relationship compared with CON (+ = individual animal data points forming the regression line). **(D)** Interleukin 1 receptor-like 1 (IL1RL1) mRNA level was also increased in the WD-AB group and **(E)** negatively correlated with LV untwisting. WD-AB animals again show a right and downward shift along this relationship compared with CON (+ = individual animal data points forming the regression line). **(F)** The collagen I/III mRNA ratio is increased in the WD-AB group. **(G)** A decrease in the more compliant N2BA titin isoform is seen in WD-AB animals with representative samples from both the CON and WD-AB groups presented alongside the bar graph. *t-test versus CON ($*p < 0.05$). n = 3 for CON and WD-AB in Figure 4A. n = 5 for the CON group and n = 4 for the WD-AB group in Figures 4B to 4G. Abbreviations as in Figures 1 and 2.

Continued on the next page

calcium transient and shortening kinetics, which resulted in a loss in dobutamine-induced functional kinetic reserve (Figures 2A to 2D). Decreases in cardiomyocyte time to peak calcium (Figures 2A and 2B) and shortening (Figures 2C and 2D) following dobutamine challenge were blunted in the WD-AB group compared with the CON group, despite showing faster cellular systolic kinetics under 0.5-Hz baseline pacing conditions. These combined data suggest that although traditional indicators of systolic function like EF appear normal, the means by which resting systolic function is maintained is substantially different in WD-AB animals.

Diastolic function was also impaired in both the whole heart and individual cardiomyocytes in WD-AB animals. The EDPVR was increased in the WD-AB

FIGURE 4 Continued

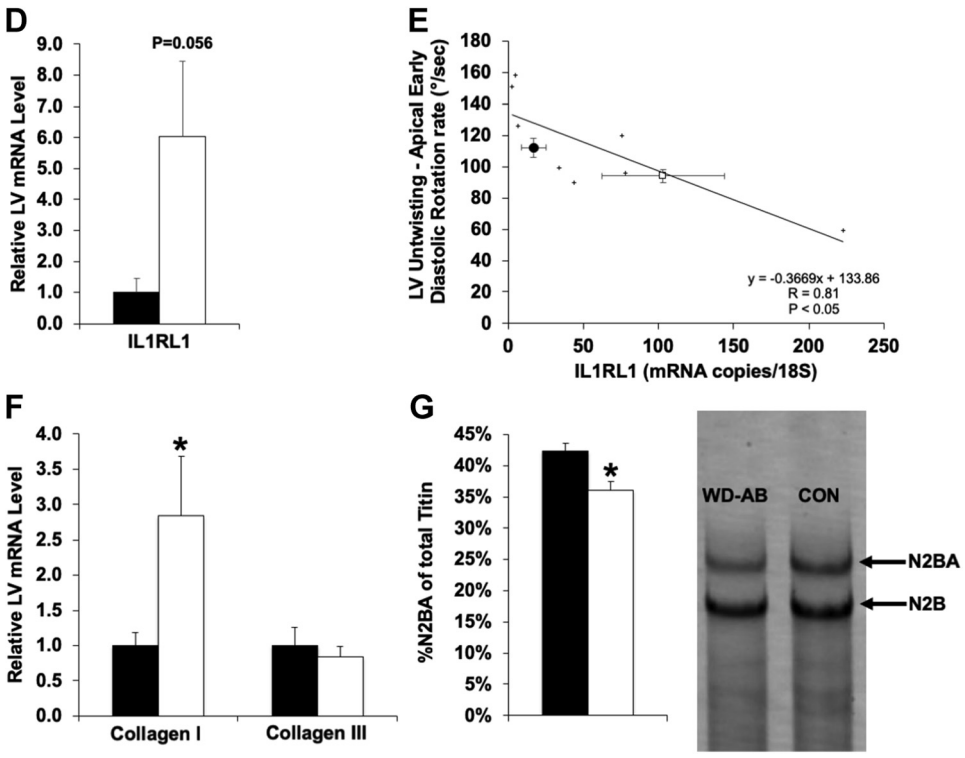

group (representative pressure–volume loops are shown in Figure 1, and quantification is shown in Table 1). This was observed in parallel with abnormal LV diastolic mechanics, including decreased LV early diastolic untwisting and increased LV late longitudinal strain rate, which were indicative of both impaired early diastolic filling and enhanced atrial systole during late diastole, respectively (Table 1). At the cellular level, dobutamine-induced enhancement in diastolic kinetic parameters, including calcium reuptake rate (Figures 2E and 2F) (tau) and relaxation rate (Figures 2G and 2H), were lost in the WD-AB group, although baseline (0.5 Hz) values were similar between groups. In addition, cardiomyocyte t-tubules were disorganized (Figures 2I and 2J), and spontaneous ryanodine receptor–mediated calcium spark frequency and amplitude were increased (Figures 2K and 2L) in WD-AB animals versus CON animals. In total, these data indicate functional and structural changes at the organ and cellular levels consistent with diastolic dysfunction.

Impaired myocardial relaxation might also have been influenced by metabolic derangement in the LV. Figure 3 shows LV mitochondrial dysfunction, including decreased complex 1- and 2-dependent respiration and *t*rifluoromethoxy carbonylcyanide phenylhydrazone (FCCP)-uncoupled maximal mitochondrial respiration (Figure 3A). Calcium-induced mitochondrial swelling was exacerbated (Figures 3B and 3C), and calcium retention capacity (Figures 3D and 3E) was also decreased in WD-AB animals, which both indicated increased susceptibility to calcium-induced mitochondrial permeability transition. Shotgun lipidomic showed the proportion of contribution of tetralinoleoyl cardiolipin to total myocardial cardiolipin levels (Figures 3F to 3H) (a phospholipid that consists of ~80% of ventricular cardiolipin in humans and is considered to reflect a healthy phospholipid phenotype in the heart) (41) was decreased in the WD-AB group. Collectively, evidence of impaired LV mitochondrial energetics is consistent with the development of HF (42).

To define the molecular signature associated with the pathological state in the WD-AB heart, transcriptome was profiled in LV tissues from WD-AB and CON animals. As presented in Table 3 and Figure 4, unbiased Ingenuity Pathway Analysis detected top gene expression changes in the WD-AB group are cardiac hypertrophy and cardiac fibrosis, which are listed as the #1 and #4 top significant toxicology lists

FIGURE 5 Ossabaw Swine Fed a WD With Chronic Pressure Overload-Induced HF Demonstrate Skeletal Muscle and Brain Vascular Dysfunction in Isolated Microvessels

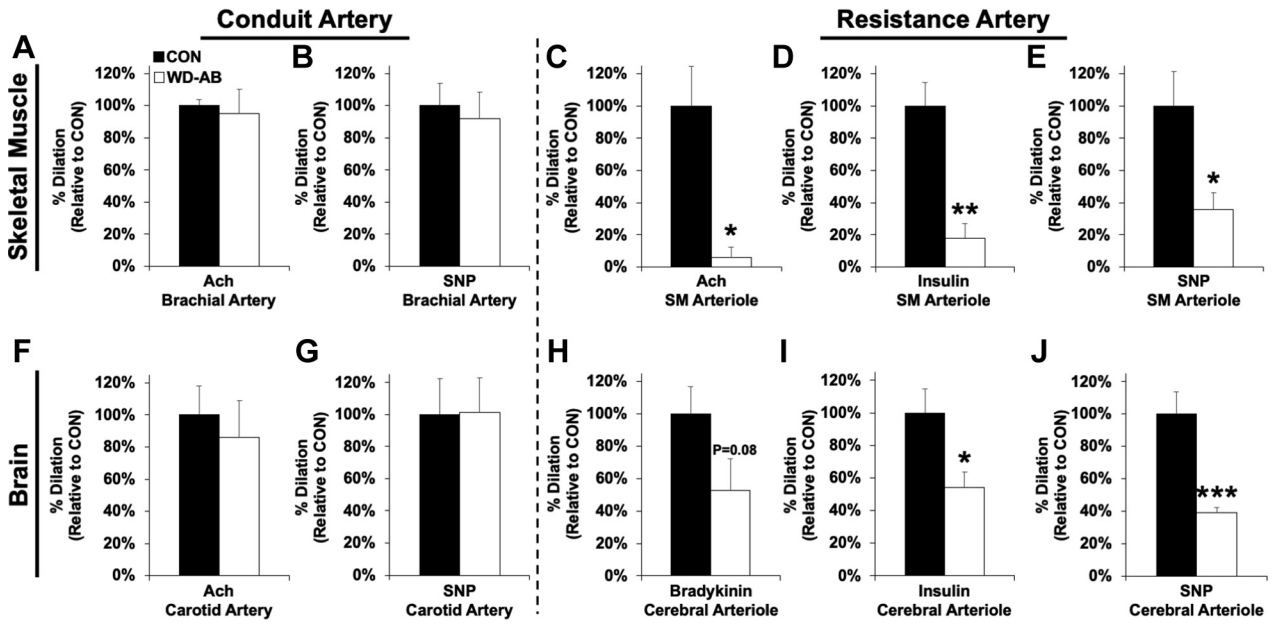

Brachial artery ring preparations indicate **(A)** endothelial and **(B)** smooth muscle–dependent function is similar between the CON and WD-AB groups. Skeletal muscle microvessel preparations show significant **(C)** endothelial, **(D)** metabolic, and **(E)** smooth muscle–dependent dysfunction in the WD-AB group. Carotid artery ring preparations reveal **(F)** endothelial and **(G)** smooth muscle–dependent function is similar between the CON and WD-AB group. Cerebral microvessel preparations show significant **(H)** endothelial, **(I)** metabolic, and **(J)** smooth muscle–dependent dysfunction in WD-AB animals. *t-test versus CON (*$p < 0.05$; **$p < 0.01$; ***$p < 0.001$). n = 5 for the CON group, and n = 4 for the WD-AB group. Ach = acetylcholine; SM = skeletal muscle; SNP = sodium nitroprusside; other abbreviations as in Figures 1 and 2.

(Table 3). Significant interaction between gene networks associated with cardiac dysfunction and fibrosis are also identified and illustrated in Figure 4A. Based on gene ontology analysis for the differentially expressed genes, a significant enrichment of several HF-related gene networks was found in the WD-AB hearts, as highlighted by numerous genes known to be implicated in HF-related cardiac fibrosis and hypertrophic remodeling, such as *NPPA*, *NPPB*, *MYH7*, as well as bone morphogenic proteins and collagens (Table 3). In addition to these well-known molecular markers for HF, a number of inflammatory genes were also implicated, including pentraxin-3 (PTX3) (43,44) and interleukin 1 receptor-like 1 (IL1RL1) (44,45), which are indicators of inflammation. The approximate 5-fold increase in PTX3 reported by RNA-seq in WD-AB animals was confirmed independently using quantitative real-time polymerase chain reaction (Figure 4B), as was an increase in IL1RL1 (Figure 4D). Cumulative group data, represented by the regression line, also showed a significant negative correlation between LV untwisting and both PTX3 (Figure 4C) and IL1RL1 (Figure 4E) mRNA levels. Group means reflected a right and downward shift along this relationship in the WD-AB group compared with the CON group, which indicated that an increase in LV expression of these markers of inflammation was associated with a decline in LV diastolic mechanical function. Cardiac remodeling in the WD-AB group was confirmed separately by 2 different measures that could influence the stiffness of individual cardiomyocytes and/or the whole heart: 1) an increase in the collagen I/III mRNA ratio (Figure 4F) (indicative of potentially increased extracellular matrix stiffness) (46); and 2) a decrease in protein expression of the N2BA isoform of titin (Figure 4G) (a more compliant isoform of the large elastic sarcomeric protein) (47-51). Total LV collagen protein was the same between the groups and visualized by representative Masson's trichrome images (Supplemental Figure 3). This suggested that differences in LV stiffness regulated by the extracellular matrix might be more related to changes in its composition (i.e., collagen isoform shift) as opposed to a general accumulation of total fibrotic components. Overall, these data are indicative of molecular signatures consistent with cardio-metabolic disease in the myocardium of WD-AB animals and suggest

FIGURE 6 Ossabaw Swine Fed a WD With Chronic Pressure Overload-Induced HF Exhibit a Systemic Inflammatory State Consistent With Common Comorbidities Seen in Experimental HF

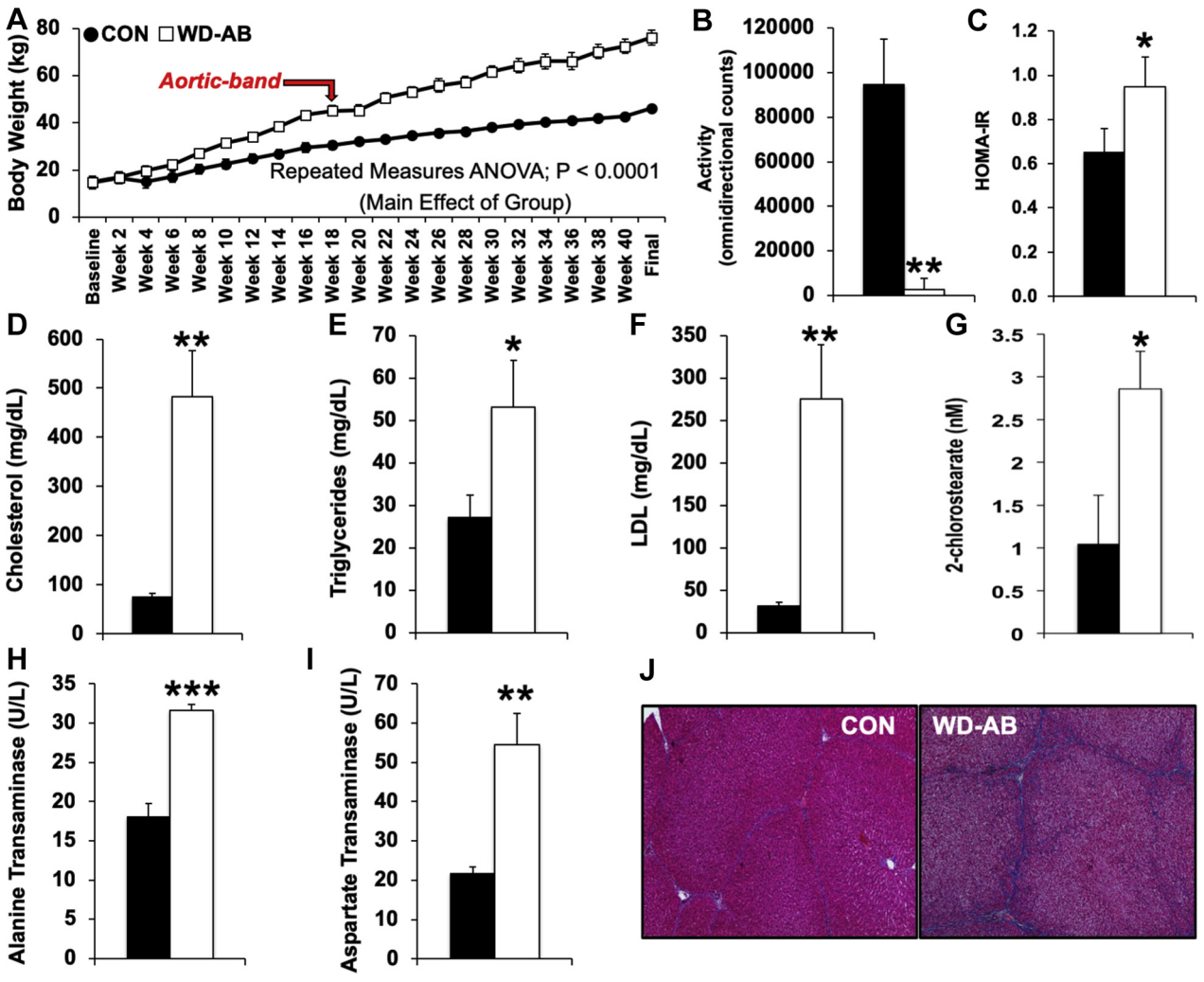

Animals in the WD-AB group were **(A)** obese, **(B)** inactive, and **(C)** insulin resistant (homeostatic model assessment of insulin resistance [HOMA-IR]). Dyslipidemia was observed in WD-AB animals as indicated by **(D)** increased plasma cholesterol, **(E)** triglycerides, **(F)** low-density lipoproteins (LDL), and **(G)** 2-chlorostearate. **(H and I)** Plasma liver enzymes were increased and evidence of (**J**; Masson's trichrome stain) increased liver fibrosis were seen in the WD-AB group. *t-test versus CON (*$p < 0.05$; **$p < 0.01$; ***$p < 0.001$). n = 5 for CON and WD. Abbreviations as in Figures 1 and 2.

that molecular mechanisms potentially relevant to HF are present in this model.

PERIPHERAL AND CENTRAL VASCULAR FUNCTION. Microvascular dysfunction, reflected by impaired vasodilatory capacity, was present in the skeletal muscle, brain, and coronary resistance vessels of WD-AB animals. Figure 5 shows conduit and resistance vessel function from the skeletal muscle and brain following exposure to endothelial (acetylcholine, bradykinin, insulin) and smooth muscle–dependent (sodium nitroprusside) vasodilators. Although conduit vessel function from both peripheral vascular beds was similar to the brachial artery (Figures 5A and 5B) and the carotid artery (Figures 5F and 5G) in the CON group, endothelial, metabolic, and smooth muscle–mediated vasodilatory capacity was impaired in the resistance arteries from isolated skeletal muscle (Figures 5C to 5E) and brain (Figures 5H to 5J) arterioles in the WD-AB group (complete dose–response curves for resistance vessels are shown in Supplemental Figures 4 to 5). In addition, in vivo evaluation of coronary vascular function demonstrated that although relative coronary blood flow was similar between groups (Supplemental Figure 6A, measured in the left

anterior descending coronary artery), myocardial oxygen extraction was greater in the WD-AB group (Supplemental Figure 6B). This was associated with impaired coronary resistance vessel vasodilatory capacity to the large conductance calcium-activated potassium (BKCa) channel agonist NS-1619 in isolated arterioles (Supplemental Figures 6C and 6D, a mediator of arterial tone abundantly expressed in vascular smooth muscle shown to provide protection against excessive vasoconstriction) (24,52-54). Gene ontology analysis revealed significant enrichment of several molecular pathways related to vascular disease, including atherosclerosis, microvascular complications, and peripheral vascular disease (Supplemental Table 2). In summary, these data indicate endothelial, metabolic, and smooth muscle–dependent microvascular dysfunction dominate vascular impairment in both the periphery and heart of WD-AB animals, which is consistent with functional vascular abnormalities seen in both cardio-metabolic disease and HF.

COMORBIDITIES AND INFLAMMATION. Before aortic banding, the body weight of WD-AB animals was significantly increased compared with CON, which indicated metabolic disease was developing at the time of surgery. The data presented in **Figures 6A to 6J and Table 2** show evidence of metabolic derangement at the time terminal experiments were performed. Specifically, obesity (body weight) (**Figures 6A, Table 2**), inactivity (decreased animal movement in the pen) (**Figure 6B**), insulin resistance (homeostatic model assessment of insulin resistance) (**Figure 6C**), and plasma hyperlipidemia (**Figures 6D to 6G**) (including chlorinated lipids [**Figure 6G**] associated with increased immune-derived reactive oxygen species production, inflammatory signaling, and endothelial dysfunction) (55-58) were seen in the WD-AB group. Wound healing in the WD-AB group following surgical intervention was excellent, and all animals were ambulatory, eating, urinating, and defecating normally within 1 week post-surgery. Thus, the significant decrease in cage activity in WD-AB animals was not related to our surgical procedures or other health concerns separate from the aortic banding or dietary interventions. Increased plasma liver enzyme levels and nonalcoholic fatty liver disease (**Figures 6H to 6J**) (evident by the combination of liver steatosis, inflammation, and fibrosis) in WD-AB animals was also consistent with nonalcoholic steatohepatitis as shown previously in WD-fed Ossabaw swine by our laboratory (14). Several reports indicate nonalcoholic steatohepatitis is related to HF and LV diastolic dysfunction (59-63). Further exploration of group differences that examined metabolic and renal disease, including immune and inflammation-related signaling pathways and phenotypes, were assessed using RNA-seq in LV tissue and is presented in Supplemental Figures 7 and 8 and Supplemental Tables 1 to 3. Enhancement of molecular pathways related to obesity, metabolic syndrome, diabetes, fatty liver disease, glomerulonephritis, and renal fibrosis were revealed following gene ontology analysis (Supplemental Table 2). A number of corresponding signaling pathways (Supplemental Table 3) and genetic phenotypes (Supplemental Table 4) highlighted immune and inflammatory involvement. Three of the top 5 significant upstream regulators identified by ingenuity pathway analysis indicated activation of well-known signaling networks that contributed to systemic inflammation, including tumor necrosis factor (Supplemental Figure 7A) ($p < 0.05$), interferon-γ (Supplemental Figure 7B) ($p < 0.05$), and toll-like receptor 3 (Supplemental Figure 7C) ($p < 0.05$). Top regulator effect gene networks that support activation (Supplemental Figure 8A) ($p < 0.05$), migration (Supplemental Figure 8A, $p < 0.05$), and adhesion (Supplemental Figure 8B) ($p < 0.05$) of immune cells potentially influenced by NF-κB signaling pathways (Supplemental Table 3, Supplemental Figure 8B) (CHUK-inhibitor of NF-κB kinase subunit-α) were also identified. Together, these findings suggest this preclinical model displays a chronic inflammatory state consistent with cardio-metabolic disease and HF.

DISCUSSION

This multidisciplinary research study showed that Ossabaw swine fed a WD and subjected to chronic cardiac pressure-overload exhibited functional, structural, and genetic characteristics consistent with cardio-metabolic HF. In this experimental setting, WD-AB animals displayed a number of cardiac and vascular features reminiscent of metabolic derangement and HF, including comorbidities associated with activation of the immune system and inflammation. Collectively, these data indicated the combination of traditional methods used to generate HF (i.e., diet, aortic-banding) imposed on the unique genetic background of Ossabaw swine resulted in a translational animal model with a distinctive constellation of findings that are conceivably useful to extending the understanding of how pre-existing cardio-metabolic syndrome can contribute to developing HF.

As hypothesized, WD-AB animals displayed cardiac characteristics fundamental to HF, including traditional indicators, myocardial remodeling, diastolic

dysfunction, and signs of altered, but compensated resting systolic function. Conventional markers of HF were observed at both system and molecular levels as shown by post-mortem, imaging, and molecular signatures that highlighted pathological cardiac remodeling (increased diastolic wall thickness), pulmonary involvement, and classic HF-related genes (e.g., natriuretic peptides, myosin heavy chain). Diastolic dysfunction was evident at the whole heart level in the WD-AB group by both an increase in the EDPVR and mechanically via abnormal diastolic strain measures, which implied difficulty filling during early diastole, with attempts to compensate for this deficiency by increasing the contributions of atrial systole to overall LV filling (64-68). Increased EDPVR and altered LV diastolic mechanics, observed in parallel with increased aortic systolic pressure, pulse pressure, and directionally consistent (but nonsignificant) increases in mean arterial pressure, effective arterial elastance, end-systolic elastance, and a decreased effective arterial elastance/end-systolic elastance ratio are evocative of HFpEF (69). LV end-diastolic pressure may not be elevated in early HFpEF (70,71); thus, our findings outline a reasonable scenario in which both vascular and ventricular stiffening could lead to the increase in the wet lung weight observed in the WD-AB group in the present study. In addition, an impaired ability of cardiomyocytes to sequester calcium and relax during diastole following β-adrenergic agonism signified a decrease in cellular diastolic cardiac reserve. Molecular signatures also indicated detrimental LV remodeling, as verified by evidence of collagen and titin isoform shifts, could increase the stiffness of the myocardium in parallel with LV mitochondrial dysfunction (via associated deficits in energetic need impairing excitation–contraction coupling).

Although compensated at rest, physiological assessment of systolic function indicated a number of paradoxical findings in the whole organ and a lack of cardiac reserve in isolated cardiomyocytes from the WD-AB group. A specific example of this inconsistency included no group differences in what would be considered a normal EF (>50%), observed in parallel with increased LV contractility (preload recruitable stroke work) and reduced systemic perfusion as indicated by the decreased stroke volume index. This contradiction also existed at the cellular level in WD-AB animals, as individual cardiomyocytes displayed normal absolute calcium transient and shortening amplitude, yet had an associated reduction in kinetic reserve capacity in response to adrenergic challenge with dobutamine. Such findings were consistent with those in rodent models of hypertrophy, in which cardiomyocyte functional parameters are maintained or enhanced (72,73), which may serve as an initial compensatory mechanism used by the heart to maintain systolic function at rest (74). However, such functional adaptations might consume a large portion of the cardiac reserve that normal healthy hearts typically maintain. This functional compensation, disguised at rest, becomes apparent during scenarios of increasing cardiovascular stress (e.g., activities of daily living, exercise), limiting the flexibility of the heart to respond to increasing hemodynamic demand. Together, this collection of data provides a solid foundation of evidence supporting the presence of experimental HF in WD-AB animals.

Increasing evidence suggests peripheral vascular dysfunction also plays a significant role in the lack of cardiovascular reserve and high prevalence of cardiogenic dementia in patients with HF. Our results indicate that at this stage of disease, a profile of primarily microvascular dysfunction reminiscent of HFpEF was observed in this translational model, as opposed to impaired conduit artery function which is more often associated with HFrEF (75-87). Novel data from the WD-AB group indicated there was a significant smooth muscle component to this profile of functional microvascular impairment in multiple vascular beds, including those supplying skeletal muscle, the brain, and the heart. Vascular mechanisms targeting smooth muscle may have therapeutic value given smooth muscle-mediated vascular dysfunction has been observed in resistance vessels from both the heart and the brain of Ossabaw swine with metabolic syndrome that did not have HF (88), and aortic-banded Yucatan mini-swine that displayed HF in the absence of metabolic comorbidities (24,26). A good deal of focus has also been placed on endothelial impairment caused by chronic inflammation as a driving force behind the development of cardiometabolic syndrome and HF. Our results likewise showed both endothelial and metabolic microvascular dysfunction in WD-AB animals (again in multiple vascular beds). A potential intersection between smooth muscle and endothelial-dependent vascular dysfunction could be nitric oxide, manifested via impaired downstream cGMP/PKG signaling that could negatively affect LV function from both a vascular and myocardial perspective (44). Diminished microvascular function, regardless of cellular mechanism, could significantly impact a patient's ability to engage in normal activities of daily living via: 1) a limited ability to increase blood flow to skeletal muscle and/or the heart in response to increased metabolic demand; or 2) by harming cognitive function potentially

leading to depression, dementia, and reduced therapeutic compliance. Together, these data indicate vascular impairment in WD-AB animals is dominated by microvascular dysfunction in multiple organs. We provide new evidence of a significant smooth muscle–mediated component to the disease process, in addition to metabolic and endothelial-dependent impairment. These findings are consistent with paradigms believed to reflect a scenario of cardio-metabolic HF.

CLINICAL PERSPECTIVES. The combination of multisystem genetic signatures, considered in parallel with a profile of metabolic disease, including obesity, inactivity, and dyslipidemia, supports the initial decision to use Ossabaw swine for this study given their genetic predisposition to this cluster of health disparities. From a molecular perspective, mRNA transcriptome signatures from the LV support our pathophysiological evidence of experimental HF and extensive cardio-metabolic disease in the WD-AB group. The molecular changes are highlighted by genes and pathways that are also implicated in numerous cardiac, vascular, metabolic, renal, immune, and inflammation-related signaling pathways. In particular, bone morphogenic protein–related pathways and NF-κB–mediated inflammatory gene induction are stimulated by transforming growth factor-β, tumor necrosis factor-α, and interleukin-1 signaling (89-91). These pathways, in addition to IL1RL1 (also part of the IL-1 super family) (92,93), were observed in the hearts of WD-AB animals. Anti-inflammatory therapy, including interleukin-1 and transforming growth factor-β inhibition, could be tested in the preclinical cardio-metabolic HF model presented here and contribute to the continuing evaluation of these therapeutic targets, which are currently being examined in clinical trials for both HFrEF and HFpEF (94-97).

In addition, ingenuity pathway analysis revealed significant gene signatures associated with activation, migration, and adhesion of immune cells potentially regulated in part by Inhibitor of NFκB Kinase Subunit Alpha (CHUK), a component of the NFκB signaling complex that, counterintuitive to its title, prompts activation of NFκB signaling (90,91). Results from unbiased '-omics'-based analysis between groups indicate a strong role for NFκB signaling in WD-AB animals, which can be activated by chlorinated lipids such as 2-chlorostearate. Chlorinated lipids can be generated from myeloperoxidase, a protein expressed in neutrophils, monocytes, and leukocytes that has been linked to inflammation and endothelial dysfunction (55-57). Therapeutic modulation of diet, including manipulation of lipid intake, has been linked to diastolic function and cardiovascular risk in HFpEF patients (98-100). Our results suggest this animal model could be a suitable platform to examine nutritional interventions as a way to modulate the pathological inflammation and vascular dysfunction associated with cardio-metabolic HF.

Systemic inflammation is highly correlated with metabolic derangement, and our results also found several gene networks reflecting inflammatory and immune signaling pathways were induced in the WD-AB group, including well-established molecular targets such as tumor necrosis factor, interferon-γ, and toll-like receptor 3 (101-105). The finding of inflammatory markers, such as PTX3 and IL1RL1, may also have potential diagnostic importance (43-45). PTX3 has been correlated with diastolic dysfunction (106,107), and IL1RL1 is mechanistically linked to the regulation of myocardial fibrosis (104,105,108). Molecular validation of these targets in WD-AB animals, and the association of PTX3 and IL1RL1 with LV untwisting during early diastole, provides further support of potential links between their levels and impaired diastolic function. These relationships warrant further mechanistic interrogation.

Other molecular targets that recently garnered attention for their therapeutic potential to treat HF include phosphodiesterase-9 (109) and histone deacetylases such as HDAC9 (110). These mechanisms appear as genes of interest in the cardiac hypertrophy and fibrosis networks presented in **Figure 4A** that are significantly altered in this translational model of cardio-metabolic HF. Considered together, the results of this study reveal a number of cellular mechanisms potentially applicable to a cardio-metabolic phenotype characterized by diet and comorbidity-driven inflammation. Accordingly, these data provide numerous avenues of exploration that we believe could be tested in this new preclinical platform of cardio-metabolic HF.

STUDY LIMITATIONS. The assessment of cardiac reserve is powerful as a diagnostic tool for assessing HF. In the present study, we assessed cardiac reserve at only the cellular level. Our group has a history of using both exercise and dobutamine dose–response protocols in the catheter laboratory to assess cardiac reserve in vivo (22-25,27,111-113). Although practical considerations (including an extensive focus on the transcriptome) limited our ability to perform these experiments, examination of cardiac reserve in future studies will be important to the continued verification of HF in this model. A comprehensive examination of cardiomyocyte calcium fluxes was not

performed, and the functional changes in calcium handling proteins in this disease model remain to be determined. We anticipate these changes are multifactorial based on our findings, and suggest complex changes in expression and/or post-translational modification of multiple calcium handling proteins. The transcriptome results presented in this study only suggest that certain molecular signatures in the heart share the same profile as observed in other diseases (e.g., renal pathology). By itself, the renal RNA-seq data observed from LV samples was not sufficient to establish etiology or mechanism, and further interrogation of kidney disease and its relationship to developing HF is warranted. A strength of this model is the statistical justification of a strong pathological phenotype in the animals, despite the large variability inherent to disease. Nevertheless, more subtle phenotypes that could be of physiological importance may be difficult to resolve with the present study design, and follow-up studies will be essential to extend the clinical translation of our initial findings.

CONCLUSIONS

Our results indicate the combination of pressure-overload and dietary intervention results in a profile of cardio-metabolic HF in Ossabaw swine. This unique preclinical animal model provides the opportunity to enhance our understanding of how metabolic disease interacts with developing HF, as well as a translational opportunity to develop new mechanistic avenues of exploration relevant to pathological conditions when symptoms of both cardio-metabolic disease and HF are present.

ACKNOWLEDGMENTS The authors would like to thank Michelle Gastecki, Grace Meers, Michelle Lambert, Rory Cunningham, Matt Panasevich, and Madeleine Dionne for their considerable technical contributions, which were essential to the successful completion of the study, and Gore for their generous gift of vascular Gore-Tex sleeves used for aortic banding. This work was supported with resources and the use of facilities at the Harry S. Truman Memorial Veterans Hospital in Columbia, Missouri.

ADDRESS FOR CORRESPONDENCE: Dr. Craig A. Emter, Dr. R. Scott Rector, Dr. Jaume Padilla, and Dr. Timothy L. Domeier, University of Missouri-Columbia, 1600 East Rollins, Columbia, Missouri 65211. E-mail: emterc@missouri.edu OR RectorS@health.missouri.edu OR padillaja@missouri.edu OR domeiert@health.missouri.edu.

PERSPECTIVES

COMPETENCY IN MEDICAL KNOWLEDGE: The development of new treatments for HF has suffered from a lack of animal models that encompass the increasingly heterogeneous disease profile of this patient population. This report provides evidence supporting the hypothesis that WD-AB Ossabaw swine displayed an integrated physiological, morphological, and genetic phenotype evocative of cardio metabolic HF.

TRANSLATIONAL OUTLOOK: This new preclinical animal model displayed a distinctive constellation of findings that are conceivably useful to extending the understanding of how pre-existing cardio-metabolic syndrome can contribute to developing HF.

REFERENCES

1. Borlaug BA, Paulus WJ. Heart failure with preserved ejection fraction: pathophysiology, diagnosis, and treatment. Eur Heart J 2011;32:670–9.

2. Maeder MT, Kaye DM. Heart failure with normal left ventricular ejection fraction. J Am Coll Cardiol 2009;53:905–18.

3. Oktay AA, Rich JD, Shah SJ. The emerging epidemic of heart failure with preserved ejection fraction. Curr Heart Fail Rep 2013;10:401–10.

4. Zhao Z, Wang H, Jessup JA, Lindsey SH, Chappell MC, Groban L. Role of estrogen in diastolic dysfunction. Am J Physiol Heart Circ Physiol 2014;306:H628–40.

5. Sharma K, Kass DA. Heart failure with preserved ejection fraction: mechanisms, clinical features, and therapies. Circ Res 2014;115:79–96.

6. Paulus WJ, van Ballegoij JJ. Treatment of heart failure with normal ejection fraction: an inconvenient truth! J Am Coll Cardiol 2010;55:526–37.

7. Burkhoff D. Mortality in heart failure with preserved ejection fraction: an unacceptably high rate. Eur Heart J 2012;33:1718–20.

8. Borlaug BA, Redfield MM. Diastolic and systolic heart failure are distinct phenotypes within the heart failure spectrum. Circulation 2011;123:2006–13. discussion 2014.

9. Zile MR, Kjellstrom B, Bennett T, et al. Effects of exercise on left ventricular systolic and diastolic properties in patients with heart failure and a preserved ejection fraction versus heart failure and a reduced ejection fraction. Circ Heart Fail 2013;6:508–16.

10. Bratz IN, Dick GM, Tune JD, et al. Impaired capsaicin-induced relaxation of coronary arteries in a porcine model of the metabolic syndrome. Am J Physiol Heart Circ Physiol 2008;294:H2489–96.

11. Dyson MC, Alloosh M, Vuchetich JP, Mokelke EA, Sturek M. Components of metabolic syndrome and coronary artery disease in female Ossabaw swine fed excess atherogenic diet. Comp Med 2006;56:35–45.

12. Neeb ZP, Edwards JM, Alloosh M, Long X, Mokelke EA, Sturek M. Metabolic syndrome and coronary artery disease in Ossabaw compared with Yucatan swine. Comp Med 2010;60:300–15.

13. Padilla J, Jenkins NT, Lee S, et al. Vascular transcriptional alterations produced by juvenile obesity in Ossabaw swine. Physiol Genomics 2013;45:434–46.

14. Panasevich MR, Meers GM, Linden MA, et al. High-fat, high-fructose, high-cholesterol feeding causes severe NASH and cecal microbiota dysbiosis in juvenile Ossabaw swine. Am J Physiol Endocrinol Metab 2018;314:E78–92.

15. Toedebusch RG, Roberts MD, Wells KD, et al. Unique transcriptomic signature of omental adipose tissue in Ossabaw swine: a model of childhood obesity. Physiol Genomics 2014;46:362–75.

16. Vieira-Potter VJ, Lee S, Bayless DS, et al. Disconnect between adipose tissue inflammation and cardiometabolic dysfunction in Ossabaw pigs. Obesity (Silver Spring) 2015;23:2421–9.

17. Olver TD, Grunewald ZI, Jurrissen TJ, et al. Microvascular insulin resistance in skeletal muscle and brain occurs early in the development of juvenile obesity in pigs. Am J Physiol Regul Integr Comp Physiol 2018;314:R252–64.

18. Fleenor BS, Ouyang A, Olver TD, et al. Saxagliptin prevents increased coronary vascular stiffness in aortic-banded mini swine. Hypertension 2018;72:466–75.

19. Hiemstra JA, Gutierrez-Aguilar M, Marshall KD, et al. A new twist on an old idea part 2: cyclosporine preserves normal mitochondrial but not cardiomyocyte function in mini-swine with compensated heart failure. Physiol Rep 2014;2:e12050.

20. Hiemstra JA, Lee DI, Chakir K, et al. Saxagliptin and tadalafil differentially alter cyclic guanosine monophosphate (cGMP) signaling and left ventricular function in aortic-banded mini-swine. J Am Heart Assoc 2016;5:e003277.

21. Hiemstra JA, Liu S, Ahlman MA, et al. A new twist on an old idea: a two-dimensional speckle tracking assessment of cyclosporine as a therapeutic alternative for heart failure with preserved ejection fraction. Physiol Rep 2013;1:e00174.

22. Hiemstra JA, Veteto AB, Lambert MD, et al. Chronic low-intensity exercise attenuates cardiomyocyte contractile dysfunction and impaired adrenergic responsiveness in aortic-banded miniswine. J Appl Physiol (1985) 2018;124:1034–44.

23. Marshall KD, Muller BN, Krenz M, et al. Heart failure with preserved ejection fraction: chronic low-intensity interval exercise training preserves myocardial O2 balance and diastolic function. J Appl Physiol (1985) 2013;114:131–47.

24. Olver TD, Edwards JC, Ferguson BS, et al. Chronic interval exercise training prevents BKCa channel-mediated coronary vascular dysfunction in aortic-banded miniswine. J Appl Physiol (1985) 2018;125:86–96.

25. Olver TD, Hiemstra JA, Edwards JC, Ferguson BS, Laughlin MH, Emter CA. The protective role of sex hormones in females and exercise prehabilitation in males on sternotomy-induced cranial hypoperfusion in aortic banded mini-swine. J Appl Physiol (1985) 2017;122:423–9.

26. Olver TD, Hiemstra JA, Edwards JC, et al. Loss of female sex hormones exacerbates cerebrovascular and cognitive dysfunction in aortic banded miniswine through a neuropeptide Y-Ca(2+)-activated potassium channel-nitric oxide mediated mechanism. J Am Heart Assoc 2017;6.

27. Olver TD, Klakotskaia D, Ferguson BS, et al. Carotid artery vascular mechanics serve as biomarkers of cognitive dysfunction in aortic-banded miniature swine that can be treated with an exercise intervention. J Am Heart Assoc 2016;5.

28. Douglas WR. Of pigs and men and research: a review of appreciation, and the logic of the pig in human medical research. Space Life Sci 1977;3:226–34.

29. Laughlin MH, Overholser KA, Bhatte MJ. Exercise training increases coronary transport reserve in miniature swine. J Appl Physiol (1985) 1989;67:1140–9.

30. Hurnik JF, Lewis NJ. Use of body surface area to set minimum space allowances for confined pigs and cattle. Can J Animal Sc 1991;71:577–80.

31. Esmay ML. Principles of animal environment. Westport, CT: AVI Publishing Co., Inc., 1978.

32. de Winter JCF. Using the Student's t-test with extremely small sample sizes. Pract Assess Res Eval 2013;18:1–12.

33. Tee MW, Won S, Raman FS, et al. Regional strain analysis with multidetector CT in a swine cardiomyopathy model: relationship to cardiac MR tagging and myocardial fibrosis. Radiology 2015;277:88–94.

34. Kim J, Seo BS. How to calculate sample size and why. Clin Orthoped Surg 2013;5:235–42.

35. Curran-Everett D, Benos DJ. Guidelines for reporting statistics in journals published by the American Physiological Society. Am J Physiol Regul Integr Comp Physiol 2004;287:R247–9.

36. Williams JL, Hathaway CA, Kloster KL, Layne BH. Low power, type II errors, and other statistical problems in recent cardiovascular research. Am J Physiol 1997;273:H487–93.

37. Yin FC, Spurgeon HA, Rakusan K, Weisfeldt ML, Lakatta EG. Use of tibial length to quantify cardiac hypertrophy: application in the aging rat. Am J Physiol 1982;243:H941–7.

38. Chirinos JA, Segers P, De Buyzere ML, et al. Left ventricular mass: allometric scaling, normative values, effect of obesity, and prognostic performance. Hypertension 2010;56:91–8.

39. Litwin SE. Cardiac "morphomics": do we need to measure LV mass and geometry in everyone? J Am Coll Cardiol Img 2015;8:1016–8.

40. Ishikawa K, Aguero J, Oh JG, et al. Increased stiffness is the major early abnormality in a pig model of severe aortic stenosis and predisposes to congestive heart failure in the absence of systolic dysfunction. J Am Heart Assoc 2015;4:e001925.

41. Sparagna GC, Chicco AJ, Murphy RC, et al. Loss of cardiac tetralinoleoyl cardiolipin in human and experimental heart failure. J Lipid Res 2007;48:1559–70.

42. Ventura-Clapier R, Garnier A, Veksler V. Energy metabolism in heart failure. J Physiol 2004;555:1–13.

43. Inoue K, Kodama T, Daida H. Pentraxin 3: a novel biomarker for inflammatory cardiovascular disease. Int J Vasc Med 2012;2012:657025.

44. Greene SJ, Gheorghiade M, Borlaug BA, et al. The cGMP signaling pathway as a therapeutic target in heart failure with preserved ejection fraction. J Am Heart Assoc 2013;2:e000536.

45. Shah SJ, Kitzman DW, Borlaug BA, et al. Phenotype-specific treatment of heart failure with preserved ejection fraction: a multiorgan roadmap. Circulation 2016;134:73–90.

46. Burgess ML, Buggy J, Price RL, et al. Exercise- and hypertension-induced collagen changes are related to left ventricular function in rat hearts. Am J Physiol 1996;270:H151–9.

47. Hidalgo C, Granzier H. Tuning the molecular giant titin through phosphorylation: role in health and disease. Trends Cardiovasc Med 2013;23:165–71.

48. Linke WA, Hamdani N. Gigantic business: titin properties and function through thick and thin. Circ Res 2014;114:1052–68.

49. Franssen C, Gonzalez Miqueo A. The role of titin and extracellular matrix remodelling in heart failure with preserved ejection fraction. Neth Heart J 2016;24:259–67.

50. Lewis GA, Schelbert EB, Williams SG, et al. Biological phenotypes of heart failure with preserved ejection fraction. J Am Coll Cardiol 2017;70:2186–200.

51. van Heerebeek L, Franssen CP, Hamdani N, Verheugt FW, Somsen GA, Paulus WJ. Molecular and cellular basis for diastolic dysfunction. Curr Heart Fail Rep 2012;9:293–302.

52. Berkefeld H, Fakler B, Schulte U. Ca2+-activated K+ channels: from protein complexes to function. Physiol Rev 2010;90:1437–59.

53. Hill MA, Yang Y, Ella SR, Davis MJ, Braun AP. Large conductance, Ca2+-activated K+ channels (BKCa) and arteriolar myogenic signaling. FEBS Lett 2010;584:2033–42.

54. Rusch NJ. BK channels in cardiovascular disease: a complex story of channel dysregulation. Am J Physiol Heart Circ Physiol 2009;297:H1580–2.

55. Ford DA. Lipid oxidation by hypochlorous acid: chlorinated lipids in atherosclerosis and myocardial ischemia. Clin Lipidol 2010;5:835–52.

56. Hartman CL, Duerr MA, Albert CJ, Neumann WL, McHowat J, Ford DA. 2-Chlorofatty acids induce Weibel-Palade body mobilization. J Lipid Res 2018;59:113–22.

57. Messner MC, Albert CJ, Ford DA. 2-Chlorohexadecanal and 2-chlorohexadecanoic acid induce COX-2 expression in human coronary artery endothelial cells. Lipids 2008;43:581–8.

58. Wang WY, Albert CJ, Ford DA. Alpha-chlorofatty acid accumulates in activated monocytes and causes apoptosis through reactive oxygen species production and endoplasmic reticulum stress. Arterioscler Thromb Vasc Biol 2014;34:526–32.

59. Chung GE, Lee JH, Lee H, et al. Nonalcoholic fatty liver disease and advanced fibrosis are associated with left ventricular diastolic dysfunction. Atherosclerosis 2018;272:137–44.

60. Mantovani A, Pernigo M, Bergamini C, et al. Nonalcoholic fatty liver disease is independently associated with early left ventricular diastolic dysfunction in patients with type 2 diabetes. PLoS One 2015;10:e0135329.

61. Simon TG, Bamira DG, Chung RT, Weiner RB, Corey KE. Nonalcoholic steatohepatitis is associated with cardiac remodeling and dysfunction. Obesity (Silver Spring) 2017;25:1313–6.

62. Takahashi T, Watanabe T, Shishido T, et al. The impact of non-alcoholic fatty liver disease fibrosis score on cardiac prognosis in patients with chronic heart failure. Heart Vessels 2018;33:733–9.

63. Yoshihisa A, Sato Y, Yokokawa T, et al. Liver fibrosis score predicts mortality in heart failure patients with preserved ejection fraction. ESC Heart Fail 2018;5:262–70.

64. Kosmala W, Plaksej R, Strotmann JM, et al. Progression of left ventricular functional abnormalities in hypertensive patients with heart failure: an ultrasonic two-dimensional speckle tracking study. J Am Soc Echocardiogr 2008;21:1309–17.

65. Park SJ, Miyazaki C, Bruce CJ, Ommen S, Miller FA, Oh JK. Left ventricular torsion by two-dimensional speckle tracking echocardiography in patients with diastolic dysfunction and normal ejection fraction. J Am Soc Echocardiogr 2008;21:1129–37.

66. Takeuchi M, Borden WB, Nakai H, et al. Reduced and delayed untwisting of the left ventricle in patients with hypertension and left ventricular hypertrophy: a study using two-dimensional speckle tracking imaging. Eur Heart J 2007;28:2756–62.

67. Morris DA, Boldt LH, Eichstadt H, Ozcelik C, Haverkamp W. Myocardial systolic and diastolic performance derived by 2-dimensional speckle tracking echocardiography in heart failure with normal left ventricular ejection fraction. Circ Heart Fail 2012;5:610–20.

68. Tan YT, Wenzelburger F, Lee E, et al. The pathophysiology of heart failure with normal ejection fraction: exercise echocardiography reveals complex abnormalities of both systolic and diastolic ventricular function involving torsion, untwist, and longitudinal motion. J Am Coll Cardiol 2009;54:36–46.

69. Borlaug BA, Kass DA. Ventricular-vascular interaction in heart failure. Heart Fail Clin 2008;4:23–36.

70. Andersen MJ, Borlaug BA. Invasive hemodynamic characterization of heart failure with preserved ejection fraction. Heart Fail Clin 2014;10:435–44.

71. Borlaug BA, Nishimura RA, Sorajja P, Lam CS, Redfield MM. Exercise hemodynamics enhance diagnosis of early heart failure with preserved ejection fraction. Circ Heart Fail 2010;3:588–95.

72. Curl CL, Danes VR, Bell JR, et al. Cardiomyocyte functional etiology in heart failure with preserved ejection fraction is distinctive-a new preclinical model. J Am Heart Assoc 2018;7.

73. Primessnig U, Schonleitner P, Holl A, et al. Novel pathomechanisms of cardiomyocyte dysfunction in a model of heart failure with preserved ejection fraction. Eur J Heart Fail 2016;18:987–97.

74. Peana D, Domeier TL. Cardiomyocyte Ca(2+) homeostasis as a therapeutic target in heart failure with reduced and preserved ejection fraction. Curr Opin Pharmacol 2017;33:17–26.

75. Lee JF, Barrett-O'Keefe Z, Garten RS, et al. Evidence of microvascular dysfunction in heart failure with preserved ejection fraction. Heart 2016;102:278–84.

76. Lee JF, Barrett-O'Keefe Z, Nelson AD, et al. Impaired skeletal muscle vasodilation during exercise in heart failure with preserved ejection fraction. Int J Cardiol 2016;211:14–21.

77. Borlaug BA, Olson TP, Lam CS, et al. Global cardiovascular reserve dysfunction in heart failure with preserved ejection fraction. J Am Coll Cardiol 2010;56:845–54.

78. Dhakal BP, Malhotra R, Murphy RM, et al. Mechanisms of exercise intolerance in heart failure with preserved ejection fraction: the role of abnormal peripheral oxygen extraction. Circ Heart Fail 2015;8:286–94.

79. Haykowsky MJ, Herrington DM, Brubaker PH, Morgan TM, Hundley WG, Kitzman DW. Relationship of flow-mediated arterial dilation and exercise capacity in older patients with heart failure and preserved ejection fraction. J Gerontol A Biol Sci Med Sci 2013;68:161–7.

80. Hundley WG, Bayram E, Hamilton CA, et al. Leg flow-mediated arterial dilation in elderly patients with heart failure and normal left ventricular ejection fraction. Am J Physiol Heart Circ Physiol 2007;292:H1427–34.

81. Athilingam P, D'Aoust RF, Miller L, Chen L. Cognitive profile in persons with systolic and diastolic heart failure. Congest Heart Fail 2013;19:44–50.

82. Cermakova P, Lund LH, Fereshtehnejad SM, et al. Heart failure and dementia: survival in relation to types of heart failure and different dementia disorders. Eur J Heart Fail 2015;17:612–9.

83. Dodson JA, Truong TT, Towle VR, Kerins G, Chaudhry SI. Cognitive impairment in older adults with heart failure: prevalence, documentation, and impact on outcomes. Am J Med 2013;126:120–6.

84. van den Hurk K, Reijmer YD, van den Berg E, et al. Heart failure and cognitive function in the general population: the Hoorn Study. Eur J Heart Fail 2011;13:1362–9.

85. Haykowsky MJ, Brubaker PH, John JM, Stewart KP, Morgan TM, Kitzman DW. Determinants of exercise intolerance in elderly heart failure patients with preserved ejection fraction. J Am Coll Cardiol 2011;58:265–74.

86. Upadhya B, Haykowsky MJ, Eggebeen J, Kitzman DW. Exercise intolerance in heart failure with preserved ejection fraction: more than a heart problem. J Geriatr Cardiol 2015;12:294–304.

87. Dryer K, Gajjar M, Narang N, et al. Coronary microvascular dysfunction in patients with heart failure with preserved ejection fraction. Am J Physiol Heart Circ Physiol 2018;314:H1033–42.

88. Borbouse L, Dick GM, Asano S, et al. Impaired function of coronary BK(Ca) channels in metabolic syndrome. Am J Physiol Heart Circ Physiol 2009;297:H1629–37.

89. Guo X, Wang XF. Signaling cross-talk between TGF-beta/BMP and other pathways. Cell Res 2009;19:71–88.

90. Hayden MS, Ghosh S. Shared principles in NF-kappaB signaling. Cell 2008;132:344–62.

91. Solt LA, May MJ. The IkappaB kinase complex: master regulator of NF-kappaB signaling. Immunol Res 2008;42:3–18.

92. Griesenauer B, Paczesny S. The ST2/IL-33 axis in immune cells during inflammatory diseases. Front Immunol 2017;8:475.

93. Sanada S, Hakuno D, Higgins LJ, Schreiter ER, McKenzie AN, Lee RT. IL-33 and ST2 comprise a critical biomechanically induced and cardioprotective signaling system. J Clin Invest 2007;117:1538–49.

94. AbouEzzeddine OF, McKie PM, Dunlay SM, et al. Suppression of tumorigenicity 2 in heart failure with preserved ejection fraction. J Am Heart Assoc 2017;6.

95. Hartman MHT, Groot HE, Leach IM, Karper JC, van der Harst P. Translational overview of cytokine inhibition in acute myocardial infarction and chronic heart failure. Trends Cardiovasc Med 2018;28:369–79.

96. McCarthy CP, Januzzi JL Jr. Soluble ST2 in heart failure. Heart Fail Clin 2018;14:41–8.

97. Panahi M, Papanikolaou A, Torabi A, et al. Immunomodulatory interventions in myocardial infarction and heart failure: a systematic review of clinical trials and meta-analysis of IL-1 inhibition. Cardiovasc Res 2018;114:1445–61.

98. Carbone S, Canada JM, Buckley LF, et al. Dietary fat, sugar consumption, and cardiorespiratory fitness in patients with heart failure with preserved ejection fraction. J Am Coll Cardiol Basic Transl Sci 2017;2:513–25.

99. Tschope C, Birner C, Bohm M, et al. Heart failure with preserved ejection fraction: current management and future strategies: expert opinion on the behalf of the Nucleus of the "Heart Failure Working Group" of the German Society of Cardiology (DKG). Clin Res Cardiol 2018;107:1–19.

100. von Bibra H, Strohle A, St John Sutton M, Worm N. Dietary therapy in heart failure with preserved ejection fraction and/or left ventricular diastolic dysfunction in patients with metabolic syndrome. Int J Cardiol 2017;234:7–15.

101. Asghar A, Sheikh N. Role of immune cells in obesity induced low grade inflammation and insulin resistance. Cell Immunol 2017;315:18–26.

102. Lauterbach MA, Wunderlich FT. Macrophage function in obesity-induced inflammation and insulin resistance. Pflugers Arch 2017;469:385–96.

103. Saltiel AR, Olefsky JM. Inflammatory mechanisms linking obesity and metabolic disease. J Clin Invest 2017;127:1–4.

104. D'Elia E, Vaduganathan M, Gori M, Gavazzi A, Butler J, Senni M. Role of biomarkers in cardiac structure phenotyping in heart failure with

preserved ejection fraction: critical appraisal and practical use. Eur J Heart Fail 2015;17:1231–9.

105. Meijers WC, van der Velde AR, de Boer RA. Biomarkers in heart failure with preserved ejection fraction. Neth Heart J 2016;24:252–8.

106. Abernethy A, Raza S, Sun JL, et al. Pro-Inflammatory biomarkers in sTable versus acutely decompensated heart failure with preserved ejection fraction. J Am Heart Assoc 2018;7.

107. Matsubara J, Sugiyama S, Nozaki T, et al. Pentraxin 3 is a new inflammatory marker correlated with left ventricular diastolic dysfunction and heart failure with normal ejection fraction. J Am Coll Cardiol 2011;57:861–9.

108. Sanders-van Wijk S, van Empel V, Davarzani N, et al. Circulating biomarkers of distinct pathophysiological pathways in heart failure with preserved vs. reduced left ventricular ejection fraction. Eur J Heart Fail 2015;17:1006–14.

109. Lee DI, Zhu G, Sasaki T, et al. Phosphodiesterase 9A controls nitric-oxide-independent cGMP and hypertrophic heart disease. Nature 2015;519:472–6.

110. Jeong MY, Lin YH, Wennersten SA, et al. Histone deacetylase activity governs diastolic dysfunction through a nongenomic mechanism. Sci Transl Med 2018;10.

111. Emter CA, Baines CP. Low-intensity aerobic interval training attenuates pathological left ventricular remodeling and mitochondrial dysfunction in aortic-banded miniature swine. Am J Physiol Heart Circ Physiol 2010;299:H1348–56.

112. Emter CA, Tharp DL, Ivey JR, Ganjam VK, Bowles DK. Low-intensity interval exercise training attenuates coronary vascular dysfunction and preserves Ca(2)(+)-sensitive K(+) current in miniature swine with LV hypertrophy. Am J Physiol Heart Circ Physiol 2011;301:H1687–94.

113. McDonald KS, Emter CA. Exploring new concepts in the management of heart failure with preserved ejection fraction: is exercise the key for improving treatment? J Appl Physiol (1985) 2015;119:724–5.

KEY WORDS cardio-metabolic disease, heart failure, integrative pathophysiology, preclinical model of cardiovascular disease

APPENDIX For an expanded Methods section and supplemental figures and tables, please see the online version of this paper.

JACC: BASIC TO TRANSLATIONAL SCIENCE VOL. 4, NO. 3, 2019

EDITORIAL COMMENT

Cardiometabolic Heart Failure and HFpEF

Still Chasing Unicorns*

Thomas E. Sharp III, PhD,[a] David J. Lefer, PhD,[a,b] Steven R. Houser, PhD[c]

Heart failure (HF) is a complex and heterogenous syndrome that is projected to affect more than 8 million adults by 2030 (1). The HF patient population can be separated into 2 general groups, those with HF with reduced ejection fraction and those with HF with preserved ejection fraction (HFpEF). HFpEF has been estimated to affect approximately one-half of the HF patient population, and this population is predicted to increase over the next decade (2). The pathophysiological drivers that cause or exacerbate HFpEF are under investigation because the precise cardiac and extracardiac pathologies that cause or exacerbate the HFpEF phenotype remain largely unknown. There are no Food and Drug Administration–approved therapeutic agents to treat patients that have HFpEF, in part because the pathobiology is still not clearly defined, and there is a lack of suitable preclinical models that can be used to define causes and test therapies (3). Complicating matters further, current clinical research suggests that HFpEF is not caused by a single pathology but is a result of multiple, distinct, and unique diseases with different primary driving factors. This was eloquently presented by Shah et al. (4), where 3 primary phenotypes were observed in patients: 1) young patients with moderate diastolic dysfunction and normal B-type natriuretic peptide (BNP) levels; 2) obese, diabetic patients with sleep apnea and worsened left ventricular (LV) relaxation; and 3) older patients with chronic kidney disease, myocardial dysfunction, and pulmonary hypertension. This characterization of distinct phenotypes may aid in better clinical trial design and outcomes but leaves the basic research community in a conundrum regarding the development of suitable translational animal models which reliably recapitulate each of these different HFpEF phenotypes. Although rodent models of HFpEF have emerged (5), the physiological differences between rodents and humans are well established and suggests that large animal models might be more predictive of therapies that could be effective in humans (6). It is imperative, that these newly developed large animal models of HFpEF recapitulate essential pathophysiological features of HFpEF and its progression to allow for translation to the clinic. In this issue of *JACC: Basic to Translational Science*, Olver et al. (7) have characterized a swine HFpEF model that includes several of the key comorbidities (obesity, early metabolic derangement, and pressure overload) observed in patients.(8,9).

SEE PAGE 404

The study was performed in Ossabaw swine, which are well characterized to have a “thrifty phenotype,” becoming obese and pre-diabetic when fed a western diet (WD) (10). The authors fed 2-month-old, female Ossabaw swine a control or WD for 10 months to induce obesity with metabolic derangements. They then placed an aortic band (AB) at 6 months of age to induce pressure overload in an attempt to induce HFpEF. Functional, morphological, and molecular endpoints were measured to assess the degree of

*Editorials published in *JACC: Basic to Translational Science* reflect the views of the authors and do not necessarily represent the views of *JACC: Basic to Translational Science* or the American College of Cardiology.

From [a]Cardiovascular Center of Excellence, School of Medicine, LSU Health Science Center, New Orleans, Louisiana; [b]Department of Pharmacology and Experimental Therapeutics, Louisiana State University Health Sciences Center, New Orleans, Louisiana; and the [c]Department of Physiology and Cardiovascular Research Center, Lewis Katz School of Medicine, Temple University, Pennsylvania. The authors have reported that they have no relationships relevant to the contents of this paper to disclose.

All authors attest they are in compliance with human studies committees and animal welfare regulations of the authors’ institutions and Food and Drug Administration guidelines, including patient consent where appropriate. For more information, visit the *JACC: Basic to Translational Science* author instructions page.

ISSN 2452-302X https://doi.org/10.1016/j.jacbts.2019.05.003

cardiac and systemic dysfunction at 12 months of age in 4 to 5 control and WD-AB swine. The authors describe the cardiac structural and functional changes observed at 10-months' post-diet and 6-months' post-aortic banding (7). The expected hypertrophic response due to aortic banding was demonstrated by increased heart weight and LV wall thickness. Furthermore, they conclude LV systolic function remained normal, whereas diastolic function was impaired based solely on the end-diastolic pressure volume relationship and isolated single cardiomyocyte T-tubule structure and function. They attribute impaired relaxation to LV mitochondrial dysfunction as previously reported in the Ossabaw swine (11). Furthermore, the investigators also explore the molecular signature through transcriptomic analysis of LV tissue, reporting alterations of a myriad of genes that are consistent with cardiovascular diseases and their related comorbidities. The authors conclude that their model recapitulates features of HFpEF.

In our view, the model in the study by Olver et al. (7) represents an early-stage of HFpEF, and as such may not faithfully mimic HFpEF in humans. Although Ossabaw swine on a WD develop dyslipidemia, immature vascular plaque formation, and hyperinsulinemia, the investigators acknowledge they do not spontaneously develop HF (12). HFpEF is recognized to also be an age-related disease, because age is a primary predictor of HFpEF's initial diagnosis (13), whereas the investigators used very young animals (2 months of age for 10 months). To induce HF in the WD-fed animals, the investigators implanted a surgical band on the aorta to produce acute pressure overload. This technique is widely used in both large and small animal models (14–17) but has caveats. More rapid pressure overload usually causes compensatory states (hypertrophic response) (18,19) or decompensation (LV dilation with reduced ejection fraction) such as in mouse transverse aortic constriction models of acute pressure overload (15). By contrast, slow, progressive pressure overload models more closely parallel the type of structural heart disease induced by aortic stenosis in humans (14). There are several alternatives to aortic banding that are more physiologically relevant, including an increase in dietary salt consumption or introduction of agonists that activate the renin-angiotensin-aldosterone system to develop a global hypertensive phenotype. The gene ontology data herein is generalized and could conceivably be altered by HF-independent cardiovascular disease (7).

Although systolic function was preserved (no change in LVEF) in the model, there was a leftward shift in the EDPVR, consistent with diastolic dysfunction, many traditional measures of LV diastolic dysfunction were not measured (i.e., E/A, E/e′, Doppler flow velocities). Moreover there was no physiological measurement of pulmonary hypertension (elevated pulmonary artery pressure or pulmonary capillary wedge pressure). Most importantly, LV end-diastolic pressure was not elevated (LVEDP), which is an essential feature of HFpEF involving pressure overload. Lastly, there was no traditional HFpEF biomarkers (i.e., cardiac troponin I, BNP, atrial natriuretic peptide) studies.

The authors also studied the cellular mechanisms that may contribute to impaired relaxation by investigating isolated single cardiomyocyte physiology in the basal state and after exposure to adrenergic agonists. Myocytes isolated from the WD-AB animals did not have significant alterations in Ca^{2+} regulation, either in the basal state or after treatment with an adrenergic agonist. This suggests the presence of the very earliest stages of adaptation to persistent disease stress. These findings are at odds with previous studies of myocytes with hypertrophy from slow progressive pressure overload, where myocyte contractile derangements are present even though global pump performance parameters (LVEF) are maintained (18). In these studies, persistent disease caused derangements of cardiac functional reserve (20,21). The absence of these changes suggests that the model fails to show any systolic defects that are present in patients with HFpEF. The absence of any significant changes in Ca^{2+} transient dynamics is also a bit surprising, given the T-tubules are disrupted in the WD-AB myocytes (7).

In conclusion, HFpEF is a complex and heterogenous clinical syndrome for which there are no effective therapies. Developing novel HPpEF therapies will require developing large animal models that faithfully mimic the HFpEF phenotype. The model developed by Olver et al. (7) combines metabolic derangements together with mechanical pressure overload in young, female swine. Although these animals develop cardiac hypertrophy and some metabolic disturbances, as noted above many of the phenotypic features characteristic of human HFpEF are not observed in this model, which raise important questions about the overall clinical utility of the model. In our view, the critical features of a large animal HFpEF model should include adverse LV structural and functional remodeling, abnormal

diastolic function, decreased systolic functional reserve, increased LV filling pressures, and pulmonary hypertension. Models with several comorbidities such as increased body mass index, dyslipidemia, moderately resistant hypertension, and metabolic derangements are also critical for the development of HFpEF models. In this regard, the study by Olver et al. (7) represents an important first step in developing an appropriate large animal model that mimics the cardiometabolic phenotype of HFPEF in humans.

ADDRESS FOR CORRESPONDENCE: Dr. David J. Lefer, Louisiana State University Health Sciences Center, Department of Pharmacology and Experimental Therapeutics, 533 Bolivar Street, CSRB Suite 408, New Orleans, Louisiana 70112. E-mail: dlefe1@lsuhsc.edu. OR Dr. Steven R. Houser, Temple University Lewis Katz School of Medicine, Medicine Education & Research Building, 3500 N. Broad Street, 10th Floor, Philadelphia, Pennsylvania 19140. E-mail: SRHouser@temple.edu.

REFERENCES

1. Benjamin EJ, Blaha MJ, Chiuve SE, et al. Heart disease and stroke statistics-2017 update: a report from the American Heart Association. Circulation 2017;135:e146–603.

2. Dunlay SM, Roger VL, Redfield MM. Epidemiology of heart failure with preserved ejection fraction. Nat Rev Cardiol 2017;14:591–602.

3. Patel RB, Shah SJ. Drug targets for heart failure with preserved ejection fraction: a mechanistic approach and review of contemporary clinical trials. Ann Rev Pharmacol Toxicol 2019;59:41–63.

4. Shah SJ, Katz DH, Selvaraj S, et al. Phenomapping for novel classification of heart failure with preserved ejection fraction. Circulation 2015;131:269–79.

5. Valero-Muñoz M, Backman W, Sam F. Murine Models of heart failure with preserved ejection fraction: a "fishing expedition". J Am Coll Cardiol Basic Trans Sci 2017;2:770–89.

6. Houser SR, Margulies KB, Murphy AM, et al. Animal models of heart failure: a scientific statement from the American Heart Association. Circulation Research 2012;111:131–50.

7. Olver TD, Edwards JC, Jurrissen TJ, et al. Western diet-fed, aortic-banded ossabaw swine: a pre-clinical model of cardio-metabolic heart failure. J Am Coll Cardiol Basic Trans Sci 2019;4:404–21.

8. Olver TD, Grunewald ZI, Jurrissen TJ, et al. Microvascular insulin resistance in skeletal muscle and brain occurs early in the development of juvenile obesity in pigs. Am J Physiol Regul Integr Comp Physiol 2018;314:R252–64.

9. Olver TD, Edwards JC, Ferguson BS, et al. Chronic interval exercise training prevents BKCa channel-mediated coronary vascular dysfunction in aortic-banded miniswine. J Appl Physiol (1985) 2018;125:86–96.

10. Martin RJ, Gobble JL, Hartsock TH, Graves HB, Ziegler JH. Characterization of an obese syndrome in the pig. Proc Soc Exp Biol Med 1973;143:198–203.

11. Zhang X, Li Z-L, Eirin A, et al. Cardiac metabolic alterations in hypertensive obese pigs. Hypertension 2015;66:430–6.

12. Dyson MC, Alloosh M, Vuchetich JP, Mokelke EA, Sturek M. Components of metabolic syndrome and coronary artery disease in female ossabaw swine fed excess atherogenic diet. Comp Med 2006;56:35–45.

13. Reddy YNV, Carter RE, Obokata M, Redfield MM, Borlaug BA. A simple, evidence-based approach to help guide diagnosis of heart failure with preserved ejection fraction. Circulation 2018;138:861–70.

14. Ishikawa K, Aguero J, Oh JG, et al. Increased stiffness is the major early abnormality in a pig model of severe aortic stenosis and predisposes to congestive heart failure in the absence of systolic dysfunction. J Am Heart Assoc 2015;4:e001925.

15. Li Z, Organ CL, Kang J, et al. Hydrogen sulfide attenuates renin angiotensin and aldosterone pathological signaling to preserve kidney function and improve exercise tolerance in heart failure. J Am Coll Cardiol Basic Trans Sci 2018;3:796–809.

16. Moorjani N, Catarino P, El-Sayed R, et al. A pressure overload model to track the molecular biology of heart failure. Eur J Cardiothorac Surg 2003;24:920–5.

17. Elrod JW, Wong R, Mishra S, et al. Cyclophilin D controls mitochondrial pore-dependent Ca(2+) exchange, metabolic flexibility, and propensity for heart failure in mice. J Clin Invest 2010;120:3680–7.

18. Bailey BA, Houser SR. Calcium transients in feline left ventricular myocytes with hypertrophy induced by slow progressive pressure overload. J Mol Cell Cardiol 1992;24:365–73.

19. Wallner M, Eaton DM, Berretta RM, et al. A feline HFpEF model with pulmonary hypertension and compromised pulmonary function. Sci Rep 2017;7:16587.

20. Haykowsky MJ, Kitzman DW. Exercise physiology in heart failure and preserved ejection fraction. Heart Fail Clin 2014;10:445–52.

21. Bailey BA, Houser SR. Sarcoplasmic reticulum-related changes in cytosolic calcium in pressure-overload-induced feline LV hypertrophy. Am J Physiol Heart Circ Physiol 1993;265:H2009–16.

KEY WORDS cardiometabolic heart failure, HFpEF, translational animal model

JACC: BASIC TO TRANSLATIONAL SCIENCE
VOL. 4, NO. 3, 2019
ISSN 2452-302X

Letters

Reduced Lipoprotein(a) Associated With the Apolipoprotein E2 Genotype Confers Cardiovascular Protection in Familial Hypercholesterolemia

There are 3 isoforms of apolipoprotein E (apo E) in humans (ε2, ε3, and ε4). They differ by single amino acid substitutions that variably affect their affinity for the low-density lipoprotein receptor (LDLR) and for the LDLR-related protein (LRP1), with ε2 having the weakest binding to these receptors (1). The plasma levels of lipoprotein(a) [Lp(a)], a highly atherogenic LDL-like lipoprotein species, are influenced by the polymorphism of apo E, with ε2/ε2 and ε4/ε4 carriers presenting with the lowest and highest Lp(a) plasma concentrations, respectively (1).

Lp(a) contains a highly polymorphic signature protein, apolipoprotein(a) [apo(a)], bound to the apolipoprotein B100 (apo B100) of an LDL particle. The proatherogenic properties of Lp(a) are mediated by its LDL moiety rich in cholesterol, as well as by its elevated content in proinflammatory oxidized phospholipids, and by the antifibrinolytic effects of its plasminogen-like apo(a) moiety. Elevated Lp(a) is an independent predictor of cardiovascular disease (CVD), particularly for patients with familial hypercholesterolemia (FH) (2,3).

To evaluate whether the modulation of Lp(a) levels by apo E isoforms affects CVD risk, we assessed apo E and apo(a) concentrations, as well as polymorphisms, in a cohort of patients at very high cardiovascular risk by liquid chromatography-tandem mass spectrometry (4). These parameters were measured in plasma samples collected at the first visit from 444 nontreated heterozygous patients with FH (all genetically confirmed carriers of a single mutated *LDLR* allele) attending the lipid clinic at Groote Schuur Hospital in Cape Town, South Africa (5). Their mean ± SD plasma levels of total cholesterol (8.9 ± 2.0 mmol/l), triglycerides (1.5 ± 0.9 mmol/l), high-density lipoprotein (HDL) cholesterol (1.3 ± 0.2 mmol/l), LDL cholesterol (7.0 ± 1.9 mmol/l), apo A-I (96 ± 28 mg/dl), apo B (155 ± 50 mg/dl), apo E (6.4 ± 2.8 mg/dl), and apo(a)/Lp(a) (52 ± 48 nmol/l) were typical of a heterozygous FH phenotype. One-third (32.9%) of these patients had experienced at least 1 cardiovascular event before the initial visit.

The majority of these patients were ε3/ε3 carriers (n = 292) and served as the control group carriers. The remaining patients were ε3/ε4 (n = 79), ε2/ε3 (n = 42), ε4/ε4 (n = 20), ε2/ε4 (n = 8), or ε2/ε2 (n = 3). The ε2/ε4 carriers were excluded from all subsequent analyses. Compared with ε3/ε3, ε2 carriers (i.e., ε2/ε3 and ε2/ε2) had increased plasma apo E levels, whereas ε4 carriers (i.e., ε3/ε4 and ε4/ε4) had reduced plasma apo E levels (**Figure 1**). LDL cholesterol levels were similar in all groups (**Figure 1**), as well as non-HDL cholesterol levels (not shown). In contrast, ε2 carriers had significantly reduced Lp(a) concentrations (median 3 nmol/l [interquartile range (IQR): 0 to 45 nmol/l]) compared with ε3/ε3 homozygotes (median 27 nmol/l [IQR: 0 to 73 nmol/l]). Lp(a) concentrations were slightly but not significantly increased in ε4 carriers (median 34 nmol/l [IQR: 0 to 104 nmol/l]) compared with the ε3/ε3 control group (**Figure 1**). The detection limit for apo(a) measurement by liquid chromatography-tandem mass spectrometry was 2 nmol/l (6). All patients with apo(a) levels lower than this limit were reported as having Lp(a) concentrations of 0 nmol/l. Thus, 48% of ε2 carriers, 28% of ε3/ε3 carriers, and 25% of ε4 carriers had Lp(a) levels lower than the detection limit. Given that Lp(a) levels are strongly influenced by the polymorphism of apo(a) resulting from the presence of a variable number of kringle IV_2 repeats in humans (1 to more than 40) (3), we verified that the number of kringle IV repeats on apo(a) was similar in ε3/ε3, ε2, and ε4 carriers, on average at a mean ± SD of 21.7 ± 7.2, 20.6 ± 8.6, and 20.4 ± 7.0 (p = 0.196), respectively, thus ruling out a chance finding.

These results confirm specifically in patients with FH a landmark observation made in the general population showing that apo E_2 is associated with reduced Lp(a) (1). Whether LDLR or LRP1 plays a role in that process is unknown. The mechanism by which apo E_2 specifically reduces Lp(a) clearly remains to be established. The percentage of patients with FH who had CVD was significantly less in ε2 carriers than

FIGURE 1 Apo E_2 Is Associated With Cardiovascular Protection in FH

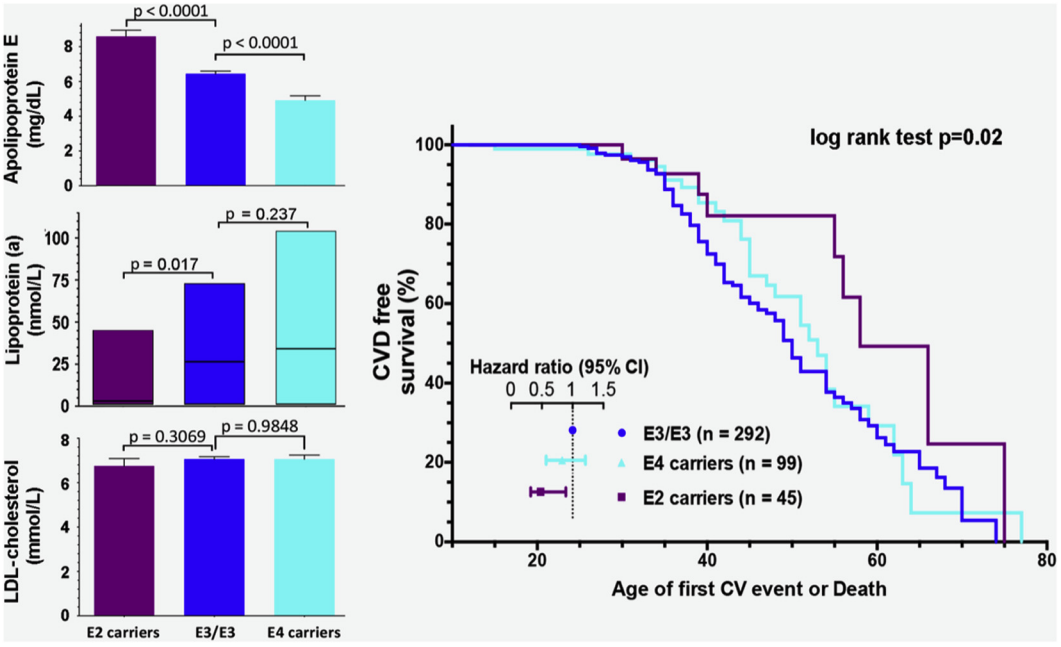

Plasma apolipoprotein E (apo E) and apolipoprotein(a) levels were measured by liquid chromatography–tandem mass spectrometry in plasma samples isolated from 444 nontreated patients with familial hypercholesterolemia (FH). Plasma low-density lipoprotein (LDL) cholesterol levels were calculated using the Friedewald formula when triglycerides levels were lower than 4.52 mmol/l (i.e., in 440 patients). Apolipoprotein E and low-density lipoprotein cholesterol are displayed as mean ± SEM, and comparisons between groups were made using Student's *t*-test. Lipoprotein(a) levels are displayed as median (interquartile range), and comparisons between groups were made using a Wilcoxon rank sum test. Cardiovascular disease (CVD)-free survivals were determined using a Kaplan-Meier estimate. Cumulative hazards for age (probability for a patient to experience a cardiovascular [CV] event or death) were compared using a log-rank test. CI = confidence interval.

in ε3/εε3 carriers (20% vs. 37%; p = 0.021) and intermediate in ε4 carriers (31%).

The reduced rate of CVD in ε2 carriers remained significant after adjustment for age, sex, tobacco use, body mass index, diabetes, HDL cholesterol, hypertension, and LDLR mutation status. We next performed a Kaplan-Meier estimate to determine the CVD-free survival time according to apo E genotypes (Figure 1). The CVD-free survival time was significantly longer in patients with FH carrying one ε2 allele compared with ε3/ε3 carriers (hazard ratio: 0.48 [95% confidence interval (CI): 0.32 to 0.89]; p = 0.02). In contrast, patients carrying one ε4 allele had similar CVD-free survival time as ε3/ε3 (hazard ratio: 0.84 [95% CI: 0.57 to 1.21]; p = 0.35). It is far-fetched to speculate that the apparent lack of increase in CVD in ε4 carriers may relate to the similar levels of Lp(a) observed in ε4 carriers and ε3/ε3 homozygotes in the present study.

These results are unique in that we investigated patients at very high cardiovascular risk, and none of these patients were taking lipid-lowering medication at the time of their first visit (5), we were able to demonstrate that apo E_2 confers a significant degree of cardioprotection. Unlike non-FH subjects, who have variable effects of apo E genotypes on LDL cholesterol (1), apo E_2 did not significantly reduce LDL in our FH cohort, thus indicating that the cardioprotection observed here stems, at least in part, from the lowering of Lp(a).

There are some limitations to our study, in particular the lack of data on the ethnic background of our patients. However, our results clearly underpin that Lp(a) should be measured systematically in all patients with FH, given that with progressively more effective pharmacological LDL reduction, Lp(a) becomes a strong predictor of CVD (3) and, as such, an important driver of residual CVD risk.

Valentin Blanchard, BS
Mikaël Croyal, PhD

Ilya Khantalin, MD
Stéphane Ramin-Mangata, BS
Kévin Chemello, BS
Brice Nativel, PhD
Dirk. J. Blom, MD, PhD
A. David Marais, MD
***Gilles Lambert, PhD**

*Inserm UMR 1188
Plateforme CYROI
2 rue Maxime Rivière
97490 Sainte Clotilde, France
E-mail: gilles.lambert@univ-reunion.fr

https://doi.org/10.1016/j.jacbts.2019.03.002

Please note: This work was funded by the program grant CHOPIN (CHolesterol Personalized Innovation) granted by the Agence Nationale de la Recherche (ANR-16-RHUS-0007). The authors have reported that they have no relationships relevant to the contents of this paper to disclose. Mr. Blanchard and Dr. Croyal contributed equally to this work and are joint first authors.

All authors attest they are in compliance with human studies committees and animal welfare regulations of the authors' institutions and Food and Drug Administration guidelines, including patient consent where appropriate. For more information, visit the *JACC: Basic to Translational Science* author instructions page.

REFERENCES

1. Moriarty PM, Varvel SA, Gordts PL, McConnell JP, Tsimikas S. Lipoprotein(a) mass levels increase significantly according to *APOE* genotype: an analysis of 431 239 patients. Arterioscler Thromb Vasc Biol 2017;37:580–8.

2. Alonso R, Andres E, Mata N, et al. Lipoprotein(a) levels in familial hipercholesterolemia: an important predictor for cardiovascular disease independent of the type of LDL-receptor mutation. J Am Coll Cardiol 2014;63:1982–9.

3. Willeit P, Ridker PM, Nestel PJ, et al. Baseline and on-statin treatment lipoprotein(a) levels for prediction of cardiovascular events: individual patient-data meta-analysis of statin outcome trials. Lancet 2018;392:1311–20.

4. Blanchard V, Ramin-Mangata S, Billon-Crossouard S, et al. Kinetics of plasma apolipoprotein E isoforms by LC-MS/MS: a pilot study. J Lipid Res 2018;59:892–900.

5. Lambert G, Petrides F, Chatelais M, et al. Elevated plasma PCSK9 level is equally detrimental for patients with nonfamilial hypercholesterolemia and heterozygous familial hypercholesterolemia, irrespective of low-density lipoprotein receptor defects. J Am Coll Cardiol 2014;63:2365–73.

6. Croyal M, Ouguerram K, Passard M, et al. Effects of extended-release nicotinic acid on apolipoprotein (a) kinetics in hypertriglyceridemic patients. Arterioscler Thromb Vasc Biol 2015;35:2042–7.

JACC: BASIC TO TRANSLATIONAL SCIENCE VOL. 4, NO. 3, 2019

TRANSLATIONAL TOOLBOX

Phase II Trials in Drug Development and Adaptive Trial Design

Gail A. Van Norman, MD

SUMMARY

Phase II clinical studies represent a critical point in determining drug costs, and phase II is a poor predictor of drug success: >30% of drugs entering phase II studies fail to progress, and >58% of drugs go on to fail in phase III. Adaptive clinical trial design has been proposed as a way to reduce the costs of phase II testing by providing earlier determination of futility and prediction of phase III success, reducing overall phase II and III trial sizes, and shortening overall drug development time. This review examines issues in phase II testing and adaptive trial design. (J Am Coll Cardiol Basic Trans Science 2019;4:428–37) © 2019 The Authors. Published by Elsevier on behalf of the American College of Cardiology Foundation. This is an open access article under the CC BY-NC-ND license (http://creativecommons.org/licenses/by-nc-nd/4.0/).

Human clinical trials for drug development traditionally progress from small toxicity trials in healthy volunteers (phase I) to proof-of-concept and dose-finding trials in somewhat larger groups of patients with the target condition (phase II) (1), and finally to randomized trials to further delineate clinical efficacy, outcomes, and adverse events in large groups of patients (phase III). The timeframe for passage of a therapeutic agent through clinical testing for Food and Drug Administration (FDA) marketing approval is approximately 12 years (2), with costs now estimated from $1 billion to $1.8 billion dollars (2,3).

A recent study by the Biotechnology Innovation Organization of clinical success rates in advancing drugs to market between 2006 and 2015 found that only 9.6% of drugs entering phase I clinical testing will reach the market (4). Following phases II and III, 30.7% and 58.1% of drugs fail, respectively (4). The picture is even worse for cardiovascular (CV) agents; 6.6% of CV drugs entering phase I advance to market, 24% that enter phase II transition to phase III, and 45% that enter phase III result in a new drug application filing (4). These late phase failure rates probably underestimate failures for first-in-class agents because the reported rates include trials that examine new indications for already-approved drugs and drugs that replicate the mechanism of another successful agent (5).

The flow of innovative agents to the marketplace is slowing significantly as the “low hanging fruit” of therapeutic targets appears to have been substantially harvested (6). Fewer blockbuster drugs and first-in-class drugs are being developed that are both effective in broad patient populations and would: 1) reap enough returns to pay for their own development costs; 2) substantially cover the cost of trials for failed drugs together; and 3) make up for patent expirations on existing drugs (3). New drugs increasingly target fewer indications, are more frequently used for second- and third-line therapy, apply to smaller patient populations, have smaller market interests, and produce a smaller margin in which to recoup costs. Drug companies are answering these challenges by focusing on therapies that are most likely to reach market approval rapidly, are less

From the Department of Anesthesiology and Pain Medicine, University of Washington, Seattle, Washington. Dr. Van Norman has received financial support from the *Journal of the American College of Cardiology*.
The author attests she is in compliance with human studies committees and animal welfare regulations of the author’s institutions and Food and Drug Administration guidelines, including patient consent where appropriate. For more information, visit the *JACC: Basic to Translational Science* author instructions page.

Manuscript received February 11, 2019; accepted February 14, 2019.

ISSN 2452-302X https://doi.org/10.1016/j.jacbts.2019.02.005

subject to pricing pressure once the market is reached, are less expensive to develop, and therefore, have higher potential to improve return on investment (7,8).

There are worries that drugs are being discarded too soon in clinical testing, either due to failure of trials to identify the right target patient population or due to commercial concerns rather than clinical concerns. Attention is turning to understanding why so few initially promising drugs fail to pass clinical testing and to reducing the time it takes for drugs that will ultimately be successful to pass through phases II and III. Phase II testing plays a pivotal role in drug development costs because so many agents "die" in phase II, and because successful completion of phase II is a poor predictor of whether a drug will complete phase III, the most expensive of clinical trials. As the CEO of GlaxoSmithKline pointed out, "if you stop failing so often, you massively reduce the cost of drug development" (7). This review examines some aspects of the phase II problem and discusses adaptive trials and statistical challenges.

WHY DRUGS FAIL IN CLINICAL TRIALS

Phase II represents the first time in which a drug is tested in actual patients, ranging from 50 to 200 patients in most heart failure (HF) studies (9). Failures in phase II testing overall usually occur because: 1) previously unknown toxic side effects occur (50%); 2) the trials show insufficient efficacy to treat the medical condition being tested (30%); or 3) commercial viability looks poor (15%) (10). For CV drugs, 44% of late trial failures are due to poor efficacy and 24% are due to safety concerns (11). Phase II trials face many challenges due to small sample size and choice of study design. In addition, the relatively short duration of phase II trials makes it difficult to identify long-term side effects and outcomes.

BIOMARKERS AS SURROGATE ENDPOINTS. Single-arm phase II (SA-II) studies are usually insufficient to test long-term outcomes because clear indications of the success or failure of a treatment can take months or years, and would extend trial times and cost (12). Phase II studies instead increasingly rely on surrogate clinical or biochemical markers to provide "interim" data about safety and efficacy, allowing faster drug approval conditioned on continued post-marketing safety and efficacy studies (9). In HF phase II trials, increasing emphasis has been placed on clinical biomarkers such as functional capacity, left ventricular ejection fraction, and chemical biomarkers of HF (e.g., B-type natriuretic peptide levels). However, validating that a given biomarker is an appropriate surrogate study endpoint is complex and requires compelling evidence (13).

The use of biomarkers has been encouraged by the FDA, which has now established means by which to qualify biomarkers for use in drug development, but there is a lack of validated biomarkers at this time (14–16). Commercial development and validation of biomarkers is slow, because development of robust and meaningful biomarkers is both time-consuming and extremely expensive (**Figures 1 and 2**) (17). Biomarkers can also fail in development, just as drugs fail in clinical trials. As with drugs, biomarker failures carry both scientific and commercial consequences—if the risks of failure are too high, research to yield successful biomarkers and therapeutics simply will not be undertaken or may be terminated prematurely.

It is unclear how well biomarkers accurately predict positive patient (and trial) outcomes. Wong et al. (18) examined the probability of success of various clinical trial phases between 2000 and 2015 by examining 185,994 unique trials from the Informa Pharma Intelligence's Trialtrove and Pharmaprojects databases. During their study period, probability of success for all indications declined until 2013, but then began to rise. The increase occurred as the use of biomarkers rose, although the authors admitted that there were many other potential causes for this trend. Even so, no significant difference was found in probability of success when phase II studies in which biomarkers were used for patient selection and/or as an indicator of therapeutic efficacy or toxicity were compared with trials that did not use biomarkers (18,19).

Examples of remarkable biomarker failures in CV therapies abound. Floseqinan increased exercise capacity of HF patients in phase II trials, but increased patient mortality in phase III (20,21). The phase III VISTA-16 (Vascular Inflammation Suppression to Treat Acute Coronary Syndrome for 16 Weeks) trial showed promising biomarker response in early phase trials, but had to be terminated early due to higher mortality in phase III (22,23). Darapladib failed to show clinical efficacy in a trial involving >15,000 patients, despite the biomarker (high-density lipoprotein) response (24). Despite evidence of reduction in B-type natriuretic peptide with aliskiren, the ASTRONAUT (Effect of Aliskiren on Postdischarge Mortality and Heart Failure Readmissions Among Patients Hospitalized for Heart Failure) trial failed to show improvement in major clinical outcomes (25,26). Tredaptive, a European therapy that combined niacin

ABBREVIATIONS AND ACRONYMS

AD = adaptive (trial) design

CV = cardiovascular

EMA = European Medicines Agency

FDA = Food and Drug Administration

FDR = false discovery rate

HF = heart failure

RP-II = randomized phase II studies

SA-II = single-arm phase II studies

JACC: BASIC TO TRANSLATIONAL SCIENCE VOL. 4, NO. 3, 2019
JUNE 2019:428–37

FIGURE 1 Timelines for Development and Validation of Various Types of Biomarkers

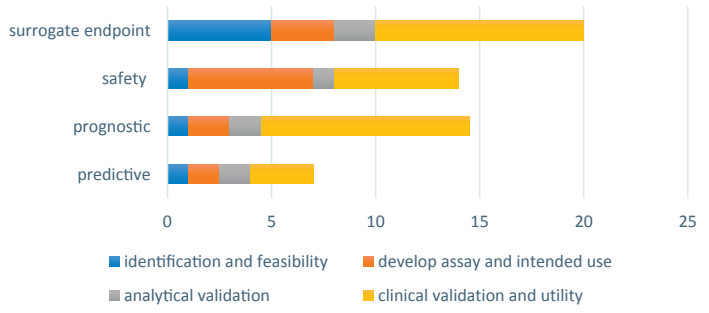

Timelines for development and validation of biomarkers by type, as estimated by the U.S. Department of Health and Human Services (17).

and laropiprant, which was demonstrated to raise high-density lipoprotein, not only found no clinical effect on CV outcomes in a trial for U.S. approval that involved >25,000 patients, but had significant toxic side effects. The drug was not approved in the United States, and the drug maker began warning overseas doctors to stop prescribing it (27,28).

PHASE II AND PHASE III ATTRITION. Once a drug or biological has passed phase II efficacy trials, less than one-half of them show sufficient efficacy in phase III to make it to market. There are many reasons this might be so; phase II and III studies often examine different endpoints. A phase II study may examine surrogate endpoints for disease, but longer term outcomes and toxicities are usually the focus of most phase III studies. Phase III studies are performed in a less homogeneous patient population than phase II trials, to better reflect real-world results. In addition, failures of phase II studies to predict phase III success may be in part due to statistical phenomena (5).

The false discovery rate. The false discovery rate (FDR) is a concept that arises from relatively simple statistical characteristics of type I (false positive) and type II (false negative) errors in clinical testing. The FDR is the ratio of false positive results to total positive results (29).

Consider a study finding in favor of a drug effect for which the p value is 0.05, a common significance level set in clinical trials. The p value is not the probability of mistakenly rejecting the null hypothesis (i.e., the odds of wrongfully attributing an effect to the drug when there is none), but rather is the probability that a random sampling error could lead to the difference that is observed. A low p value indicates that the data are unlikely to have occurred in the presence of a true null, but the p value does not evaluate: 1) whether the null is actually true, that is, there actually is no drug effect, but the study sample was unusual or flawed; and 2) whether the null hypothesis is false. In the case of our drug, the correct conclusion is that there is a 5% chance that the apparent effect shown in the study is due to a random sampling error, regardless of whether other features of the study are flawed. The odds of incorrectly rejecting the null hypothesis (and therefore incorrectly concluding the drug has an effect when it does not) in a study with a p value of 0.05 is at least to 23% and typically closer to 50%. Even at a p value of 0.01, the odds of incorrectly deciding the drug has an effect are still 7% to 15% (30).

The multiplicity problem. Another issue in statistical analysis is the "multiplicity problem": the odds of a false positive result rise as the number of tests rises (31). If a test has a 5% significance level ($p = 0.05$), and the test is run only 20 times, the odds of seeing a false positive result are >64% (32).* Repeating the test multiple times increases the FDR by increasing the number of false positive tests (Table 1). Put another way, repeat a test enough times, and you are guaranteed to find an effect, but the effect you see is increasingly likely to be a false positive as the number of repetitions grows. Most phase II clinical studies have enrollments of 100 to 200 patients and multiple tests; therefore, the odds of multiple false positive results are high. An obvious answer seems to be to decrease the accepted p value, but then the number of tests must be increased to reach significance. Controlling for type I errors (false positives) furthermore causes the complementary errors (type II, false negatives) to increase. The study starts to risk not identifying the true effects that are present, and therefore, misidentifies a drug as being ineffective when it is actually effective, which is an equally undesirable false conclusion.

Challenges in clinical design. Traditionally, phase II clinical trials have been SA-II studies, many of which use historical controls. Selection bias is common, because these trials are often carried out in a single institution or a small group of academic institutions where the patient population differs

*This number is arrived at using the binomial formula to calculate the probability of having a zero (0) FDR at a 5% ($p = 0.05$) significance level for 20 tests. The odds of a zero FDR is approximately 36%, and therefore, the odds of a false positive is 64%.

$$P(0) = \frac{20!}{(20-0)!0!}(0.05)^0 \times (0.95)^{20-0} = 0.358$$

FIGURE 2 Costs (in $ Millions) for Development and Validation of Various Types of Biomarkers

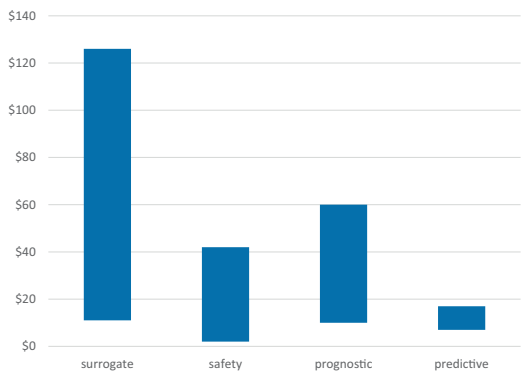

Costs for development and validation of biomarkers by type, as estimated by the U.S. Department of Health and Human Services (17).

significantly from the at-large phase III target population. Multicenter community-based studies partially overcome this issue.

The historical controls are also problematic. They do not consider the fluidity of patient outcomes over time due to changes in supportive care, changes in the quality of diagnostic "trial entry" studies, or changes in other standards of care over time. They also do not account for interim advances in understanding of disease biology that permit subclassifications of diseases (which might respond optimally to different therapies), as well as advances in surgical, radiological, and other nondrug interventions that are also constantly evolving. Even the criteria used to grade disease response are evolving, and this adds complexities to interpreting time-related endpoints (33).

SA-II trials using historical controls do not account for the heterogeneity of real-world patients for whom the treatment will be targeted and assume that the study patients are identical to historical patients. The true success rates of a drug tested in SA-II design against historical controls can only be incompletely known. This is because even a small variance (e.g., 5%) of the actual control success rate away from the historical success rate rockets the false positive rate in single-arm studies by 2- to 3-fold (34). Thus, the drug may falsely appear in a phase II study to demonstrate the level of efficacy that is required to survive phase III studies. Trying to compensate for this issue by increasing the sample size in the SA-II study actually inflates the false positive error rate further, by as much as 50% (34).

TABLE 1 Adaptive Designs*

Adaptive Design	Description
Dose-finding	After interim analysis, a randomized trial with multiple dosing arms assigns more patients to dose groups of higher interest.
Hypothesis	After interim analysis, the study hypothesis is altered (e.g., a pre-specified swap of primary and secondary endpoints).
Sequential or group sequential	After interim analysis, adaptations include pre-specified options of changing sample size, modification of existing treatment arms, elimination or addition of treatment arms, changes in endpoints, changes in randomization schedules.
Randomization	Randomization is adjusted after interim analysis so that patients enrolled later in the study have a higher probability of assignment to a treatment arm that appeared successful earlier.
Seamless phase II/III	Study moves from phase I to phase II without stopping the patient enrollment process.
Treatment switching	Investigator is allowed to switch patients to a different treatment arm based on lack of efficacy, disease progression, or safety issues.
Biomarker adaptive	Interim analysis of treatment responses of biomarkers allows pre-specified adaptations to trial design
Pick-the-winner and drop-the-loser designs	After interim analysis, treatment arms are modified, added, or eliminated.
Sample size re-estimation	Interim analysis allow sample size adjustment or re-estimation.
Multiple adaptive	Multiple adaptive design characteristics applied in a single study.

*See references 36,42,73.

One way to theoretically manage this problem is to actually include a control arm of contemporary patients in the phase II study in place of historical controls (a so-called randomized phase [RP-II] study) (35). RP-II trials guarantee better matching of patients and control patients, and that similar assessment methods and supportive medical care occur in the trial arms contemporaneously. Although RP-II trials increase the size, complexity, and costs of phase II studies, they mitigate the problem of inflating the false positive rate (34,35). However, the increased size randomization makes RP-II studies less suitable as screening trials. RP-II trials can require 4-fold more patients that SA-II trials (33).

The concept of an RP-II trial also raises the question: if a RP-II trial generates sufficiently robust clinical data, why could it not be used alone to achieve full drug approval and avoid a phase III trial altogether? If sufficiently compelling data are obtained in RP-II, would not the performance of a phase III trial, which includes possibly randomizing patients to a nontreatment arm, be unethical? A definitive RP-

JACC: BASIC TO TRANSLATIONAL SCIENCE VOL. 4, NO. 3, 2019
JUNE 2019:428–37

TABLE 2 Magnification of Type I Error With Multiple Tests*

No. of Tests	Type I Error (approximate %)
1	5
2	10
3	14
10	40
20	64

For p = 0.05, the odds of type I error (false identification of an effect where none exists) as the number of tests increases. *See reference 31.

II trial might be appropriate for approval of a drug that treats a sufficiently rare disease for which a conventional phase III trial might be difficult or impossible to conduct. An important challenge rests in determining what would define a "sufficiently robust" data set for a given drug to bypass phase III. The concept is not without precedent. The FDA has based initial approval of a few oncology drugs on the outcome of SA-II trials (33).

RP-II trials are larger and more complex than traditional phase II trials; more than one-quarter have been shown to require major amendments during the trial (33). This has led to calls for the development and acceptance of "seamless" trials—strategies that in effect allow a phase II trial to fold seamlessly into a phase III trial by combining elements and data analysis of both in a single innovative trial design (36,37).

INNOVATIVE TRIAL DESIGN

In March 2004, the FDA issued a report recognizing that the approval of innovative medical therapies had slowed over the preceding years (38). The estimated phase II failure rate in 2006 was 50% versus 20% 10 years earlier (39).

A result of the critical pathway initiative of the FDA was increased interest in innovative trial designs. In December 2016, the U.S. Congress passed the 21st Century Cures Act, allotting $500 million to the FDA to establish an "innovation account" for National Institutes of Health funding to speed regulatory approval of medical therapies (40). Since then, the FDA has devoted efforts to exploring modern trial design and evidence development, including the use of adaptive trial designs (ADs) and real-world evidence (41).

A number of different designs fall under the category of innovative trial design, all of which allow interim data analysis and modification of the trial (**Table 2**) (42). Examples include enrichment trials, adaptive trials, and flexible trials.

ENRICHMENT TRIALS. Enrichment trials allow patient enrollment by clinical criteria, and each is then assayed for a pre-specified drug target (1). After that, several different trial strategies can be pursued: 1) randomize all enrolled patients and analyze the patients carrying the target in a subgroup analysis; 2) continue the trial with patients who only express the target; or 3) split the trial into 2 groups (those with the target and those without) and randomize and analyze each group separately. Enrichment trials may hasten to market therapeutics that benefit a specific patient subpopulation rather than a more heterogeneous population with a broad disease designation, but they depend in part on knowing in advance what factors may contribute to disease progression, and then constructing trial populations that contain the various factors. A downside of enrichment trials are that they identify agents that work in enriched populations but may show less efficacy in unselected populations. Such trials may also inadvertently exclude patient subpopulations that are responsive to the drug, because a characteristic common to that subpopulation was not recognized in trial design and patient selection. A therapy that might be effective in an untested patient subpopulation would then be inadvertently discarded from further development for lack of efficacy (1).

ADAPTIVE TRIALS. ADs have been discussed for 30 years (43–45). The FDA defines an AD as a clinical trial design that allows for prospectively planned modifications to ≥1 aspects of the design based on accumulating data from subjects in the trial (46,47).

In ADs, the goal is to learn from accumulating data in the trial and apply what is learned as quickly as possible in a prospectively specified way during the trial itself to hone flexible aspects of the study while it is still ongoing. ADs can be classified as prospective, continuously adjusted or concurrent (ad hoc), and retrospective (9,42,48). In prospective ADs, there is a pre-specified protocol to alter aspects of the study, such as size, follow-up period, and clinical endpoints following interim data analysis. This might lead to early termination of a study based on futility or unacceptable toxicity, or, alternatively, might require a change in sample size. A platform study or master protocol design is a type of adaptive trial in which multiple treatment arms are simultaneous studies, and interim analysis allows early termination of various arms due to futility or lack of efficacy (49). Concurrent or ad hoc study designs allow flexibility to alter multiple parameters in a study in a pre-specified way based on interim results. In ad hoc design, investigators are allowed to hone their hypothesis

based on interim results and re-steer the study accordingly. Both retrospective and prospective data following changes are used in analysis. Retrospective ADs allow the investigators to change the primary study endpoint or analysis methodology in a pre-specified way after a study is closed.

ADs must be approached cautiously. Seamless progression of an AD study from phase II proof-of-concept and dose-finding stages into phase III studies of efficacy and safety in large populations implies that an efficacious outcome was seen in phase II. This "unblinding" can bias both investigators and caregivers going forward. Also, because the patient population is adjusting throughout the trial, patients enrolled earlier in the trial are likely to show a different magnitude of outcomes than those enrolled later, and this effect must be carefully accounted for in a more complex statistical analysis.

Adaptation in ADs is a design feature and not a cure for poor trial design and inadequate planning (50,51). The PhRMA Working Group on Adaptive Design in Clinical Drug Development identified statistical, logistical, and procedural issues that can arise in ADs and made recommendations for meeting these challenges (50). For ADs to take full advantage of the efficiencies they supposedly offer, they recommended that: 1) study endpoints in ADs should have short follow-up time relative to the overall duration of the trial; 2) data accrual should occur in real time or rapidly, making electronic data collection a priority; and 3) use of databases must incorporate case-by-case decisions regarding how well the data must be "cleaned" (a potentially time-consuming enterprise) versus making adaptation decisions based on all available data. They and other authors also emphasize that data monitoring committees that carry out interim analyses must be constituted in such a way as to minimize bias, including commercial bias (50,52). This can be challenging, because such committees usually need representation from the commercial sponsor itself, to provide input on practical aspects of trial design and commercialization. They strongly recommend that such data monitoring committees be "firewalled" from project personnel, that sponsor representatives on the committee be isolated from all trial activities, and that sponsor access to interim data be minimized.

ADs are slowly achieving increasing regulatory acceptance. Both the European Medicines Agency (EMA) and the FDA have published papers and guidance documents addressing the limitations of ADs in the regulatory context (47,53,54). Regulatory guidances all agree that strict control of the type I error rate is a regulatory prerequisite for acceptance of a clinical trial (55). In a review of >5 years of EMA and FDA advice letters regarding proposed AD phase II or phase II/III studies, 20% of the 59 studies were not accepted, and the most frequently cited concerns raised by the agencies were, not unexpectedly, insufficient justifications for the adaptation, inadequate type I error rate control, and study bias (53).

FLEXIBLE DESIGN TRIALS

The term flexible design (FD) is not entirely synonymous with adaptive design, and there is some confusion of these terms in the literature (56–58). FDs are a subset of ADs that allows both planned and unplanned changes. Flexible aspects of such trials might include inclusion and/or exclusion criteria, sample size, randomization ratios, analytic methods, drug dose, treatment schedule, and endpoints. For example, if the incidence of a primary endpoint is much lower than expected, a FD would allow a mid-trial increase of sample size. The primary endpoint itself could be altered by including additional outcomes in a composite primary outcome. Protocol changes might be made based on unblended interim results.

AD is complex, must be undertaken carefully to minimize bias, and tends to draw greater regulatory scrutiny. In 2006, the FDA strongly recommended ADs to address the decline in innovative medical products being submitted for approval (47). FDs have been criticized as being subject to both more perceived and more actual bias, and present more complex challenges to regulators (58,59). However, such designs could theoretically speed study efficiency, reduce the number of subjects needed (thus, saving time and money), and expose fewer patients to ineffective or even harmful treatment by allowing intra-trial adjustment of pre-determined parameters.

ARE AD TRIALS MORE ETHICAL? Randomization is believed to enhance the validity of clinical research. However, many researchers now question whether traditional randomization is actually ethical. Asking a patient with a serious medical condition to submit to randomization is only ethical if the investigator is truly uncertain about the efficacy of the 2 study arms. Zelen (60) originated the idea of the "play the winner" rule, an example of an AD in which if a patient in a comparative study responded to treatment, the next patient would be assigned to that study arm. Zelen pointed out the ethical implications of this method: 1) patients would tend to be increasingly assigned to the successful arm during the course of the trial; 2) fewer patients would theoretically receive

JACC: BASIC TO TRANSLATIONAL SCIENCE VOL. 4, NO. 3, 2019
JUNE 2019:428–37

ineffective or less effective treatment; and 3) trial duration would theoretically be lessened, thus minimizing the time to get effective drugs to market.

Despite arguments that adaptive trials are more ethical (42,60), strong arguments are advanced that they are not. It is not clear that actual patient burden is reduced, because contemporary adaptive trials must often rely on intermediate markers of response that will not be validated or repudiated until late in phase II or even later in phase III, if at all. Unless phase II studies actually lead to faster approval of more effective therapies (a hypothesis yet to be proven), adaptive trials may not improve patient burdens (61). At this point, no studies have shown that adaptive trials improve patient outcomes overall.

Ethical controversies regarding adaptive trials are numerous, and include problems of informed consent, the importance of maintaining the validity of research, and many other issues (49,62–69). However, determining whether adaptive phase II trials accomplish their goals by actually improving patient outcomes and/or shortening trial duration and costs are key to answering the ethical concerns.

DO ADs ACCOMPLISH THEIR GOALS? The goals of ADs include reduction of overall costs of drug development through several mechanisms: 1) potentially shorter phase II trial durations due to early termination for futility or efficacy; 2) elimination of phase III trials through adequate proof of efficacy and safety via RP-II trials; 3) less expensive studies due to smaller total sample sizes for phase II and phase III studies; and 4) more accurate prediction of success in phase III trials. All of this must be accomplished while holding type I error rates at bay. But do ADs accomplish these goals?

Statistical issues in ADs are complex. Tsong et al. (70) demonstrated that dropping a treatment arm could increase the type I error rate, unless certain precautions are taken in design. Hung et al. (57) pointed out problems in interpreting noninferiority might be problematic in ADs that compare a new treatment with established treatments (nonplacebo comparison trials).

In a review of 60 AD medical trials published between 1989 and 2004, Bauer and Einfalt (71) found that 60% ended after interim analysis, with 20% stopped for futility. However, it is difficult to know if that is actually an improvement from non-AD trials; for example, only 24% of CV drugs pass traditional phase II testing. Moreover, 44% of CV drugs fail in phase III trials due to lack of efficacy (i.e., "futility"). The authors did not detail how many of the trials were stopped because of concerns over commercial viability (71).

Lin et al. (72) from the Center for Biologics Evaluation and Research at the FDA, reviewed AD features of investigational device exemptions applications to the FDA between 2008 and 2013. ADs consisted of only approximately 11% of all studies. The number of AD trials in submissions fluctuated during that period between 10 and 40 per year, which did not represent a clear increase in applications using ADs despite release of FDA draft guidance. Multiple authors agreed that real or even perceived excess regulatory scrutiny might be discouraging commercial sponsors from embracing nontraditional ADs (52). Lin et al. (72) pointed out several problematic features of AD studies that might adversely affect costs. AD studies might not necessarily be of short duration: they must be long enough to allow the adaptation called for in the design. Complex ADs might be neither time- nor cost-efficient for sponsors because they often require detailed justification, extensive simulation studies, and multiple review cycles, all of which can significantly delay the start of a study. Studies stopped too early for success might not have accumulated sufficient safety information, which is an important issue, because for early phase studies, regulators are more concerned with safety than efficacy. International trials pose special problems. Local regulators may require significant in-country trial data; substantial differences in standard of care between countries and regions and substantial differences in populations may exist.

There is conflicting evidence about whether ADs shorten study duration or enroll fewer patients. One survey published in 2018 examined 245 AD clinical trials between 2012 and 2015 (46). ADs in this study resulted in shorter study durations and smaller numbers of subjects. More than 80% of the adaptive phase II trials resulted in early termination at interim analysis, with more than one-half ending up with fewer randomized patients than initially planned (46). However, early termination of some trials occurred for reasons unrelated to study findings, such as poor study enrollment or commercial considerations.

Another analysis included 31 adaptive phase II or III clinical trials at the EMA (55). In contrast to the study by Sato et al. (46), planned and actual study sizes ended up being similar, and ADs did not result in significantly smaller numbers of subjects. Whether ADs led to shorter durations of study was not clear. Only 4 of 23 completed trials (17.4%) were terminated early, 2 of which were stopped due to difficulty recruiting subjects, and 2 of which (8.7%) were stopped according to a pre-planned stopping-for-

futility analysis—a much smaller percentage of trials than those in the Sato et al. (46) study. It is unknown if this means that more drugs were successful in passing to market, or if more drugs were passed through, only to fail in later phase trials.

Bothwell et al. (73) reviewed 142 AD clinical trials. In 9% of cases, adaptive trials were used for FDA product approval consideration and in 12% for EMA product approval consideration. In 8% and 5% of cases, ADs were the final or pivotal trials used for FDA and EMA approvals, respectively. Review times for the FDA and EMA for adaptive trials was a median of 12.2 and 14 months, respectively, which exceeded estimates of review times of non-AD studies by the FDA and EMA by 6 to 7 weeks. Frequently cited problems in reviews were lack of sufficient statistical power, risk of ineffectively evaluating doses, risk of falsely detecting treatment effects (type I errors), and inadequate blinding. Some sample sizes were deemed at times to be too small to draw robust conclusions by both the FDA and EMA. Both agencies cited inadequate sample sizes in adaptive trials to gather sufficient subpopulation effects, such as outcomes on race and sex. Lengthy review correspondence was noted at both agencies in many adaptive trials. At the FDA, 9% (n = 13) and at the EMA 7% (n = 10) of AD trials tested drugs that were later approved at least in part, but not solely through reliance on the adaptive trial data. However, most of these trials involved orphan drugs at both these agencies (9 and 6, respectively), in which the challenges of traditional trial design and population sizes might have mitigated some of the samples size concerns of the ADs.

The question of whether the success of AD trials in phase II better predict that all-important success in subsequent phase III trials is entirely unanswered. One 2016 review of 143 adaptive design studies found that 30% and 50% of early terminations of phase II and III AD studies, respectively, were due to findings of futility, but did not provide information of what preceded these failures (i.e., was a termination in an AD phase III preceded by a successful AD in phase II?) (74). To date, the average costs of bringing a drug to market via AD trials relative to traditional trials are also unknown.

SUMMARY

Adaptive trials are a proposed way to shorten clinical trial phases, reduce the number of patients needed for enrollment, better predict later drug success, and reduce drug development costs. Criticisms of ADs have included increased risks of falsely detecting treatment effects (type I errors), premature dismissal of promising therapies as falsely ineffective (type II errors), statistical challenges and bias, and operational bias. Use of ADs has been limited due to lack of inadequate information regarding completed adaptive trials, a lack of practical understanding of how to implement an adaptive trial, and worries about excessive regulatory scrutiny and nonapproval. To date, analysis of AD trials gives conflicting results with regard to their effects on study size and duration. Data regarding whether phase II ADs permit more accurate prediction of successful completion of phase III and whether ADs reduce overall costs of drug development are needed.

ADDRESS FOR CORRESPONDENCE: Dr. Gail A. Van Norman, Department of Anesthesiology and Pain Medicine, University of Washington, 2141 8th Avenue West, Seattle, Washington 98119. E-mail: lbsparrow@yahoo.com.

REFERENCES

1. Cummings JL. Optimizing phase II of drug development for disease-modifying compounds. Alzheimers Dement 2008;4 1 Suppl 1:S15–20.

2. Paul SM, Myteka DS, Dunwiddie CT, et al. How to improve R&D productivity: the pharmaceutical industry's grand challenge. Nature Rev Drug Dis 2010;9:203–14.

3. Van Norman G. Drugs, Devices and the FDA: Part 1. An overview of approval processes for drugs. J Am Coll Cardiol Basic Transl Sci 2016;1:170–9.

4. Thomas DW, Burns J, Audette J, et al. Clinical development success rates 2006-2015. Biotechnology Innovation Organization, Washington DC. June 2016. Available at: https://www.bio.org/sites/default/files/Clinical%20Development%20Success%20Rates%202006-2015%20-%20BIO,%20Biomedtracker,%20Amplion%202016.pdf. Accessed December 7, 2018.

5. Grainger D. Why too many clinical trials fail—and a simple solution that could increase returns on Pharma R&D. Pharma and Health Care. Forbes. January 29, 2015. Available at: https://www.forbes.com/sites/davidgrainger/2015/01/29/why-too-many-clinical-trials-fail-and-a-simple-solution-that-could-increase-returns-on-pharma-rd/#46e76ff1db8b. Accessed December 23, 2018.

6. Van Norman G. Overcoming the declining trends in innovation and investment in cardiovascular therapies: beyond Eroom's law. J Am Coll Cardiol Basic Trans Sci 2017:613–25.

7. Huss R. The high price of failed clinical trials: time to rethink the model. Clinical Leader October 3, 2016. Available at: https://www.clinicalleader.com/doc/the-high-price-of-failed-clinical-trials-time-to-rethink-the-model-0001. Accessed December 7, 2018.

8. Honig P, Huang SM. Intelligent pharmaceuticals: beyond the tipping point. Clin Pharm Ther 2014;94:455–9.

9. Lavine KJ, Mann D. Rethinking phase II clinical trial design in heart failure. Clin Investig (London) 2013;3:57–68.

10. Tufts Center for the Study of Drug Development. Causes of clinical failures vary widely by therapeutic class, phase of study. Tufts CSDD study assessed compounds entering clinical testing in 2000–09. Tufts CSDD Impact Rep 2013;15(5).

11. Hwang TJ, Lauffenburger JL, Franklin JM, Kesselheim AS. Temporal trends and factors associated with cardiovascular drug development. J Am Coll Cardiol Basic Trans Sci 2016;1:301–30.

12. Marius, Nico, Saswati. The role of a statistician in drug development: phase II. Ideas: improving drug development. February 20, 2017. Available at: http://www.ideas-itn.eu/the-role-of-a-statistician-in-drug-development-phase-ii. Accessed December 20, 2018.

13. Strimbu K, Tavel J. What are biomarkers? Curr Opin HIV AIDS 2010;5:463–6.

14. Amur S. FDA's efforts to encourage biomarker development and qualification. M-CERSI Symposium, Baltimore, MD. August 21, 2015. Available at: https://c-path.org/wp-content/uploads/2015/08/EvConsid-Symposium-20150821-I-01-SAmur-FINAL.pdf. Accessed February 6, 2019.

15. U.S. Food and Drug Administration. CDER Biomarker Qualification Program. U.S. FDA. Available at: https://www.fda.gov/Drugs/DevelopmentApprovalProcess/DrugDevelopmentToolsQualificationProgram/BiomarkerQualificationProgram/default.htm. Accessed February 6, 2019.

16. Rosenblatt M, Austin CP, Boutin M, et al. Innovation in development, regulatory review and use of clinical advances. A vital direction for health and health care. Discussion Paper. National Academy of Medicine. September 19, 2016. Available at: https://nam.edu/innovation-in-development-regulatory-review-and-use-of-clinical-advances-a-vital-direction-for-health-and-health-care. Accessed August 20, 2017.

17. Rubens E. Office of the Assistant Secretary of Planning and Evaluation. Cost Drivers in the development and validation of biomarkers used in drug development. Final report. U.S. Department of Health and Human Services. July 20, 2018. Available at: https://aspe.hhs.gov/system/files/pdf/260031/FinalBiomarkersReport.pdf. Accessed February 6, 2019.

18. Wong CH, Siah KW. Estimation of clinical trial success rates and related parameters. Biostatistics 2018;00:1–14.

19. Lowe D. A new look at clinical success rates. In the Pipeline. February 2, 2018. Available at: https://blogs.sciencemag.org/pipeline/archives/2018/02/02/a-new-look-at-clinical-success-rates?r3f_986=https://r.search.yahoo.com/_ylt=AwrgDmlXuF9c7PQAb4RXNyoA;_ylu=X3oDMTExa2MyY3N1BGNvbG8DZ3ExBHBvcwMxBHZOaWQDVUlDMV8xBHNlYwNzcg-/RV=2/RE=1549805783/RO=10/RU=http%3a%2f%2fblogs.sciencemag.org%2fpipeline%2farchives%2f2018%2f02%2f02%2fa-new-look-at-clinical-success-rates/RK=2/RS=8zeDvGgvYPlubMYc.WDTzh1ZVPU. Accessed January 27, 2019.

20. Packer M, Narahara KA, Elkayam U, et al. Double-blind, placebo-controlled study of the efficacy of flosequinan in patients with chronic heart failure. Principal investigators of the REFLECT study. J Am Coll Cardiol 1993;22:65–72.

21. Packer M, Pitt B, Rouleau JL, Swedberg K, DeMets DL, Fisher L. Long-term effects of flosequinan on the morbidity and mortality of patients with severe chronic heart failure: primary results of the PROFILE trial after 24 years. J Am Coll Cardiol HF 2017;5:399–407.

22. O'Donoghue ML. Targeting inflammation—what has the VISTA-16 trial taught us? Nature Rev Cardiol 2014;11:130–2.

23. O'Riordan M. VISTA-16 at last: investigators allege misconduct by sponsor. Medscape. November 18. 2013. Available at: https://www.medscape.com/viewarticle/814530. Accessed January 10, 2019.

24. Karabina S, Ninio E. Plasma PAFAH/PLA2G7 genetic variability, cardiovascular disease and clinical trials. In: Tamanoi F, editor. The Enzymes, Volume 38. Amsterdam: Elsevier Inc., 2015: 145–55.

25. Gheorghiade M, Bohm M, Greene SJ, et al. Effect of aliskiren on postdischarge mortality and heart failure readmissions among patients hospitalized for heart failure: the ASTRONAUT randomized trial. JAMA 2013;309:1125–35.

26. Mentz R, Felker GM, Ahmad T, et al. Learning from recent trials and shaping the future of acute heart failure trials. Am Heart J 2013;166:629–35.

27. Lapook J. Study: Heart drug Tredaptive is ineffective. CBS News July 29, 2013. Available at: https://www.cbsnews.com/news/study-heart-drug-tredaptive-is-ineffective/. Accessed March 18, 2019.

28. Merrill J. Surprise! It's a phase III failure! Scrip Pharma Intelligence Pink Sheet. August 12, 2016. Available at: https://scrip.pharmaintelligence.informa.com/SC097113/Surprise-Its-A-Phase-III-Failure. Accessed January 10, 2019.

29. Benjamini Y, Hochberg Y. Controlling the false discovery rate: a practical and powerful approach to multiple testing. J Royal Stat Soc Series B (Methodological) 1995;57:289–300.

30. Sellke T, Bayarri MJ, Berger JO. Calibration of p values for testing precise null hypotheses. Am Statist 2001;55:62–71.

31. U.S. Food and Drug Administration. Multiple endpoints in clinical trials: guidance for industry. US DHHS Center for Drug Evaluation and Research. January 2017. Available at: https://www.fda.gov/downloads/Drugs/GuidanceComplianceRegulatoryInformation/Guidances/UCM536750.pdf. Accessed February 2, 2019.

32. Statistics How To: False discovery rate: simple definition, adjusting for FDR. Available at: https://www.statisticshowto.datasciencecentral.com/false-discovery-rate. Accessed February 6, 2019.

33. Gan HK, Grothey A, Pond GR, Moore MJ, Siu LL, Sargent D. Randomized phase II trials: inevitable or inadvisable? J Clin Oncol 2010;28:2641–7.

34. Tang H, Foster NR, Grothey A, Ansell SM, Sargent DJ. Excessive false-positive errors in single-arm phase II trials: a simulation-based analysis. J Clin Oncol 2009;27:A6512.

35. Thall PF, Simon R. Incorporating historical control data in planning phase II clinical trials. Stat Med 1990;9:215–28.

36. Bretz F, Schmidli H, Konig F, Racine A, Maurer W. Confirmatory seamless phase II/III clinical trials with hypotheses selection at interim: general concepts. Biom J 2006;4:623–34.

37. Schmidli H, Bretz F, Racine A, Maurer W. Confirmatory seamless phase II/III clinical trials with hypotheses selection at interim: applications and practical considerations. Biom J 2006;48:635–43.

38. U.S. Food and Drug Administration. Innovation or stagnation? Challenge and opportunity on the critical path to new medical products. 2004. Available at: http://wayback.archive-it.org/7993/20180125035500/https://www.fda.gov/downloads/ScienceResearch/SpecialTopics/CriticalPathInitiative/CriticalPathOpportunitiesReports/UCM113411.pdf. Accessed February 6, 2019.

39. O'Neill RT. FDA's critical path initiative: a perspective on contributions in biostatistics. Biom J 2006;48:559–64.

40. H.R. 34—114th Congress (2015-2016). The 20th Century Cures Act. . Available at: https://www.congress.gov/bill/114th-congress/house-bill/34. Accessed January 10, 2019.

41. Gottlieb S. Submission to Congress: Food and Drug Administration Work Plan and Proposed Funding Allocations of FDA Innovation Account. June 6, 2017. Available at: https://www.fda.gov/downloads/RegulatoryInformation/LawsEnforcedbyFDA/SignificantAmendmentstotheFDCAct/21stCenturyCuresAct/UCM562852.pdf. Accessed January 10, 2019.

42. Chow SC, Chang M. Adaptive design methods in clinical trials—a review. Orphanet J Rare Dis 2008;3:11.

43. Bauer P. Multistage testing with adaptive designs. Biomet Informatik Medizin Biol 1989;20:130–48.

44. Bauer P, Kohne K. Evaluation of experiments with adaptive interim analyses. Biometrics 1994;50:1029–41.

45. Bauer P, Bretz F, Dragalin V, Konig F, Wassmer G. Twenty-five years of confirmatory adaptive designs; opportunities and pitfalls. Stat Med 2016;35:325–47.

46. Sato A, Shimura M, Gosho M. Practical characteristics of adaptive design in phase 2 and 3 clinical trials. J Clin Pharm Ther 2018;43:170–80.

47. U.S. Food and Drug Administration. Adaptive designs for clinical trials of drugs and biologics: guidance for industry. U.S. FDA. Center for Drug Evaluation and Research. September 2018. Available at: https://www.fda.gov/downloads/Drugs/GuidanceComplianceRegulatoryInformation/Guidances/UCM201790.pdf. Accessed February 6, 2019.

48. Pong A, Shein-Chung C. Adaptive trial design in clinical research. Biopharm Appl Stat Symp 2014:5–99.

49. Korn EL, Freidlin B. Adaptive clinical trials: advantages and disadvantages of various adaptive design elements. J National Cancer Inst 2017;109:6.

50. Gallo P, Chuang-Stein C, Dragalin V, Gaydos B, Krams M, Pinheiro J. Adaptive designs in clinical drug development—an executive summary of the PhRMA working group. J Biopharm Stats 2006;16:275–83.

51. Weichung JS. Plan to be flexible: a commentary on adaptive designs. Biom J 2006;48:656–9.

52. Mehta CR, Jemiai Y. A consultant's perspective on the regulatory hurdles to adaptive trials. Biom J 2006;48:604–8.

53. Elsaßer A, Regnstrom J, Vetter T. Adaptive clinical trial designs for European marketing authorization: a survey of scientific advice letters from the European Medicines Agency. Trials 2014; 15:383.

54. European Medicines Agency. Reflection paper on methodological issues in confirmatory clinical trials for drugs and biologics planned with an adaptive design. 2007. Available at: https://www.ema.europa.eu/en/documents/scientific-guideline/reflection-paper-methodological-issues-confirmatory-clinical-trials-planned-adaptive-design_en.pdf. Accessed March 18, 2019.

55. Collignon O, Koenig F, Koch A, et al. Adaptive designs in clinical trials: from scientific advice to marketing authorisation to the European Medicine Agency. Trials 2018;19:642.

56. Gallo P, Chuang-Stein C, Dragalin V, et al. Rejoinder. J Biopharm Stats 2006;16:311–2.

57. Hung HMJ, O'Neill RT, Want SJ, Lawrence J. A regulatory view on adaptive/flexible clinical trial design. Biom J 2006;48:565–73.

58. Jennison C, Turnbull BW. Discussion of "executive summary of the PhRMA working group on adaptive designs in clinical drug development. J Biopharm Stats 2006;16:293–8.

59. Gould AL. How practical are adaptive designs likely to be for confirmatory trials? Biom J 2006; 48:644–9.

60. Zelen M. Play the winner rule and the controlled clinical trial. J Am Stat Assoc 1969;64:131–46.

61. Hey SP, Kimmelman J. Are outcome-adaptive allocations trials ethical? Clin Trials 2015;12:102–6.

62. Hey SP, Kimmelman J. Rejoinder. Clin Trials 2015;12:125–7.

63. Korn EL, Friedlin B. Commentary on Hey and Kimmelman. Clin Trials 2015;12:122–4.

64. Buyse M. Commentary on Hey and Kimmelman. Clin Trials 2015;12:119–21.

65. Saxman SB. Commentary on Hey and Kimmelman. Clin Trials 2015;12:113–5.

66. Berry DA. Commentary on Hey and Kimmelman. Clin Trials 2015;12:107–9.

67. Li Y, Mick R, Heitjan DF. Suspension of accrual in phase II cancer clinical trials. Clin Trials 2015;12: 128–38.

68. Joffe S, Ellenber SS. Commentary on Hey and Kimmelman. Clin Trials 2015;12:16–8.

69. Begg CB. Ethical concerns about adaptive randomization. Clin Trials 2015;12:101.

70. Tsong Y, Hung HMJ, Wong SJ, Dui L, Nuri WA. Dropping a treatment arm in clinical trial with multiple arms. In: Proceedings of Biopharmaceutical Section. Alexandria, VA: American Statistics Association, 1997:58–63.

71. Bauer P, Enfalt J. Application of adaptive designs—a review. Biom J 2006;48: 493–506.

72. Lin M, Lee S, Zhen B, et al. CBER's experience with adaptive design clinical trials. Therap Innov Reg Sci 2016;50:195–203.

73. Bothwell L. Adaptive design clinical trials; a review of the literature and clinicalTrials.gov. BMJ Open 2018;8:e018320.

74. Hatfield I, Allison A, Flight L, Julious SA, Munyaradzi D. Adaptive designs undertaken in clinical research: a review of registered clinical trials. Trials 2016;17:150.

KEY WORDS adaptive design, biomarker studies, false discovery rate, multiplicity problem, phase II clinical trials

JACC: BASIC TO TRANSLATIONAL SCIENCE VOL. 4, NO. 3, 2019

STATE-OF-THE-ART REVIEW

Emerging Therapeutics for the Treatment of Light Chain and Transthyretin Amyloidosis

Kathleen W. Zhang, MD,[a] Keith E. Stockerl-Goldstein, MD,[b] Daniel J. Lenihan, MD[a]

HIGHLIGHTS

- **Cardiac amyloidosis has high associated morbidity and, until recently, limited treatment options.**
- **This review discusses the mechanism and clinical trial performance of multiple emerging therapies.**
- **Additional studies should identify optimal treatment paradigms and biomarker strategies for cardiac response to therapy.**

SUMMARY

Cardiac amyloidosis is a restrictive cardiomyopathy that results from the deposition of misfolded light chain or transthyretin proteins, most commonly, in cardiac tissue. Traditionally, treatment options for light chain (AL) and transthyretin (ATTR) amyloidosis have been limited. However, there are now multiple novel therapeutics in development and several therapeutics recently approved that promise to revolutionize clinical management of AL and ATTR. Most of these agents disrupt specific stages of amyloidogenesis such as light chain or transthyretin protein production, formation of amyloidogenic intermediates, or amyloid fibril aggregation. Others aim to remove existing amyloid tissue deposits using monoclonal antibody technology. Although these advances represent an important step forward in the care of cardiac amyloidosis patients, additional studies are needed to define the optimal treatment paradigms for AL and ATTR and to validate clinical, imaging, or serum biomarker strategies that may confirm a cardiac response to therapy. (J Am Coll Cardiol Basic Trans Science 2019;4:438–48) © 2019 The Authors. Published by Elsevier on behalf of the American College of Cardiology Foundation. This is an open access article under the CC BY-NC-ND license (http://creativecommons.org/licenses/by-nc-nd/4.0/).

Cardiac amyloidosis is a restrictive cardiomyopathy that results from the deposition of amyloid fibrils in cardiac tissue, causing progressive heart failure (HF) with median survival of 2 to 4 years (1,2). Two types of amyloid protein cause more than 95% of cardiac amyloidosis: immunoglobulin light chain, which causes light chain amyloidosis (AL), and transthyretin, which causes hereditary or wild-type (previously called senile systemic amyloidosis) transthyretin amyloidosis (ATTR).

Although hereditary ATTR (3) and AL (4) are uncommon conditions, wild-type ATTR is likely underdiagnosed particularly among patients with HF with preserved ejection fraction (EF) and calcific

From the [a]Division of Cardiology, Cardio-Oncology Center of Excellence, Washington University in St. Louis School of Medicine, Saint Louis, Missouri; and the [b]Division of Oncology, Washington University in St. Louis School of Medicine, Saint Louis, Missouri. Dr. Stockerl-Goldstein is on the advisory board for Celgene; has stock equity in Abbott and AbbVie; and has received grants from Millenium Pharmaceuticals, Janssen Pharmaceuticals, BioLineRx Ltd., Pfizer Inc., and GlaxoSmithKline. Dr. Lenihan has received personal fees from Pfizer, Prothena, Akcea, and Takeda. Dr. Zhang has reported that she has no relationships relevant to the contents of this paper to disclose.

All authors attest they are in compliance with human studies committees and animal welfare regulations of the authors' institutions and U.S. Food and Drug Administration guidelines, including patient consent where appropriate. For more information, visit the *JACC: Basic to Translational Science* author instructions page.

Manuscript received November 1, 2018; revised manuscript received February 16, 2019, accepted February 19, 2019.

ISSN 2452-302X https://doi.org/10.1016/j.jacbts.2019.02.002

aortic stenosis (5-9). Despite growing clinical recognition of the disease, availability of reliable noninvasive diagnostic techniques (10), and significant associated morbidity and mortality, pharmacologic agents have yet to receive regulatory approval specifically for AL or ATTR with cardiac involvement.

This review highlights the new and emerging therapies for AL and ATTR with emphasis on their mechanistic effects on the amyloid disease-producing process and performance in early clinical trials. It is apparent that additional studies are needed to define the optimal treatment paradigms and to measure therapeutic cardiac response in light chain (AL-CA) and transthyretin (ATTR-CA) cardiac amyloidosis.

LIGHT CHAIN AMYLOIDOSIS

BACKGROUND. AL results from the extracellular deposition of amyloid fibrils composed of monoclonal immunoglobulin light chains, which are produced by an underlying clonal plasma cell proliferative disorder such as multiple myeloma (MM) (**Central Illustration**, panel A). Ten percent to 15% of patients with MM develop AL; however, the majority of AL patients have <10% plasma cells in the bone marrow (11). Monoclonal gammopathy of undetermined significance (MGUS) is a known precursor of both MM and AL, and progresses to AL in 1.0% of cases with a relative risk of 8.8 as compared to the general population (12). The light chain amyloid fibrils in AL derive mostly from N-terminal amino acid residues of light chain immunoglobulin variable regions, and arise more commonly from λ light chains than κ (11).

The exact mechanism of AL pathogenesis and the resultant pathophysiological changes that lead from MGUS or MM to AL are currently unknown. The monoclonal plasma cells in AL share many genetic abnormalities with the plasma cells in MM and MGUS, namely, gain of chromosomes 7, 9, 11, 15, and 18, loss of chromosome 18 (13), translocation of the immunoglobulin heavy chain gene at 14q32 (14,15), and deletion of the long arm of chromosome 13 [del(13q)] (16). However, functional gene expression analyses show a unique molecular profile for AL as compared with MM including higher expression of CD27 SDF-1 (17). AL clonal plasma cells also show a number of deregulated genes and pathways involving protein processing and folding.

Current standard-of-care for newly diagnosed AL is based on antimyeloma therapy and consists of autologous stem cell transplantation (ASCT) for eligible patients or bortezomib-based chemotherapy for high-risk patients who are transplant-ineligible. Five-year survival with upfront bortezomib-based regimens lags behind that with upfront ASCT (55% versus 84%) (18,19), although the 2 strategies have not been compared in a clinical trial setting and the transplant-ineligible population is generally sicker with more comorbidities. Additionally, up to 45% of patients have progression of cardiac disease despite complete hematologic response with initial therapy (20), possibly related to obstructive intramural coronary amyloidosis, subendocardial ischemia, and/or interstitial fibrosis (21,22). There remains a critical need for novel therapeutic agents that improve cardiac response to AL therapy.

PROTEASOME INHIBITORS. Protein degradation is an essential cellular function carried out by the proteasome. Proteasome inhibition causes cell cycle arrest and cellular apoptosis, with proliferating malignant cells showing higher susceptibility than normal cells (23). Bortezomib is a boronic acid dipeptide that inhibits the 20S proteasome by binding to the catalytic β subunits lining the inner ring of the 20S core particle in a reversible manner (23,24).

Ixazomib is a second-generation boronic acid dipeptide proteasome inhibitor that binds reversibly to the 20S proteasome. Because of a shorter proteasome dissociation half-life, ixazomib has significantly larger volume of distribution and greater tumor proteasome inhibition than bortezomib in vivo, allowing for higher doses of administration and greater plasma exposure (24). Compared to lenalidomide and dexamethasone alone, addition of ixazomib reduced disease progression or death in patients with relapsed/refractory MM with a hazard ratio (HR) of 0.74 (25). No excess of adverse events was seen with ixazomib. A phase I/II trial of ixazomib in 27 patients with relapsed/refractory AL showed encouraging hematologic (52%) and organ (56%) response rates with only 3 patients experiencing dose-limiting toxicity (NCT01318902) (26). A phase III trial of ixazomib in the AL population is ongoing (NCT01659658) (**Table 1**).

Carfilzomib is a modified epoxyketone that binds the 20S proteasome irreversibly and with higher selectivity than bortezomib. As compared with lenalidomide and dexamethasone alone, the addition of carfilzomib in relapsed MM improved 24-month survival by 21% and also led to significant improvement in hematologic response rate (27). Cardiovascular toxicities (hypertension, cardiac failure, and ischemic heart disease) were among the major adverse effects. In a phase I/II trial of carfilzomib monotherapy in 28 patients with previously treated AL, 63% showed

ABBREVIATIONS AND ACRONYMS

AL = light chain amyloidosis

ATTR = transthyretin amyloidosis

ASCT = autologous stem cell transplantation

CA = cardiac amyloidosis

GLS = global longitudinal strain

MGUS = monoclonal gammopathy of undetermined significance

MM = multiple myeloma

MMP = matrix metalloproteinase

NT-proBNP = N-terminal prohormone of brain natriuretic peptide

SAP = serum amyloid P

hematologic response although pulmonary, renal, and cardiac toxicities were common (28) (NCT01789242). Because of advanced cardiac disease in many AL patients, the role of carfilzomib in standard AL treatment paradigms remains to be determined.

IMMUNOMODULATORY AGENTS. The immunomodulatory agents (IMiDs) include thalidomide and its analogues, and have therapeutic efficacy in a wide range of malignancies. Recent studies have shown that the IMiDs exert antimyeloma activity by activating the E3 ubiquitin ligase activity of the protein cereblon. Binding of the IMiDs to cereblon results in the rapid ubiquitination and degradation of Ikaros (IKZF1) and Aiolos (IKZF3), 2 key transcriptional regulators of B and T cell development (29). Lenalidomide is a second-generation synthetic thalidomide that has been in use for AL. In 69 patients with AL treated with lenalidomide and dexamethasone, 16% of patients achieved a complete response (CR) in an intent-to-treat analysis (NCT00091260) (30). The median time to achieve a CR was 6 months with 60% of CRs considered durable.

Pomalidomide is a newer thalidomide analogue with more potent antimyeloma activity than lenalidomide. As with lenalidomide, it inhibits proinflammatory cytokine production and angiogenesis, induces apoptosis and cell cycle arrest, and activates T cells and natural killer cells (31). A phase I trial of pomalidomide and dexamethasone in 33 patients with previously treated AL showed hematologic response rate of 48% and organ response rate of 15% (32) (NCT01807286). Twenty-seven patients (82%) had cardiac involvement but only 4 showed cardiac response. This trial was terminated early during the phase I portion without continuation to phase II.

Trials using the IMiDs thalidomide, lenalidomide, and pomalidomide have repeatedly shown that patients with AL have a poor tolerance for these agents when used at the standard doses typically prescribed for MM, although it is unclear why this occurs (33). The precise role and optimal sequence of the IMiDs in the treatment of AL remains unclear.

MONOCLONAL ANTIBODIES. CD38 and SLAMF7 (also known as CD319 and CS1) are cell surface antigens specific to MM cells that are being evaluated as targets of monoclonal antibody (mAb) therapeutics in MM and AL.

CD38 is a type II transmembrane glycoprotein that associates with cell-surface receptors in lipid rafts, regulates cytoplasmic Ca^{2+} flux, and mediates signal transduction in lymphoid and myeloid cells (34). It is expressed at low level on normal lymphoid and myeloid cells and in some tissues of nonhematopoietic origin, but it is highly and uniformly expressed on plasma cells in patients with MM and AL (35,36). Daratumumab is a human immunoglobulin (Ig) G1κ mAb that targets the extracellular domain of CD38 (37). In vitro, daratumumab kills MM cells by antibody-dependent cellular cytotoxicity and complement-dependent cytotoxicity, and is highly efficacious in both early- and late-treatment settings in in vivo tumor models (37). Two large phase III trials showed improved progression-free survival (PFS) with daratumumab in combination with either lenalidomide and dexamethasone or bortezomib and dexamethasone in patients with relapsed/refractory MM (38,39). A retrospective analysis of 25 patients with refractory AL who received daratumumab and dexamethasone showed overall hematologic response rate of 76% including CR in 36% (40). Therapy was well tolerated without any grade 3 or 4 reactions observed, even among the 72% of patients with cardiac involvement. A phase III trial of daratumumab, cyclophosphamide, bortezomib, and dexamethasone in patients with newly diagnosed AL is ongoing (NCT03201965).

Isatuximab is a chimeric IgG1 monoclonal antibody that targets CD38 as an allosteric antagonist (41). In vivo, isatuximab showed antitumor activity in multiple cancer models including MM, lymphoma, and leukemia. In a phase Ib trial of isatuximab, lenalidomide, and dexamethasone for relapsed/refractory multiple myeloma, the overall hematologic response rate was 56% and median PFS was 8.5 months, indicative of clinical benefit without significant toxicity (42). A phase II trial of isatuximab in patients with relapsed/refractory AL is ongoing (NCT03499808).

SLAMF7 is a member of the Signaling Lymphocyte Activation Molecule Family and is expressed at low level on natural killer cells, CD8+ T cells, B cells, and mature dendritic cells (43). Normal plasma cells and MM cells express high levels of SLAMF7 mRNA and protein (44), and targeting of SLAMF7 using mAbs led to antibody-dependent cellular cytotoxicity and reduction in myeloma activity in vivo. Although the mechanism of SLAMF7 upregulation in MM is unknown, small interfering RNA inhibition of SLAMF7 expression inhibited MM cell adhesion to bone marrow stromal cells (45). Elotuzumab is a humanized recombinant IgG1κ mAb that targets the extracellular region of SLAMF7 (44). In patients with relapsed/refractory MM, the addition of elotuzumab to lenalidomide and dexamethasone improved median PFS from 14.9 to 19.4 months, with overall

response rate (ORR) of 79% (improved from 66%) (46). Elotuzumab gained U.S. Food and Drug Administration approval for relapsed/refractory MM in 2015, and is currently in a phase II trial for patients with relapsed AL (NCT03252600).

SMALL MOLECULE INHIBITORS. Modulation of intrinsic apoptotic pathways offers an additional mechanism by which to treat AL amyloidosis. BCL-2 is a central regulator of programmed cell death that binds and sequesters pro-apoptotic proteins (47). Elevated expression of anti-apoptotic proteins is common in MM and associated with resistance to therapy (48). Venetoclax is a small molecule that binds with high affinity to the binding pocket on BCL-2 specific for the BH3 region of intrinsic pro-apoptotic proteins (47). In vitro, venetoclax inhibits interaction of BCL-2 with pro-apoptotic proteins within the mitochondria, and induces apoptosis in lymphoma and leukemia cells as well as tumor regression in in vivo solid tumor models (47). In human myeloma cell lines and primary MM samples, sensitivity to venetoclax was highest in the presence of the (11;14) translocation, which correlated with higher ratios of *BCL2* and *MCL1* mRNA (49). t(11;14) is seen in 15% to 20% of patients with MM, and may be a marker of intermediate-risk disease (50).

A phase I trial of venetoclax monotherapy in 66 patients with relapsed/refractory MM showed an ORR of 21%; among patients with t(11;14), the ORR was doubled at 40% (51). Similarly, time to progression of disease was 6.6 months in patients with t(11;14) and 1.9 months in those without t(11;14). There were no adverse cardiac events, and changes in cardiac parameters with therapy were not evaluated. A separate phase Ib trial of venetoclax in combination with bortezomib and dexamethasone showed better ORR at 67%, with time to progression of 9.7 months (52). Again, patients with higher *BCL2* expression had a higher ORR (94%) as compared to patients with low *BCL2* expression (59%). A phase I trial of venetoclax and dexamethasone in patients with relapsed/refractory AL is ongoing (NCT03000660).

DOXYCYCLINE. Matrix metalloproteinases (MMPs) and their tissue inhibitors are key regulators of cardiac extracellular matrix homeostasis, which is disrupted by amyloid infiltration resulting in thickening and stiffening of the myocardium. Elevation in MMP and tissue inhibitor of matrix metalloproteinase serum levels and tissue expression have been associated with renal and cardiac damage in AL (53,54), suggesting that inhibition of the MMP pathway may mitigate the cardiotoxic effects of light chain amyloid fibril deposition. Doxycycline is a semisynthetic tetracycline antibiotic that inhibits bacterial protein synthesis and, separately, also acts as an inhibitor of MMPs. Doxycycline inhibits the formation of light chain amyloid fibrils in vivo and ex vivo in a dose-dependent manner, and prevented light chain amyloid deposition in a mouse model of AL (55). In a retrospective cohort study of 103 patients with AL-CA, 24-month survival improved from 40% to 82% by administering doxycycline along with chemotherapy whereas cardiac response to therapy improved 3-fold to 60% (56). Multiple clinical trials of doxycycline in conjunction with plasma cell-directed therapy in patients with AL are ongoing (NCT02207556, NCT03474458, and NCT03401372).

CLEARANCE OF AMYLOID DEPOSITS. Mouse models of human AL amyloidomas showed spontaneous tumor regression in association with neutrophil infiltration and production of antibodies targeted to κ and λ light chain extracts (57), suggesting that exogenous administration of anti-amyloid antibodies may expedite clearance of amyloid deposits.

11-1F4 (CAEL-101) is a chimeric monoclonal IgG1 antibody that targets the V_L fragment of human κ Bence Jones protein, with stronger affinity for κ light chain than λ (57,58). 11-1F4 interacts immunohistochemically with human AL deposits in hepatocytes, proximal renal tubules, and myocytes, and facilitates regression of AL amyloidomas in vivo (58). In a phase Ia/b dose-escalation study in 27 patients with relapsed/refractory AL, 62% of patients showed organ response at a median of 2 weeks after starting treatment (NCT02245867) (59). In patients with cardiac involvement, 11-1F4 led to a statistically significant improvement in global longitudinal strain (GLS) after 12 weeks of follow-up (60). A randomized phase II/III trial for newly diagnosed AL patients is planned, inclusive of a high-risk patient cohort with N-terminal prohormone of brain natriuretic peptide (NT-proBNP) $>$ 8,500 ng/L. Additionally, a radiolabeled peptide comprising a 11-1F4 epitope and a pan-amyloid-reactive peptide is in development which may enable the use of 11-1F4 as a diagnostic imaging agent for AL and other forms of amyloidosis (61).

NEOD001 is a humanized mAb originally developed for secondary amyloidosis but found to target AL deposits with high affinity. It targets the C-terminal amino acid sequence of murine serum amyloid A protein, which is exposed during the process of AA amyloid deposition and is not accessible in the full-length serum amyloid A molecule (62). NEOD001 binds AL amyloid deposits in situ, induces phagocytic clearance of AL deposits, and expedites clearance of AL amyloidomas (63,64).

JACC: BASIC TO TRANSLATIONAL SCIENCE VOL. 4, NO. 3, 2019
JUNE 2019:438–48

CENTRAL ILLUSTRATION **Pathophysiology of Light Chain and Transthyretin Amyloidosis and Mechanism of Action of Novel Therapeutics**

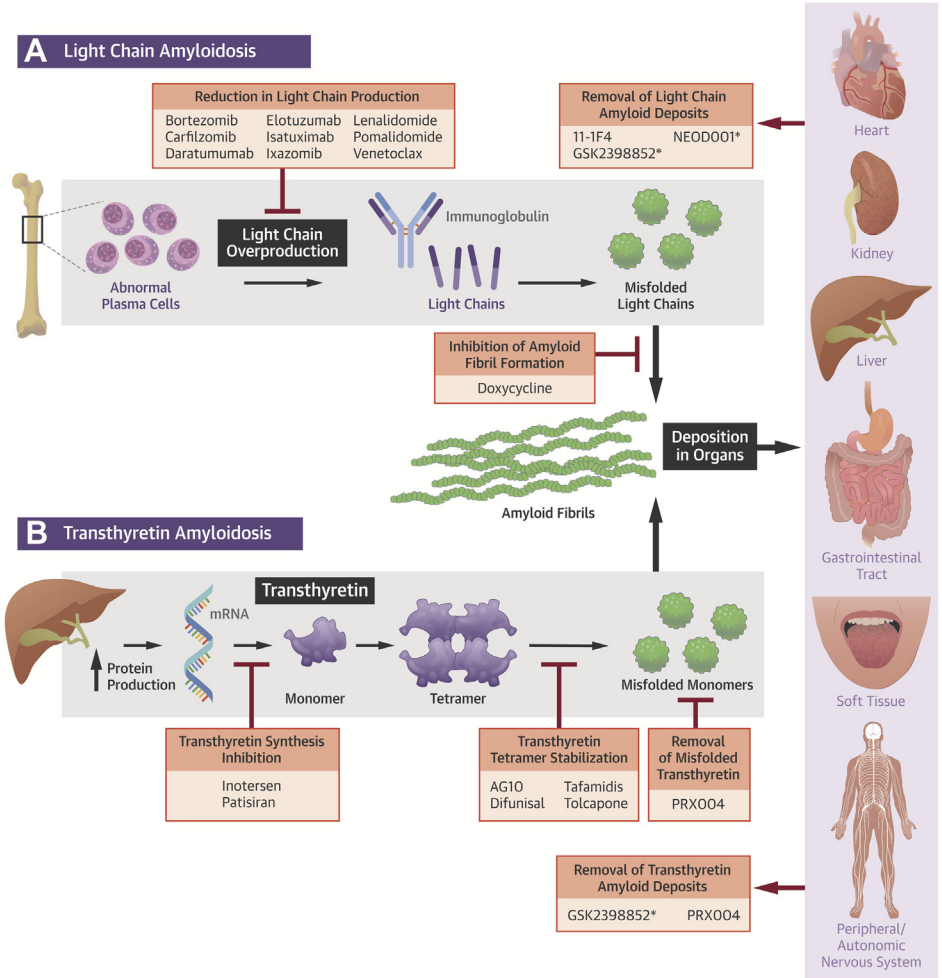

Zhang, K.W. et al. J Am Coll Cardiol Basic Trans Science. 2019;4(3):438–48.

(A) Abnormal plasma cells overproduce κ or λ light chains, which misfold and aggregate into amyloid fibrils. The light chain amyloid fibrils deposit in multiple end-organs causing organ dysfunction. Carfilzomib, daratumumab, elotuzumab, isatuximab, ixazomib, pomalidomide, and venetoclax reduce light chain production; doxycycline inhibits formation of light chain amyloid fibrils; 11-1F4, GSK2398852, and NEOD001 remove light chain amyloid deposits from tissue. **(B)** Transthyretin is synthesized in hepatocytes as a homotetramer, which dissociates into alternatively folded monomers that self-assemble to form insoluble amyloid fibrils. The transthyretin amyloid fibrils deposit in multiple end-organs causing organ dysfunction. Patisiran and inotersen inhibit transthyretin synthesis by targeting transthyretin mRNA; AG10, diflunisal, tafamidis, and tolcapone stabilize the transthyretin tetramer; PRX004 targets misfolded transthyretin and removes tissue amyloid deposits; GSK2398852 removes amyloid deposits from tissue. *Drug development has been suspended or terminated.

NEOD001 performed well in a phase I/II trial of patients with AL and persistent organ dysfunction after therapy (65). However, a phase II trial failed to meet its primary endpoint of cardiac response as measured by NT-proBNP (NCT02632786), and a subsequent phase III trial was discontinued prematurely for futility (NCT02312206) (66). Failure of these late-phase clinical trials may have stemmed from issues with study design, such as the use of biomarker-based endpoints in NCT02632786 and a composite clinical endpoint in NCT02312206 as opposed to best response analysis. Further development of NEOD001 for AL was halted in April 2018.

TABLE 1 Emerging Therapeutics for Light Chain and Transthyretin Amyloidosis

Mechanism of Action	Drug Name	Route	Frequency	FDA Approved?	FDA Approved For Amyloid?	Latest Amyloidosis Clinical Trial Phase	NCT Clinical Trial Number
Light chain amyloidosis							
Reduction in light chain production							
Proteasome Inhibitor	Carfilzomib	IV	Twice weekly for 3 weeks per 28-day cycle	Yes	No	I/II	NCT01789242
	Ixazomib	PO	Once weekly for 3 weeks per 28-day cycle	Yes	No	III	NCT01659658
Immunomodulator	Pomalidomide	PO	Once daily for 3 weeks per 28-day cycle	Yes	No	I/II (terminated)	NCT01807286
Anti-CD38 mAb	Daratumumab	SQ	Once weekly (then once) per 28-day cycle	Yes	No	III	NCT03201965
	Isatuximab	IV	Weekly (then biweekly) per 28-day cycle	No	No	II	NCT03499808
Anti-SLAMF7	Elotuzumab	IV	Weekly (then biweekly) per 28-day cycle	Yes	No	II	NCT03252600
BCL2 Inhibitor	Venetoclax	PO	Daily	Yes	No	I	NCT03000660
Inhibition of amyloid fibril formation							
	Doxycycline	PO	Twice daily	Yes	No	II/III	NCT02207556, NCT03474458, NCT03401372
Clearance of amyloid deposits							
	11-1F4	IV	Once weekly	No	No	I	NCT02245867
	NEOD001	IV	Once every 28 days	No	No	III (terminated)	NCT02312206
Transthyretin amyloidosis							
Transthyretin tetramer stabilizer							
	AG10	PO	Twice daily	No	No	II	NCT03458130
	Diflunisal	PO	Twice daily	Yes	No	III	NCT00294671
	Tafamidis	PO	Daily	No	No	III	NCT01994889
	Tolcapone	PO	Daily	Yes	No	II	NCT02191826
Transthyretin synthesis inhibitor							
	Inotersen	SQ	Weekly	Yes	Yes	III	NCT01737398
	Patisiran	IV	Once every 3 weeks	Yes	Yes	III	NCT01960348
Removal of amyloid deposits							
	PRX004	IV	Once every 28 days	No	No	I	NCT03336580
Light chain and transthyretin amyloidosis							
Removal of amyloid deposits							
	GSK2398852	IV	Once per 11-day cycle	No	No	II (suspended)	NCT03044353

FDA = U.S. Food and Drug Administration; IV = intravenous; mAb = monoclonal antibody; NCT = National Clinical Trial; PO = oral; SQ = subcutaneous.

TRANSTHYRETIN AMYLOIDOSIS

BACKGROUND. Transthyretin is a 55,000-Dalton protein that is synthesized primarily in the liver, and serves as the primary serum transport protein for holo-retinol-binding protein and a minor transport protein for thyroxine. In plasma, <1% of transthyretin is thyroxine-bound due to higher binding affinity of thyroxine for thyroid binding globulin and albumin (67). Transthyretin is also synthesized in the choroid plexus and secreted into the cerebrospinal fluid (CSF), where it serves as the primary carrier of thyroxine (68).

The transthyretin protein contains 4 identical subunits rich in β-sheets that assemble into 2 αβ dimers. The αβ dimers contact one another at an extended β-sheet that forms 2 funnel-shaped hormone binding sites, where thyroxine binds with negative cooperativity (68,69). Formation of transthyretin amyloid fibrils requires dissociation of the tetramer into alternatively folded monomers, which then self-assemble to form insoluble amyloid fibrils (**Central Illustration**, panel B) (70,71). Binding of thyroxine stabilizes the native conformation of the transthyretin tetramer, preventing its dissociation into monomer units and subsequent aggregation into amyloid fibrils (72). In CSF, where transthyretin is highly thyroxine bound, transthyretin fibril formation is generally not observed (72).

The kinetics of tetramer dissociation also explain the predilection of mutant transthyretin for amyloid

formation. L55P and V122I-mutant transthyretin dissociate rapidly to the monomeric amyloidogenic intermediate and aggregate to form amyloid fibrils at a correspondingly high rate, leading to nearly 100% disease penetrance with severe systemic disease (73). In comparison, the V30M mutant dissociates more slowly even than wild-type transthyretin and results in a milder disease phenotype (polyneuropathy) with penetrance as low as 2% (74,75). The protective T119M variant exhibits extremely slow tetramer dissociation and fibril formation rates (73); compound heterozygotes expressing both T119M and V30M transthyretin exhibit either normal phenotype or only mild pathology of late onset (76).

TRANSTHYRETIN TETRAMER STABILIZERS. Because of the disease-modifying effect of tetramer stabilization, transthyretin tetramer stabilizers have emerged as a novel class of therapeutics for ATTR. Nonsteroidal anti-inflammatory drugs such as diflunisal were among the first transthyretin tetramer stabilizers identified, binding with higher efficacy to the central hormone-binding funnel than thyroxine (77). Administration of diflunisal 250 mg twice daily in healthy subjects slowed transthyretin aggregation in vitro by 3-fold (78). In familial amyloid polyneuropathy, a phase III clinical trial of diflunisal 250 mg twice daily reduced the rate of progression of neurologic impairment and preserved quality of life over 2 years (NCT00294671) (79). Diflunisal was well tolerated in an open-label study of 13 patients with wild-type and hereditary ATTR-CA; hemoglobin, mean arterial pressure, and glomerular filtration rate remained stable over 0.9 years of follow-up without significant change in cardiac structure, function, or biomarkers (80). Larger randomized studies of diflunisal in the ATTR-CA population are needed.

Tafamidis is a small molecule ligand in the benzoxazole family that exhibits potent and selective transthyretin binding, and lacks nonsteroidal anti-inflammatory drugs activity. Tafamidis inhibits wild-type transthyretin amyloidogenesis in a dose-dependent manner, and also stabilizes the 2 most clinically significant amyloidogenic mutant homotetramers (V30M and V122I) with comparable potency and efficacy (81). In a phase III trial of 441 patients with wild-type and hereditary ATTR-CA, tafamidis led to a reduction in all-cause mortality (HR: 0.70, 95% confidence interval: 0.51 to 0.96) and cardiovascular-related hospitalization (HR: 0.68, 95% confidence interval: 0.56 to 0.81), with a number-needed-to-treat for the combined endpoint of all-cause mortality and cardiovascular-related hospitalization of 7.5 (82). It remains unknown whether tafamidis is effective in advanced amyloid disease, as patients with New York Heart Association (NYHA) functional class IV HF were excluded; a small study of patients with advanced familial amyloid polyneuropathy showed no significant clinical improvement with tafamidis (83).

AG10 is a synthetic small molecule transthyretin ligand whose basic protein structure was identified by high-throughput screen, and subsequently modified with a carboxylic acid group on the 2-fluorophenyl ring to optimize binding energetics to transthyretin (84). AG10 binds to wild-type transthyretin with higher affinity than tafamidis or diflunisal; furthermore, AG10 stabilizes V122I mutant transthyretin tetramers more effectively than tafamidis and is also more effective in preventing V122I amyloid fibril formation (84). Both tafamidis and AG10 protect cardiomyocytes from the proteotoxic effects of amyloidogenic V122I transthyretin in vitro. AG10 is currently in a phase II clinical trial for hereditary and wild-type ATTR-CA (NCT03458130); a phase III trial in ATTR-CA is projected to open in early 2019.

Tolcapone is a catechol-O-methyltransferase inhibitor originally approved as an adjunct to levodopa and carbidopa for the treatment of Parkinson's disease. It binds to the thyroxine binding pocket at the transthyretin dimer-dimer interface with higher affinity than tafamidis, and is a stronger aggregation inhibitor than tafamidis (85). Similar to tafamidis, tolcapone inhibits aggregation of the V122I-transthyretin variant although with less efficacy than wild-type transthyretin. When incubated with human plasma, tolcapone prevents transthyretin tetramer dissociation for wild-type and V30M transthyretin with greater stabilizing activity than tafamidis. The unique ability of tolcapone to cross the blood-brain barrier indicates that it may treat transthyretin leptomeningeal amyloidosis, noting that the majority of transthyretin in the CSF is thyroxine bound. A phase II trial of tolcapone in familial amyloid polyneuropathy is ongoing (NCT02191826).

TRANSTHYRETIN SYNTHESIS INHIBITORS. Patisiran is a second-generation, double-stranded small interfering RNA that targets the 3' untranslated region of the transthyretin gene, which is conserved among wild-type transthyretin and all reported transthyretin mutations. Patisiran is modified with 2'-O-methyl ribonucleosides for improved stability and formulated in a lipid nanoparticle, which enables passage through the fenestrated vascular endothelium of the liver and targeted organ delivery (86). Endosomal endocytosis of the lipid nanoparticle delivers patisiran to the cytoplasm, where it triggers endogenous cellular pathways for controlling gene expression through RNA

interference. Specifically, binding of patisiran to the RNA-induced silencing complex triggers separation of the 2 RNA strands and allows for binding of the antisense strand to transthyretin mRNA. The double-stranded RNA substrate is then cleaved and targeted for degradation, leading to a reduction in transthyretin protein levels (87). In animal models, patisiran reduced transthyretin deposition and facilitated regression of existing transthyretin deposits, with the extent of deposit regression correlating with the level of RNA interference-mediated knockdown (88).

In a phase III trial of patients with hereditary ATTR with polyneuropathy, patisiran significantly improved neuropathy and quality of life after 18 months of therapy in the overall cohort and in the subgroup with cardiac involvement (56%; NYHA functional class III/IV were excluded) (86). Within the cardiac subpopulation, patisiran led to a statistically significant reduction in NT-proBNP level, left ventricular (LV) wall thickness, and reduced worsening in GLS, suggestive of cardiac benefit (89). Further study of patisiran in the ATTR-CA population with the use of clinically relevant cardiac endpoints is needed.

Inotersen is a second-generation antisense oligonucleotide that targets the 3' untranslated region of transthyretin mRNA. Its single-stranded synthetic oligomer contains 20 nucleotides with a modified phosphorothioate backbone as well as 2'-*O*-methoxyethyl modified ribonucleotides at each terminus, which confer increased hybridization affinity to target RNA, increased resistance to nuclease degradation, and reduced immunostimulatory activity (90). Systemically administered inotersen distributes at high levels to the liver, where it gains access to the intracellular space via endosome activity and then moves to the nucleus by passive diffusion and active transport due to its phosphorothioate backbone (91,92). Once bound to the target RNA through Watson-Crick base-pairing, inotersen forms an RNA-DNA hybrid that triggers target mRNA degradation by RNase H via a central region of 10 2'-deoxynucleotide residues that is recognized by the enzyme (93).

In a phase III trial of patients with hereditary ATTR with polyneuropathy, inotersen significantly improved neuropathy and quality of life after 16 months of therapy in the overall cohort and in the subgroup with cardiomyopathy (68%; NYHA functional class III/IV were excluded) (94). Within the cardiomyopathy subgroup, there was no significant change in LVEF, GLS, LV wall thickness, LV mass, or lateral E/E' ratio after 16 months of inotersen therapy, although baseline LVEF and GLS were relatively preserved at 64% and −14%, respectively. Thrombocytopenia and, rarely, glomerulonephritis are important safety concerns and should be monitored on a regular basis. The safety of inotersen in patients with a prior liver transplant for hereditary ATTR is not established. As with patisiran, further study of inotersen in the ATTR-CA population is needed.

CLEARANCE OF AMYLOID DEPOSITS. GSK2398852 is an anti-serum amyloid P component (SAP) antibody whose epitope is a glycoprotein in the pentraxin family, a group of highly evolutionarily conserved proteins that activate the innate immune response upon binding to microbial ligands, apoptotic cells, and amyloid fibrils (95,96). The pentraxins have also been found to promote amyloid deposition and disease progression in vivo (97). In a mouse model of systemic amyloidosis, depletion of circulating SAP followed by administration of anti-SAP monoclonal IgG1 antibody led to infiltration of macrophages and other monocytic inflammatory cells into tissue amyloid deposits in a complement-dependent fashion (98). The inflammatory process was characterized by high-phagocyte endocytotic activity and engulfment of amyloid deposits by multinucleated giant cells, culminating in complete clearance of amyloid tissue deposits and restoration of normal tissue architecture.

In a phase I trial, 16 subjects with systemic amyloidosis and significant amyloid infiltration of the liver and spleen received GSK2398852 after depletion of circulating SAP without excess toxicity (99). Patients with cardiac involvement were excluded from this study, and there were no significant changes in extracellular volume of the heart, troponin T, or NT-proBNP. However, a phase II trial of GSK2398852 in patients with biopsy- or bone scintigraphy-proven ATTR-CA was suspended prematurely due to an adverse risk/benefit profile (NCT03044353).

PRX004 is a humanized IgG1 mAb that targets an epitope exposed on abnormal transthyretin protein. In preclinical models, PRX004 neutralized soluble cytotoxic forms of transthyretin, prevented amyloid fibril formation, and promoted clearance of organ amyloid deposits via phagocytosis (unpublished data, courtesy of Prothena Corporation, May 2018). A phase I dose escalation trial is currently ongoing (NCT03336580).

FUTURE DIRECTIONS

With the emergence of multiple novel therapeutics for AL and ATTR, there is an urgent need to define optimal drug combinations and sequences of drug delivery to reduce morbidity and mortality amongst patients with AL-CA and ATTR-CA. This is particularly important in the treatment of AL-CA, although large randomized clinical trials in this population are challenging due to low disease prevalence and poor

performance status. Although initial therapy for AL with a bortezomib-based regimen versus ASCT is generally accepted, it remains unclear which regimens are optimal for relapsed/refractory disease (100) and how the novel AL therapeutics will fit into the treatment paradigm. It is likely that a multipronged treatment approach will be optimal for both AL-CA and ATTR-CA, and carefully executed clinical trials are needed to determine the optimal approach.

The impact of each novel therapeutic on cardiac biomarkers also requires clarification. NT-proBNP is an important cardiac biomarker that correlates inversely with prognosis in AL-CA and ATTR-CA (2,20). A paradoxical increase in NT-proBNP has been described in AL patients on lenalidomide despite hematologic response and absence of cardiac symptoms, possibly reflecting IMiD-induced fluid retention as opposed to direct cardiotoxicity (101,102). Additionally, a significant increase in NT-proBNP has been described in patients with advanced AL-CA on bortezomib, although it is unclear whether this represents drug toxicity or worsening of pre-existing cardiac disease (103). The utility of alternate cardiac biomarkers, such as troponin T, for assessment of drug-induced cardiotoxicity should be explored.

Finally, validated biomarkers that track with cardiac response to therapy are needed to rigorously assess the cardiac efficacy of emerging therapeutics in AL and ATTR. Challenges associated with NT-proBNP have been discussed, and also include optimal timing of NT-proBNP assessment (104). Whereas serial cardiac magnetic resonance imaging studies may be useful in clinical trials, this strategy is unlikely to be feasible in clinical practice. GLS by echocardiography has shown value for prognosis and diagnosis in CA, but its utility for tracking cardiac response to therapy has yet to be explored (105,106). Six-minute walk distance was better on tafamidis as compared with placebo in clinical trials and correlated with cardiac response to chemotherapy in AL (82,107), and could be implemented in future clinical trials and clinical practice as a marker of cardiac response to therapy.

CONCLUSIONS

Cardiac amyloidosis is a restrictive cardiomyopathy with high morbidity and mortality, and is increasingly recognized as an underdiagnosed condition. Although no therapies have been approved for AL- or ATTR-CA, a number of therapeutics targeted at neoplastic plasma cells, transthyretin protein production, and amyloid fibril formation are currently in clinical trials. Additionally, mAbs aiming to remove existing amyloid deposits may improve outcomes for patients with more advanced cardiac disease. Future efforts should define the optimal treatment paradigms for cardiac response in AL-CA and ATTR-CA, and identify effective clinical, imaging, and serum biomarker strategies that reflect cardiac response to therapy.

ADDRESS FOR CORRESPONDENCE: Dr. Kathleen W. Zhang, Division of Cardiology, Washington University in St. Louis School of Medicine, Campus Box 8086, 660 South Euclid Avenue, St. Louis, Missouri 63110-1093. E-mail: kwzhang@wustl.edu.

REFERENCES

1. Cibeira MT, Sanchorawala V, Seldin DC, et al. Outcome of AL amyloidosis after high-dose melphalan and autologous stem cell transplantation: long-term results in a series of 421 patients. Blood 2011;118:4346–52.

2. Gillmore JD, Damy T, Fontana M, et al. A new staging system for cardiac transthyretin amyloidosis. Eur Heart J 2017;44:1–8.

3. Hawkins PN, Ando Y, Dispenzeri A, Gonzalez-Duarte A, Adams D, Suhr OB. Evolving landscape in the management of transthyretin amyloidosis. Ann Med 2015;47:625–38.

4. Maurer MS, Elliott P, Comenzo R, Semigran M, Rapezzi C. Addressing common questions encountered in the diagnosis and management of cardiac amyloidosis. Circulation 2017;135:1357–77.

5. Mohammed SF, Mirzoyev SA, Edwards WD, et al. Left ventricular amyloid deposition in patients with heart failure and preserved ejection fraction. J Am Coll Cardiol HF 2014;2:113–22.

6. González-López E, Gallego-Delgado M, Guzzo-Merello G, et al. Wild-type transthyretin amyloidosis as a cause of heart failure with preserved ejection fraction. Eur Heart J 2015;36:2585–94.

7. Scully PR, Treibel TA, Fontana M, et al. Prevalence of cardiac amyloidosis in patients referred for transcatheter aortic valve replacement. J Am Coll Cardiol 2018;71:463–4.

8. Treibel TA, Fontana M, Gilbertson JA, et al. Occult transthyretin cardiac amyloid in severe calcific aortic stenosis: prevalence and prognosis in patients undergoing surgical aortic valve replacement. Circ Cardiovasc Imaging 2016:1–11.

9. Castano A, Narotsky DL, Hamid N, et al. Unveiling transthyretin cardiac amyloidosis and its predictors among elderly patients with severe aortic stenosis undergoing transcatheter aortic valve replacement. Eur Heart J 2017;38:2879–87.

10. Gillmore JD, Maurer MS, Falk RH, et al. Nonbiopsy diagnosis of cardiac transthyretin amyloidosis. Circulation 2016;133:2404–12.

11. Muller AMS, Geibel A, Neumann HPH, et al. Primary (AL) amyloidosis in plasma cell disorders. Oncologist 2006;11:824–30.

12. Kyle RA, Larson DR, Therneau TM, et al. Long-term follow-up of monoclonal gammopathy of undetermined significance. N Engl J Med 2018;378:241–9.

13. Fonseca R, Ahmann GJ, Jalal SM, et al. Chromosomal abnormalities in systemic amyloidosis. Br J Haematol 1998;103:704–10.

14. Avet-Loiseau H, Daviet A, Saunier S, Bataille R. Chromosome 13 abnormalities in multiple myeloma are mostly monosomy 13. Br J Haematol 2000;111:1116–7.

15. Perfetti V, Coluccia AML, Intini D, et al. Translocation t(4;14)(p16.3;q32) is a recurrent genetic lesion in primary amyloidosis. Am J Pathol 2001;158:1599–603.

16. Harrison CJ, Mazzullo H, Ross FM, et al. Translocations of 14q32 and deletions of 13q14 are common chromosomal abnormalities in systemic amyloidosis. Br J Haematol 2002;117:427–35.

17. Abraham RS, Ballman KV, Dispenzieri A, et al. Functional gene expression analysis of clonal

plasma cells identifies a unique molecular profile for light chain amyloidosis. Blood 2005;105:794.

18. Palladini G, Sachchithanantham S, Milani P, et al. A European collaborative study of cyclophosphamide, bortezomib, and dexamethasone in upfront treatment of systemic AL amyloidosis. Blood 2015;126:612–5.

19. Sidiqi MH, Aljama MA, Buadi FK, et al. Stem cell transplantation for light chain amyloidosis: decreased early mortality over time. J Clin Oncol 2018;36:1323–9.

20. Palladini G, Dispenzieri A, Gertz MA, et al. New criteria for response to treatment in immunoglobulin light chain amyloidosis based on free light chain measurement and cardiac biomarkers: Impact on survival outcomes. J Clin Oncol 2012; 30:4541–9.

21. Hashimura H, Ishibashi-Ueda H, Yonemoto Y, et al. Late gadolinium enhancement in cardiac amyloidosis: attributable both to interstitial amyloid deposition and subendocardial fibrosis caused by ischemia. Heart Vessels 2016;31:990–5.

22. Dubrey S, Falk RH. Amyloidosis and the heart. Br J Cardiol 1995;2:193–9.

23. Rajkumar SV, Richardson PG, Hideshima T, Anderson KC. Proteasome inhibition as a novel therapeutic target in human cancer. J Clin Oncol 2005;23:630–9.

24. Kupperman E, Lee EC, Cao Y, et al. Evaluation of the proteasome inhibitor MLN9708 in preclinical models of human cancer. Cancer Res 2010;70: 1970–80.

25. Moreau P, Masszi T, Grzasko N, et al. Oral ixazomib, lenalidomide, and dexamethasone for multiple myeloma. N Engl J Med 2016;374: 1621–34.

26. Sanchorawala V, Palladini G, Kukreti V, et al. A phase 1/2 study of the oral proteasome inhibitor ixazomib in relapsed or refractory AL amyloidosis. Blood 2017;130:597–606.

27. Stewart AK, Rajkumar SV, Dimopoulos MA, et al. Carfilzomib, lenalidomide, and dexamethasone for relapsed multiple myeloma. N Engl J Med 2015;372:142–52.

28. Cohen AD, Landau H, Scott EC, et al. Safety and efficacy of carfilzomib (CFZ) in previously-treated systemic light-chain (AL) amyloidosis. Blood 2016;128:645.

29. Stewart AK. How thalidomide works against cancer. Science 2014;343:256–7.

30. Sanchorawala V, Finn KT, Fennessey S, et al. Durable hematologic complete responses can be achieved with lenalidomide in AL amyloidosis. Blood 2010;116:1990–1.

31. Gay F, Mina R, Troia R, Bringhen S. Pharmacokinetic evaluation of pomalidomide for the treatment of myeloma. Expert Opin Drug Metab Toxicol 2013;9:1517–27.

32. Dispenzieri A, Buadi F, Laumann K, et al. Activity of pomalidomide in patients with immunoglobulin light-chain amyloidosis. Blood 2012;119: 5397–404.

33. Dispenzieri A, Lacy MQ, Zeldenrust SR, et al. The activity of lenalidomide with or without dexamethasone in patients with primary systemic amyloidosis. Blood 2007;109:465–70.

34. Deaglio S, Vaisitti T, Billington R, et al. CD38/CD19 : a lipid raft – dependent signaling complex in human B cells. Blood 2007;109:5390–8.

35. Lin P, Owens R, Tricot G, Wilson CS. Flow cytometric immunophenotypic analysis of 306 cases of multiple myeloma. Am J Clin Pathol 2004;121:482–8.

36. Lisenko K, Schönland SO, Jauch A, et al. Flow cytometry-based characterization of underlying clonal B and plasma cells in patients with light chain amyloidosis. Cancer Med 2016;5:1464–72.

37. de Weers M, Tai Y-T, van der Veer MS, et al. Daratumumab, a novel therapeutic human CD38 monoclonal antibody, induces killing of multiple myeloma and other hematological tumors. J Immunol 2011;186:1840–8.

38. Dimopoulos MA, Oriol A, Nahi H, et al. Daratumumab, lenalidomide, and dexamethasone for multiple myeloma. N Engl J Med 2016;375: 1319–31.

39. Palumbo A, Chanan-Khan A, Weisel K, et al. Daratumumab, bortezomib, and dexamethasone for multiple myeloma. N Engl J Med 2016;375: 754–66.

40. Kaufman GP, Schrier SL, Lafayette RA, Arai S, Witteles RM, Liedtke M. Daratumumab yields rapid and deep hematologic responses in patients with heavily pretreated AL amyloidosis. Blood 2017; 130:900–2.

41. Deckert J, Wetzel MC, Bartle LM, et al. SAR650984, a novel humanized CD38-targeting antibody, demonstrates potent antitumor activity in models of multiple myeloma and other CD38+ hematologic malignancies. Clin Cancer Res 2014; 20:4574–83.

42. Martin T, Baz R, Benson DM, et al. A phase 1b study of isatuximab plus lenalidomide and dexamethasone for relapsed/refractory multiple myeloma. Blood 2017;129:3294–303.

43. Malaer JD, Mathew PA. CS1 (SLAMF7, CD319) is an effective immunotherapeutic target for multiple myeloma. Am J Cancer Res 2017;7: 1637–41.

44. Hsi ED, Steinle R, Balasa B, et al. CS1, a potential new therapeutic antibody target for the treatment of multiple myeloma. Clin Cancer Res 2008;14:2775–84.

45. Tai Y-T, Dillon M, Song W, et al. Anti-CS1 humanized monoclonal antibody HuLuc63 inhibits myeloma cell adhesion and induces aritibody-dependent cellular cytotoxicity in the bone marrow mitieu. Blood 2008;112:1329–37.

46. Lonial S, Dimopoulos M, Palumbo A, et al. Elotuzumab therapy for relapsed or refractory multiple myeloma. N Engl J Med 2015;373:621–31.

47. Oltersdorf T, Elmore SW, Shoemaker AR, et al. An inhibitor of Bcl-2 family proteins induces regression of solid tumours. Nature 2005;435: 677–81.

48. Bodet L, Gomez-Bougie P, Touzeau C, et al. ABT-737 is highly effective against molecular subgroups of multiple myeloma. Blood 2011;118: 3901–10.

49. Touzeau C, Ryan J, Guerriero J, et al. BH3 profiling identifies heterogeneous dependency on Bcl-2 family members in multiple myeloma and predicts sensitivity to BH3 mimetics. Leukemia 2016;30:761–4.

50. Kaufman GP, Gertz MA, Dispenzieri A, et al. Impact of cytogenetic classification on outcomes following early high-dose therapy in multiple myeloma. Leukemia 2016;30:633–9.

51. Kumar S, Kaufman JL, Gasparetto C, et al. Efficacy of venetoclax as targeted therapy for relapsed/refractory t(11;14) multiple myeloma. Blood 2017;130:2401–9.

52. Moreau P, Chanan-Khan A, Roberts AW, et al. Promising efficacy and acceptable safety of venetoclax plus bortezomib and dexamethasone in relapsed/refractory MM. Blood 2017;130: 2392–400.

53. Keeling J, Herrera GA. Matrix metalloproteinases and mesangial remodeling in light chain-related glomerular damage. Kidney Int 2005;68:1590–603.

54. Biolo A, Ramamurthy S, Connors LH, et al. Matrix metalloproteinases and their tissue inhibitors in cardiac amyloidosis: relationship to structural, functional myocardial changes and to light chain amyloid deposition. Circ Heart Fail 2008;1:249–57.

55. Ward JE, Ren R, Toraldo G, et al. Doxycycline reduces fibril formation in a transgenic mouse model of AL amyloidosis. Blood 2011;118:6610–7.

56. Wechalekar AD, Whelan C. Encouraging impact of doxycycline on early mortality in cardiac light chain (AL) amyloidosis. Blood Cancer J 2017;7: 89–91.

57. Hrncic R, Wall J, Wolfenbarger DA, et al. Antibody-mediated resolution of light chain-associated amyloid deposits. Am J Pathol 2000; 157:1239–46.

58. Solomon A, Weiss DT, Wall JS. Therapeutic potential of chimeric amyloid-reactive monoclonal antibody 11-1F4. Clin Cancer Res 2003;9. 3831s LP–8s.

59. Edwards CV, Gould J, Langer AL, et al. Final analysis of the phase 1a/b study of chimeric fibril-reactive monoclonal antibody 11-1F4 in patients with relapsed or refractory AL amyloidosis. Blood 2017;130 suppl 1. 509 LP-509.

60. Shames S, Jeff G, Maurer MS, Lentzsch S. Cardiac response to chimeric fibril-reactive monoclonal antibody 11-1F4 in patients with AL amyloidosis with global longitudinal strain: results from the phase 1b trial. J Am Soc Echocardiogr 2018;31:B14.

61. Stuckey A, Williams A, Richey T, et al. Preliminary pharmacokinetic study of a bispecific peptide for pretargeting immunotherapy of amyloidosis using PreClinical SPECT/CT. J Nucl Med 2018;59 suppl 1:1834.

62. Wall JS, Kennel SJ, Richey T, et al. Generation and characterization of anti-AA amyloid-specific monoclonal antibodies. Front Immunol 2011;2: 1–11.

63. Renz M, Torres R, Dolan PJ, et al. 2A4 binds soluble and insoluble light chain aggregates from AL amyloidosis patients and promotes clearance of

amyloid deposits by phagocytosis. Amyloid 2016;23:168–77.

64. Wall JS, Kennel SJ, Williams A, et al. AL amyloid imaging and therapy with a monoclonal antibody to a cryptic epitope on amyloid fibrils. PLoS One 2012;7.

65. Gertz MA, Landau H, Comenzo RL, et al. First-in-human phase I/II study of NEOD001 in patients with light chain amyloidosis and persistent organ dysfunction. J Clin Oncol 2016;34:1097–103.

66. Varga C, Lentzsch S, Comenzo RL. Beyond NEOD001 for systemic light-chain amyloidosis. Blood 2018;132:1992–3.

67. Purkey HE, Dorrell MI, Kelly JW. Evaluating the binding selectivity of transthyretin amyloid fibril inhibitors in blood plasma. Proc Natl Acad Sci U S A 2001;98:5566–71.

68. Hamilton JA, Benson MD. Transthyretin: a review from a structural perspective. Cell Mol Life Sci 2001;58:1491–521.

69. Klabunde T, Petrassi HM, Oza VB, Raman P, Kelly JW, Sacchettini JC. Rational design of potent human transthyretin amyloid disease inhibitors. Nat Struct Biol 2000;7:312–21.

70. Colon W, Kelly JW. Partial denaturation of transthyretin is sufficient for amyloid fibril formation in vitro. Biochemistry 1992;31:8654–60.

71. Lai Z, Colón W, Kelly JW. The acid-mediated denaturation pathway of transthyretin yields a conformational intermediate that can self-assemble into amyloid. Biochemistry 1996;35:6470–82.

72. Miroy GJ, Lai Z, Lashuel HA, Peterson SA, Strang C, Kelly JW. Inhibiting transthyretin amyloid fibril formation via protein stabilization. Proc Natl Acad Sci U S A 1996;93:15051–6.

73. Hammarstrom P, Jiang X, Hurshman AR, Powers ET, Kelly JW. Sequence-dependent denaturation energetics: a major determinant in amyloid disease diversity. Proc Natl Acad Sci U S A 2002;99 suppl 4:16427–32.

74. Coelho T. Familial amyloid polyneuropathy: new developments in genetics and treatment. Curr Opin Neurol 1996;9:355–9.

75. Holmgren G, Costa PM, Andersson C, et al. Geographical distribution of TTR met30 carriers in northern Sweden: discrepancy between carrier frequency and prevalence rate. J Med Genet 1994;31:351–4.

76. Hammarström P, Schneider F, Kelly JW. Trans-suppression of misfolding in an amyloid disease. Science 2001;293:2459–62.

77. Peterson SA, Klabunde T, Lashuel HA, Purkey H, Sacchettini JC, Kelly JW. Inhibiting transthyretin conformational changes that lead to amyloid fibril formation. Proc Natl Acad Sci U S A 1998;95:12956–60.

78. Sekijima Y, Dendle MA, Kelly JW. Orally administered diflunisal stabilizes transthyretin against dissociation required for amyloidogenesis. Amyloid 2006;1:236–49.

79. Berk JL, Suhr OB, Obici L, et al. Repurposing diflunisal for familial amyloid polyneuropathy. JAMA 2013;310:2658.

80. Castaño A, Helmke S, Alvarez J, Delisle S, Maurer MS. Diflunisal for ATTR cardiac amyloidosis. Congest Hear Fail 2012;18:315–9.

81. Bulawa CE, Connelly S, DeVit M, et al. Tafamidis, a potent and selective transthyretin kinetic stabilizer that inhibits the amyloid cascade. Proc Natl Acad Sci U S A 2012;109:9629–34.

82. Maurer MS, Schwartz JH, Gundapaneni B, et al. Tafamidis treatment for patients with transthyretin amyloid cardiomyopathy. N Engl J Med 2018;379:1007–16.

83. Lozeron P, Théaudin M, Mincheva Z, Ducot B, Lacroix C, Adams D. Effect on disability and safety of tafamidis in late onset of Met30 transthyretin familial amyloid polyneuropathy. Eur J Neurol 2013;20:1539–45.

84. Penchala SC, Connelly S, Wang Y, et al. AG10 inhibits amyloidogenesis and cellular toxicity of the familial amyloid cardiomyopathy-associated V122I transthyretin. Proc Natl Acad Sci U S A 2013;110:9992–7.

85. Sant'Anna R, Gallego P, Robinson LZ, et al. Repositioning tolcapone as a potent inhibitor of transthyretin amyloidogenesis and associated cellular toxicity. Nat Commun 2016;7:10787.

86. Adams D, Gonzalez-Duarte A, O'Riordan WD, et al. Patisiran, an RNAi therapeutic, for hereditary transthyretin amyloidosis. N Engl J Med 2018;379:11–21.

87. Bumcrot D, Manoharan M, Koteliansky V, Sah DWY. RNAi therapeutics: a potential new class of pharmaceutical drugs. Nat Chem Biol 2006;2:711–9.

88. Butler JS, Chan A, Costelha S, et al. Preclinical evaluation of RNAi as a treatment for transthyretin-mediated amyloidosis. Amyloid 2016;23:109–18.

89. Solomon SD, Adams D, Kristen A, et al. Effects of patisiran, an RNA interference therapeutic, on cardiac parameters in patients with hereditary transthyretin-mediated amyloidosis: an analysis of the APOLLO study. Circulation 2019;139:431–43.

90. Rinaldi C, Wood MJA. Antisense oligonucleotides: the next frontier for treatment of neurological disorders. Nat Rev Neurol 2018;14:9–21.

91. Hartig R, Shoeman RL, Janetzko A, Grub S, Traub P. Active nuclear import of single-stranded oligonucleotides and their complexes with nonkaryophilic macromolecules. Biol Cell 1998;90:407–26.

92. Lorenz P, Misteli T, Baker BF, Bennett CF, Spector DL. Nucleocytoplasmic shuttling: a novel in vivo property of antisense phosphorothioate oligodeoxynucleotides. Nucleic Acids Res 2000;28:582–92.

93. Wu H, Lima WF, Zhang H, Fan A, Sun H, Crooke ST. Determination of the role of the human RNase H1 in the pharmacology of DNA-like antisense drugs. J Biol Chem 2004;279:17181–9.

94. Benson MD, Waddington-Cruz M, Berk JL, et al. Inotersen treatment for patients with hereditary transthyretin amyloidosis. N Engl J Med 2018;379:22–31.

95. Wade WF. Pattern Recognition Receptors and the Innate Immune Network. In: Tang W-F, editor. Molecular Medical Microbiology (Second Edition) Vol. 1. Philadelphia, Pennsylvania: Elsevier Ltd., 2015:449–74.

96. Pepys MB, Dyck RF, de Beer FC, Skinner M, Cohen AS. Binding of serum amyloid P-component (SAP) by amyloid fibrils. Clin Exp Immunol 1979;38:284–93.

97. Botto M, Hawkins PN, Bickerstaff MC, et al. Amyloid deposition is delayed in mice with targeted deletion of the serum amyloid P component gene. Nat Med 1997;3:855–9.

98. Bodin K, Ellmerich S, Kahan MC, et al. Antibodies to human serum amyloid P component eliminate visceral amyloid deposits. Nature 2010;468:93–7.

99. Richards DB, Cookson LM, Berges AC, et al. Therapeutic clearance of amyloid by antibodies to serum amyloid P component. N Engl J Med 2015;373:1106–14.

100. Milani P, Gertz MA, Merlini G, Dispenzieri A. Attitudes about when and how to treat patients with AL amyloidosis: an international survey. Amyloid 2017;24:213–6.

101. Dispenzieri A, Dingli D, Kumar SK, et al. Discordance between serum cardiac biomarker and immunoglobulin-free light-chain response in patients with immunoglobulin light-chain amyloidosis treated with immune modulatory drugs. Am J Hematol 2010;85:757–9.

102. Tapan U, Seldin DC, Finn KT, et al. Increases in B-type natriuretic peptide (BNP) during treatment with lenalidomide in AL amyloidosis. Blood 2010;116:3021.

103. Hussain AS, Hari P, Brazauskas R, et al. Changes in cardiac biomarkers with bortezomib treatment in patients with advanced cardiac amyloidosis. Am J Hematol 2015;90:E212–3.

104. Wechalekar A, Foard D, Whelan C, et al. Challenges of using NT-Probnp for response assessment in systemic AL amyloidosis — analysis of a prospective study. Blood 2016;128:4511.

105. Barros-Gomes S, Williams B, Nhola LF, et al. Prognosis of light chain amyloidosis with preserved LVEF: added value of 2D speckle-tracking echocardiography to the current prognostic staging system. J Am Coll Cardiol Img 2017;10:398–407.

106. Phelan D, Collier P, Thavendiranathan P, et al. Relative apical sparing of longitudinal strain using two-dimensional speckle-tracking echocardiography is both sensitive and specific for the diagnosis of cardiac amyloidosis. Heart 2012;98:1442–8.

107. Decker I, Goodman SA, Phillips SE, Lenihan DJ, Cornell RF. The six-minute walk test is a valuable measure of functional change following chemotherapy for AL (light-chain) cardiac amyloidosis. Br J Haematol 2017;177:481–3.

KEY WORDS cardiac amyloidosis, clinical trials, therapeutics

JACC: BASIC TO TRANSLATIONAL SCIENCE VOL. 4, NO. 3, 2019

STATE-OF-THE-ART REVIEW

Fibroblasts in the Infarcted, Remodeling, and Failing Heart

Claudio Humeres, PhD, Nikolaos G. Frangogiannis, MD

HIGHLIGHTS

- **Cardiac fibroblasts become activated following injury and participate in repair and remodeling of the heart.**
- **The authors discuss the phenotypic alterations and role of fibroblasts in infarcted and failing hearts.**
- **In failing hearts, fibroblasts may deposit ECM proteins, increasing myocardial stiffness, but may also exert protective and reparative actions.**
- **Future studies will focus on characterization of the phenotypic heterogeneity of cardiac fibroblasts that may explain their functional diversity.**

SUMMARY

Expansion and activation of fibroblasts following cardiac injury is important for repair but may also contribute to fibrosis, remodeling, and dysfunction. The authors discuss the dynamic alterations of fibroblasts in failing and remodeling myocardium. Emerging concepts suggest that fibroblasts are not unidimensional cells that act exclusively by secreting extracellular matrix proteins, thus promoting fibrosis and diastolic dysfunction. In addition to their involvement in extracellular matrix expansion, activated fibroblasts may also exert protective actions, preserving the cardiac extracellular matrix, transducing survival signals to cardiomyocytes, and regulating inflammation and angiogenesis. The functional diversity of cardiac fibroblasts may reflect their phenotypic heterogeneity. (J Am Coll Cardiol Basic Trans Science 2019;4:449–67) © 2019 The Authors. Published by Elsevier on behalf of the American College of Cardiology Foundation. This is an open access article under the CC BY-NC-ND license (http://creativecommons.org/licenses/by-nc-nd/4.0/).

Most myocardial conditions are associated with "fibrosis," expansion of the cardiac interstitium, due to deposition of extracellular matrix (ECM) proteins (1-3). In human patients with a wide variety of cardiac diseases, the extent of fibrotic changes is a strong predictor of adverse outcome. In patients with heart failure with reduced ejection fraction, and in those with heart failure with preserved ejection fraction, prominent fibrotic remodeling is associated with higher mortality, increased hospitalization rates, and an increased incidence of adverse cardiac events (4-7). Moreover, in subjects with diabetes, expansion of the myocardial interstitial space is associated with mortality and with heart failure hospitalizations (8). The association between fibrosis and poor prognosis may reflect the adverse functional consequences of ECM deposition on systolic and diastolic function or the proarrhythmic effects of fibrotic myocardial lesions. However, because the adult mammalian heart

From The Wilf Family Cardiovascular Research Institute, Department of Medicine (Cardiology), Albert Einstein College of Medicine, Bronx, New York. Dr. Frangogiannis's laboratory is supported by National Institutes of Health grants R01 HL76246 and R01 HL85440 and by U.S. Department of Defense grants PR151134 and PR151029. Dr. Humeres is supported by American Heart Association post-doctoral award 19POST34450144. The authors have reported that they have no relationships relevant to the contents of this paper to disclose.

All authors attest they are in compliance with human studies committees and animal welfare regulations of the authors' institutions and U.S. Food and Drug Administration guidelines, including patient consent where appropriate. For more information, visit the *JACC: Basic to Translational Science* author instructions page.

Manuscript received November 19, 2018; revised manuscript received February 15, 2019, accepted February 19, 2019.

ISSN 2452-302X https://doi.org/10.1016/j.jacbts.2019.02.006

ABBREVIATIONS AND ACRONYMS

AT1 = angiotensin type 1

ECM = extracellular matrix

FAK = focal adhesion kinase

FGF = fibroblast growth factor

IL = interleukin

lncRNA = long noncoding ribonucleic acid

MAPK = mitogen-activated protein kinase

miRNA = micro-ribonucleic acid

MRTF = myocardin-related transcription factor

PDGF = platelet-derived growth factor

RNA = ribonucleic acid

ROCK = Rho-associated coiled-coil containing kinase

ROS = reactive oxygen species

SMA = smooth muscle actin

TGF = transforming growth factor

TRP = transient receptor potential

lacks significant endogenous regenerative capacity, cardiac fibrosis may also reflect activation of reparative mechanisms in response to primary cardiomyocyte injury. To what extent fibrotic cardiac remodeling represents a primary myocardial disease that mediates dysfunction and causes adverse outcome remains unknown.

Fibroblasts are the main effector cells of cardiac fibrosis. The adult mammalian heart contains abundant fibroblasts that expand following injury and can produce large amounts of ECM proteins. Animal model studies have identified cardiac fibroblasts both as critical reparative cells that maintain the structural integrity of the infarcted ventricle and as cellular effectors of heart failure that deposit stiff ECM in the interstitium, reducing myocardial compliance. The functional heterogeneity of fibroblast populations, their remarkable phenotypic plasticity, and the limited information on the characteristics and properties of fibroblasts in human myocardial diseases have hampered dissection of reparative and maladaptive fibroblast actions. In this review we describe the role of fibroblasts in failing and remodeling hearts. We discuss the dynamic alterations of fibroblasts in injury and repair of the infarcted heart and their role in remodeling and dysfunction of the ventricle in conditions associated with chronic heart failure.

FIBROBLASTS IN CARDIAC HOMEOSTASIS

Fibroblasts are defined and identified on the basis of functional and morphological criteria as cells of mesenchymal origin that lack a basement membrane and are involved in the formation and maintenance of connective tissues by producing a wide range of ECM proteins (9). Although several fibroblast markers have been proposed (**Table 1**), their specificity is limited. Moreover, considering that resident fibroblast populations in many tissues are heterogeneous (10) and undergo dynamic phenotypic changes following injury, identification of reliable markers that label all fibroblast subsets is a major challenge. Thus, characterization of fibroblasts typically requires the combined use of fibroblast-related markers (including ECM proteins that reflect their matrix-synthetic function) and exclusion criteria reflecting the absence of expression of endothelial, hematopoietic cell and vascular mural cell-specific proteins.

The myocardium contains a large population of resident fibroblasts enmeshed within the ECM network (11,12). For many years, fibroblasts were considered the most abundant noncardiomyocytes in the adult mammalian myocardium. A study using flow cytometry in adult mice identified 27% of myocardial cells as discoidin domain-containing receptor 2-positive fibroblasts and only 7% of the cells as $CD31^{+}$ endothelial cells (13), a finding quite surprising considering the high vascular content of the mammalian heart. In contrast, a more recent study using a combination of fibroblast reporter mouse models and cell-specific antibodies suggested that cardiac fibroblasts represent <20% of noncardiomyocytes and are greatly outnumbered by endothelial cells (which represent more than 60% of noncardiomyocytes) (14). Differences in the strategies used for cardiac cell isolation, and variability in the sensitivity and specificity of the methodological approaches used for cellular identification, may account, at least in part, for conflicting results in various investigations. Moreover, the relative numbers of various interstitial cell populations in the myocardium are also dependent on the age, sex, and species of the subjects studied. It should be emphasized that most of our knowledge on the characteristics of cardiac fibroblasts is based on studies in rodents, and relatively little is known regarding the density, phenotype, and distribution of fibroblasts in normal human hearts.

What is the function of resident fibroblasts in normal mammalian hearts? In the developing myocardium, cardiac fibroblasts have been suggested to regulate cardiomyocyte proliferation through a fibronectin/β_1-integrin-mediated pathway (15). In adult hearts, normal cardiac function may require interactions between cardiomyocytes and the surrounding ECM. Cardiac fibroblasts, enmeshed into the endomysium and perimysium, may play an important role in regulation of the synthesis and turnover of ECM components, thus preserving the structural integrity of the ventricle (16–18). Mice with global germline loss of transcription factor 21, which is essential for cardiac fibroblast development, had greatly decreased collagen levels in the cardiac interstitium and exhibited dysmorphic hearts that lacked a distinct apex (19). Although these findings are consistent with an important role of fibroblasts in cardiac development, the consequences of fibroblast depletion on cardiac homeostasis in adult mice have not been investigated.

In addition to their critical role in the formation of the cardiac ECM network, fibroblasts may also contribute to cellular communication in the cardiac

TABLE 1 Sensitivity and Specificity of Markers Used to Identify Cardiac Fibroblasts

Marker	Sensitivity	Specificity
Vimentin	Labels all fibroblasts (180,181).	Also expressed by other cells of mesenchymal origin (endothelial cells [182], vascular smooth muscle cells [183], etc.).
α-SMA	Expressed by activated myofibroblasts in fibrotic hearts (22,41,138). Not expressed by quiescent fibroblasts (137).	Also expressed by vascular mural cells.
Col1α1	Synthesis of structural collagens is a hallmark of fibroblasts in normal and remodeling hearts (42,141).	Although synthesis of structural collagens by cells other than fibroblasts has been reported, expression of Col1α1 in cardiac endothelial cells, immune cells, vascular smooth muscle cells, and pericytes is negligible when compared to fibroblasts (141). Because of labeling of the surrounding matrix, antibodies to collagens may be suboptimal for fibroblast identification. Col1α1-GFP reporter mice represent a robust tool for identification of fibroblasts in many organs, including the heart (42).
Periostin	Expressed by fibroblasts in neonatal hearts but not by fibroblasts in normal adult hearts (184). Highly expressed in activated cardiac fibroblasts after injury (185,186).	May also be expressed by subsets of vascular smooth muscle cells (187).
Fibronectin ED-A	Highly expressed by activated myofibroblasts (188).	Deposited in the matrix (189). May also colocalize with macrophages, endothelial cells, and other cell types (190,191).
PDGFRα	Highly expressed in cardiac fibroblasts in normal (41) and pressure-overloaded myocardium (141).	Although vascular smooth muscle cells have been reported to express PDGFRα, especially under conditions of stress (192), PDGFRα-GFP reporter lines seem to predominantly identify cells with fibroblast-like characteristics (193).
DDR2	High expression in cardiac fibroblasts in normal adult hearts (194), colocalizing with vimentin and col1α1 (195). May also be expressed in various subpopulations of infarct fibroblasts and myofibroblasts (196).	DDR2 expression has been reported in activated endothelial cells (197) and in stretched vascular smooth muscle cells (198). It is unclear whether this affects the specificity of DDR2 for fibroblasts in injured and remodeling hearts.
Antigen recognized by MEFSK4	The MEFSK4 antibody labels through flow cytometry almost all PDGFRα+, Col1α1+ cardiac fibroblasts (14). No antibodies are available for immunohistochemistry.	MEFSK4 has been reported to label a small subpopulation of pericytes (14).
Cluster of differentiation 90 (Thy1)	Identifies a subpopulation of fibroblasts in the normal and remodeling myocardium (14,141,199,200).	Also expressed by immune cells, lymphatic endothelial cells, and pericytes (201).
Sca1	Identifies a subpopulation (~60%) of PDGFRα+, Col1α1+ fibroblasts in the murine heart (14).	Lacks specificity. In Sca1-GFP reporter mice, Sca1 expression colocalized with endothelial and pericyte markers (202).
Tcf21	Labels the majority of fibroblast-like cells in normal myocardium (19). In infarcted and pressure-overloaded hearts, accumulation of Tcf21+ fibroblast-like cells is noted; however, according to a single report, Tcf21 may not label activated α-SMA+ myofibroblasts (203).	Relatively specific for fibroblast populations. Not expressed by immune cells (CD45+) (203), endothelial cells, and vascular smooth muscle cells (19).
FSP1	No expression in fibroblasts in the normal adult myocardium. In the infarcted and pressure-overloaded heart, there is a marked expansion of FSP1+ cells. The majority of these cells cannot be identified as α-SMA+ myofibroblasts (141,184).	Lacks specificity. The majority of FSP1+ cells in injured and remodeling hearts are endothelial cells, macrophages, and vascular smooth muscle cells (184,204).
FAP	Not expressed in normal cardiac fibroblasts (174). Labels many activated fibroblasts in infarcted rat hearts and in human myocardial samples from patients with post-infarction heart failure (205).	Specific for activated fibroblasts. However, in human failing hearts, FAP expression has been reported in small populations of inflammatory cells and endothelial cells (205).

Col1α1 = collagen 1α1; DDR2 = discoidin domain receptor 2; FAP = fibroblast-activation protein; FSP1 = fibroblast-specific protein 1; GFP = green fluorescent protein; PDGFRα = platelet-derived growth factor α; Sca1 = stem cell antigen-1; SMA = smooth muscle actin; Tcf21 = transcription factor 21.

syncytium. Given their strategic location in the interstitium, cardiac fibroblasts have been suggested to facilitate communication between myocardial layers (20). Cardiac fibroblasts express high levels of connexins (connexin-40, connexin-43, and connexin-45) and establish functional gap junctional channels with neighboring cardiomyocytes, modulating their electrophysiological properties (21). Thus, fibroblasts may act as electric couplers of myocytes from different regions that would normally be isolated by connective tissue, contributing to the synchronization of the contraction.

PHENOTYPIC CHANGES AND ROLE OF CARDIAC FIBROBLASTS IN THE INFARCTED MYOCARDIUM

Fibroblasts exhibit remarkable phenotypic plasticity and undergo dramatic alterations in their gene expression profile and functional properties in response to mechanical stress or to stimulation with soluble mediators. In vitro, cardiac fibroblasts cultured in the low-tension environment of a collagen-based pad have dendritic morphology, synthesize low levels of collagen, and have negligible

expression of myofibroblast markers, such as α-smooth muscle actin (SMA) (22). In contrast, when cultured in plates, fibroblasts undergo conversion to myofibroblasts, exhibiting activation of mechanosensitive signaling pathways that trigger incorporation of α-SMA into stress fibers and induce synthesis of ECM proteins. In vivo, cardiac fibroblasts respond to changes in their microenvironment by acquiring a wide range of phenotypic profiles, thus serving as inflammatory, matrix-synthetic, or proangiogenic cells depending on the context (**Central Illustration**).

In myocardial infarction, sudden occlusion of a coronary artery results in the death of up to 1 billion cardiomyocytes, triggering an intense inflammatory reaction (23). Because the massive loss of cardiomyocytes overwhelms the extremely limited regenerative potential of the adult mammalian heart, the infarcted myocardium heals through formation of a scar. Thus, repair of the infarcted heart is dependent on a well-orchestrated cellular response, composed of 3 distinct but overlapping phases. During the inflammatory phase, innate immune activation in response to release of damage-associated molecular patterns by dying cardiomyocytes and degraded ECM triggers cytokine and chemokine induction and recruits leukocytes that clear the infarct from necrotic and apoptotic cells and remove matrix debris (24). Macrophages phagocytosing apoptotic cells undergo transition to an anti-inflammatory phenotype, mediating suppression of inflammation and activation of a reparative program that orchestrates the proliferative phase of cardiac repair, characterized by expansion of myofibroblasts and vascular cells. The maturation phase follows and is associated with quiescence of fibroblasts, recruitment of mural cells by infarct neovessels, and formation of a crosslinked collagenous scar (25). During the 3 phases of infarct healing, cardiac fibroblasts undergo rapid phenotypic transitions from quiescence to a pro-inflammatory and matrix-degrading phenotype to a matrix-synthetic myofibroblast phenotype, only to revert to quiescence as the scar matures. Emerging evidence suggests that fibroblasts do not simply follow the changes in their microenvironment but serve as critical regulators of the cellular events in every phase of cardiac repair (26).

THE FIBROBLASTS IN THE INFLAMMATORY PHASE OF INFARCT HEALING. Fibroblasts are capable of producing large amounts of proinflammatory cytokines and chemokines in response to stimulation with reactive oxygen species (ROS), Toll-like receptor ligands, or interleukin (IL)-1β (27–29). During the early post-ischemic phase, interstitial fibroblasts may sense damage-associated molecular patterns released by dying cardiomyocytes, activating a proinflammatory program (**Figure 1**). Considering that several other cell types, including cardiomyocytes, endothelial cells, immune cells, and vascular mural cells, can also secrete proinflammatory mediators (30), the relative role of resident cardiac fibroblasts as inflammatory cells remains unclear. In vivo studies have suggested that infarct fibroblasts may exhibit activation of the NRLP3 inflammasome (31,32), thus serving as an important source of active IL-1β, a critical proinflammatory cytokine in the infarcted myocardium (33). A recent study suggested that fibroblasts may stimulate leukocyte recruitment in the infarcted myocardium by secreting large amounts of granulocyte/macrophage colony-stimulating factor (34). To what extent proinflammatory fibroblasts also contribute other chemokines or cytokines to the infarct environment remains unknown. Cytokine-activated proinflammatory fibroblasts also secrete proteases that play an important role in clearance of the infarct from matrix debris (35). Associative data have suggested that in addition to their role as proinflammatory and matrix-degrading cells, fibroblasts may protect cardiomyocytes from ischemic injury (36). The molecular signals responsible for the prosurvival actions are unclear.

THE ROLE OF FIBROBLASTS IN THE PROLIFERATIVE PHASE OF INFARCT HEALING. The potential role of infarct fibroblasts in phagocytosis and suppression of inflammation. Activation of the post-infarction inflammatory reaction is followed by rapid suppression of proinflammatory gene synthesis and subsequent resolution of the leukocytic infiltrate, marking the transition to the proliferative phase of infarct healing. Phagocytosis of apoptotic cells plays a key role in downmodulation of inflammation, stimulating release of anti-inflammatory signals, such as IL-10 and transforming growth factor (TGF)-β. To what extent fibroblasts participate in repression and resolution of post-infarction inflammation remains unknown. A recent study suggested that activated fibroblasts may serve as phagocytes, engulfing apoptotic cells from the infarct zone (37). Considering the abundance of phagocytic macrophages in the healing infarct (38), the relative contribution of fibroblasts in clearance of dead cells is unclear. Whether any phagocytic actions of fibroblasts are accompanied by secretion of IL-10 or TGF-β and by acquisition of an anti-inflammatory phenotype has not been investigated.

CENTRAL ILLUSTRATION **Functional Diversity of Fibroblasts in the Infarcted Myocardium**

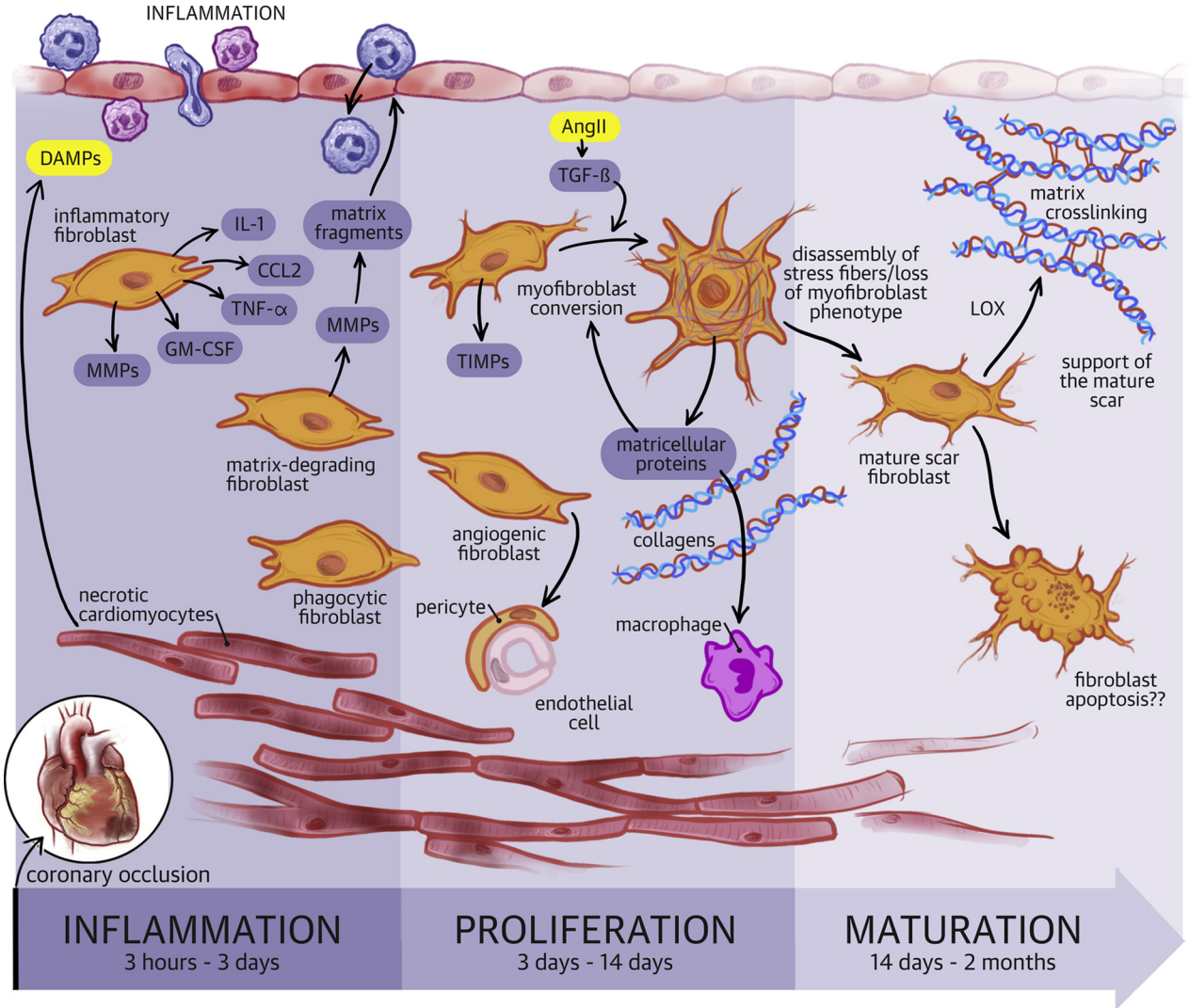

Humeres, C. et al. J Am Coll Cardiol Basic Trans Science. 2019;4(3):449–67.

In the dynamic environment of the infarcted heart, cardiac fibroblasts expand, undergo phenotypic changes, and are implicated in a wide range of functions. Coronary occlusion causes death of cardiomyocytes in the area of injury. During the inflammatory phase of infarct healing, Damage-Associated Molecular Patterns (DAMPs) released by dying cells activate a pro-inflammatory phenotype in cardiac fibroblasts that secrete cytokines (such as IL-1, TNF-α, and GM-CSF), and chemokines (such as CCL2) contributing to recruitment and activation of leukocytes. Cytokine-stimulated fibroblasts also secrete matrix metalloproteinases (MMPs), promoting extracellular matrix degradation and release of pro-inflammatory matrix fragments. Some studies have suggested that infarct fibroblasts may also function as phagocytic cells; however, considering the abundance of macrophages in the healing infarct the relative contribution of "phagocytic fibroblasts" remains unclear. Clearance of the infarcted heart from dead cells stimulates anti-inflammatory signals, leading to suppression of inflammation and transition to the proliferative phase of infarct healing. Fibroblasts expand, predominantly through recruitment of resident populations and undergo myofibroblast conversion, incorporating α-SMA into cytoskeletal stress fibers. Activated myofibroblasts are the main matrix-synthetic cells in the infarcted heart and produce both structural extracellular matrix proteins and matricellular macromolecules. In addition to their contribution in matrix production, fibroblast populations may also contribute to regulation of the angiogenic response and may regulate macrophage phenotype. During scar maturation fibroblasts exhibit disassembly of α-SMA-decorated stress fibers, and may produce matrix-crosslinking enzymes such as lysyl-oxidases (LOX). Reduction of fibroblast numbers in mature scars has been suggested to involve activation of apoptosis. The molecular basis for the phenotypic transitions of cardiac fibroblasts in the phases of infarct healing remains poorly understood. The functional diversity of fibroblasts in the infarcted heart may reflect sequential activation of distinct fibroblast subpopulations, or may result from coordinated responses of the fibroblasts to the dynamic changes in their microenvironment.

FIGURE 1 Fibroblasts in the Inflammatory Phase of Infarct Healing

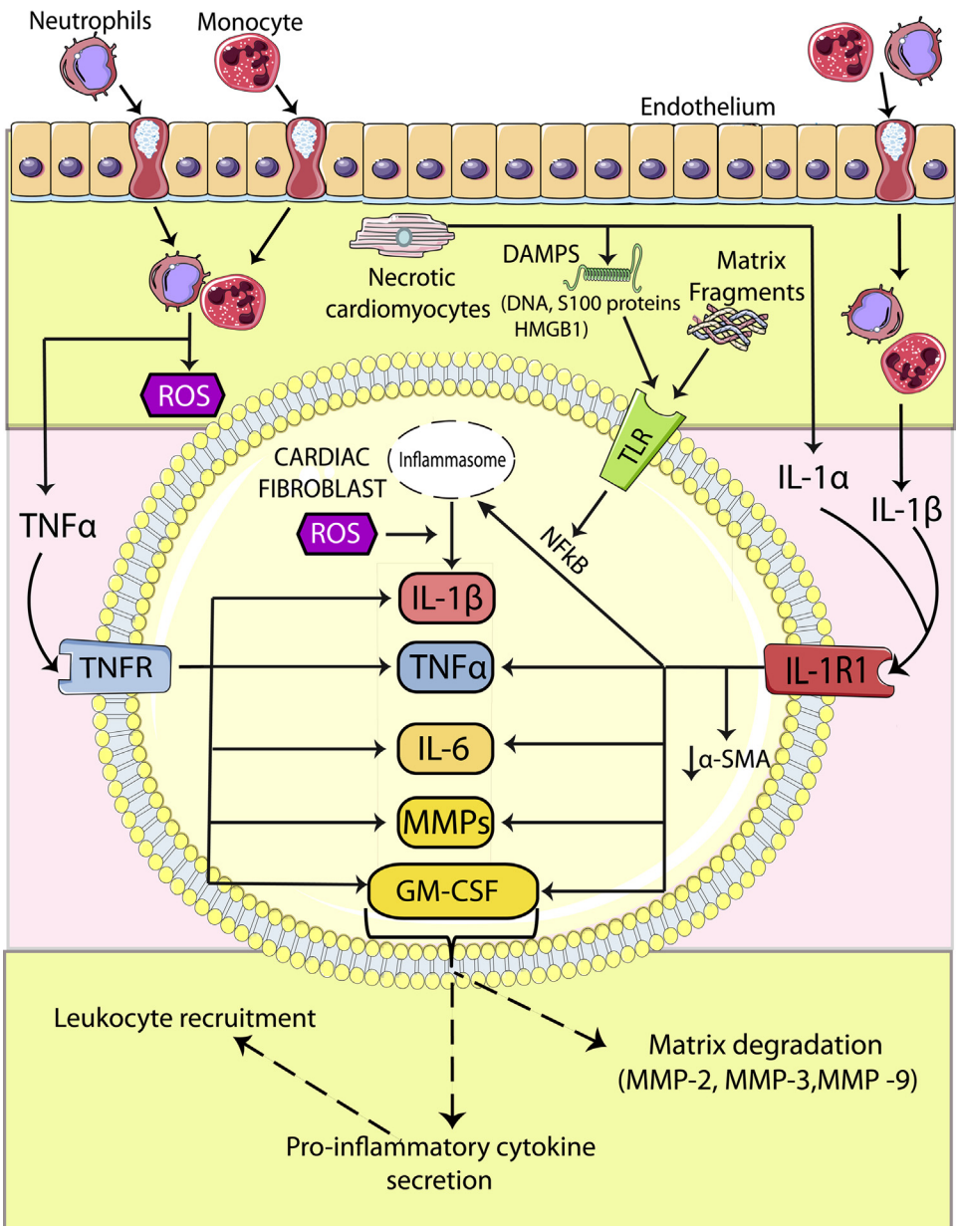

During the inflammatory phase of infarct healing, cardiac fibroblasts secrete proinflammatory mediators and matrix-degrading proteases. Damage-associated molecular patterns (DAMPs) released by necrotic cells and matrix fragments activate Toll-like receptor signaling in cardiac fibroblasts. Proinflammatory cytokines (such as interleukin [IL]-1β and tumor necrosis factor [TNF]-α) released by endothelial cells, immune cells, and cardiomyocytes and activation of reactive oxygen species (ROS) accentuate fibroblast inflammatory activity. IL-1/IL-1RI signaling has been suggested to reduce α-smooth muscle actin (α-SMA) expression, preventing myofibroblast conversion. Cytokines and chemokines (such as IL-1β, TNF-α, IL-6, and granulocyte/macrophage colony-stimulating factor [GM-CSF]) secreted by activated fibroblasts may contribute to the recruitment of leukocytes, whereas protease release may promote matrix degradation. Considering that several other cell types are capable of secreting inflammatory mediators, the relative contribution of fibroblasts is unclear. The cartoon was designed using Servier Medical Art (https://smart.servier.com). DNA = deoxyribonucleic acid; HMGB1 = high-mobility group protein B1; MMP = matrix metalloproteinase; TNFR = tumor necrosis factor receptor.

TABLE 2 Cellular Origin of Fibroblasts in Myocardial Infarction

Reference #	Main Conclusions of the Study	Strategies Used to Study the Cellular Origin of Infarct Fibroblasts	Markers Used for Fibroblast Identification
(41)	Activated fibroblasts in infarcted and remodeling hearts are derived from Tcf21^{+} tissue-resident fibroblasts. Endothelial cells, myeloid cells, and smooth muscle cells do not significantly contribute to the activated fibroblast population.	Lineage-tracing analysis using Cre drivers to study the fate of resident cardiac fibroblasts (Tcf21^{MCM}), activated myofibroblasts (Postn^{MCM}), myeloid cells (LysM^{Cre}), endothelial cells (Cdh5^{Cre}), and vascular smooth muscle cells (Myh11^{CreERT2}).	Vimentin, PDGFRα, α-SMA, FSP1
(137)	Resident Tcf21^{+} cardiac fibroblasts become activated and proliferative within 2–4 days after nonreperfused infarction, then undergo myofibroblast conversion, secreting large amounts of ECM proteins. Finally in mature scars, fibroblasts show reduced expression of α-SMA and express tendon genes.	The fate of fibroblasts was studied using 3 different lineage-tracing models: Tcf21$^{MCM/+}$ (resident cardiac fibroblasts), *Postn*-^{MCM} (activated fibroblasts), and *Acta2*-^{CreERT2} (activated myofibroblasts).	Vimentin, α-SMA
(206)	Epicardial-derived resident mesenchymal cells, not bone marrow cells, are the main source of fibroblasts in the infarcted heart.	WT1Cre mice were used for permanent genetic tracing of epicardium-derived cells. Mice reconstituted with RFP^{+} bone marrow cells were used to study bone marrow origin.	Collagen I, FSP1, DDR2, CD90, α-SMA
(207)	Following nonreperfused infarction, subsets of epicardium-derived cells differentiate into fibroblasts and smooth muscle cells.	Lineage tracing of epicardium derived cells by using inducible WT1^{CreERT2} mice.	FSP1, procollagen I, collagen III, fibronectin, α-SMA
(42)	The vast majority of activated collagen-producing fibroblasts (~96%) in nonreperfused infarcts are derived from epicardial cells. Hematopoietic, bone marrow lineages, and endothelial cells do not significantly contribute to the fibroblast population.	Lineage-tracing models to label epicardial cells (Wt1-Cre), endothelial cells (Tie2-Cre), hematopoietic cells (Vav-Cre). Transplantation with RFP^{+} bone marrow to study bone marrow origin.	Breeding with collagen 1α1-GFP reporter mice, α-SMA
(39)	Post-infarction, 35%–40% of α-SMA^{+} mesenchymal cells are derived from endothelial cells, possibly through endothelial-to-mesenchymal transition.	The endothelial cell-specific endothelial-SCL^{CreERT} mouse line was used to trace endothelial cells.	α-SMA expression, Snail, FSP1, vimentin and collagen I mRNA expression
(208)	24% of myofibroblasts in nonreperfused myocardial infarcts originate from bone marrow cells.	Transplantation with EGFP-tagged bone marrow, or bone marrow from proCol1α2 gene-driven luciferase or β-Gal reporter mice.	αSMA staining, β galactosidase activity in pro-Col1α2-driven chimeric mice
(40)	25% of vimentin^{+} fibroblasts and 57% of α-SMA^{+} myofibroblasts in nonreperfused infarcts are derived from bone marrow cells.	Transplantation with bone marrow from EGFP reporter mice to document bone marrow origin.	α-SMA, vimentin
(209)	Blood-derived cells contributed to the myofibroblast population. Treatment with G-CSF enhances recruitment of bone marrow–derived myofibroblasts.	Transplantation of GFP^{+} bone marrow.	Vimentin, α-SMA
(210)	Gli-1^{+} perivascular cells contribute to the myofibroblast population in the infarcted myocardium (approximately 60% of activated myofibroblasts are derived from Gli1^{+} cells).	Lineage tracing using Gli1^{CreERT2} mice.	Collagen I, PDGFRα, α-SMA

ECM = extracellular matrix; EGFP = enhanced green fluorescent protein; G-CSF = granulocyte-colony stimulating factor; mRNA = messenger ribonucleic acid; other abbreviations as in Table 1.

Expansion of activated fibroblasts in the infarcted myocardium. Expansion of cardiac fibroblasts and acquisition of a matrix-synthetic myofibroblast phenotype are prominent features of the proliferative phase of infarct healing. In addition to the abundant resident cardiac fibroblasts that can respond to activating signals, several other cell types have been proposed as important cellular sources for the expanding infarct myofibroblast population. Endothelial cells can undergo endothelial-to-mesenchymal transition in response to growth factor stimulation, acquiring a matrix-synthetic phenotype. Hematopoietic fibroblast progenitors can also contribute to the expansion of activated fibroblasts in injury sites. Pericytes and vascular smooth muscle cells can undergo fibroblast conversion, contributing to fibrotic responses. Over the past 10 years, studies combining bone marrow transplantation experiments, parabiosis, and lineage tracing strategies have attempted to explore the cellular origin of fibroblasts in the infarcted heart (Table 2). Although earlier investigations had suggested important contributions of endothelial cells and hematopoietic progenitors to the infarct myofibroblast population (39,40), recent studies using lineage-tracing approaches with several different Cre drivers demonstrated that resident cardiac fibroblasts are the main source for activated myofibroblasts in the infarcted heart, with much smaller contributions of endothelial and hematopoietic cells (41,42). It should be emphasized that the studies investigating the origin of infarct myofibroblasts have several limitations that may explain, at least in part, conflicting findings (43). First, the use of nonspecific fibroblast markers or Cre drivers with questionable specificity may limit the reliability of the findings. For example, some of the studies suggesting major contributions of endothelial cells to the myofibroblast population

FIGURE 2 Fibroblasts in the Proliferative Phase of Infarct Healing

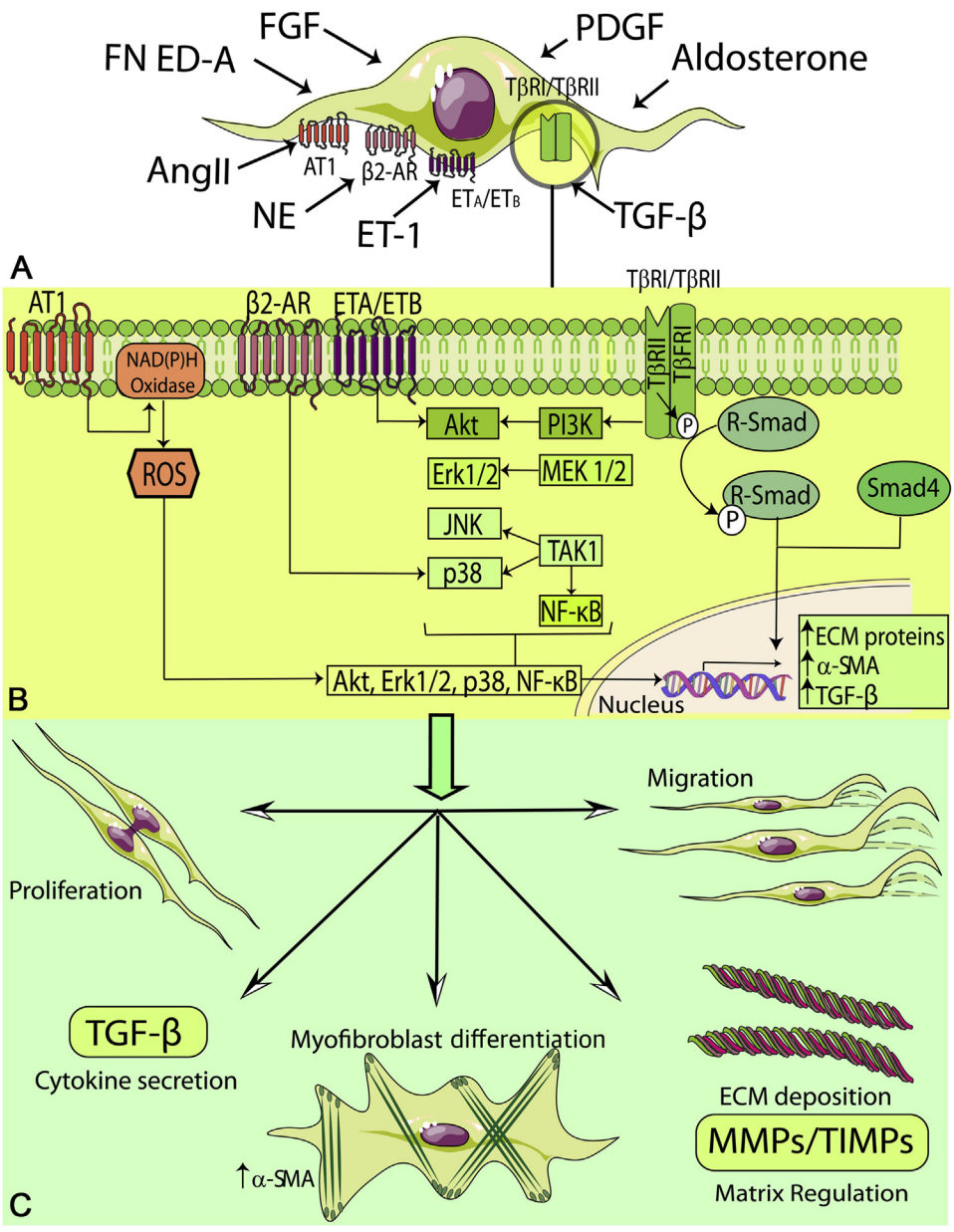

During the proliferative phase of infarct healing, fibrogenic growth factors and neurohumoral mediators trigger myofibroblast conversion and stimulate fibroblast proliferation, migration, and activation. A wide range of fibrogenic mediators, induced during the proliferative phase of cardiac repair, are implicated in myofibroblast activation. Neurohumoral mediators, such as angiotensin II (AngII), aldosterone, and norepinephrine (NE), growth factors (transforming growth factor [TGF]-βs, fibroblast growth factors [FGFs], platelet-derived growth factors [PDGFs]), and specialized matrix proteins, such as ED-A fibronectin and matricellular proteins cooperate to activate intracellular signaling pathways that promote myofibroblast conversion and proliferation and modulate expression of extracellular matrix (ECM) proteins and of genes associated with matrix metabolism. The cartoon was designed using Servier Medical Art (https://smart.servier.com). AR = adrenergic receptor; ET = endothelin; MMP = matrix metalloproteinase; NF = nuclear factor; ROS = reactive oxygen species; SMA = smooth muscle actin; TIMP = tissue inhibitor of metalloproteinase.

were based on nonspecific Cre drivers (such as the Tie1-Cre line) (44). Identification of fibroblasts represents another major challenge due to the absence of specific markers (**Table 1**). Thus, in many cases, conclusions regarding conversion of other lineages into fibroblasts are based on immunofluorescence data showing expression of nonspecific markers, such as fibroblast-specific protein-1 or α-SMA (40,44).

Second, the timing of reperfusion may have dramatic effects on the fate of resident myocardial cells and on recruitment of blood-derived progenitors, thus altering the relative contribution of various cell types to the expansion and activation of fibroblasts. Early reperfusion results in accentuated and accelerated leukocyte influx and could also augment infiltration of the infarct zone with bone marrow–derived fibroblast progenitors. Prolonged coronary occlusion, in contrast, may cause ischemic death of large numbers of interstitial and vascular cells in the infarct zone, thus reducing their relative contribution to myofibroblast expansion.

Third, considering that all lineage-tracing studies were performed in mouse models, there is practically no information on the origin of myofibroblasts in human myocardial infarction.

Myofibroblast migration in the border zone of the infarct. In the healing infarct, fibroblasts undergo conversion to myofibroblasts, expressing contractile proteins, such as α-SMA and the embryonic isoform of smooth muscle myosin heavy chain, synthesizing periostin, and secreting large amounts of ECM proteins (22,45). In animal models of myocardial infarction, myofibroblasts are localized predominantly in the border zone, forming well-organized arrays (46). Fibroblast migration to the infarct border zone may be mediated by growth factors, such as TGF-β and fibroblast growth factors (FGFs) (47,48), and by proinflammatory cytokines, such as IL-1β, tumor necrosis factor-α, and cardiotrophin-1 (27,49). It has also been suggested that chemokines, such as monocyte chemoattractant protein-1/C-C motif chemokine ligand 2, may promote the migration of bone marrow–derived fibroblast progenitors in injured tissues. Considering the robust evidence documenting no significant contribution of hematopoietic cells on infarct fibroblast populations (42), the potential significance of this mechanism is unclear. C-C motif chemokine ligand 2 may contribute to fibrosis through recruitment and activation of fibrogenic monocytes and macrophages (50,51) rather than through recruitment of circulating fibroblast progenitors or modulation of fibroblast function. A recently published investigation identified a subpopulation of atypical monocytes with a critical contribution in bleomycin-induced pulmonary fibrosis (52). Whether fibrogenic monocyte subsets with distinct phenotypic profiles are recruited in remodeling hearts has not been investigated. Other members of the chemokine family, such as the CXC chemokine interferon-γ–inducible protein-10/CXCL10, may inhibit fibroblast migration, serving as an endogenous inhibitory signal that restrains the fibrotic response following injury (53,54).

Fibroblast migration is dependent on the continuous formation and disruption of adhesive interactions between fibroblast surface proteins and the surrounding cardiac ECM. Migration involves well-orchestrated activation of integrins on cardiac fibroblast cytoplasmic membrane (55), linked with the production of proteases that degrade the matrix (56) and expression of specialized matrix proteins that locally activate or transduce growth factor–mediated signals (57).

The effects of neurohumoral pathways on activation of infarct myofibroblasts. After migrating to the infarct border zone, fibroblasts acquire a proliferative matrix-synthetic phenotype through the local induction of fibrogenic mediators (**Figure 2**). Neurohumoral pathways are critically implicated in regulation of fibroblast function following myocardial infarction. Potent activation of the renin-angiotensin-aldosterone system in infarcted hearts (58) stimulates myofibroblast conversion, proliferation, and ECM protein synthesis both through direct actions, and via induction of TGF-β (59,60). The fibrogenic actions of angiotensin II are mediated predominantly through engagement of the angiotensin type 1 (AT1) receptor (61–64). In contrast, the AT2 receptor may exert inhibitory functions, suppressing fibroblast proliferation and ECM synthesis (65), and has been suggested to restrain profibrotic signaling (66). Although extensive in vivo evidence supports the profibrotic actions of AT1 signaling in experimental models of myocardial infarction (67), to what extent the prosurvival effects of angiotensin-converting enzyme inhibition and AT1 blockade in patients with acute myocardial infarction are mediated through attenuation of angiotensin-induced fibrosis remains unknown.

Both animal model studies and investigations in human patients suggest that aldosterone contributes to myocardial fibrosis (68). Mineralocorticoid receptor inhibition attenuated fibrosis in experimental models of nonreperfused myocardial infarction (69) and reduced levels of biomarkers reflecting collagen synthesis in patients with acute myocardial infarction (70). The cellular basis for these effects remains unclear. Aldosterone-mediated signaling has been

JACC: BASIC TO TRANSLATIONAL SCIENCE VOL. 4, NO. 3, 2019
JUNE 2019:449–67

suggested to modulate the phenotype of all cells involved in cardiac repair, driving macrophages toward a fibrogenic phenotype (71), activating T cells (72), inducing cardiomyocyte-derived fibrogenic signals (73), and directly stimulating fibroblast proliferation and collagen synthesis (74,75).

The adrenergic system is also prominently activated following myocardial infarction. Stimulation of β_2-adrenergic receptor signaling directly stimulates proliferation of cardiac fibroblasts through effects that may involve p38 mitogen-activated protein kinase (MAPK) signaling (76–78). Chronic pharmacological stimulation or transgenic overexpression of β-adrenergic receptor causes myocardial fibrosis (79); whether fibrotic remodeling is due to direct activation of fibroblasts or reflects reparative fibrosis in response to cardiomyocyte death remains unknown. Activation of G protein-coupled receptor kinase 2 in cardiac fibroblasts may transduce, at least in part, the fibrogenic actions of β-adrenergic receptors in the infarcted myocardium (80,81).

The role of TGF-βs in fibroblast activation. The fibrogenic growth factor TGF-β is a central mediator in myofibroblast conversion following myocardial infarction. All 3 TGF-β isoforms are markedly upregulated in the infarcted heart; TGF-β1 and TGF-β2 are induced earlier, whereas TGF-β3 exhibits a late peak and a prolonged time course of expression (82). Whether TGF-β isoforms play distinct roles following infarction remains unknown. Most myocardial cell types are capable of secreting TGF-β as an inactive complex bound to the latency-associated peptide (forming the small latent complex), and latent TGF-β-binding protein (forming the large latent complex). Several mediators, including ROS, cell surface integrins, proteases, and matricellular proteins (such as thrombospondin-1), have been implicated in generation of active TGF-β in the healing infarct (83–87). The active TGF-β dimer binds and sequentially transphosphorylates type II and type I TGF-β receptors, activating downstream canonical signaling pathways through receptor-activated Smad proteins (R-Smads-Smad2/3) and Smad-independent pathways (88). Both Smad-dependent and non-Smad pathways have been implicated in α-SMA and ECM protein upregulation, triggering myofibroblast conversion and activation in healing myocardial infarction (89). In the infarcted heart, activation of Smad3-dependent signaling in cardiac fibroblasts plays a crucial role in formation of well-organized fibroblast arrays in the infarct border zone by inducing integrin expression (90).

Endothelin-1. The endothelium-derived peptide endothelin-1 is a potent vasoconstrictor but has also been reported to exert fibroblast-activating effects. Endothelin-1 secreted by TGF-β- or angiotensin II-stimulated endothelial cells may stimulate fibroblast proliferation, myofibroblast conversion, and ECM synthesis through activation of the endothelin-A receptor and downstream Rac/PI3K/Akt signaling pathways (91). In vivo, cardiac-specific endothelin-1 overexpression caused myocardial fibrosis associated with biventricular systolic and diastolic dysfunction (92), whereas endothelin antagonism attenuated adverse fibrotic remodeling following myocardial infarction (93).

The role of FGFs and platelet-derived growth factors in the activation of infarct fibroblasts. FGF2 may stimulate a proliferative phenotype in infarct fibroblasts through activation of p38 MAPK and protein kinase Cδ signaling pathways (94). In vivo, FGF2-knockout mice had reduced proliferation of infarct fibroblasts, associated with decreased ECM synthesis. These defects resulted in impaired scar formation and infarct expansion. In contrast, FGF2 overexpression increased fibroblast proliferation and accentuated ECM deposition (95). PDGFs and PDGF receptors (PDGFRs) are also overexpressed in the infarcted myocardium and may play role in regulation of fibroblast function (96). Activation of PDGFRα signaling may promote fibroblast activation; in contrast, PDGFRβ actions are important for maturation of the infarct vasculature. In vitro, PDGF-AA potently stimulates cardiac fibroblast proliferation and ECM protein synthesis (97). In vivo, PDGFRα and PDGFRβ neutralization reduced collagen deposition in reperfused myocardial infarcts (96); however, PDGFRβ inhibition also prevented the recruitment of mural cells by infarct neovessels, perturbing maturation of the infarct vasculature (96).

The role of specialized ECM proteins in the regulation of infarct fibroblast phenotype. Tissue injury is associated with induction of specialized matricellular proteins that do not play a primary structural role but regulate cellular responses by transducing or modulating signaling cascades. Fibroblasts are important cellular targets of specialized ECM proteins. The ED-A domain of fibronectin plays an important role in conversion of fibroblasts into myofibroblasts (98–100). Moreover, several matricellular macromolecules, including thrombospondins (87), osteopontin (101), tenascin-C (102), secreted protein acidic and rich in cysteine (103), periostin (104), and osteoglycin (105), have been implicated in activation of myofibroblasts in healing infarcts. Nonfibrillar collagens, such as collagen VI, are also involved in the activation of a myofibroblast phenotype following myocardial infarction (106). Most

specialized matrix proteins act by binding to fibroblast surface molecules, such as integrins and syndecans, or by modulating activity of growth factors and proteases.

Intracellular molecular pathways involved in fibroblast activation. In the healing infarct, induction of fibrogenic stimuli, such as damage-associated molecular patterns, cytokines and growth factors, neurohumoral mediators, and matricellular proteins cooperate to stimulate intracellular cascades involved in myofibroblast conversion, migration, proliferation, and induction of a matrix-synthetic transcriptional program (107). Experimental studies have identified several essential intracellular pathways that contribute to fibroblast activation.

The ROS system acts as a common effector of many fibrogenic signals (108). Angiotensin II activates downstream ROS-sensitive kinases (109) and stimulates collagen synthesis through ROS generation (110). Aldosterone-induced fibroblast activation is mediated, at least in part, through oxidative stress (111). Moreover, extensive evidence suggests that ROS mediate the fibrogenic actions of TGF-β and critically regulate matrix metabolism by modulating synthesis and activity of proteases involved in ECM degradation (112).

Ca^{2+} oscillations have also been implicated in the regulation of fibroblast phenotype and function (113). Angiotensin II or TGF-β may induce fibrogenic actions, at least in part through activation of members of the transient receptor potential (TRP) family of cationic channels. In cardiac fibroblasts, the calcium channel TRPC6 has been implicated in myofibroblast conversion by activating a calcineurin-nuclear factor of activated T cells cascade (114,115).

MAPKs exhibit a broad range of functions in many different cellular responses, including cell proliferation, survival, migration, and differentiation. Both in vitro and in vivo studies suggest an important role for MAPK signaling pathways in fibroblast activation. Fibroblast-specific loss-of-function approaches suggested that activation of p38α MAPK, the major isoform expressed in cardiac fibroblasts (116), promotes myofibroblast conversion following infarction through activation of the transcription factor serum response factor and the signaling effector calcineurin (78,117). The serum response factor/myocardin-related transcription factor (MRTF) axis plays a dominant role in regulation of α-SMA transcription and subsequent myofibroblast conversion (118,119). In vivo, mice with global loss of MRTF-A had attenuated fibrosis following myocardial infarction (120). Whether these observations reflect abrogation of MRTF-dependent effects on fibroblasts remains unclear, considering that MRTF-A may also modulate cardiomyocyte and vascular cell phenotype and function (121,122).

Noncoding ribonucleic acids in regulation of infarct fibroblasts. A growing body of evidence demonstrates that noncoding ribonucleic acids (RNAs), including small noncoding microRNA (miRNAs) and long noncoding RNA (lncRNA), may be implicated in the regulation of fibroblast activity in the infarcted heart (123,124). MiRNAs may act by modulating several profibrotic target pathways, including the TGF-β/Smad system, angiotensin II/MAPK signaling, the RhoA/Rho-associated coiled-coil containing kinase (ROCK) cascade, the MRTF/serum response factor axis, and the cationic channels regulating calcium responses (125). Several miRNAs, such as miR-29 and miR-101, function as negative regulators of cardiac fibroblasts; repression of these miRNAs by fibrogenic stimuli, such as TGF-β, may activate a fibrogenic program in response to infarction (126,127). Members of the miR-15 family have also been suggested to exert antifibrotic actions by inhibiting the TGF-β pathway (128). In contrast to other antifibrotic miRNAs, miR-15 is up-regulated following cardiac injury and may play a role in restraining the fibrotic response.

Other miRNAs may function as activators of the fibrogenic cascade, promoting myofibroblast conversion and activation in the infarcted heart. MiR-21 is markedly induced in infarct fibroblasts (129) and may exert fibrogenic actions by stimulating MAPK activation in cardiac fibroblasts (130) or by targeting the TGF-β cascade (131). In addition to its effects on the fibrotic response, fibroblast-derived miR-21, packaged into exosomes, may exert paracrine effects on cardiomyocyte hypertrophy and immune cell activation (132).

Evidence on the role on lncRNAs in fibroblast activation following infarction is limited (133). Wisp2 superenhancer-associated RNA, a cardiac fibroblast-enriched lncRNA, has been implicated in fibroblast proliferation, activation, and survival following myocardial infarction (134). The species specificity of lncRNAs (only 15% of mouse lncRNAs are expressed in humans and vice versa) is a major limiting factor in the use of animal models to understand their role in human diseases (135).

FIBROBLASTS IN SCAR MATURATION. In healing infarcts, secretion of structural ECM proteins by activated myofibroblasts is followed by induction of matrix crosslinking enzymes that contribute to scar maturation. As the scar matures, the density of activated myofibroblasts is dramatically reduced (45).

FIGURE 3 The Phenotypic Heterogeneity of Cardiac Fibroblast Populations May Explain Their Functional Diversity in Injured and Remodeling Hearts

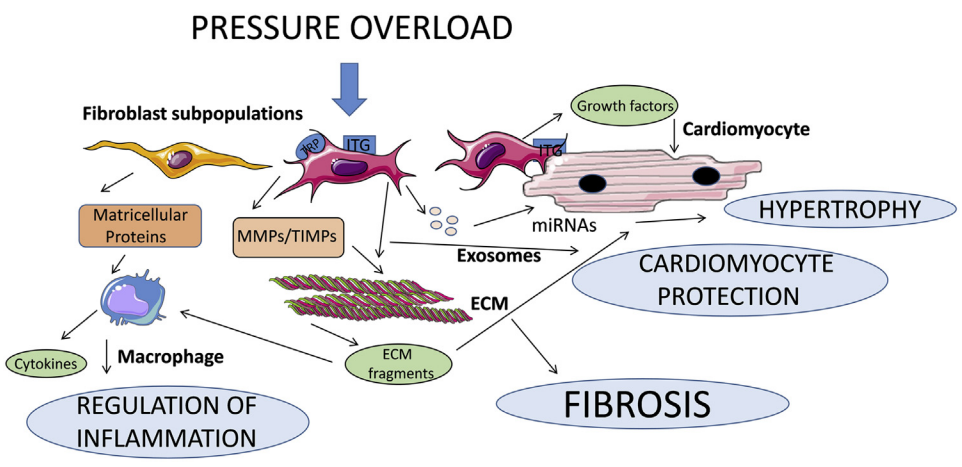

In the pressure-overloaded myocardium, mechanical stress activates mechanosensitive signaling pathways in cardiac fibroblasts that may involve integrins (ITGs) and stress-activated ion channels (such as transient receptor potential [TRP] channels). Traditional views consider the fibroblasts as matrix-producing cells that secrete large amounts of fibrillar and nonfibrillar collagens, increasing extracellular matrix (ECM) deposition and promoting fibrosis and diastolic dysfunction. However, recent evidence challenges this unidimensional view of fibroblasts, suggesting that they may also play protective roles, by preserving the ECM, thus preventing generation of proinflammatory matrix fragments and by transducing prosurvival cascades in cardiomyocytes. Secretion of matricellular proteins that bind to the structural components of the ECM and modulate signaling responses and release of micro-ribonucleic acid (miRNA)–containing exosomes that may modulate cardiomyocyte responses represent major additional mechanisms implicated in fibroblast actions. The diverse effects of fibroblasts in vivo may reflect their phenotypic heterogeneity, as different fibroblast subsets may exert distinct actions. MMP = matrix metalloproteinase; TIMP = tissue inhibitor of metalloproteinase.

Depletion of myofibroblasts from the mature scar may reflect apoptosis of fibroblasts (136) or loss of α-SMA expression and acquisition of a distinct fibroblast phenotype, characterized by high expression of tendon genes (137). The molecular signals responsible for apoptosis, or deactivation of scar myofibroblasts remain unknown.

CHRONIC ACTIVATION OF FIBROBLASTS IN THE REMODELING NONINFARCTED MYOCARDIUM. As the infarcted heart heals, the surviving myocardium exhibits chronic remodeling, associated with cardiomyocyte hypertrophy and interstitial fibrotic changes. Increased wall stress in noninfarcted myocardial segments may activate interstitial fibroblasts, promoting a matrix-synthetic phenotype and contributing to segmental dysfunction. Although chronic fibrotic changes have been reported in remodeling noninfarcted segments, and some studies have suggested persistence of myofibroblasts for many years in patients surviving an acute infarction (138), the relative contribution of chronic fibroblast activation in the pathogenesis of post-infarction heart failure remains unknown.

THE FIBROBLASTS IN THE PRESSURE-OVERLOADED MYOCARDIUM

Increased afterload is a common pathophysiologic companion of many cardiac pathologic conditions, including hypertensive heart disease and aortic stenosis. A pressure load imposes mechanical stress on all myocardial cells and triggers a series of molecular events leading to hypertrophic and fibrotic ventricular remodeling and ultimately heart failure (139). Expansion of resident cardiac fibroblast populations is a prominent characteristic of cardiac pressure overload (140,141) and is associated with activation of a matrix-synthetic program and subsequent deposition of collagens in interstitial and perivascular areas. Neurohumoral activation has been critically implicated in pressure overload-induced cardiac fibrosis. Angiotensin II-mediated AT1 activation mediates interstitial fibrosis in models of left ventricular pressure overload (142), through direct actions and via induction of inflammatory cytokines and growth factors. Although fibrogenic actions of proinflammatory cytokines, such as tumor necrosis

factor-α and IL-6, have been reported in pressure-overload models, whether these effects involve direct modulation of fibroblast phenotype or reflect indirect actions on macrophages or cardiomyocytes remains unknown (143,144). Moreover, TGF-β-driven activation of Smad-dependent signaling has been implicated in fibroblast activation in the pressure-overloaded heart (145).

Considering that mechanical stress is the primary insult in the pressure-overloaded myocardium, activation of mechanosensitive signaling pathways in cardiac fibroblasts may be the critical initial event involved in the pathogenesis of interstitial fibrosis. The focal adhesion-integrin complex is a primary mechanosensor in fibroblasts and transduces molecular signals that promote ECM gene transcription and myofibroblast conversion (146). Focal adhesion kinase (FAK) is a critical molecular link between mechanical stress and fibroblast activation. In vitro, FAK activation has been demonstrated to mediate mechanosensitive or growth factor–induced myofibroblast conversion (147–149). In vivo, FAK knockdown attenuated fibrotic changes in a model of cardiac pressure overload (150). However, considering the broad effects of FAK activation on cardiomyocytes and vascular and interstitial cells, the cellular basis for these effects is unclear. Evidence documenting the role of fibroblast-specific FAK activation in cardiac fibrosis is lacking.

Mechanosensitive ion channels have also been implicated in pressure overload–induced fibroblast activation (146). TRPC3 and TRPV4 have been implicated in myofibroblast conversion in response to mechanical stress or to growth factor stimulation (151,152). A recent study demonstrated a critical role for fibroblast-specific activation of the TWIK-related potassium channel in the activation of a fibrogenic response in the pressure-overloaded myocardium (153).

Mechanosensitive or neurohumoral activation of the small GTP-binding protein RhoA may also play an important role in fibroblast proliferation and activation following pressure overload, signaling through the ROCKs, ROCK1 and ROCK2 (154,155). In an experimental model of cardiac pressure overload, pharmacological inhibition of the RhoA-ROCK pathway attenuated fibrosis (156). Fibroblast-specific ROCK2 signaling has been suggested to mediate angiotensin II–mediated fibrosis, through induction of FGF2 and of the matricellular protein CCN2 (157). In addition to the direct fibrogenic actions of mechanosensitive signaling pathways, pressure overload may activate fibroblasts indirectly, through mechanical stress–induced actions on cardiomyocytes, T lymphocytes, or macrophages (158,159).

It should be emphasized that the contribution of fibroblasts in the pressure-overloaded myocardium is not limited to synthesis of ECM proteins and subsequent increase in ventricular stiffness. Activated fibroblasts may function as potent modulators of cardiomyocyte prosurvival and hypertrophic responses by secreting growth factors or through the release of miRNA-containing exosomes (160,161). Recent work suggested that TGF-β/Smad–dependent matrix-preserving actions of activated myofibroblasts prevent the generation of proinflammatory ECM fragments and play a critical role in protection of the pressure-overloaded myocardium from inflammation and systolic dysfunction (162). Thus, activated fibroblasts in the pressure-overloaded heart are not unidimensional cells that mediate fibrosis and dysfunction but may also exert protective actions preventing myocardial injury (**Figure 3**). Whether the diverse actions of fibroblasts in the remodeling myocardium are mediated through distinct fibroblast subpopulations remains unknown.

FIBROBLASTS IN THE VOLUME-OVERLOADED HEART

Conditions associated with volume overload, such as severe aortic or mitral valve regurgitation, are associated with marked ventricular dilation and progressive systolic dysfunction. Studies in experimental models of chordal rupture–induced mitral regurgitation in the dog (163,164) and of aortocaval fistula in the rat (165,166) suggest that volume overload causes unique interstitial perturbations that may contribute to adverse remodeling. In contrast to the marked increase in collagen deposition noted in pressure-overloaded hearts, the volume-overloaded myocardium exhibits a marked loss of interstitial collagen associated with increased MMP expression (163,164), reduced collagen synthesis (167), and accentuated collagen degradation (166,168). The matrix-degrading phenotype of interstitial cells in volume-overloaded hearts has been attributed to release of cardiomyocyte-derived TNF-α (165) or to down-modulation of TGF-β signaling (163). Whether these changes reflect perturbations of fibroblast phenotype and function in response to volume overload–induced stretch remains unknown.

FIBROBLAST ACTIVATION IN THE AGING AND DIABETIC HEART

Aging, diabetes, obesity, and metabolic dysfunction are associated with progressive interstitial and perivascular fibrosis that may contribute to the

pathogenesis of heart failure with preserved ejection fraction (5,169–173). In contrast to the rapid accumulation of α-SMA-expressing myofibroblasts in models of acute cardiac injury, diabetes and aging do not typically trigger myofibroblast conversion but may cause induction of a matrix-preserving program in cardiac interstitial cells (174). The cellular events and molecular mechanisms mediating fibrosis in senescent and diabetic hearts remain poorly understood. In aging hearts, fibroblast activation may involve the cooperation of several distinct pathways, including age-associated induction of the ROS system, activation of neurohumoral mediators, and stimulation of cytokine and TGF-β-mediated responses (175). In diabetic subjects, in contrast, hyperglycemia may result in accumulation of advanced glycation end-products that crosslink the cardiac ECM, while directly activating fibroblasts by triggering receptor for advanced glycation end-product-mediated signals (176) and accentuating age-associated changes. Diabetes-associated induction of matricellular proteins, such as thrombospondin-1, may also promote fibrosis by activating growth factor-dependent signaling in cardiac fibroblasts (177). Fibroblast activation in diabetic hearts may also reflect microvascular inflammation or resident macrophage stimulation and subsequent secretion of fibrogenic signals (5,178). It should be emphasized that although aging is associated with increased basal interstitial and perivascular collagen deposition, senescent animals exhibit perturbed fibroblast responses following injury, associated with blunted activation of growth factor signaling pathways (179).

CONCLUSIONS AND FUTURE DIRECTIONS

Expansion and activation of resident fibroblast populations play an important role in repair and remodeling of the injured heart and are implicated in the pathogenesis of systolic and diastolic dysfunction in chronic heart failure. Emerging evidence suggests that activated fibroblasts are not unidimensional matrix-producing cells but exhibit a wide range of phenotypes and may regulate inflammatory, hypertrophic, and prosurvival responses. Several important questions remain to be answered. Does the diversity of functional effects of cardiac fibroblasts in the remodeling heart reflect actions of distinct fibroblast subpopulations? If so, what are the phenotypic characteristics, origin, and fate of these fibroblast subsets? Does the functional pluralism of fibroblasts reflect their high responsiveness to changes in their microenvironment? Which molecular signals and environmental cues drive the dramatic phenotypic changes of cardiac fibroblasts in remodeling hearts? Do cell biological processes documented in mouse models recapitulate the phenotypic changes of fibroblasts in human hearts? Answering these questions is critical in order to design novel therapeutic approaches for patients with heart failure.

ADDRESS FOR CORRESPONDENCE: Dr. Nikolaos G. Frangogiannis, The Wilf Family Cardiovascular Research Institute, Albert Einstein College of Medicine, 1300 Morris Park Avenue, Forchheimer G46B, Bronx, New York 10461. E-mail: nikolaos.frangogiannis@einstein.yu.edu.

REFERENCES

1. Frangogiannis NG. Cardiac fibrosis: cell biological mechanisms, molecular pathways and therapeutic opportunities. Mol Aspects Med 2019;65:70–99.

2. Berk BC, Fujiwara K, Lehoux S. ECM remodeling in hypertensive heart disease. J Clin Invest 2007;117:568–75.

3. Kong P, Christia P, Frangogiannis NG. The pathogenesis of cardiac fibrosis. Cell Mol Life Sci 2014;71:549–74.

4. Aoki T, Fukumoto Y, Sugimura K, et al. Prognostic impact of myocardial interstitial fibrosis in non-ischemic heart failure. Comparison between preserved and reduced ejection fraction heart failure. Circ J 2011;75:2605–13.

5. Paulus WJ, Tschope C. A novel paradigm for heart failure with preserved ejection fraction: comorbidities drive myocardial dysfunction and remodeling through coronary microvascular endothelial inflammation. J Am Coll Cardiol 2013;62:263–71.

6. Kato S, Saito N, Kirigaya H, et al. Prognostic significance of quantitative assessment of focal myocardial fibrosis in patients with heart failure with preserved ejection fraction. Int J Cardiol 2015;191:314–9.

7. Roy C, Slimani A, de Meester C, et al. Associations and prognostic significance of diffuse myocardial fibrosis by cardiovascular magnetic resonance in heart failure with preserved ejection fraction. J Cardiovasc Magn Reson 2018;20:55.

8. Wong TC, Piehler KM, Kang IA, et al. Myocardial extracellular volume fraction quantified by cardiovascular magnetic resonance is increased in diabetes and associated with mortality and incident heart failure admission. Eur Heart J 2014;35:657–64.

9. Ivey MJ, Tallquist MD. Defining the cardiac fibroblast. Circ J 2016;80:2269–76.

10. Phipps RP, Borrello MA, Blieden TM. Fibroblast heterogeneity in the periodontium and other tissues. J Periodont res 1997;32:159–65.

11. Souders CA, Bowers SL, Baudino TA. Cardiac fibroblast: the renaissance cell. Circ Res 2009;105:1164–76.

12. Zak R. Development and proliferative capacity of cardiac muscle cells. Circ Res 1974;35 Suppl II:17–26.

13. Banerjee I, Fuseler JW, Price RL, Borg TK, Baudino TA. Determination of cell types and numbers during cardiac development in the neonatal and adult rat and mouse. Am J Physiol Heart Circ Physiol 2007;293:H1883–91.

14. Pinto AR, Ilinykh A, Ivey MJ, et al. Revisiting cardiac cellular composition. Circ Res 2016;118:400–9.

15. Ieda M, Tsuchihashi T, Ivey KN, et al. Cardiac fibroblasts regulate myocardial proliferation through beta1 integrin signaling. Dev Cell 2009; 16:233–44.

16. Eghbali M, Blumenfeld OO, Seifter S, et al. Localization of types I, III and IV collagen mRNAs in rat heart cells by in situ hybridization. J Mol Cell Cardiol 1989;21:103–13.

17. Brown RD, Ambler SK, Mitchell MD, Long CS. The cardiac fibroblast: therapeutic target in myocardial remodeling and failure. Annu Rev Pharmacol Toxicol 2005;45:657–87.

18. Spinale FG. Myocardial matrix remodeling and the matrix metalloproteinases: influence on cardiac form and function. Physiol Rev 2007;87: 1285–342.

19. Acharya A, Baek ST, Huang G, et al. The bHLH transcription factor Tcf21 is required for lineage-specific EMT of cardiac fibroblast progenitors. Development 2012;139:2139–49.

20. Weber KT. Cardiac interstitium in health and disease: the fibrillar collagen network. J Am Coll Cardiol 1989;13:1637–52.

21. Kohl P, Camelliti P, Burton FL, Smith GL. Electrical coupling of fibroblasts and myocytes: relevance for cardiac propagation. J Electrocardiol 2005;38:45–50.

22. Shinde AV, Humeres C, Frangogiannis NG. The role of alpha-smooth muscle actin in fibroblast-mediated matrix contraction and remodeling. Biochim Biophys Acta 2017;1863:298–309.

23. Frangogiannis NG. Pathophysiology of myocardial infarction. Compr Physiol 2015;5: 1841–75.

24. Shinde AV, Frangogiannis NG. Fibroblasts in myocardial infarction: A role in inflammation and repair. J Mol Cell Cardiol 2014;70C:74–82.

25. Prabhu SD, Frangogiannis NG. The biological basis for cardiac repair after myocardial infarction: from inflammation to fibrosis. Circ Res 2016;119: 91–112.

26. Chen W, Frangogiannis NG. Fibroblasts in post-infarction inflammation and cardiac repair. Biochim Biophys Acta 2013;1833:945–53.

27. Mitchell MD, Laird RE, Brown RD, Long CS. IL-1beta stimulates rat cardiac fibroblast migration via MAP kinase pathways. Am J Physiol Heart Circ Physiol 2007;292:H1139–47.

28. Richter K, Kietzmann T. Reactive oxygen species and fibrosis: further evidence of a significant liaison. Cell Tissue Res 2016;365:591–605.

29. Boza P, Ayala P, Vivar R, et al. Expression and function of toll-like receptor 4 and inflammasomes in cardiac fibroblasts and myofibroblasts: IL-1beta synthesis, secretion, and degradation. Mol Immunol 2016;74:96–105.

30. Frangogiannis NG, Lindsey ML, Michael LH, et al. Resident cardiac mast cells degranulate and release preformed TNF-alpha, initiating the cytokine cascade in experimental canine myocardial ischemia/reperfusion. Circulation 1998;98: 699–710.

31. Kawaguchi M, Takahashi M, Hata T, et al. Inflammasome activation of cardiac fibroblasts is essential for myocardial ischemia/reperfusion injury. Circulation 2011;123:594–604.

32. Sandanger O, Ranheim T, Vinge LE, et al. The NLRP3 inflammasome is up-regulated in cardiac fibroblasts and mediates myocardial ischaemia-reperfusion injury. Cardiovasc Res 2013;99: 164–74.

33. Bujak M, Dobaczewski M, Chatila K, et al. Interleukin-1 receptor type I signaling critically regulates infarct healing and cardiac remodeling. Am J Pathol 2008;173:57–67.

34. Anzai A, Choi JL, He S, et al. The infarcted myocardium solicits GM-CSF for the detrimental oversupply of inflammatory leukocytes. J Exp Med 2017;214:3293–310.

35. Saxena A, Chen W, Su Y, et al. IL-1 induces proinflammatory leukocyte infiltration and regulates fibroblast phenotype in the infarcted myocardium. J Immunol 2013;191:4838–48.

36. Abrial M, Da Silva CC, Pillot B, et al. Cardiac fibroblasts protect cardiomyocytes against lethal ischemia-reperfusion injury. J Mol Cell Cardiol 2014;68:56–65.

37. Nakaya M, Watari K, Tajima M, et al. Cardiac myofibroblast engulfment of dead cells facilitates recovery after myocardial infarction. J Clin Invest 2017;127:383–401.

38. DeBerge M, Yeap XY, Dehn S, et al. MerTK cleavage on resident cardiac macrophages compromises repair after myocardial ischemia reperfusion injury. Circ Res 2017;121:930–40.

39. Aisagbonhi O, Rai M, Ryzhov S, Atria N, Feoktistov I, Hatzopoulos AK. Experimental myocardial infarction triggers canonical Wnt signaling and endothelial-to-mesenchymal transition. Dis Model Mech 2011;4:469–83.

40. Mollmann H, Nef HM, Kostin S, et al. Bone marrow-derived cells contribute to infarct remodelling. Cardiovasc Res 2006;71:661–71.

41. Kanisicak O, Khalil H, Ivey MJ, et al. Genetic lineage tracing defines myofibroblast origin and function in the injured heart. Nat Commun 2016;7: 12260.

42. Moore-Morris T, Cattaneo P, Guimaraes-Camboa N, et al. Infarct fibroblasts do not derive from bone marrow lineages. Circ Res 2018;122: 583–90.

43. Alex L, Frangogiannis NG. The cellular origin of activated fibroblasts in the infarcted and remodeling myocardium. Circ Res 2018;122: 540–2.

44. Zeisberg EM, Tarnavski O, Zeisberg M, et al. Endothelial-to-mesenchymal transition contributes to cardiac fibrosis. Nat Med 2007;13:952–61.

45. Frangogiannis NG, Michael LH, Entman ML. Myofibroblasts in reperfused myocardial infarcts express the embryonic form of smooth muscle myosin heavy chain (SMemb). Cardiovasc Res 2000;48:89–100.

46. Blankesteijn WM, Essers-Janssen YP, Verluyten MJ, Daemen MJ, Smits JF. A homologue of Drosophila tissue polarity gene frizzled is expressed in migrating myofibroblasts in the infarcted rat heart. Nat Med 1997;3:541–4.

47. Detillieux KA, Sheikh F, Kardami E, Cattini PA. Biological activities of fibroblast growth factor-2 in the adult myocardium. Cardiovasc Res 2003; 57:8–19.

48. Stawowy P, Margeta C, Kallisch H, et al. Regulation of matrix metalloproteinase MT1-MMP/MMP-2 in cardiac fibroblasts by TGF-beta1 involves furin-convertase. Cardiovasc Res 2004; 63:87–97.

49. Freed DH, Chilton L, Li Y, et al. Role of myosin light chain kinase in cardiotrophin-1-induced cardiac myofibroblast cell migration. Am J Physiol Heart Circ Physiol 2011;301:H514–22.

50. Dewald O, Zymek P, Winkelmann K, et al. CCL2/monocyte chemoattractant protein-1 regulates inflammatory responses critical to healing myocardial infarcts. Circ Res 2005;96:881–9.

51. Frangogiannis NG, Dewald O, Xia Y, et al. Critical role of monocyte chemoattractant protein-1/CC chemokine ligand 2 in the pathogenesis of ischemic cardiomyopathy. Circulation 2007;115: 584–92.

52. Satoh T, Nakagawa K, Sugihara F, et al. Identification of an atypical monocyte and committed progenitor involved in fibrosis. Nature 2017;541: 96–101.

53. Bujak M, Dobaczewski M, Gonzalez-Quesada C, et al. Induction of the CXC chemokine interferon-gamma-inducible protein 10 regulates the reparative response following myocardial infarction. Circ Res 2009;105:973–83.

54. Saxena A, Bujak M, Frunza O, et al. CXCR3-independent actions of the CXC chemokine CXCL10 in the infarcted myocardium and in isolated cardiac fibroblasts are mediated through proteoglycans. Cardiovasc Res 2014;103:217–27.

55. Manso AM, Kang SM, Ross RS. Integrins, focal adhesions, and cardiac fibroblasts. J Investig Med 2009;57:856–60.

56. Ghersi G, Dong H, Goldstein LA, et al. Regulation of fibroblast migration on collagenous matrix by a cell surface peptidase complex. J Biol Chem 2002;277:29231–41.

57. Murphy-Ullrich JE. The de-adhesive activity of matricellular proteins: is intermediate cell adhesion an adaptive state? J Clin Invest 2001;107: 785–90.

58. Weber KT, Sun Y, Bhattacharya SK, Ahokas RA, Gerling IC. Myofibroblast-mediated mechanisms of pathological remodelling of the heart. Nat Rev Cardiol 2012;10:15–26.

59. Kagami S, Border WA, Miller DE, Noble NA. Angiotensin II stimulates extracellular matrix protein synthesis through induction of transforming growth factor-beta expression in rat glomerular mesangial cells. J Clin Invest 1994;93: 2431–7.

60. Campbell SE, Katwa LC. Angiotensin II stimulated expression of transforming growth factor-beta1 in cardiac fibroblasts and myofibroblasts. J Mol Cell Cardiol 1997;29:1947–58.

61. Schorb W, Booz GW, Dostal DE, Conrad KM, Chang KC, Baker KM. Angiotensin II is mitogenic in neonatal rat cardiac fibroblasts. Circ Res 1993;72: 1245–54.

62. Sadoshima J, Izumo S. Molecular characterization of angiotensin II-induced hypertrophy of cardiac myocytes and hyperplasia of cardiac fibroblasts. Critical role of the AT1 receptor subtype. Circ Res 1993;73:413–23.

63. Crabos M, Roth M, Hahn AW, Erne P. Characterization of angiotensin II receptors in cultured adult rat cardiac fibroblasts. Coupling to signaling systems and gene expression. J Clin Invest 1994;93:2372–8.

64. Thibault G, Lacombe MJ, Schnapp LM, Lacasse A, Bouzeghrane F, Lapalme G. Upregulation of alpha(8)beta(1)-integrin in cardiac fibroblast by angiotensin II and transforming growth factor-beta1. Am J Physiol Cell Physiol 2001;281:C1457–67.

65. Ohkubo N, Matsubara H, Nozawa Y, et al. Angiotensin type 2 receptors are reexpressed by cardiac fibroblasts from failing myopathic hamster hearts and inhibit cell growth and fibrillar collagen metabolism. Circulation 1997;96:3954–62.

66. Kurisu S, Ozono R, Oshima T, et al. Cardiac angiotensin II type 2 receptor activates the kinin/NO system and inhibits fibrosis. Hypertension 2003;41:99–107.

67. Schieffer B, Wirger A, Meybrunn M, et al. Comparative effects of chronic angiotensin-converting enzyme inhibition and angiotensin II type 1 receptor blockade on cardiac remodeling after myocardial infarction in the rat. Circulation 1994;89:2273–82.

68. Lijnen P, Petrov V. Induction of cardiac fibrosis by aldosterone. J Mol Cell Cardiol 2000;32:865–79.

69. van den Borne SW, Isobe S, Zandbergen HR, et al. Molecular imaging for efficacy of pharmacologic intervention in myocardial remodeling. J Am Coll Cardiol Img 2009;2:187–98.

70. Hayashi M, Tsutamoto T, Wada A, et al. Immediate administration of mineralocorticoid receptor antagonist spironolactone prevents post-infarct left ventricular remodeling associated with suppression of a marker of myocardial collagen synthesis in patients with first anterior acute myocardial infarction. Circulation 2003;107:2559–65.

71. Rickard AJ, Morgan J, Tesch G, Funder JW, Fuller PJ, Young MJ. Deletion of mineralocorticoid receptors from macrophages protects against deoxycorticosterone/salt-induced cardiac fibrosis and increased blood pressure. Hypertension 2009;54:537–43.

72. Li C, Sun XN, Zeng MR, et al. Mineralocorticoid receptor deficiency in T cells attenuates pressure overload-induced cardiac hypertrophy and dysfunction through modulating T-cell activation. Hypertension 2017;70:137–47.

73. Rickard AJ, Morgan J, Bienvenu LA, et al. Cardiomyocyte mineralocorticoid receptors are essential for deoxycorticosterone/salt-mediated inflammation and cardiac fibrosis. Hypertension 2012;60:1443–50.

74. Neumann S, Huse K, Semrau R, et al. Aldosterone and D-glucose stimulate the proliferation of human cardiac myofibroblasts in vitro. Hypertension 2002;39:756–60.

75. Brilla CG, Zhou G, Matsubara L, Weber KT. Collagen metabolism in cultured adult rat cardiac fibroblasts: response to angiotensin II and aldosterone. J Mol Cell Cardiol 1994;26:809–20.

76. Kim J, Eckhart AD, Eguchi S, Koch WJ. Beta-adrenergic receptor-mediated DNA synthesis in cardiac fibroblasts is dependent on transactivation of the epidermal growth factor receptor and subsequent activation of extracellular signal-regulated kinases. J Biol Chem 2002;277:32116–23.

77. Turner NA, Porter KE, Smith WH, White HL, Ball SG, Balmforth AJ. Chronic beta2-adrenergic receptor stimulation increases proliferation of human cardiac fibroblasts via an autocrine mechanism. Cardiovasc Res 2003;57:784–92.

78. Molkentin JD, Bugg D, Ghearing N, et al. Fibroblast-specific genetic manipulation of p38 mitogen-activated protein kinase in vivo reveals its central regulatory role in fibrosis. Circulation 2017;136:549–61.

79. Nguyen MN, Kiriazis H, Ruggiero D, et al. Spontaneous ventricular tachyarrhythmias in beta2-adrenoceptor transgenic mice in relation to cardiac interstitial fibrosis. Am J Physiol Heart Circ Physiol 2015;309:H946–57.

80. Woodall MC, Woodall BP, Gao E, Yuan A, Koch WJ. Cardiac fibroblast GRK2 deletion enhances contractility and remodeling following ischemia/reperfusion injury. Circ Res 2016;119:1116–27.

81. Travers JG, Kamal FA, Valiente-Alandi I, et al. Pharmacological and activated fibroblast targeting of gbetagamma-GRK2 after myocardial ischemia attenuates heart failure progression. J Am Coll Cardiol 2017;70:958–71.

82. Dewald O, Ren G, Duerr GD, et al. Of mice and dogs: species-specific differences in the inflammatory response following myocardial infarction. Am J Pathol 2004;164:665–77.

83. Liu RM, Desai LP. Reciprocal regulation of TGF-β and reactive oxygen species: a perverse cycle for fibrosis. Redox Biol 2015;6:565–77.

84. Nishimura SL. Integrin-mediated transforming growth factor-beta activation, a potential therapeutic target in fibrogenic disorders. Am J Pathol 2009;175:1362–70.

85. Annes JP, Munger JS, Rifkin DB. Making sense of latent TGFbeta activation. J Cell Sci 2003;116:217–24.

86. Rifkin DB, Mazzieri R, Munger JS, Noguera I, Sung J. Proteolytic control of growth factor availability. APMIS 1999;107:80–5.

87. Frangogiannis NG, Ren G, Dewald O, et al. Critical role of endogenous thrombospondin-1 in preventing expansion of healing myocardial infarcts. Circulation 2005;111:2935–42.

88. Derynck R, Zhang YE. Smad-dependent and Smad-independent pathways in TGF-beta family signalling. Nature 2003;425:577–84.

89. Meng XM, Nikolic-Paterson DJ, Lan HY. TGF-β: the master regulator of fibrosis. Nat Rev Nephrol 2016;12:325–38.

90. Kong P, Shinde AV, Su Y, et al. Opposing actions of fibroblast and cardiomyocyte Smad3 signaling in the infarcted myocardium. Circulation 2018;137:707–24.

91. Shi-Wen X, Chen Y, Denton CP, et al. Endothelin-1 promotes myofibroblast induction through the ETA receptor via a rac/phosphoinositide 3-kinase/Akt-dependent pathway and is essential for the enhanced contractile phenotype of fibrotic fibroblasts. Mol Biol Cell 2004;15:2707–19.

92. Mueller EE, Momen A, Masse S, et al. Electrical remodelling precedes heart failure in an endothelin-1-induced model of cardiomyopathy. Cardiovasc Res 2011;89:623–33.

93. Miyauchi T, Fujimori A, Maeda S, et al. Chronic administration of an endothelin-A receptor antagonist improves exercise capacity in rats with myocardial infarction-induced congestive heart failure. J Cardiovasc Pharmacol 2004;44 Suppl 1:S64–7.

94. House SL, Branch K, Newman G, Doetschman T, Schultz JJ. Cardioprotection induced by cardiac-specific overexpression of fibroblast growth factor-2 is mediated by the MAPK cascade. Am J Physiol Heart Circ Physiol 2005;289:H2167–75.

95. Virag JA, Rolle ML, Reece J, Hardouin S, Feigl EO, Murry CE. Fibroblast growth factor-2 regulates myocardial infarct repair: effects on cell proliferation, scar contraction, and ventricular function. Am J Pathol 2007;171:1431–40.

96. Zymek P, Bujak M, Chatila K, et al. The role of platelet-derived growth factor signaling in healing myocardial infarcts. J Am Coll Cardiol 2006;48:2315–23.

97. Simm A, Nestler M, Hoppe V. Mitogenic effect of PDGF-AA on cardiac fibroblasts. Basic Res Cardiol 1998;93 Suppl 3:40–3.

98. Dugina V, Fontao L, Chaponnier C, Vasiliev J, Gabbiani G. Focal adhesion features during myofibroblastic differentiation are controlled by intracellular and extracellular factors. J Cell Sci 2001;114:3285–96.

99. Kohan M, Muro AF, White ES, Berkman N. EDA-containing cellular fibronectin induces fibroblast differentiation through binding to alpha4beta7 integrin receptor and MAPK/Erk 1/2-dependent signaling. FASEB J 2010;24:4503–12.

100. Arslan F, Smeets MB, Riem Vis PW, et al. Lack of fibronectin-EDA promotes survival and prevents adverse remodeling and heart function deterioration after myocardial infarction. Circ Res 2011;108:582–92.

101. Lenga Y, Koh A, Perera AS, McCulloch CA, Sodek J, Zohar R. Osteopontin expression is required for myofibroblast differentiation. Circ Res 2008;102:319–27.

102. Tamaoki M, Imanaka-Yoshida K, Yokoyama K, et al. Tenascin-C regulates recruitment of myofibroblasts during tissue repair after myocardial injury. Am J Pathol 2005;167:71–80.

103. Schellings MW, Vanhoutte D, Swinnen M, et al. Absence of SPARC results in increased cardiac rupture and dysfunction after acute myocardial infarction. J Exp Med 2009;206:113–23.

104. Oka T, Xu J, Kaiser RA, et al. Genetic manipulation of periostin expression reveals a role

in cardiac hypertrophy and ventricular remodeling. Circ Res 2007;101:313–21.

105. Van Aelst LN, Voss S, Carai P, et al. Osteoglycin prevents cardiac dilatation and dysfunction after myocardial infarction through infarct collagen strengthening. Circ Res 2015;116:425–36.

106. Naugle JE, Olson ER, Zhang X, et al. Type VI collagen induces cardiac myofibroblast differentiation: implications for postinfarction remodeling. Am J Physiol Heart Circ Physiol 2006;290:H323–30.

107. Roche PL, Filomeno KL, Bagchi RA, Czubryt MP. Intracellular signaling of cardiac fibroblasts. Compr Physiol 2015;5:721–60.

108. Cheng TH, Cheng PY, Shih NL, Chen IB, Wang DL, Chen JJ. Involvement of reactive oxygen species in angiotensin II-induced endothelin-1 gene expression in rat cardiac fibroblasts. J Am Coll Cardiol 2003;42:1845–54.

109. Ohtsu H, Frank GD, Utsunomiya H, Eguchi S. Redox-dependent protein kinase regulation by angiotensin II: mechanistic insights and its pathophysiology. Antioxid Redox Signal 2005;7:1315–26.

110. Lijnen P, Papparella I, Petrov V, Semplicini A, Fagard R. Angiotensin II-stimulated collagen production in cardiac fibroblasts is mediated by reactive oxygen species. J Hypertens 2006;24:757–66.

111. Iglarz M, Touyz RM, Viel EC, Amiri F, Schiffrin EL. Involvement of oxidative stress in the profibrotic action of aldosterone. Interaction with the renin-angiotensin system. Am J Hypertens 2004;17:597–603.

112. Siwik DA, Pagano PJ, Colucci WS. Oxidative stress regulates collagen synthesis and matrix metalloproteinase activity in cardiac fibroblasts. Am J Physiol Cell Physiol 2001;280:C53–60.

113. Mukherjee S, Ayaub EA, Murphy J, et al. Disruption of calcium signaling in fibroblasts and attenuation of bleomycin-induced fibrosis by nifedipine. Am J Respir Cell Mol Biol 2015;53:450–8.

114. Nishida M, Onohara N, Sato Y, et al. Galpha12/13-mediated up-regulation of TRPC6 negatively regulates endothelin-1-induced cardiac myofibroblast formation and collagen synthesis through nuclear factor of activated T cells activation. J Biol Chem 2007;282:23117–28.

115. Davis J, Burr AR, Davis GF, Birnbaumer L, Molkentin JD. A TRPC6-dependent pathway for myofibroblast transdifferentiation and wound healing in vivo. Dev Cell 2012;23:705–15.

116. Sinfield JK, Das A, O'Regan DJ, Ball SG, Porter KE, Turner NA. p38 MAPK alpha mediates cytokine-induced IL-6 and MMP-3 expression in human cardiac fibroblasts. Biochem Biophys Res Commun 2013;430:419–24.

117. Bageghni SA, Hemmings KE, Zava N, et al. Cardiac fibroblast-specific p38alpha MAP kinase promotes cardiac hypertrophy via a putative paracrine interleukin-6 signaling mechanism. FASEB J 2018;32:4941–54.

118. Tomasek JJ, McRae J, Owens GK, Haaksma CJ. Regulation of alpha-smooth muscle actin expression in granulation tissue myofibroblasts is dependent on the intronic CArG element and the transforming growth factor-beta1 control element. Am J Pathol 2005;166:1343–51.

119. Lighthouse JK, Small EM. Transcriptional control of cardiac fibroblast plasticity. J Mol Cell Cardiol 2016;91:52–60.

120. Small EM, Thatcher JE, Sutherland LB, et al. Myocardin-related transcription factor-a controls myofibroblast activation and fibrosis in response to myocardial infarction. Circ Res 2010;107:294–304.

121. Weng X, Yu L, Liang P, et al. Endothelial MRTF-A mediates angiotensin II induced cardiac hypertrophy. J Mol Cell Cardiol 2015;80:23–33.

122. Trembley MA, Quijada P, Agullo-Pascual E, et al. Mechanosensitive gene regulation by myocardin-related transcription factors is required for cardiomyocyte integrity in load-induced ventricular hypertrophy. Circulation 2018;138:1864–78.

123. Creemers EE, van Rooij E. Function and therapeutic potential of noncoding RNAs in cardiac fibrosis. Circ Res 2016;118:108–18.

124. Thum T. Noncoding RNAs and myocardial fibrosis. Nat Rev Cardiol 2014;11:655–63.

125. Piccoli MT, Bar C, Thum T. Non-coding RNAs as modulators of the cardiac fibroblast phenotype. J Mol Cell Cardiol 2016;92:75–81.

126. van Rooij E, Sutherland LB, Thatcher JE, et al. Dysregulation of microRNAs after myocardial infarction reveals a role of miR-29 in cardiac fibrosis. Proc Natl Acad Sci U S A 2008;105:13027–32.

127. Pan Z, Sun X, Shan H, et al. MicroRNA-101 inhibited postinfarct cardiac fibrosis and improved left ventricular compliance via the FBJ osteosarcoma oncogene/transforming growth factor-beta1 pathway. Circulation 2012;126:840–50.

128. Tijsen AJ, van der Made I, van den Hoogenhof MM, et al. The microRNA-15 family inhibits the TGFbeta-pathway in the heart. Cardiovasc Res 2014;104:61–71.

129. Roy S, Khanna S, Hussain SR, et al. MicroRNA expression in response to murine myocardial infarction: miR-21 regulates fibroblast metalloprotease-2 via phosphatase and tensin homologue. Cardiovasc Res 2009;82:21–9.

130. Thum T, Gross C, Fiedler J, et al. MicroRNA-21 contributes to myocardial disease by stimulating MAP kinase signalling in fibroblasts. Nature 2008;456:980–4.

131. Yuan J, Chen H, Ge D, et al. Mir-21 promotes cardiac fibrosis after myocardial infarction via targeting Smad7. Cell Physiol Biochem 2017;42:2207–19.

132. Bang C, Batkai S, Dangwal S, et al. Cardiac fibroblast-derived microRNA passenger strand-enriched exosomes mediate cardiomyocyte hypertrophy. J Clin Invest 2014;124:2136–46.

133. Jiang X, Zhang F. Long noncoding RNA: a new contributor and potential therapeutic target in fibrosis. Epigenomics 2017;9:1233–41.

134. Micheletti R, Plaisance I, Abraham BJ, et al. The long noncoding RNA Wisper controls cardiac fibrosis and remodeling. Sci Transl Med 2017;9:eaai9118.

135. Paralkar VR, Mishra T, Luan J, et al. Lineage and species-specific long noncoding RNAs during erythro-megakaryocytic development. Blood 2014;123:1927–37.

136. Hayakawa K, Takemura G, Kanoh M, et al. Inhibition of granulation tissue cell apoptosis during the subacute stage of myocardial infarction improves cardiac remodeling and dysfunction at the chronic stage. Circulation 2003;108:104–9.

137. Fu X, Khalil H, Kanisicak O, et al. Specialized fibroblast differentiated states underlie scar formation in the infarcted mouse heart. J Clin Invest 2018;128:2127–43.

138. Willems IE, Havenith MG, De Mey JG, Daemen MJ. The alpha-smooth muscle actin-positive cells in healing human myocardial scars. Am J Pathol 1994;145:868–75.

139. Frohlich ED, Susic D. Pressure overload. Heart Fail Clin 2012;8:21–32.

140. Ali SR, Ranjbarvaziri S, Talkhabi M, et al. Developmental heterogeneity of cardiac fibroblasts does not predict pathological proliferation and activation. Circ Res 2014;115:625–35.

141. Moore-Morris T, Guimaraes-Camboa N, Banerjee I, et al. Resident fibroblast lineages mediate pressure overload-induced cardiac fibrosis. J Clin Invest 2014;124:2921–34.

142. Dickstein K. The role of losartan in the management of patients with heart failure. Clin Ther 2001;23:1456–77.

143. Nakajima S, Roswit WT, Look DC, Holtzman MJ. A hierarchy for integrin expression and adhesiveness among T cell subsets that is linked to TCR gene usage and emphasizes V delta 1+ gamma delta T cell adherence and tissue retention. J Immunol 1995;155:1117–31.

144. Zhao L, Cheng G, Jin R, et al. Deletion of interleukin-6 attenuates pressure overload-induced left ventricular hypertrophy and dysfunction. Circ Res 2016;118:1918–29.

145. Khalil H, Kanisicak O, Prasad V, et al. Fibroblast-specific TGF-beta-Smad2/3 signaling underlies cardiac fibrosis. J Clin Invest 2017;127:3770–83.

146. Saucerman JJ, Tan PM, Buchholz KS, McCulloch AD, Omens JH. Mechanical regulation of gene expression in cardiac myocytes and fibroblasts. Nat Rev Cardiol 2019;16:361–78.

147. Leask A. Focal adhesion kinase: a key mediator of transforming growth factor beta signaling in fibroblasts. Adv Wound Care (New Rochelle) 2013;2:247–9.

148. Zhang P, Wang W, Wang X, et al. Focal adhesion kinase mediates atrial fibrosis via the AKT/S6K signaling pathway in chronic atrial fibrillation patients with rheumatic mitral valve disease. Int J Cardiol 2013;168:3200–7.

149. Chan MW, Arora PD, Bozavikov P, McCulloch CA. FAK, PIP5KIgamma and gelsolin cooperatively mediate force-induced expression of alpha-smooth muscle actin. J Cell Sci 2009;122:2769–81.

150. Clemente CF, Tornatore TF, Theizen TH, et al. Targeting focal adhesion kinase with small interfering RNA prevents and reverses load-induced cardiac hypertrophy in mice. Circ Res 2007;101:1339–48.

151. Adapala RK, Thoppil RJ, Luther DJ, et al. TRPV4 channels mediate cardiac fibroblast differentiation by integrating mechanical and soluble signals. J Mol Cell Cardiol 2013;54:45–52.

152. Harada M, Luo X, Qi XY, et al. Transient receptor potential canonical-3 channel-dependent fibroblast regulation in atrial fibrillation. Circulation 2012;126:2051–64.

153. Abraham DM, Lee TE, Watson LJ, et al. The two-pore domain potassium channel TREK-1 mediates cardiac fibrosis and diastolic dysfunction. J Clin Invest 2018;128:4843–55.

154. Loirand G, Sauzeau V, Pacaud P. Small G proteins in the cardiovascular system: physiological and pathological aspects. Physiol Rev 2013;93:1659–720.

155. Shimizu T, Liao JK. Rho kinases and cardiac remodeling. Circ J 2016;80:1491–8.

156. Phrommintikul A, Tran L, Kompa A, et al. Effects of a Rho kinase inhibitor on pressure overload induced cardiac hypertrophy and associated diastolic dysfunction. Am J Physiol Heart Circ Physiol 2008;294:H1804–14.

157. Shimizu T, Narang N, Chen P, et al. Fibroblast deletion of ROCK2 attenuates cardiac hypertrophy, fibrosis, and diastolic dysfunction. JCI Insight 2017;2:93187.

158. Nishida M, Sato Y, Uemura A, et al. P2Y6 receptor-Galpha12/13 signalling in cardiomyocytes triggers pressure overload-induced cardiac fibrosis. EMBO J 2008;27:3104–15.

159. Laroumanie F, Douin-Echinard V, Pozzo J, et al. $CD4^+$ T cells promote the transition from hypertrophy to heart failure during chronic pressure overload. Circulation 2014;129:2111–24.

160. Xiang FL, Fang M, Yutzey KE. Loss of β-catenin in resident cardiac fibroblasts attenuates fibrosis induced by pressure overload in mice. Nat Commun 2017;8:712.

161. Lyu L, Wang H, Li B, et al. A critical role of cardiac fibroblast-derived exosomes in activating renin angiotensin system in cardiomyocytes. J Mol Cell Cardiol 2015;89:268–79.

162. Russo I, Cavalera M, Huang S, et al. Protective effects of activated myofibroblasts in the pressure-overloaded myocardium are mediated through smad-dependent activation of a matrix-preserving program. Circ Res 2019;124:1214–27.

163. Zheng J, Chen Y, Pat B, et al. Microarray identifies extensive downregulation of noncollagen extracellular matrix and profibrotic growth factor genes in chronic isolated mitral regurgitation in the dog. Circulation 2009;119:2086–95.

164. Nagatomo Y, Carabello BA, Coker ML, et al. Differential effects of pressure or volume overload on myocardial MMP levels and inhibitory control. Am J Physiol Heart Circ Physiol 2000;278:H151–61.

165. Chen Y, Pat B, Zheng J, et al. Tumor necrosis factor-alpha produced in cardiomyocytes mediates a predominant myocardial inflammatory response to stretch in early volume overload. J Mol Cell Cardiol 2010;49:70–8.

166. Chancey AL, Brower GL, Peterson JT, Janicki JS. Effects of matrix metalloproteinase inhibition on ventricular remodeling due to volume overload. Circulation 2002;105:1983–8.

167. Childers RC, Sunyecz I, West TA, Cismowski MJ, Lucchesi PA, Gooch KJ. Role of the cytoskeleton in the development of a hypofibrotic cardiac fibroblast phenotype in volume overload heart failure. Am J Physiol Heart Circ Physiol 2018;316:H596–608.

168. Cox MJ, Hawkins UA, Hoit BD, Tyagi SC. Attenuation of oxidative stress and remodeling by cardiac inhibitor of metalloproteinase protein transfer. Circulation 2004;109:2123–8.

169. Cavalera M, Wang J, Frangogiannis NG. Obesity, metabolic dysfunction, and cardiac fibrosis: pathophysiological pathways, molecular mechanisms, and therapeutic opportunities. Transl Res 2014;164:323–35.

170. Russo I, Frangogiannis NG. Diabetes-associated cardiac fibrosis: Cellular effectors, molecular mechanisms and therapeutic opportunities. J Mol Cell Cardiol 2016;90:84–93.

171. Biernacka A, Cavalera M, Wang J, et al. Smad3 signaling promotes fibrosis while preserving cardiac and aortic geometry in obese diabetic mice. Circ Heart Fail 2015;8:788–98.

172. Sorop O, Heinonen I, van Kranenburg M, et al. Multiple common co-morbidities produce left ventricular diastolic dysfunction associated with coronary microvascular dysfunction, oxidative stress and myocardial stiffening. Cardiovasc Res 2018;114:954–64.

173. Chen F, Chen D, Zhao X, et al. Interleukin-6 deficiency facilitates myocardial dysfunction during high fat diet-induced obesity by promoting lipotoxicity and inflammation. Biochim Biophys Acta 2017;1863:3128–41.

174. Alex L, Russo I, Holoborodko V, Frangogiannis NG. Characterization of a mouse model of obesity-related fibrotic cardiomyopathy that recapitulates features of human heart failure with preserved ejection fraction. Am J Physiol Heart Circ Physiol 2018;315:H934–49.

175. Chen W, Frangogiannis NG. The role of inflammatory and fibrogenic pathways in heart failure associated with aging. Heart Fail Rev 2010;15:415–22.

176. Zhao J, Randive R, Stewart JA. Molecular mechanisms of AGE/RAGE-mediated fibrosis in the diabetic heart. World J Diabetes 2014;5:860–7.

177. Gonzalez-Quesada C, Cavalera M, Biernacka A, et al. Thrombospondin-1 induction in the diabetic myocardium stabilizes the cardiac matrix in addition to promoting vascular rarefaction through angiopoietin-2 upregulation. Circ Res 2013;113:1331–44.

178. Packer M. Derangements in adrenergic-adipokine signalling establish a neurohormonal basis for obesity-related heart failure with a preserved ejection fraction. Eur J Heart Fail 2018;20:873–8.

179. Bujak M, Kweon HJ, Chatila K, Li N, Taffet G, Frangogiannis NG. Aging-related defects are associated with adverse cardiac remodeling in a mouse model of reperfused myocardial infarction. J Am Coll Cardiol 2008;51:1384–92.

180. Camelliti P, Green CR, LeGrice I, Kohl P. Fibroblast network in rabbit sinoatrial node: structural and functional identification of homogeneous and heterogeneous cell coupling. Circ Res 2004;94:828–35.

181. Chang HY, Chi JT, Dudoit S, et al. Diversity, topographic differentiation, and positional memory in human fibroblasts. Proc Natl Acad Sci U S A 2002;99:12877–82.

182. Franke WW, Schmid E, Osborn M, Weber K. Intermediate-sized filaments of human endothelial cells. J Cell Biol 1979;81:570–80.

183. Gabbiani G, Schmid E, Winter S, et al. Vascular smooth muscle cells differ from other smooth muscle cells: predominance of vimentin filaments and a specific alpha-type actin. Proc Natl Acad Sci U S A 1981;78:298–302.

184. Kong P, Christia P, Saxena A, Su Y, Frangogiannis NG. Lack of specificity of fibroblast-specific protein 1 in cardiac remodeling and fibrosis. Am J Physiol Heart Circ Physiol 2013;305:H1363–72.

185. Shimazaki M, Nakamura K, Kii I, et al. Periostin is essential for cardiac healing after acute myocardial infarction. J Exp Med 2008;205:295–303.

186. Takeda N, Manabe I, Uchino Y, et al. Cardiac fibroblasts are essential for the adaptive response of the murine heart to pressure overload. J Clin Invest 2010;120:254–65.

187. Snider P, Hinton RB, Moreno-Rodriguez RA, et al. Periostin is required for maturation and extracellular matrix stabilization of noncardiomyocyte lineages of the heart. Circ Res 2008;102:752–60.

188. Santiago JJ, Dangerfield AL, Rattan SG, et al. Cardiac fibroblast to myofibroblast differentiation in vivo and in vitro: expression of focal adhesion components in neonatal and adult rat ventricular myofibroblasts. Dev Dyn 2010;239:1573–84.

189. Dobaczewski M, Bujak M, Zymek P, Ren G, Entman ML, Frangogiannis NG. Extracellular matrix remodeling in canine and mouse myocardial infarcts. Cell Tissue Res 2006;324:475–88.

190. Doddapattar P, Gandhi C, Prakash P, et al. Fibronectin splicing variants containing extra domain a promote atherosclerosis in mice through Toll-like receptor 4. Arterioscler Thromb Vasc Biol 2015;35:2391–400.

191. Chang ML, Chen JC, Alonso CR, Kornblihtt AR, Bissell DM. Regulation of fibronectin splicing in sinusoidal endothelial cells from normal or injured liver. Proc Natl Acad Sci U S A 2004;101:18093–8.

192. Hu Y, Bock G, Wick G, Xu Q. Activation of PDGF receptor alpha in vascular smooth muscle cells by mechanical stress. FASEB J 1998;12:1135–42.

193. Chen L, Acciani T, Le Cras T, Lutzko C, Perl AK. Dynamic regulation of platelet-derived growth factor receptor alpha expression in alveolar fibroblasts during realveolarization. Am J Respir Cell Mol Biol 2012;47:517–27.

194. Goldsmith EC, Hoffman A, Morales MO, et al. Organization of fibroblasts in the heart. Dev Dyn 2004;230:787–94.

195. Chang Y, Guo K, Li Q, Li C, Guo Z, Li H. Multiple directional differentiation difference of neonatal rat fibroblasts from six organs. Cell Physiol Biochem 2016;39:157–71.

196. Squires CE, Escobar GP, Payne JF, et al. Altered fibroblast function following myocardial infarction. J Mol Cell Cardiol 2005;39:699–707.

197. Zhang S, Bu X, Zhao H, et al. A host deficiency of discoidin domain receptor 2 (DDR2) inhibits both tumour angiogenesis and metastasis. J Pathol 2014;232:436–48.

198. Shyu KG, Chao YM, Wang BW, Kuan P. Regulation of discoidin domain receptor 2 by cyclic mechanical stretch in cultured rat vascular smooth muscle cells. Hypertension 2005;46:614–21.

199. Furtado MB, Costa MW, Pranoto EA, et al. Cardiogenic genes expressed in cardiac fibroblasts contribute to heart development and repair. Circ Res 2014;114:1422–34.

200. Hudon-David F, Bouzeghrane F, Couture P, Thibault G. Thy-1 expression by cardiac fibroblasts: lack of association with myofibroblast contractile markers. J Mol Cell Cardiol 2007;42:991–1000.

201. Jurisic G, Iolyeva M, Proulx ST, Halin C, Detmar M. Thymus cell antigen 1 (Thy1, CD90) is expressed by lymphatic vessels and mediates cell adhesion to lymphatic endothelium. Exp Cell Res 2010;316:2982–92.

202. Uchida S, De Gaspari P, Kostin S, et al. Sca1-derived cells are a source of myocardial renewal in the murine adult heart. Stem Cell Rep 2013;1:397–410.

203. Braitsch CM, Kanisicak O, van Berlo JH, Molkentin JD, Yutzey KE. Differential expression of embryonic epicardial progenitor markers and localization of cardiac fibrosis in adult ischemic injury and hypertensive heart disease. J Mol Cell Cardiol 2013;65:108–19.

204. Schneider M, Kostin S, Strøm CC, et al. S100A4 is upregulated in injured myocardium and promotes growth and survival of cardiac myocytes. Cardiovasc Res 2007;75:40–50.

205. Tillmanns J, Hoffmann D, Habbaba Y, et al. Fibroblast activation protein alpha expression identifies activated fibroblasts after myocardial infarction. J Mol Cell Cardiol 2015;87:194–203.

206. Ruiz-Villalba A, Simón AM, Pogontke C, et al. Interacting resident epicardium-derived fibroblasts and recruited bone marrow cells form myocardial infarction scar. J Am Coll Cardiol 2015;65:2057–66.

207. Zhou B, Honor LB, He H, et al. Adult mouse epicardium modulates myocardial injury by secreting paracrine factors. J Clin Invest 2011;121:1894–904.

208. van Amerongen MJ, Bou-Gharios G, Popa E, et al. Bone marrow-derived myofibroblasts contribute functionally to scar formation after myocardial infarction. J Pathol 2008;214:377–86.

209. Fujita J, Mori M, Kawada H, et al. Administration of granulocyte colony-stimulating factor after myocardial infarction enhances the recruitment of hematopoietic stem cell-derived myofibroblasts and contributes to cardiac repair. Stem Cells 2007;25:2750–9.

210. Kramann R, Schneider RK, DiRocco DP, et al. Perivascular $Gli1^{+}$ progenitors are key contributors to injury-induced organ fibrosis. Cell Stem Cell 2015;16:51–66.

KEY WORDS cytokines, extracellular matrix, fibroblast, infarction, remodeling

JACC: BASIC TO TRANSLATIONAL SCIENCE VOL. 4, NO. 3, 2019

EDITOR'S PAGE

Q4 Vital Signs

Can Machine Learning Protect Patients From the Machinery of Modern Medicine?

Douglas L. Mann, MD, *Editor-in-Chief: JACC: Basic to Translational Science*

> *While I sleep I have no fear, nor hope, nor trouble, nor glory. God bless the inventor of sleep, the cloak that covers all man's thoughts, the food that cures all hunger, the water that quenches all thirst, the fire that warms the cold, the cold that cools the heart; the common coin, in short, that can purchase all things, the balancing weight that levels the shepherd with the king, and the simple with the wise.*
>
> —Miguel de Cervantes (1)

I recently had the opportunity to engage the American health care system as an inpatient. Although I am exceedingly grateful to all of my health care providers (including the well-meaning resident who decided that I required a blood transfusion at 5 AM) for the excellent care that I received in the hospital, I must confess that being awakened for vital signs every 4 h reminded me of the sleep deprivation technique (*tormentum vigilae* [waking torture]) used by the Romans to extract information from their enemies. My inpatient experience evoked a number of memories about being sleep deprived as a resident, which in turn made me curious about the origin of q4 vital signs: surely there must be a logical medical explanation for why we sleep deprive inpatients by waking them up every 4 h.

Although collecting vital signs every 4 h has been practiced in hospitalized patients since 1893, the evidence base that supports the clinical utility of this practice is scant (2,3). A recent systematic review of the literature concluded that "There are suggestions that vital sign monitoring has become a routine procedure, but little useful information was identified in regard to the optimal frequency of vital sign measurement. It was noted that many of the important issues related to vital sign measurement have not been investigated through research" (4). In contrast to the paucity of evidence that supports the need for frequent vital signs, there is large body of evidence that shows that poor sleep quality in hospitalized patients can lead to impaired immune responses, hypertension, increased pain sensitivity, changes in metabolic and endocrine regulation, and increased delirium (5). Sleep deprivation has also been linked to the post-hospitalization syndrome, which has been implicated as a cause for 30-day readmissions (6). While there are a number of reasons why hospitalized patients are sleep deprived, checking vital signs is the most important factor that contributes to sleep fragmentation (7).

Given that there are multiple reasons for sleep deprivation in hospitalized patients, it is unlikely that there is a simple fix. This statement notwithstanding, the advent of wearable sensors that can monitor vital signs and that can be coupled with either track and trigger systems or with supervised machine learning-based prediction models will likely have a significant impact on how hospitalized patients are monitored in the future. A recent prospective study showed that a modified track and trigger system (Modified Early Warning Score) was able to identify a low-risk subset of patients who had significantly fewer adverse events than high-risk patients, suggesting that the frequency of nighttime vital signs could be reduced for low-risk inpatients (2). The U.S. Food and Drug Administration (FDA) has approved a wireless device (ViSi Mobile, Sotera Wireless, San Diego, California) for monitoring the vital signs of inpatients including

The author attests they are in compliance with human studies committees and animal welfare regulations of the authors' institutions and Food and Drug Administration guidelines, including patient consent where appropriate. For more information, visit the *JACC: Basic to Translational Science* author instructions page.

ISSN 2452-302X https://doi.org/10.1016/j.jacbts.2019.05.002

blood pressure, heart rate, 3- or 5-lead electrocardiograms, functional oxygen saturation, respiratory rate, and skin temperature (8), thereby allowing health care providers to review real-time transmissions of a complete panel of vital signs, regardless of whether the patient is in bed or is ambulatory. Currently the ViSi Mobile device requires interfacing with a track and trigger monitoring system. The FDA has also approved an artificial intelligence-enabled wearable device (Current, Current Health, Edinburgh, Scotland) for inpatients and outpatients that monitors everything except blood pressure (9). The Current also allows health care providers to monitor a patient's vital signs in real time, with the added benefit that their artificial intelligence algorithms may, in the future, be able to predict which patients are more likely to deteriorate clinically in the immediate future. Although the FDA and other regulatory agencies have not established benchmarks for the predictive accuracy of machine learning algorithms, it is noteworthy that a recent study by Google (Menlo Park, California), in which they obtained deidentified data from 216,221 adults, showed that deep learning models were able to predict in-hospital mortality with an area under the receiver operator curve of 0.93 to 0.94 and 30-day unplanned readmission with an area under the receiver operator curve of 75 to 0.76. Remarkably, these models outperformed the traditional clinically used predictive models (10).

Q4 NO MORE?

Despite decades of research detailing the deleterious effects of sleep deprivation in hospitalized patients, surprisingly few changes have been made by health care systems to remedy this problem. With the advent of wearable technologies that can reliably monitor vital signs, as well as the advent of machine learning algorithms that can accurately predict clinical events based on data in the electronic health record, there is no reason technically why these types of machine learning algorithms cannot be used to predict real-time clinical events in hospitalized patients based on data from wearable devices. As with any high-tech-low-touch approach, artificial intelligence has the potential to further remove patients from the human connection that they have with their health care providers. The question is whether this is something we should lose sleep over—and if so, how much? As always, we welcome your thoughts about the impact of machine learning on health care, either through social media (*#JACC:BTS; #Q4NoMore*) or by e-mail (jaccbts@acc.org).

ADDRESS FOR CORRESPONDENCE: Dr. Douglas L. Mann, Editor-in-Chief, *JACC: Basic to Translational Science,* American College of Cardiology, Heart House, 2400 N Street NW, Washington, DC 20037. E-mail: JACC@acc.org.

REFERENCES

1. de Cervantes M. Don Quixote. New York, NY: Penguin Classics, 2003.

2. Yoder JC, Yuen TC, Churpek MM, Arora VM, Edelson DP. A prospective study of nighttime vital sign monitoring frequency and risk of clinical deterioration. JAMA Intern Med 2013;173:1554–5.

3. Zeitz K, McCutcheon H. Evidence-based practice: to be or not to be, this is the question! Int J Nurs Pract 2003;9:272–9.

4. Lockwood C, Conroy-Hiller T, Page T. Vital signs. JBI Libr Syst Rev 2004;2:1–38.

5. Watson PL, Ceriana P, Fanfulla F. Delirium: is sleep important? Best Pract Res Clin Anaesthesiol 2012;26:355–66.

6. Dharmarajan K, Hsieh AF, Lin Z, et al. Diagnoses and timing of 30-day readmissions after hospitalization for heart failure, acute myocardial infarction, or pneumonia. JAMA 2013;309:355–63.

7. Freedman NS, Kotzer N, Schwab RJ. Patient perception of sleep quality and etiology of sleep disruption in the intensive care unit. Am J Respir Crit Care Med 1999;159:1155–62.

8. Dolan B. FDA OKs Sotera's Full Wireless Patient Monitoring System. Mobihealth News 2012. Available at: https://www.mobihealthnews.com/18291/fda-oks-soteras-full-wireless-patient-monitoring-system. Accessed May 8, 2019.

9. Carfagno J. First AI Medical Monitoring Wearable Approved by FDA for Home Use. Docwire. 2019. Available at: https://www.docwirenews.com/docwire-pick/future-of-medicine-picks/first-ai-wearable-approved-by-fda-for-home-use-monitoring-vitals. Accessed May 8, 2019.

10. Rajkomar A, Oren E, Chen K, et al. Scalable and accurate deep learning for electronic health records. npj Digital Medicine 2018;1:18; https://doi.org/10.1038/s41746-018-0029-1.